ASPECTS OF THE MEASUREMENT OF SOIL STRENGTH USING ROTATING SHEAR DEVICES, WITH PARTICULAR REFERENCE TO THE VANE TEST

A thesis submitted to the University of London
(Imperial College of Science, Technology and Medicine)

in partial fulfilment of the requirements for the degree of
Doctor of Philosophy
in the Faculty of Engineering

by

Mahmoud Mahmoud, B.Sc. (Eng.), M.Sc., DIC

September 1989

To my parents

ABSTRACT

This thesis describes an experimental and a semi-analytical study of some of the fundamental aspects of the measurement of the strength of clays using rotating shear devices. The majority of the investigation is concerned with the vane test, but it is extended to examine the results of rotation of model piles.

Normally consolidated samples of Speswhite kaolin and London clay, as well as a bentonite/London clay mixture, have been used in the vane test experimental programme to study:

(a) the effect of strain rate on the measured vane strength;
(b) the effect of the number of blades on strength;
(c) the pattern of soil deformation induced by the vane.

The effect of the rate of vane rotation on the measured strength is explored by means of a hypothetical model in which consolidation effects are related to the square of the drainage path length, whilst viscous effects are a function of the diameter of the vane. Theoretical drainage curves, originally derived by Blight (1968) and extended by the writer, may be used for the selection of the rate of rotation required to ensure undrained conditions during vane shear.

Increasing the number of vane blades leads to the mobilisation of lower shear strengths at smaller angles of rotation. This effect is explained in terms of vane insertion disturbance effects and the Farrent–Arnold interpretation of the vane test, in which an exponential shear stress distribution is assumed along the vertical shearing surface of adjacent blades.

The progressive development of microfabric features with vane rotation in clay is investigated using petrological techniques observing thin-sections under cross polarised light. This examination is conducted with vanes having two, three and six blades as well as the conventional four, with vanes having a height to diameter (H/D) ratio of 1. The thin-section observations show that the shear structures propagate both in front of and behind each vane blade tip, exhibiting features which resemble logarithmic spirals. The shear structures extend beyond the periphery of the vane and are analogous to those observed by Morgenstern & Tchalenko (1967) in the shear box test. A similar conclusion is inferred, namely that simple shear conditions apply at peak vane stress.

The formation of a continuous cylindrical shear surface around the vane periphery is shown to be a post-peak phenomenon, with the implication that direct shear conditions apply at that stage.

Photoelastic studies, conducted in order to determine both the distribution and the directions of maximum shearing stresses during vane testing, are compared with the results of the thin-section observations, and good agreement is observed.

A specially adapted hydraulic stress path cell is used in order to examine the mode of deformation associated with 4-bladed vanes of H/D = 2 under drained conditions. The same apparatus is used for the examination of the second rotating shear device, namely a model pile. Rigid piles are installed with a minimum of disturbance to the clay, and subjected to rotation under drained conditions. The results show a continuous shear band around the pile at residual shear stress conditions. At peak shear stress, the shear structures are similar to those observed at maximum torque in the vane test. Similar observations are made at both peak and residual shear stress for axial 'wished-in-place' pile load tests. Considerable similarities between the observed microfabric features suggest that simple shear conditions probably also apply at peak shear stress for piles subjected to torsion, as well as for axial pile load tests (Martins, 1983). The soil strengths measured with the vane and model pile are compared, showing good agreement, as do the shear stress – circumferential/axial displacement curves for corresponding torsionally and axially loaded piles.

ACKNOWLEDGEMENTS

The work described in this Thesis was carried out in the Soil Mechanics Section of the Department of Civil Engineering, under the joint supervision of Dr. R.J. Chandler and Professor J.B. Burland (Head of Section). Their constructive comments on the draft version of the Thesis is greatly appreciated, as is the financial support provided by my father over the years and by the Department during the last two years of my Ph.D.

My very special thanks go to Dick Chandler for his guidance, considerable assistance, numerous stimulating discussions from which I have much benefitted, and particularly for his friendship and support throughout the period of this research programme. I would also like to thank him for his help and advice in many other respects, not directly related to the Ph.D.

I am indebted to Prof. Burland for the special interest which he has taken in my work and for keeping a fatherly eye on its progress for the period of its duration. His support, kindness and continuing encouragement are sincerely acknowledged. I am also grateful to him for many fruitful discussions.

I wish to express my gratitude to Professor P.J. Dowling (Head of Department), Professor P.R. Vaughan, Dr. S.K. Sarma, Professor N.N. Ambraseys and Dr. A.E. Skinner, for their interest and assistance, and particularly for their advice, support and encouragement during a difficult period of my research. Special thanks are also due to Dr. David Hight for his friendship and generosity with ideas, and to Dr. David Potts for his co-operation and also for reading the section of the Thesis on the analysis of the vane test in terms of earth pressures.

I am most grateful to Professor E.H. Brown (Structures Section) for his enthusiasm, willingness to help, and assistance with the photoelastic analysis of the vane test and also for reading those sections of the Thesis concerned with photoelastic aspects associated with the vane test. I have learnt a great deal from Prof. Brown, and also from Professor I.M. Allison (Head, Department of Mechanical Engineering, University of Surrey), who kindly provided facilities for the photoelastic experiments on polyurethane rubber, and broadened my knowledge of photoelasticity.

I should also like to extend my thanks to Professor A.W. Skempton, Dr. Richard Jardine and Professor J.N. Hutchinson for their interest and co-operation.

Dr. G. Stephenson (Department of Mathematics) provided valuable assistance with mathematical aspects connected with the analysis of consolidation effects in the vane test.

I would like to express my thanks to my friend and colleague, Andrew Bond, for his comradeship and assistance, and particularly for proof-reading Chapters 2 to 8 of the Thesis.

The technical staff of the Soil Mechanics Research Laboratory provided help with apparatus development. Alan Bolsher manufactured all the vanes and piles tested in the experimental programme. His quick response to most of my requests, not only those connected with the research programme, is much appreciated. The technical assistance of Steve Ackerley, Lou Spall, Graham Keefe and Roger Hare is also acknowledged.

Kevin Schrapel, Department of Earth Sciences, Queen Mary College, University of London, prepared all the thin-sections skilfully and promptly, with due care and attention.

The rubber 'packer' membranes were prepared in the Soil Mechanics Research Laboratory at University College, University of London.

The photoelastic rigs were constructed at the Soil Mechanics Research Laboratory. Technical staff of the Structures Section provided valuable assistance with the setting up of the photoelastic optical bench. Technical staff of the Mechanical Engineering Department of Surrey University helped with the photoelastic experiments conducted on polyurethane rubber.

Ahmed M. El-Sharief assisted the writer during the triaxial compression tests on remoulded London clay.

Andrew Chipling and Richard Packer advised on photographic matters. The photographs for the Thesis have been produced with the invaluable assistance of Ms. Romy Driscoll (Department of Materials), who undertook the task most enthusiastically.

Ciril de Quadros (Sir William Halcrow and Partners Ltd.) traced most of the drawings presented in the Thesis.

I am glad to acknowledge the help and assistance of my friends and colleagues, Drs. Najwa Yassir, Dalmas Nyaro, Jan Hellings, Tony Addis, Kunle Onabolu, Satoru Shibuya, Deneys Schreiner, Dave Toll, Theodora Tika, George Dounias, Marciano Maccarini, Luis Lemos, Ephrain Ovando-Shelley, Justice Maswoswe, Jose Ziolkowski, and particularly Ms. Sherry Nabijou and Messrs. David French, Nicholas Ninis and Phil Smith. Thanks are also due to Luis Bressani, Mike Crilly, Rob Day, Chris Menkiti and Mike Leddra.

Miss. Kathy Evans and Mrs. Eileen Gibbs assisted on many occasions.

I would also like to thank Mrs. Kay Crooks and Miss. Jessica Underhill for their assistance in the departmental library.

My deepest gratitude goes to my parents, brother and sister for their support and continuous encouragement throughout this research programme.

NOTATION

A	rate of change of pore water volume per unit time per unit volume of soil
A_0	rate of generation of heat per unit time per unit volume
A_r	'area ratio' of vane
a	length of leading shear structures; radius of cylindrical triaxial sample; radius of 'sphere of influence' centred at mid-point of vane (in Blight's (1968) consolidation theory)
$a_{p,r}$	number of soil segments at peak and residual shear stress conditions
a_v	coefficient of compressibility of soil
a_{1-4}	relative orientations of thin-section slide between two polarising filters
av	average of test results
C	speed of light in a vacuum or in air; a constant
C_c	compression index of soil
c	specific heat of a solid; cohesion intercept
c'	effective cohesion intercept
$c_{p,r}$	peak and residual shear strength of soil 'element'
c_s	coefficient of swelling of soil
c_u	undrained shear strength
c_{uh}	undrained shear strength along the horizontal direction
c_{uv}	undrained shear strength along the vertical direction
c_v	coefficient of consolidation of soil
D	diameter
D_f	outer diameter of the vane failure zone
D_r	'disturbance ratio'
d	drainage path length; diameter of vane shaft
dM	moment of resistance of an 'element' along surface of shearing
ds	length of an 'element' along surface of shearing
E	initial stiffness of soil
e	voids ratio
e_λ	voids ratio at effective pressure $p' = 1$ kPa
F_R	total resultant force on the entire length of 'wall'
G_s	specific gravity of soil; shear modulus of soil
H	height
I_B	Bishop's brittleness index
I_D	disturbance index ($= D_r/A_r$)
I_L	liquidity index
I_P	plasticity index

i	individual test results
K	stiffness parameter (= $\{\tau_m/\sigma_{vo}'\}/\theta_m$ or τ_m/θ_m)
K_A	coefficient of active earth pressure
K_P	coefficient of passive earth pressure
K_0	coefficient of earth pressure at rest; ratio of radial and axial stresses on soil
k	coefficient of permeability
L	('wall') length
l	length of vane shaft; segmental distance between adjacent blades around the vane periphery (= $2\pi R/n$)
M	(maximum) torque measured with the vane
M_R	torque about the top of the 'wall'
M_0	torque with zero drainage
M_1	torque with full drainage
m	contribution of each vane blade to the total torque
m_v	coefficient of volume change of soil
N	fringe order; number of leading shear structures
n	number of vane blades; number of test results
n.c.	normally consolidated soil
OCR	overconsolidation ratio
o.c.	over-consolidated soil
P_A	active thrust acting behind the 'wall'
P_P	passive resistance acting in front of the 'wall'
P_R	resultant force on 'retaining wall'
p'	mean effective stress (= $\{\sigma_1' + 2\sigma_3'\}/3$)
q	surcharge
$(q/p')_f$	failure stress ratio
R	radius of vane
r	radius from centre of 'sphere of influence' at which pore pressure generation/ dissipation is considered
S_r	'shear area ratio'
S_t	sensitivity
S_2	kinematic discontinuity (Morgenstern & Tchalenko, 1967)
S_6	strength normalised with respect to that measured at standard rate of 6 °/min (= τ_f/τ_{f0})
T	time; time factor
T_f	time factor corresponding to the time to failure
t	time; thickness of vane blade; time to reach a given average degree of consolidation
t_f	time to failure

U	average degree of consolidation / pore pressure dissipation
u	(excess) porewater pressure
u_0	maximum excess porewater pressure (generated due to vane rotation)
u_f	excess porewater pressure at failure
V	τ_f/σ_{vo}' normalised with respect to $(\tau_f/\sigma_{vo}')_{max}$
V_r	ratio of field vane and K_0-consolidated triaxial compression strengths
V_0	V at undrained conditions
V_1	V at fully drained conditions
v	temperature; velocity of vane tip (= $R\omega$)
W_4	normalised soil shear strength measured with an n-bladed vane (= $\{\tau_f/\sigma_{vo}'\}_n/\{\tau_f/\sigma_{vo}'\}_4$; τ_{fn}/τ_{f4}; M_n/M_4)
w	water content
w_L	liquid limit
w_P	plastic limit
z	depth of penetration of top of rotating shear device below soil surface
α	orientation of the crossed polaroids; vane 'perimeter ratio' (La Rochelle et al., 1973)
α_n	positive roots of the transcendental equation, $J_0(a\alpha_n) = 0$
β	angle between adjacent blades for vane with n equally spaced blades (= $2\pi/n$)
γ_s	saturated unit weight of soil
γ_w	unit weight of water
$\Delta\sigma_v$	change in total stress
δ	retardation between 'components' of light (= $N\lambda$); 'wall' friction angle
$\dot{\varepsilon}$	strain rate
ε_f	axial strain at failure
θ	(measured) angle of rotation of vane; variation in the vertical plane of a sphere
θ_b	twist of vane blade
θ_c	compliance of torsional load cell
θ_f	angular rotation to failure
θ_m	angle of rotation corresponding to τ_m
θ_s	twist of vane shaft
θ_t	'exact' ('true') angular rotation of vane
κ	thermal conductivity
λ	wavelength of colour fringe
λ_n	positive roots of Bessel's function of order zero, $J_0(\lambda_n) = 0$
Ω	angle of propagation of leading shear structures
ρ	average density

σ_a'	axial effective stress
σ_h	normal total stress
σ_h'	normal effective stress acting on the vane; effective (radial) horizontal stress
σ_{ho}'	'in situ' horizontal effective stress
σ_r'	radial effective stress
σ_v	(total) vertical stress
σ_v'	(current) vertical effective stress
σ_{vo}'	maximum consolidation pressure; initial vertical effective stress
σ_1	major principal stress
σ_3	minor principal stress
τ	shear stress
τ/σ_{vo}'	normalised shear stress
τ_A	shear stress mobilised along the vertical shearing surface at vane blade A
τ_f	measured peak (vane) shear strength
τ_f/σ_{vo}'	normalised vane strength
τ_{f0}	strength measured at 'standard' rate of rotation
τ_h	maximum shear stress mobilised across the top and bottom horizontal surfaces circumscribed by the vane
τ_m	mobilised shear stress
$\tau_{p,r}$	soil peak and residual shear strength for a progressive failure model
τ_r	'residual' (large displacement) shear strength (corresponding to an angle of rotation of 360°)
τ_v	maximum shear stress mobilised along the vertical cylindrical surface circumscribing the vane
τ_{vf}	maximum shear stress mobilised along the vertical cylindrical surface circumscribing the vane
ϕ	angle of shearing resistance of soil
ϕ'	effective angle of shearing resistance of soil
ϕ_{ps}	plane-strain angle of shearing resistance of soil
ϕ_r'	effective residual angle of shearing resistance of soil
ω	rate of rotation

TABLE OF CONTENTS

ABSTRACT iii

ACKNOWLEDGEMENTS v

NOTATION viii

TABLE OF CONTENTS xii

CHAPTER 1 INTRODUCTION 1

1.1 SCOPE OF THE THESIS 1
1.2 OUTLINE OF THE THESIS 4

CHAPTER 2 LITERATURE REVIEW 6

2.1 INTRODUCTION 6
2.2 THE VANE SHEAR TEST 6
2.3 THE VANE SHEAR STRENGTH 9
2.4 STRAIN-RATE EFFECTS IN THE VANE TEST 10
2.5 THE EFFECT OF THE NUMBER OF BLADES ON THE VANE SHEAR STRENGTH 16
2.6 THE VANE FAILURE MECHANISM 21
2.6.1 Extent of the Vane Failure Surface 21
2.6.2 Evidence for Progressive Failure 27
2.7 PILES SUBJECTED TO ROTATION 29

CHAPTER 3 EXPERIMENTAL APPARATUS, SAMPLE PREPARATION AND TESTING PROCEDURES 35

3.1 INTRODUCTION 35
3.2 EXPERIMENTAL APPARATUS 35
3.2.1 Introduction 35
3.2.2 Vane Shear and Pile Testing 36

	3.2.2A	Vanes	36
		3.2.2A(i) Laboratory-vanes	36
		3.2.2A(ii) Triaxial-vanes	37
	3.2.2B	The laboratory vane shear apparatus	39
	3.2.2C	Triaxial-vane and model pile test cell	41
		3.2.2C(i) Introduction	41
		3.2.2C(ii) Apparatus layout	41
		3.2.2C(iii) Sample loading	46
		3.2.2C(iv) Vane insertion and rotation	47
		3.2.2C(v) Piles	47
		3.2.2C(vi) Pile loading systems	48
3.2.3	Triaxial Apparatus		48
	3.2.3A	Introduction	48
	3.2.3B	The conventional triaxial cell	49
3.2.4	Consolidometers		49
	3.2.4A	Introduction	49
	3.2.4B	The loading frame	49
	3.2.4C	The large oedometer	50
3.2.5	Instrumentation		50
	3.2.5A	Introduction	50
	3.2.5B	Load cells	51
	3.2.5C	Pressure transducers	51
	3.2.5D	Displacement transducers	54
	3.2.5E	Data acquisition units	54
	3.2.5F	'Exact' angular rotation of the vane	55
	3.2.5G	Axial stresses on samples in the large stress path cell	56
	3.2.5H	Miscellaneous	56
3.3	SAMPLE PREPARATION		56
3.3.1	Materials Selected for the Experimental Programme		56
	3.3.1A	Introduction	56
	3.3.1B	Reasons for the clays selected	57
	3.3.1C	Characteristics of Speswhite kaolin	58
	3.3.1D	Characteristics of London clay	58
	3.3.1E	Characteristics of the bentonite/London clay mixture	58
3.3.2	Sample Preparation		58
	3.3.2A	Introduction	58
	3.3.2B	Slurry preparation	63

3.3.2B(i) Kaolin 63
3.3.2B(ii) London clay 64
3.3.2B(iii) The bentonite/London clay mixture 64
3.3.2C Slurry consolidation 64
3.3.2C(i) Displacement-controlled consolidation 64
3.3.2C(ii) Stress-controlled consolidation 69
3.3.2D Consolidation in the stress path cell 69
3.4 TESTING PROCEDURES 71
3.4.1 Introduction 71
3.4.2 Laboratory-vane Tests 72
3.4.2A Introduction 72
3.4.2B Tests to investigate strain-rate effects in the vane test 72
3.4.2C Tests to study the effect of different numbers of blades 73
3.4.2D Tests to examine the vane failure mechanism 73
3.4.2E Tests to study other effects 76
3.4.2E(i) Tests to study the effect of sample storage time 76
3.4.2E(ii) Tests to examine the effect of shaft friction 76
3.4.3 Triaxial-vane Tests 77
3.4.3A Introduction 77
3.4.3B Unloading the sample 77
3.4.3C Vane insertion 77
3.4.3D Re-application of total radial stresses to the sample 78
3.4.3E Vane rotation 78
3.4.4 Model Pile Tests 79
3.4.4A Introduction 79
3.4.4B Installation of model piles 80
3.4.4C Pile loading procedures 81
3.4.5 Triaxial Compression Tests 81
3.4.6 Thin-section Preparation 82
3.4.6A Introduction 82
3.4.6B Impregnation procedure 82
3.4.6C Preparation of thin-sections 83
3.4.6D Examination of thin-sections 83
3.5 PHOTOELASTIC STUDY OF THE VANE TEST 86
3.5.1 Introduction 86
3.5.2 Experimental Procedures 86
3.5.2A The polariscope 86
3.5.2B The photoelastic materials 88

3.5.2B(i) Gelatine 88
3.5.2B(ii) Polyurethane rubber 89
3.5.2C The model experiments 90
3.5.2C(i) Gelatine 90
3.5.2C(ii) Polyurethane rubber 92

CHAPTER 4 STRAIN-RATE EFFECTS IN THE VANE TEST 95

4.1 INTRODUCTION 95
4.2 TESTING PROGRAMME 95
4.2.1 Introduction 95
4.2.2 Tests on Speswhite Kaolin 96
4.2.3 Tests on London Clay and the Bentonite/London Clay Mixture 96
4.3 SHEAR STRESS – ROTATION BEHAVIOUR AT DIFFERENT RATES OF VANE ROTATION 97
4.3.1 Introduction 97
4.3.2 Parameters Used for the Presentation and Analysis of Results 97
4.3.3 Shear Stress – Rotation Characteristics 98
4.3.3A Kaolin test results 98
4.3.3B London clay and the bentonite/London clay mixture test results 102
4.3.4 Summary 124
4.3.4A The effect of vane size 124
4.3.4B The effect of clay type 125
4.4 RATE OF ROTATION TO ENSURE UNDRAINED CONDITIONS 130
4.4.1 Intoduction 130
4.4.2 Tests on Kaolin 133
4.4.2A Introduction 133
4.4.2B The 12 mm vane test results 133
4.4.2C The 18 mm vane test results 135
4.4.2D The 24 mm vane test results 135
4.4.2E Summary of the results 137
4.4.2F Discussion of the results 139
4.4.2F(i) Introduction 139
4.4.2F(ii) The effect of sample storage time 139
4.4.2F(iii) The effect of the depth of vane insertion 141
4.4.2F(iv) Comparison of results with published data 143
4.4.2F(v) Summary 146

4.4.3 Tests on London Clay 146
4.4.3A Introduction 146
4.4.3B Normally consolidated London clay 147
4.4.3C Remoulded London clay 149
4.4.4 Tests on the Bentonite/London Clay Mixture 154
4.4.5 Analysis of the Results 155
4.4.5A Introduction 155
4.4.5B Theoretical considerations 155
4.4.5B(i) Blight's (1968) theory 155
4.4.5B(ii) Gibson & Henkel's (1954) theory 157
4.4.5C Experimental considerations 159
4.4.5C(i) Kaolin 159
4.4.5C(ii) London clay 162
4.4.6 Summary 164

CHAPTER 5 THE BEHAVIOUR OF VANES WITH DIFFERENT NUMBERS OF BLADES 166

5.1 INTRODUCTION 166
5.2 TESTING PROGRAMME 167
5.3 SHEAR STRESS – ROTATION CHARACTERISTICS 167
5.3.1 Introduction 167
5.3.2 Kaolin Test Results 168
5.3.3 London Clay Test Results 170
5.3.4 Summary 171
5.4 DISCUSSION OF THE RESULTS 181
5.4.1 Introduction 181
5.4.2 Progressive Failure Effects 181
5.4.3 Insertion Disturbance Effects 190
5.4.4 The Farrent–Arnold Interpretation of the Vane Test 192
5.4.5 Summary 194

CHAPTER 6 STUDY OF THE VANE FAILURE MECHANISM 195

6.1 INTRODUCTION 195
6.2 TESTING PROGRAMME 196
6.2.1 Laboratory-vane Tests 196
6.2.2 Triaxial-vane Tests 197

6.3 TEST RESULTS 198
6.3.1 Introduction 198
6.3.2 Insertion Disturbance 198
6.3.3 The 4-bladed Vane 203
6.3.3A Development of shear structures 203
6.3.3B Conditions close to peak torque 214
6.3.4 The Effect of Different Numbers of Blades 219
6.3.4A The 2-bladed vane 219
6.3.4B The 3-bladed vane 223
6.3.4C The 6-bladed vane 227
6.3.4D Summary 230
6.3.5 Sample Water Content Effects 232
6.3.6 Clay-type Effects 233
6.4 QUANTIFICATION OF THE RESULTS 235
6.4.1 Shear Structure Characteristics 235
6.4.1A Length 235
6.4.1B Angle of propagation 237
6.4.1C Number 237
6.4.2 Diameter of the Vane Failure Surface 237
6.4.3 Size of the Vane Failure Zone 241
6.4.4 Summary 243
6.5 FAILURE MECHANISMS IN THE VANE TEST 244
6.5.1 Simple Shear Conditions 244
6.5.2 Comparison of Vane and Shear Box Tests 246
6.6 ANALYSIS OF THE 2-BLADED VANE IN TERMS OF EARTH PRESSURES 250

CHAPTER 7 PHOTOELASTIC MODELLING OF THE VANE TEST 253

7.1 INTRODUCTION 253
7.2 TESTING PROGRAMME 254
7.3 EXPERIMENTAL RESULTS 254
7.3.1 The Isochromatics 255
7.3.2 The Isoclinics 257
7.3.3 Shear Stress Directions 260

CHAPTER 8 ROTATING SHEAR DEVICES UNDER SIMULATED IN SITU CONDITIONS 262

8.1 INTRODUCTION 262
8.2 TESTING PROGRAMME 263
8.3 TRIAXIAL-VANE TEST RESULTS 264
8.3.1 Introduction 264
8.3.2 Shear Stress – Rotation Relationships 264
8.4 MODEL PILE TEST RESULTS 270
8.4.1 Piles Subjected to Rotation 270
8.4.1A Installation disturbance 270
8.4.1B Conditions close to peak shear stress 273
8.4.1C Residual conditions 275
8.4.2 Axially Loaded Pile 275
8.5 DISCUSSION OF THE RESULTS 279
8.5.1 The Behaviour of Rotating Shear Devices 279
8.5.1A Vanes with different H/D ratios 279
8.5.1B Comparison of vane and pile rotation 281
8.5.1C Effective stress analysis of the vane test 284
8.5.2 Comparison of the Behaviour of Torsionally and Axially Loaded Piles 286

CHAPTER 9 CONCLUDING REMARKS 288

9.1 CONCLUSIONS 288
9.1.1 The Vane Shear Test 288
9.1.1A Strain-rate effects in the vane test 288
9.1.1B Effect of the number of blades 290
9.1.1C Vane failure mechanism 291
9.1.2 Model Pile Tests 293
9.2 PRACTICAL IMPLICATIONS 295
9.2.1 The Vane Shear Test 295
9.2.2 Piles Subject to Torsion 296
9.3 SUGGESTIONS FOR FURTHER RESEARCH 297

REFERENCES 298

APPENDIX A1 BASIC PHOTOELASTICITY 306

APPENDIX A2 THEORIES OF CONSOLIDATION FOR THE VANE TEST 310

A2.1 INTRODUCTION 310
A2.2 BLIGHT'S THEORY (THE SPHERICAL CASE) 311
A2.3 THE CYLINDRICAL CASE 315
A2.4 CRITICISMS OF BLIGHT'S THEORY 316

APPENDIX A3 INTERPRETATION OF THE VANE TEST FOR c–ϕ MATERIALS 318

APPENDIX A4 ANALYSIS OF THE VANE TEST IN TERMS OF EARTH PRESSURES 322

CHAPTER 1

INTRODUCTION

1.1 SCOPE OF THE THESIS

The possibility of using rotation of piles for the measurement of the shaft carrying capacity has received very little attention in the past, despite the greater ease of operation and significantly reduced cost of torsional, as opposed to axial, pile load tests (see, e.g. Stoll, 1972). Clearly, therefore, there is scope in examining the behaviour of piles subjected to rotation, and in comparing the observed mode of failure with that associated with axially loaded piles, with a view to developing an in situ test method for the determination of pile shaft friction. In this light, it is also of considerable value to study the mechanism of failure of other rotating shear devices, of which the most well-known is the vane.

Since the 1940s, the vane shear test has been used worldwide for the determination of the undrained strength of soft clays, particularly in the field. Despite its advantages (in terms of its low cost and ease of use), a body of people, mainly in the research community (e.g. Schmertmann, 1975), have criticised the reliability of the undrained strength measured with the vane, following differences between the vane strength and the undrained strength measured using other test methods. Two reasons which are often quoted for the observed discrepancies are:

(a) that the cylindrical rupture surface has a diameter larger than that of the vane, thus implying that the vane overestimates the soil strength; and
(b) that the vane failure mode is progressive, which infers that the vane underestimates the undrained shear strength.

Therefore, it is clearly of considerable importance for the interpretation of the vane test to examine the conventional assumption that the mobilisation of the peak soil strength occurs both fully and instantaneously along the entire cylindrical surface circumscribing the vane.

It is surprising that the vane failure mechanism has not so far been clearly established, since (a) the available test data indicate a 'vane-sized' circular failure plane in most instances, but with some cases presuming a rupture surface with a diameter extending beyond the vane perimeter, and (b) there are two 'schools of thought'

regarding the progressive or non-progressive nature of the mode of failure in the vane test. Thus it is important to investigate the soil deformation patterns induced by the rotating vane at different stages of the shear stress – rotation curve, in order to examine the validity of the assumptions related to both the extent and the mode of formation of the vane failure surface.

One or two authors have in the past suggested that progressive failure probably occurs with vanes with fewer blades than four, although almost all of the studies into the vane failure mechanism have been conducted using a four-bladed vane. Moreover, the universal acceptance of the 4-bladed vane as standard has not been fully substantiated. Hence there is obvious merit in investigating the behaviour of vanes with different numbers of blades, both fewer and greater than four. Ideally, both the shear stress – rotation characteristics and the mode(s) of failure of such vanes should be examined.

Adoption of a standard rate of vane rotation of 6 (or 12) degrees per minute (°/min) as standard in the laboratory, as well as in the field, is based on a large number of studies into strain-rate effects in the vane test, conducted primarily in the field. This rate corresponds to the measurement of the smallest shear strength for most soft clays. Blight (1968) found that the 'undrained' vane strength of soils does not always occur at the rate of 6 °/min, since the soil coefficient of consolidation (c_v) plays an important role, with strengths inconsistent with undrained conditions being measured at this rate in soils having high values of c_v. Blight derived theoretical drainage curves (Fig. 2.3) for the vane test, and obtained good agreement between experimental and theoretical relationships. These studies involved vanes with a height to diameter (H/D) ratio of 2, which is standard. Therefore it is also of interest to examine whether Blight's theoretical drainage curve holds for vanes with other H/D ratios.

As part of the present research programme, 'laboratory-vane' (Section 3.2.2A(i)), 'triaxial-vane' (Section 3.2.2A(ii)) and model pile tests have been performed, together with photoelastic experiments and unconsolidated undrained triaxial compression tests. Examination of petrological thin-sections of soil sheared by a laboratory-vane forms a major part of the work. Speswhite kaolin has been used for most tests, with both London clay and a bentonite/London clay mixture also having been tested extensively. The samples have all been prepared in the laboratory, following a normally consolidated stress history, or they have been remoulded. A number of pieces of equipment have been specifically designed and constructed for the investigations undertaken.

Strain-rate effects in the vane test are established from a study of vanes having H/D ratios of 1, with diameters in the range D = 12 to 24 mm, rotated through 360° at rates between about 1 and 1100 °/min. Shear stress – rotation behaviour at different rates of rotation of samples of a number of soft clays are explored, and a hypothetical model is proposed in order to explain the variation of measured vane strength with time to failure and/or rate of rotation. The rate of rotation to ensure undrained conditions is established by extending Blight's (1968) theoretical relationship for vanes with H/D = 2, to vanes with H/D = 1. The importance of the vane H/D ratio on the appropriateness of a given theoretical drainage curve is also considered, albeit briefly.

The behaviour of vanes with different numbers of blades in the range 2 to 12, as well as the use of a solid rod to simulate a multi-bladed vane, is investigated with a view to identifying the relative significance on the measurement of the vane shear strength of insertion disturbance effects, as opposed to progressive failure effects which are demonstrated using a simple model. Relevance of the use as standard of a 4-bladed vane, and validity of the assumption of exponentially, rather than uniformly, distributed shear stresses between adjacent blades along the vertical vane periphery is also examined.

Failure mechanisms associated with 2-, 3-, 4- and 6-bladed vanes are established from an examination of thin-sections prepared from 12mm 'square' (i.e. H/D = 1) laboratory-vanes. The assumptions related to the shape, size and mode of formation of the vane failure surface are thus examined. Results from 12mm x 24mm long 4-bladed triaxial-vane tests provide verification of the laboratory-vane test results. Comparison of the deformation patterns at or near maximum shear stress in the vicinity of the vane with corresponding features in the shear box test show considerable similarities, thus suggesting that simple shear conditions probably also apply in the vane test. Analysis of the 2-bladed vane in terms of earth pressures is successful in demonstrating that the measured peak torque is related to the resultant of the passive and active earth pressures which develop around each vane blade.

Photoelastic modelling of the vane has enabled an examination of both the distribution and directions of maximum shearing stresses in the vicinity of vane blades. The photoelastic materials used were gelatine and polyurethane rubber. There is support for exponentially distributed shear stresses between adjacent blades, with good agreement between directions of maximum shearing stresses and orientations of shear structures observed from thin-sections.

By considering that a pile is equivalent to a multi-bladed vane, a natural progression from the study of the vane test is that of rotation of piles. 'Wished-in-place' rigid model piles — installed with little or no disturbance to the soil fabric — have been subjected to torsion. The results confirm the validity of the presumption regarding a multi-bladed vane representing a pile. Conditions at peak and residual shear stress for axial and torsional pile load tests are compared, and show considerable similarities, with simple shear conditions applying at maximum shear stress.

1.2 OUTLINE OF THE THESIS

The Thesis has nine Chapters and four Appendices. Each Chapter/Appendix has a number of Sections and Sub-sections; the Tables and Figures for each Chapter/Appendix are presented within that Chapter/Appendix, as closely as possible to where reference is first made to a Table or Figure.

Chapter 2 presents a review of the literature with respect to (a) the vane shear test, concentrating on three major aspects, including the effect on the measured shear strength of both the rate of vane rotation and the number of vane blades, as well as the mode of deformation associated with the vane test, and (b) the behaviour of piles subjected to torsion.

Experimental apparatus, sample preparation and testing procedures are described in detail in Chapter 3.

A detailed presentation of the effect of the rate of vane rotation on the measured shear strength is given in Chapter 4. The experimental results are discussed in the light of a hypothetical model, in the first instance, and then, comparisons are made between experimental results and theoretical relationships derived by extending and modifying Blight's (1968) interpretation of the vane test.

Chapter 5 is concerned with an investigation of the shear stress – rotation characteristics of vanes with different numbers of blades, in order to examine the appropriateness of the use of the 4-bladed vane as standard. The relative dominance of vane insertion disturbance effects over progressive failure effects on the measurement of soil shear strength is illustrated with the aid of a simple progressive failure model and an extension of the Farrent–Arnold interpretation of the vane test.

A comprehensive account of the failure mechanism associated with both laboratory- and triaxial-vanes is given in Chapter 6. Deformation patterns around 2-, 3- and 6-bladed laboratory-vanes, as well as the conventional 4-bladed vane, are presented, discussing variations in the failure modes. Implications of the results are discussed in the light of direct shear box test results and retaining wall analyses.

Analysis of the vane test using photoelasticity is described in Chapter 7. Both the distribution and directions of shearing stresses around the vane blades are established, and discussed with respect to the Farrent–Arnold interpretation and deformation patterns around 4-bladed vanes, respectively.

Chapter 8 presents the results of torsional pile load tests, together with the results of triaxial-vane and axial pile load tests, with discussions centred on a comparison of the behaviour of piles subjected to torsion with both that of vanes and that of axially loaded piles.

Conclusions and suggestions for further research are outlined in Chapter 9.

Appendix A1 provides a summary of the basics of photoelasticity, while Appendix A2 gives a detailed description of Blight's (1968) theory of consolidation for the vane test; an alternative version of Blight's theory, as well as criticisms of that theory, is also presented. Interpretation of the vane test for c–ϕ materials, with the assumption of a logarithmic spiral shearing surface (Arnold, 1978) is given in Appendix A3. Analysis of the vane test in terms of earth pressures is outlined in Appendix A4.

CHAPTER 2

LITERATURE REVIEW

2.1 INTRODUCTION

The vane shear test is one of the most widely used methods for the determination of the undrained strength of soft clays, particularly in the field. Despite its advantages (in terms of its low cost and ease of use), a number of people have heavily criticised the reliability of the undrained shear strength measured with the vane (see, e.g. Schmertmann, 1975). These criticisms have centred on differences between the measurement of the undrained strength using the vane and by other test methods (see, e.g. Chandler, 1988).

This Chapter concentrates on those aspects of the vane test which are investigated in the proceeding Chapters, following a layout similar to that of the Thesis (see Section 1.2). A brief review of the vane test is followed by an examination of some factors which are important to the interpretation of the test. Three major aspects of the vane test are considered. These include: (a) the effect of the rate of rotation of the vane; (b) the influence of the number of vane blades; (c) the vane failure mechanism. The discussion is confined to the conventional rectangular/square vane, with little or no consideration of either 'diamond' vanes (Aas, 1965; Menzies & Mailey, 1976) or 'elliptical' vanes (Selvadurai, 1979). Finally, the subject of rotation of piles is reviewed.

2.2 THE VANE SHEAR TEST

An historical review of the vane shear test is given by Merrifield (1980) and Flodin & Broms (1981) in which the development of the Olsson vane borer in the 1910s and its first use in 1919 are described. Although the use of the Olsson vane borer and other vane-type instruments probably continued in the 1920s and 30s, the vane test was developed in its modern form during the 1940s by such people as Carlson (1948) and Skempton (1948), who believed that it would provide a direct and accurate measurement of the undrained shear strength of soft clays in situ. However, the various possible factors expected to affect the vane strength measurement were not fully considered until Cadling & Odenstad (1950) conducted an extensive investigation of the vane test. They examined the influence of the dimensions of the vane, the number of vane blades, the rate of vane rotation, and the possibility of progressive failure. On the basis of this

pioneering work, Cadling & Odenstad suggested certain standards, which were:

(a) that the height to diameter (H/D) ratio should be 2;
(b) that the vane should have four blades;
(c) that the rate of rotation should be 6 degrees per minute (°/min).

It was further stated that the possibility of progressive failure in the vane test was small. These recommendations have subsequently been adopted on a worldwide basis (see, e.g. Chandler, 1988).

In addition, there seems to be international agreement concerning the conventional interpretation of the vane test (Fig. 2.1), in which the maximum torque (M) recorded by the vane is related to the undrained shear strength (c_u) of the soil by the expression:

$$c_u = \frac{2M}{\pi D^2 H\left[1 + \frac{D}{3H}\right]} \qquad \text{Eq. 2.1.}$$

The basic assumptions made are:

(a) that the test is undrained;
(b) that vane insertion causes no disturbance to the soil fabric;
(c) that the soil is isotropic with respect to undrained strength;
(d) that the shear stress distribution around the vane failure surface is uniform;
(e) that the soil strength is mobilised fully and instantaneously along the entire failure surface;
(f) that the vane failure surface is defined by the vane diameter.

The main purpose of this Thesis is to examine the validity of the above assumptions by considering certain aspects which, despite their fundamental nature, have not so far been fully explored.

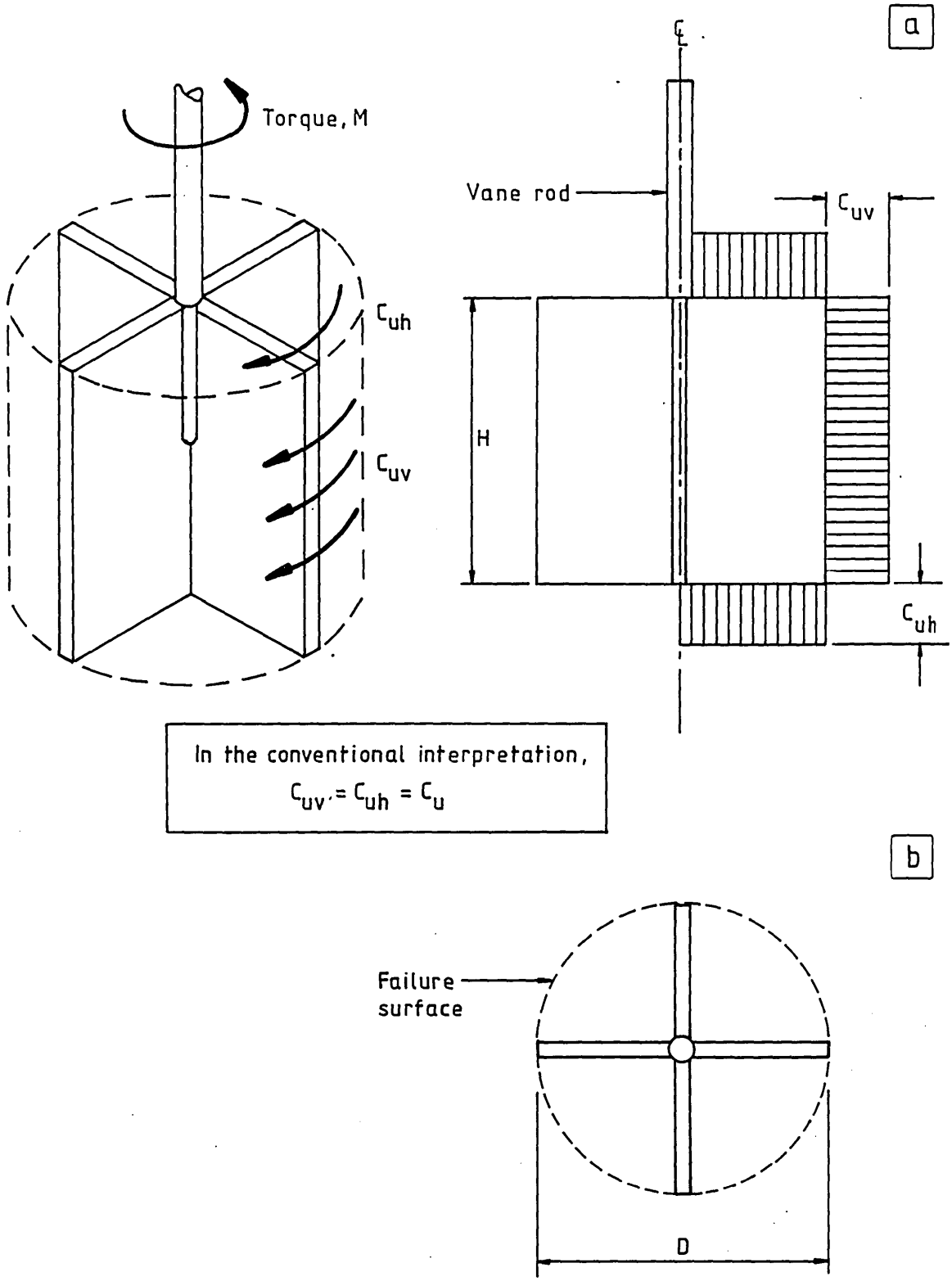


Fig. 2.1 Fundamental assumptions made in the interpretation of the vane test.
(a) Distribution of shear stresses along the vertical cylindrical surface and the two horizontal end-surfaces.
(b) Shape and extent of the cylinder of revolution circumscribing the vane at failure.

2.3 THE VANE SHEAR STRENGTH

In order to establish whether or not the vane shear test provides an accurate measurement of the undrained shear strength of soils, it is necessary to compare the measured vane strength with the strength measured in other tests. In practice, the ratio of the (4-bladed) vane shear strength to other measurements of undrained strength does not usually equal unity. In early work it was generally assumed that agreement between vane and unconfined compression test results was to be expected. More recently, however, it has been realised that various factors are involved, and that there will not necessarily be agreement between two different measurements of strength. Factors which may be important in controlling the magnitude of the vane shear strength ratio include sensitivity (S_t), anisotropy with respect to undrained strength, and shear strain rate amongst others.

As would be expected, the disturbance to the soil fabric during vane insertion is greater for the more sensitive clays, for which the available strength in the vicinity of the vane may be significantly reduced and thus, it is reasonable to expect low vane strength ratios (Chandler, 1988); the more sensitive clays are those with low I_p. Therefore, the amount of local destruction of interparticle bonds within the soil surrounding the vane is a dominating factor in the measurement of the vane strength ratio. In this light, it is important to note that the more blades the vane has, the greater the disturbance caused to the soil fabric. The significance of the effect of the number of blades on the measured vane strength is discussed later in Section 2.5.

It is well-known that the undrained shear strength of soils may be anisotropic, particularly for normally consolidated clays with low plasticity. Since the conventional interpretation of the vane test assumes uniform shear stress distribution on both the horizontal and vertical shear surfaces of the vane (Section 2.2), the measurements of soil strength in different directions would be reliable only if the assumption holds. However, it has been shown by Menzies & Merrifield (1980) that, although the above assumption is valid with regard to the vertical periphery of the vane, the shear stress distribution on the top and bottom horizontal surfaces is far from uniform. Hence, there is little justification in the procedure in which the undrained strength anisotropy of the soil is determined graphically (see, e.g. Aas, 1965) using the expression:

$$\frac{2M}{\pi D^2 H} = c_{uv} + \left[\frac{D}{3H}\right] c_{uh} \qquad \text{Eq. 2.2,}$$

where the results of tests using vanes with different H/D ratios are plotted in

terms of $2M/\pi D^2H$ versus $D/3H$, with c_{uv} and c_{uh} respectively given by the intercept and slope of the straight line through the data.

It is noteworthy that Merrifield's (1980) work led to the conclusion that the calculation of the undrained strength in the vertical and horizontal planes using vanes with different H/D ratios might be seriously in error (see also Mahmoud, 1988).

2.4 STRAIN-RATE EFFECTS IN THE VANE TEST

The effect of the rate of vane rotation on the measurement of shear strength has in the past been the subject of a large number of studies (Cadling & Odenstad, 1950; Sridharan & Madhav, 1964; Bhandari, 1970; Wiesel, 1973; Perlow & Richards, 1977; Torstensson, 1977; Pugh, 1978; Sharifounnasab & Ullrich, 1985; Roy & Leblanc, 1988). Table 2.1 summarises the relevant soil and vane test parameters corresponding to each study.

The pioneering study of Cadling & Odenstad (1950) is important since it led to many of the standards now used for the field vane test. They found a 20% increase in the measured strength when the rate of rotation of 2-bladed field vanes was increased from 6 °/min to 60 °/min. At unspecified rates of rotation less than 6 °/min, higher vane strengths were measured — an effect attributed to consolidation of the soil in the vicinity of the vane. They subsequently recommended the rate of rotation of 6 °/min as standard, since they found that this rate corresponded both to the measurement of the smallest shear strength, and to the time of loading in laboratory tests, where times to failure (t_f) of between 2 and 15 minutes are typical. [Chandler (1988) reports that t_f = 30–60 secs when the field vane is rotated at 6 °/min.] Since then, the field vane test has almost invariably been carried out at the standard rate of 6 °/min, which has also been adopted as a standard in the laboratory.

Most studies suggest that higher shear strengths would result at higher rates of rotation — a trend which is explained either in terms of rheological phenomena (see, e.g. Bjerrum, 1973), or in terms of pore pressure effects (see, e.g. Bjerrum et al., 1958). As the rate of rotation increases under undrained conditions, it is considered that the measurement of a higher shear strength is probably as a consequence of either (a) viscous effects related to the clay content of the soil, or (b) the generation of lower pore pressures, with both (a) and (b) subsequently leading to the mobilisation of higher shear stresses at failure. However, the range of rotation rates over which the measured strength increases with increasing rates of strain is not quite clear.

Table 2.1 Strain-rate effects in the vane shear test: Published data.

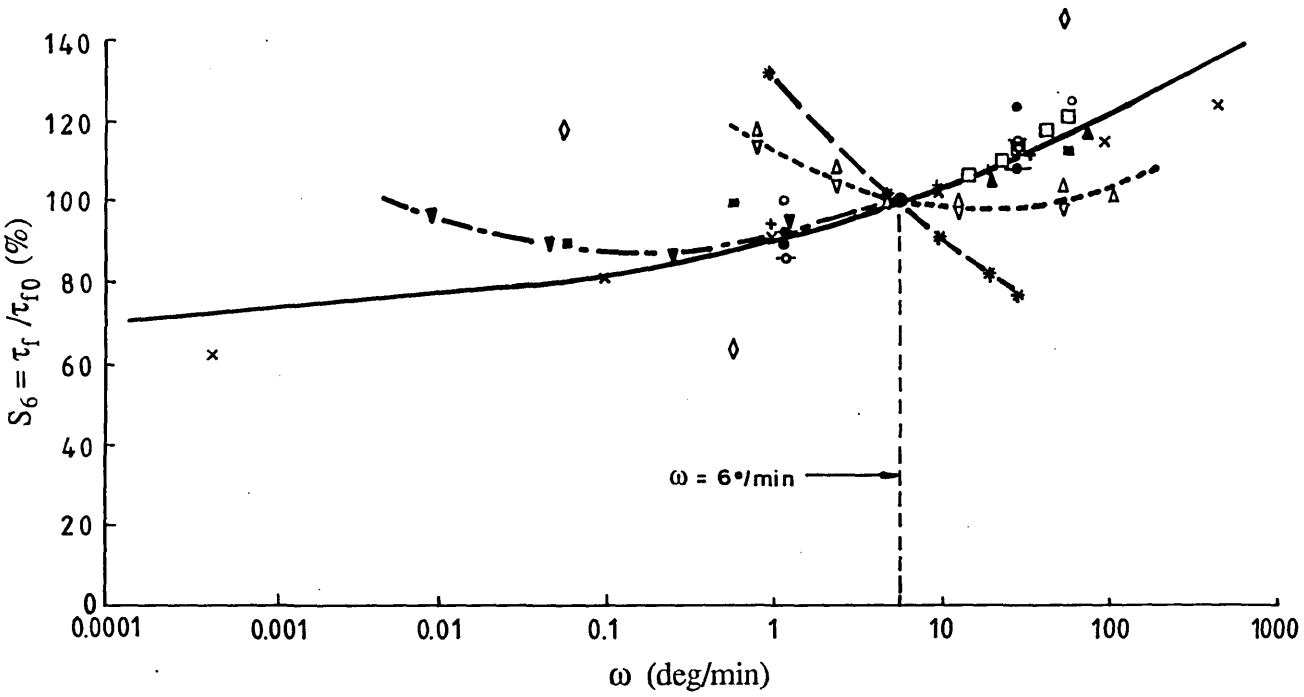
Reference	Test Site and/or (Soil Type)	Liquid Limit (%)	Plastic Limit (%)	Plasticity Index (%)	Clay Fraction (%)	Vane Dimensions D (mm)	Vane Dimensions H/D	Range of Values of z	Range of Rates of Rotation (°/min)
Cadling & Odenstad* (1950)	Bromma, Sweden	-	-	38	-	80	2.5	2–10 m	6–60
Sridharan & Madhav (1964)	n.c. silty clay (undisturbed & remoulded)	75–135	37–51	38–92	20–44	12.7	1.5	2 m	1.2–30
Bhandari (1970)	London clay (remoulded)	65	25	40	43	12.7	1.5	-	1.2–30
	Reading Beds (remoulded)	45	20	25	45	"	"	-	1.2–64
Wiesel (1973)	Ska Edeby, Sweden (n.c. varved clay)	-	-	42	-	65	2	5–11 m	0.06–60
Perlow & Richards (1977)	San Diego Trough (clayey silt)	111	47	64	35	12.7	2	1.5 m	21–79
Torstensson (1977)	Backebol, Sweden (n.c./lightly o.c. inorganic clay)	-	-	50–65	-	65	2	3–14 m	0.00047–470
	Askim, Sweden (n.c./lightly o.c. organic clay)	-	-	80–90	-	"	"	2–4 m	0.0047–470
Pugh (1978)	Stanford-le-hope (mucking clay)	-	-	40–70	30–60	254	2	4–6 m	0.011–6.7
Sharifounnasab & Ullrich (1985)	(n.c. kaolinite)	48	34	14	43	12.7	1, 1.5, 2	38.1–63.5 mm	1–30
	(n.c. Pierre Shale)	138	35	103	73	"	"	38.1 mm	1–35
Roy & Leblanc (1988)	Saint-Louis de Bonsecours (silty clay)	42	22–28	13–19	69–80	65	2	7–11 m	0.84–57
	Saint-Alban (highly organic silty clay)	22–39	16–21	6–18	60–65	"	"	"	"

* using a 2-bladed vane

Therefore, there is obvious merit in comparing the results of different vane tests, taken from the literature, and shown in Table 2.1. The values of the measured strength, τ_f, have in each case been normalised to the vane strength measured at the standard rate of rotation of 6 °/min, τ_{fo}, and plotted against the corresponding rate of rotation, ω, in Fig. 2.2; rates of rotation extend over seven logarithmic cycles in the range 10^{-4}–10^3 °/min. The general trend of the data is that the strength increases with increasing rates of rotation. At values of ω = 0.6 °/min and 60 °/min, which are respectively ten-times slower and faster than the standard rate of rotation, the effect of the rate of vane rotation on the measured strength is demonstrated by the corresponding decrease and increase in the measured strength of about 12% and 17% respectively. The difference between the strength measured at the standard rate and that at a rate of rotation of 12 °/min — which is also extensively used in the field — is about 5%.

It is important to note that three sets of data in Fig. 2.2 do not show the measurement of higher strengths at faster rates of rotation. On the one hand, there are the kaolinite data of Sharifounnasab & Ullrich (1985), which exhibit the opposite trend of decreasing strengths with increasing rates of rotation. On the other hand, a more complicated relationship is evident from both Pugh's (1978) data obtained from tests on Mucking clay, and the results of Roy & Leblanc (1988) corresponding to soils from both St. Alban and St. Louis; these data illustrate that, although higher strengths are measured with increasing rates of rotation, the strength reduces at decreasing rates of rotation until a minimum is reached at a rate beyond which higher strengths are once again measured. The rate of rotation corresponding to the measurement of the minimum strength is $\omega \approx$ 0.15 and 20 °/min for Pugh's and Roy & Leblanc's data, respectively. Therefore, the use as standard of the rate of rotation of 6 °/min is open to question, since it apparently does not always result in the measurement of the smallest undrained shear strength.

There is an indication that S_6 ($= \tau_f/\tau_{fo}$) is related in some manner to I_p in Fig. 2.2. The kaolinite data of Sharifounnasab & Ullrich (1985) and both the St. Alban and St. Louis data of Roy & Leblanc (1988), with low I_p values of 14%, 6–18%, and 13–19%, respectively, show trends which may be explained by drainage effects at slow rates of rotation and by viscous effects at fast rates (see Sections4.4.1, 4.4.5 and 4.4.6). Although the Mucking clay that Pugh tested had relatively high values of I_p in the range 40–70%, it also had a high coefficient of consolidation ($c_v \approx 60$ m^2/yr), which might have resulted in consolidation in the vicinity of the vane as a consequence of reducing rotation rates.



		I_p (%)
□	CADLING & ODENSTAD (1950), BROMMA NEAR STOCKHOLM	38
-○-	SRIDHARAN & MADHAV (1964), UNDISTURBED	38-92
-●-	REMOULDED	
•	BHANDARI (1970), LONDON CLAY	40
○	READING BEDS	25
■	WIESEL (1973), SKA EDEBY NEAR STOCKHOLM	42
×	TORSTENSSON (1977), BÄCKEBOL	50-65
▲	PERLOW & RICHARDS (1977), SAN DIEGO TROUGH	64
▼	PUGH (1978), MUCKING CLAY	40-70
◊	SHIBUYA (1981), CYLINDER SHEAR TESTS, OSAKA ALLUVIAL LAYER	56
*	SHARIFOUNNASAB & ULLRICH (1985), KAOLINITE	14
+	PIERRE SHALE	103
Δ	ROY & LEBLANC (1988), ST. LOUIS	13-19
▽	ST. ALBAN	6-18

Fig. 2.2 Variation of normalised (vane) shear strength with rate of rotation: Comparison of published results.

In summary, it is evident that the soil type, as characterised by its physical (i.e. I_p) and consolidation (i.e. c_v) properties has an important influence on the variation of the measured vane strength with the rate of vane rotation. It is therefore concluded that a single standard rate of vane rotation to obtain undrained strength cannot be valid for all soils.

Blight (1968) was the first to acknowledge this fact. In an attempt to establish the rates of vane rotation required for both drained (and undrained) conditions to apply, he developed a simple theory of consolidation (Appendix A2.2). This approximate theory assumes that the volume of soil which will be influenced by pore pressure effects associated with vane rotation is a sphere of radius a, centred on the mid-height of the vane, with hydrostatic conditions prevailing at the surface of this sphere of influence (also see Section 4.4.5B). [The other assumptions made by Blight are outlined in Appendix A2.2, while their validity is discussed in Appendix A2.4.] By considering the dissipation of excess pore pressures at a radius, r, within the 'sphere', and assuming that the maximum torque, M, is related to the average degree of consolidation, U, Blight derived relationships between U and the time factor, T ($= c_v t_f/D^2$, in which t_f = the time to failure in the vane test, and D = the diameter of the vane failure surface; see also Eqs. 4.3 and 4.9).

Blight carried out a series of tests in a well-graded cohesionless silt ($k = 1 \times 10^{-7}$ m/sec; $c_v = 370$ m^2/yr) at a depth of 3 m, using rectangular (H/D = 2) field vanes of three different diameters (D = 30, 45 and 60 mm). The measured torques in slow tests ($t_f \approx 35$ mins) were about 35% greater than those measured in rapid tests ($t_f = 0.1$ mins). Very fast tests with a time to failure of 1 second ($t_f = 0.017$ mins) resulted in the measurement of torques similar to those at the slowest rate. Fig. 2.3 shows Blight's test results in terms of U and T. It can be seen that there is good agreement between the experimental results and the theoretical relationship for a 'sphere' of radius a = D, the vane diameter, with r = D/2 (see also Appendix A2.2). Blight, therefore, concluded that the above relationship would apply to any size vane with H/D = 2 operating in soil with any consolidation characteristics.

In this connection, it is of interest to note that Matsui & Abe (1981), who carried out laboratory tests using 15mm diameter vanes of H/D = 2 in reconstituted kaolin (I_p = 20%; $k = 5 \times 10^{-9}$ m/sec), have also concluded that their data also support Blight's theory. Moreover, Roy & Leblanc's (1988) results of field vane tests in St. Alban and St. Louis at rates of rotation in the range ω = 0.4–30 °/min also show acceptable agreement with Blight's approximate theory (see Fig. 2.3). Consequently, it may be concluded that Blight's simple theory can be used to determine the rate of vane rotation

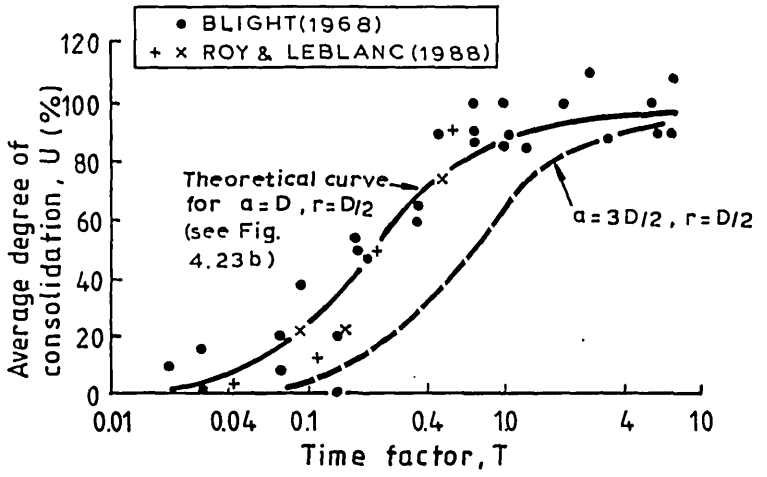


Fig. 2.3 Comparison of theoretical drainage curves for vanes with H/D = 2 with experimental results (after Chandler, 1988).

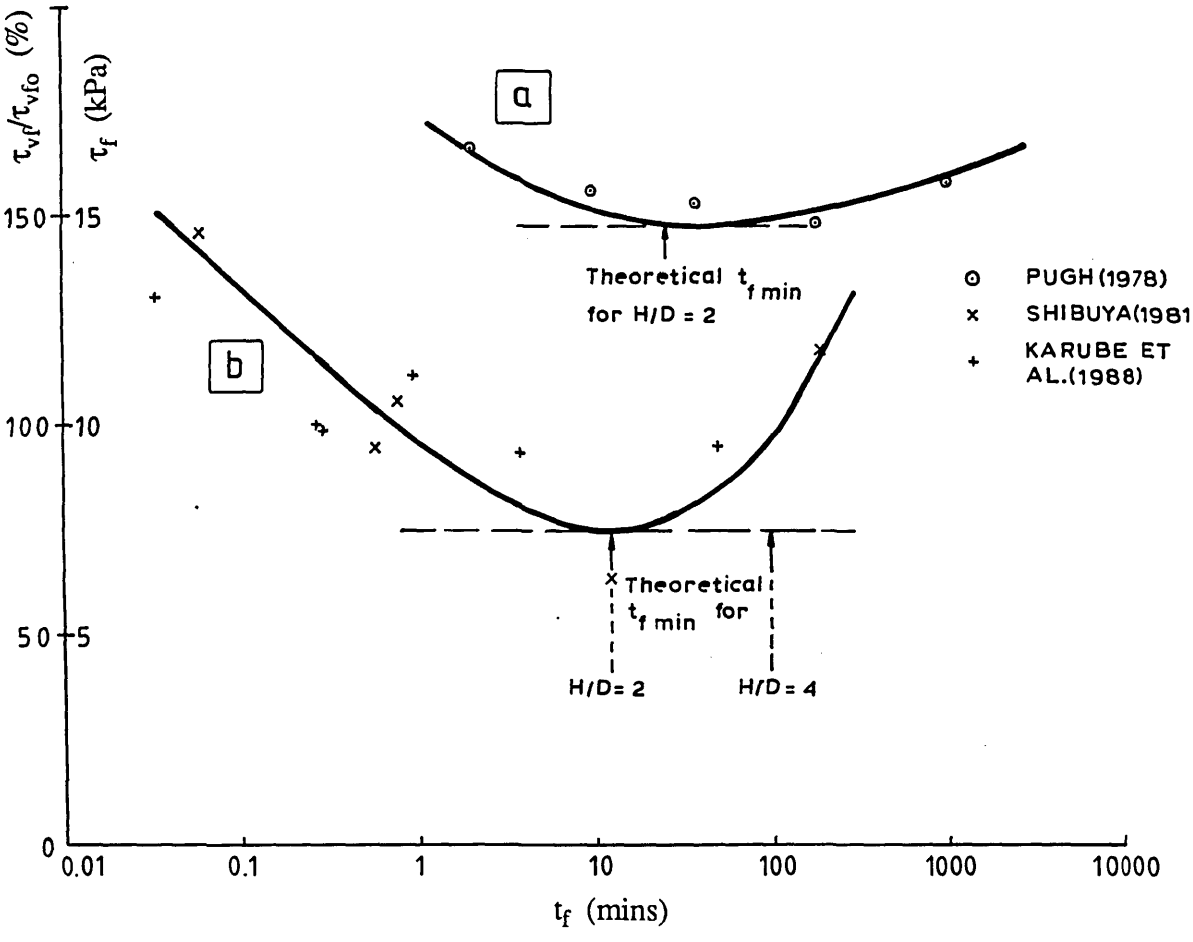


Fig. 2.4 Comparison of experimental results from rotating shear tests with theoretical times to failure corresponding to undrained conditions.

corresponding to substantially undrained conditions during the test. According to the above theoretical relationship, undrained conditions (i.e. $U \leq 5\%$) apply at $T \leq 0.04$.

Now, it is considered useful to apply Blight's theory to both Pugh's (1978) field vane test data, and the results of Shibuya (1981) and Karube et al. (1988), obtained from laboratory cylinder shear rod tests in normally consolidated samples of an alluvial marine clay (see Section 2.7). There is very good agreement between the times to failure at which the minimum vane strengths are seen to occur experimentally and those predicted using Blight's theoretical relationship, as follows:

(a) $t_f \approx 25$ mins for Pugh's data, since $t_f = TD^2/c_v$, $T = 0.04$, $D = 254$ mm, and $c_v = 60$ m^2/yr (see Fig. 2.4a);

(b) Fig. 2.4b shows the results of Shibuya and Karube et al. in terms of S_6 versus t_f, with the two sets of data normalised with respect to τ_{fo}, and then treated as one data set, since Shibuya's samples were at lower stress levels than those of Karube et al. Given that $D = 15$ mm, and $c_v = 0.38$ m^2/yr (Shibuya, 1981), the theoretical time to failure (for $H/D = 2$) is $t_{f\,min} = 12.5$ mins. It is of particular interest to note that the appropriate theoretical relationship for the cylinder shear rod ($H/D \approx 4$; Table 8.3) test data may be considered to be that corresponding to the 'sphere' with $a = 2D$ (Section 4.4.5; Figs. 4.23a and b), for which $U \leq 5\%$ corresponds to $T \leq 0.3$, giving $t_{f\,min} \approx 95$ mins. However, $t_{f\,min} \approx 95$ mins (corresponding to $a = 2D$) does not fit Shibuya and Karube et al.'s data as well as $t_{f\,min} = 12.5$ mins (corresponding to $a = D$). This suggests that for vanes (and other rotating shear devices) with $H/D \geq 2$, the volume of soil which is affected by the vane is probably that corresponding to a sphere with $a = D$.

2.5 THE EFFECT OF THE NUMBER OF BLADES ON THE VANE SHEAR STRENGTH

Only a few researchers have investigated the effect of the number of vane blades on the measurement of the vane shear strength and the corresponding shear stress – rotation characteristics (Vey & Schlesinger, 1949; Cadling & Odenstad, 1950; Farrent, 1960; Goughnour & Sallberg, 1964; Cox, 1967; Helenelund, 1967; Wiesel, 1973; Menzies & Simons, 1977). The soil and vane test parameters relevant to each study are summarised in Table 2.2.

Table 2.2 Effect of the number of blades in the vane test: Published data.

Reference	Test Site and/or (Soil Type)	Liquid Limit (%)	Plastic Limit (%)	Plasticity Index (%)	Vane Dimensions D (mm)	H/D	Rate of Rotation (°/min)	Range of Values of z	Values of n Tested
Vey & Schlesinger (1949)	Chicago (n.c. glacial tills)	31	-	11.5	88.9	1.29	1	6.1–13.7 m	2 and 4
Cadling & Odenstad (1950)	Bromma, Sweden	-	-	38	80	2.5	6	2–4 m	2 and 4
Farrent (1960)	Noarlunga (sand)	-	-	-	38.1	1.33	40–80	25.4–38.1 mm	3, 4 and 6
Goughnour & Sallberg (1964)	remoulded loam,	36	28	8	6.35	2	12	12.7 mm	2, 4 and 6
	clay loam,	42	19	23	"	"	"	"	"
	silty clay loams	48	26	22	"	"	"	"	"
	and sandy loams	34	28	6	"	"	"	"	"
Cox (1967)	(sand/kaolinite mixture)	-	-	-	12.7	1–2?	6?	-	3, 4 and 6
Helenelund (1967)	Espoo, Helsinki (fibrous peat)	-	-	-	16.5	2	-	1.0–1.2 m	2, 3, 4 and 6
Menzies & Simons (1977)	Brent Knoll	-	-	37*	70 (diamond vane)	2	-	2 m	4 and 8

* after Merrifield (1980)

Vey & Schlesinger (1949) carried out a number of 2- and 4-bladed field vane (H/D ≈ 1.3) tests on normally consolidated Chicago glacial clays ($I_p \approx 12\%$) at depths in the range 6.1–13.7 m; the vanes were rotated at a rate of (ω =) 1 °/min. Their results indicate that the strengths measured with the 2-bladed vane were about 20% higher than those measured with the 4-bladed vane.

Cadling & Odenstad (1950) conducted a total of six 2-bladed and three 4-bladed field vane tests (H/D = 2.5) at Bromma near Stockholm ($I_p = 38\%$) at depths of 2, 3 and 4 m. Despite a large degree of scatter in the 2-bladed vane test data, they found that the 4-bladed vane resulted in the measurement of slightly higher strengths than the former. This is in agreement with the average values of vane strength of 8.94 and 9.93 kPa, extracted from their paper, which respectively correspond to the 2- and 4-bladed vanes. Although the large scatter in the very small number of test results leads one to doubt the repeatability of the data, Cadling & Odenstad recommended the 4-bladed vane as standard (because of its greater stiffness and suitability for practical use), and added: "The discrepancy in the strength measurement using a vane with four blades instead of the ideal number would probably be of little practical importance."

Cadling & Odenstad also studied the deformation patterns at different angles of rotation of a 4-bladed vane and concluded that there was little or no evidence of progressive failure, since the pattern of deformation was found to be comparatively uniform across the whole surface of rupture. However, the average strength measured with the 4-bladed vane was about 11% greater than that measured with the 2-bladed one, which suggests that there probably was a progressive failure element present. This inference is contrary to the conclusion drawn by Cadling & Odenstad from their studies of the vane failure mechanism (Section 2.6.2).

In a study of the vane test in 'free-draining' soils, Farrent (1960) carried out a series of laboratory tests with 3-, 4- and 6-bladed vanes. Noarlunga sand was compacted — with an addition of 10% of water by weight — into California Bearing Ratio and Standard Proctor moulds. The vanes had H/D ratios of about 1.3 and were rotated at a rate of (ω =) 40–80 °/min. The average torques measured with the 3- and 6-bladed vanes were respectively 24% greater and 39% less than the average torque measured with the 4-bladed vane.

Goughnour & Sallberg's (1964) study involved a number of laboratory tests with 2-, 4- and 6-bladed vanes having H/D = 2. The vanes were inserted to a depth of (z =) 12.7 mm below the surface of the samples and rotated at a constant rate of (ω =) 12 °/min. Results of tests on remoulded samples of a loam, a clay loam, silty clay loams

and sandy loams all showed that the 6- and 4-bladed vanes gave strengths respectively 9 and 2% greater than the 2-bladed vane, which suggested to the authors that progressive failure was taking place.

In a review of the theory and practice of the vane test in c–ϕ materials, Cox (1967) reports the results of a number of 3-, 4- and 6-bladed miniature vane tests on a sand/kaolinite mixture. The experimental torque ratios, M_3/M_6 and M_3/M_4, which were derived from average torque curves, were found to vary between the limits of 1.15 and 1.40, being relatively constant over a wide range of ϕ values.

Helenelund (1967) carried out an investigation to examine the influence of the number of vane blades on the development of shearing resistance in a fibrous peat at Espoo near Helsinki (w = 950–1050%). The averaged strengths measured with 2-, 3- and 6-bladed field vanes were respectively 71, 63 and 48% higher than that measured with the 4-bladed vane.

Although Wiesel (1973) apparently performed 4- and 8-bladed vane tests at Ska Edeby near Stockholm, the results of the tests were unfortunately not presented.

The results of a series of 4- and 8-bladed diamond-shaped field vane tests in the Brent Knoll trial embankment (I_p = 37%, as given by Merrifield, 1980) have been reported by Menzies & Simons (1977). Although the 8-bladed vane tests were carried out two weeks after the 4-bladed ones, it was concluded that the two data sets were indistinguishable. However, a closer examination of the test results reveals that the strengths measured with the 8-bladed vane were on average 6% less than those measured with the 4-bladed vane.

In summary, apart from Farrent (1960), Cox (1967) and Helenelund (1967), all investigators suggest that the effect of the number of blades on the measured vane strength is not very significant. In this light, it is important to note that Cadling & Odenstad (1950) and Goughnour & Sallberg (1964) have concluded, albeit only in a qualitative manner, that progressive failure effects are enhanced as the number of blades decreases, whilst with increasing number of blades the vane insertion effects become significant. Both these effects are thought to result in the measurement of lower shear strengths. Nevertheless, it is clear that none of the above studies has involved an extensive testing programme aimed at a systematic investigation of the effect of the number of blades on the measurement of the vane shear strength. Consequently, the conclusions drawn in connection with the influence of the number of vane blades on the measured vane strength are open to criticism, since there is no evidence that either

progressive failure effects or vane insertion disturbance effects are so dominant that they would significantly influence the measurement of soil strength in tests with vanes having a different number of blades.

The data summarised in Table 2.2 are plotted in Fig. 2.5, in which the measured torques/strengths have been normalised with respect to the torques/strengths measured with a 4-bladed vane, i.e. $W_4 = \tau_{fn}/\tau_{f4}$ or $= M_n/M_4$, where n is the number of blades on the vane. In spite of the scatter in the results, the general trend of the data suggests that higher strengths are measured with a 2-bladed vane, whilst the measured strengths are lower as the number of blades increases; the observed trend is contrary to the overall conclusions previously made in the literature.

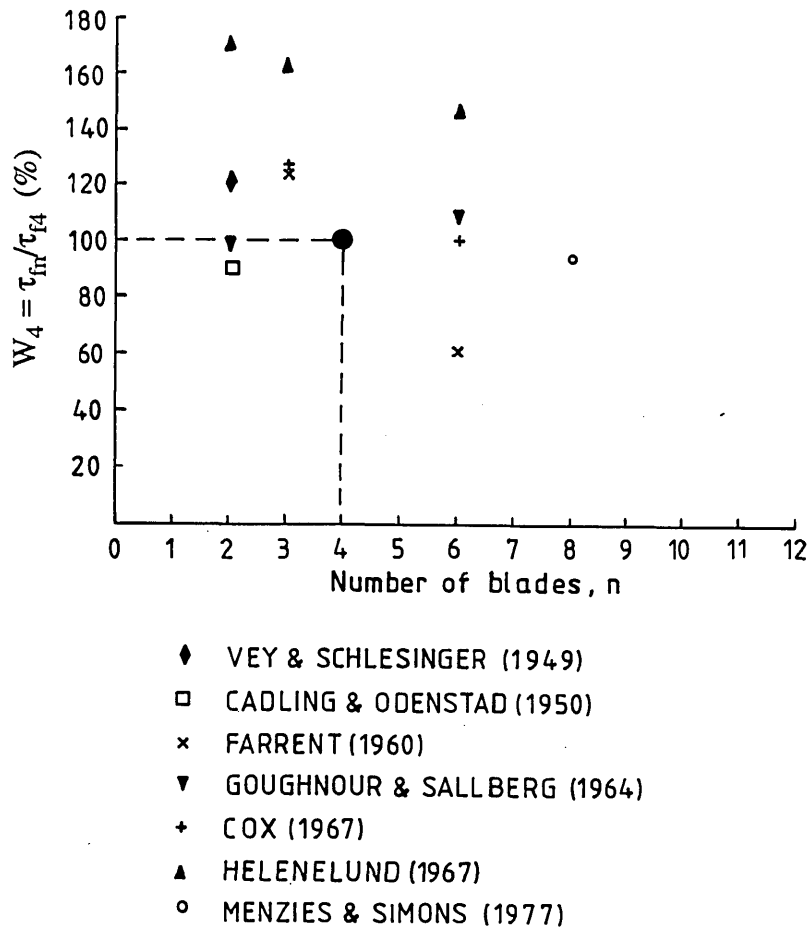


Fig. 2.5 Effect of the number of blades on the measured vane strength : Comparison of published results.

2.6 THE VANE FAILURE MECHANISM

2.6.1 Extent of the Vane Failure Surface

Since it is normally postulated that the mobilisation of the vane shear strength will occur on both the vertical cylindrical surface and the horizontal end-surfaces of the vane (Section 2.2; Fig. 2.1), it implicitly follows that the vane failure surface will be defined by the cylindrical circumscription of the vane blades (see, e.g. Hansen & Gibson, 1948). While a few investigators have questioned the validity of this assumption (Skempton, 1948; Vey & Schlesinger, 1949), others have found supporting evidence concerning its appropriateness. Since the diameter of the vane failure surface is of fundamental importance in the interpretation of the vane test (see Eq. 2.1), it is vital to determine the reasons for the contradictory conclusions expressed in the literature.

A comparison of field vane and unconfined compression test strength data led Skempton (1948) to suggest that the vane rupture surface had a diameter 5% larger than the vane diameter. Evidently, at that time it was not appreciated that vane and unconfined compression tests need not necessarily yield identical strength measurements (see, e.g. Section 2.3). Although Vey & Schlesinger (1949) were convinced that the diameter of the cylindrical shear surface would depend on soil plasticity and hence might not always be defined by the vane diameter, they concluded that the difference between the actual diameter of the shear surface and that used in the conventional test interpretation would probably be small and within the accuracy of the test. However, it is important to acknowledge that neither Skempton nor Vey & Schlesinger had any direct experimental evidence for anything other than the assumption of a 'vane-sized' failure surface.

Subsequently, many attempts have been made to examine the shape and size of the vane failure surface, primarily as a consequence of observed discrepancies between the measurements of the soil shear strength using the vane and by other test methods (Cadling & Odenstad, 1950; Mohan & Jain, 1957; Gibbs, 1960; Jones, 1961; Karlsson, 1961; Wilson, 1963; Kenney & Landva, 1965; Arman et al., 1975; Roy, 1975; Rush, 1975; Veneman, 1977; Fukuda, 1980; Merrifield, 1980; Cheah, 1981; Kimura & Saitoh, 1983; Hoeg, 1985; Roy & Leblanc, 1988; Veneman & Edil, 1988). It is clear from this literature review that there are still conflicting views in connection with the validity of the assumption that the vane failure surface circumscribes the vane periphery. There are two major 'schools of thought':

(1) Those who have concluded that failure occurs on a surface tangential to the vane blades and leads to the formation of a cylindrical surface falling on the circumscribing circle of rotation. These scholars therefore accept that the assumption of a cylindrical 'vane-sized' failure surface is applicable to the analysis of the vane test (Vey & Schlesinger, 1949; Cadling & Odenstad, 1950; Mohan & Jain, 1957*; Gibbs, 1960; Jones, 1961; Karlsson, 1961; Wilson, 1963; Kenney & Landva, 1965; Rush, 1975; Veneman, 1977; Fukuda, 1980; Merrifield, 1980; Cheah, 1981; Hoeg, 1985). [* Note: Although Mohan & Jain apparently observed a very fine 38mm diameter circular air gap and some indication that soil was slightly pushed out beyond the periphery of the vane, they concluded that the diameter of the vane failure surface was 'just equal' to the vane diameter, D, where D = 50.8 mm.]

(2) Those who have concluded that the vane failure surface, though circular in shape, is not defined exactly by the vane dimensions but extends beyond the vane perimeter (Skempton, 1948; Arman et al., 1975; Kimura & Saitoh, 1983; Roy & Leblanc, 1988). [Roy's (1975) studies led him to doubt the assumption of a cylindrical failure surface in the conventional interpretation of the vane test.]

These contradictory conclusions have been drawn from studies of the vane failure mechanism using a number of different experimental techniques. Therefore, it is considered useful to examine the possible significance of the different test procedures on the observed extent of the vane failure surface.

A 4-bladed vane was used by all the investigators, except Cadling & Odenstad (1950) who used a 2-bladed field vane as well as a 4-bladed laboratory vane.

The field investigations by Mohan & Jain (1957) and Gibbs (1960) involved the examination of the soil mass after retrieval from the test location and thus, the shapes of the observed failure surfaces may have been influenced by sampling disturbance.

In the laboratory, various techniques have been employed to observe the patterns of failure around the vane. On the one hand, there is the use of wet patterned tissue paper placed in the soil at the vane mid-height (Cadling & Odenstad, 1950), while on the other hand, there is the relative sophistication of radiographic techniques (Arman et al., 1975; Roy, 1975; Rush, 1975; Fukuda, 1980; Merrifield, 1980; Cheah, 1981; Kimura & Saitoh, 1983; Hoeg, 1985; Roy & Leblanc, 1988).

The 'smoked plate' and 'layered' methods were both used by Jones (1961) in his investigation of the mode of failure and the zone of influence of the vane in sands. The 'smoked plate' technique involves the introduction, positioning, and finally recovery of a smoked perspex plate in the horizontal plane containing the top edge of the vane. The plate is then photographed, thus revealing the removal of smoke particles caused by grain movements which result from the shearing action of the vane. In the 'layered' technique, the position of the rupture surface is indicated by disturbance of very thin marker layers of dyed sand. Capillary tension resulting from the subsequent introduction of water into the deposit enables the sand to stand unsupported while the marker layers are examined.

Gibbs (1960) polished and then lacquered air-dried test samples in order to examine the clay texture.

Other workers have observed the vane failure surface directly. Karlsson (1961) cut out the volume of clay above the vane, while Wilson (1963) simply inserted the vane in the soil to a depth equal to its height, and examined the disturbance at the ground surface.

Studies in which radiographic techniques were used in order to examine the vane failure mechanism fall into two groups: (1) those which used lead shot for the measurement of displacements (Rush, 1975; Merrifield, 1980; Kimura & Saitoh, 1983), and (2) those which did not (Kenney & Landva, 1965; Arman et al., 1975; Roy, 1975; Fukuda, 1980; Merrifield, 1980; Cheah, 1981; Hoeg, 1985; Roy & Leblanc, 1988).

In the latter, the slip surfaces appear as light areas on the radiographs, and indicate easier passage of X-rays through the soil. The light areas have been attributed to either (a) orientation of the clay particles parallel to the direction of irradiation (Hoeg, 1985), or (b) a lower density of the soil structure resulting from the dilation of clay (Hoeg, 1985) or sand (Merrifield, 1980) as a consequence of lower stress levels.

There have been various degrees of success with radiographic studies using lead shot. The results of investigations carried out by Rush (1975) on kaolin led to limited interpretations due to absence of any dilation patterns, although these patterns were clearly demonstrated by the results of his tests on sand. Figs. 2.6a and b are radiographs, reproduced by Rush, respectively taken after clockwise angles of rotation of 2 and 12° during 4-bladed vane tests in fine Washed Beach sand; the three-dimensional image of the vanes in the radiographs is probably due to non-axial alignment of the X-ray machine. Figs. 2.6a and b show dilation behind each blade, with

a circular rupture surface circumscribing the vane; the movement of lead shot placed between the blades can also be seen. Fig. 2.6a, which according to Rush corresponds to conditions just prior to failure, shows the development of a few very fine straight shear planes at the blade tips (see also Fig. 6.13a). These shear structures had apparently increased in length with further rotation until the formation of a complete circular failure surface at approximately 12° rotation (see Fig. 2.6b and also Fig. 6.13 b); the straight shear structures remain as relic features after failure.

Based on an examination of the displacements of lead shot at various angles of rotation, Merrifield (1980; repeated in part in Menzies & Merrifield, 1980) derived contours of maximum shear strain which at small angles of rotation ($\theta = 5°$), showed a flattened arc approximating a chord between the blade tips, but at larger rotations ($\theta = 20°$) moved towards the circumscribing cylinder of rotation.

Photoelastic techniques were used by Merrifield (1980) in a qualitative study of the shear stress distribution around the vane (see also Section 7.3.1). Eccogel 1265 transparent epoxy gel — a linear elastic material, with Poisson's ratio of 0.5 and very low creep properties — was used to simulate a saturated clay subjected to a two-dimensional rapid loading condition. On the basis of observations from contours of maximum shear stress corresponding to angles of rotation in the range $\theta = 0–10°$, Merrifield states that at small rotations ($\theta < 5°$), the direction of 'growth' of maximum shear strains was along a chord joining each blade tip and not along the vane circumference, with contours of maximum shear stress extending both within and beyond the cylindrical surface enclosing the vane blades.

The only previous examination of the vane failure mechanism using petrological techniques is that carried out unsuccessfully by Veneman (1977). Figs. 2.7a–d show the soil deformation patterns observed from tracings obtained from slide projections of the thin-sections prepared from freeze-dried, plastic-impregnated samples. According to Veneman, these show that the failure surface is a very thin circular zone with a diameter equal to that of the vane. However, Veneman's observations must be in doubt since he made no distinction between 'shrinkage cracks' formed during freeze-drying, and microfabric features developed as a consequence of the shearing action of the vane (see Figs. 2.7a–d).

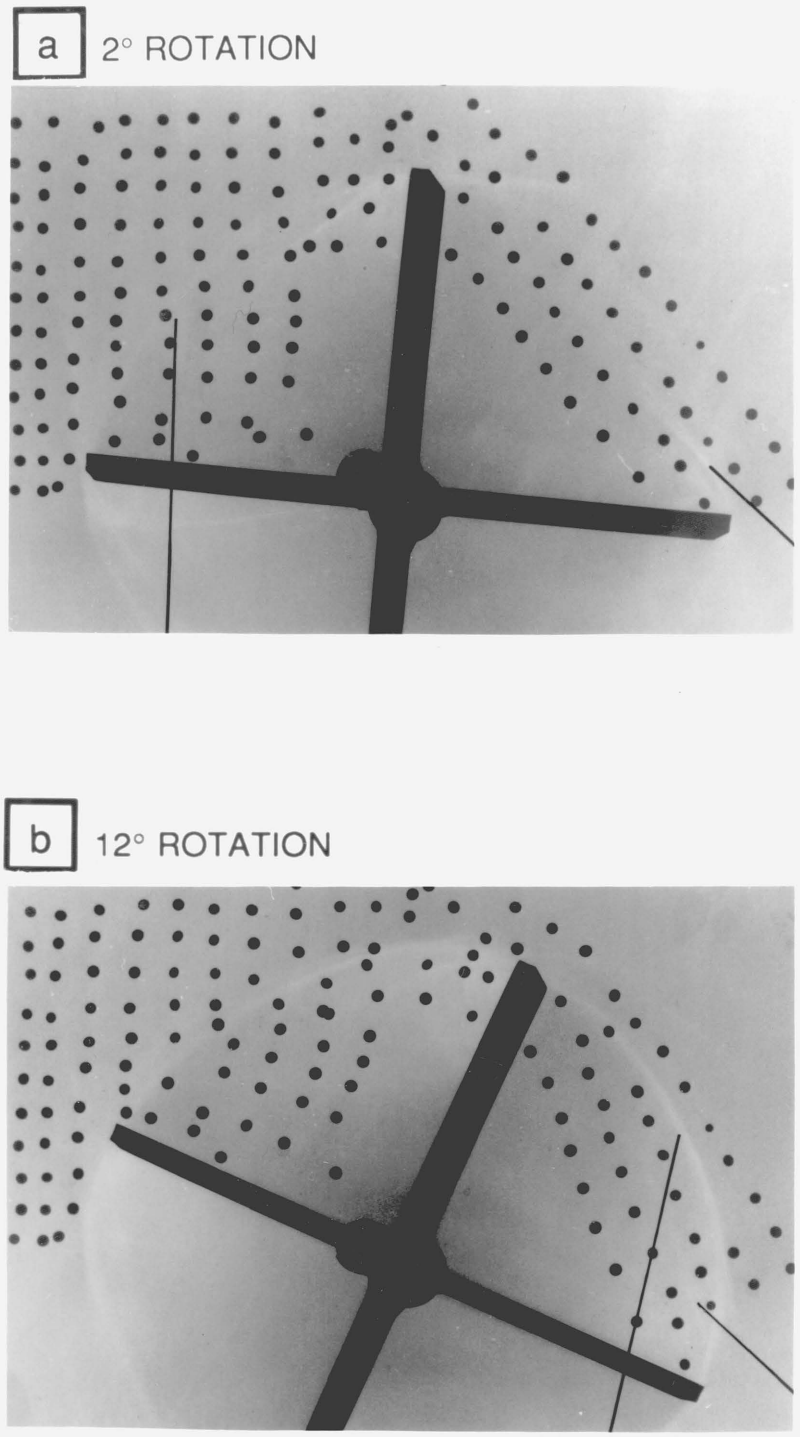
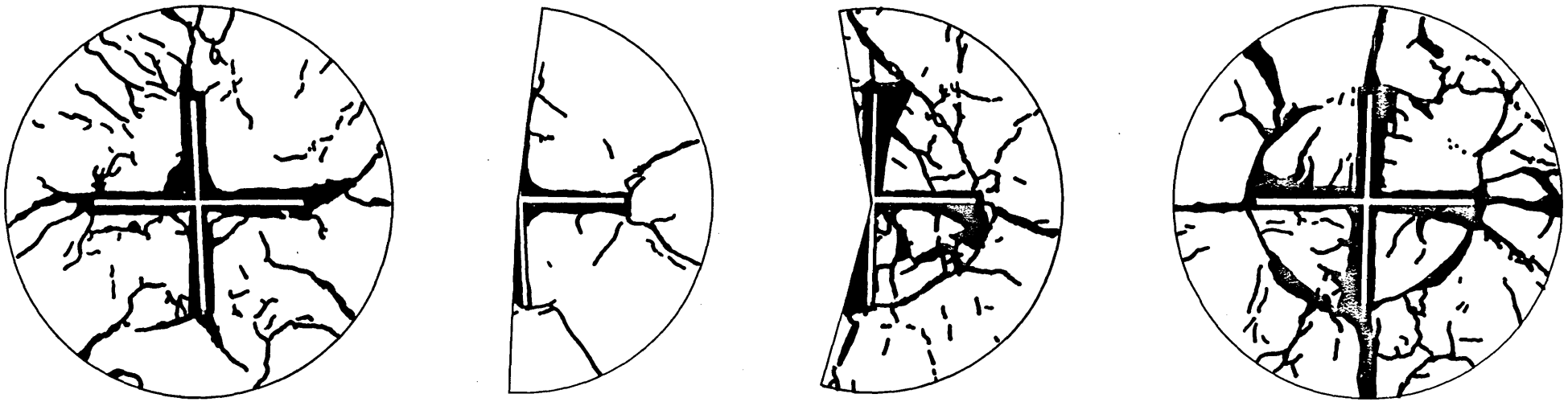


Fig. 2.6 Radiographs of 4-bladed vane rotated in Washed Beach sands through clockwise angles of rotation (after Rush, 1975).



10° rotation
(a)

17.5° rotation
(b)

45° rotation
(c)

70° rotation
(d)

Fig. 2.7 Deformation patterns around 4-bladed vane tests in illite (after Veneman, 1977)

In brief, a large number of attempts have in the past been made to examine the vane failure mechanism in different soils, mostly in the laboratory and with a 4-bladed vane. These investigations have employed a variety of techniques ranging from the simple direct visual observation of the development of the rupture zone, to the sophisticated technique of X-ray radiography. With the exception of the results of radiographic studies carried out on sand by Rush (1975), none of the test results may be regarded as having improved our limited understanding of the actual failure pattern around the vane. They conclude either (a) that the diameter of the vane failure surface is defined by the vane diameter, or (b) that it has a diameter which, apparently depending on the soil type, is between 5 and 30% greater than that of the vane. These conclusions are based on unsatisfactory evidence.

2.6.2 Evidence for Progressive Failure

Another basic assumption in the conventional interpretation of the vane test is that the peak strength is mobilised fully and instantaneously along the entire failure surface (Section 2.2), thus implying that progressive failure does not occur.

Based on observed, comparatively uniform soil deformation patterns across the whole surface of rupture around the vane, Cadling & Odenstad (1950) concluded that there was little or no evidence of progressive failure associated with vane tests on Swedish clays. On the other hand, from a study of the vane test on cemented Canadian clays, it has been hypothesised by both La Rochelle & Lefebvre (1971) and La Rochelle et al. (1973) that a progressive action would initiate at the tips of the vane blades where the clay is more intensely strained than in the rest of the shear zone. Although this suggestion is not supported by Roy's (1975) data, from which there was no evidence of any shear structures until the onset of peak strength, both Veneman's (1977) thin-section observations and the results of the researchers at the Norwegian Geotechnical Institute (NGI; Hoeg, 1985) show that the vane failure surface had propagated over a peripheral distance approximately equal to the amount of vane rotation. Veneman studied the vane failure mechanism on laboratory-prepared samples of both a stiff illite ($I_p \approx 19\%$) and a normally consolidated soft illite/sand mixture ($I_p \approx 17\%$), both tested at zero confining stress, and found that progressive failure was of some importance along the surface of rupture, especially in the stiff illite; remoulded kaolin was used by the researchers at the NGI.

The validity of the assumption of an instantaneous mobilisation of the vane shear strength has also been examined indirectly by studying the effect of the number of blades

on the measured vane strength (Cadling & Odenstad, 1950; Goughnour & Sallberg, 1964; Section 2.5). These investigations were also inconclusive, although both Cadling & Odenstad (1950) and Goughnour & Sallberg (1964) concluded that progressive failure was more likely to occur when the number of blades was small, from which it may be inferred that some progressive failure may take place in the vane test.

Clearly therefore, there is no agreement as to whether the vane failure mechanism is progressive or non-progressive. However, there is very little evidence to support either viewpoint since (a) neither La Rochelle & Lefebvre (1971) nor La Rochelle et al. (1973) provide any test results, and (b) the results of Cadling & Odenstad (1950), the researchers at the NGI (Hoeg, 1985), Roy (1975), Veneman (1977), and Roy & Leblanc (1988) are open to question in the following respects:

(i) Cadling & Odenstad's (1950) photographs show that the soil deformations in front of each blade were somewhat larger than behind it, although the contrary could also be seen;

(ii) the researchers at the NGI (Hoeg, 1985), Roy (1975), and Roy & Leblanc (1988) all used radiographic techniques, whose applicability to the study of the vane failure mode is open to question, since such methods probably do not detect small strains in the soil (Roy & Leblanc, 1988);

(iii) Veneman's (1977) results are obscured by the apparent dominance of shrinkage cracks (Figs. 2.7a–d).

The results of Kimura & Saitoh's (1983) radiographic study of the movement of lead shot at various angles of rotation are also of particular interest. They concluded that the vane failure mode was similar to that observed in direct shear tests, without defining their interpretation of the mechanism of failure associated with such tests. It is difficult to see how such a conclusion could be reached on the basis of the results presented. Consequently, the implication that simple shear conditions would apply at failure (Morgenstern & Tchalenko, 1967; Potts et al., 1987; Section 6.5) cannot be immediately accepted, since it is not at all clear whether Kimura & Saitoh meant that the conditions at failure were those of simple shear or direct shear.

2.7 PILES SUBJECTED TO ROTATION

Torsional pile load tests have similarities with the vane test, since a pile may be regarded as simulating a multi-bladed vane (see Sections 5.4 and 8.1). Thus, the measurement of the pile shaft capacity from a torsional load test may be compared with the undrained shear strength(s) measured with vanes with different numbers of blades.

Torsional load tests have been used because they are often simpler and more economic to perform than axial load tests on piles (see, e.g. Stoll, 1972; Kishida et al., 1986). Despite these obvious advantages, however, the subject of torsionally loaded piles is one which has received very little attention in the research community, with the result that only a handful of publications are cited in the literature (Stoll, 1972, 1976; Poulos, 1975; O'Neill & Dutt, 1976; Randolph, 1981; Gens & Potts, 1984; Kishida et al., 1986; Tominaga & Hanzawa, 1986; Hache & Valsangkar, 1988; Karube et al., 1988).

Stoll (1972) devised a simple field torsional load test, applicable to any cylindrical pipe pile of sufficient structural rigidity, with the aim of determining the required depth of penetration of friction piles from the measured torsional resistance, which he suggested should be on the conservative side when applied to axially loaded piles; it was assumed that there was a strong likelihood that the pile torsional resistance would not generally exceed the axial resistance. The key feature of the test apparatus was that torque was applied by small capacity hydraulic jacks reacting horizontally against adjoining job piles, approximately a metre apart; this utilising the large mechanical advantage available. A number of full-scale torsional pile load tests were carried out in variable soil conditions, ranging from a clayey silt to a clayey sand and gravel, with the result that the measurements of pile shaft friction were not unreasonable for the given soil conditions; comparative axial load tests were not however conducted.

Poulos (1975) presents an analysis for the determination of the response of a single pile subjected to torsion, and reports the results of a series of axial and torsional model pile tests in kaolin (w_L = 55%; w_P = 33%) consolidated from an initial water content of about 55% to a vertical stress in the range σ_v' = 138–372 kPa; undrained conditions were assumed to have prevailed during loading. The piles, which were of solid aluminium (D = 13–38 mm, L = 152–508 mm), were installed by jacking after unloading the samples which had consolidated to a vertical effective stress of σ_v' = 138 kPa. Upon completion of pile installation, σ_v' was increased to the final required value. The piles were then tested in stress-relieved samples (in which σ_v = 0). The ratio of the maximum shear stress (τ_f) measured from torsional tests to that from axial tests was

0.96, with a range of 0.54–1.32, which Poulos attributed to variations in the sample water contents and the nature of the pile surfaces. [However, cavitation effects are more likely to have given rise to the observed discrepancies, since the piles were tested in stress-relieved samples which had apparently also undergone sample storage time effects (see Section 4.4.2F(ii))]. For each test, an average value of the soil shear modulus (G_s) was obtained from the axial load tests, and then used to calculate the rotation of the piles subjected to torsion; G_s was assumed constant with depth, and the value of torsion for which the rotation was calculated was in the linear range of the observed torque–rotation curve. The average ratio of calculated to observed rotation was 0.88, with a range of 0.31–1.47, which — in view of the small scale of the tests and possible experimental errors in measuring the small rotations involved — led Poulos to conclude that it would be possible to use axial pile load test data to predict both the working load and the ultimate behaviour of piles subjected to torsion, or vice versa. It is unfortunate that Poulos did not present the shear stress – displacement/rotation curves.

Randolph's (1981) closed-form solutions for the torsional stiffness of a pile were consistent with Stoll's back-analysed results of torsion tests on full-scale piles. Randolph thereby concluded that due to the similarity between the soil parameters deduced from torsional and axial pile load tests, it was reasonable to suggest using torsional pile load tests in investigating qualitatively the behaviour of piles under axial loading, thus giving further support to the conclusions reached by Poulos (1975).

The numerical analysis carried out by Gens & Potts (1984) is of interest. They used simple two-dimensional axisymmetric finite element formulations to study the behaviour of a long rigid pile under both torsional and axial loading. The soil was modelled by means of an elastoplastic constitutive law of the Cam-clay type as a horizontal disc with an external radius of 345 mm assumed to be normally consolidated under radial and vertical effective stresses of about 200 and 286 kPa respectively, with a rigid co-axial pile of 7.5mm radius; the soil parameters adopted were those appropriate for remoulded kaolin, and drained conditions were assumed to exist throughout the analyses. Fig. 2.8 presents the shear stress/radial effective stress – axial/circumferential displacement curves. It can be seen that a rigid pile under torsion has a much stiffer response than an axially loaded pile, with the mobilised maximum shear stress being about 3% lower in the case of the former. The difference in the respective radial effective stress – displacement relationships of the two modes of shear should be noted, since it may be inferred that different failure mechanisms operate in the two cases (see also Section 8.5.2).

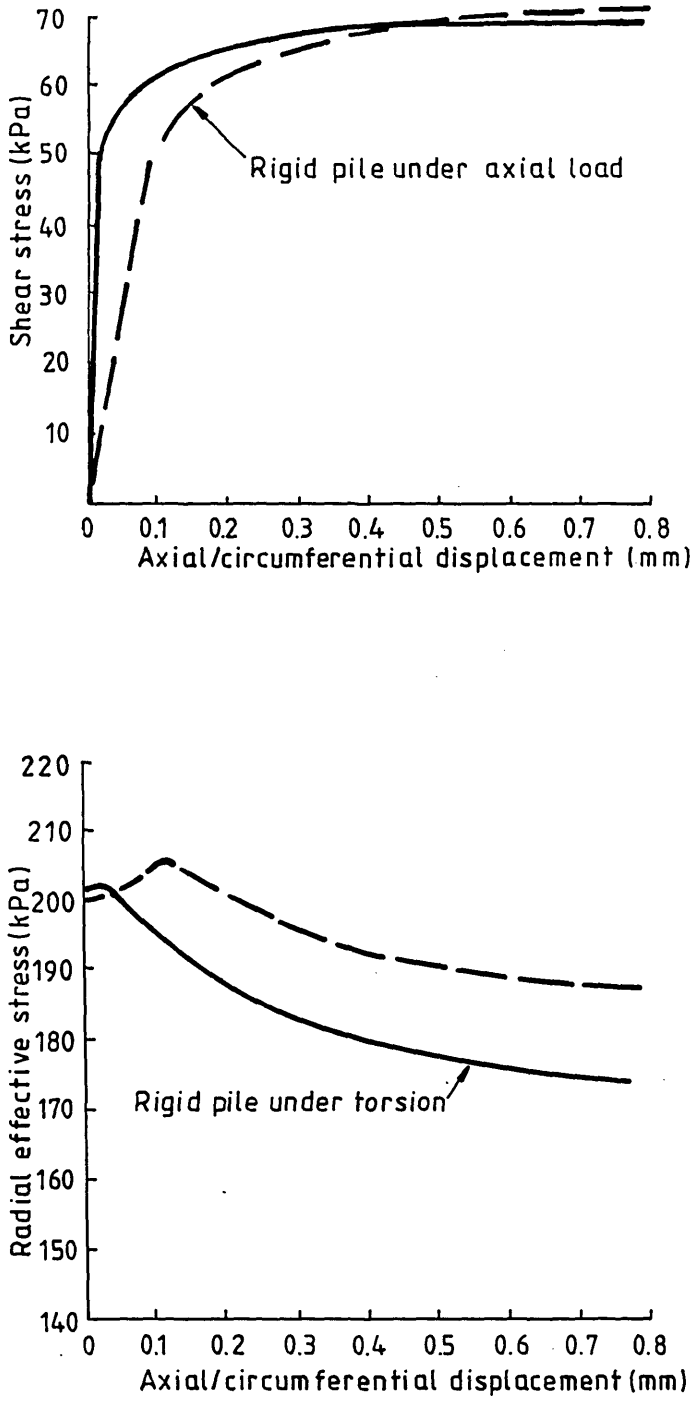


Fig. 2.8 Comparison of the behaviour of axial and torsional pile load tests : Finite element analyses (after Gens and Potts, 1984)

Kishida et al. (1986) criticised the accuracy of the analytical methods available for predicting the skin friction of a pile in dense sand and hard clay, and also pointed out that it would sometimes be difficult to predict accurately the shaft adhesion even from an axial load test, since the test would often be stopped once the bearing capacity requirement considered in the design had been satisfied; this occurring before the onset of the ultimate load. Consequently, Kishida et al. developed a device, named the "friction meter", for the direct evaluation of the maximum shear stress mobilised along a pile; the friction meter, which is 100mm in diameter with a measurement sleeve 100mm long, is portable and therefore suitable for routine site investigations. From tests carried out in hard Pleistocene clay, a comparison was made between the measurements of skin friction according to the friction meter test and load tests on 400mm diameter driven piles; this demonstrated that the values obtained from the friction meter were about 8 ± 6% higher than those measured from the axial load tests.

Tominaga & Hanzawa (1986) also report the results of friction meter tests conducted on a site underlain by alluvial sand and clay, and Pleistocene sand and clay, which they compare both with data obtained from axial load tests on an 800mm diameter pile and with values according to the analytical methods currently practised in Japan. The maximum shaft adhesion measured with the friction meter was about 9% higher than that measured with the pile test. However, the value obtained analytically was considered far too conservative as it was about 80% smaller than that measured with the friction meter.

Hache & Valsangkar (1988) have developed simple mathematical solutions for a torsionally loaded pile in a layered soil, and present non-dimensional design charts based on Randolph's (1981) simplified elastic model of a beam on elastic foundation.

Karube et al. (1988) developed a 'cylinder shear' apparatus in an attempt to analyse the vane test. The cylinder shear rod had a diameter of D = 15 mm and a total of sixteen V-shaped grooves engraved around its perimeter, which likens it to a multi-bladed vane, and hence to a pile. The apparatus was used to carry out a suite of laboratory tests on samples of an alluvial marine clay (w_L = 107%; I_p = 70%) from the north of Osaka Bay, Japan, reconstituted from a slurry water content of about 120%. The soil was consolidated around the shear rod to a vertical stress of about 74 kPa, and then sheared under undrained conditions at a rate of rotation of (ω =) 6 °/min. Due to the similarity between the maximum vertical shear stresses in the cylinder shear tests and in a 4-bladed vane (D = 15 mm) test, it was suggested that the shearing mechanism of the cylinder shear test is compatible with that observed on the vertical shear surface of the vane test (see also Sections 8.5.1B and 8.5.2).

In summary, the behaviour of torsionally loaded piles has been studied because (a) rotating a pile is considered to be a relatively easier and less expensive method of determining the pile shaft friction than loading the pile axially, and (b) it has been suggested that pile response under torsion is similar to that under axial load (Stoll, 1972; Poulos, 1975; Randolph, 1981; Kishida et al. 1986). In this light, Stoll (1972) proposed that the subject of torsionally loaded piles was worthy of further investigation, although he himself did not compare the behaviour of piles under both axial load and torsion.

Despite the obvious merits of examining the response of piles under torsion, however, very little work has so far been carried out on this subject. In particular, only Poulos (1975) has attempted to examine whether there is any justification either in the suggestion of similarities between the behaviour of axially and torsionally loaded piles, or in assuming that both modes of testing a pile would result in similar measurements of skin friction. Poulos' laboratory results showed that the maximum shear stresses measured in torsionally loaded piles were about $4 \pm 41\%$ less than the values obtained from piles subjected to axial loading, whilst from his analytical study it can be seen that the calculated angles of rotation were about $12 \pm 66\%$ lower than those measured experimentally. However, both these results show a very large scatter, thus making it difficult to draw any firm conclusions regarding the similarity of the two test modes. On the other hand, Kishida et al.'s (1986) and Tominaga & Hanzawa's (1986) field studies showed that the values of the skin friction measured by rotating the friction meter were respectively about $8 \pm 6\%$ and 9% higher than those measured from axial load tests, whilst the values of skin friction obtained from Gens & Potts' (1984) finite element analyses were, in the case of torsionally loaded piles, about 3% lower compared to the axially loaded piles. There is therefore no definite consensus among the available experimental data. Consequently, there is a need for a comprehensive examination of the similarities/differences between the behaviour of torsionally and axially loaded piles.

It is rather unfortunate that Poulos (1975) did not present the experimental shear stress – displacement/rotation plots, and Kishida et al. (1986) only present the shear stress – rotation curves. In order to gain a better insight into the behaviour of axially and torsionally loaded piles it is important to compare the shear stress – circumferential/vertical displacement relationships, as shown in Fig. 2.8 using Gens & Potts' (1984) numerical results.

The study of piles under torsion has led to two interesting developments, namely the friction meter device (Kishida et al., 1986) which is used in the field, and the laboratory cylinder shear apparatus (Karube et al., 1988). Further investigtions using

these devices, in conjunction with axial pile load tests, will undoubtedly lead to an improved understanding of the similarities between axially and torsionally loaded piles. Only then will it be possible to conclude whether or not torsional pile load test data provide an accurate measurement of the pile shaft friction which may be used in the determination of the load carrying capacity of axially loaded piles.

CHAPTER 3

EXPERIMENTAL APPARATUS, SAMPLE PREPARATION AND TESTING PROCEDURES

3.1 INTRODUCTION

This Chapter is concerned with a detailed description of the experimental programme undertaken in the laboratory in order to study some aspects of the measurement of soil strength using rotating shear devices. It is divided into three major sections dealing with the experimental apparatus employed, the sample preparation techniques adopted, and the testing procedures followed. A fourth section gives details of a photoelastic study initiated at Imperial College and completed at Surrey University.

3.2 EXPERIMENTAL APPARATUS

3.2.1 Introduction

This Section describes the test equipment used in the experimental investigation. To save space, no mention will be made of the standard apparatus used for gradings, specific gravity, Atterberg limits, or the standard oedometers, except to say that (a) the standard fall-cone test (BS1377: 1975) was used for all liquid limit determinations, and (b) every oedometer cell and loading frame was calibrated before use, with calibration corrections subsequently applied to compression dial gauge readings in order to allow for elasticity of each apparatus (see Head, 1982); both the "square root of time" and "logarithm of time" fitting methods were used in calculating coefficients of consolidation.

The laboratory vane apparatus and the vanes used in both the laboratory-vane and triaxial-vane* tests will be discussed first, then the triaxial-vane and model pile test cell, followed by the conventional triaxial equipment used for undrained compression tests of London clay, and finally the sample tube and the large oedometer used for the preparation of reconstituted clay. The instrumentation employed will be described at the end of this Section. [* Note: Triaxial-vane tests are vane tests conducted in soil samples under one major and two minor principal stresses. For details of a triaxial-vane apparatus, reference should be made to Law (1979).]

3.2.2 Vane Shear and Pile Testing

3.2.2A Vanes

3.2.2A(i) Laboratory-vanes

Based on the standards adopted by Cadling & Odenstad (1950) and subsequently by many other researchers, it was initially proposed to manufacture vanes with a height to diameter (H/D) ratio of 2. [Following a fundamental line of argument, Chandler (1988) has also recommended that this height to diameter ratio be adopted for field vane testing; see Section 3.2.2A(ii), below.]

In order to study the progressive development of deformation patterns in clay, the main requirement was to obtain a complete picture of the propagation of the shear structures at different stages of the shear stress – rotation curve. Hence, at least three tests, stopped at conditions corresponding to pre-peak, peak and 'residual' shear stress, had to be performed in each sample. After considering side effects and selecting a vane diameter, D = 12 mm, this meant that a minimum of three vane tests could be done in samples reconstituted in U100 tubes. Head (1982) suggests that up to five tests can be carried out when 12.7mm diameter vanes and 100mm diameter samples are used (see Fig. 3.13a).

Sample end effects also had to be considered. In this regard, Cadling & Odenstad (1950) suggest that the influence of surface interference effects can be disregarded at a depth below the surface of five times the vane diameter in the case of the field vane, whilst Head (1982) states that the top of the laboratory vane should not be less than four blade lengths below the clay surface. According to Head's recommendation, a vane of 24mm height (with D = 12 mm) should be pushed to a depth of 96 mm below the clay surface, requiring a sample about 215 mm high. However, the laboratory vane apparatus used in this investigation imposed a limitation of 150 mm on the sample height. Therefore, it was decided to test vanes having H/D = 1 (i.e. *square* vanes), with D = 12 mm. This is also in accordance with Head (1982) who states that the standard laboratory apparatus has a 12.7mm square vane.

The results of the thin-section work described in Sections 6.3 and 6.4 show that the limits suggested by Head (1982) in relation to the side and end effects are unnecessarily restrictive, since the soil deformation patterns, corresponding to 12mm square vanes with varying number of blades, propagate only a few millimetres, less than a tenth of the vane diameter beyond the top and bottom surfaces of the vane in the

vertical direction (Section 6.3.3A), and extend a maximum distance approximately equal to 50% of the vane diameter beyond the periphery of the vane in the horizontal direction (Sections 6.4.2 and 6.4.4).

All the vanes used in the experimental programme were constructed using 0.018" (0.457 mm) thick brass shim. A guillotine was used to cut the brass shim into the approximate blade sizes of 12 mm x 12 mm, 18 mm x 18 mm, or 24 mm x 24 mm. The vane shafts had diameters, d = 1/8" (= 3.175 mm), although vanes with d = 3/16" (= 4.763 mm) were also used as part of the investigation into the effect of shaft friction on soil strength (see Chapter 5).

Brass rods were first cut to a length of approximately 110 mm before cutting slots — equal to the number of blades on the vane — along 10 mm of the lengths of the rods using a vertical milling machine. Soft soldering was then used to assemble the shaft and blades, with 10 mm of the shaft length extending into the vane blades, before the complete vane was placed into specially manufactured jigs for final machining to the exact sizes on a lathe. Using a hand file, the uppermost part of the shaft was filed so that it would fit in the screw assembly of the vane apparatus (see Section 3.2.2B). Finally the burrs were cleaned with emery cloth and the vane was grit-blasted in order to achieve a consistent roughness.

The area ratio (A_r) of vanes (BS 1377: 1975; Section 5.4.3, and Fig. 5.11a) with shaft diameters of 3.175 mm and blade diameters between 12 and 24 mm was in the range 6–14%; a limiting value of 12% is recommended by the American, British and Norwegian standards for the field vane (Geise et al., 1988).

3.2.2A(ii) Triaxial-vanes

After reviewing both Donald et al.'s (1977) three-dimensional finite element analysis of the vane test and the experimental results of Menzies and Merrifield (1980), Wroth (1984) pointed out that for vanes with H/D = 2, the peak shear stress, τ_f, measured by the vane in an isotropic soil is given by:

$$\tau_f = \frac{0.94M}{\pi D^3} \qquad \text{Eq. 3.1}$$

where M is the maximum torque recorded during the test.

For vanes having H/D = 2, the conventional interpretation of the vane test (Section 2.2) expresses the soil strength as

$$\tau_f = \frac{0.86M}{\pi D^3} \qquad \text{Eq. 3.2}$$

It follows, therefore, that in an isotropic soil the conventional analysis would appear to underestimate the soil strength by about 9% (see also Mahmoud, 1988). Similarly, it can be seen from Table 3.1 that for vanes with H/D = 1, the conventional analysis would underestimate the soil strength by about 19% compared to Wroth's interpretation. Consequently, the latter may be considered more appropriate for the analysis of the results of the triaxial-vane tests presented in Sections 8.3 and 8.5.1 (see also Table 8.1).

Three tests had to be carried out in each sample in order to have a comprehensive picture of the shear structure development corresponding to pre-peak, peak and 'residual' shear stress conditions. These results would subsequently be compared with the soil deformation patterns observed at similar stages of the laboratory-vane tests.

The stress path cell only accommodated vane tests through the central portion of each sample. However, provided that the vanes had D ≤ 15 mm and H/D ≤ 3, it was possible to do the tests at three different heights in the centre of each sample; thin-section observations (Section 6.3.3A) show that the disturbance caused by the vane in the vertical direction is almost negligible. Consequently, the triaxial-vanes were chosen to have D = 12 mm, with H/D = 2, in preference to 1, because the former will lead to a 10% (= 19% – 9%) less underestimation of the soil strength measured when the conventional, as opposed to Wroth's interpretation, is used (Table 3.1).

The vanes were constructed from the same brass thickness as the laboratory-vanes, but with a shaft diameter of 4.763 mm, instead of 3.175 mm, since the latter could not accommodate blades of 24mm height without adversely affecting the rigidity of the vanes. The triaxial-vanes had area ratios of about 21.5%.

A 'long' triaxial-vane having H = 120 mm and D = 12 mm was also constructed (see Section 8.2).

Table 3.1 A comparison of vane strength formulae.

Interpretation	Vane Height to Diameter Ratio (H/D) 1	2	10
'Conventional' ($x\ M/\pi D^3$)	1.5	0.86	0.194
'Wroth', 1984 ($x\ M/\pi D^3$)	1.78	0.94	0.198
'Chandler', 1988 ($x\ M/\pi D^3$)	1.66	0.91	–
Difference by which 'Conventional' underestimates			
'Wroth' (%)	18.7	9.3	2.1
'Chandler' (%)	10.7	5.8	–

3.2.2B The laboratory vane shear apparatus

The laboratory vane shear apparatus used throughout this investigation was a modified version of the Wykeham Farrance Eng. Ltd. motor-driven apparatus. The apparatus will hereafter be referred to as the Imperial College Laboratory Vane Apparatus, ICLVA.

In contrast to the standard type of laboratory vane equipment (in which the vane rotates relative to the soil), in ICLVA the platform, and hence the sample rotate relative to the vane via a system of shafts and gears connected to the platform, and thereby, the actual sample rotation is recorded (also see Section 3.2.5F). The major elements of ICLVA which are shown in Fig. 3.1 are:

(a) torsional load cell
(b) vane shaft and its connection to the torsional load cell
(c) moving platform
(d) shaft and gearing mechanism connected to a stepping motor capable of applying rates of rotation in the range 0.0043–1075 °/min
(e) control panel
(f) recording instrument
(g) equipment used to calibrate the torsional load cell.

To connect the vane shaft to the torsional load cell, the former was fitted into its socket and the fixing screw was tightened. The vane would then be pushed into the sample by manually raising the platform at a slow constant rate. On completion of a test, the vane was either retracted from the clay or left in place, as appropriate. The latter occurred when the investigation was concerned with the pattern of soil deformation around the vane, the former with the effect of the rate of vane rotation and number of blades on soil strength.

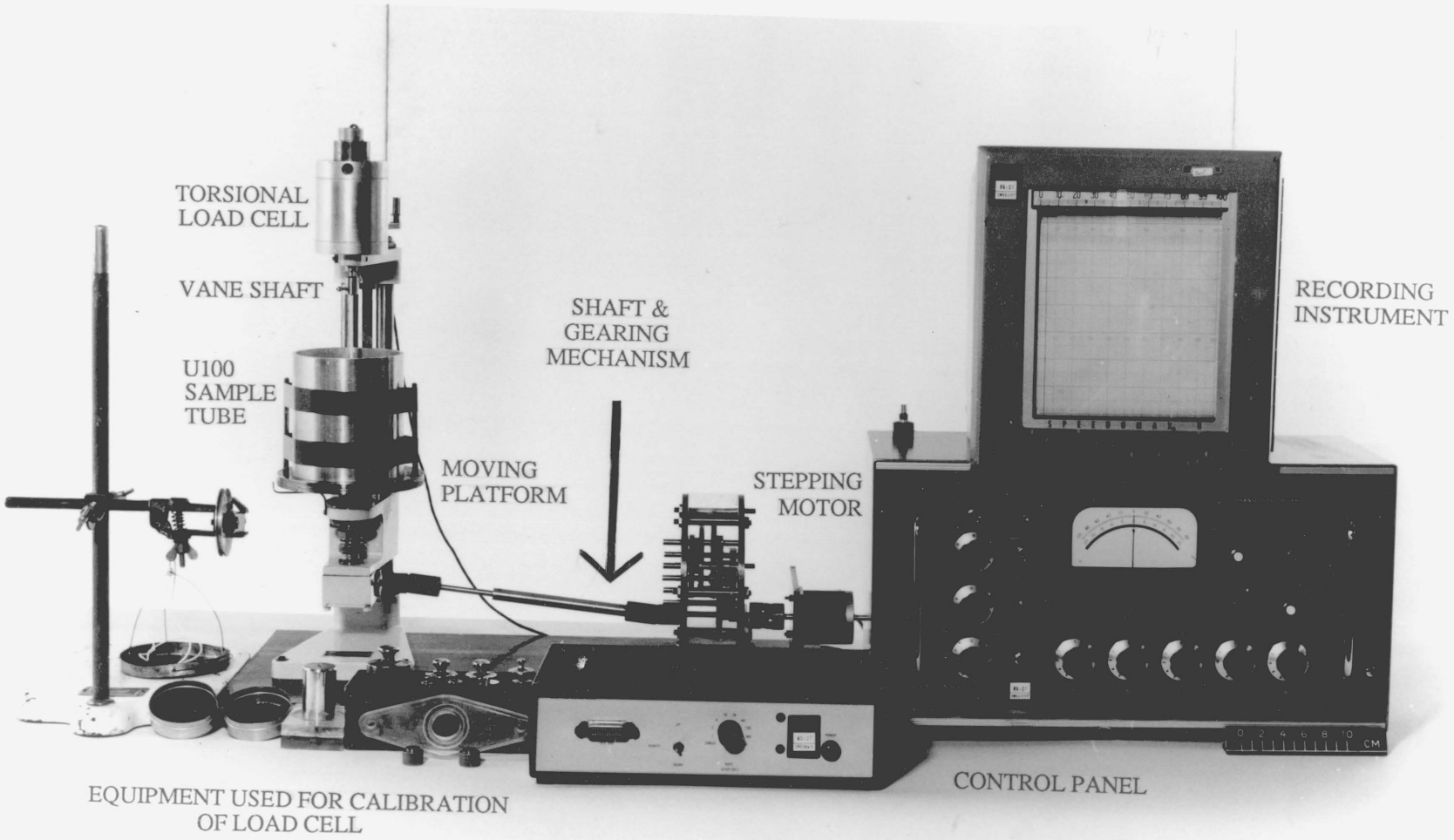


Fig. 3.1 The Imperial College Laboratory Vane Apparatus (ICLVA).

3.2.2C Triaxial-vane and model pile test cell

3.2.2C(i) Introduction

The triaxial-vane and model pile tests were performed using the same stress path cell in which Martins (1983) had conducted axial loading of model piles. Martins has given a detailed account of the aspects of the stress path cell, while Bishop & Wesley (1975) have presented a description of the operation of stress path cells. Therefore, only a brief description of the test equipment will be given here. This will be followed by an account of the modifications which were carried out with respect to the sample loading system, and the vane and model pile loading systems.

3.2.2C(ii) Apparatus layout

The triaxial-vane and model pile test cell used in this investigation is presented schematically in Figs. 3.2a–c. The major components of the apparatus are the stress path cell, the hydraulic system for sample loading, the vane and model pile, and the vane and model pile loading systems. A Solartron Data Transfer Unit (DTU) was used to record all the data from the experimental tests. The output from the DTU was on a paper tape print-out.

Following consolidation in a 100mm diameter cylinder (Sections 3.2.4B and 3.3.2C), the final consolidation of the samples (nominally 102mm diameter x 150mm long) was carried out in the stress path cell. The cell pressure applied to the circumferential boundary of the sample controlled the radial stress, whilst the axial stress was governed by the ram pressure. The controlling pressures were supplied by means of air pressure, via air/water interfaces.

Bottom drainage was provided by a filter paper – metal gauze sandwich (Fig. 3.2c). The two drainage connections at each end of the drainage system allowed gentle flushing of the system with air or water, depending on whether free water had to be removed from the ends of the samples or flushed through the samples. The water expelled from the samples during consolidation was measured by means of a burette; no back pressures were used. Fig. 3.3 shows a schematic diagram of the hydraulic system of the test equipment; this was designed by the writer.

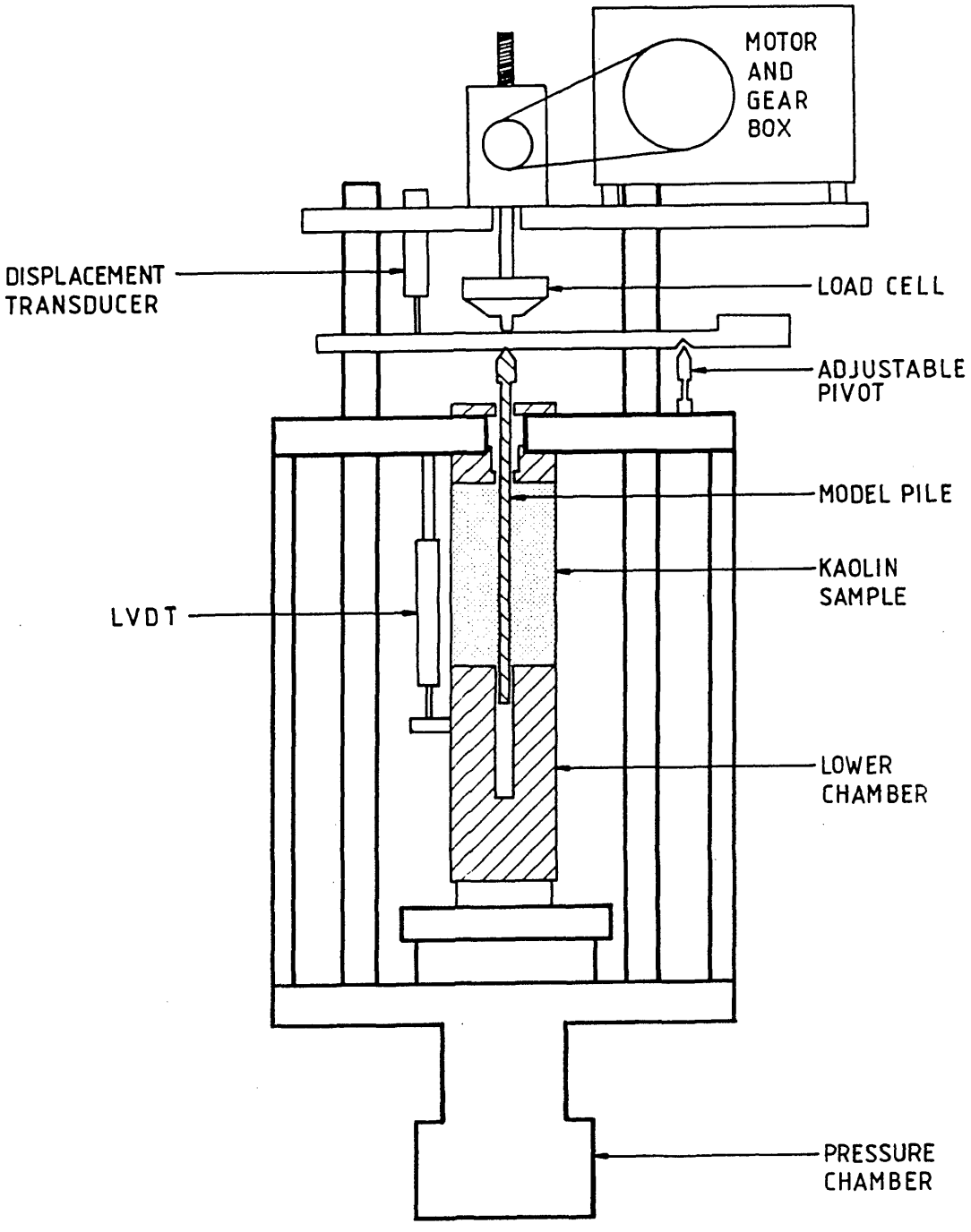


Fig. 3.2a Apparatus layout for an axial pile load test.
Note: Pile installation was the same for both torsionally and axially loaded piles.

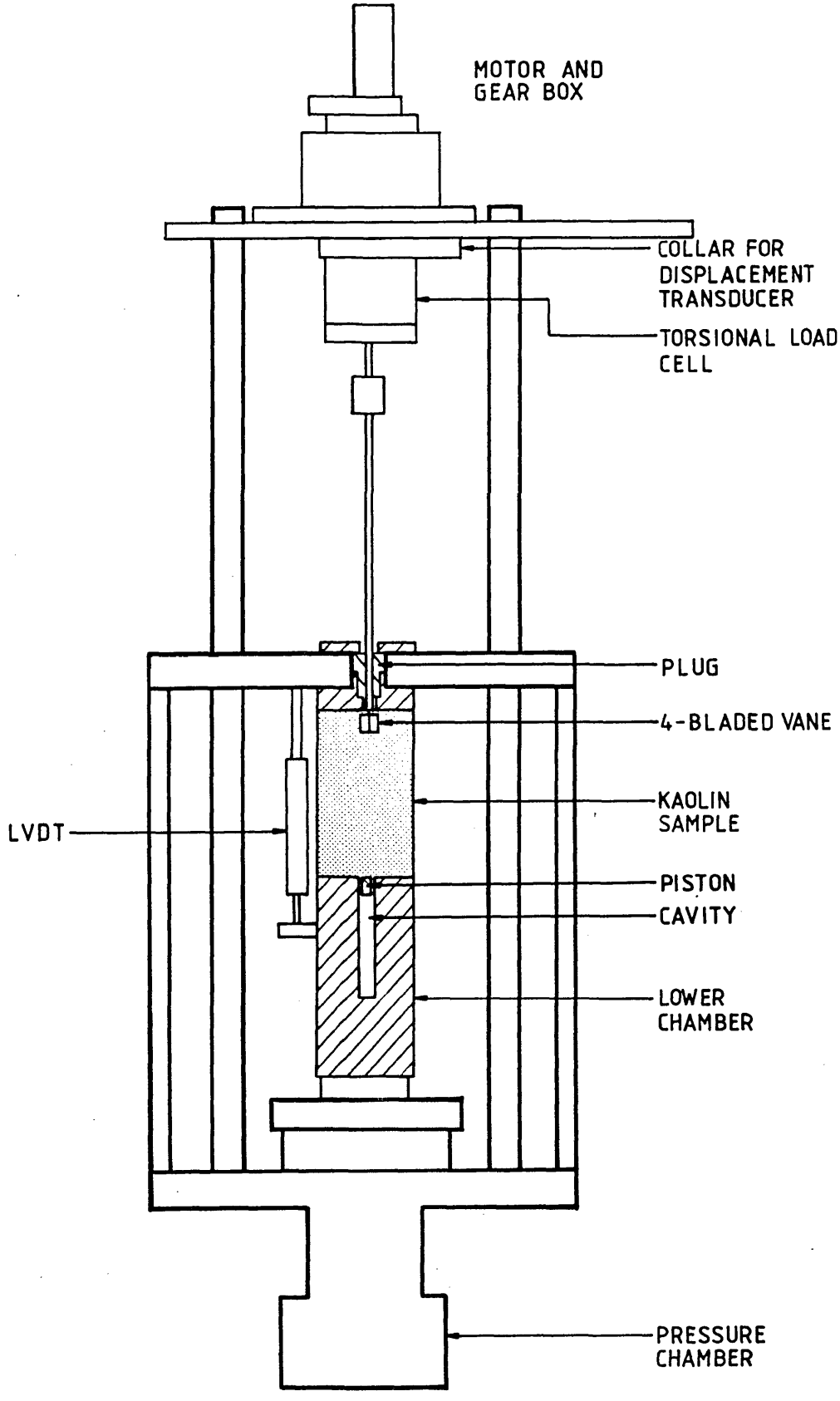


Fig. 3.2b Apparatus layout for a triaxial-vane test.

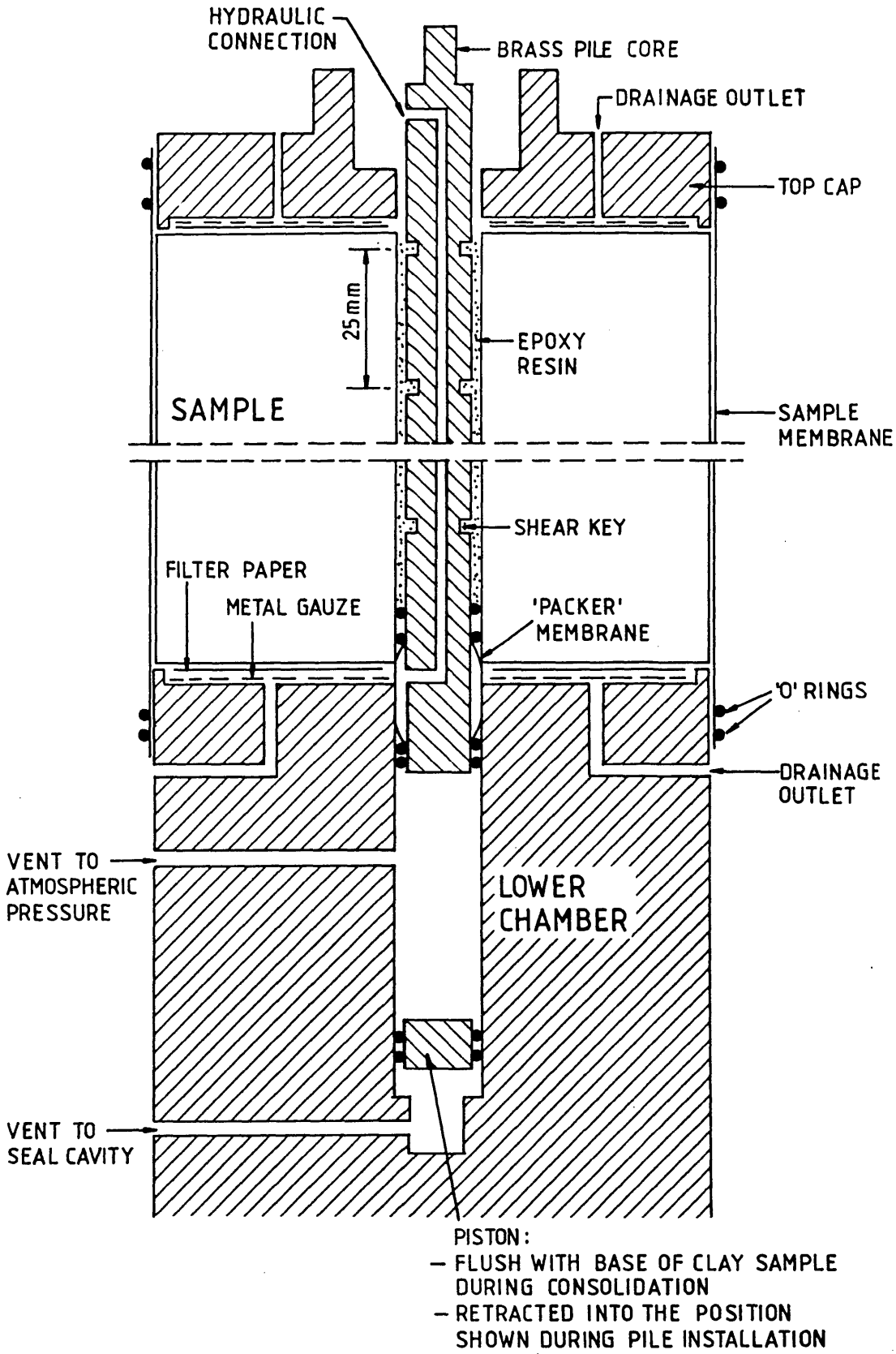


Fig. 3.2c Detail at the top, bottom and central core of clay samples tested in the large stress path cell. A general view of a model pile is also shown.

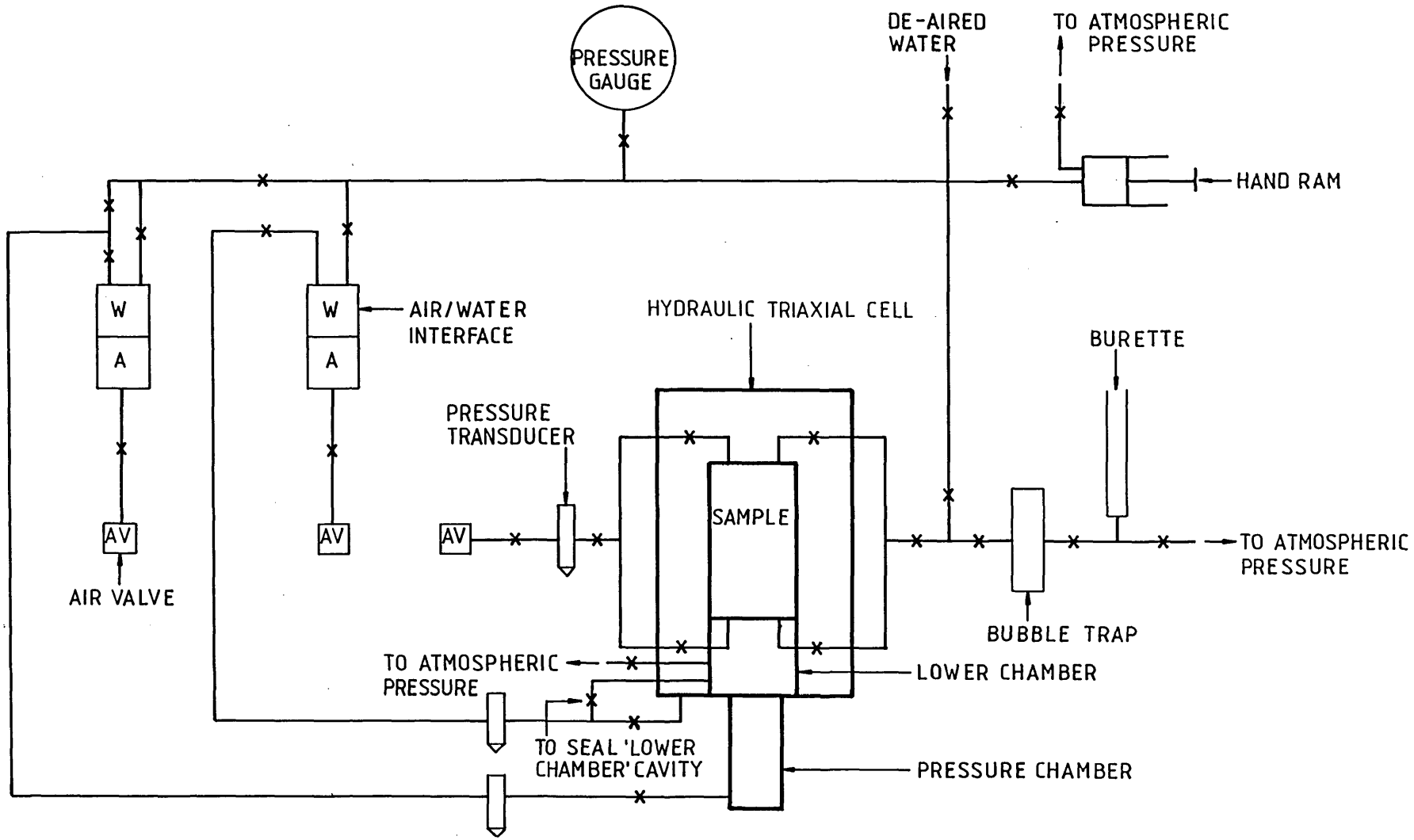


Fig. 3.3 Hydraulic system of the triaxial-vane and model pile test cell.

The bottom platen had a central cavity into which the pile tip would protrude through the base of the samples so that only shaft resistance would be mobilised during axial loading of model piles (see Martins, 1983, and Fig. 3.2a). During sample consolidation — before the installation of the model pile — a small piston was held flush with the surface of the platen hydraulically, sealing the cavity in the bottom platen (see Fig. 3.2b). A simpler screw-in plug arrangement was used in the top platen. During pile loading, the top platen was retracted and the bottom platen piston was pushed down in the cavity after the latter was vented to atmospheric pressure (see Fig. 3.2c). For the triaxial-vane tests, the piston was held flush with the bottom platen surface throughout each test (Fig. 3.2b).

3.2.2C(iii)Sample loading

For a complete description of the important aspects of the stress path cell regarding sample consolidation, reference should be made to Martins (1983).

As discussed by Martins, the available axial travel of the hydraulic piston imposed constraints on the height of samples which could be tested in the stress path cell; thus, each sample was cut nominally to 102mm diameter and 150mm long. All the samples underwent anisotropic (K_0) consolidation up to a radial stress of about 220 kPa. The cell pressure was controlled manually, and monitored by means of a 1000kPa Bell and Howell transducer. An air/water interface enabled the pressure applied to the cell to be accurately pre-set before application (see Fig. 3.3).

The axial stress was supplied through a hydraulically controlled piston. Details of the hydraulic ram have been described by Atkinson (1973). Martins found that the friction in the system was very small and hence measurements of axial stress using a 1000kPa pressure transducer connected to the hydraulic ram were considered acceptable (see Section 3.2.5G). The axial deformation of the sample was monitored by means of a linear variable differential transducer (LVDT) connected between the top and bottom platens (Figs. 3.2a and b). On completion of sample consolidation, the height of the sample was maintained for the rest of the test by means of a hand ram connected to the pressure chamber of the stress path cell (Fig. 3.3).

3.2.2C(iv) Vane insertion and rotation

The requirement was to be able to carry out a minimum of three vane tests in each sample, with the tests stopped at pre-peak, peak and 'residual' shear stress conditions.

To insert the vane into the sample, the vane shaft was connected to the torsional load cell which had been specially designed and constructed for this part of the investigation (see Fig. 3.2b). The top platen screw-in plug arrangement was replaced by a push-in plug with a central hole through which the vane shaft would pass. When the push-in plug was placed over the vane blades, vertical penetration of the vane was ensured. With the top of the blades just below the top surface of the sample, the push-in plug was absolutely flush with the top platen. The vane was manually pushed into the sample at a constant rate, using a spirit level to ensure its vertical insertion.

Rotation of vanes was applied via a regulator which controlled the DC motor with tacho-feedback through a high reduction gear box (see Fig. 3.2b); the tacho generator ensured that the rotation speed was kept constant, while the gear box allowed the motor to run at a variety of speeds. The electric motor was driven at a constant rate of rotation of 1.4 °/hr ($\approx$ 0.15 mm/hr, since D = 12 mm). A collar placed around the torsional load cell provided the seating for a displacement transducer employed to measure the angular rotation of the vane.

3.2.2C(v) Piles

The piles were of similar design to those of Martins (1983). In order to instal the piles with minimal disturbance to the clay fabric, they were cast in place by carefully drilling a 15mm diameter hole through the central portion of the sample, and placing a rigid brass core of 11mm diameter which was subsequently grouted in situ with a strong, low shrinkage epoxy resin (Araldite CY219, HY219 and AY219). A general view of a model pile can be seen in Fig. 3.2c; the overall length of the piles was approximately 250 mm. Shear keys, spaced regularly along the length of the rigid core, helped to minimise any possible longitudinal shrinkage of the resin around the brass core. To fit the screw assembly of the torsional load cell (Fig. 3.2b) and/or the knife-edged cap used for the axial pile load tests (Fig. 3.2a), the top 10 mm of the pile was machined.

In order to prevent injected resin from escaping into the cavity in the bottom platen, a 3mm diameter hole was drilled down the centre of the brass core so that water could be passed through it to inflate a small 12mm diameter latex rubber 'packer' membrane at the base of the pile (Fig. 3.2c). The membranes were prepared — according to procedures outlined by Menzies & Phillips (1972) — by dipping a degreased aluminium former first into a coagulant solution and then into a solution of pre-vulcanised rubber (Revultex); after each dipping, the former was put in an oven kept at 60 °C. Each membrane was then removed from the former, allowed to leach in a bath of tap-water for 24 hours, dried, dusted with French chalk, and stored in the dark until required for use.

3.2.2C(vi) Pile loading systems

Except for two model piles which were to be subjected to axial loading, all other piles were to undergo rotation at the same rate as the triaxial-vane tests, where $\omega = 1.4$ °/hr ≈ 0.18 mm/hr, since D = 15 mm.

The axial pile load tests were carried out at a displacement rate of 0.36 mm/hr, using the equipment that Martins (1983) had employed in his investigation. A stainless-steel bar of rectangular cross-section was lowered onto a stainless-steel knife-edged cap placed on the pile. The rectangular bar was then levelled using a knife-edged support which was adjustable in height (see Fig. 3.2a). The load was applied to the upper face of the bar immediately above the pile cap, through a ball-ended extension to a 4500N Imperial College load cell, via an electric motor driven through a reduction gear box and a restrained worm gear. Thus, axial load was applied without the introduction of bending moments. Pile displacements were measured to an accuracy of 0.01 mm by means of a displacement transducer (see Fig. 3.2a).

3.2.3 Triaxial Apparatus

3.2.3A Introduction

The conventional triaxial cell was used to perform a series of unconsolidated undrained triaxial compression tests on samples of remoulded London clay. These tests enabled a comparison of the strength* – water content relationships obtained from triaxial compression and vane shear tests. [* The 'right cylinder' assumption was made in calculating the deviator stress at failure (see Section 4.4.3C).]

3.2.3B The conventional triaxial cell

The conventional triaxial apparatus which was used for testing 38mm diameter (76mm high) clay samples was similar to that described by Bishop and Henkel (1962).

The confining pressure on the samples was supplied by air pressure which was monitored by a pressure gauge calibrated against a Budenberg dead weight tester. Undrained compression tests were performed at a constant rate of strain of 0.81 %/min (= 0.64 mm/min, since sample height ≈ 76 mm); this being equivalent to the rate of rotation of 6.27 °/min (≈ 0.66 mm/min, since D = 12 mm) at which the vane tests were carried out. Loading was applied through a 1tonne frame, with a servo-controlled electric motor acting through a gear box. The deviator stresses were determined internally with a 4500N Imperial College load cell. Axial displacements of the samples were observed externally by means of a dial gauge.

3.2.4 Consolidometers

3.2.4A Introduction

In order to reconstitute the samples selected for the experimental programme, two pieces of equipment were employed: one involved displacement-controlled consolidation in a U100 sample tube, while the other was a large 229mm diameter oedometer which operated under conditions of stress control.

Slurries were prepared using a motor-driven rotary mixer. De-airing of the slurry was carried out prior to one-dimensional consolidation of the slurry, using a new piece of equipment designed by the writer. This consisted of a circular perspex container with an electric motor (capable of slow rates of rotation) attached to a paddle. Provision was made for the application of vacuum and/or air pressure.

3.2.4B The loading frame

Except for one large sample of London clay, slurry consolidation of all other samples was performed in a 330mm long 108mm diameter sample tube, by means of a 5tonne loading frame and a servo-controlled electric motor. Using a reduction gear box, constant rates of displacement between 0.0274 and 76.2 mm/hr could be applied.

Continuous variation of strain, however, was not possible with this apparatus as displacement rates could only be varied at every major gear change in ratios of 1 : 5; each of these fixed rate gear changes could be modified by means of a Kopp variator.

3.2.4C The large oedometer

A large 229mm diameter cell was used for the purpose of one-dimensional consolidation of London clay samples from a slurry. A firm block of uniform consistency was thus obtained providing samples for a series of laboratory-vane tests.

The load was applied to a rigid top platen via a knife-edged lever system which ensured vertical loading at all times. Top and bottom drainage were provided through coarse porous stones, and sample compression was monitored with a long-throw dial gauge.

3.2.5 Instrumentation

3.2.5A Introduction

The experimental results of the laboratory-vane tests were recorded using an X–Y chart recorder (Fig. 3.1). The triaxial-vane and model pile experimental results were monitored using a Solartron DTU.

The torsional load cells employed were calibrated before and after each series of tests and there was good agreement between the calibrations. Calibrations of all the other transducers employed were repeated at regular intervals during the testing programme, and the differences found in their response and 'zero drift' were negligible. For each device, the calibration cycle consisted of three load–unload loops covering the likely range of values in the experiments; 20 points being typically recorded at each cycle.

The calibration data were analysed using a statistics package and by running linear regression routines to find best-fit straight line relationships between strain gauge readings and torque, force, pressure or displacement. For each of the recorded points the deviation from the determined relationship was calculated and the mean errors were assessed.

3.2.5B Load cells

Two torsional load cells were used: one for the laboratory-vane tests and the other for the triaxial-vane and model pile experiments; the former was available and the latter was designed by the writer and manufactured in the workshops. The triaxial-vane torsional load cell had a capacity of 5 N-m, with rates of rotation in the range $\omega = 1$ °/hr to 8.325 °/hr. Both load cells were calibrated by applying known torques and measuring the corresponding responses. Typical calibration curves obtained from both torsional load cells are shown in Fig. 3.4. Over the range of torques used in each case, the responses were linear.

A total of three 'Imperial College' 4500N load cells (El-Ruwayih, 1976) were used in the testing programme. (The deflections of the strain gauges which connect to form a full bridge circuit are directly related to the deviator force in a triaxial test. The strain gauges are placed on a 'star', housed in an oil-filled cavity.) The load cells were calibrated using the Budenberg dead weight tester.

One load cell was employed to monitor the one-dimensional consolidation of samples from slurry in a sample tube. A second load cell was used to monitor the axial loads on model piles. The third load cell was used to monitor deviatoric stresses during unconsolidated undrained shearing of remoulded London clay samples in a conventional triaxial cell. The responses of these load cells were linear (see Fig. 3.5).

3.2.5C Pressure transducers

Altogether three Bell and Howell 1000kPa pressure transducers, made by Senso-metrics Inc. of California, were used in the experimental programme; the devices use unbonded strain gauges connected to a pressure sensing diaphragm. One such transducer was employed during the one-dimensional consolidation of samples from a slurry in order to monitor pore pressures at the base of the sample, while another two were employed to monitor cell pressure and ram pressure in the large stress path cell used for the triaxial-vane and model pile tests.

The calibration of the transducers was carried out using a Budenberg dead weight tester. As can be seen from typical calibration plots of the pressure transducers (Fig. 3.6), the responses were linear. All the transducers performed well.

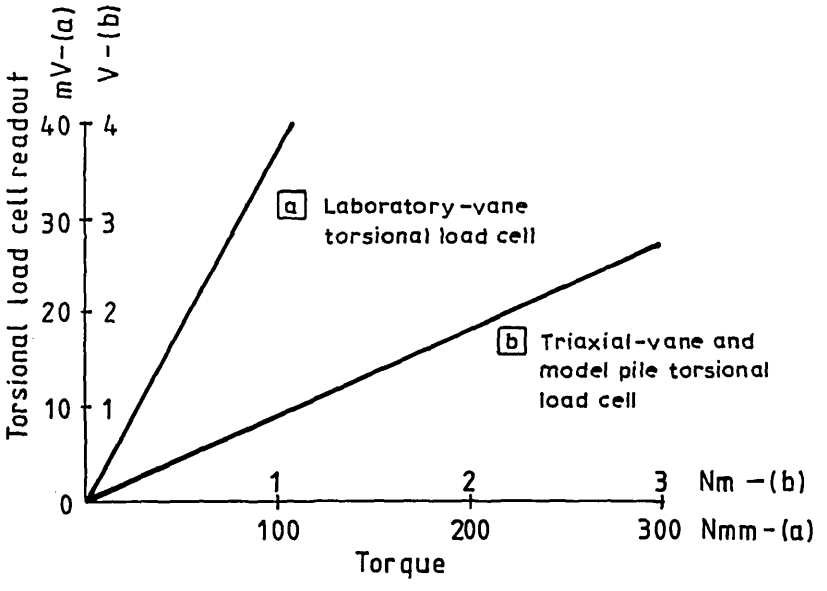


Fig. 3.4 Responses of torsional load cells.

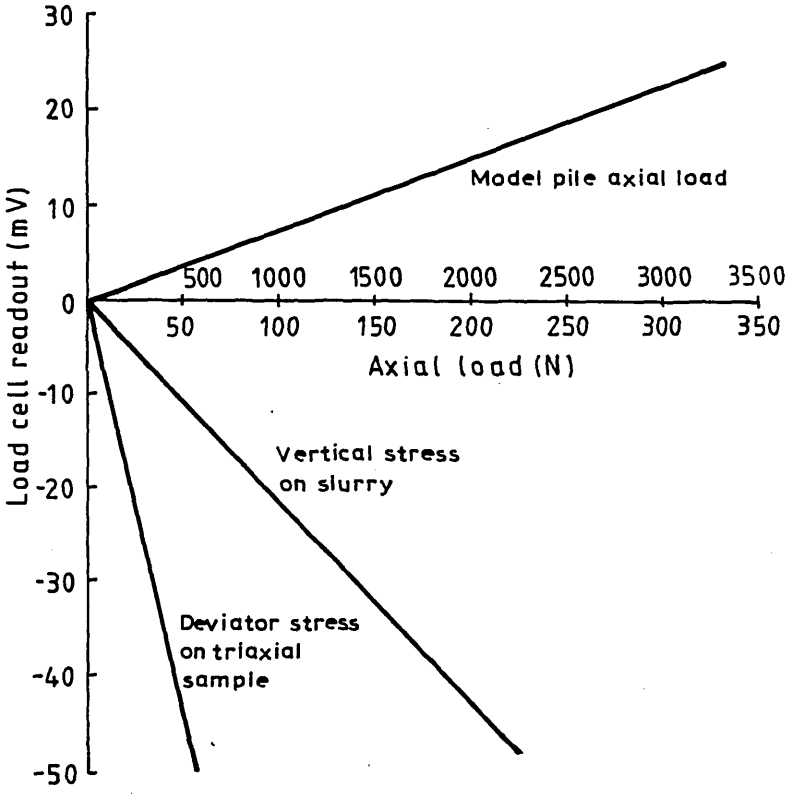


Fig. 3.5 Calibration curves for Imperial College load cells.

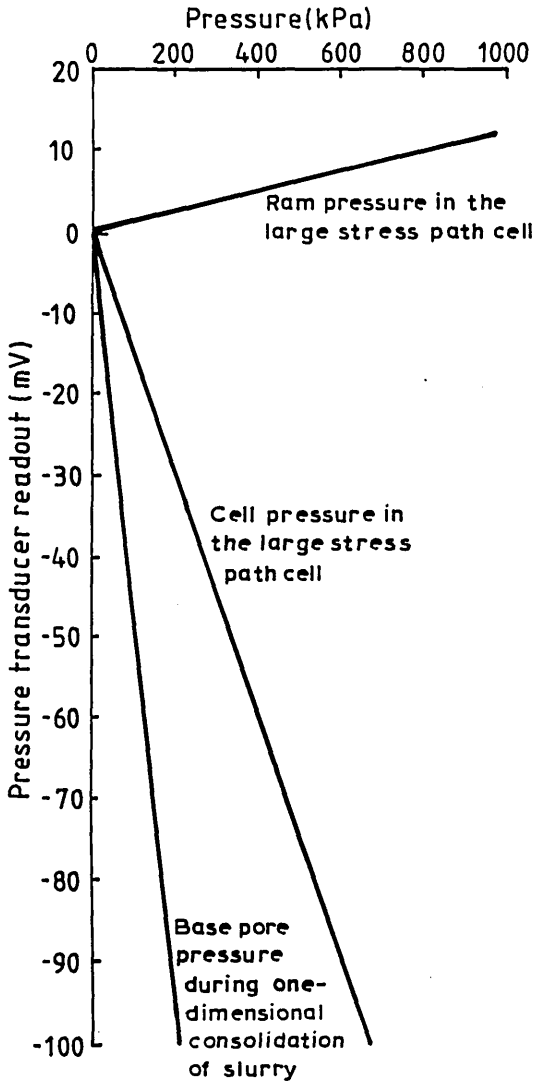


Fig. 3.6
Responses of pressure transducers.

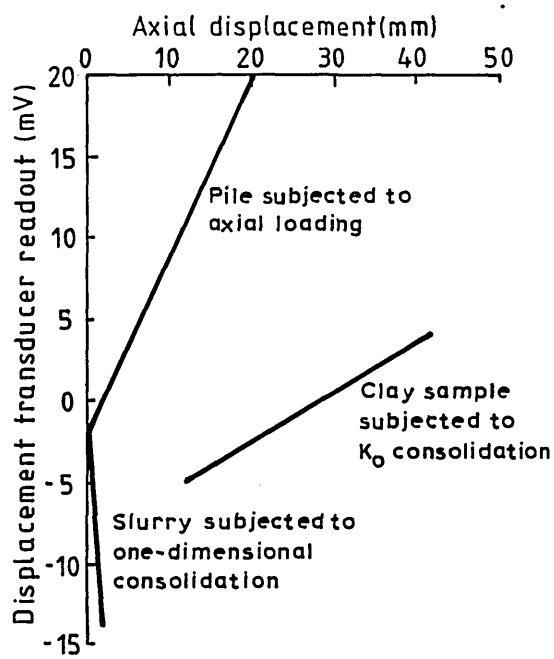


Fig. 3.7
Displacement transducer calibration curves.

3.2.5D Displacement transducers

Three LVDTs, supplied by Minster Precision Engineering, were used in the course of this investigation. They consist of a stainless-steel shell, housing a pair of strain-gauged cantilever arms whose deflections are dependent on the linear movement of a tapered wedge.

One transducer was employed to monitor the rate of displacement during one-dimensional consolidation in a sample tube; digital voltmeters connected to a printer were used for data acquisition. A similar transducer was used during triaxial-vane and model pile testing in order to monitor the angle of rotation of vanes or model piles as well as the vertical displacement of piles subjected to axial loading; a Solartron DTU was used to monitor the data. The third transducer was a submersible LVDT used to monitor the consolidation of samples within the large stress path cell; the data were recorded via a Sangamo C30 modulator–demodulator unit connected to the Solartron DTU. Apart from the submersible LVDT, the other two devices had a range of about 25 mm.

The transducers were calibrated by means of a bench-mounted high accuracy vernier micrometer and the responses were linear (Fig. 3.7). The performance of all the transducers was excellent.

3.2.5E Data acquisition units

A digital voltmeter and an X–Y chart recorder (see Fig. 3.1) were employed to monitor the response of the ICLVA torsional load cell.

During one-dimensional slurry consolidation, three transducer boxes — with digital read-out — were used to monitor axial load, base pore pressure and axial displacement. The voltmeters were connected to a printer which could take readings at rates between 1 per second and 1 per 99 hours.

All the electrical transducers employed during the triaxial-vane and model pile tests were connected to a Solartron DTU. The DTU provided a constant current power supply of 10 mA and could print data at rates between 1 per second and 1 per 2 hours.

3.2.5F 'Exact' angular rotation of the vane

Due to the flexibility of the vane shaft, and to a lesser extent that of the vane blades, as well as the compliance of the torsional load cell, the angle of rotation which is measured during the vane test (θ) will inevitably be greater than the 'exact' ('true') angular rotation (θ_t) through which the soil undergoes vane shear. Hence, both experimental calibration and structural theory were used to correct for the twist of the vane shaft, vane blades and that associated with the load cell.

The calibration exercise involved pushing the vane — connected to the torsional load cell — inside an aluminium cylinder which had four concentrically orthogonal slots cut along both its diameter and the upper portion of its length (see Fig. 3.1); the metal cylinder — securely fixed on the ICLVA platform — accommodated the vane blades, with the platform disconnected from the shaft and gearing mechanism. Consequently, both the twist of the vane and the compliance of the torsional load cell were measured as known torques were applied; it is assumed that the vane blades could not twist since they were held rigidly within the metal cylinder.

For a shaft diameter and length of d = 3.175 mm and l = 10 cm respectively, the experimentally determined angular rotation of a 12mm diameter 4-bladed vane was about 25° per 1 N-m. From elastic torsion formulae (see, e.g. Coates et al., 1980), the calculated angle of rotation of the laboratory vane shaft (θ_s) was found to equal 15° per 1 N-m ($= \theta_s/M = l/GJ$, where G = 39 GPa, and $J = \pi d^4/32$), which thus indicates that the compliance of the torsional load cell (θ_c) was approximately 10 °/N-m.

The twist of each vane blade was calculated — by considering the deflection of the tip of a cantilever beam with a triangular pressure distribution (see Section 2.3; Reynolds & Steedman, 1981) — as $\theta_b = 2.5$ °/N-m.

Hence, the total twist of the laboratory vane apparatus was ignored, since it only amounted to about 27.5 °/N-m, which is rather small as a proportion of the measured angle of rotation, θ; e.g. for a typical maximum torque of 0.05 N-m (see Section 6.6), $\{\theta_s + \theta_c + \theta_b\} = 27.5 \times 0.05 < 1.5°$.

3.2.5G Axial stresses on samples in the large stress path cell

Martins (1983) found that the friction within the hydraulic ram of the large stress path cell was so low that only an error of 0.2% would be incurred by neglecting it. He thus assumed that the axial stresses acting on a sample within the cell were equivalent to the pressure in the cell pressure chamber. The same assumption has also been made in this study.

3.2.5H Miscellaneous

The Budenberg dead weight tester provides a calibration system which is free from friction and stick-slip problems. It is fitted with electric motors which slowly rotate the calibrated piston and ram cylinders.

A standard dial gauge, which was used for the triaxial compression test had a range of 12 mm, while the long-throw dial gauge used during one-dimensional consolidation of London clay had a range of 75 mm; both dial gauges had a resolution of around 0.01 mm.

Air pressure was used in the control of all cell pressures and ram pressures applied in the conventional triaxial apparatus and the triaxial-vane and model pile test cell. The air pressure system consisted of a mains pressure supply and air valves. Air/water interfaces converted air pressure into the required cell and ram pressures.

The experiments were conducted in a temperature-controlled laboratory at 20 ± 1°C.

3.3 SAMPLE PREPARATION

3.3.1 Materials Selected for the Experimental Programme

3.3.1A Introduction

The use of laboratory soils consolidated under controlled conditions has the advantage of reducing variability and providing 'standard' homogeneous test materials, with subsequent repeatability of results. It is also of advantage to use clays whose properties have been well established. For these reasons, the majority of tests reported

here were carried out using normally consolidated samples of Speswhite kaolin. Additionally, both normally consolidated and remoulded samples of London clay were tested for comparison with the tests on kaolin. While investigating strain-rate effects in the vane test, a series of laboratory-vane tests was also conducted using normally consolidated samples of a bentonite/London clay mixture.

3.3.1B Reasons for the clays selected

Speswhite kaolin supplied by English China Clays, Lovering Pochin and Co. Ltd., Cornwall, was used throughout this investigation. This material has a rapid consolidation rate (its coefficient of consolidation is of the order of 10 m^2/yr — Table 3.3, and Fig. 3.9a) and thus the relatively large samples required for the test programme could be consolidated in realistic times (about one month for each sample). In addition, the mechanical properties of the material are similar to Spestone kaolin (Mair, 1979; Davies, 1981) whose fundamental characteristics have been extensively explored by other research workers, principally at Cambridge. It is further noted that kaolin particles are large and consequently exhibit excellent optical properties for microfabric studies (Morgenstern & Tchalenko, 1967; Martins, 1983).

To examine whether the results of tests on kaolin were generally applicable to the vane test, a parallel series of tests was carried out using London clay. London clay has both a much smaller particle size and a higher plasticity than kaolin and consequently, consolidation of London clay samples of a similar size to the kaolin samples took considerably longer.

The difference between the consolidation characteristics of the clays is particularly important when the effects of strain rate in vane testing are investigated (see Sections 4.3 and 4.4). Although microfabric studies are also possible with London clay (see, e.g. Garga, 1970), because of the smaller surface area to thickness ratio of the particles, London clay is not as suitable as kaolin for such purposes (see, e.g. Section 6.3.6).

Bentonite has a very low coefficient of consolidation and while examining the effects of the rate of rotation on vane strength, normally consolidated samples of a bentonite/London clay mixture were also tested.

3.3.1C Characteristics of Speswhite kaolin

Speswhite kaolin is an inorganic clay of relatively high plasticity and permeability. Its chemical composition is presented in Table 3.2a and its index properties are summarised in Table 3.2b. A review of the available data on the properties of Speswhite kaolin is presented in Table 3.3. Fig. 3.8 shows the particle size distribution, whilst Fig. 3.9a presents relationships between coefficient of consolidation, c_v, and vertical effective stress, σ_v'.

3.3.1D Characteristics of London clay

The physical properties and consolidation characteristics of London clay are presented in Table 3.4; the results of oedometer tests on samples with two different initial water contents of about 85% ('slurry' state) and 40% ('normally consolidated' state) are plotted in Fig. 3.9b. The clay from Canons Park, North London, had a different particle size distribution to that obtained from Wraysbury (see Fig. 3.8).

3.3.1E Characteristics of the bentonite/London clay mixture

Table 3.5 summarises the properties of the bentonite/London clay mixture used in this investigation. Fig. 3.9c shows the results of oedometer tests on samples having two different initial water contents of about 190% ('slurry' state) and 130% ('normally consolidated' state).

3.3.2 Sample Preparation

3.3.2A Introduction

The majority of samples were consolidated to the desired water contents from a slurry condition, with water contents exceeding twice the liquid limit (giving liquidity indices in the range $I_L \approx 3$–3.5). Except for one large cake of reconstituted London clay prepared in a 229mm diameter oedometer, one-dimensional consolidation in a 100mm diameter tube was employed, with sample preparation techniques aimed at producing consolidated samples of uniform water content distributions.

Remoulded samples of London clay were also tested.

Table 3.2 Characteristics of kaolin.

(a) Chemical composition.

Reference	Rosenfarb (1975)	Odeh (1980)	This Study*
Kaolin Brand Name	Kaolinite Hydrite 10	SPS	Speswhite
Symbol of Compound	Weight (%)	Weight (%)	Weight (%)
SiO_2	45.3	46.2	46.2
Al_2O_3	38.38	38.7	38.7
K_2O	0.04	1.01	1.01
Fe_2O_3	0.3	0.56	0.56
CaO	0.05	0.2	0.2
MgO	0.25	0.2	0.2
TiO_2	1.44	0.09	0.09
Na_2O	0.27	0.07	0.07
Loss on Ignition	13.97	13.14	13.14

* from English China Clays

(b) Physical properties.

Reference	Rosenfarb 1975	Odeh 1980	Steenfelt et al. 1981	Francescon 1983	Martins 1983	Kirkpatrick & Khan 1984	Taylor 1984	This Study
Kaolin Brand Name	Kaolinite Hydrite 10	SPS	Speswhite	Speswhite	Speswhite	–	Spestone	Speswhite
Property								
Liquid Limit (%)	62	65.2	69	74	62	–	74	66*
Plastic Limit (%)	34	34.8	38	42	32	–	42	32
Plasticity Index (%)	28	30.4	31	32	30	30.4	32	34
Clay Fraction (%)	96	77–83	–	–	–	–	–	75
Specific Gravity of Solids	2.64	2.62	2.61	2.61**	–	2.62	2.61	2.66
γ_s at w = 50% (kN/m^3)	–	–	16.67	16.67**	–	–	–	–

* using the fall-cone test
** after Steenfelt et al. (1981)

Table 3.3 Strength and consolidation characteristics of Speswhite kaolin: A review.

Reference	Khan 1979	Odeh 1980	Steenfelt et al. 1981	Francescon 1983	Martins 1983	Kirkpatrick & Khan 1984
Kaolin Brand Name	SPS	SPS	Speswhite	Speswhite	Speswhite	SPS
Property						
ϕ' (deg)	21	24	≈ 23	23	≈ 23	21
c' (kPa)	0	2.5	–	–	–	–
ϕ'_r (deg)	–	–	–	–	11.5–12	–
e_λ	–	–	2.58	–	2.52	–
K_0	0.56*	0.56**	0.64 ± 0.01	0.69	0.65 ± 0.01	0.56
$(c_u/\sigma_v')_{nc}$	–	–	–	0.22	–	0.29
k (m/sec)	10^{-9}	6×10^{-10}	–	–	–	1.36×10^{-9}
corresponding to σ_v' (kPa)	552	552				552
C_c	–	–	–	–	0.25–0.18	0.482
corresponding to p′ (kPa)					5 ≤ p′ ≤ 350	
c_v (m^2/yr)	–	–	8–13.5	15.78	5–10	–
corresponding to p′ (kPa)			54 ≤ p′ ≤ 430		50 ≤ p′ ≤ 300	
c_s (m^2/yr)	–	–	31	–	22	–
corresponding to p′ (kPa)			250		250	

* measured in Rowe cell
** from Khan (1979)

Table 3.4 Characteristics of London clay.

Reference	Bishop et al. 1965			Jardine 1985	This Study	
London Clay Site	Ashford Common	Bradwell	Waterloo Bridge	Canons Park	Canons Park	Wraysbury
Property						
Liquid Limit (%)	67	95	77	87–67	70	74
Plastic Limit (%)	27	30	27	31–25	29	32
Plasticity Index (%)	40	65	50	–	41	42
Clay Fraction (%)	54	52	53	96	87.5	54
Specific Gravity of Solids	–	–	–	2.64	2.66	2.69
c_v (m^2/yr)	–	–	–	0.2	see Fig. 3.9b	–
Bulk Unit Weight (kN/m^3)	–	–	–	19.66 ± 0.35	–	–

Table 3.5 Characteristics of a bentonite/London clay mixture.

Reference		Schreiner* 1977	This Study
Property			
Liquid Limit	(%)	–	175
Plastic Limit	(%)	–	30
Plasticity Index	(%)	–	145
Specific Gravity of Solids		2.63	2.76
c_v	(m^2/yr)	0.2	see Fig. 3.9c

* for bentonite

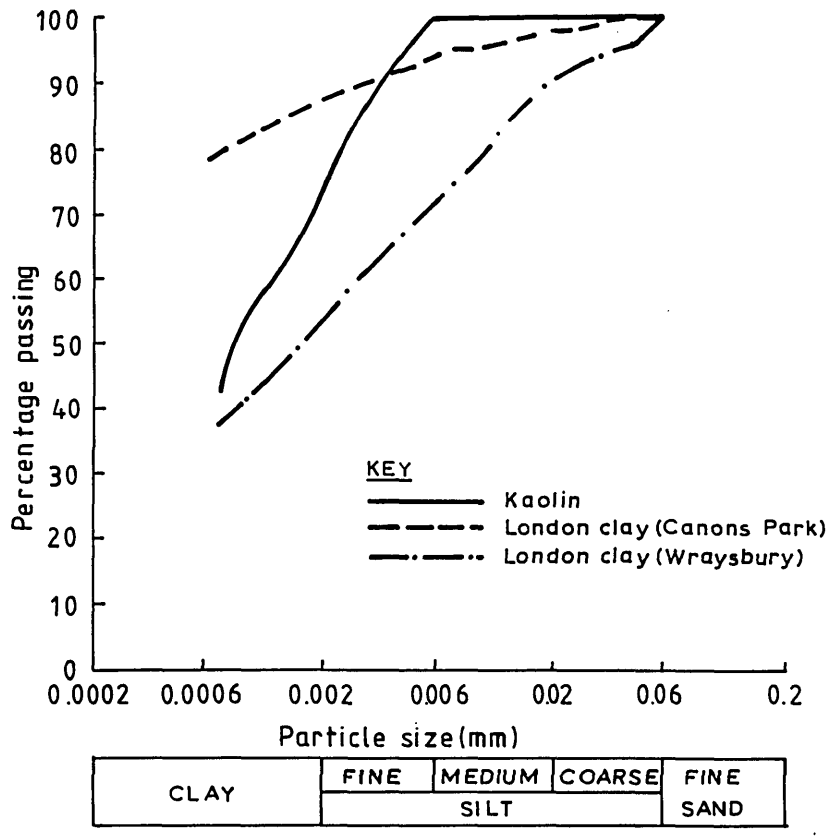


Fig. 3.8 Particle size distribution curves.

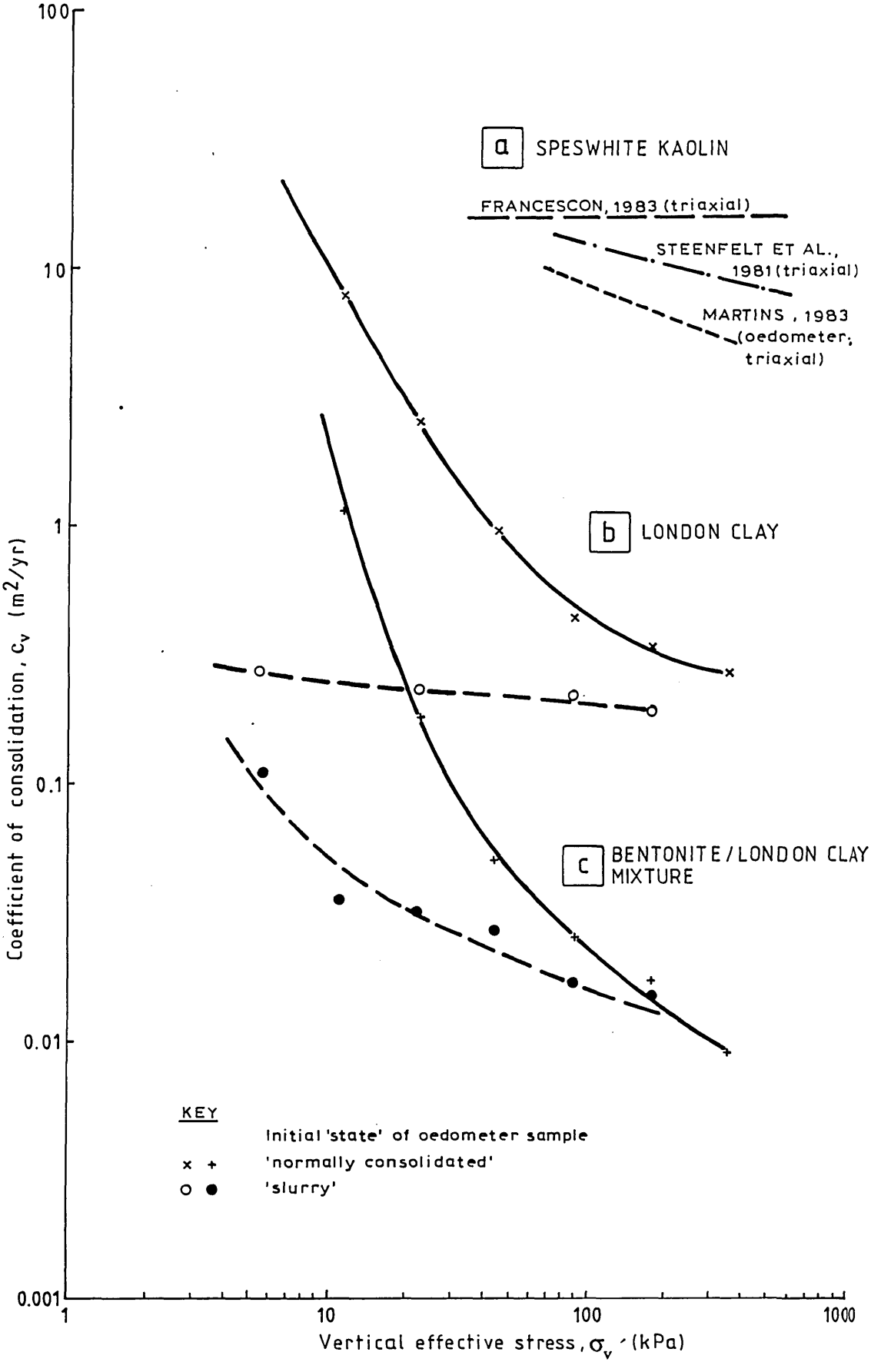


Fig. 3.9 $C_v - \sigma_v'$ relationships.

3.3.2B Slurry preparation

3.3.2B(i) Kaolin

Before outlining the slurry preparation technique used in this investigation, a short review of the literature will be presented in order to illustrate the reasons for the selection of the technique adopted.

Rosenfarb (1975) perfected a slurry consolidation technique (Krizek et al., 1975) and obtained consolidated samples of kaolin which were homogeneous and reasonably free from any slurry placement effects. To achieve such samples, dry Kaolinite Hydrite 10 (Georgia Kaolin Company) was mixed with distilled water to a water content of about 250 ± 10% (i.e. roughly four times the liquid limit (Table 3.2b), resulting in $I_L \approx$ 7.5–8); the mixture was thoroughly stirred for about 20 minutes using a motor-driven rotary mixer. To saturate the slurry completely, it was stored for about two to four weeks until equilibrium conditions were attained.

Kirkpatrick & Khan (1981) found that slurry water contents of 1.5 times the liquid limit ($I_L \approx 2$) were suitable for the mechanical mixing and the sample preparation processes which they employed, while Martins (1983) used a slurry water content just over twice the liquid limit (with initial water content values of between 140 and 150%) and allowed the slurry to stand for several weeks to ensure full hydration.

At Cambridge, kaolin is consolidated from a slurry water content of about 125%; this is just under twice the liquid limit and gives a liquidity index less than 3 (see, e.g. Cheah, 1981).

Thus, homogeneous samples of kaolin may be obtained from a slurry water content in the range 100–250%, corresponding to 1.5–4 times the liquid limit and liquidity indices in the range I_L = 2–8. For each mix in this investigation, 5 kg of dry Speswhite kaolin powder was mixed with distilled water (by adding kaolin to water, and not vice-versa) to form a slurry with a water content of about 150%, this being less than 2.5 times the liquid limit and resulting in $I_L \approx 3.5$. To achieve this, an electric paddle mixer was used for a period of about five hours. To ensure full hydration of the slurry, it was stored for 5–10 weeks and manually stirred once a week prior to consolidation.

3.3.2B(ii) London clay

For the programme of reconstituted* soil testing, intact samples of London clay from Canons Park were air-dried, ground and passed through a 420μm sieve. Based on the experience gained from the preparation of kaolin slurry, dry London clay was thoroughly mixed with distilled water to give a slurry of about 150% water content (≈ $2w_L$, with $I_L \approx 3$). Similarly, the slurry was allowed to stand for about ten weeks to ensure full hydration; during this time it was stirred once a week. [* Remoulded samples of London clay (obtained from Wraysbury) were also tested in the experimental programme. These needed no preparation other than allowing several weeks for hydration.]

3.3.2B(iii)The bentonite/London clay mixture

As part of the investigation into the strain-rate effects associated with the vane test, a mixture consisting of equal parts of London clay from Canons Park and commercially available bentonite was prepared. The dry mixture was added to distilled water to give a slurry of about 350% water content (= $2w_L$, with $I_L \approx 2$). Prior to consolidation, the slurry was stored, being stirred once a week for about 20 weeks.

3.3.2C Slurry consolidation

Two different types of slurry consolidation technique were employed. Stress-controlled consolidation of a large cake of London clay involved the use of a 229mm diameter oedometer, while all the other samples were consolidated one-dimensionally in a 100mm diameter tube under conditions of displacement control.

3.3.2C(i) Displacement-controlled consolidation

The procedure adopted by Rosenfarb (1975) involved re-stirring and de-airing the slurry under a vacuum for about four to six hours prior to its placement in a consolidometer chamber.

Martins (1983) introduced the slurry into a 330mm long, 108mm diameter sample tube after it was stirred under vacuum for at least one week. In order to reduce side friction during consolidation, the inner wall of the sample tube was lightly smeared

with soft white paraffin (and not silicone grease, as suggested by Martins). Drainage at both ends was provided in the form of a sandwich of filter paper and metal gauze. Having filled the bottom drainage system with distilled water, it was sealed before the slurry was gently poured down the sides of the tube. The tube was gradually rotated to ensure uniform distribution of the slurry, whilst great care was taken to avoid trapping any air bubbles. After pouring each 50mm thick layer of slurry, the tube was 'rocked' in order to level the surface and thus to minimise transverse bedding structures from the final sample. The tube full of slurry was then placed in a displacement-controlled press before consolidation was effected by compressing the sample at constant rates of displacement commencing with 0.6 mm/hr, followed by 0.48, 0.37 and finally 0.15 mm/hr. These rates were selected such that excess pore pressures generated at the centre of the sample were minimised.

A sample of 180mm final height was prepared using Martins' procedure, but a difference of the order of ± 1% was found in water contents along the length of the sample. This variation did not agree with Martins' figure of less than 0.5%, this being apparently equivalent to a 5% loss of axial stress due to friction down the sample. It is of interest to note that Kirkpatrick & Khan (1981) also observed variations of about 0.5% between average water contents along the length of 90mm thick samples. They found that this difference was reduced by a more gradual application of consolidation pressure, and achieved this by lowering the load increment ratio in oedometer consolidation to below unity. Consequently, it was decided to check the rates of sample compression chosen by Martins, since a water content variation with depth of the order of ± 1% was not considered acceptable.

As part of the improvements to the sample preparation techniques, a new piece of equipment (Section 3.2.4A) was designed in order to be used for slurry preparation prior to its placement in a sample tube. This allowed the slurry to be continuously stirred under a vacuum of about 50 kPa. [Love (1984) had found that any vacuum greater than about 60 kPa would give rise to many small bubbles appearing within the slurry.] After stirring for about five hours the electric motor was switched off, the vacuum removed, and the slurry slowly expelled from the container via a plastic tube of 3/4" (19.1 mm) diameter under a small air pressure of about 10 kPa. The plastic tube was placed at the bottom of the tube in which the sample was subsequently consolidated, being gradually raised as the level of the slurry approached the top of the sample tube. It is believed that this method of placing of the slurry in the sample tube (a) reduces trapped air bubbles to an absolute minimum and, (b) results in samples that retain the least number of the early structural features (see, e.g. Tchalenko, 1967, and Martins, 1983). [There is no evidence to suggest that the early structures, which are attributed to

slurry placement effects, in any way influence the behaviour of the samples, although they may confuse the interpretation of the thin-sections (see, e.g. Martins, 1983).] The above procedure was used during the preparation of all the soils tested in this study.

Finally, one-dimensional consolidation of the sample was effected by placing the tube full of slurry in a displacement-controlled loading frame (Section 3.2.4B). In order to control the excess pore pressures generated within the sample, rates of compression were varied while excess pore pressures were monitored at the base; drainage was provided at the top. The criterion adopted was that the base pore pressures were not allowed to exceed the vertical stress measured at the top of the sample by more than about (u/σ_v =) 10% during any stage of sample consolidation, except for the initial and final stages, when $u/\sigma_v \approx 20$ and 2% respectively (see Fig. 3.10).

One-dimensional consolidation to a water content of about 50% took about six weeks; Martins (1983) reports that it took ten days to consolidate the samples to a water content of 53%. At the end of this period, free water was removed from the top drainage system while the pore pressure transducer was disconnected from the bottom drainage system. The motor was switched off, the tube taken from the loading frame, the bottom cap removed and the sample, still inside the sample tube, was wrapped in cling-film and sealed with wax before being stored. As a result of these improved procedures, the variation in the water content of the samples was found to have reduced to 0.25%.

The relation between sample water content (w) and vertical effective stress (σ_v') during one-dimensional slurry consolidation of all three clay types tested in this investigation can be seen in Fig. 3.11 which also presents a number of published w–σ_v' relationships for Speswhite kaolin. It is worthy of note that the slope of the 'virgin' consolidation line is the same for both one-dimensional consolidation of Speswhite kaolin and isotropically consolidated samples (Mair, 1979), thus inferring that Speswhite kaolin is isotropic with respect to strength; although Davies (1981) found that the failure stress ratio, $(q/p')_f$, for undrained triaxial tests conducted on K_0 consolidated samples was the same as that for undrained triaxial tests on isotropically consolidated samples, he reports that both the axial strain at failure, ε_f, and the initial stiffness, E, of isotropically and K_0 consolidated samples were different, with ε_f equal to 12 and 4% respectively, and the former having a lower E.

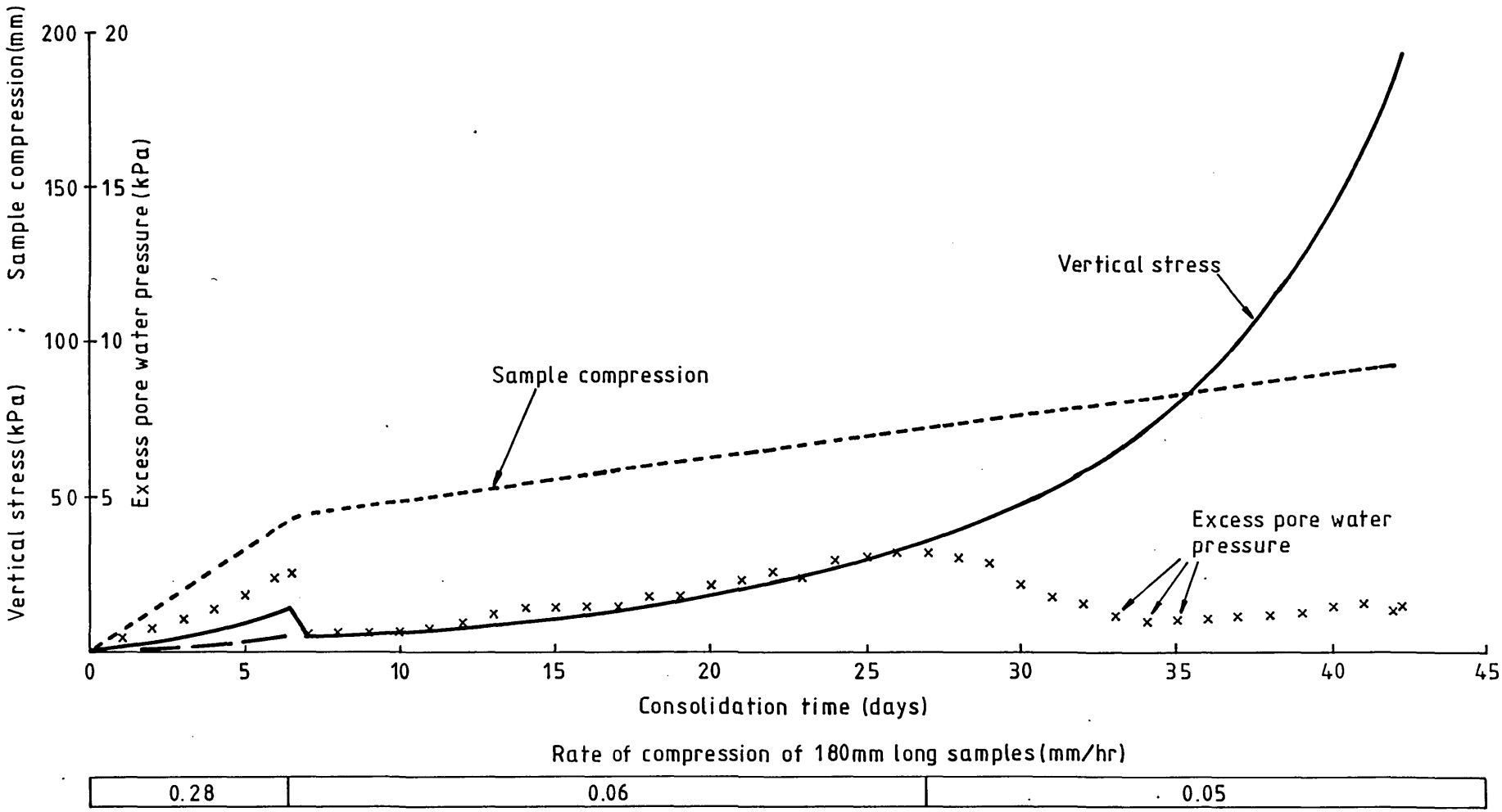


Fig. 3.10 Displacement-controlled one-dimensional consolidation of kaolin from slurry.

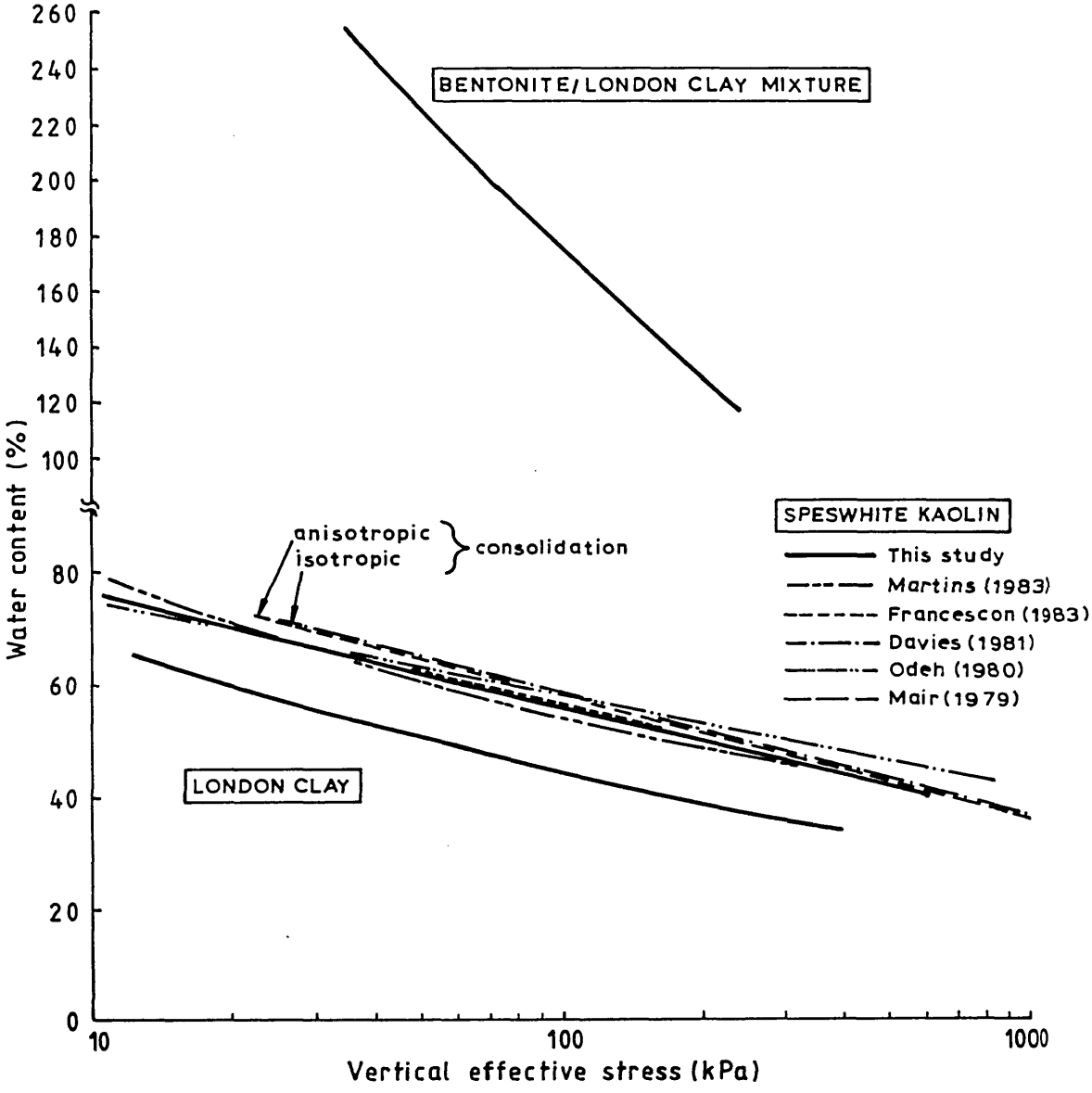


Fig. 3.11 Water content-vertical effective stress relationships obtained from slurry consolidation.

3.3.2C(ii) Stress-controlled consolidation

One large cake of London clay was reconstituted under conditions of stress control. The slurry was mechanically stirred under vacuum using the same procedures outlined in Section 3.3.2C(i), above. Before transferring the slurry to the 229mm diameter oedometer cell, the porous stones were de-aired and the side walls lubricated with soft white paraffin. The oedometer cell was mounted in its loading frame and the slurry was allowed to consolidate under its own weight for two days; the top of the cell having been cling-filmed. The cling-film was then removed and a wooden cap placed over the slurry; further consolidation was allowed for another two days. Thereafter, the top cap was gently placed over the slurry. Table 3.6 indicates the loading sequence which was subsequently followed.

A cake of normally consolidated London clay was obtained after two months. This was taken from the oedometer by shutting off the drainage valves and rapidly unloading the cell, thus avoiding water being sucked into the sample from the porous stones. The base plate was subsequently disconnected from the side walls and the cake placed on a loading frame whereupon three U100 thin-walled tubes, with lubricated surfaces, were carefully pushed into it. The tubes were wrapped in cling-film, coated in wax and stored in a sealed container until required for testing.

3.3.2D Consolidation in the stress path cell

A series of tests of both a model pile and a triaxial-vane was carried out in a large stress path cell capable of taking 100mm diameter samples. A detailed account of the procedures adopted for consolidating samples of kaolin in this stress path cell is given by Martins (1983). For the sake of completeness, however, a brief outline of the procedures followed is given below.

Kaolin samples consolidated one-dimensionally using the loading frame were trimmed nominally to 102mm diameter and 150mm long by means of a soil lathe and a split mould. The dimensions of the sample were measured with vernier callipers, the sample weighed and water content samples taken from the trimmings. Each sample was jacketed with a rubber membrane (which had already been checked for leaks) and equipped with top and bottom drainage, each comprising two sheets of filter paper and a metal gauze disc.

Day No.	σ_v' (kPa)
11	11.1
18	22.2
25	44.3
32	88.6
39	177.2
60	0

Table 3.6

Stress-controlled consolidation of London clay in a 229mm diameter oedometer.

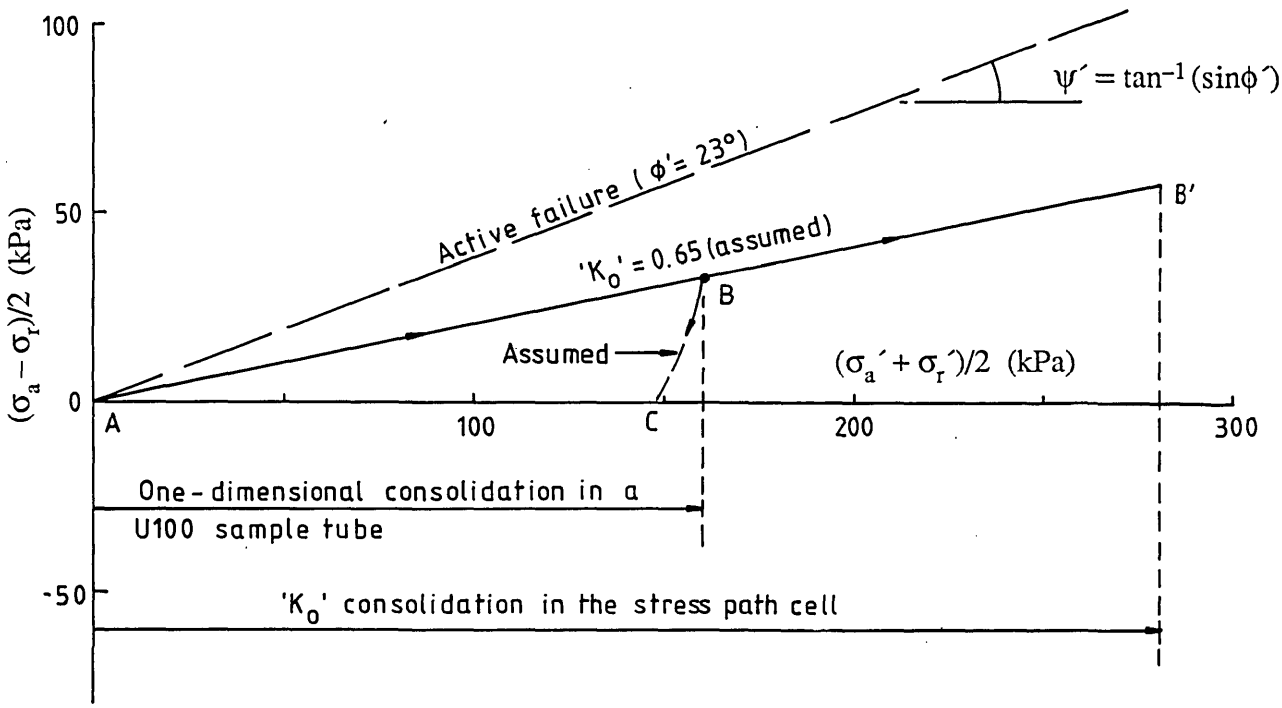


Fig. 3.12 Consolidation of kaolin

Anisotropic consolidation along a 'K_0' path (= σ_3'/σ_1' = 0.65) followed, in accordance with the procedures outlined by Bishop & Wesley (1975), as shown in Fig. 3.12. The initial one-dimensional consolidation stage (see Section 3.3.2C(i)) is represented by path AB, and the path that the sample is assumed to have followed during stress relief is indicated by BC. All the samples were normally consolidated to a radial effective stress ($\sigma_3' = \sigma_r'$) of about 220 kPa, with $\sigma_a' \approx 340$ kPa $\approx$ 1.7 times the maximum previous (one-dimensional) consolidation stress of approximately 200 kPa, thus resulting in samples which would behave in a normally consolidated fashion (see Gens, 1982).

The experimental procedures which were adopted included flushing the bottom drainage system with water before placing, first a metal gauze – filter paper sandwich and then, the one-dimensionally consolidated sample on the bottom cap; the metal gauze disc had a 20mm diameter hole at its centre. A second metal gauze – filter paper sandwich was placed on top of the sample, and the top cap mounted before securing the assembly at the top and bottom with rubber 'o' rings. The cell top platen which was guided by tie rods was positioned on the top cap before finally lowering the stress path cell perspex cylinder into place. The cell was filled with de-aired water and a cell pressure of 20 kPa immediately applied before flushing both the top and bottom drainage systems with de-aired distilled water, thereby removing as much free air as possible. The radial stresses applied to the sample were increased in steps of about 15 kPa every 24 hours until the final stress level of 220 kPa (point B' in Fig. 3.12) was reached; the axial stresses on the sample were increased such that the sample followed a stress path along the 'K_0' (= 0.65) line.

A 25cc burette was used to measure the volume of water expelled during sample consolidation, while changes in the length of the sample were measured with a submersible LVDT.

3.4 TESTING PROCEDURES

3.4.1 Introduction

The experimental details associated with the laboratory-vane tests, the triaxial-vane tests, the model pile tests, the triaxial compression tests, and the thin-section preparation techniques are described below.

3.4.2 Laboratory-vane Tests

3.4.2A Introduction

A suite of laboratory-vane tests were conducted to examine

(i) the effect of strain rate on the measured vane strength;
(ii) the effect of the number of blades on strength;
(iii) the pattern of soil deformation around n-bladed vanes, where n = 2, 3, 4 and 6.

Specimens of Speswhite kaolin and London clay which were consolidated in U100 sample tubes were tested in the laboratory (in free air, i.e. at zero confining stress).

Great care was taken to avoid the sample being jacked even part way out of the tube once the end seal, consisting of wax and cling-film, had been removed. The upper end of the sample was cut flat and perpendicular to the tube axis and then waxed to minimise moisture loss. The tube was then securely fixed on the ICLVA platform (Section 3.2.2B). Having measured the dimensions* of the vane, the vane shaft was fitted into its socket and the fixing screw tightened such that there was no possibility for the shaft to slip or rotate. The vane was then pushed squarely through the wax into the sample and after a 'delay' of less than one minute, rotation of the vane was started. [*Note: Differences between the actual and nominal (e.g. 12 mm x 12 mm) vane dimensions were found to result in a maximum discrepancy in the measured shear strength of only 5%, and consequently the nominal dimensions of vanes were used in the calculation of shear strengths.]

A series of pilot tests was conducted before deciding how each separate test programme would be run.

3.4.2B Tests to investigate strain-rate effects in the vane test

In order to study the effect of the rate of rotation on the measured vane strength, an experimental programme was devised to test samples of both Speswhite kaolin and London clay over a range of rates of rotation of (ω =) 1.075–1075 °/min, as dictated by the stepper motor which was available. A supplementary series of tests was conducted on normally consolidated samples of a bentonite/London clay mixture.

In the majority of the tests the 4-bladed 12mm square vane was employed. In an attempt to determine the rate of rotation at which undrained conditions would apply, tests were also carried out using the 4-bladed 18 and 24mm square vanes.

Each test was continued for 360° rotation.

3.4.2C Tests to study the effect of different numbers of blades

A series of tests was carried out in order to examine the effect of the number of vane blades on both the measured strength and the shear stress – rotation characteristics of soft clays. The vanes used were primarily of dimensions 12 mm x 12 mm, with 2, 3, 4, 6, 8 and 12 blades, as well as a solid brass rod to simulate the effect of an infinite number of blades; brass vanes with H = D = 24 mm were also included in the test programme. Both Speswhite kaolin and London clay samples were tested.

The vanes were all rotated through 360° at a constant rate of 6.27 °/min. At the end of each test, the vane was taken out of the sample and cleaned. The next test was conducted at a different location within the sample and with a vane with a different number of blades. In each sample, up to ten tests could be carried out with the 12mm square vane (see Section 3.2.2A(i), and Fig. 3.13b). Consequently, two tests each were conducted with 2-, 3-, 4- and 6-bladed vanes. It was therefore possible to check the repeatability of the results obtained with each vane in each sample. If it seemed necessary, one or two more tests could also be carried out in the same sample. To check sample homogeneity and reproducibility of results, the 4-bladed vane was tested in two positions in each sample.

With the 24mm square vanes, up to five tests could be done in each U100 sample, with two 'control' tests conducted using 2- and 4-bladed 12mm vanes.

3.4.2D Tests to examine the vane failure mechanism

A series of tests was conducted with vanes having two, three, and six blades, as well as the conventional four, in order to study the development of the deformation patterns at different stages of vane rotation.

The effect of sample water content on the development of shear structures around the vane was investigated by testing 2-, 3- and 4-bladed vanes in samples of Speswhite

kaolin having water contents in the range 40–60%, corresponding to liquidity indices between 0.25 and 0.82.

The effect of clay type on the propagation of the microfabric features was examined by testing a 4-bladed vane in a sample of London clay having a similar liquidity index of $I_L \approx 0.25$.

Each vane, with nominal dimensions of 12 mm x 12 mm, was pushed through the wax seal into the sample — inside the container fixed on to the ICLVA platform (Section 3.2.2B) — so that the top of the vane was at a depth of 50 mm below the surface of the sample (see Section 3.2.2A(i)). There was a delay time of less than one minute before vane rotation at a rate of 6.27 °/min. This rate of rotation was chosen since it corresponds to the rate of rotation of 6 °/min at which both Skempton (1948) and Cadling & Odenstad (1950) had measured the lowest field vane strength (see Section 2.4).

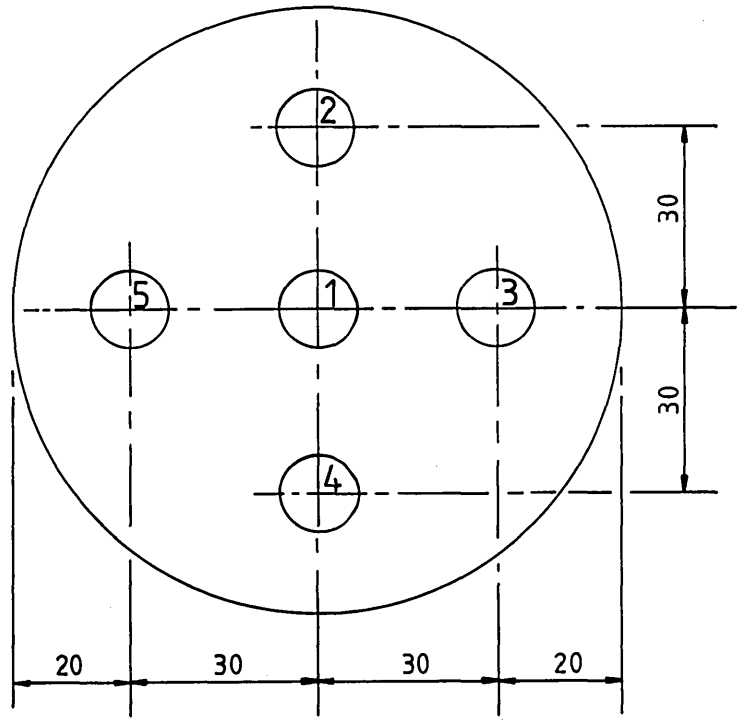
Using five identical vanes, the tests were carried out at five locations within each U100 sample, as indicated in Fig. 3.13a: at the centre (location 1) and on two diameters at right angles, 20 mm from the edge of the container (locations 2–5). At location 1, the vane rotation was continued past the maximum torque, until 'residual' conditions (corresponding to large displacements) appeared to have been approached. This test result provided a likely torque–rotation relationship for the sample, and was helpful in deciding when to stop the subsequent tests at locations 2 to 5.

In order to establish the vane failure mode precisely, tests were also stopped *just before* and *just after* the peak shear stress. Consequently, once the thin-sections were prepared, a picture of the propagation of shear structures defining the vane failure mechanism was available.

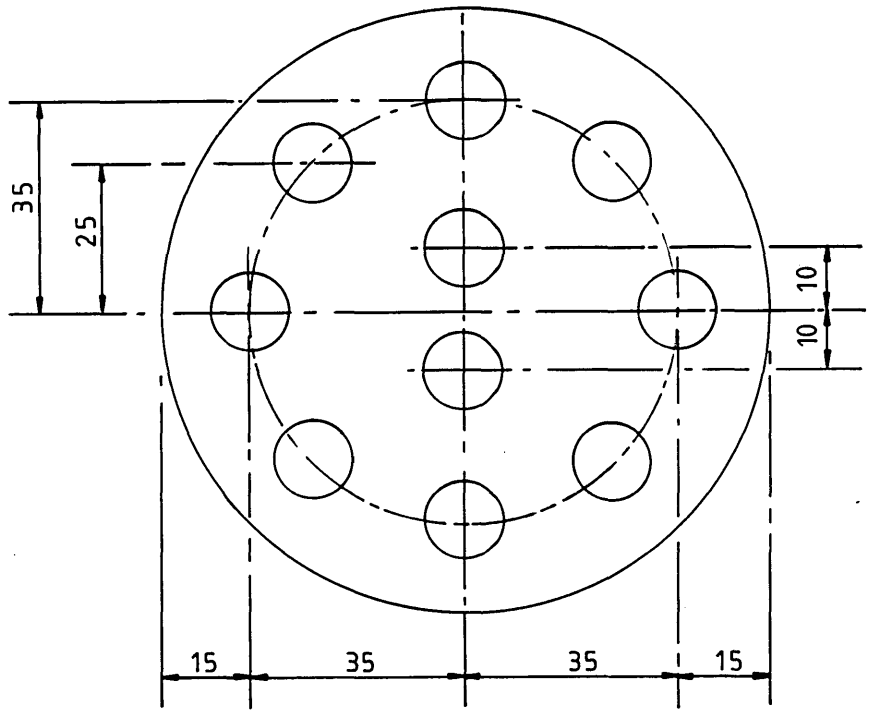
At the end of each test (after stopping the vane rotation), the screw connecting the vane shaft to the torsional load cell was very carefully slackened so as to avoid any further disturbance to the soil sample. With the vane left in its position, the platform was lowered and another vane, identical to the first one, was fitted into the vane shaft socket. The sample tube was carefully moved to the next test position, and the above procedure repeated at the other test locations.

On completion of each series of tests, the wax seals at the top and bottom of the sample tube were broken and the sample was allowed to slide out of the tube under its own weight. Subsequently, thin-sections were prepared (Section 3.4.6).

a (after Head, 1982)



b



ALL DIMENSIONS ARE IN MILLIMETRES.

Fig. 3.13 12mm diameter vane test locations in U100 tube

3.4.2E Tests to study other effects

3.4.2E(i) Tests to study the effect of sample storage time

Tests were conducted using soil samples which were one-dimensionally consolidated to specified stress levels and then subjected to total vertical stress relief. The samples were then waxed and stored, and used for testing when required. The duration for which the samples were stored prior to testing is referred to as the "sample storage time".

Based on the work conducted by Kirkpatrick & Khan (1981), the strength of soil samples subjected to total stress relief drops as the sample storage time increases (see Section 4.4.2F(ii)). To examine the validity of this observation, a series of tests was conducted using normally consolidated samples of Speswhite kaolin subjected to total vertical stress relief. After unloading the samples to zero total stress, they were stored for 1 day, 10 days and 50 days before being tested at zero confining stress using a 4-bladed 12mm square vane. The vane was rotated for 360° at rates of rotation of 5.375, 107.5 and 1075 °/min. Repeatability of results was checked (see Section 4.4.2F(ii)).

3.4.2E(ii) Tests to examine the effect of shaft friction

A series of tests was carried out to determine the frictional resistance along the vane shaft as a percentage of the total torque measured by the vane. This was done by inserting vane rods having diameters d = 3.175 and 4.763 mm into kaolin; the rods were rotated through 360° at a rate of rotation of 6.27 °/min. The shaft friction was found to be a small percentage of the total mobilised torque and was therefore neglected (see also Section 5.4.3 and Fig. 5.11b).

In addition, the effect of rod penetration distance was investigated by inserting vanes into samples to a variety of depths, z, where z denotes the height of soil above the top of the vane blades. For z in the range 10–60 mm, it was found that the depth of vane insertion had no noticeable effect on the measured vane strength (see Section 4.4.2F(iii)).

3.4.3 Triaxial-vane Tests

3.4.3A Introduction

In order to examine the validity of the results of the laboratory-vane tests, an experimental programme was devised primarily aimed at investigating the soil deformation patterns associated with the rotation of vanes in samples of kaolin under known triaxial stress conditions, as a check on the 'unknown' stress conditions of the main series of (laboratory-vane) tests.

The principles adopted for the insertion of vanes were similar to those used by Martins (1983) when installing model piles. The procedures which were followed during the triaxial-vane tests involved unloading the fully consolidated sample under undrained conditions, vane insertion to the desired depth, re-application of the initial total radial stress of about 220 kPa on the sample, equilibration, and vane rotation under drained conditions; Section 3.4.3D, below, deals with the re-application of the axial stresses.

3.4.3B Unloading the sample

Once the kaolin sample had undergone 'K_0' consolidation within the stress path cell to a radial effective stress of about 220 kPa, the burette was isolated and the top and bottom drainage systems were gently flushed through with air (under a pressure of about 15 kPa) in order to remove as much free water as possible. The drainage valves were shut off and the cell pressure reduced to zero in decrements of about 15 kPa under undrained conditions. During this operation, the height of the sample was kept constant with the aid of a manually operated ram (Fig. 3.3) which controlled the hydraulic piston of the stress path apparatus; the submersible LVDT monitored the sample height while the ram pressure corresponding to every decrement in cell pressure was being recorded.

Unloading of the sample from the radial stress of 220 to 0 kPa took about two hours.

3.4.3C Vane insertion

When the cell pressure had been reduced to zero, the plug at the centre of the top cap was removed; there was no extrusion of the clay. The vane was fixed to the

torsional load cell and inserted very slowly into the sample with the aid of a guide which ensured central positioning of the vane; a spirit level was used to ensure that the vane was inserted absolutely vertically. Simultaneously, the torsional load cell platform was lowered (by turning the nuts underneath it) until the top of the vane blades was just below the top of the sample (Fig. 3.2b). The vane guide was then fitted in the centre of the top cap and securely screwed in place. Lowering the vane to a depth of 25 mm took about an hour.

As in the laboratory-vane tests, no grease was applied to the vane shaft.

3.4.3D Re-application of total radial stresses to the sample

Once the vane was inserted inside the sample, the cell pressure was increased in increments of about 15 kPa up to 220 kPa while the hand-ram was used to maintain the sample height at a constant value; the ram pressure was monitored throughout this operation and it was assumed that, since undrained conditions were maintained, the axial stress acting on the sample would return to its initial value. However, at the end of the re-application of the total radial stresses to the sample, the ram pressure that resulted was lower than the original ram pressure of about 340 kPa (see Tables 8.1 and 8.2); this observation was also made by Martins (1983) in his model pile experiments. Nevertheless, the ram pressure was not adjusted, for to have done so would probably have resulted in some axial displacement of the sample, and thus relative movement between the clay and the vane.

3.4.3E Vane rotation

Once the cell pressure of 220 kPa was re-applied on the sample, a period of 24 hours was allowed to elapse in order that the sample would reach a state of equilibrium. The vane was then vertically lowered a further 30 mm to test position 1. After a further 24 hours had been allowed to elapse for the sample to equilibrate, the vane was rotated through 360° at a constant rate of rotation of 1.4 °/hr (≈ 0.023 °/min) using the vane rotating equipment described in Section 3.2.2C; the drainage valves were open during the vane test.

The rate of vane rotation of 0.023 °/min provided a peripheral displacement of 0.0025 mm/min and was thus sufficiently slow to ensure that shearing occurred under fully drained conditions. [Martins (1983) had used a rate of pile displacement of 0.25

mm/hr (≈ 0.0042 mm/min) in the drained axial loading of his model piles.]

The shear stress – rotation variation during the test was monitored by means of the Solartron DTU (see Section 3.2.5E).

At the end of the test, the vane shaft was disconnected from the torsional load cell and after 24 hours, it was again reconnected and slowly pushed another 30 mm into the sample, thus leaving a 5–10mm gap between test position 1 and 2. Again, 24 hours was allowed to elapse so that the sample would equilibrate before the vane was rotated at test position 2. This time, however, the test was stopped as soon as the peak shear stress was reached. Following the above procedures, the vane was pushed to test position 3 and rotated until pre-peak shear stress conditions were attained.

At the end of the third vane test, the sample was unloaded under the same conditions as those used before the vane was inserted into the sample (see Section 3.4.3B). The vane shaft was disconnected from the torsional load cell and the latter very carefully raised in the same manner in which it had been lowered (Section 3.4.3C); undue contact with the vane shaft was therefore avoided. The stress path cell was disassembled, and the dimensions of the sample and water contents within it were determined. The sample was then trimmed and placed in a bath of Breox Peg 8000 so that thin-sections could be prepared from horizons within the sample corresponding to the vane test positions.

Repeatability of results was checked by conducting similar tests on a second sample.

In an attempt to investigate whether the radial stresses acting on the vane would vary during rotation, a 'long' vane of 120mm height (and 12mm diameter) was rotated through 360° in a third sample.

3.4.4 Model Pile Tests

3.4.4A Introduction

The second rotating shear device to be studied was the model pile. It was hypothesised that, when subjected to rotation, the pile would behave as a multi-bladed vane. Model piles were therefore subjected to rotation in order to examine both the soil deformation patterns and the shear stress – rotation characteristics. Axially loaded pile

tests were also conducted, firstly to provide a check with the work of Martins (1983), and secondly, to compare their behaviour with that of piles subjected to rotation.

The pile installation procedure was the same as that described by Martins. However, a brief account of the experimental details involved in the installation of model piles is given below. This is followed by a description of the pile loading procedures.

3.4.4B Installation of model piles

At the end of full consolidation of the sample, the cell pressure was reduced to zero and the sample unloaded as described in Section 3.4.3B. Access to the sample was obtained by removing the plug at the centre of the top cap.

After mounting a drilling guide on the top platen of the cell, a hand-turned twist-drill was slowly advanced, thus coring a 13mm diameter hole through the centre of the sample; the twist-drill was cleared after increments of about 15mm advance. The waste clay was used for water content determinations which showed a uniform variation along the length of the sample.

Once the full length along the centre of the sample was drilled, the hydraulic system retaining the small piston in the lower platen was vented to the atmosphere (Fig. 3.2c). A small diameter rod was then used to push the piston to the bottom of its chamber, taking great care not to touch the sides of the borehole. Using a sharp reaming tool, the hole was enlarged to a diameter of 15 mm. It is shown in Section 8.4.1A that the drilling and reaming operations caused very little disturbance to the local soil fabric.

To instal the model pile, an 11.1mm diameter brass pile-core was degreased and subsequently attached to the torsional load cell mounted on the adjustable platform (Fig. 3.2b). Using the procedure described for inserting vanes into samples (Section 3.4.3C), the model pile was carefully lowered into the hole until the centre of the 'packer' membrane – at the lower end of the pile – was level with the base of the sample, as illustrated in Fig. 3.2c; taking great care, it was ensured that the pile did not touch the sides of the hole. The borehole sealing membrane – having always been tested before use – was then inflated to a pressure of about 35 kPa, with water via the hole through the pile. The pile-core was grouted into the hole by injecting a low shrinkage epoxy resin via a small-bore stainless-steel tubing attached to a hypodermic syringe; the tubing was 'housed' in the groove cut along the top 4 cm of the length of the model pile, and care was taken not to trap any air bubbles. The resin was then left to set overnight.

3.4.4C Pile loading procedures

After the resin had set hard, the total radial stress of about 220 kPa was re-applied to the sample, as outlined in Section 3.4.3D, above.

For the torsional pile load tests, the electric motor was switched on and the pile rotated at the same rate of rotation (of 1.4 °/hr, equivalent to 0.003 mm/min) as that used for the vane tests (see Section 3.4.3E). The tests were stopped either after 360° rotation or as soon as conditions of peak or pre-peak shear stress were reached.

For the axial load tests, the pile was detached from the torsional load cell once the resin had set hard. Using the equipment described in Section 3.2.2C(vi), the pile was loaded axially at a rate of displacement of 0.006 mm/min which was equivalent to the rate (of 0.003 mm/min) at which the torsional pile load tests were carried out; drained conditions applied during the tests which were continued to a displacement of about 11 mm, approximately corresponding to 'residual' conditions.

At the end of the model pile tests (whether subjected to axial loading or rotation), the unloading of samples, disassembling of the cell, and other procedures which followed were as described in Section 3.4.3E.

3.4.5 Triaxial Compression Tests

For the purpose of establishing how the vane strength relates to other measures of undrained strength, a series of vane and unconsolidated undrained triaxial compression tests was carried out on remoulded London clay.

Samples of London clay with water contents in the range $35\% \leq w \leq 55\%$ were tested; at each water content, four samples were tested at cell pressures in the range of 70–275 kPa. The dimensions of the samples and their weights were recorded, and the tests carried out using standard procedures for setting up 38mm diameter 76mm long remoulded triaxial specimens (Head, 1982). Each sample was subsequently sheared at a constant rate of strain of 0.81 %/min, i.e. equivalent to the rate of rotation of 6.27 °/min. Readings of deviator stress and axial displacement were taken at 10-second intervals for the first two minutes, then at 20-second intervals for the next four minutes, and thereafter at 30-second intervals, until the sample had undergone 25% axial strain. At the end of each test, the sample was cut into five horizontal slices for water content determinations.

3.4.6 Thin-section Preparation

3.4.6A Introduction

Thin-sections were prepared in order to examine the soil deformation patterns associated with the laboratory-vane test, the triaxial-vane test, and the model piles subjected to both rotation and axial loading. The technique employed for the preparation of thin-sections was similar to that used by Tchalenko (1967).

Specimens of clay were completely immersed in a bath of Breox Peg 8000 — a material which is miscible with water. The bath was kept at a temperature of about 65 °C and the samples were left there for various lengths of time depending on their size. Through diffusion, Breox Peg 8000 slowly replaced the water inside the specimens until the pores were filled with wax-rich fluid. On removal of the samples from the bath, solidification of the wax inside the samples resulted in rock-like specimens from which thin-sections were subsequently prepared by grinding with paraffin. An optical microscope (Tchalenko, 1967) and a macro-photography system were used to examine the microfabric features on the thin-sections.

3.4.6B Impregnation procedure

At the end of each test, a fine wire was used to cut the sample systematically so that finally only the vane/pile with a mass of soil around it remained. The clay specimen was then placed in a tightly-fitting steel-gauze box and completely immersed in a large bath of Breox Peg 8000; the volume of fresh wax employed being about 20 times that of the specimen. The wax was stirred once a day. After the first week, the specimens were transferred to a fresh bath; the 'laboratory-vane' specimens remaining in this bath for another week, while the 'triaxial-vane' and 'model pile' specimens were left there for a further two weeks. The specimens were then removed from the bath and allowed to cool slowly at room temperature for a day before thin-sections were prepared.

While impregnating London clay samples, it was necessary to wrap the specimens in two layers of tissue paper protected by elastic bands to ensure that the samples did not collapse in the warm bath.

When a defective batch of wax resulted in an imperfectly impregnated specimen, surface impregnation was used, proving satisfactory.

3.4.6C Preparation of thin-sections

For ease of handling during preparation of the thin-sections, extraneous lengths of brass, such as vane shafts, were immediately cut off. The rock-like specimen was then cut perpendicular* to the mid-height of the brass vane/pile using a diamond saw and a Kerosene-based oil as the cutting fluid. [* Note: To prepare longitudinal thin-sections the specimens were cut parallel to the vertical axes of the vanes (Section 3.2.2A(ii)).]

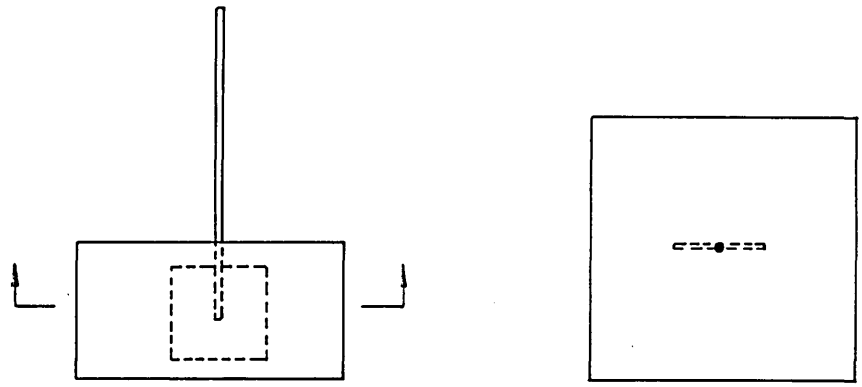
The required surface of the specimen was ground flat using a horizontal diamond lap and paraffin, followed by aluminium oxide on a glass plate. Subsequently, the specimen was cleaned using petroleum ether in an ultra-sonic bath, and mounted on a ground glass slide using Loctite 358. Once cured, the bulk of the specimen was cut from the glass slide, leaving a 2–3mm thick section which was ground down to about 50 μm. Great care was taken to prevent removal of the brass vanes from the thin-section slides, whilst the model piles were gently tapped out of the cut specimens (see also Martins, 1983). The sample was continually checked with a polarising microscope until it was ground evenly to a 30μm thin section. Finally, it was cleaned, covered with a coverslip, and labelled. As an example, Fig. 3.14 presents the sequence in which the cutting and grinding processes were carried out when preparing a thin-section slide from a specimen in which a 2-bladed vane was tested.

3.4.6D Examination of thin-sections

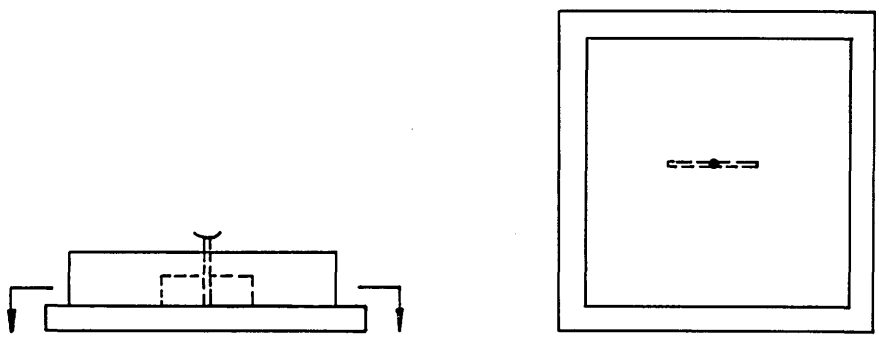
To study the thin-section slides, they were photographed using a macro-photography system incorporating an Illumitran, a 35mm camera, and two polarising filters so that all thin-section observations were made under crossed polarised light.

Each thin-section slide was photographed at exposure compensations of +1 and +2, and at two different slide positions, one at 45° to the other, thus providing the maximum amount of information available on the slides. Fig. 3.15 shows the manner in which the microfabric features around a 4-bladed vane go in and out of extinction as the orientation of the thin-section slide is varied under polarised light.

An optical microscope (Tchalenko, 1967) was used when greater detail of the microfabric features was required, e.g. in the London clay thin-sections.



(a) Sample cut along the horizontal plane at vane mid-height.

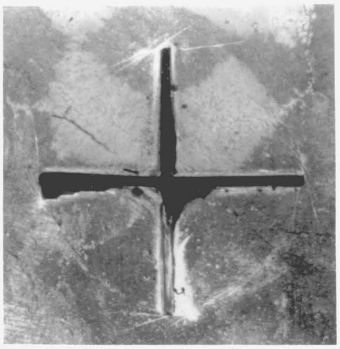


(b) Cut-sample ground flat and mounted on a glass slide, and then cut to give a 2 to 3mm thick section.



(c) Sample ground to a 30μm thin section, polished and covered with a coverslip.

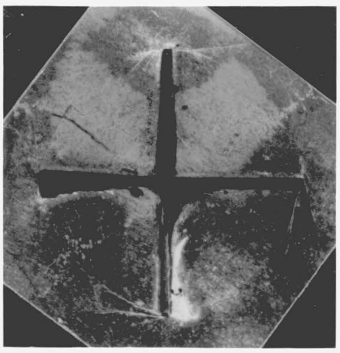
Fig. 3.14 Stages involved in preparing a thin-section slide.





a_1 = Datum

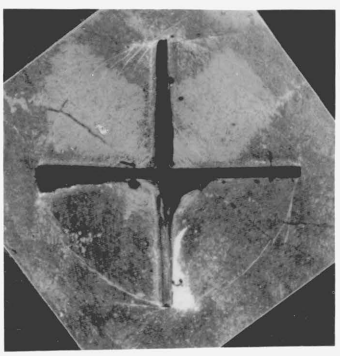
VANE BLADE, 'A', ASSUMING THE VERTICAL ORIENTATION.





$a_2 = a_1 + 30°$

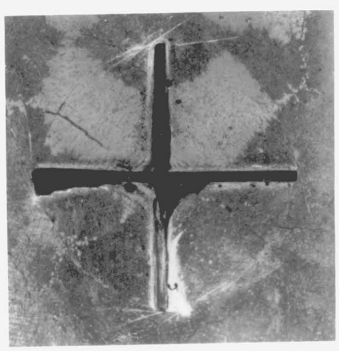
SLIDE TURNED THROUGH 30° IN THE ANTI-CLOCKWISE DIRECTION RELATIVE TO a_1.





$a_3 = a_1 + 60°$

SLIDE AT AN ORIENTATION OF 60° RELATIVE TO a_1.





$a_4 = a_1 + 90°$

SLIDE AT AN ORIENTATION OF 90° RELATIVE TO a_1.

Fig. 3.15 Effect of thin-section orientation on the observation of shear structures (Re: Figs. 6.17a and b).

3.5 PHOTOELASTIC STUDY OF THE VANE TEST

3.5.1 Introduction

Study of the stress field generated within a photoelastic material, as a consequence of the application of a torque in the elastic range, may be considered an appropriate model of the stress and strain distributions within a soil sample when strains are small and the soil is consequently in its elastic range of behaviour. Therefore, in order to gain further insight into the mechanism of formation of the initial ('first series') shear structures at the blade tips during vane rotation, a series of photoelastic experiments was carried out aimed at determining the directions of shear stresses around the periphery of vanes subjected to axial plane-strain loading conditions.

Two photoelastic materials — gelatine and polyurethane rubber — were used in the present experiments. Consequently, the model experiments on gelatine (Section 3.5.2C(i)) differed from those on polyurethane rubber (Section 3.5.2C(ii)).

A description of the components of the polariscopes used at both Imperial College (Department of Civil Engineering) and Surrey University (Department of Mechanical Engineering) is given in Section 3.5.2A, followed by an outline of the aspects of gelatine for use as the photoelastic material in the present investigation and particulars of the gelatine model experiments (Sections 3.5.2B(i) and C(i)), and details of the polyurethane rubber model experiments (Sections 3.5.2B(ii) and C(ii)).

Essential aspects of photoelasticity, such as definitions of the "isochromatics" and "isoclinics", are given in Appendix A1.

3.5.2 Experimental Procedures

3.5.2A The polariscope

The collimated light transmission polariscope used in the photoelastic experiments is shown in Figs. 3.16a and b. It was chosen in preference to the diffused light transmission polariscope because it enables measurements of the full field to be made from a photograph. The principle of operation of the polariscope is exactly the same as that of a polarising microscope (Hendry, 1966), in which the polarisation axes of the polariser and analyser are always at right angles to each other (Fig. 3.16a).

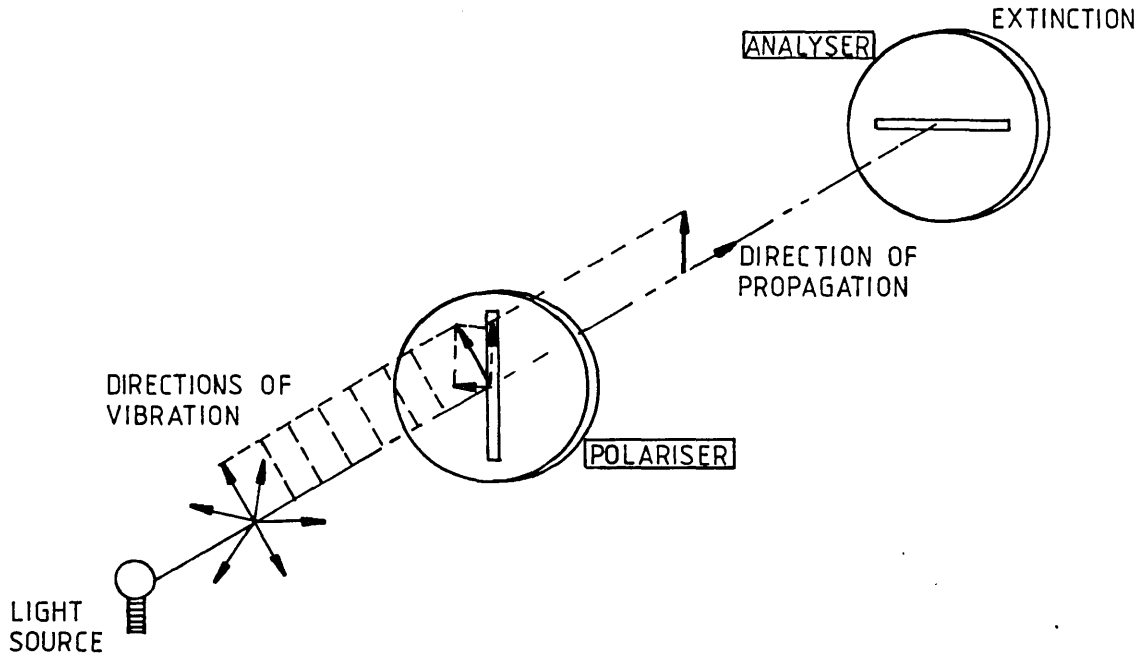


Fig. 3.16a Initial orientations of polaroid filters; when the polaroid axes are crossed, complete extinction occurs (after Photolastic, 1969).

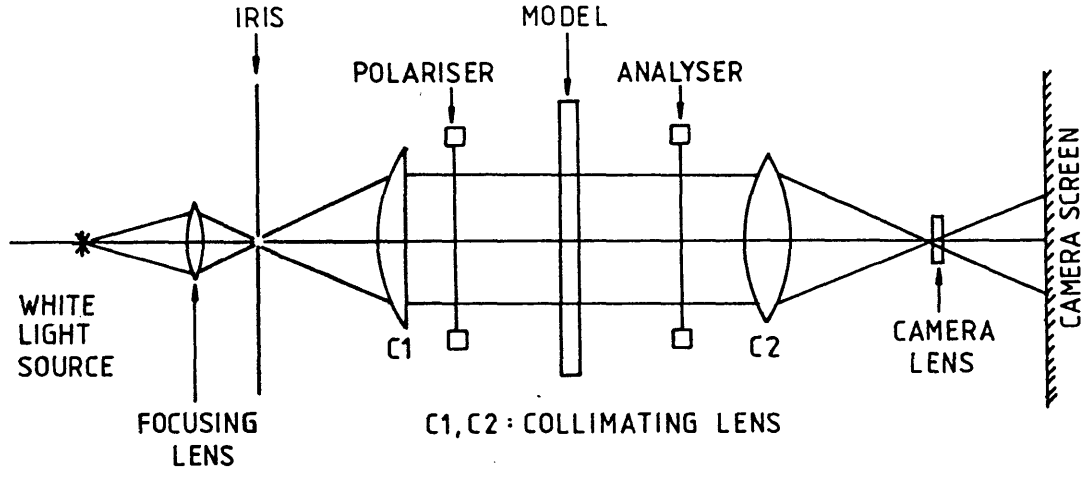


Fig. 3.16b Schematic diagram of the optical system of collimated light polariscope (after Hendry, 1966).

The collimated light polariscopes used at both Imperial College and Surrey University were similar, with each one consisting of a white light source, a small focusing lens, an iris, two 6" diameter biconvex collimating lenses, polarising assembly, analysing assembly and a mechanical drive coupling system for remote control of the simultaneous rotation of the polaroid filters for inspection of the isoclinics. The rotation was indicated on a precision engraved ring which was graduated in degrees. These various components were mounted on an optical bench which maintained alignment of the components whilst permitting their adjustment in the longitudinal, transversal and vertical directions.

A white light point source was formed by using a focusing lens and an iris, followed by a second lens — one of the 6" diameter lenses, positioned with the point light source at its focal point — to generate a parallel beam. The polaroid filter subsequently polarised the light along its axis of polarisation, with the result that the light passage was 'parallel' throughout the field, passing through the polariser, then the model, emerging from the model and then through the analyser. The camera lens was placed at the focal point of the other 6" diameter collimating lens (C2 in Fig. 3.16b), which was of good quality, free from internal strains, and positioned behind the analyser. The model photoelastic image appeared on the ground glass camera screen.

To carry out a detailed study of the "isochromatics" — photoelastic patterns which represent points of constant principal stress difference (Appendix A1) — circularly-polarised light was used by incorporating two quarter-wave plates in the polariscope, with each plate placed between the model and one of the polaroids (Fig. A1.2); the quarter-wave plates were crossed in order to obtain isochromatics of integral, as opposed to intermediate, parameter.

3.5.2B The photoelastic materials

3.5.2B(i) Gelatine

The optical sensitivity of gelatine greatly exceeds that of any other photoelastic material (see, e.g. Stimpson, 1970). For this reason, and because of its relative ease of preparation, together with its suitability for modelling real soil behaviour in the elastic range (see, e.g. Merrifield, 1980), gelatine was initially chosen as the photoelastic model material.

Ordinary household gelatine was allowed to settle into a solution of glycerine — a non-evaporating solvent, which also increases both the strength and elasticity of gelatine — and boiling water. The relative proportions by weight were 15% gelatine, 25% glycerine and 60% water, with the aim that the elastic modulus should be at an optimum (low) value, the geometrical shape of the model would not alter appreciably under load, and ultimately the maximum possible photoelastic effect would be achieved (see, e.g. Kuske & Robertson, 1974). The gelatine solution was thoroughly mixed and left to cure for two hours in an oven at 60 °C, before being transferred to the vane test container. The mixture was considered linearly viscoelastic with Poisson's ratio equal to 0.5 and a relaxation time of several hours (Richards & Mark, 1966). Thus, in the short term, i.e. when stressed for less than two hours, gelatine may be assumed to behave as an incompressible perfectly elastic solid and subsequently, purely elastic behaviour can be studied; thereafter, gelatine will undergo permanent deformations.

The experimentation was carried out with great diligence, since the photoelastic and mechanical properties of gelatine are known to be very markedly influenced by any physical or mechanical manipulation of the gel solution. As a result of the great care taken in preparation, model non-uniformity and possible initial stresses were avoided.

Owing to "time-edge" effects — which result from evaporation or absorption of water from the surfaces of gelatine models, causing changes of volume and resulting in tensile or compressive stresses in a narrow zone bordering the edges of the model, together with small equilibrating stresses distributed through the interior — the stress field in the material was affected and the photoelastic patterns were somewhat obscured. Hence, it was decided to carry out an additional series of tests with another photoelastic material. Polyurethane rubber, which has the advantage that it does not suffer from time-edge effects (Allison, 1987), was subsequently used as the photoelastic model material.

3.5.2B(ii) Polyurethane rubber

Polyurethane rubber is a highly transparent amber-coloured rubber-like plastic of very low elastic modulus and very high optical sensitivity, which is practically free from time-edge effects. Its behaviour is linear over a wide range (similar to gelatine), and at room temperature, its optical and mechanical creep are negligible after a few seconds following the application of load.

The polyurethane rubber model material was cast using 100 parts by weight of resin to 120 parts of hardener, which were thoroughly mixed. The mixture was then left for half an hour in an oven kept at 60 °C, during which time air bubbles were allowed to escape. It was subsequently poured into its mould (Section 3.5.2C) and allowed to cure at room temperature for one week. Although the mixture was free from air bubbles before it was poured into the mould, the process of pouring resulted in the entrapment of some air bubbles within the model; these did not, however, obscure the observation of the photoelastic patterns (see Section 7.3.2, and Figs. 7.2 and 7.3).

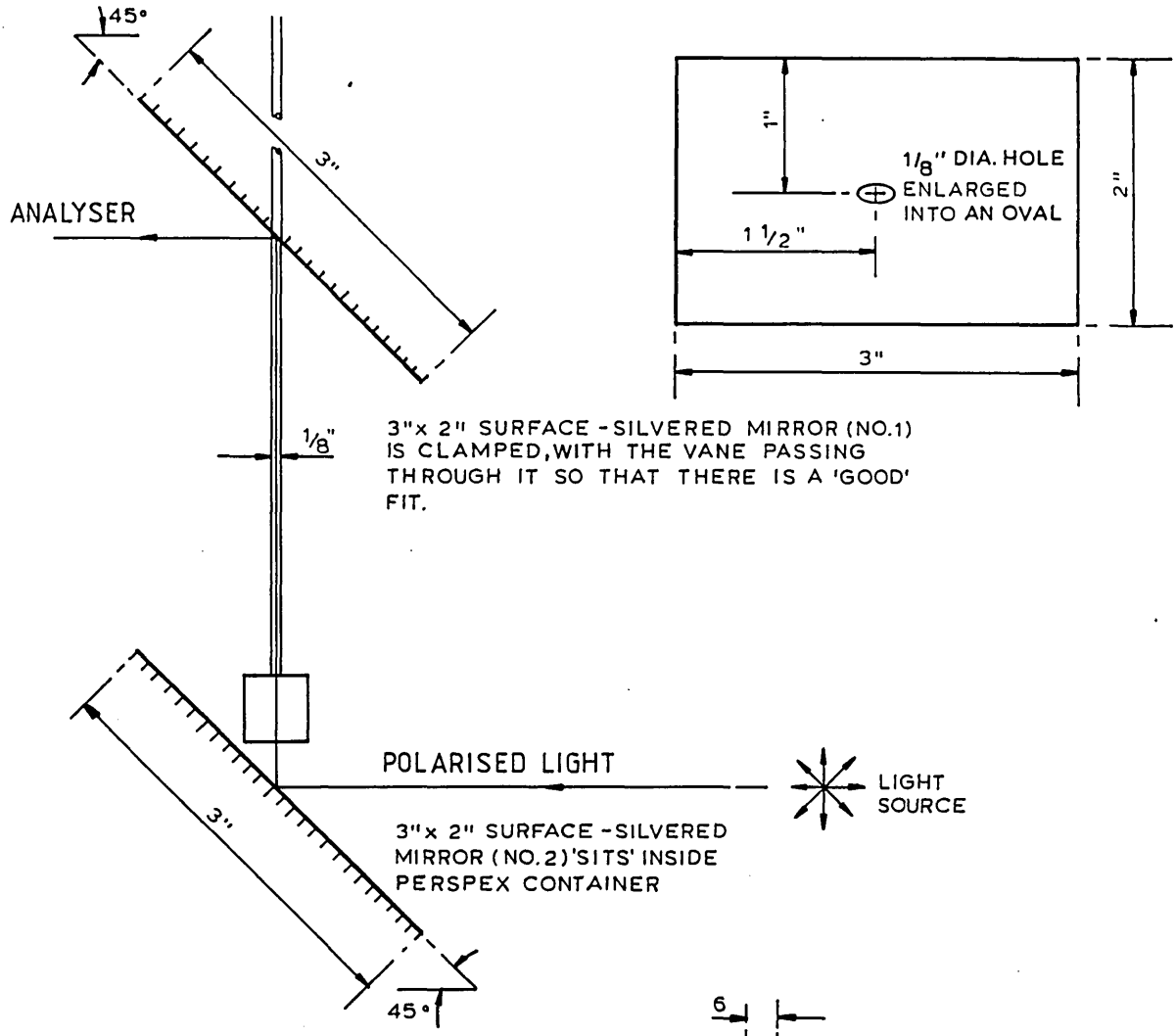
3.5.2C The model experiments

3.5.2C(i) Gelatine

The gelatine model, designed to study the stress field in the horizontal plane of the vane, is schematically presented in Fig. 3.17.

A container (67 mm x 55 mm x 26 mm) was constructed from 6mm thick perspex and supported on two columnar perspex sheets. This is shown in position in the polariscope in Fig. 3.16b. Apart from the top of the model which was a free surface, the model was bounded by rigid perspex. Plane-strain conditions were attained by making the container as high as the vane so that any deformation in the vertical direction would only result in negligible strains. A system of high quality surface-silvered mirrors was implemented and this allowed direct observation of the stress field in the horizontal plane of the vane during its rotation.

The base of the container was smeared uniformly with a thin layer of silicone grease. Hence, once gelatine had set in the container, little or no shear stress could result along the container base – gelatine interface. The vane (24mm high x 12mm diameter) was positioned in the centre of the container so that it was within 1 mm from the container base; the vane blades having been coated uniformly with a thin film of silicone grease in order to minimise the shear stresses along the blades, which might subsequently interfere with the stress field generated during vane rotation. The container and vane were then located on the platform of the vane apparatus and put in a 60 °C oven. Warm gelatine (at 60 °C) was poured into the mould covering the whole vane height. The oven temperature was gradually lowered to room temperature before the model vane apparatus was taken out of the oven and positioned in the polariscope.



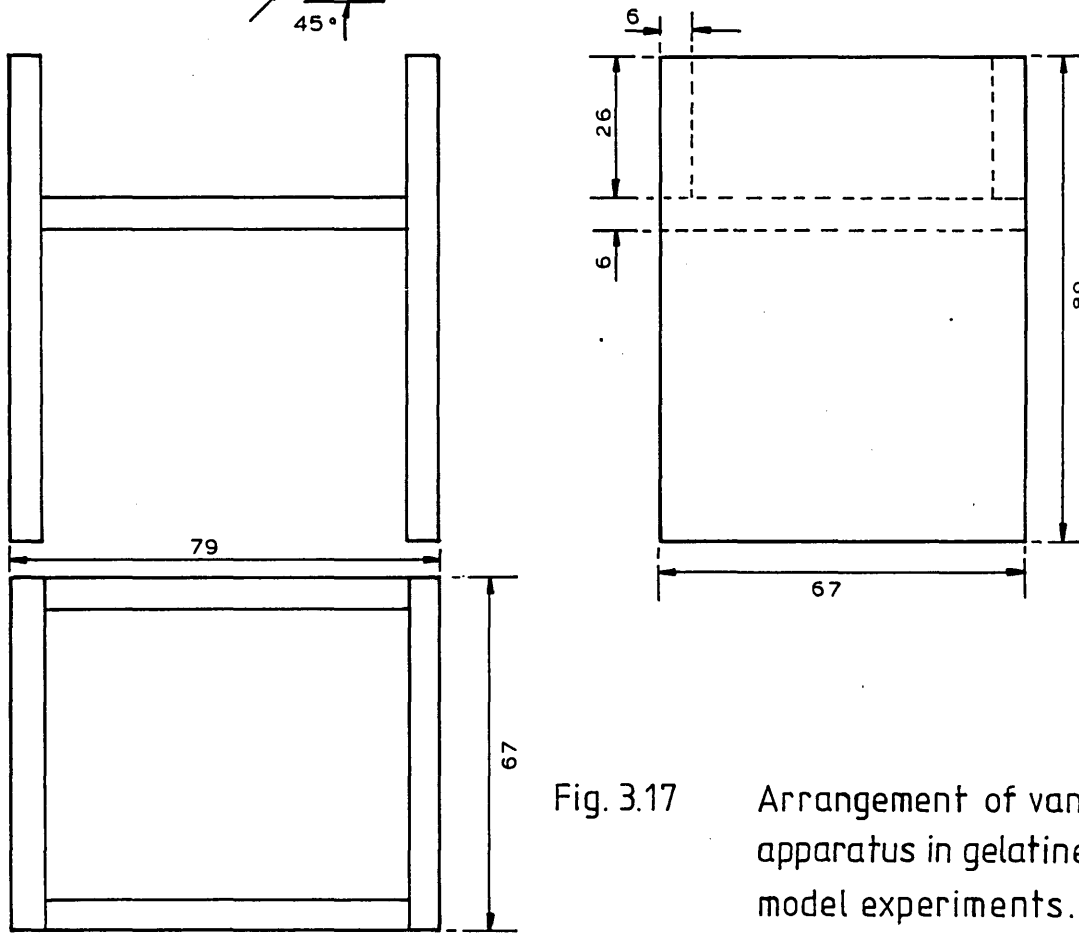


Fig. 3.17 Arrangement of vane apparatus in gelatine model experiments.

The polarisation axis of the polariser and analyser was adopted with reference to the plane orthogonal to the axis of the polariscope, such that the "isoclinics" — dark bands which occur when the direction of one of the principal stresses coincides with the reference axis (see Appendix A1) — were measured with respect to the line bisecting the vane blades. The gelatine was allowed to solidify around the vane and after 24 hours had elapsed, it was loaded at room temperature by rotating the vane in a clockwise direction. At increasing rotations of the vane, the stress state in the entire model was photoelastically determined by mapping the isoclinics using plane-polarised light. The principal stress directions ("stress trajectories"; see Appendix A1) were established from a direct examination of the isoclinics, in relation to the selected reference datum — the line at 45° to the vane blades. The directions of the shearing stresses were constructed at 45° to the stress trajectories. The isochromatics were obtained by incorporating the quarter-wave plates in the polariscope (see Fig. A1.2).

3.5.2C(ii) Polyurethane rubber

Fig. 3.18 shows the polyurethane rubber model vane test rig. Two parallel 3/8" thick perspex plates were used to support the model to ensure that the polyurethane casting had plane faces. The material was contained within a 1/4" thick disc, with inside and outside diameters of 3 and 4" respectively, positioned on the centre of the perspex plates. For ease of fabrication, the vane assembly was made from brass, having four blades with a diameter of 24 mm and a height of 1/4". The vane shaft, with a diameter of 1/8", extended an equal distance of 3/2" on each side of the vane; the 1/4" wide x 1/8" thick crossbar accommodated 3/2" offsets for the applied load, and was accordingly 7/2" long. The application of torque to the vane was by two equal 1/2lb weights attached to the crossbar offsets, with one of the weights being applied via a 3/2" diameter pulley mounted on the perspex support frame. All the parts described above were 'separate' in order to facilitate cleaning. Nuts and bolts passing through the perimeter of the perspex annulus were used to hold the test rig together.

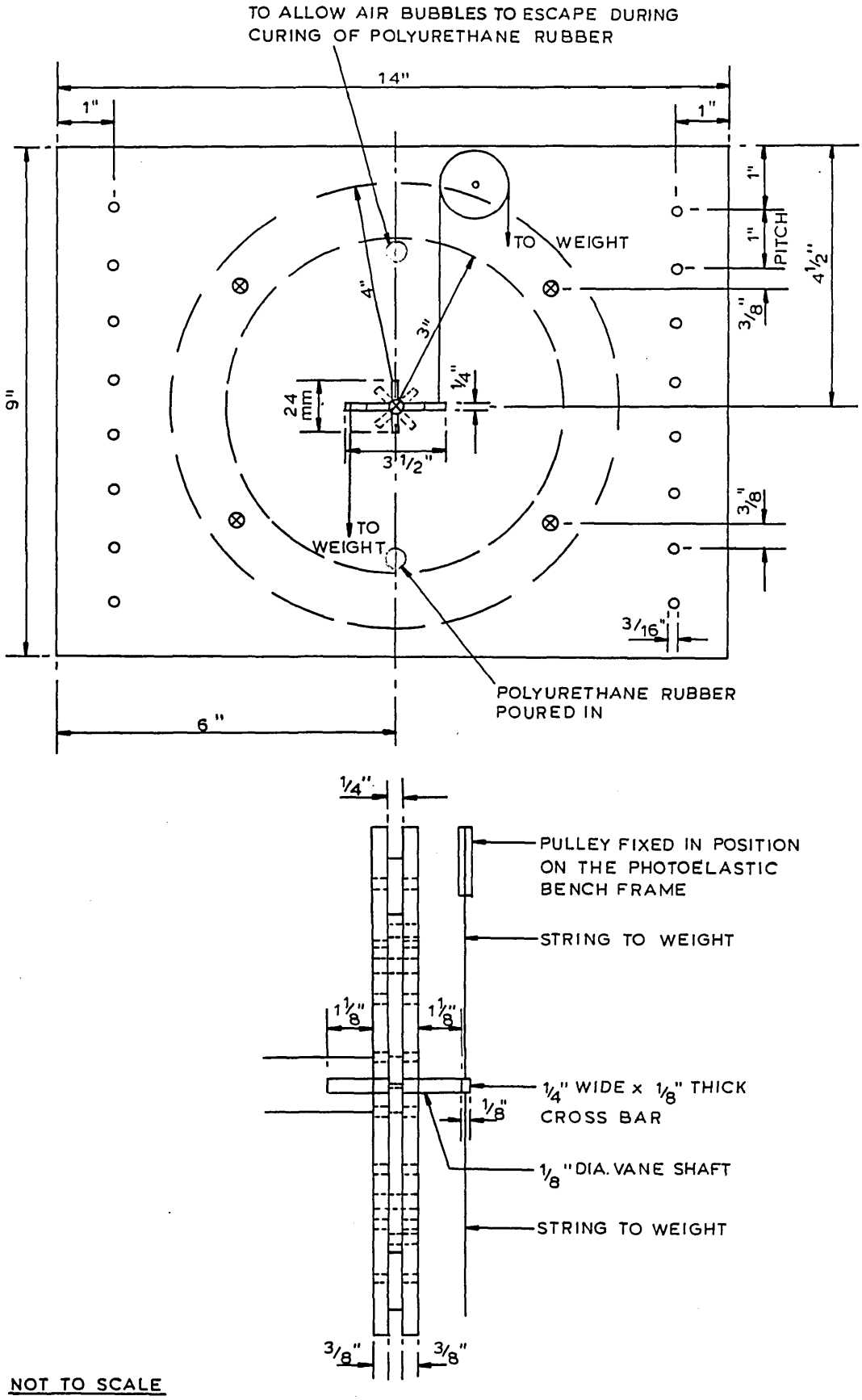


Fig. 3.18 Polyurethane rubber vane test rig.

The model experiments were similar to the gelatine model experiments, comprising:

(a) lightly smearing Releasil silicone grease on the vane blades and the two plane faces of the 'perspex disc', thus lubricating the contacting surfaces (the vane/perspex plates and the model), and aiding to eliminate the corresponding shear stresses;

(b) assembly of the model vane test rig, with the vane blades assuming orientations of 45° to the crossbar, and the vane located centrally inside the perspex disc, and supported by two parallel perspex plates (Fig. 3.18);

(c) mixing of the constituent parts of the polyurethane rubber, and carefully pouring the mixture around the vane through one of the two holes on the face of one of the parallel perspex plates;

(d) allowing the polyurethane rubber to set and cure;

(e) simultaneous rotation of the axis of the crossed polaroid filters to an orientation orthogonal to the axis of the polariscope bench and parallel to the axis of the crossbar, and selection of this orientation as the reference axis with respect to which the orientations of the isoclinics were to be measured;

(f) positioning of the experimental model on the polariscope bench so that the vane blades were at 45° to the selected reference axis;

(g) application of load on the vane using two 1/2lb dead weights, and photographically recording the stress field within the entire model at 10°-interval orientations, in the range 0–90°, of the polaroids;

(h) determination of the shear stress directions from an examination of the photographs at certain 'points of interest' in the model.

During the course of the experiments the model test rig performed satisfactorily.

CHAPTER 4

STRAIN-RATE EFFECTS IN THE VANE TEST

4.1 INTRODUCTION

It is well-known that the undrained shear strength of soils is not a unique parameter but is dependent on factors such as stress history, test type, and strain rate.

In general two phenomena are considered to be associated with strain-rate effects in the vane test. On the one hand, Kenney & Landva (1965) have suggested that the effect of the rate of strain on the vane shear strength is such that it results in changes in pore water movement thus resulting in changes of pore pressure, u, in the shear zone, and/or changes of the total stress, σ_n, acting across the shear zone, resulting from volumetric strains. Pore pressure effects are also important at fast rates of shearing, where the generation of lower pore pressures will subsequently lead to the mobilisation of higher effective stresses at failure (see, e.g. Mahmoud, 1988). On the other hand, Bjerrum (1973) has explained the measurement of higher shear strengths at higher rates of strain in terms of rheological phenomena related to the viscous nature of clays. Consequently, due to differences in the rate of peripheral rotation resulting from differences in vane size, one would not expect field and laboratory measurements of vane strength to be similar. Therefore, it is important to establish the rate of vane rotation required for the measurement of the undrained shear strength.

This Chapter describes a laboratory investigation into the influence of the rate of vane rotation on the behaviour of soft clay samples. It will be shown that at different rates of shear, both clay type and vane size have a marked influence on the shear stress – rotation behaviour. In addition, it will be demonstrated that the relationships between rotation rate and measured vane strength are consistent with drainage effects being dominant at slow rates of rotation, and viscous effects dominant at high rates.

4.2 TESTING PROGRAMME

4.2.1 Introduction

The test procedure has been described in Section 3.4.2D; 4-bladed square vane tests were carried out at a variety of rates of rotation in the range 1.075–1075 °/min.

Tests were conducted on both normally consolidated and remoulded samples of soft clay prepared in the laboratory using the procedures described in Section 3.3.2. The normally consolidated samples included Speswhite kaolin, London clay and a bentonite/London clay mixture; in addition, remoulded samples of London clay were also tested. All the samples were tested at zero confining stress (Section 3.4.2A) and in each test the vane rotation was continued through 360°. The above clay types were selected for this study for the reasons given in Section 3.3.1B.

Bulk of the experimental programme involved testing kaolin. A shorter series of tests was also done using samples of London clay as well as the bentonite/London clay mixture. The latter clay types were tested so that their results could be compared with the results of tests on kaolin. The testing programmes for the two series of tests are considered separately.

4.2.2 Tests on Speswhite Kaolin

All the tests on Speswhite kaolin were carried out using samples which had been normally consolidated to given maximum consolidation pressures ($\sigma_{vo}' = 265–315$ kPa) corresponding to liquidity indices of 0.41–0.45. In the majority of the tests, the 12mm square vane (i.e. the 'standard' laboratory vane; Section 3.2.2A(i)) was used, at rates of rotation of ($\omega =$) 1.075, 5.375, 26.875, 53.75, 107.5, 268.75, 537.5 and 1075 °/min.

In order to examine the effects of the size of blade on the measured vane strength, two shorter series of tests were conducted using vanes of dimensions 18 mm x 18 mm and 24 mm x 24 mm.

4.2.3 Tests on London Clay and the Bentonite/London Clay Mixture

To examine strain-rate effects on the measured vane strength of different clay types, tests were conducted on samples of London clay. Samples were normally consolidated to maximum consolidation pressures of ($\sigma_{vo}' =$) 145–190 kPa, resulting in liquidity indices in the range 0.22–0.28. Tests were done on remoulded samples in order to see whether remoulding would have any effect on the behaviour of London clay. The remoulded samples were stored for 2 and 47 days before being tested; thereby, the effect of the 'age' of remoulded samples was also examined.

To study the effects of vane size on the measured strength, tests were done using the 18mm square vane as well as the 'standard' 12mm one.

A series of tests similar to the above was conducted using samples of a bentonite/London clay mixture. The samples were consolidated to maximum vertical effective stresses in the range $\sigma_{vo}' = 100–190$ kPa, which resulted in liquidity indices in the range 0.70–1.03.

4.3 SHEAR STRESS – ROTATION BEHAVIOUR AT DIFFERENT RATES OF VANE ROTATION

4.3.1 Introduction

The effect of the rate of vane rotation and the influence of vane size on the shear stress – rotation behaviour of three soft clays are considered. The soils included Speswhite kaolin, London clay and a bentonite/London clay mixture, all of which had followed a normally consolidated stress history; vane tests were also carried out on 2-day old and 47-day old remoulded samples of London clay. Small diameter (D = 12–24 mm) 4-bladed square vanes were rotated through 360° at a variety of rates in the range $\omega = 1.075–1075$ °/min.

4.3.2 Parameters Used for the Presentation and Analysis of Results

Although the primary aim of this study was to establish the rate of vane rotation at which undrained conditions would be ensured, it was appreciated that it is more usual to conduct rate-effect investigations with reference to the rate of strain in preference to any other measure of the shearing rate — such as the rate of vane rotation. However, the nature of the vane test is such that the amount of strain that the soil undergoes is a difficult parameter to determine, since (a) soil displacements caused by the rotation of the vane are not easy to quantify (see, e.g. Section 6.4), and (b) the original volume of soil and thus the initial soil surface, which is subsequently subjected to deformation at the onset of vane rotation, are extremely difficult to establish. Consequently, it is impossible to present vane test results in terms of strains and strain rates.

The only parameter comparable to the rate of strain which is easily controlled and can be quantified precisely is the rate at which the vane is rotated. However, the rate of vane rotation takes no account of the amount of displacement to which the soil is subjected before it reaches failure; time to failure, t_f — which is equal to the amount of rotation to peak torque, θ_f, divided by the rate of vane rotation, ω — is a better parameter, since it is a measure of the amount of soil displacement to failure for a given vane size. Units of t_f which have been adopted in this thesis are minutes. It is noteworthy that t_f has also been used by many other researchers who have undertaken investigations on strain-rate effects, particularly in association with triaxial testing of soils. Furthermore, data presented in terms of time to failure can be (a) readily compared with available triaxial and other test results, and (b) used to check a simple theory of consolidation discussed in Section 4.4.5B.

The vane strengths were deduced from the measured peak torques using the conventional interpretation of the vane test presented in Section 2.2. In order to take account of any differences in the sample water contents of each soil type, the vane strengths, τ_f, have all been normalised with respect to the maximum stress that each sample had experienced during consolidation, σ_{vo}'. Normalising the results in this way is usual when normally consolidated samples are employed in an investigation (see, e.g. Berre & Bjerrum, 1973), since it enables a comparison of the strengths of samples with different water contents; for every soil undergoing a particular consolidation history there is a unique relationship between voids ratio and consolidation pressure. Thus, the majority of the results presented in this Chapter are in terms of normalised vane strength, τ_f/σ_{vo}', versus either rate of rotation, ω, or time to failure, t_f.

4.3.3 Shear Stress – Rotation Characteristics

4.3.3A Kaolin test results

Individual shear stress – rotation curves for samples subjected to similar rates of rotation are presented in Figs. 4.1a–c which show respectively the relationships between normalised shear stress, τ/σ_{vo}', and angle of rotation, θ, at three different rates of rotation of ω = 5.375, 107.5 and 1075 °/min. It can be seen that the shear stress – rotation characteristics, as portrayed by the shapes of the curves in Figs. 4.1a–c, are similar for any given rate of rotation. Therefore, it is justifiable to average the data (neglecting any anomalous results).

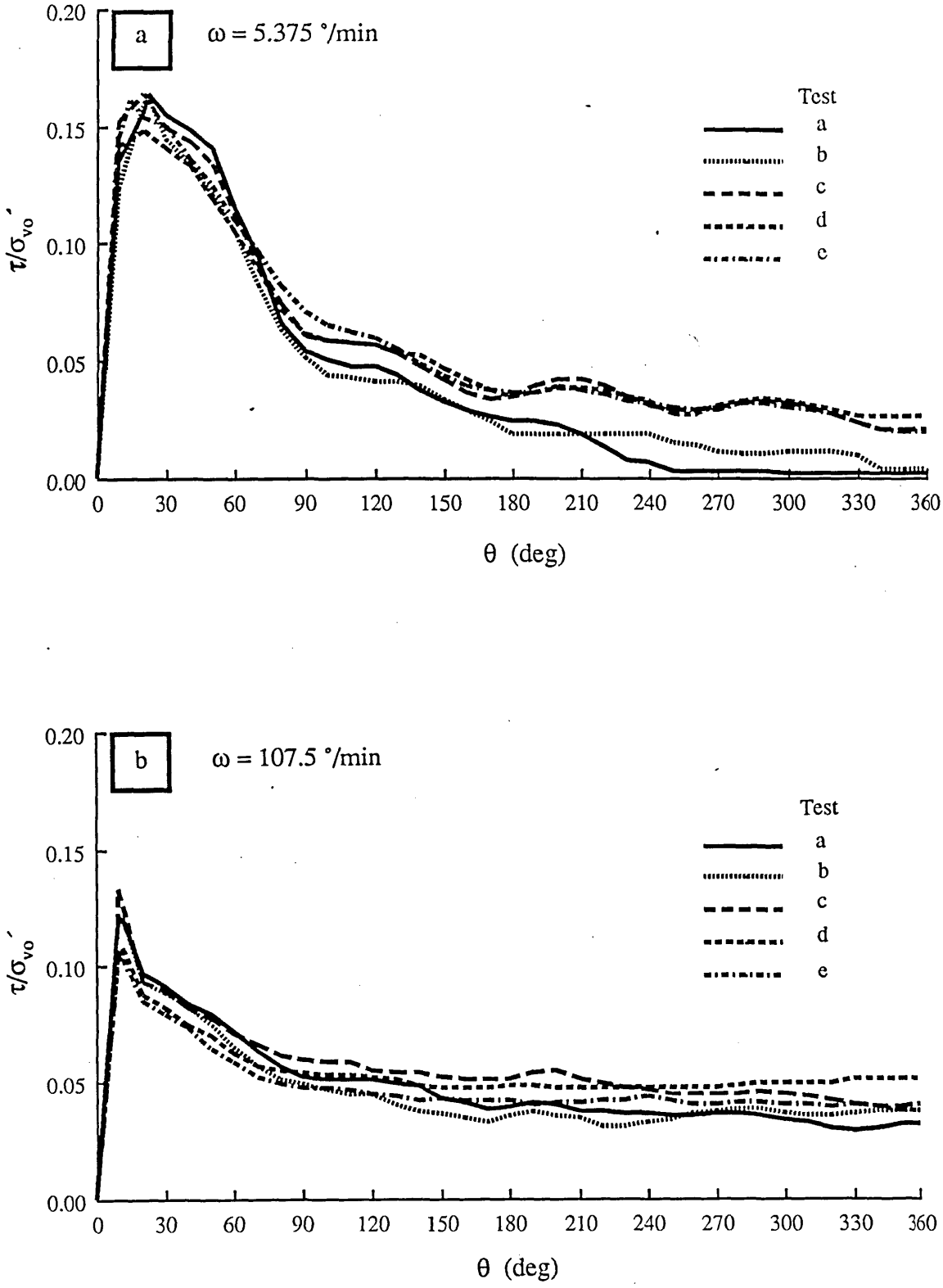


Fig. 4.1 Normalised shear stress — rotation curves for 4-bladed 12mm square vane tests in kaolin : Typical test results.

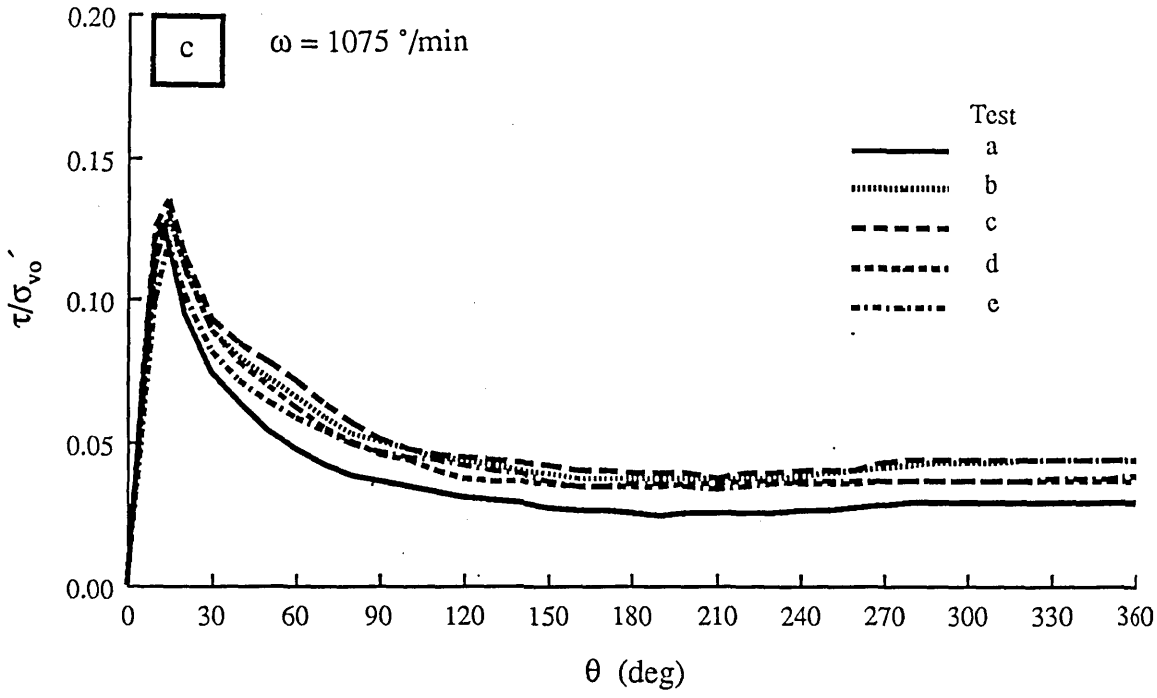


Fig. 4.1 Normalised shear stress — rotation curves for 4-bladed 12mm square vane tests in kaolin : Typical test results.

Table 4.1a gives a summary of the results of 12mm square vane tests, including both the mean values [= $(\tau_f/\sigma_{vo}')_{av} = \Sigma(\tau_f/\sigma_{vo}')_i/n$] and the range of values of normalised vane strength, τ_f/σ_{vo}', angle of rotation at failure, θ_f, and time to failure, t_f, corresponding to given rates of vane rotation (ω). The results corresponding to different rates of rotation are presented in Fig. 4.2a in terms of normalised shear stress, τ/σ_{vo}', versus angle of rotation, θ. Each curve represents the mean of between two and ten individual shear stress – rotation plots (see Table 4.1a).

The variation in the measured 12mm vane strength, τ_f/σ_{vo}', with the rate of vane rotation, ω, is presented in Fig. 4.3a, together with data from the 24mm vane tests; however, for a detailed description and discussion of these results reference should be made to Section 4.4.2 (Figs. 4.12–4.15).

An immediately obvious feature of the shear stress – rotation curves in Figs. 4.2a and a′ is that the rate of vane rotation has a significant influence on the angle of rotation at peak shear stress (θ_f). Fig. 4.4a shows the relationship between θ_f and ω. For the 12mm square vane the trend is that at slow rates of rotation (i.e. ω = 1.075 °/min), θ_f has large values which decrease with increasing rates of rotation until a minimum of about θ_f = 12.5° is reached at approximately ω = 55 °/min ± 50%; thereafter θ_f increases with increasing rates of rotation. The influence of the rate of vane rotation on θ_f is also seen in the 24mm vane test data presented in Fig. 4.4a; the average shear stress – rotation curves are shown in Fig. 4.2a′, while Table 4.1a′ summarises the mean and range of values of τ_f/σ_{vo}', θ_f and t_f associated with the 24mm square vane tests. The observed trend is similar to that for the 12mm vane, although the minimum angle of rotation (of about θ_f = 25°) occurs at a rate of rotation of about ω = 20 °/min ± 50%. At similar rates of rotation, the 24mm vane shows higher values of θ_f than the 12mm one. Furthermore, the 24mm vane gives minimum values of τ_f/σ_{vo}' and θ_f at lower values of ω than those minimum values given by the 12mm vane (see Figs. 4.3a and 4.4a).

The variation in the initial slope of the shear stress – rotation curves in Figs. 4.2a and a′ is expressed in terms of a stiffness parameter K, where K is the normalised mobilised shear stress, τ_m/σ_{vo}', divided by the angle of rotation (θ_m) at which τ_m/σ_{vo}' occurs. The slope of the curves was determined at τ_m/σ_{vo}' = 0.05, corresponding to the straight portion of the curve. It is seen from Fig. 4.5a that as the rate of rotation increases, the slope of the initial part of the curve decreases; this effect being more pronounced in the case of the 12mm vane test results, for which, values of K are large at ω = 1 °/min, but decrease, first gradually and then at a fast rate, with increasing values of ω. The 24mm vane test data show that K has a much lower value which remains almost constant in the range ω = 1–100 °/min, but then decreases steadily with increases

in ω. The above trend implies that as the rate of shearing in the vane test increases, kaolin behaves in a less stiff manner. A likely explanation for this observation is that as the rate of vane rotation increases, so less dissipation of pore pressures takes place during the test and consequently a more undrained response results. In this respect, it is important to note, however, that the undrained response of normally consolidated clays is typically much stiffer than the drained one (see, e.g. Gens, 1982).

Fig. 4.6a shows the relationship between normalised 'residual' — large displacement — shear strength (corresponding to an angle of rotation of 360°), τ_r/σ_{vo}', and the rate of rotation, ω. Despite the scatter in the test data, it is evident that τ_r/σ_{vo}' values increase with increasing values of ω. At slow rates of rotation in the range $1 \leq \omega \leq 10$ °/min, both the 12mm and the 24mm vane test data show constant values of τ_r/σ_{vo}' (of about 0.012 and 0.007, respectively). At faster rates of rotation, both vane sizes show increasing values of τ_r/σ_{vo}' as ω increases, with the 12mm vane exhibiting a faster rate of increase than the 24mm one. Moreover, the 12mm vane test results show higher values of τ_r/σ_{vo}' than the 24mm ones at similar values of ω (e.g. at $\omega = 1000$ °/min, $\tau_r/\sigma_{vo}' = 0.035$ and 0.018, respectively).

4.3.3B London clay and the bentonite/London clay mixture test results

This Section presents the results of 12 and 18mm vane tests on normally consolidated samples of London clay (Tables 4.1b and b′, and Figs. 4.2b and b′), 2-day old (Tables 4.1c and c′, and Figs. 4.2c and c′) and 47-day old (Tables 4.1d and d′, and Figs. 4.2d and d′) samples of remoulded London clay, and normally consolidated samples of a bentonite/London clay mixture (Tables 4.1e and e′, and Figs. 4.2e and e′); the above Tables summarise the results, whilst the respective Figures show the shear stress – rotation relationships in terms of (normalised) shear stress, (τ/σ_{vo}') or τ, and angle of rotation, θ, of the averaged results. It is clear from these Figures that the shear stress – rotation characteristics of normally consolidated samples of both London clay and the bentonite/London clay mixture are strongly influenced by the rate of rotation of the vane. Strain-rate effects on the shear stress – rotation behaviour are quantified in the same manner as that outlined for kaolin in Section 4.3.3A, above (see Figs. 4.3–4.6). Similar results were obtained to those for kaolin, except in the following respects:

(i) Although Figs. 4.3b and d show that the measured shear strengths (τ_f/σ_{vo}' or τ_f) decrease as ω increases, Figs. 4.3c and e exhibit the opposite trend of increasing strength with increasing ω, with no evidence of points of minima in any of the above Figures. In this connection, it is useful to compare the results presented in Figs. 4.3c and e, respectively, with (a) the results of tests carried out by Bhandari (1970) on samples of remoulded London clay (I_P = 40%), and (b) the relationship corresponding to the laboratory vane tests carried out by Sharifounnasab & Ullrich (1985) on stress-relieved normally consolidated samples of slaked Pierre shale (I_P = 103%) (see Sections 4.4.2F and 4.4.5). Furthermore, it is of interest to note that at a given rate of rotation, strengths measured with the smaller vane size are higher than those measured with the larger vane, whereas Figs. 4.3d and e show the opposite, in which the 18mm vane gives higher values of peak strength than the 12mm vane.

(ii) It appears from Fig. 4.4b that θ_f reaches a minimum value at ω = 30–40°/min, increases slightly as ω decreases to 5 °/min, but increases dramatically for $\omega \geq$ 500 °/min, with the rate of increase being much faster for the 18mm vane than the 12mm one (see Table in Fig. 4.4b). In addition, a similar trend can be seen for both the 2-day old and 47-day old samples of remoulded London clay, where θ_f is almost constant at slow rates of rotation (corresponding to ω < 10 °/min) for both sample ages, although it is more dramatically influenced at larger values of ω in the case of the 47-day old samples. A similar trend can also be seen from the results of tests carried out by Sridharan & Madhav (1964) on a remoulded silty clay (I_P = 38–92%) using a 12.7mm diameter vane (H/D = 1.5).

(iii) The initial stiffness of the 47-day old remoulded London clay samples (Fig. 4.5d) is seen to be influenced by ω to a larger degree than that of 2-day old samples (Fig. 4.5c), with values of K decreasing almost linearly with increasing values of ω in the case of the former. However, the manner in which K is influenced by ω in Fig. 4.5e suggests a very different trend, with the bentonite/London clay mixture indicating higher values of K with increasing rates of rotation; also, there is little or no vane-size effect.

(iv) Figs. 4.6b and c both show that there is little or no vane-size effect for either normally consolidated samples of London clay or 2-day old samples of remoulded London clay tested at the same rate of rotation. However, at similar rates of rotation, the 47-day old samples of remoulded London clay indicate that the larger vane measures higher residual strengths than the smaller one. This effect is more clearly demonstrated in Fig. 4.6e.

Table 4.1a 12mm square vanes rotated at different rates in normally consolidated kaolin.

Rotation Rate (°/min)	No. of Tests	θ_f			t_f			τ_f/σ_{vo}'			τ_r/σ_{vo}'
		Average (deg)	Range (deg)		Average (mins)	Range (mins)		Average	Range		Average
1.075	4	23.6	15.6	27.7	21.95	14.5	25.8	0.185	0.1317	0.2556	0.0074
5.375	10	16.1	13.4	24	3	2.5	4.5	0.1553	0.1111	0.1904	0.0106
26.875	5	14.5	13.2	16.6	0.54	0.49	0.62	0.1309	0.1053	0.1554	0.0064
53.75	3	12.3	10	13.4	0.27	0.19	0.25	0.1124	0.1063	0.1203	0.0131
107.5	7	11.5	9.1	16	0.11	0.085	0.15	0.1129	0.0845	0.1329	0.0338
268.75	2	15	14.7	15.3	0.056	0.055	0.057	0.0891	0.0845	0.0936	0.0211
537.5	3	15.1	10	23.4	0.031	0.019	0.044	0.1007	0.0978	0.104	0.0235
1075	9	19.63	12.1	36	0.018	0.011	0.033	0.12	0.0866	0.1373	0.0334

Table 4.1a´ 24mm square vanes rotated at different rates in normally consolidated kaolin.

Rotation Rate (°/min)	No. of Tests	θ_f			t_f			τ_f/σ_{vo}'			τ_r/σ_{vo}'
		Average (deg)	Range (deg)		Average (mins)	Range (mins)		Average	Range		Average
1.075	3	31.8	25.4	37.7	29.6	23.6	35.1	0.0857	0.0826	0.0901	0.0178
5.375	2	26.6	24.3	28.8	5	4.5	5.4	0.0901	0.0896	0.0905	0.0335
26.875	3	29.6	25.3	34.7	1.1	0.94	1.3	0.0836	0.074	0.0905	0.0087
107.5	1	25.8	–	–	0.24	–	–	0.0775	–	–	0.0144
268.75	1	26.3	–	–	0.098	–	–	0.0883	–	–	0.0113
1075	2	37	34	40	0.034	0.032	0.037	0.0909	0.0898	0.0919	0.0127

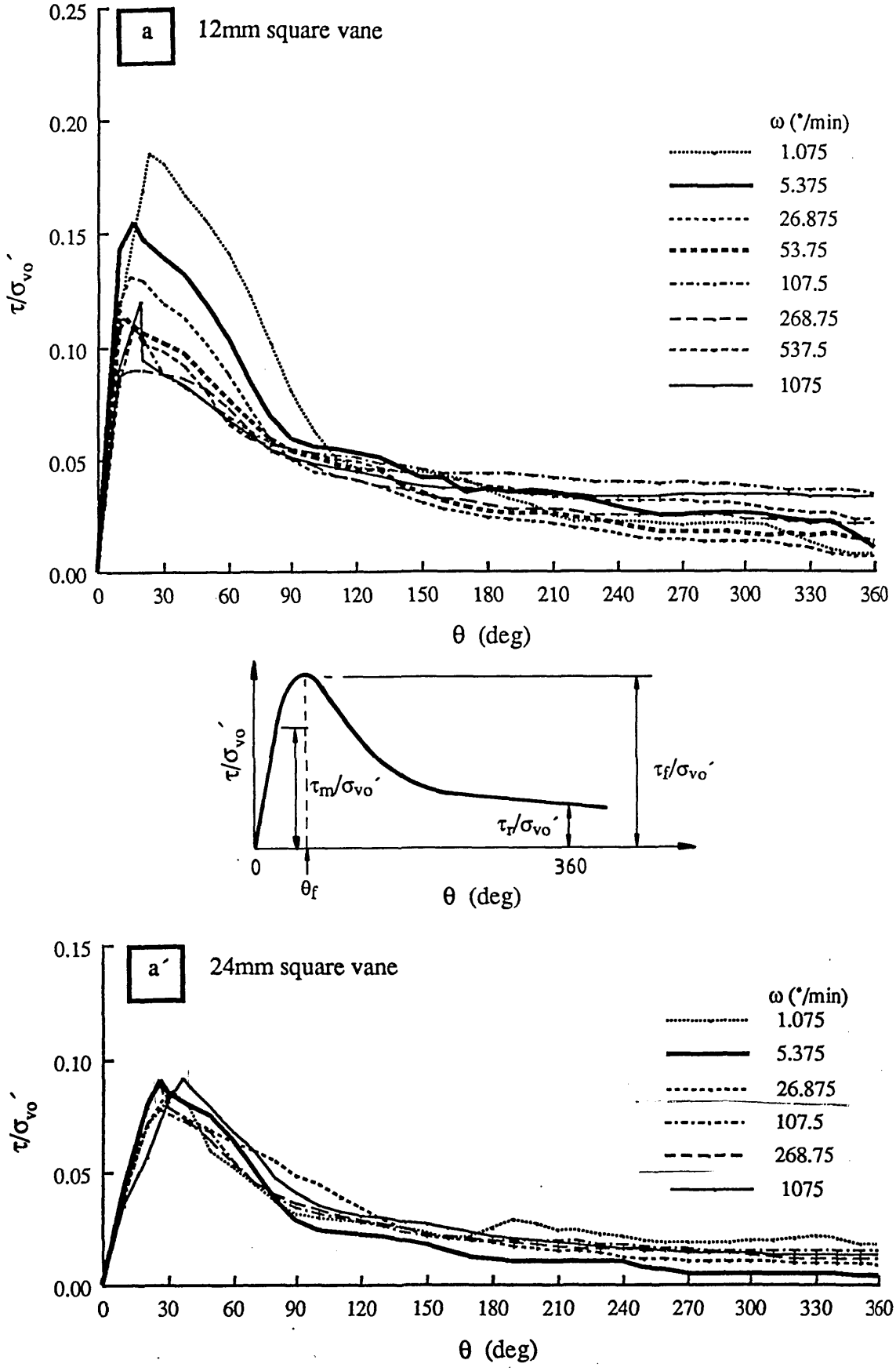


Fig. 4.2 Normalised shear stress – rotation curves for 4-bladed vane tests in normally consolidated kaolin : Averaged test results.

Table 4.1b 12mm square vanes rotated at different rates in normally consolidated London clay.

Rotation Rate (°/min)	No. of Tests	θ_f			t_f			τ_f/σ_{vo}'			τ_r/σ_{vo}'
		Average (deg)	Range (deg)		Average (mins)	Range (mins)		Average	Range		Average
5.375	3	13.3	12.1	15.5	2.47	2.3	2.9	0.212	0.1967	0.23	0.0418
26.875	3	9	8.2	10	0.34	0.31	0.37	0.1924	0.1854	0.1971	0.0968
53.75	5	12.4	11.7	13.1	0.23	0.22	0.24	0.1947	0.1849	0.2035	0.1071
107.5	4	14.5	12.2	17.9	0.14	0.11	0.17	0.1936	0.1849	0.2026	0.1083
537.5	3	22.2	16.6	30	0.041	0.031	0.056	0.1707	0.1628	0.1862	0.1137
1075	3	42	36	40	0.039	0.034	0.037	0.156	0.1538	0.1582	0.1245

Table 4.1b′ 18mm square vanes rotated at different rates in normally consolidated London clay.

Rotation Rate (°/min)	No. of Tests	θ_f			t_f			τ_f/σ_{vo}'			τ_r/σ_{vo}'
		Average (deg)	Range (deg)		Average (mins)	Range (mins)		Average	Range		Average
5.375	2	20.8	20	21.6	3.87	3.72	4.02	0.1981	0.1973	0.1988	0.103
26.875	3	18.5	17.2	20	0.69	0.64	0.74	0.1852	0.1748	0.1962	0.0928
107.5	2	20.9	20	21.7	0.2	0.19	0.2	0.1929	0.1883	0.1975	0.0945
1075	5	104	90	110	0.095	0.084	0.1	0.1182	0.1092	0.1309	0.1067

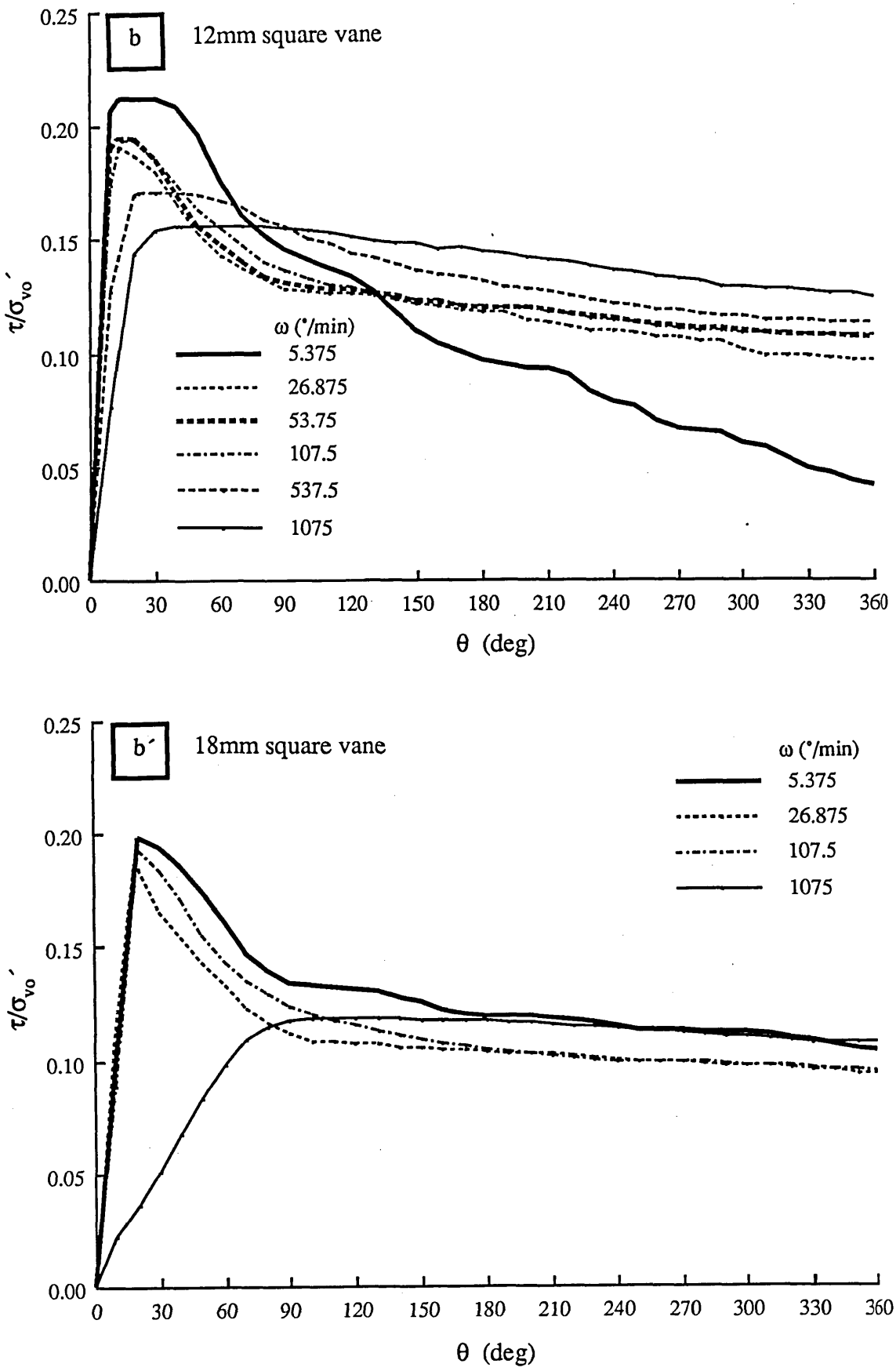


Fig. 4.2 Normalised shear stress – rotation curves for 4-bladed vane tests in normally consolidated London clay : Averaged test results.

Table 4.1c 12mm square vanes rotated at different rates in 2-day old remoulded London clay.

Rotation Rate (°/min)	No. of Tests	θ_f			t_f			τ_f			τ_r
		Average (deg)	Range (deg)		Average (mins)	Range (mins)		Average (kPa)	Range (kPa)		Average (kPa)
5.375	4	11.3	10	13.3	2.1	1.9	2.5	31.9	29.3	34.2	11.9
26.875	3	13.2	12.6	13.7	0.49	0.47	0.51	32.4	31.2	34.2	12.9
107.5	3	18.9	16.6	20	0.18	0.15	0.19	36.7	36.3	37.2	12.1
537.5	3	50	40	60	0.093	0.074	0.11	30.7	29	32	20.5
1075	2	85	80	90	0.079	0.074	0.084	26.7	26.5	26.8	20.8

Table 4.1c´ 18mm square vanes rotated at different rates in 2-day old remoulded London clay.

Rotation Rate (°/min)	No. of Tests	θ_f			t_f			τ_f			τ_r
		Average (deg)	Range (deg)		Average (mins)	Range (mins)		Average (kPa)	Range (kPa)		Average (kPa)
5.375	2	18.2	16.4	20	3.39	3.05	3.72	27.4	26.9	27.9	12.6
26.875	2	23.1	22.1	24	0.86	0.82	0.89	28.95	28.3	29.6	11.5
107.5	3	27.8	26	30	0.26	0.24	0.28	31.63	30.8	32.7	15.97
537.5	3	45	40	50	0.084	0.074	0.093	32.77	31.6	34.7	19.93
1075	2	90	90	90	0.084	0.084	0.084	25.9	25	26.8	19.9

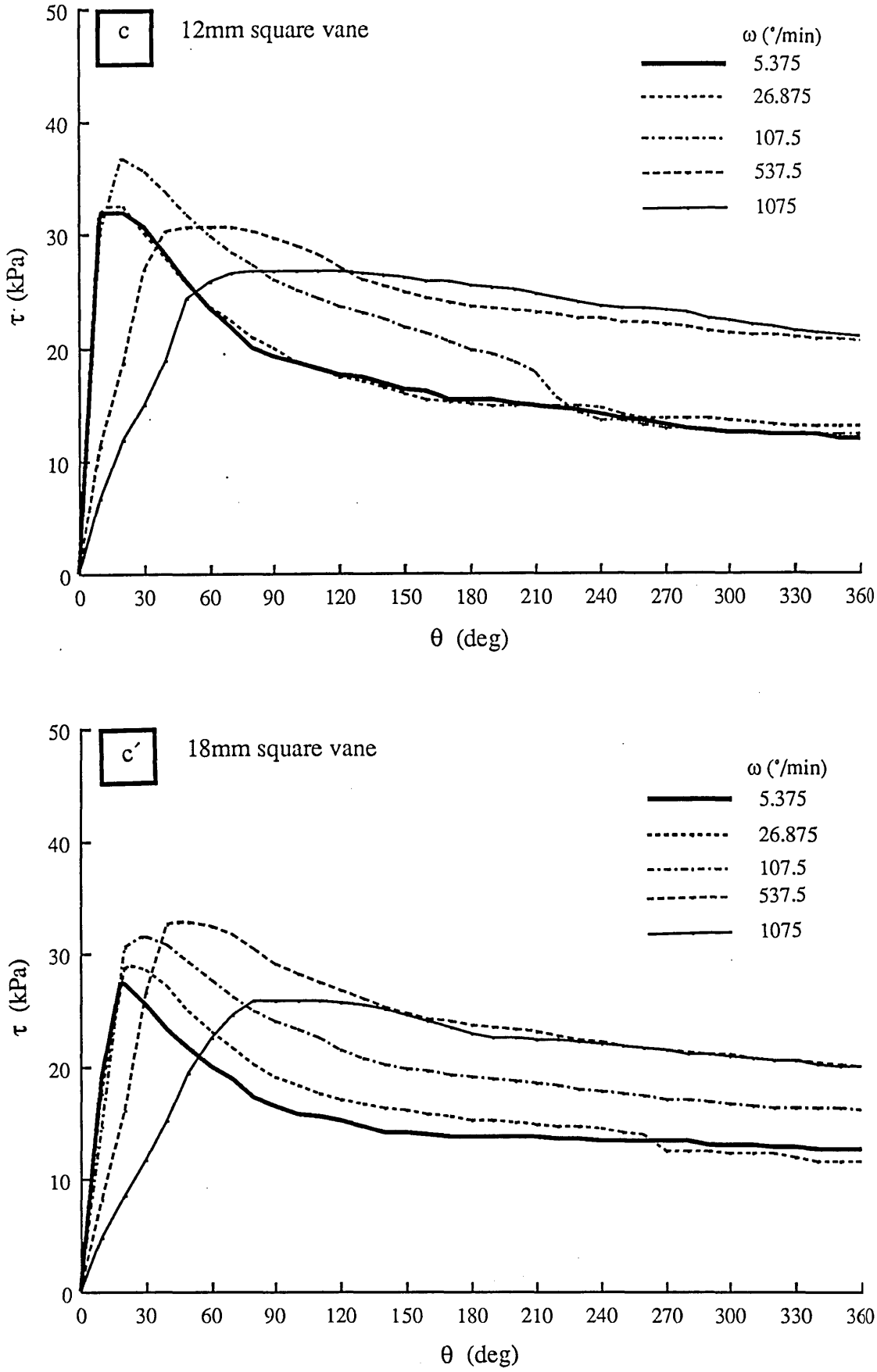


Fig. 4.2 Shear stress – rotation curves for 4-bladed vane tests in 2-day old remoulded London clay : Averaged test results.

Table 4.1d 12mm square vanes rotated at different rates in 47-day old remoulded London clay.

Rotation Rate (°/min)	No. of Tests	θ_f			t_f			τ_f			τ_r
		Average (deg)	Range (deg)		Average (mins)	Range (mins)		Average (kPa)	Range (kPa)		Average (kPa)
5.375	3	16.1	12.5	20	3	2.3	3.7	20.6	18.91	21.61	9.9
26.875	2	14.1	13.7	14.4	0.53	0.51	0.54	20.1	20.06	20.06	10.8
107.5	3	53.3	40	80	0.5	0.37	0.74	20.5	17.98	24.31	14.3
537.5	3	137.7	120	150	0.26	0.22	0.28	17.2	16.67	17.75	16.7
1075	3	195	150	240	0.18	0.14	0.22	14	13.51	16.98	15.1

Table 4.1d´ 18mm square vanes rotated at different rates in 47-day old remoulded London clay.

Rotation Rate (°/min)	No. of Tests	θ_f			t_f			τ_f			τ_r
		Average (deg)	Range (deg)		Average (mins)	Range (mins)		Average (kPa)	Range (kPa)		Average (kPa)
5.375	3	16.3	15	17.4	3.03	2.79	3.24	25.73	24.49	27.99	11.59
26.875	2	23.6	22.9	24.2	0.88	0.85	0.9	28.92	28.61	29.22	13.69
107.5	3	48.4	45.2	50	0.45	0.42	0.47	25.31	24.9	25.93	15.37
537.5	3	206.7	180	230	0.39	0.34	0.43	20.03	19.35	20.58	19.28
1075	3	340	320	360	0.32	0.3	0.34	18.25	16.67	20.58	18.25

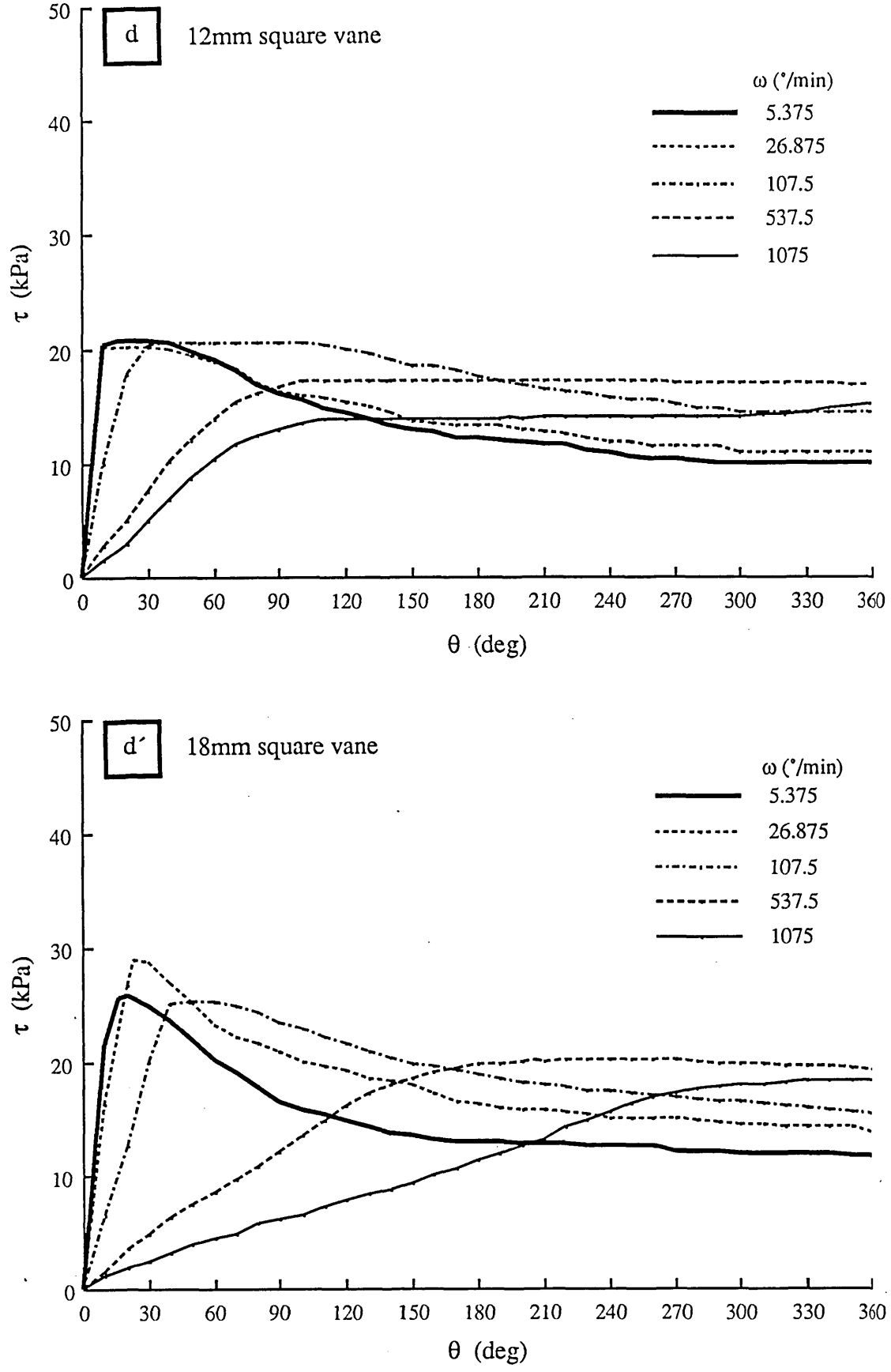


Fig. 4.2 Shear stress - rotation curves for 4-bladed vane tests in 47-day old remoulded London clay: Averaged test results.

Table 4.1e 12mm square vanes rotated at different rates in normally consolidated bentonite/London clay mixture.

Rotation Rate (°/min)	No. of Tests	θ_f			t_f			τ_f/σ_{vo}'			τ_r/σ_{vo}'
		Average (deg)	Range (deg)		Average (mins)	Range (mins)		Average	Range		Average
5.375	3	6.13	5.8	6.7	1.14	1.09	1.25	0.141	0.1301	0.1495	0.0222
26.875	3	5.13	4.3	6.6	0.19	0.16	0.25	0.1627	0.1441	0.1817	0.0289
107.5	3	6.84	5.2	8.2	0.064	0.048	0.076	0.1618	0.1363	0.1764	0.0279
537.5	2	6.43	5.7	7.1	0.012	0.011	0.013	0.1567	0.1486	0.1648	0.0311
1075	2	8.75	8.2	9.3	0.0081	0.0076	0.0086	0.171	0.1492	0.1928	0.0389

Table 4.1e´ 18mm square vanes rotated at different rates in normally consolidated bentonite/London clay mixture.

Rotation Rate (°/min)	No. of Tests	θ_f			t_f			τ_f/σ_{vo}'			τ_r/σ_{vo}'
		Average (deg)	Range (deg)		Average (mins)	Range (mins)		Average	Range		Average
5.375	3	11.9	10	14.5	2.21	1.86	2.69	0.1395	0.1325	0.1468	0.031
26.875	3	13.6	10.9	16	0.51	0.41	0.6	0.167	0.151	0.1896	0.0385
107.5	3	14	11.8	17.1	0.13	0.11	0.16	0.1693	0.1535	0.1894	0.0354
537.5	3	13.6	10	16.8	0.025	0.019	0.031	0.1861	0.1791	0.1945	0.0431
1075	3	13.8	11.6	17.1	0.013	0.011	0.016	0.1885	0.1609	0.2142	0.0455

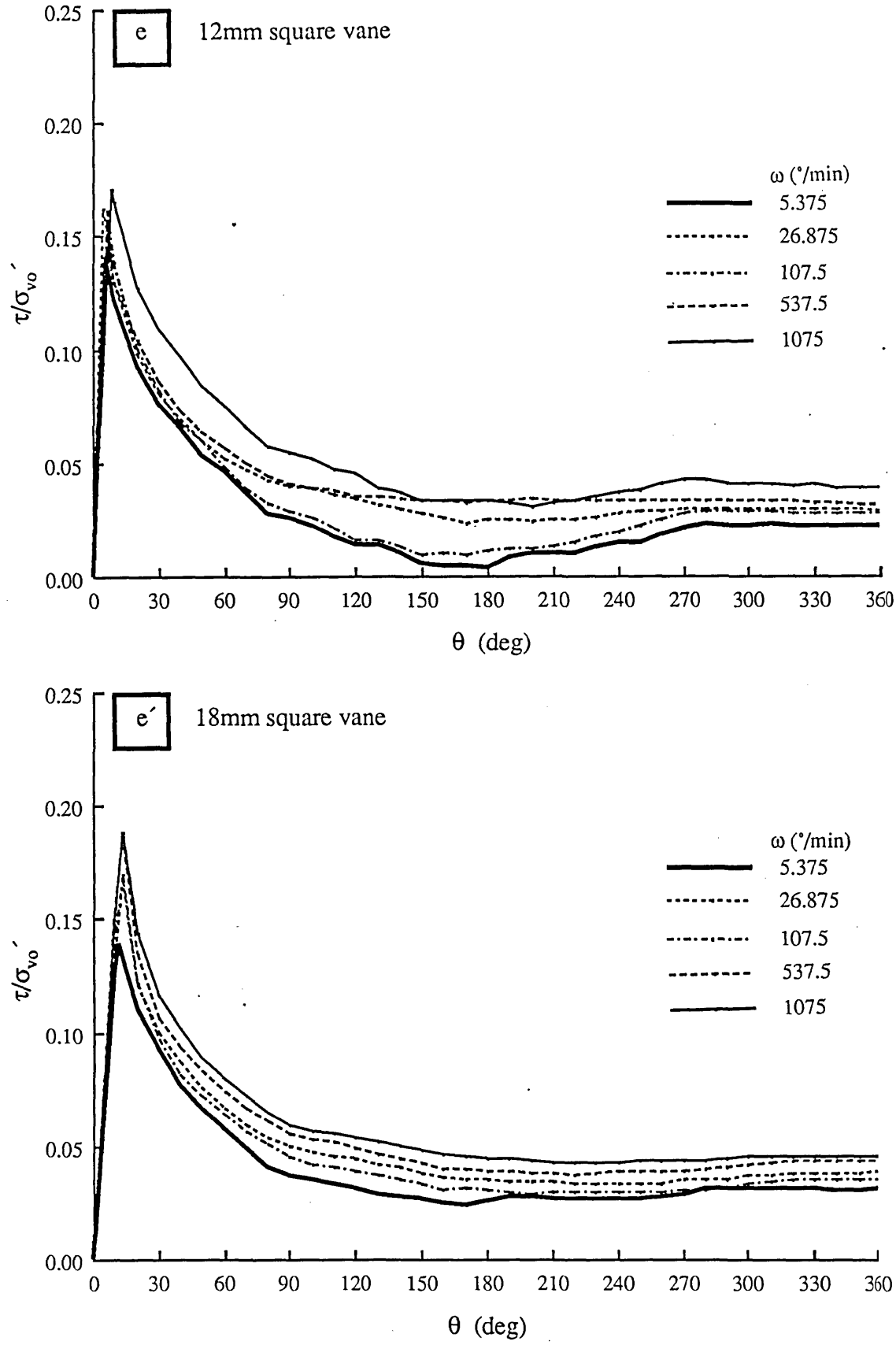


Fig. 4.2 Normalised shear stress — rotation curves for 4-bladed vane tests in normally consolidated bentonite/London clay mixture: Averaged test results.

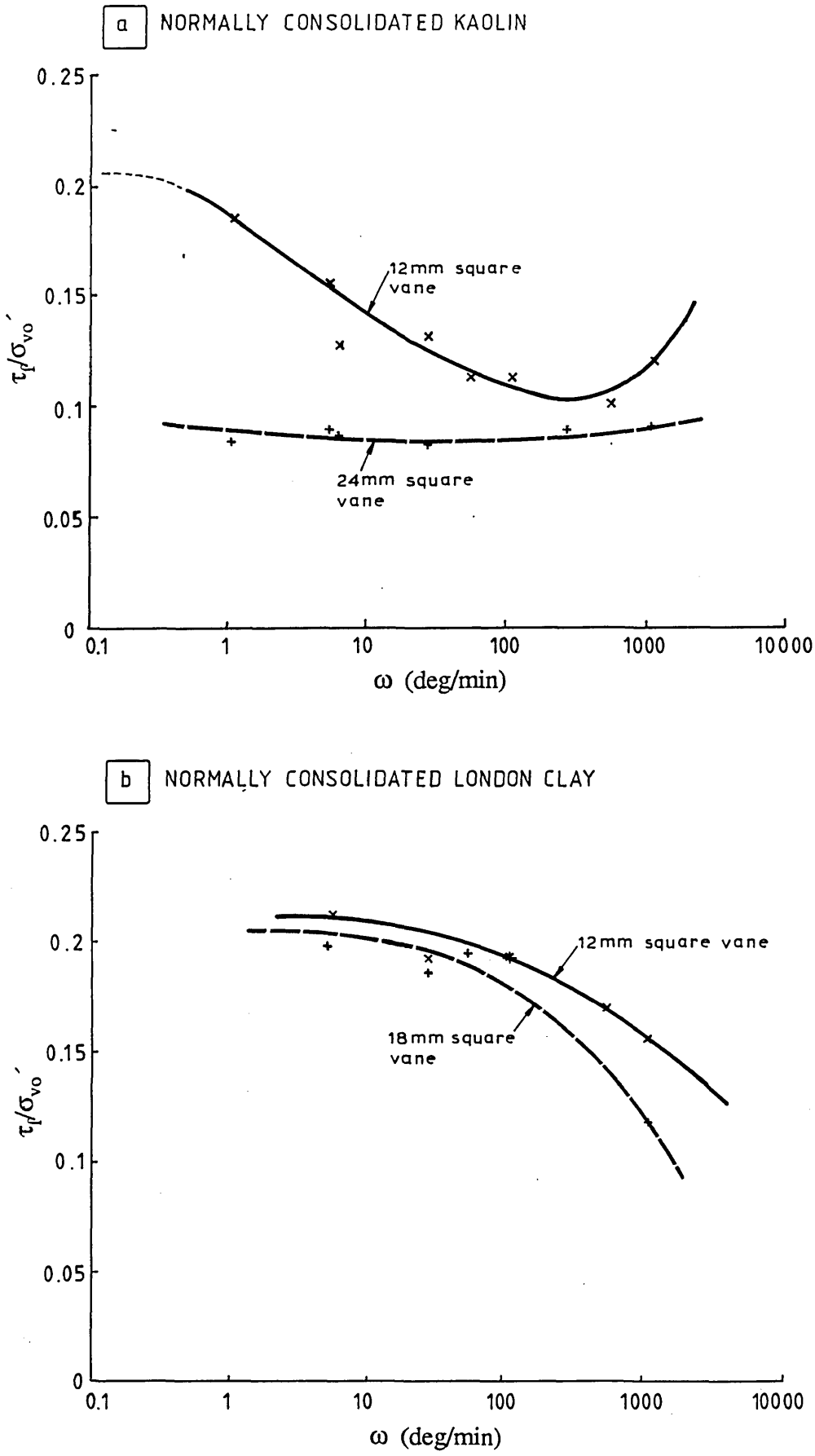


Fig. 4.3 Effect of rate of rotation on the measured peak vane strength.

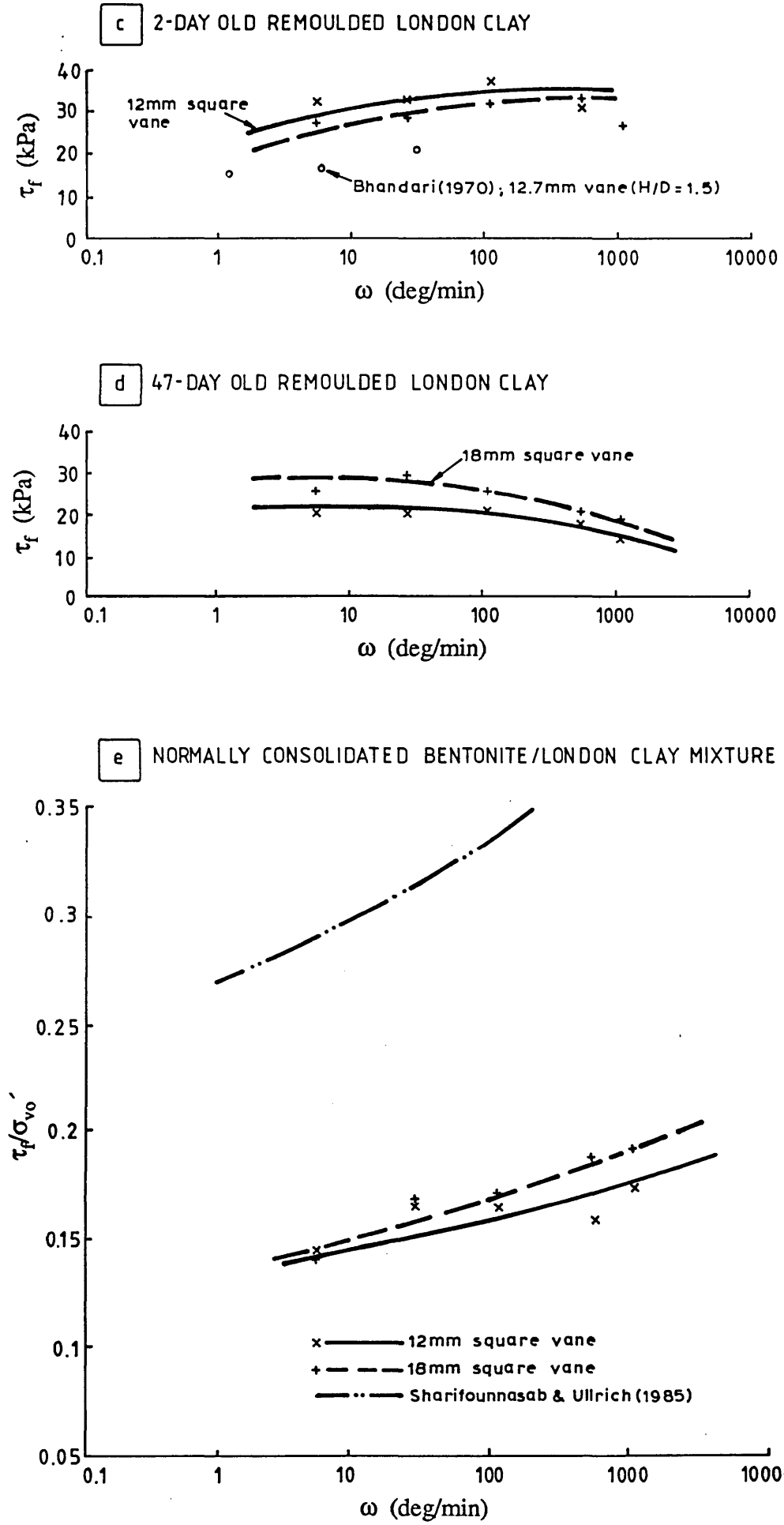


Fig. 4.3 Effect of rate of rotation on the measured peak vane strength.

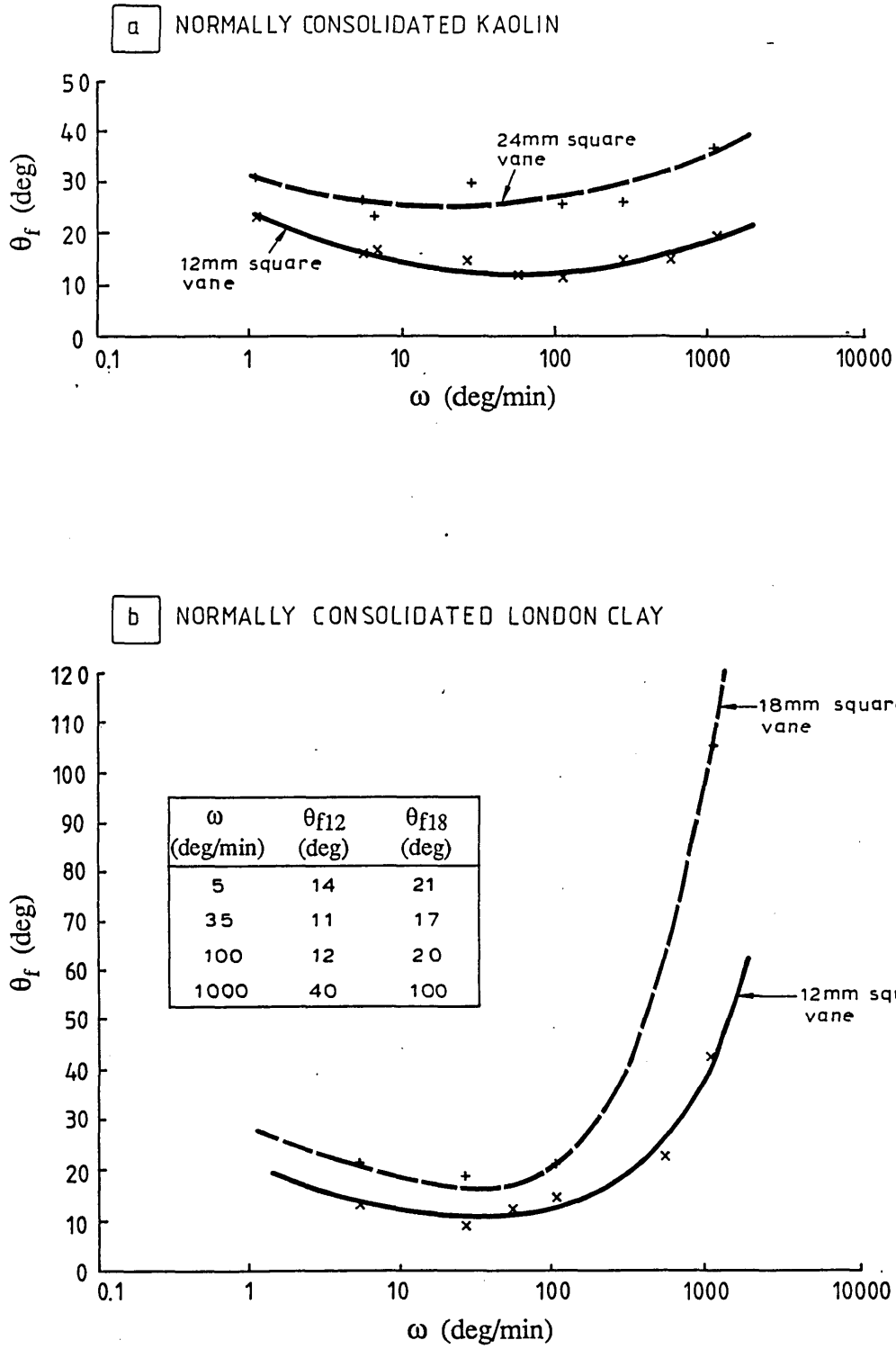


Fig. 4.4 Effect of rate of vane rotation on the measured angle of rotation at failure.

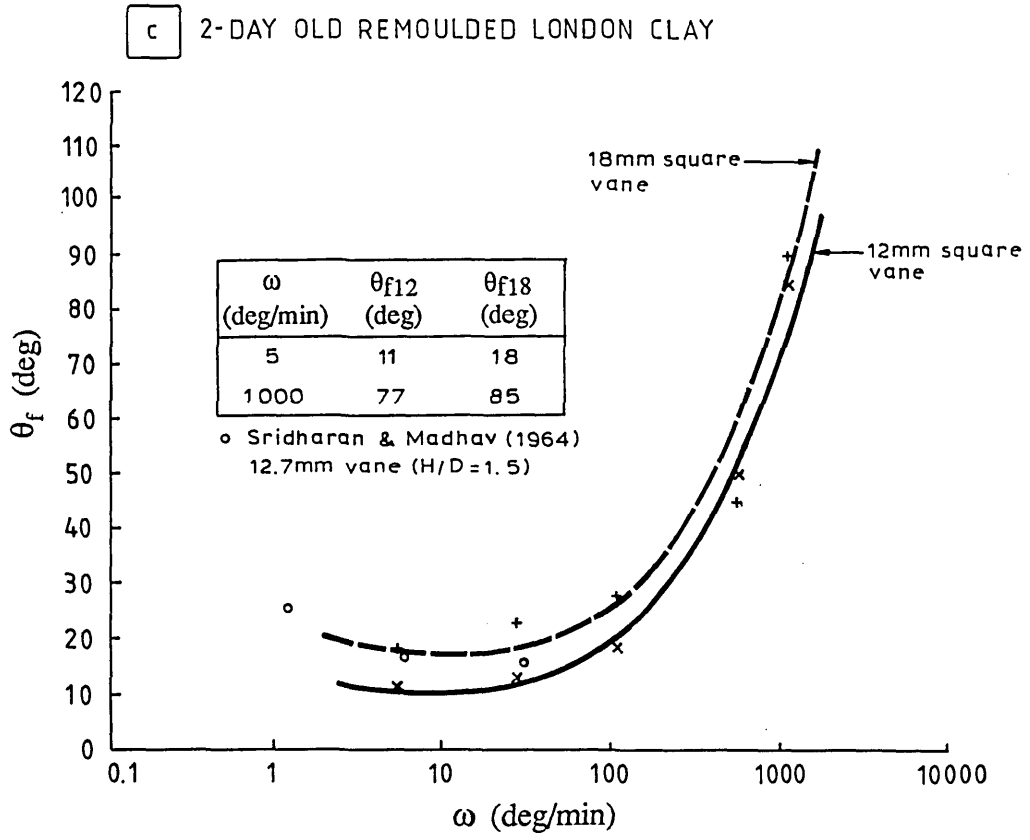


Fig. 4.4 Effect of rate of vane rotation on the measured angle of rotation at failure.

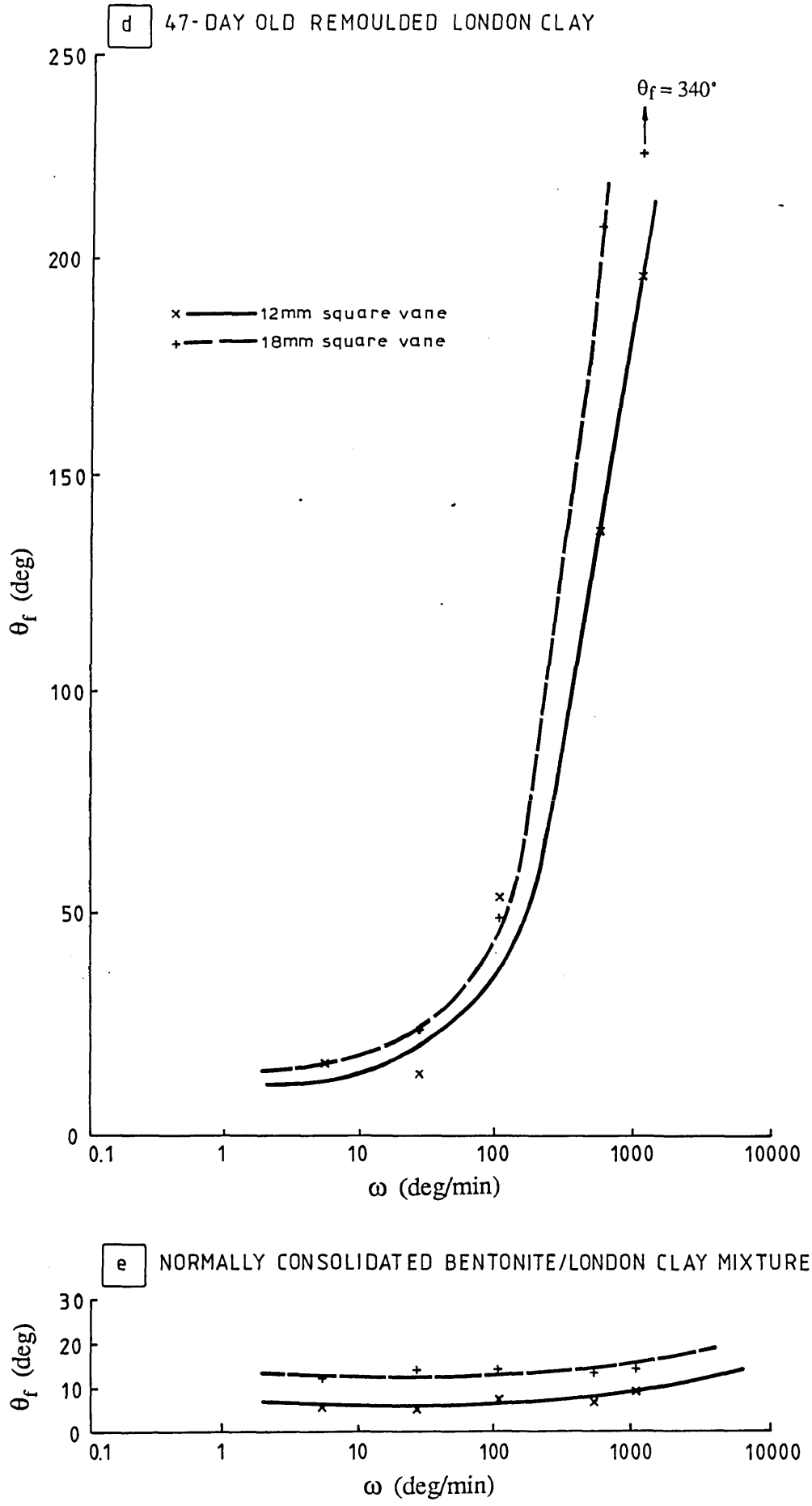


Fig. 4.4 Effect of rate of vane rotation on the measured angle of rotation at failure.

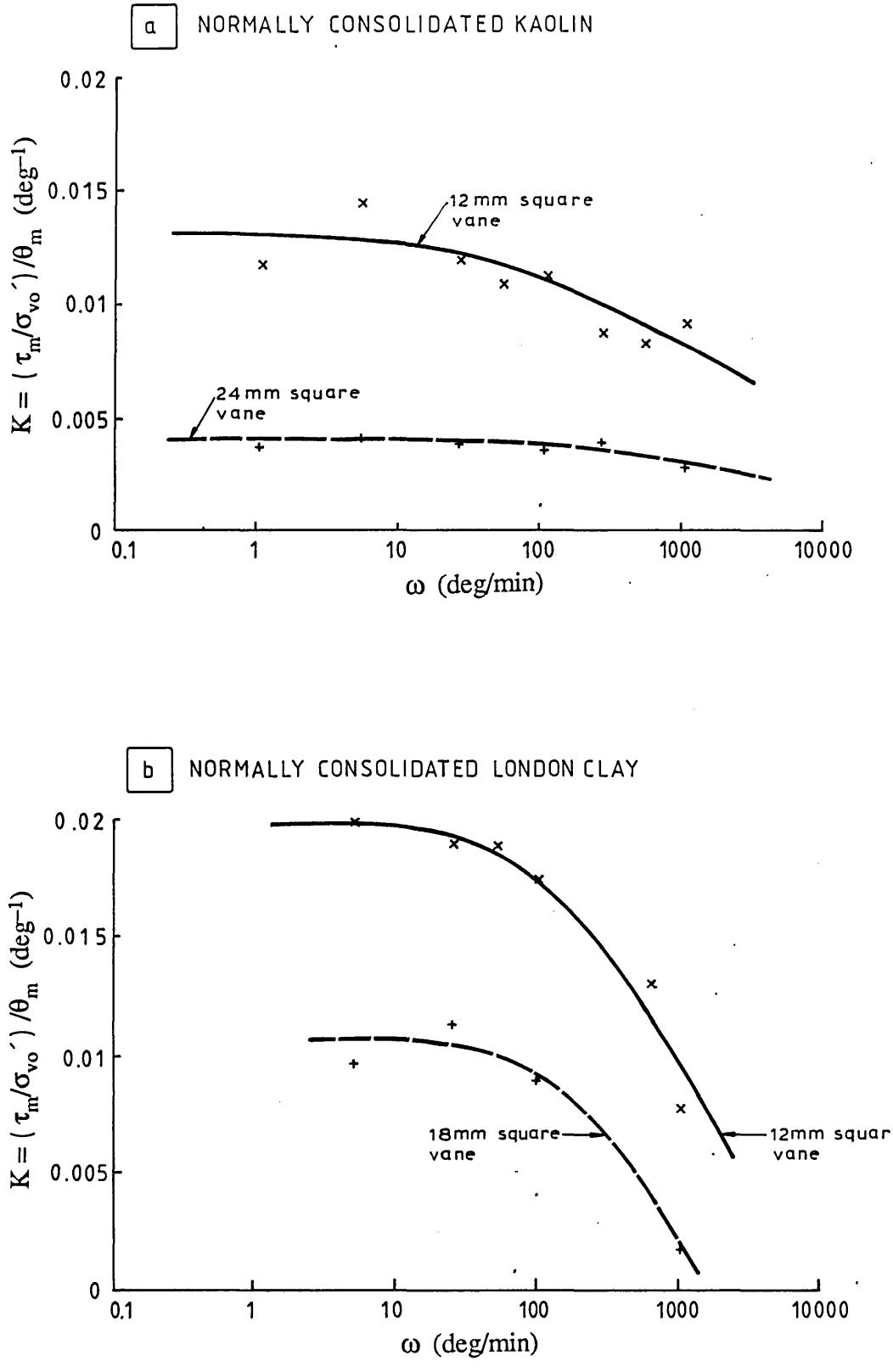
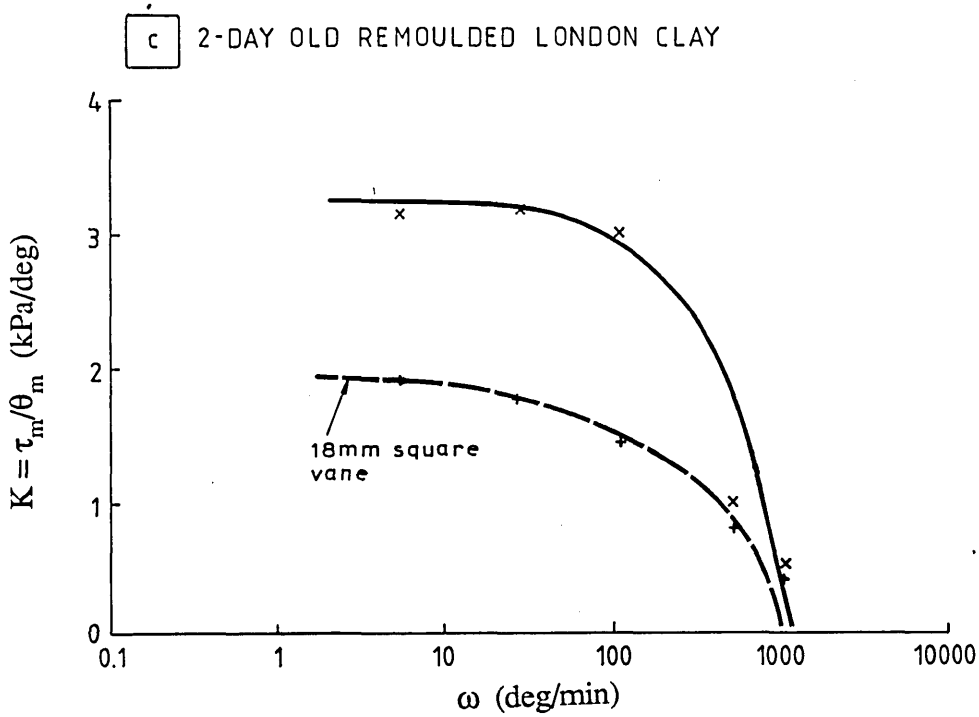


Fig. 4.5 Effect of rate of vane rotation on the measured initial soil stiffness, K.



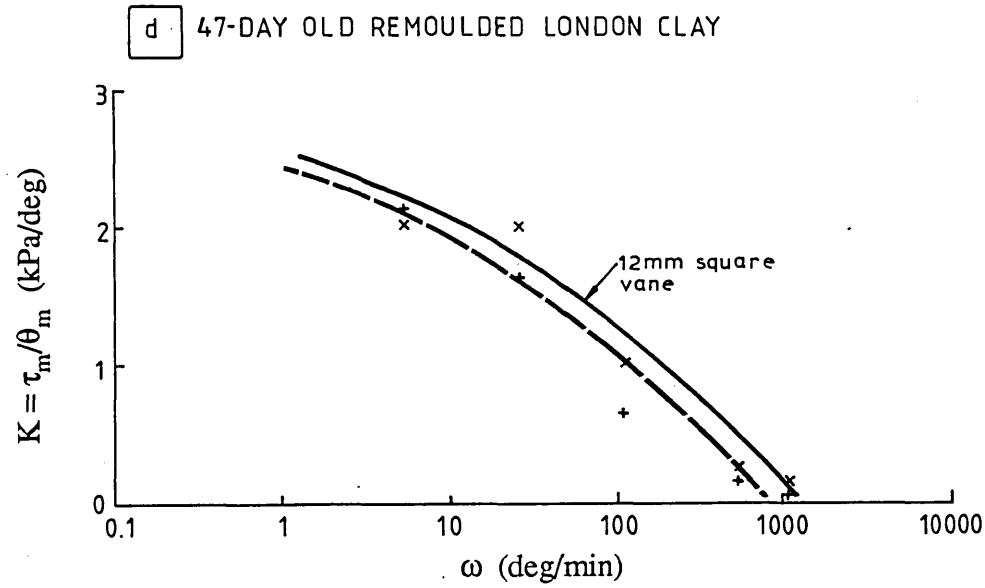


Fig. 4.5 Effect of rate of vane rotation on the measured initial soil stiffness, K.

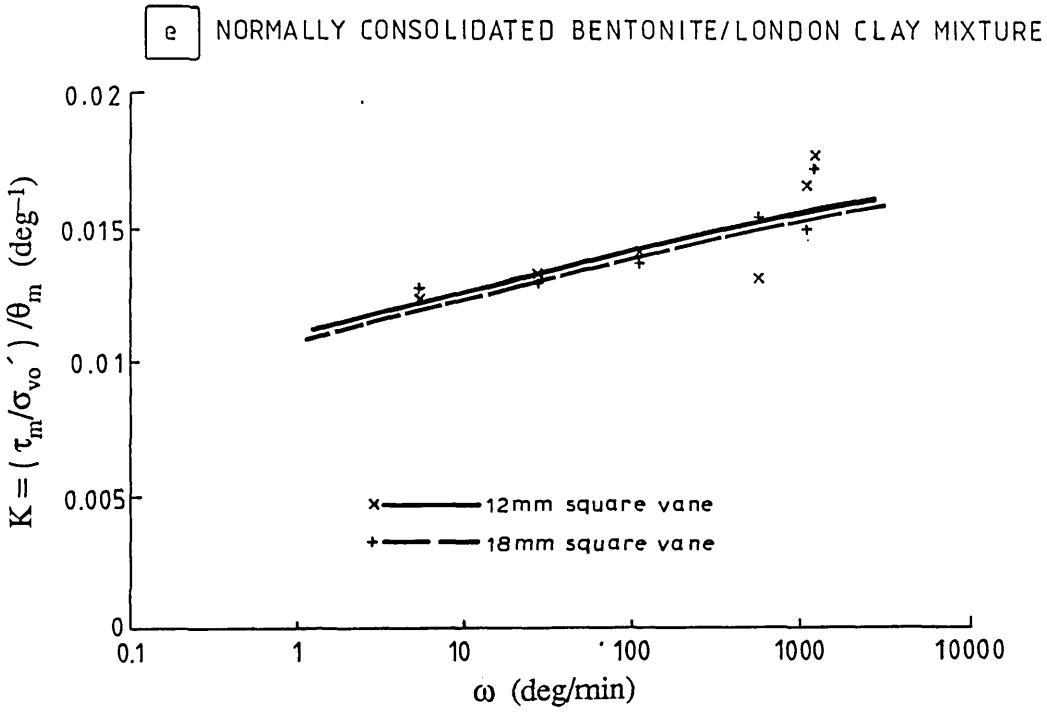


Fig. 4.5 Effect of rate of vane rotation on the measured initial soil stiffness, K.

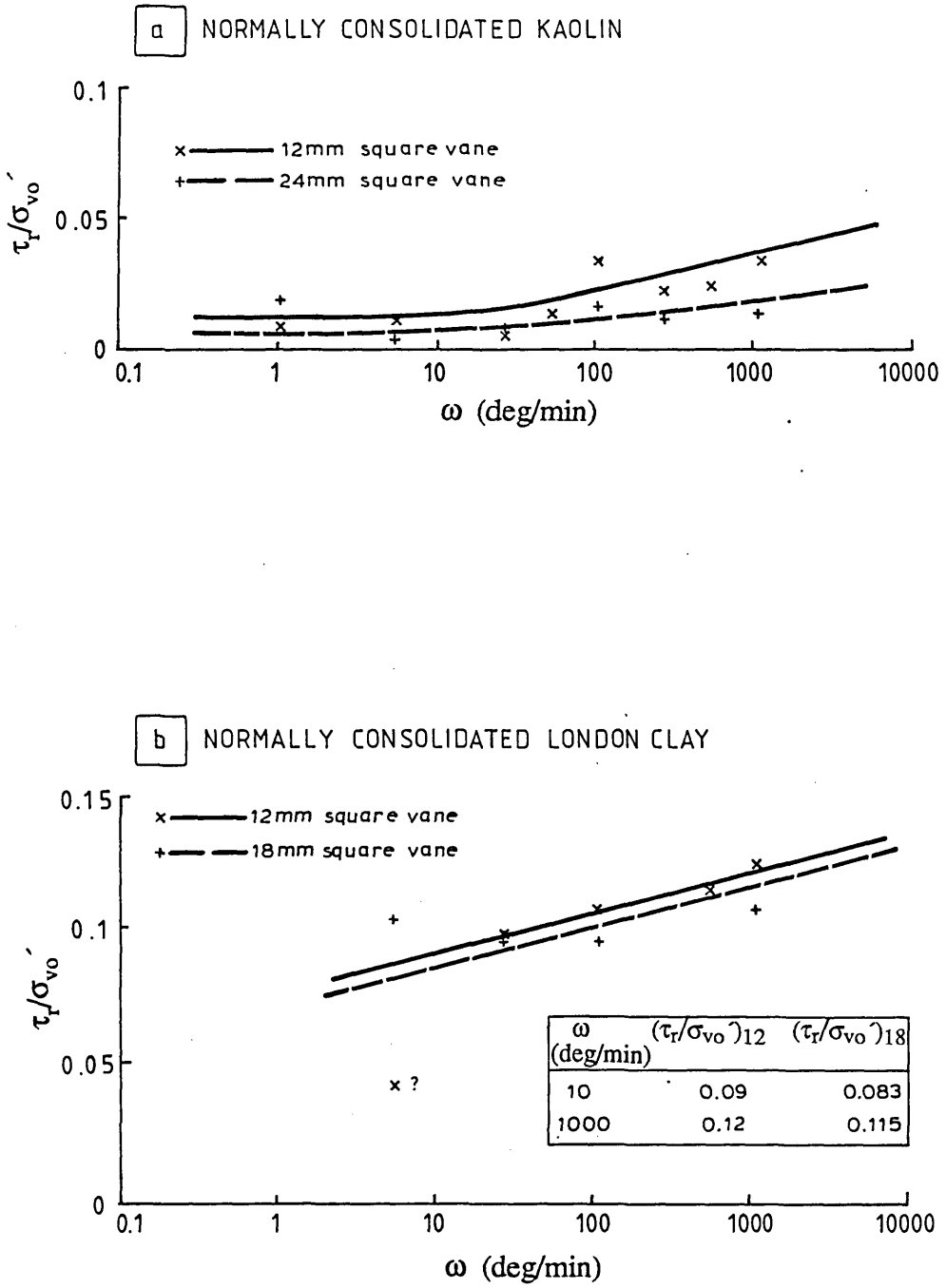


Fig. 4.6 Effect of rate of rotation on the measured residual vane strength.

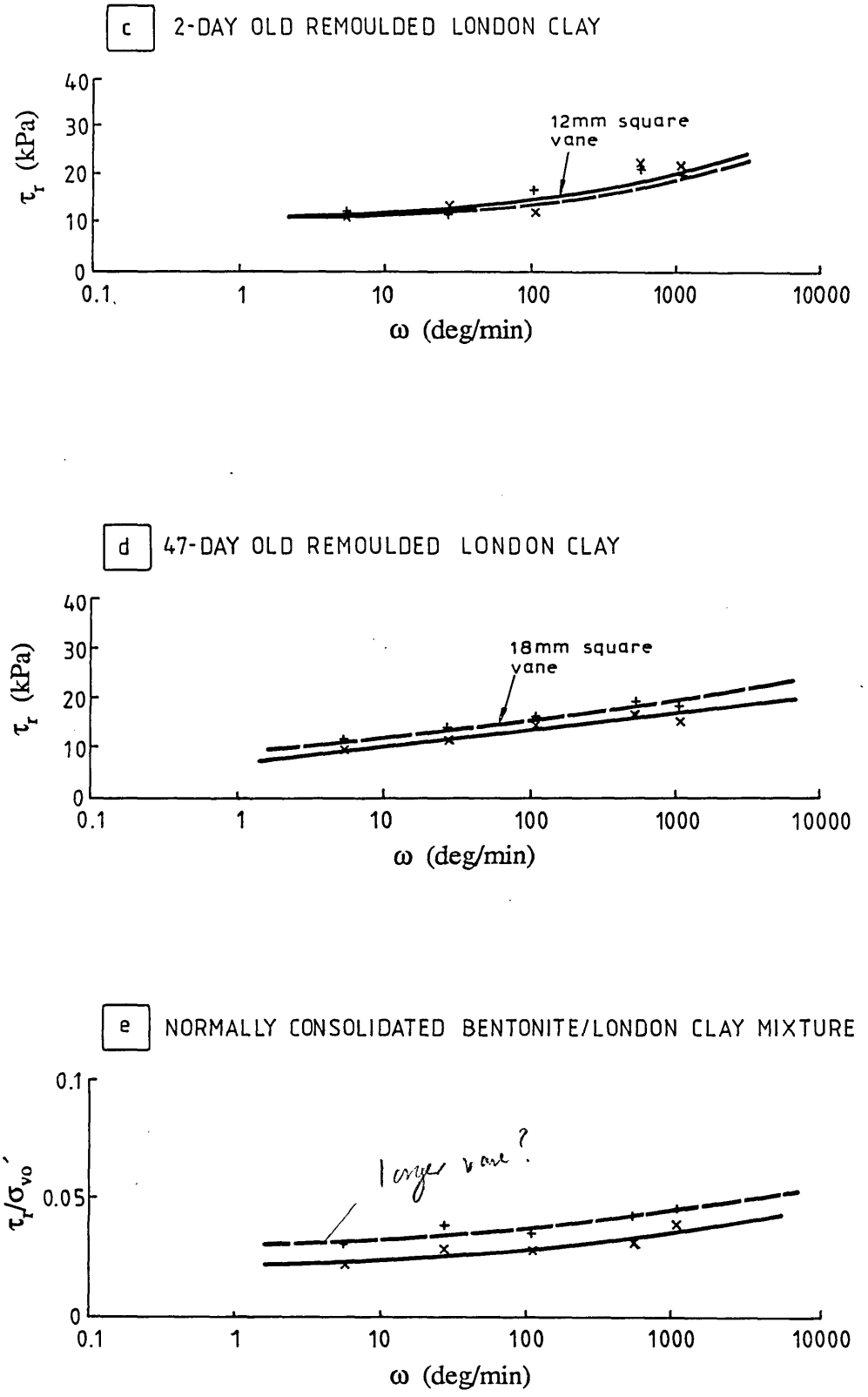


Fig. 4.6 Effect of rate of rotation on the measured residual vane strength.

4.3.4 Summary

In this Section the trends observed in Sections 4.3.3A and B, above, will be considered on a global basis. The shear stress – rotation characteristics described above include the peak shear strength (τ_f/σ_{vo}' or τ_f), the angle of rotation at failure (θ_f), the initial soil stiffness ($K = (\tau_m/\sigma_{vo}')/\theta_m$ or τ_m/θ_m), and the residual shear strength (τ_r/σ_{vo}' or τ_r). The effects of vane size and clay type on the above parameters will be discussed separately.

4.3.4A The effect of vane size

The effect of vane size on the peak shear strength, as a consequence of the effect of the rate of vane rotation (see Figs. 4.3a–e), will be discussed in detail in Sections 4.4.2E, 4.4.3 and 4.4.4. However, it should be mentioned that, except for the results of tests on remoulded samples of London clay, the peak shear strength – rate of rotation relationships are consistent with the hypothetical model outlined in Section 4.4.1 (see Section 4.4.5).

Strain-rate effects on the angle of rotation at failure for all the clays tested in this investigation show the trend that larger angles of rotation are required to reach failure with the larger vane size than with the smaller one (Figs. 4.4a–e). A likely explanation for this observation is that progressive failure might be in operation, thus implying that a larger rotation would be required for the formation of a continuous surface between adjacent blades for a vane with a larger diameter. The possibility of progressive failure in the vane test is explored in Chapters 5 and 6.

The effect of vane size on the relationship between the initial soil stiffness and rate of vane rotation can be seen in Figs. 4.5a–e, which show that the smaller vane size consistently measures a stiffer soil response than the larger one; the exception to this trend being that of the samples of the bentonite/London clay mixture in which there is little or no vane-size effect. The reason for the above observations is not clear.

The effect of vane size on the residual shear strength has been presented in Figs. 4.6a–e. Normally consolidated samples of kaolin and London clay, as well as the 2-day old samples of remoulded London clay, show that the smaller vane gives rise to higher values of residual strength, whilst samples of the 47-day old remoulded London clay and normally consolidated bentonite/London clay mixture portray an opposite trend, with the larger vane yielding higher residual strengths than the smaller one.

4.3.4B The effect of clay type

Section 4.4.6 describes the effect of clay type on the measured peak strength. In this Section, Figs. 4.7a and b are presented in order to show the effect of clay type on the shear stress – rotation curves obtained from 12mm vane tests at two different rates of rotation of $\omega = 5.375$ and 1075 °/min. Only the results of tests on normally consolidated samples of kaolin, London clay and the bentonite/London clay mixture are considered. It is seen that London clay has a 'perfectly plastic' shear stress – rotation curve initially, while the bentonite/London clay mixture shows a comparatively brittle response; kaolin lies somewhere in between these two.

Fig. 4.8 shows the relationship between θ_f and ω for all the clays tested; a log-log plot is used so that all the results could be compared on the same Figure. The effect of clay type on the angle of rotation at failure is quite evident. Over the range of rates of rotation of $1 \leq \omega \leq 1000$ °/min, the bentonite/London clay mixture reaches failure after an angle of rotation of about $\theta_f = 5–10°$, this being smaller than the angle of rotation required to reach failure in the case of both London clay and kaolin, for which $10° \leq \theta_f \leq 40°$ and $10° \leq \theta_f \leq 25°$, respectively; the remoulded samples of London clay reach failure at comparatively higher angles of rotation than the above, where $10° \leq \theta_f \leq 200°$, with θ_f increasing dramatically with increasing sample age.

The results of vane tests on normally consolidated samples of Speswhite kaolin carried out by Cheah (1981) are also presented in Fig. 4.8 (see Section 4.4.2F(iv)). Cheah's θ_f–ω relationship is very similar to that found for the normally consolidated samples of kaolin tested in this study. As the rate of rotation increases from 4 to 30 °/min, θ_f reduces and reaches a minimum value of about 20° at $\omega \approx 40$ °/min, but then continues to increase with increasing values of ω; values of θ_f lying in the range 20–1000°. At the same rate of rotation, Cheah found higher values of θ_f than those found in this investigation. This is primarily due to the bigger vane size (D = 19 mm; H/D ≈ 1.5) which Cheah used.

However, Torstensson (1977) has reported that the vane angular rotation at failure was independent of the rate of rotation for field tests on two highly plastic ($I_P \approx$ 58% and 85%) normally consolidated Swedish clays.

A summary plot of the relationships between the initial soil stiffness (K) and ω is presented in Fig. 4.9. Although both kaolin and London clay show a similar trend with K reducing as ω increases, the bentonite/London clay mixture indicates increasing values of K with increasing rates of rotation, thus inferring that some highly plastic normally

consolidated soils display an increase in stiffness as the rate of shearing increases. Consequently, since at slow rates of rotation corresponding to $\omega = 1$ °/min, London clay is stiffer than both kaolin and the bentonite/London clay mixture which show similar stiffnesses, it may be suggested that the initial soil stiffness reflects the degree of drained/undrained nature of the behaviour of the soil.

This is consistent with the $\tau_f/\sigma_{vo}' - t_f$ relationships presented in Fig. 4.27, where at slow rates of rotation, both London clay and kaolin exhibit a drained behaviour which becomes less and less drained as the rate of rotation increases. In Fig. 4.27, the curve for the bentonite/London clay mixture shows that the mixture displays undrained behaviour even at the slow rate of rotation of 1 °/min.

The effect of clay type in relation to the effect of the strain rate on the measurement of the 'residual' (large displacement) shear strength (τ_r/σ_{vo}') is presented in Fig. 4.10, where higher values of τ_r/σ_{vo}' occur at higher rates of rotation, with the rate of increase being similar for all three soils. The London clay curve shows comparatively higher values of τ_r/σ_{vo}' at given rates of rotation than the other two.

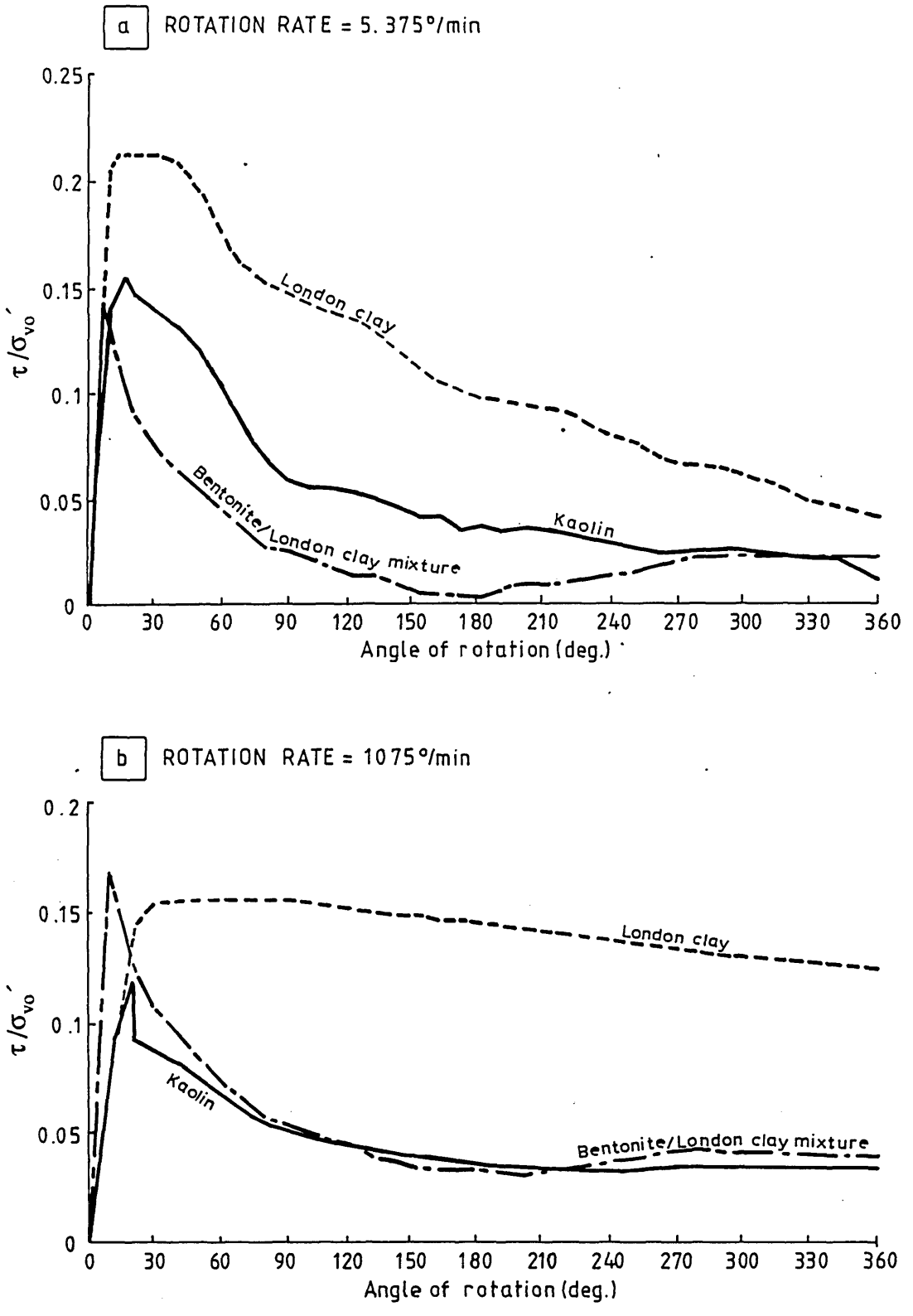


Fig. 4.7 Shear stress-rotation curves for 12mm square vane tests in different clays.

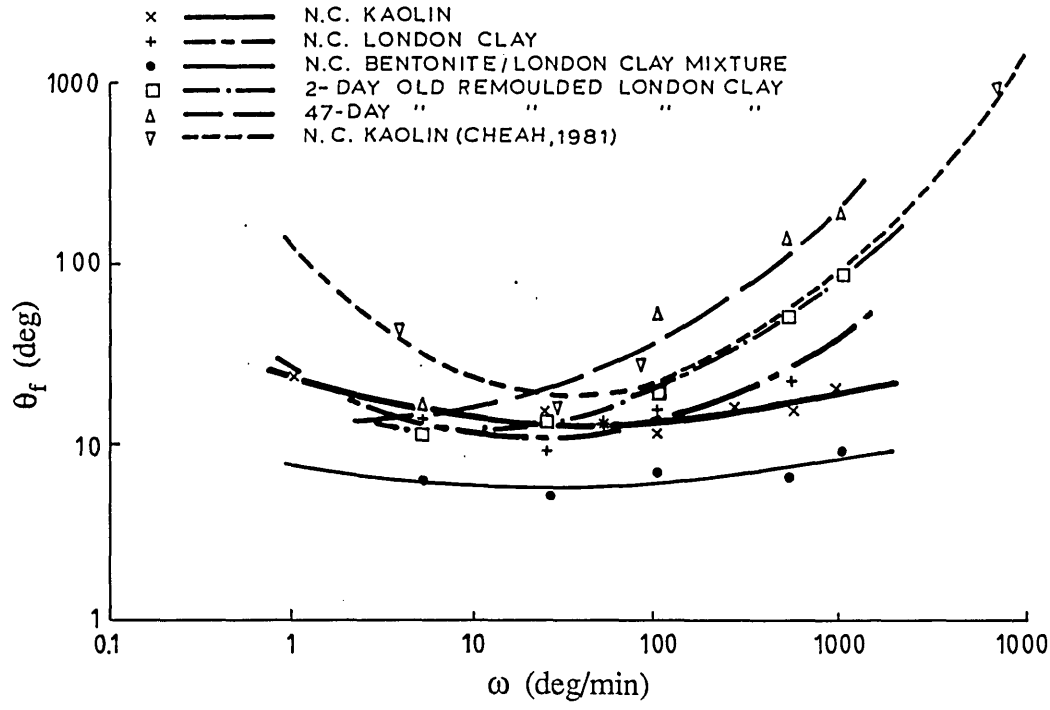


Fig. 4.8 Relationships between angle of rotation at failure and rate of rotation for 12mm square vanes in different clays.

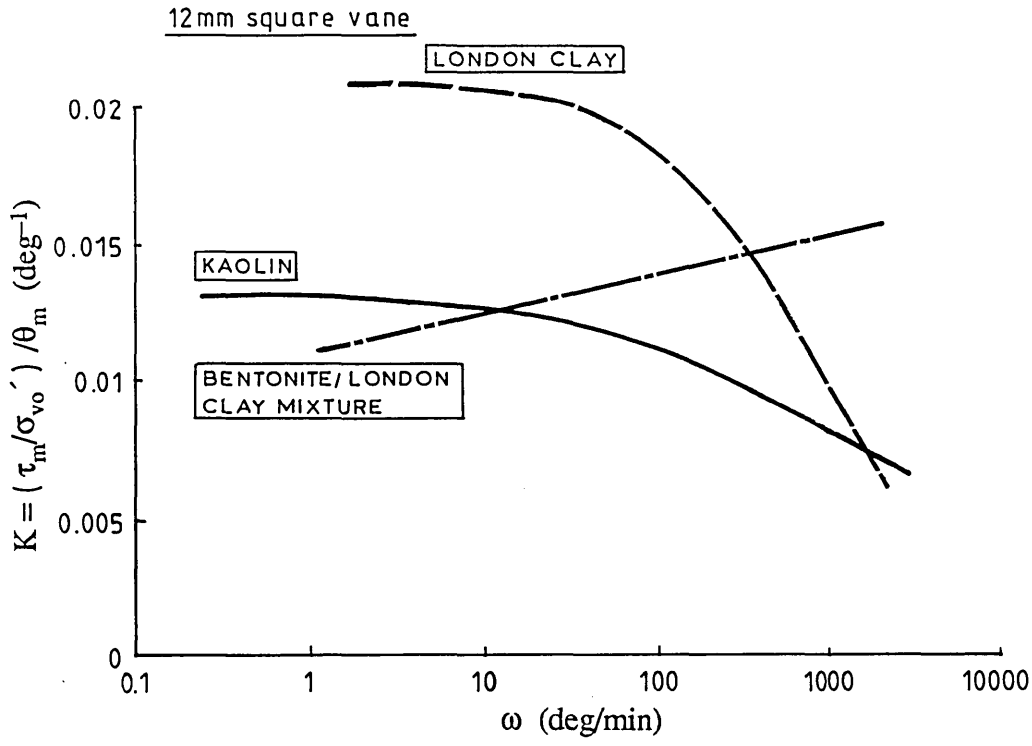


Fig. 4.9 Initial soil stiffness — rate of vane rotation relationships.

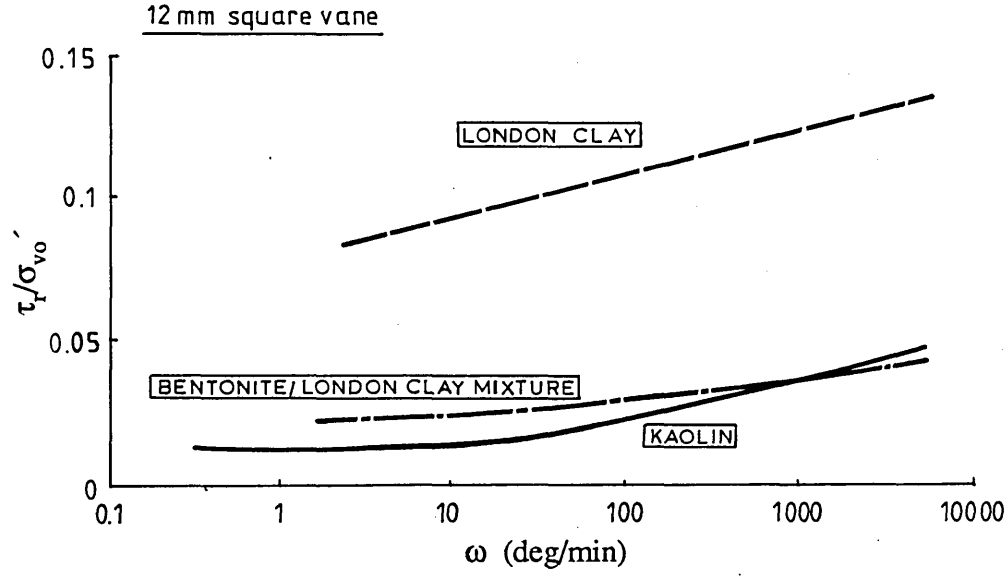


Fig. 4.10 Residual vane strength — rate of rotation relationships.

4.4 RATE OF ROTATION TO ENSURE UNDRAINED CONDITIONS

4.4.1 Introduction

The main objective of this aspect of the study was to examine the effects of varying rotation rate and size of blade on the measured vane strength, in an attempt to identify the rate of vane rotation to ensure undrained conditions.

Fig. 4.11 shows a hypothetical model representing the relationship between the measured (normalised) shear strength and (logarithmic) time to failure. Curves are presented for soils in which the normal effective stress on the shear zone increases (curves 1a and 2a), and for soils in which it decreases (curves 1b and 2b), under partially and fully drained conditions.

For 'dilatant' soils, in which the effective radial stress on the shear zone (σ_h') increases as the soil is sheared under drained conditions, higher strengths are measured at slower rates of shearing (corresponding to larger values of t_f), since with the dissipation of excess pore pressures higher degrees of consolidation will be achieved. However, degrees of consolidation will be less with increasing shear strain rates, and thus lower strengths will be measured. At some point, as the rate of vane rotation is increased, complete undrained conditions will apply and a minimum strength will be measured. Beyond this, as shear strain rates are increased further, viscous effects are assumed to begin to dominate the behaviour and the measured strength once again increases.

For a given soil and given drainage boundary conditions, Terzaghi's theory of one-dimensional consolidation states that the time taken to reach a given average degree of consolidation, t, is proportional to the square of the drainage path length, d^2, since the time factor, T ($= c_v t/d^2$) is a constant for any particular average degree of consolidation. The time factor appropriate to the time to failure (t_f) is, therefore, $T_f = c_v t_f/d^2$. If it is assumed that the drainage path length in the vane test is related to the vane diameter, D, and that there is a common degree of consolidation at failure regardless of vane diameter, then T_f is a constant and $t_f \propto D^2$, since c_v is also a constant. Hence, when using two vanes, one twice the diameter of the other, the same value of shear strength would be obtained at different times to failure (for a given average degree of consolidation) such that

$$\frac{t_{f1}}{t_{f2}} = \frac{D_1^2}{D_2^2} \qquad \text{Eq. 4.1}$$

$$\therefore \quad t_{f2} = 4t_{f1}$$

where subscripts 1 and 2 respectively denote the dimensions of a given vane size and one twice as large.

At shear strain rates greater than required to ensure undrained behaviour, viscous effects dominate, since it may be hypothesised that soil strength is a function of the rate of shearing and soil viscosity.

The viscosity of soils is dependent, inter alia, on both the type and amount of clay present. For a given soil, viscosity, and hence the soil strength, is probably proportional to the rate at which the soil is sheared. In the vane test, most of the shearing is imposed by the tip of the vane blades and consequently it is more appropriate to consider the vane tip velocity rather than the rate of vane rotation as the controlling test rate (Perlow & Richards, 1977). The vane tip velocity is given by the product of the rate of vane rotation, ω, and the vane radius, R. Therefore, when the soil behaviour is governed by viscous effects, it is reasonable to suggest that the faster the vane is rotated the more quickly a given value of soil strength is mobilised. If it is assumed that both the soil viscosity and the angle of rotation to reach peak torque remain constant regardless of the rate of vane rotation, it follows that the same value of soil strength would be obtained at different times to failure such that

$$t_f \propto D$$

$$\frac{t_{f1}}{t_{f2}} = \frac{D_1}{D_2} \qquad \text{Eq. 4.2}$$

$$\therefore \quad t_{f2} = 2t_{f1}$$

Curve 1a of Fig. 4.11 shows schematically the proposed relationship between normalised shear strength, τ_f/σ_{vo}', and (logarithmic) time to failure, t_f, for a given square vane size, while curve 2a corresponds to the relationship for a square vane of twice the linear dimension. At strain rates where drainage effects dominate the soil behaviour, curve 2a is shifted to the right of curve 1a by a factor of four, with its minimum point corresponding to a time to failure four times longer than that of curve 1a. On the other hand, where viscous effects control the soil response, curve 2a is shifted to the right of curve 1a by a factor of two.

Curves 1b and 2b show the corresponding relationships for 'contractant' soils in which the effective normal stress on the shear surface (σ_h') decreases when conditions of partial or full drainage apply. Note that when undrained/viscous conditions govern, the relationships between the normalised shear strength and time to failure are the same for both 'dilatant' and 'contractant' soils, and hence both curves 1a and b and curves 2a and b coincide.

In order to see whether or not this hypothetical model could be verified, an experimental programme was designed and undertaken, as described in Section 4.2. Consequently, tests were performed in order to examine the shear strength versus rate of rotation relationships for different clay types. The results of tests on each clay type and their respective interpretations are presented separately.

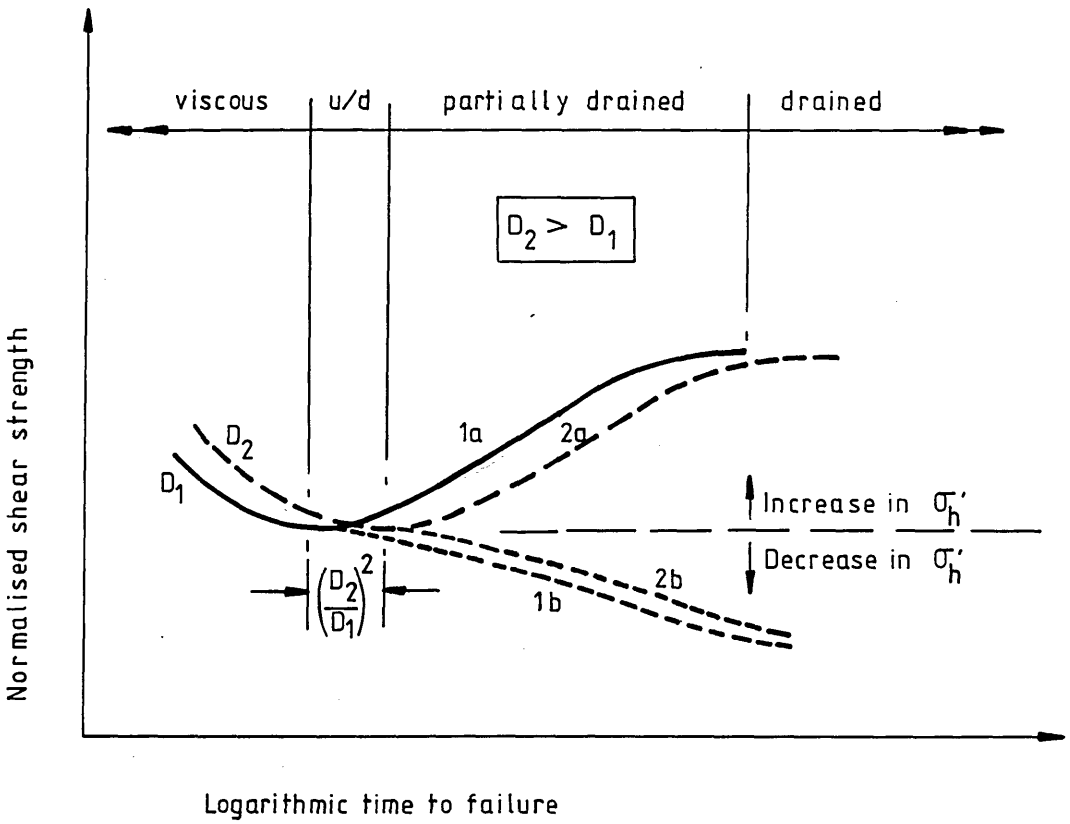


Fig. 4.11 Hypothetical model for the relationship between normalised vane shear strength and (logarithmic) time to failure.

4.4.2 Tests on Kaolin

4.4.2A Introduction

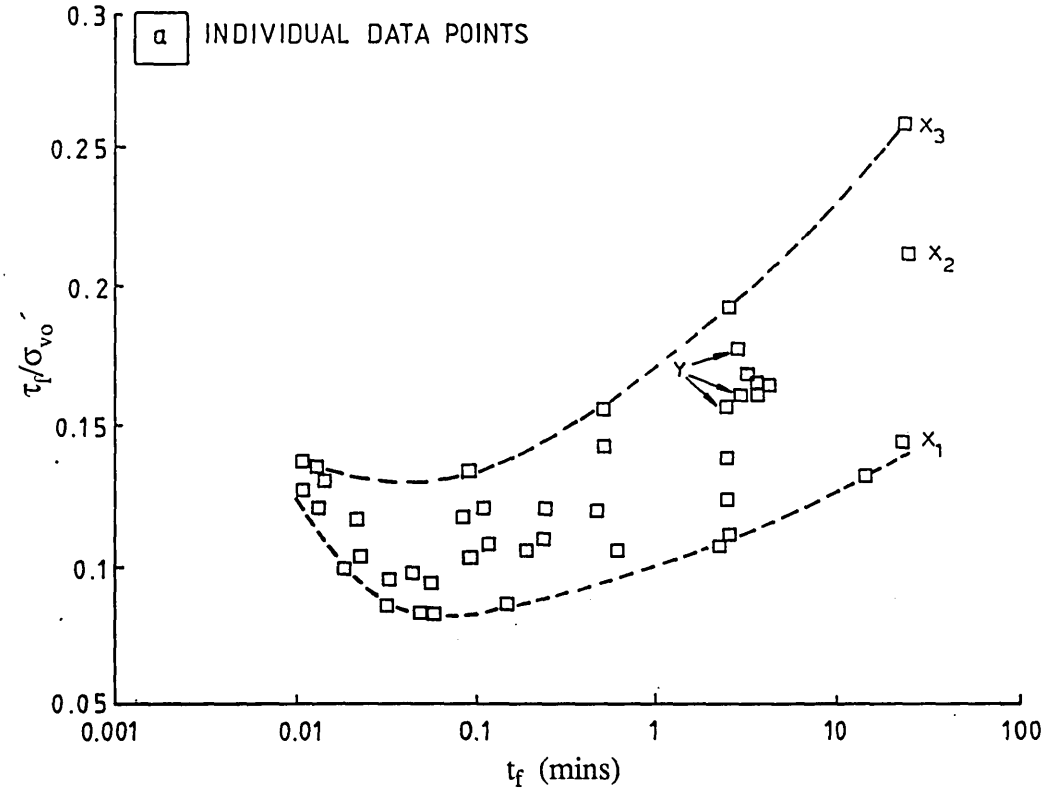
Fig. 4.12 presents the results of 12mm square vane tests on normally consolidated samples of Speswhite kaolin, in terms of τ_f/σ_{vo}' and t_f, while the results corresponding to the 18 and 24mm vanes are shown in Figs. 4.13 and 4.14, respectively. It will be seen from Figs. 4.12–4.14 that the relationships between normalised vane strength and time to failure are in broad agreement with that suggested in Section 4.4.1 and Fig. 4.11.

4.4.2B The 12mm vane test results

Fig. 4.12a shows a total of 46 test results obtained using the 12mm vane. Despite a moderately high degree of scatter (of the order of about ± 20 to 30% of the mean) in the results, it is apparent that a relationship exists between the normalised vane strength, τ_f/σ_{vo}', and time to failure, t_f. It is evident that the strength is high at long times to failure, decreases as t_f reduces (i.e. rate of vane rotation increases) and reaches a minimum before increasing with further decreases in t_f.

In an attempt to establish the time to failure at which undrained conditions would prevail, it is necessary to consider the scatter in the data points. (Possible reasons for the scatter are discussed in Section 4.4.2F.) Thus, curves are drawn through the lower and upper extremes in Fig. 4.12a. It can be seen that the minima of these curves occur at different values of τ_f/σ_{vo}' and at correspondingly different values of t_f.

It was seen in Section 4.3.3A that individual results can be justifiably averaged when samples subjected to the same rate of rotation display similar shear stress – rotation characteristics. Since no anomalous behaviour was identified, averaged values of τ_f/σ_{vo}' and corresponding averaged values of t_f are presented in Fig. 4.12b. The curve drawn through the points shows a clearly defined minimum of about $\tau_f/\sigma_{vo}' = 0.1 \pm 0.01$at about $t_f = 0.06$ mins ± 30%. At long times to failure, drained conditions will prevail (for a 'dilatant' soil) and the maximum strength would be measured. However, the fully drained value of τ_f/σ_{vo}' is not clearly defined and thus a dotted curve is drawn in; $(\tau_f/\sigma_{vo}')_{\text{fully drained}} \geq 0.19$ and requires $t_f \geq 50$ mins.



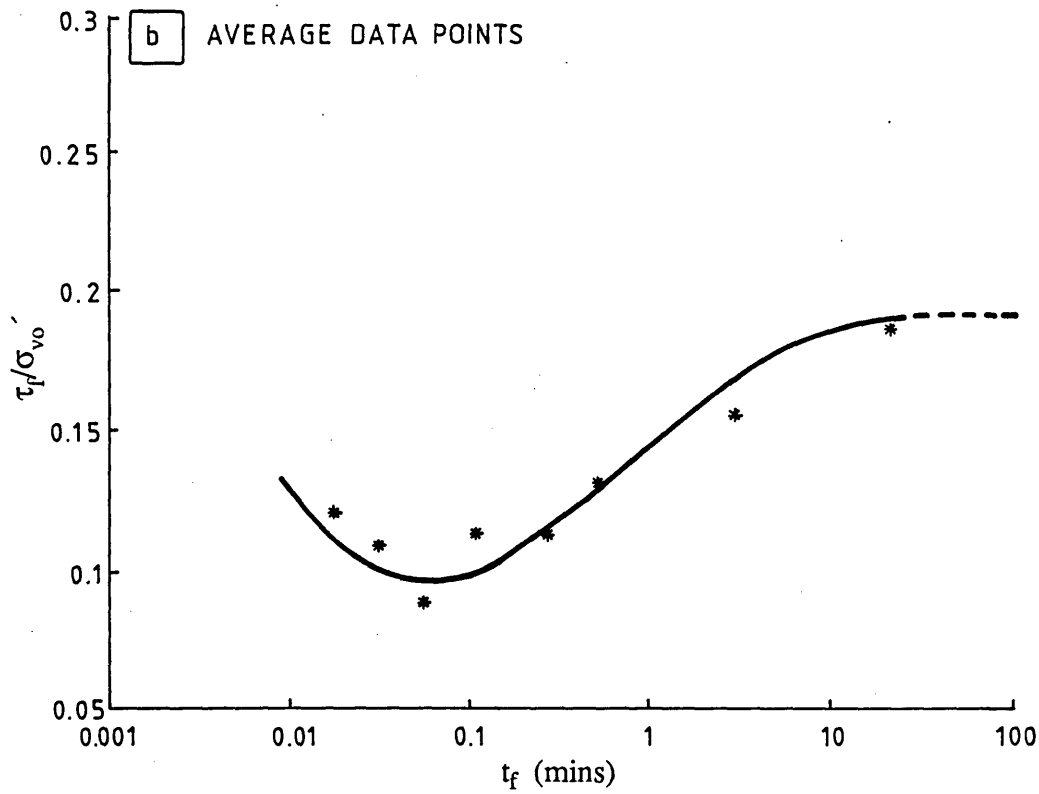


Fig 4.12 Variation of normalised peak strength with time to failure: 12mm square vane tests on normally consolidated kaolin.

4.4.2C The 18mm vane test results

Only five tests were carried out using the 18mm vane. The limited data for this vane size (see Fig. 4.13) made it extremely difficult to determine the time to failure required to ensure conditions under which undrained behaviour would result.

4.4.2D The 24mm vane test results

A total of 15 tests were conducted with the 24mm vane and the results are presented in Fig. 4.14. A feature of this set of data which is immediately striking is the lower degree of scatter (of the order of ± 20% of the mean) in the results compared to that found in Figs. 4.12 and 4.13, although it is acknowledged that fewer results would in general give rise to less scatter.

The time to failure required to ensure undrained conditions for this vane size was identified in the same manner described in Section 4.4.2B, above. The curve drawn through the averaged data (Fig. 4.14b) shows that the normalised vane strength is not greatly influenced by the rate at which the vane is rotated, giving a minimum of about $\tau_f/\sigma_{vo}' = 0.08 \pm 0.005$ at $t_f \approx 0.3$ mins ± 60%.

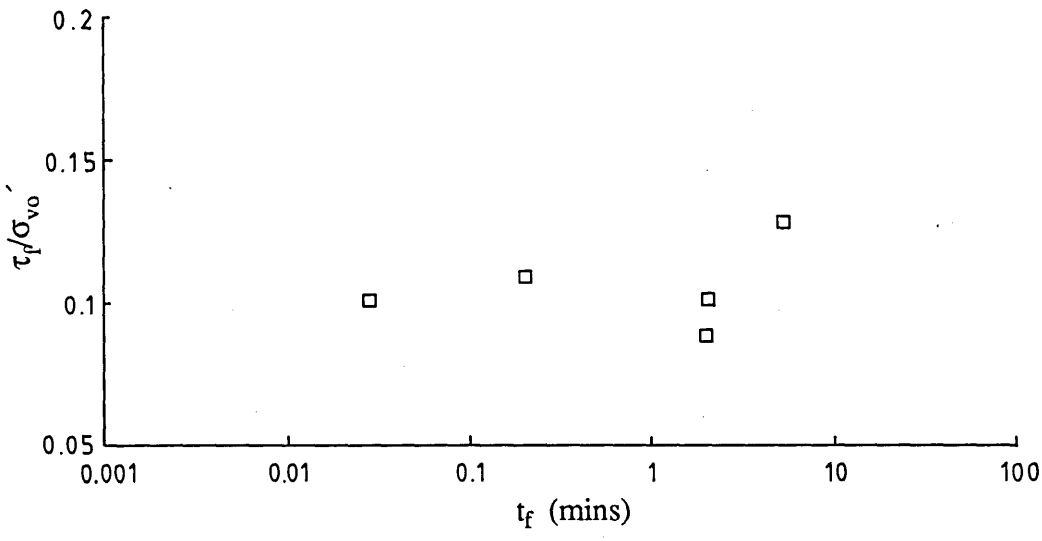


Fig. 4.13 Variation of normalised peak strength with time to failure: 18mm square vane tests on normally consolidated kaolin.

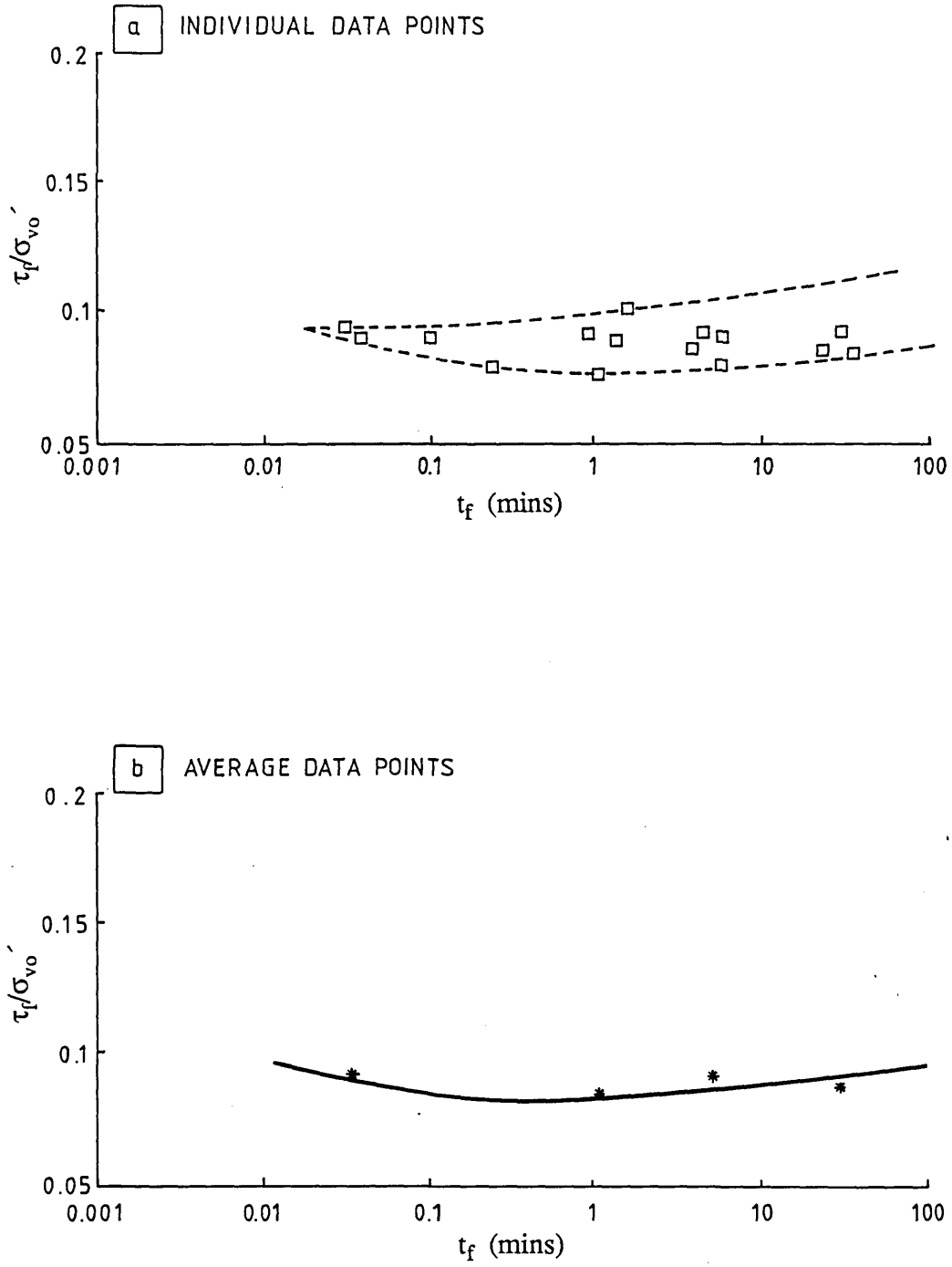


Fig. 4.14 Variation of normalised peak strength with time to failure: 24mm square vane tests on normally consolidated kaolin.

4.4.2E Summary of the results

The experimental relationships between τ_f/σ_{vo}' and t_f for the 12 and 24mm vanes (Figs. 4.12 and 4.14) indicate that the larger the vane size, the lower the minimum value of τ_f/σ_{vo}', the higher the value of t_f at which the minimum occurs (and the lower the scatter of results).

Fig. 4.15 shows the 'hypothetical 24mm vane' curve, drawn on the basis that (a) $t_f \propto D^2$ at times to failure > 0.24 mins (= $t_{f24} = 4t_{f12}$), and (b) $t_f \propto D$ at times to failure < 0.24 mins, with $(\tau_f/\sigma_{vo}')_{min} = 0.1$. It can be seen that the experimental curves are in broad agreement with the predictions of the hypothetical model described in Section 4.4.1 (Fig. 4.11) in the following respects:

(i) Terzaghi's theory of one-dimensional consolidation and viscoelastic soil behaviour models both assist in explaining the relationships between τ_f/σ_{vo}' and t_f. With increasing vane size the 'experimental' curves show both
   (a) lower values of τ_f/σ_{vo}' for $t_f > t_{f\,undrained}$, and
   (b) higher values of τ_f/σ_{vo}' for $t_f < t_{f\,undrained}$.

(ii) Although there is general agreement between the minimum values of τ_f/σ_{vo}', the 24mm vane test data suggest that $(\tau_f/\sigma_{vo}')_{min} = 0.08 \pm 0.005$, while the 12mm square vane test data suggest that $(\tau_f/\sigma_{vo}')_{min} = 0.1 \pm 0.01$, thus implying that lower minima may result as the vane size increases.

(iii) The times to failure at which the minima points occur in the 'experimental' curves of the 12 and 24mm vane test data are $t_f = 0.06$ mins ± 30% and 0.3 mins ± 60%, respectively. This suggests that t_f is proportional to D_1^2, where $D_1 > D$ (= the vane diameter). (See also Fig. 6.41, Section 6.4.2.)

(iv) The rate at which τ_f/σ_{vo}' decreases and increases with reducing t_f in the 'experimental 12mm vane' curve supports the hypothetical model illustrated in Fig. 4.11, but a corresponding trend cannot be seen in the 'experimental 24mm vane' curve, where there is a 50–100% discrepancy between the experimental and hypothetical curves at $t_f > 10$ mins.

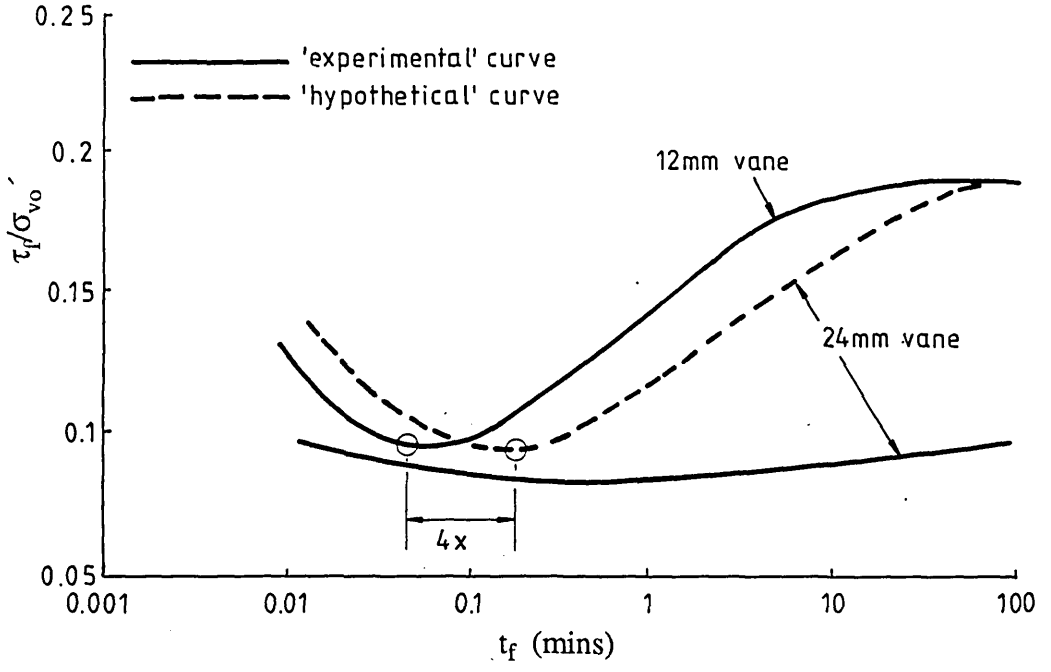


Fig. 4.15 Normalised peak vane strength – time to failure relationships : Comparison of experimental results with hypothetical curve.

4.4.2F Discussion of the results

4.4.2F(i) Introduction

The feature which is common to the test results of all three vane sizes is the noticeable amount of scatter of data. This Section explores the possible reasons for the observed scatter.

The samples were all prepared in accordance with the strict guidelines laid out in Section 3.3.2 and thus there is no reason to consider the likelihood of differences between any of the samples. Water content determinations made both along the length of the samples and from various horizons show a variation of less than 0.5%. Furthermore, the tests were all carried out in an identical manner (see Section 4.2.2) in order to ensure repeatability of results.

The likely causes of the scatter of data in Figs. 4.12a, 4.13 and 4.14a are investigated from a consideration of (a) factors which might have affected the overall stress state of the samples prior to testing, but were unaccounted for, and (b) parameters which varied during the tests and whose influence on the test results was considered negligible. In connection with the above, it is important to note that (a) the sample storage time could not be kept constant, since to have done so would have required the use of a number of consolidation cells which were not available, and (b) the vane insertion depths (z) were varied while the influence of this parameter on the measured strength was studied. These two effects will now be examined.

4.4.2F(ii) The effect of sample storage time

The experimental programme concerned with an investigation of the effect of the sample storage time on the measured vane strength has been described in Section 3.4.2E. It involved testing 1-day old, 10-day old and 50-day old samples of normally consolidated Speswhite kaolin at zero confining stress (Section 3.4.2A). Only the 12mm square vane and rotation rates of 5.375, 107.5 and 1075 °/min were used.

It can be seen from Fig. 4.16 that the longer the sample storage time, the greater the drop in the measured strength of kaolin. Furthermore, the rate of vane rotation has a significant influence on the measured strength, with reductions in strength between 1-day old and 50-day old samples tested at rates of rotation of 5.375, 107.5 and 1075 °/min of about 30, 20 and 10%, respectively. Fig. 4.16 also shows the results of

unconsolidated undrained triaxial tests performed by Odeh (1980) on samples of kaolin stored for different lengths of time. There is very good agreement between the triaxial and vane test data at similar 'strain rates' of 0.6 mm/min (Odeh) and 0.56 mm/min (writer).

A detailed study of the effect of the sample storage time on the measured strength of kaolin has been carried out by Kirkpatrick & Khan (1984). The samples were normally consolidated to a final consolidation stress of $\sigma_{vo}' = 552$ kPa, then subjected to undrained unloading, and stored for different lengths of time before being tested in the triaxial compression cell. It was found that the strength of 50-day old samples was about 29% less than that corresponding to 1-day old samples, which shows a very close agreement with the results of vane tests at a similar rate of shearing ($\omega = 5.375$ °/min). Kirkpatrick & Khan explained this loss in strength with sample storage time in terms of the loss in the negative pore water pressures with time — a phenomenon which according to Kirkpatrick & Khan involved processes that are not fully understood but appear to be related to cavitation and diffusion effects.

The concept of cavitation is generally associated with the process whereby air bubbles come out of solution as a consequence of the failure of the pore water to sustain the negative pressures which are set up following the removal of total stresses on the sample. Mair (1979) has described cavitation in terms of vaporisation of a certain proportion of the sample pore water as a result of total stress relief.

Blight (1961) could see no reason to doubt the ability of soil water to sustain large absolute tensions, since he had attained absolute tensions in tap water of up to about 275 kPa.

Bishop et al. (1975) considered the influence of total stress relief and found that for kaolin the divergence in strength of samples subjected to total stress relief compared to those which were not, occurred when the total stress change ($\Delta\sigma_v$) exceeded 1800 kPa. They suggested that the pore water failed to sustain higher tensions without a departure from the condition of full saturation. In addition, they found that on removal of stress-relieved samples from the triaxial cell, the samples showed no significant tendency to change in volume with time (until drying took place). This suggested that once initiated, the propagation of cavitation within the pore water was fairly rapid and complete. However, Davies (1981) suggests that, if it is assumed that the clay behaves elastically and isotropically on unloading, the process which involves gases coming out of solution may be progressive, with the drop in pressure in the gas-filled voids encouraging further gas to come out of solution. Consequently, the air or water vapour

present in the voids might lead to some progressive deterioration in negative pore pressure.

Mair (1979) reports a series of tests which were conducted on kaolin using very similar procedures to those adopted in Bishop et al.'s (1975) study. It was concluded that for samples consolidated to confining stresses lower than 100 kPa, cavitation effects appeared to be reversible if the total stresses were re-applied. However, this was not the case for specimens exposed to air prior to the reapplication of the total stresses. Moreover, the cavitation process appeared to propagate from the free boundaries, having less effect on the strength of larger specimens.

The samples tested in this study were consolidated to vertical effective stresses in the range $\sigma_{vo}' = 265–315$ kPa. Therefore, on the basis of Bishop et al.'s experimental data, it is highly unlikely that these samples had undergone cavitation as a result of the failure of the pore water to sustain the negative pressures set up on unloading, since the highest reduction in total stress was only 315 kPa. However, the samples were stored for various lengths of time and were subsequently exposed to air during vane testing. It is therefore difficult to escape from the conclusion that the samples had cavitated as a consequence of the effects of both exposure to air (Mair, 1979) and sample storage time (Kirkpatrick & Khan, 1984); since the scatter of data would only be slightly minimised after correction for sample storage time effects, e.g. by correcting back to '1 day', it was considered that there would be little or no justification in any further manipulation of the data.

4.4.2F(iii) The effect of the depth of vane insertion

Once it was realised that the limits suggested by Head (1982) for minimising the end effects associated with the vane test were too restrictive experimentally (see Sections 3.2.2A and 6.3), vanes were inserted into the samples to a variety of depths, z, in the range 10–60 mm. The minimum difference in the depths at which two successive tests were conducted was always 1.5 times the height of the vane which was being tested.

Fig. 4.17 shows the results of 12mm vane tests on kaolin at similar rates of rotation of 5.375 and 6.27 °/min. It had been expected that higher values of τ_f/σ_{vo}' would be measured with increasing values of z, since the deeper the position at which the vane is tested, the more the frictional resistance which would be mobilised along the vane shaft. However, the scatter of data, even after correcting back to '1 day', is too large to draw any conclusion regarding the depth of penetration.

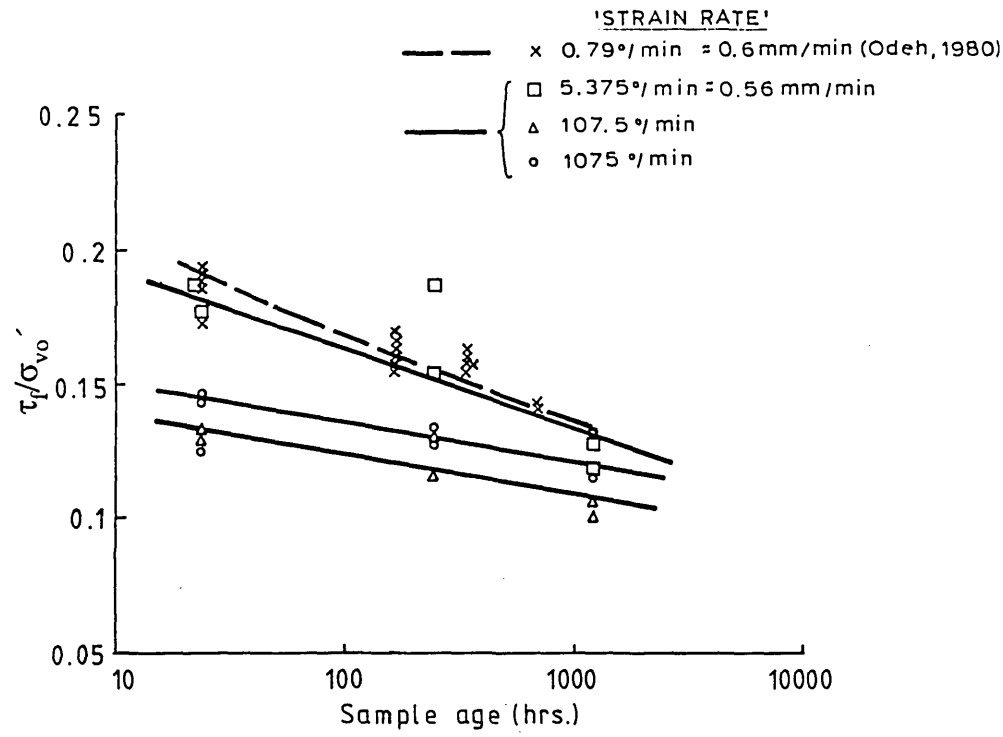


Fig. 4.16 Effect of sample storage time on the measured peak vane strength.

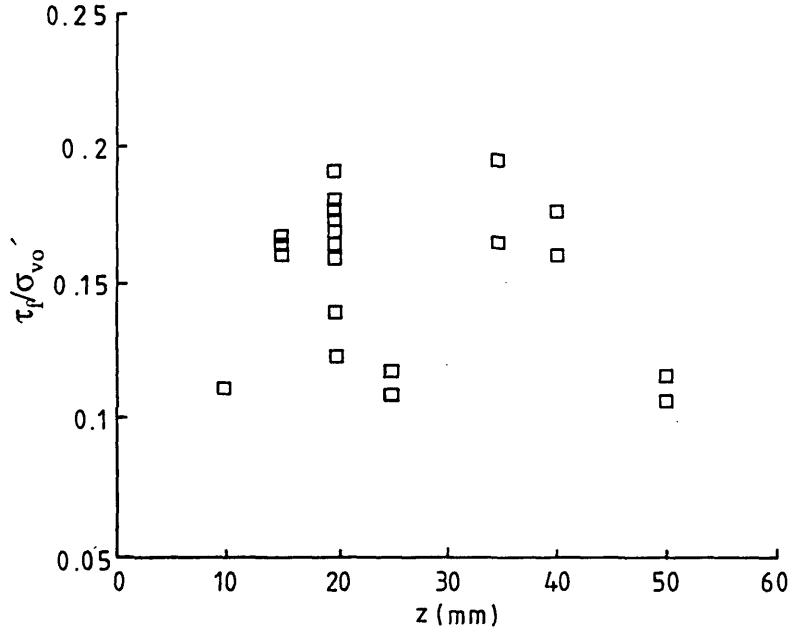


Fig. 4.17 Effect of depth of vane insertion on the measured shear strength.

4.4.2F(iv) Comparison of results with published data

The results of the 12mm vane tests on kaolin (Fig. 4.12) are re-presented in Fig. 4.18 in terms of the maximum shear stress mobilised along the vertical cylindrical surface circumscribing the vane, τ_{vf}, normalised with respect to the maximum consolidation stress, σ_{vo}', versus the rate of vane rotation, ω. These axes are used because the results of other investigators (e.g. Sharifounnasab & Ullrich, 1985) are presented in such a way that cannot be evaluated in terms of τ_f/σ_{vo}' and t_f.

Since uniform isotropic conditions are assumed in the conventional interpretation of the vane test (Section 2.2), the vertical and horizontal maximum shear stresses are taken as equal and as defining the maximum shear stress which is mobilised during the test (see Fig. 2.1). Hence, $\tau_{vf}/\sigma_{vo}' = \tau_f/\sigma_{vo}'$. Fig. 4.18b shows averaged values of τ_{vf}/σ_{vo}' at given rates of rotation. The curve drawn through the average data points is the same as that in Fig. 4.12b, with a minimum value of $\tau_{vf}/\sigma_{vo}' = 0.1 \pm 0.01$ at ω = 300 °/min ± 30%. The 'drained' value of τ_{vf}/σ_{vo}' is about 0.2 at $\omega \leq 0.2$ °/min.

Sharifounnasab & Ullrich (1985) reported laboratory vane tests on stress-relieved normally consolidated samples of kaolinite (w_L = 48%, w_P = 34%) which had not suffered from sample storage time effects; the vane having been inserted at the end of consolidation of each sample. Vanes of three different H/D ratios of 1, 1.5 and 2 (with D = 12 mm) were used but no account was taken of the influence of the vane H/D ratio on the measured strength (see Table 3.1).

The results of Sharifounnasab & Ullrich are plotted in Fig. 4.18a. Although at the time of testing, their samples all had the same 'age', the degree of scatter of this data is as much if not more than that encountered in the present investigation. Different H/D ratios can give rise to a certain amount of scatter (Table 3.1), but it is inconceivable that the scatter is primarily due to the discrepancy in the H/D ratios. However, it is highly probable that cavitation effects had attributed to most of the scatter. A best-fit second order polynomial curve through the data set shows a very similar trend to that observed in the results of this study, with decreasing vane strengths as the rate of rotation increases in the range $1 \leq \omega \leq 25$ °/min (see Fig. 4.18b).

The results of the work carried out by Cheah (1981) are also presented in Fig. 4.18b. He tested samples of Speswhite kaolin which had three different stress histories, namely (a) normally consolidated to σ_{vo}' = 150 kPa, allowed to swell back to σ_v' = 50 kPa (i.e. OCR = 3) and subjected to total stress relief, (b) normally consolidated to σ_{vo}' = 150 kPa and allowed to swell back to σ_v' = 50 kPa (i.e. OCR = 3) and (c) normally

consolidated to $\sigma_{vo}' = 150$ kPa. Only the results of the normally consolidated samples can be considered for comparative purposes, since these were not influenced by overconsolidation effects. A vane of D = 19 mm, with H/D = 1.47, was inserted into the samples and rotated at ω = 4, 30, 86 and 6480 °/min. The best-fit second order polynomial curve through Cheah's data shows a trend very similar to that observed in this study, with τ_{vf}/σ_{vo}' decreasing with increasing ω until it reaches a minimum of about $\tau_{vf}/\sigma_{vo}' = 0.14$ at ω = 215 °/min ± 50%, after which it increases with further increases in ω. The sparsity of Cheah's data should be noted.

So far, the results obtained by other researchers working with kaolin show that the relationship between τ_{vf}/σ_{vo}' and ω is similar to that found in this study. However, the contrary is seen from Khan's (1979) data (see Fig. 4.18b). Samples of normally consolidated kaolin were tested under an effective vertical stress of 552 kPa, using a 12.7mm square vane over a range of rates of rotation between 0.44 and 8 °/min. The best-fit second order polynomial curve through Khan's results shows that τ_{vf}/σ_{vo}' increases with increasing ω. Khan offered no explanation for this observation.

Perlow & Richards (1977) observed differences between field and laboratory vane strength measurements obtained using a range of vane sizes (H = 12.7–203.2 mm, D = 12.7–101.6 mm, with H/D = 2), and rotation rates (ω = 7–79 °/min) on clayey-silt (San Diego Trough; I_P = 64%) and silty-clay (Gulf of Maine; I_P = 78%) soils. Although it was acknowledged that factors such as disturbance effects, soil anisotropy, drainage effects, and progressive failure might be important in the measurement of the strength of certain soil types, they believed that the effect of the above would be small compared to the influence of the vane tip velocity, v (= Rω), resulting from differences in the vane size and rotation rate. Subsequently, it was recommended that a vane tip velocity of v = 0.15 mm/sec be adopted as standard. However, this value of v corresponds to a rate of rotation of ω = 86 °/min for a 12mm square vane and would consequently result in the measurement of a partially drained strength when kaolin is tested.

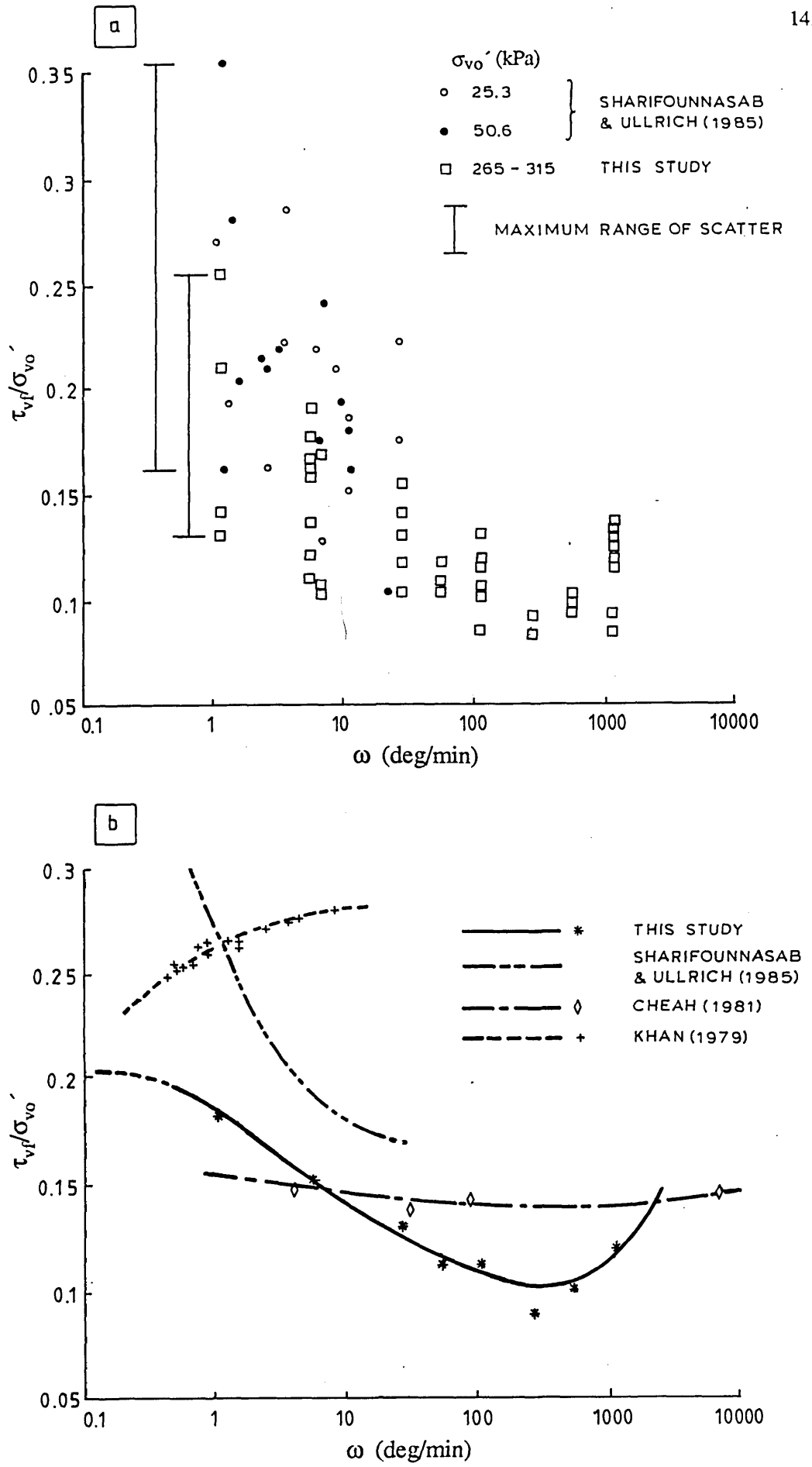


Fig. 4.18 Comparison of results of vane strain-rate effect studies using kaolin.

4.4.2F(v) Summary

Clearly, some of the scatter in the results of this study is due to differences in the age of the samples at the time of testing. However, even when this effect is considered, there remains significant differences between results of tests on the same sample, at the same rate of shearing, and at the same depth in the sample (see, e.g. test results denoted by X and Y on Fig. 4.12a). These differences are attributed to cavitation effects related to both diffusion effects during sample storage, and exposure of the samples to air during testing. Moreover, it is also highly likely that an appreciable amount of scatter is due to sample 'end effects', although no discernible trend could be found relating strength to the vane insertion depth.

The results of Sharifounnasab & Ullrich are only affected by different H/D ratios; there were no sample storage time effects. Nevertheless, these show as much if not more scatter than the results of this study, possibly as a result of cavitation effects following total stress removal.

Cheah presents only four data points and therefore no comment can be made about the scatter in his results.

The trend shown by Khan's data can be explained in terms of the value of the coefficient of consolidation, c_v; given that the samples were under a 552kPa vertical stress, it is reasonable to expect lower values of c_v compared to those for samples tested by the other investigators (see Fig. 3.9 and Section 4.4.5).

It is interesting that with increasing vane size the scatter in the results becomes less — the results of the 24mm vane tests show much less scatter than the 12mm vane test data, while Cheah's 19mm vane test results exhibit minimal scatter. In this regard, it is useful to note that when bigger vanes are used a larger volume of soil is subjected to shear, with the result that small-scale variations in the properties of the homogeneous samples tested are averaged out.

4.4.3 Tests on London clay

4.4.3A Introduction

London clay has different consolidation characteristics compared to kaolin (Sections 3.3.1A–D, and Tables 3.3 and 3.4) and therefore, series of tests were

conducted in order to (a) examine the effects of the rate of rotation on the measured strength, (b) determine the time to failure at which undrained conditions would prevail, and (c) verify and/or modify the hypothetical model outlined in Section 4.4.1 (Fig. 4.11).

The results of 12 and 18mm square vane tests on both normally consolidated and remoulded samples of London clay are presented herein. Although these results are not prone to 'sample age' effects (see Section 4.4.2F(ii)), the tests were carried out at different depths in the range z = 15–60 mm. Fig. 4.19 shows the results of tests on the former, in terms of τ_f/σ_{vo}' and t_f, while the data corresponding to tests on 2-day old and 47-day old remoulded samples are presented in Figs. 4.20a and b in terms of τ_f and t_f.

The coefficient of consolidation of London clay is low (Table 3.4) and consequently it was expected that the relationship between normalised vane strength and time to failure would show a minimum at a larger value of t_f than that found for kaolin. The relationships observed in Figs. 4.19 and 4.20 are discussed in the following Sections.

4.4.3B Normally consolidated London clay

In Section 4.3.3A it was shown that it is reasonable to average the results of vane tests carried out at the same rate of rotation as long as the individual shear stress – rotation ($\tau/\sigma_{vo}' - \theta$) curves were similar. Since this is the case here too, the averaged results are presented in Fig. 4.19, showing 12 and 18mm vane test data points in terms of mean values of τ_f/σ_{vo}' and corresponding mean values of t_f. The six 12mm and four 18mm vane test results were obtained from a total of 21 and 12 individual tests, respectively (see Tables 4.1b and b').

The curve through the 12mm vane test results shows a much better fit to the data than that corresponding to the 18mm vane. Nevertheless, it is evident that the results from both vane sizes conform to the general picture depicted by the 'drained side' of the hypothetical model illustrated in Fig. 4.11, where at a given time to failure lower strengths are measured with the larger vane. There is no indication of viscous rate effects at short times to failure. A similar $\tau_f/\sigma_{vo}' - t_f$ relationship was earlier observed in Section 4.4.2E when kaolin was tested at slow rates of rotation.

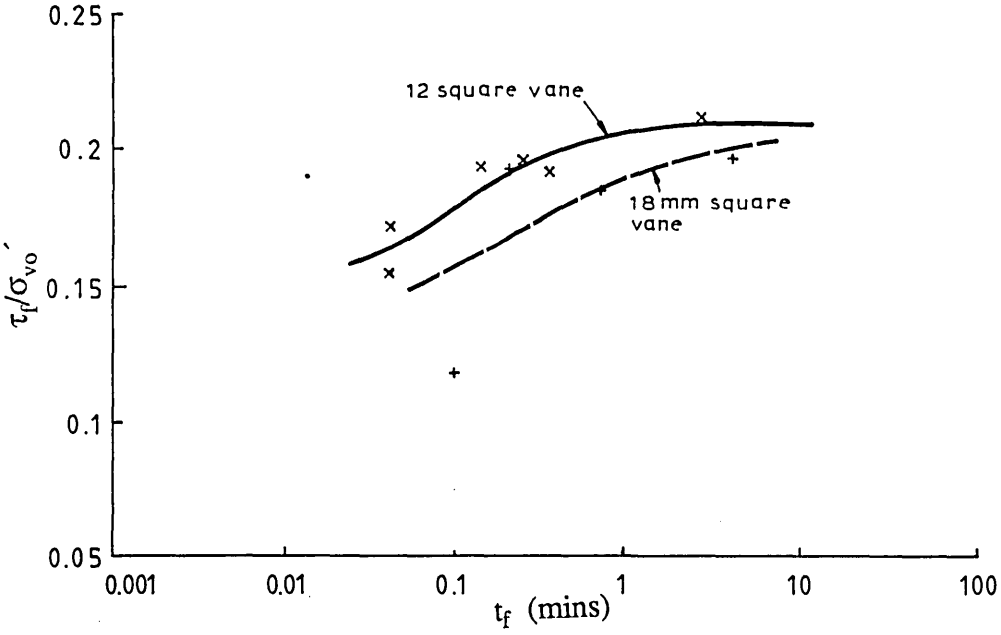


Fig. 4.19 Variation of peak vane strength with time to failure: Normally consolidated London clay.

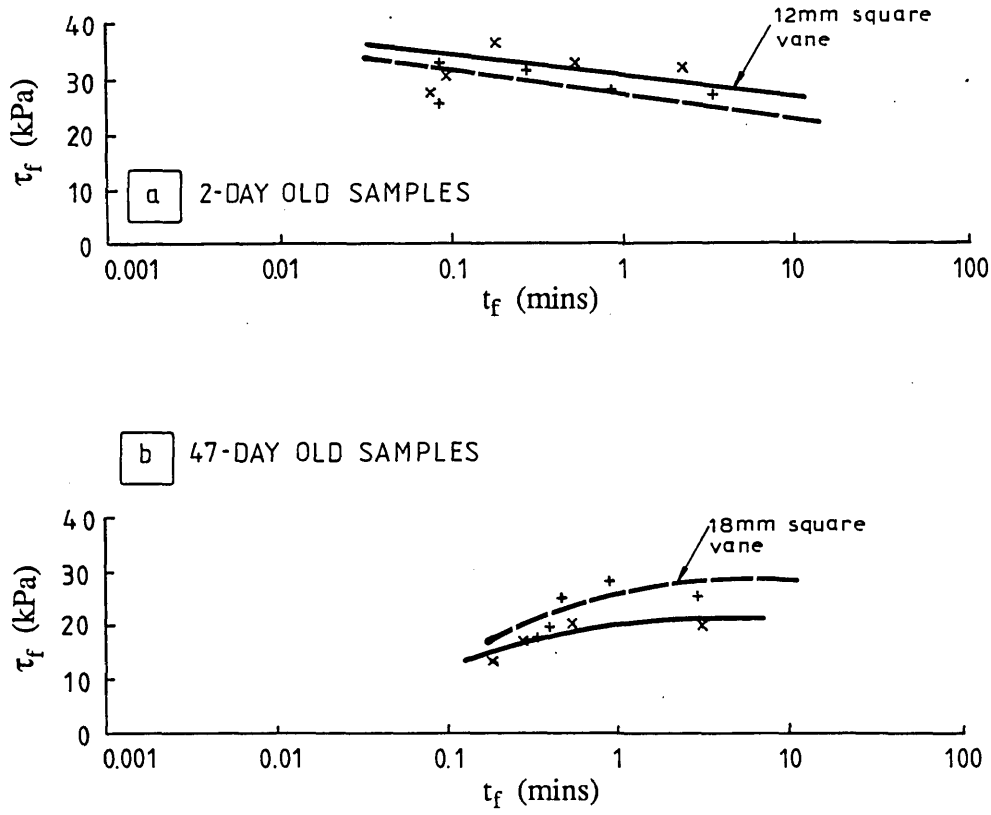


Fig. 4.20 Variation of peak vane strength with time to failure : Remoulded London clay.

4.4.3C Remoulded London clay

The results of 12 and 18mm vane tests on 2-day old and 47-day old samples of remoulded London clay are presented, in terms of mean values of τ_f* and t_f in Figs. 4.20a and b, respectively (see Tables 4.2c, c´, d and d´). Each data point represents an average of between two to four individual test results. [* The measured strengths are not normalised because the samples were remoulded and thus values of maximum consolidation stress (σ_{vo}´) were not known.]

Fig. 4.20a shows that as the time to failure decreases the measured vane strength generally increases, thus suggesting that viscous rate effects probably dominate the strength measurements. Both the 12mm and the 18mm vane test data portray this trend, although at given values of t_f, the 18mm vane strengths are slightly lower than those measured with the 12mm vane. It should be noted that at $t_f < 0.1$ mins, much lower strengths were measured than those suggested by the curves drawn through the data points.

It is particularly interesting that 47-day old samples show the opposite trend to that of 2-day old samples. Fig. 4.20b indicates the measurement of higher strengths as t_f increases, irrespective of vane size, and suggests the influence of drainage effects. It can be seen that the strengths measured at a given time to failure with the 18mm vane are higher than those corresponding to the 12mm one, thus inferring that greater pore pressure dissipation occurs with the larger vane size. Clearly, this observation is contrary to the relationship outlined in the hypothetical model in Fig. 4.11.

In order to explore possible reasons for this apparent difference in the behaviour of 2- and 47-day old specimens, the sample water contents (w) are plotted against the measured vane strengths (τ_f) in Figs. 4.21a and b respectively. It can be seen that there is little or no correlation between w and τ_f for samples of the same 'age', although there is a distinct division between the results for 2-day old samples and those for 47-day old samples.

However, Figs. 4.21c and d — which present the results of tests from 12mm vanes rotated at the standard rate of 6.27 °/min in 3-day old and 30-day old samples respectively (Section 3.4.5) — show the more commonly observed relationship between τ_f and w, with τ_f increasing as w decreases (see, e.g. Skempton & Northey, 1952). The results of 2- and 47-day old samples in which 12mm vanes were rotated at ω = 5.375 °/min are also shown in Figs. 4.21c and d respectively. For similar rates of rotation, the results from tests on 2-day old samples are more similar to those for 30-day old samples

than those for 3-day old samples, with a similar observation made with 47-day old samples showing greater consistency with the results of 3-day old samples than those of 30-day old samples.

The results of unconsolidated undrained (UU) triaxial compression tests* on 3-day old samples sheared at a rate of strain of 0.81 %/min (≈ 6.08 °/min) are shown in Fig. 4.21e, whilst Fig. 4.21f re-presents the lines of best-fit through the data in Figs. 4.21c–e. It can be seen that the strengths measured with the vane ($c_{u\,vane}$) are between 5 and 10% higher than those measured in the triaxial compression test ($c_{u\,UU}$) for the 3-day old samples. [* Note: In calculating the unconsolidated undrained triaxial strengths, it was assumed that the specimens deformed as 'right cylinders', i.e. allowance was made for the increase in cross-sectional area of each sample, with the assumption of no volume change during shear.]

The ratio of vane and UU strengths (of 1.05–1.10) is in good agreement with Chandler's (1988) relationship between V_r (= the ratio of field vane and K_0 consolidated triaxial compression strengths) and plasticity index, I_P, with V_r (= 0.55 + 0.008I_P) = 0.89, since I_P = 42% (Table 3.4). In this regard, it is of interest that the ratio of field vane to the UU strength measurements for an Indonesian silty clay having I_P = 60% is 0.89 (Mahmoud, 1988), which is lower than the value of V_r of 1.08. A comparison of vane and triaxial strengths will not be pursued further in this Thesis. Useful discussions on this topic can be found in Chandler (1988) and Mahmoud (1988).

Fig. 4.21f also shows that the vane strengths corresponding to 30-day old samples are between 8 and 20% higher than those corresponding to 3-day old samples, thus suggesting that the longer the sample is left in the perspex cylinder prior to testing, the stronger become the bonds between individual particles, and the higher is the strength which is subsequently measured with the vane.

In summary, the τ_f–t_f relationships observed in Figs. 4.20a and b show opposite trends for the same soil type, with viscous rate effects appearing to control the response of 2-day old samples, whilst consolidation effects seem to dominate the behaviour of 47-day old samples. It may be that the consolidation characteristics of remoulded London clay change significantly with time, exhibiting a behaviour similar to that of reconstituted London clay (see Figs. 4.19 and 4.20b); it can be seen from Fig. 3.9b that a 'normally consolidated' sample — which has inevitably 'aged' during one-dimensional consolidation from a slurry state initially — yields higher values of c_v during oedometer testing than a sample that is tested in an oedometer from a 'slurry' state.

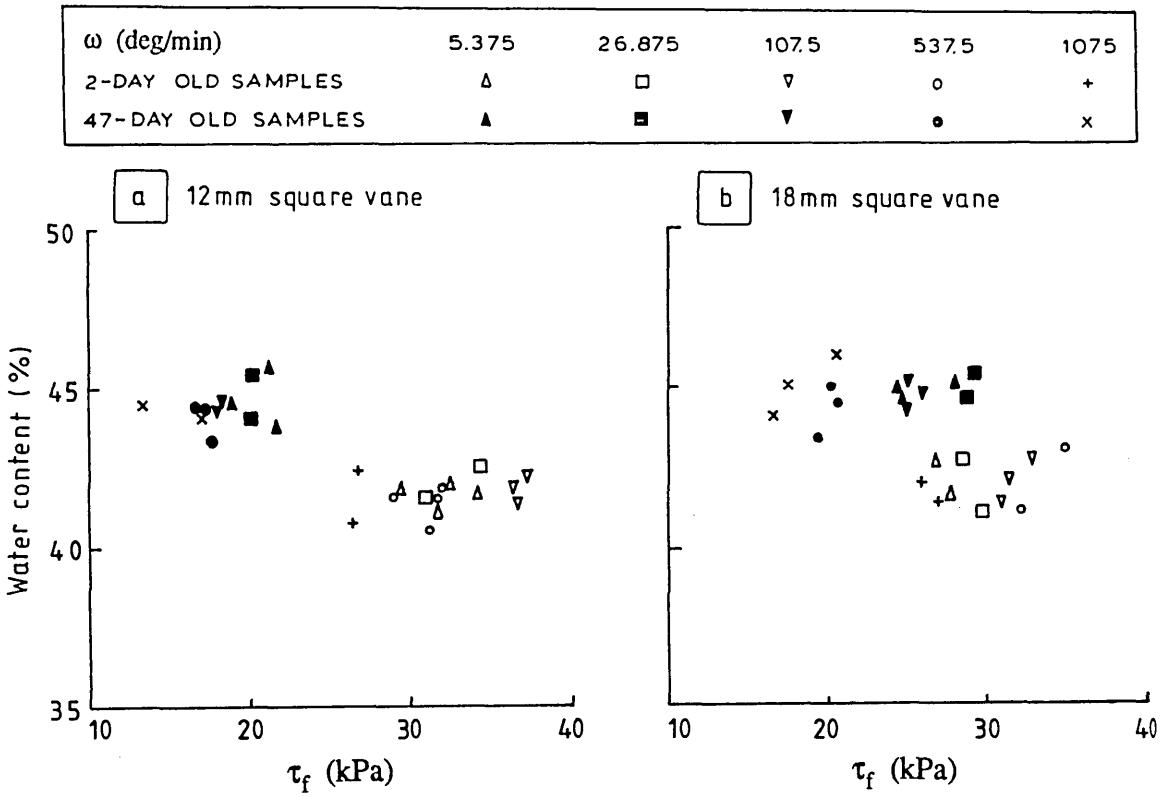


Fig. 4.21 Relation between sample water content and measured peak vane strength: Remoulded London clay.

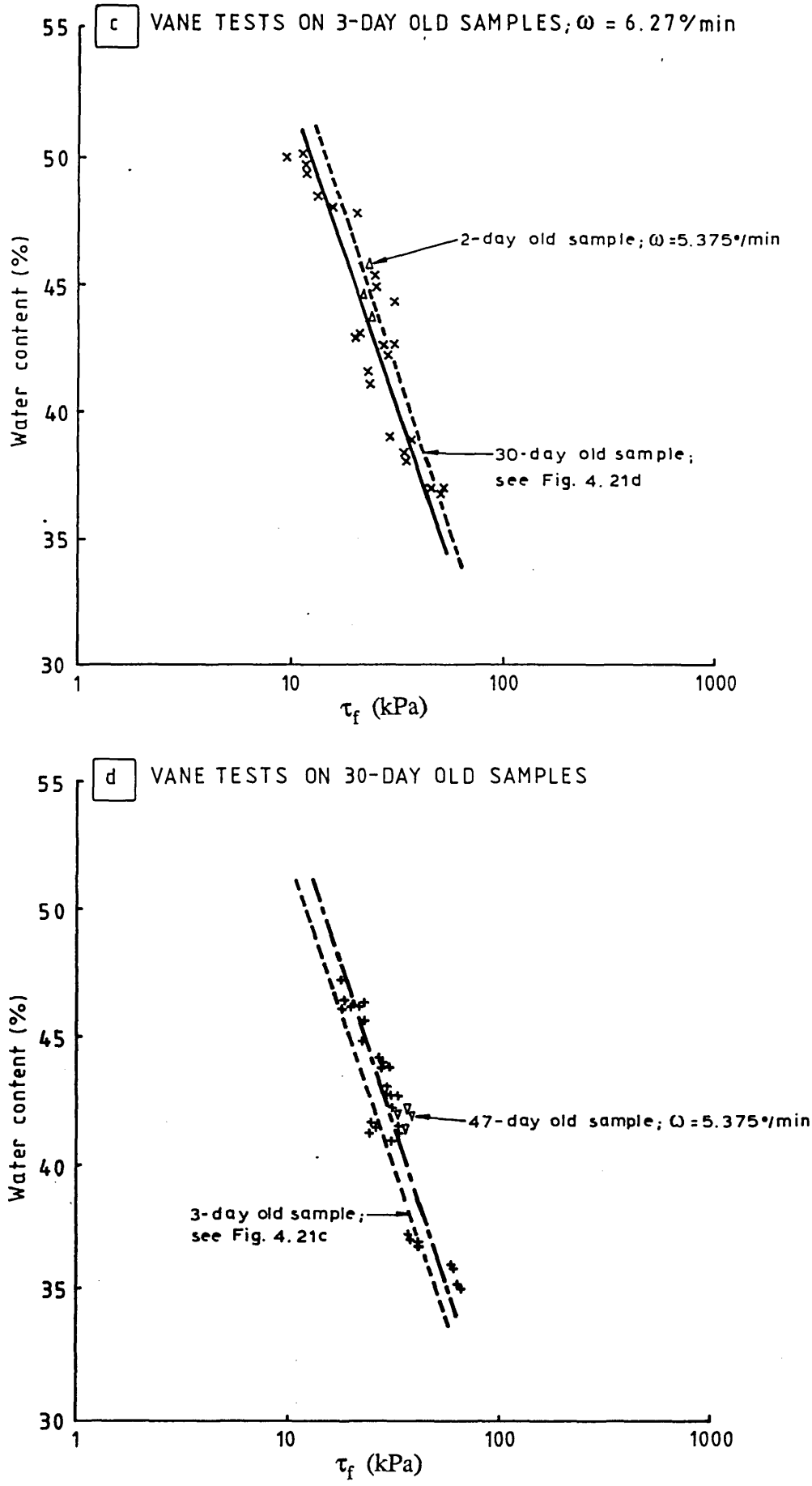
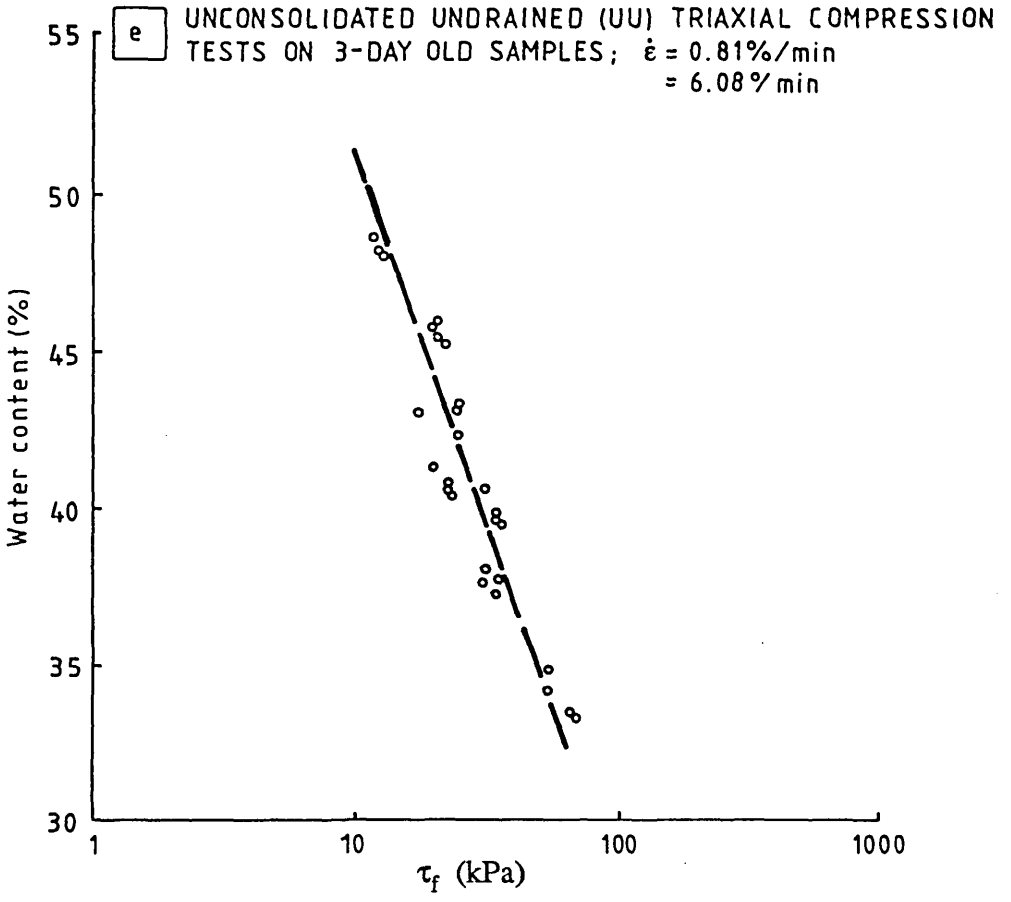


Fig. 4.21 Sample water content – measured strength relationships: Remoulded London clay.



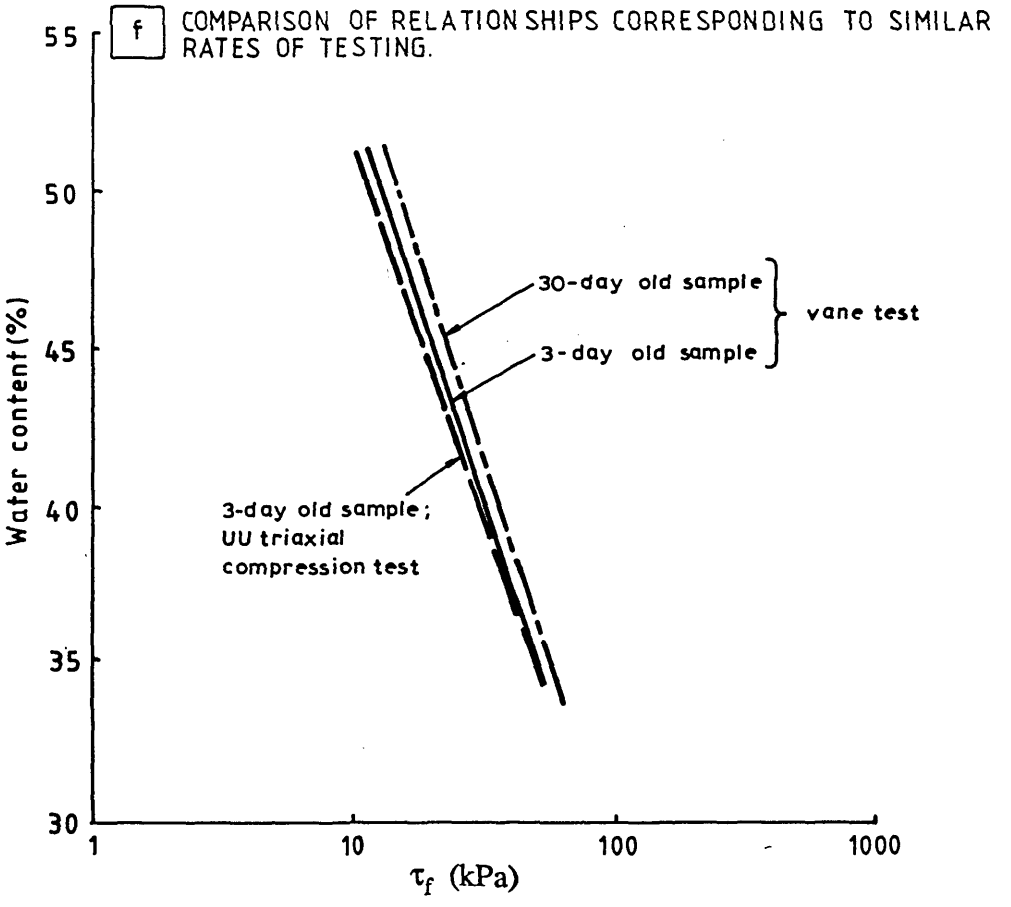


Fig. 4.21 Sample water content — measured strength relationships: Remoulded London clay.

However, as far as vane-size effects are concerned, the relationships for the 12 and 18mm vane test data of both the 2-day old and the 47-day old samples appear to deviate from the hypothetical model illustrated in Fig. 4.11. The writer is unable to offer an explanation for this apparent contradiction.

4.4.4 Tests on the Bentonite/London Clay Mixture

The results of 12 and 18mm square vane tests on normally consolidated samples of a bentonite/London clay mixture (Section 3.3.1E) are presented in Fig. 4.22 in terms of mean values of τ_f/σ_{vo}' and corresponding mean values of t_f. Each data point represents an average of two or three individual test results (see Tables 4.1e and e'). The storage time was 75 days for all the samples, while the vane insertion depths varied in the range z = 15–60 mm.

Fig. 4.22 shows higher values of τ_f/σ_{vo}' with decreasing times to failure for both vane sizes, with only a small amount of scatter in the results. The observed trends are typical of soils influenced by viscous rate effects, in accordance with the hypothetical model presented in Fig. 4.11, with the 18mm vane test data giving higher strengths than the 12mm vane at given values of t_f.

Samples of the bentonite/London clay mixture had a plasticity index of I_P = 145% (Table 3.5) and a coefficient of consolidation of about c_v = 0.018 m²/yr (Fig. 3.9).

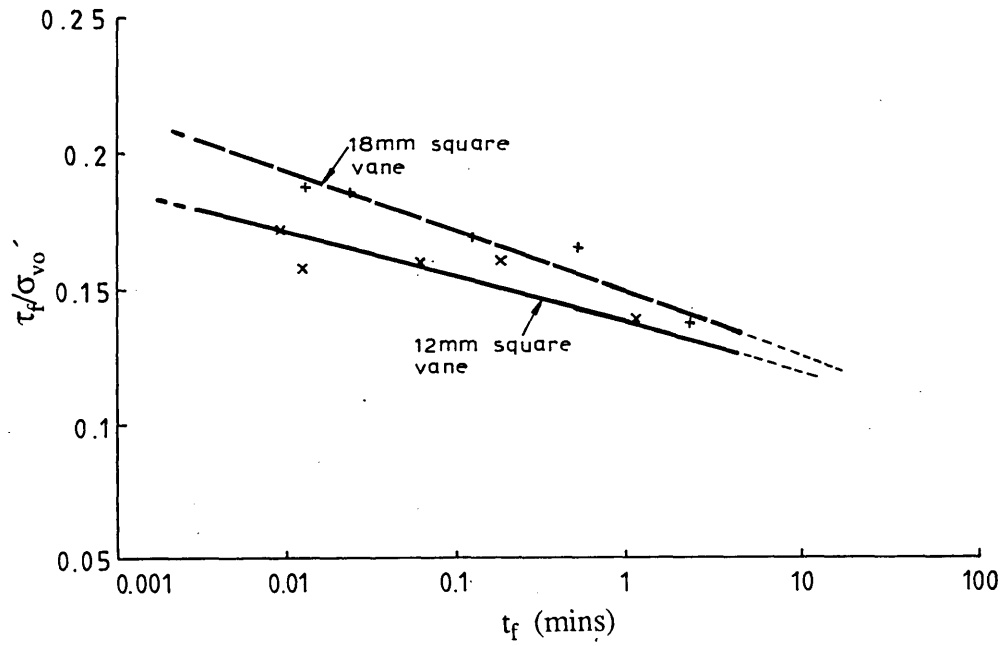


Fig. 4.22 Variation of peak vane strength with time to failure: Normally consolidated bentonite/London clay mixture.

4.4.5 Analysis of the Results

4.4.5A Introduction

Having verified the validity of the results of this study and consequently the trends observed, it is now the aim of this Section to see how the results compare with a number of theoretical considerations. Primarily, reference is made to the results of 12mm square vane tests on samples of normally consolidated Speswhite kaolin (see Section 4.4.2), since these showed good agreement with the hypothetical model described in Section 4.4.1.

4.4.5B Theoretical considerations

This Section presents two theories, due to Blight (1968) and Gibson & Henkel (1954), which can be considered to relate the influence of the rate of rotation on the measured vane strength to the amount of consolidation which occurs in the vicinity of the rotating vane.

4.4.5B(i) Blight's (1968) theory

Blight (1968) suggested a theory for the analysis of the vane test (see Appendix A2.2) and found that it agreed well with the experimental results of field vane tests in a silt. Although the theory is based on a number of simplifying assumptions (discussed in Appendix A2.4), Matsui & Abe (1981) concluded that their experimental data from reconstituted kaolin supported Blight's theory (Section 2.4). In addition, Chandler (1988) found the theory to yield good agreement with other field vane test data obtained by Roy & Leblanc (1988). It has further been shown that both the results of Pugh (1978) and those of Shibuya (1981) and Karube et al. (1988) agree well with the theory (Section 2.4).

Blight assumed that the maximum torque measured with the vane, M, is related to the degree of consolidation, U, at the vane periphery (and hence at radius R), such that:

$$U = \frac{M - M_0}{M_1 - M_0} \qquad \text{Eq. 4.3}$$

where M_0 is the torque with zero drainage, and

M_1 is the torque measured in very slow tests, in which U = 100%.

Consequently, it is possible to compare the theoretical solution, relating U to the time factor, T, with the results of vane tests of varying rates of rotation.

Blight's theory assumes that the excess pore pressures generated due to vane rotation are uniform within a 'sphere of influence' of radius a, centred on the mid-point of the vane. The pore pressures at a radius r (see Fig. 4.23a) from the centre of the sphere of influence are then given by:

$$u = \frac{A\gamma_w}{k}\left[\frac{(a^2 - r^2)}{6} + \frac{2}{\pi^3}\frac{a^3}{r}\sum_{n=1}^{\infty}\frac{(-1)^n}{n^3}\sin\frac{n\pi r}{a}\, e^{-n^2\pi^2 c_v t / a^2}\right] \qquad \text{Eq. 4.4}$$

where A = rate of change of pore water volume per unit time per unit volume of soil and thus has dimensions of $[T]^{-1}$ (see Appendix A2.2).

The degree of dissipation of pore pressures is given by Gibson & Henkel (1954) as:

$$U = 1 - \frac{u_f}{u_o} \qquad \text{Eq. 4.5}$$

where u_f = excess pore pressure at failure, i.e. at $t = t_f$, and
u_o = maximum excess pore pressure generated due to vane rotation.

At $t = t_f$, therefore, Eq. 4.4 becomes:

$$u_f = \frac{A\gamma_w}{k}\left[\frac{(a^2 - r^2)}{6} + \frac{2}{\pi^3}\frac{a^3}{r}\sum_{n=1}^{\infty}\frac{(-1)^n}{n^3}\sin\frac{n\pi r}{a}\, e^{-n^2\pi^2 c_v t_f / a^2}\right] \qquad \text{Eq. 4.6}$$

But it is shown in Appendix A2.2 that:

$$\frac{A\gamma_w}{k} = \frac{u_o}{c_v t_f} \qquad \text{Eq. 4.7}$$

Hence, Eq. 4.6 may be written as:

$$\frac{u_f}{u_o} = \frac{1}{c_v t_f}\left[\frac{(a^2 - r^2)}{6} + \frac{2}{\pi^3}\frac{a^3}{r}\sum_{n=1}^{\infty}\frac{(-1)^n}{n^3}\sin\frac{n\pi r}{a}\, e^{-n^2\pi^2 c_v t_f / a^2}\right] \qquad \text{Eq. 4.8}$$

Given that stress concentrations occur predominantly at the tips of the blades of the vane (Menzies & Merrifield, 1980) and thus the vane shears the soil primarily at its periphery, the maximum excess pore pressures can also be expected to develop along the

vane perimeter. It follows, therefore, that the value of the excess pore pressure which is of immediate importance in the analysis is that at r = D/2, where D = vane diameter.

In the assumptions made by Blight (Appendix A2.2), the surface of the sphere of influence is considered to be a drainage boundary, where excess pore pressures will equal zero. Blight suggested that the drainage boundary would probably lie between a = D and a = 3D/2.

After substituting for a and r in Eq. 4.8, the following expression was obtained for U when a = D and r = D/2:

$$U = 1 - \frac{1}{T}\left[\frac{1}{8} + \frac{4}{\pi^3}\sum_{n=1}^{\infty}\frac{(-1)^n}{n^3}\sin\frac{n\pi}{2}\,e^{-n^2\pi^2 T}\right] \qquad \text{Eq. 4.9}$$

Reasonable agreement was observed between the theoretical curve for a = D and the experimental one relating U (Eq. 4.9) to T*. On the basis of this evidence, Blight concluded that the empirical ('experimental') curve would be perfectly general and would apply to soils with any consolidation characteristics tested with any size vane, provided that the vanes have H/D = 2 (see Fig. 4.23b). [* In Blight's (1968) Fig. 5, the lower parts of the theoretical curve for a = D and the experimental curve should be transposed.]

4.4.5B(ii) Gibson & Henkel's (1954) theory

The solution for consolidation as a result of radial pore pressure dissipation in a triaxial sample with a height to diameter ratio of 2:1 has been presented by Gibson & Henkel (1954). The expression which relates the average degree of consolidation, U, to the time factor, T, for this case is:

$$U = 1 - \frac{1}{8\,T_a}\left[1 - 32\sum_{n=1}^{\infty}\frac{1}{\lambda_n^4}\,e^{-\lambda_n^2 T_a}\right] \qquad \text{Eq. 4.10}$$

where $T_a = c_v t_f / a^2$,

a = radius of a cylindrical triaxial sample, and

λ_n are the positive roots of Bessel's function of order zero (see Appendix A2.3).

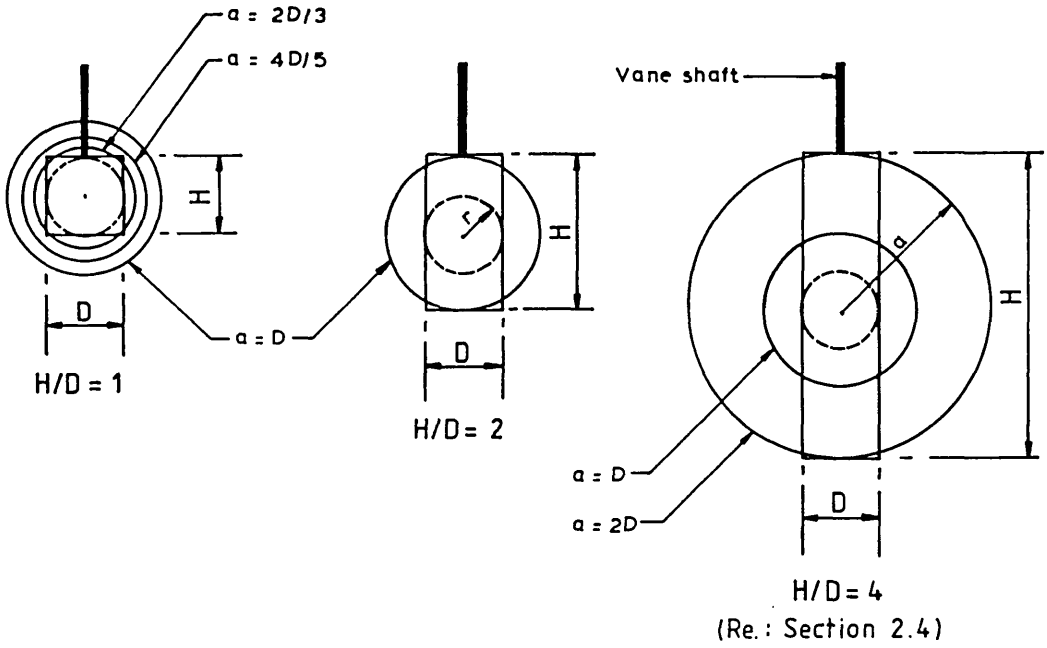


Fig. 4.23a 'Spheres of influence' for vanes of different H/D ratios.

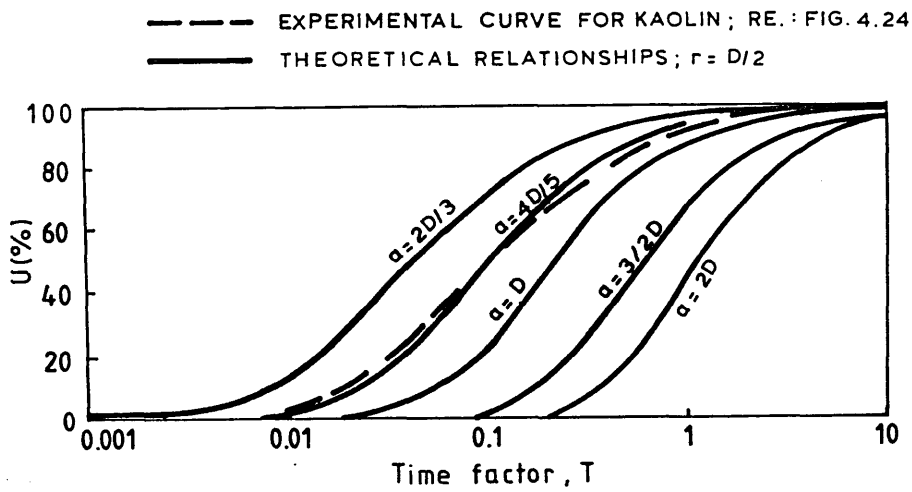


Fig. 4.23b Experimental and theoretical relationships, between average degree of consolidation, U and time factor, T.

4.4.5C Experimental considerations

The results of the vane tests in this study have been presented in terms of normalised maximum shear stresses, τ_f/σ_{vo}'. In order to compare the experimental results with both Blight's (1968) and Gibson & Henkel's (1954) theoretical relationships, values of τ_f/σ_{vo}' have to be related to the degree of consolidation, U. Therefore, Eq. 4.3 is expressed as follows:

$$U = \frac{V - V_0}{V_1 - V_0} \qquad \text{Eq. 4.11}$$

where $V = \tau_f/\sigma_{vo}'$ normalised with respect to $(\tau_f/\sigma_{vo}')_{max} = 0.19$ (Fig. 4.12b), and V_0 and V_1 are V at undrained conditions, and V at fully drained conditions corresponding to complete (i.e. 100%) consolidation, respectively.

By presenting the results in terms of V versus t_f, it is possible to establish V_0.

4.4.5C(i) Kaolin

Fig. 4.24 shows the relationship between average values of V and corresponding average values of t_f for the 12mm square vane test results. The curve through the data is equivalent to the curve established in Fig. 4.12b and is hereafter referred to as the 'experimental curve' for the 12mm vane test data. The value of V_0 is given as 50%. The experimental curve is replotted in terms of U and T in Fig. 4.23b; c_v having been taken as 9 m^2/yr, which is an average value for the range of consolidation stresses used in this study (see Fig. 3.9).

Figs. 4.23b and 4.25 show a number of theoretical curves together with the experimental curve. These include curves which correspond to

(a) Blight's theory with a variety of boundary conditions,
(b) an alternative theory based on Blight's approach, and
(c) Gibson and Henkel's theory for the relationship between average degree of consolidation and time factor for a triaxial sample with radial drainage conditions.

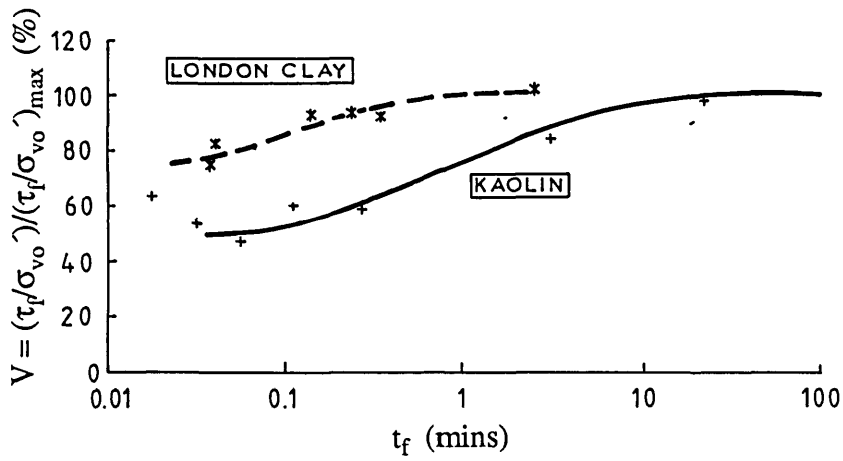


Fig. 4.24 Normalised vane strength, V versus time to failure, t_f.

Fig. 4.23b shows the theoretical curve for a = D and r = D/2, obtained using Eq. 4.9 (and not by superimposing Blight's corresponding curve). Although the experimental curve obtained from the results of this study shows a similar trend to the above theoretical relationship, the former lies to the left of the theoretical curve. This is due to the difference in the H/D ratios of the vanes. Blight used vanes with H/D = 2, for which the sphere of influence of radius a = D encompasses the vane and represents the zone affected by the vane, whilst in this study, the vanes had H/D = 1. For the latter (see Fig. 4.23a), a sphere of influence of radius a = D suggests that a comparatively bigger volume of soil is involved in the consolidation process. The 'sphere' whose radius appears to encompass a vane with H/D = 1 is that for which a = 2D/3.

The relationship between U and T for the case where a = 2D/3 and r = D/2 has been derived by the writer and is presented in Appendix A2.2 (see Eq. A2.15). The corresponding curve is shown in Fig. 4.23b; it lies to the left of the experimental curve, thus suggesting that the radius of the sphere of influence for vanes with H/D = 1 probably lies between a = 2D/3 and a = D. The expression for U in terms of T for the case of a sphere with a = 4D/5 and r = D/2 has also been derived by the writer (Eq. A2.16). Fig. 4.23b shows that this theoretical relationship is in close agreement with the experimental curve.

However, if the size of the vane relative to the sample height is of comparable proportions, it is more appropriate to analyse the vane test in terms of analogy to an infinite cylinder rather than a sphere. Under such circumstances, migration of the pore water away from the shear zone would occur mainly radially. Consequently, an alternative simplified theory of consolidation for the vane test might assume that pore pressure generation would occur within an infinite cylinder circumscribed by the vane diameter. The theoretical solution for the case of an infinite cylinder with a = 4D/5 and r = D/2 is presented as Eq. A2.20 in Appendix A2.3. It can be seen from Fig. 4.25 that there is little difference between the 'infinite cylindrical' relationship and the 'spherical' relationship with a = 4D/5 and r = D/2, since the experimental curve lies between these theoretical curves at values of T in the range 0.1 to 10. However, at values of $T < 0.1$, the experimental curve lies to the left of both these theoretical relationships, showing a better agreement with that corresponding to the spherical case.

Nevertheless, the zone affected by the vane is in most cases rather small compared to the volume of soil surrounding the vane, and therefore, it is more likely that the generation of pore pressures would occur within a three-dimensional zone more similar to the sphere than the infinite cylinder. Fig. 4.25 seems to support the above supposition.

Fig. 4.25 also shows the theoretical relationship corresponding to Gibson & Henkel's (1954) consolidation expression (Eq. 4.10). At values of T > 0.06, there seems to be good agreement between this theoretical curve and that corresponding to the spherical case with a = 2D/3 and r = D/2.

4.4.5C(ii) London clay

The experimental results of 12mm square vane tests are presented in terms of V (= $(\tau_f/\sigma_{vo}')/(\tau_f/\sigma_{vo}')_{max}$) against t_f in Fig. 4.24; according to Fig. 4.19, $(\tau_f/\sigma_{vo}')_{max}$ = 0.21. The curve drawn through the data is equivalent to the curve in Fig. 4.19 and gives V_0 = 75%. This same ('experimental') curve is replotted in terms of U and T in Fig. 4.26; the value of c_v having been taken as 0.275 m^2/yr (see Fig. 3.9). It is clear that the 'experimental' curve does not at all agree with the theoretical relationship with a = 4D/5 and r = D/2. However, this large disagreement would be rectified if the 'experimental' curve is shifted through approximately two log cycles. This requires the value of the coefficient of consolidation of London clay to be about two orders of magnitude higher than the value measured in the laboratory, thus implying that the London clay tested probably had c_v values in the range 25–75 m^2/yr . Although it is reasonable to presume that the London clay tested might have had c_v values higher than 0.275 m^2/yr — especially in the horizontal (radial) direction — by as much as one order of magnitude, it is difficult to believe that they might be as much as two orders of magnitude greater.

Despite this, there is no doubt that the results show a variation of measured strength with time to failure typical of a clay influenced by drainage effects. Therefore, part of the disagreement between the 'experimental' and 'theoretical' curves would be explained by suggesting that the c_v value was higher than 0.275 m^2/yr by one order of magnitude. This, however, would still leave the 'experimental' curve lying to the left of the theoretical relationship by one log cycle, and it is this discrepancy between the experimental and theoretical curves which the writer is unable to explain.

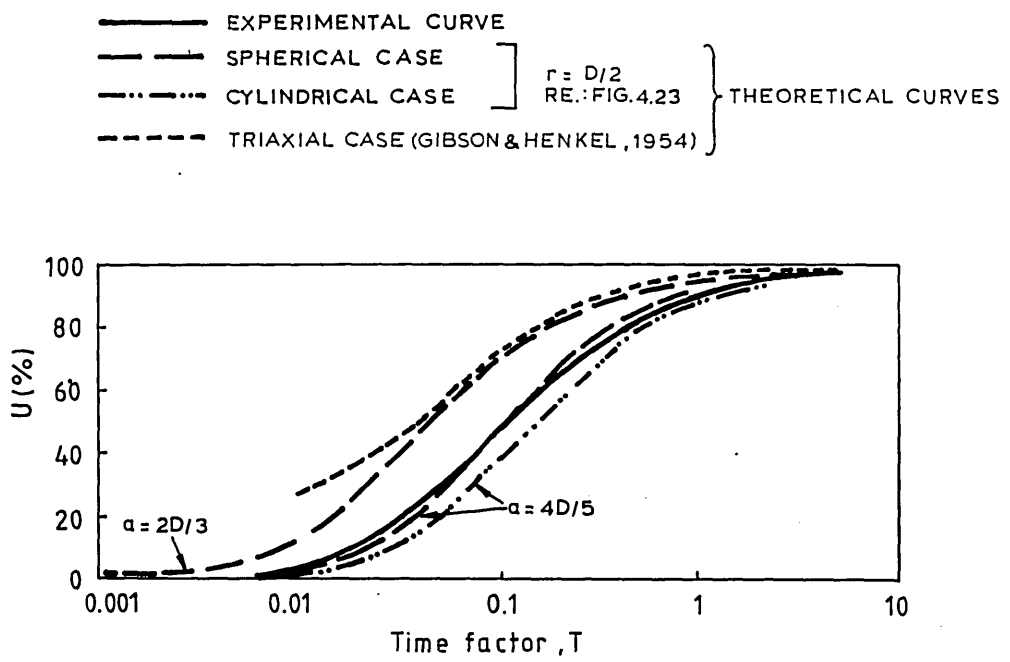


Fig. 4.25 Comparison of theoretical and experimental drainage curves: Normally consolidated kaolin.

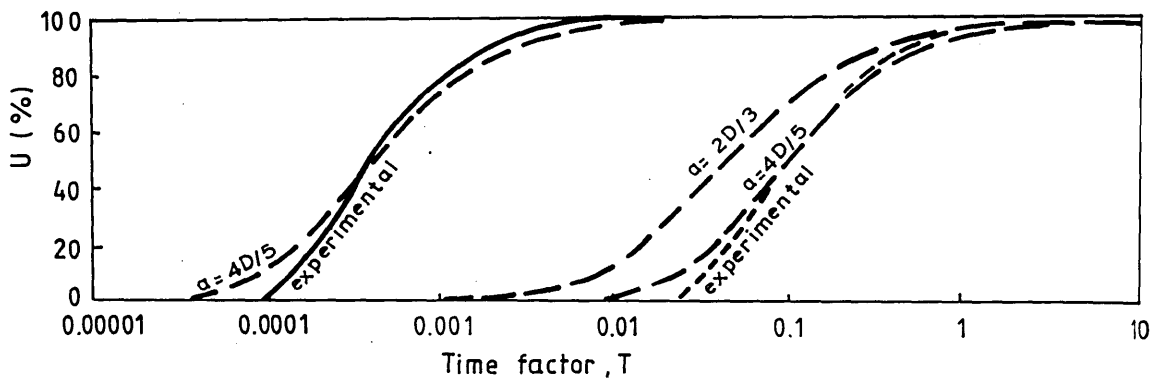


Fig. 4.26 Comparison of theoretical and experimental drainage curves: Normally consolidated London clay.

4.4.6 Summary

It has been seen in Sections 4.4.2, 4.4.3 and 4.4.4 that the rate of vane rotation (which results in different times to failure) has a marked influence on the measurement of the vane shear strength (see Figs. 4.12–4.14, 4.19, 4.20 and 4.22). The relationship between the measured vane strength and time to failure is apparently governed by drainage effects at long times to failure, and viscous effects at short times to failure. Good agreement is found when the relationships are compared in terms of a hypothetical model (Fig. 4.11). For soils in which the effective normal stresses acting on the shear zone increase with increasing times to failure, this model suggests that:

(a) at slow rates of rotation which result in drainage around the vane, the time to failure is a function of the square of the diameter of the vane, since it is presumed that the drainage path length is proportional to the vane diameter, D, while

(b) at fast rates of rotation, with subsequent viscous effects governing soil behaviour, the time to failure is a function of D.

Since the main objective of this study was to establish the rate of vane rotation required to ensure undrained conditions, the experimental results lying on the drained side of the hypothetical model (Fig. 4.11) were compared with a number of theoretical relationships (Figs. 4.23–4.26). It was found that Blight's (1968) simple theory agreed well with the experimental results of vane tests on normally consolidated samples of kaolin, provided that the H/D ratio of the vane being used was taken into account.

Fig. 4.27 is a summary diagram showing the relationships between τ_f/σ_{vo}' and t_f corresponding to the results of 12mm square vane tests on normally consolidated samples of kaolin, London clay and the bentonite/London clay mixture. The times to failure at which undrained conditions would be ensured have been established for all three soils. It is suggested from the theoretical relationship with a = 4D/5 (and r = D/2) that undrained conditions would apply at $T \leq 0.015$, corresponding to an average degree of dissipation of pore pressure, $U \leq 5\%$ (Fig. 4.23b). From $t_f = TD^2/c_v$, estimates of times to failure at which the minimum strength would be measured have been calculated using the measured values of c_v = 9, 0.275 and 0.018 m^2/yr, as t_f = 0.126, 4.2 and 63 mins, respectively for kaolin, London clay and the bentonite/London clay mixture. In the case of kaolin there is good agreement between the time to failure at which the minimum strength is measured experimentally and that calculated using the above theoretical relationship. Also, the experimental curve of the bentonite/London clay mixture may be extrapolated to give a minimum strength at the 'estimated' time to failure of 63 minutes. However, in the case of London clay, there is a large discrepancy

between the experimental and theoretical estimates of the time to failure at which the minimum strength would be obtained.

In this regard, it should also be noted that the unexpected vane strength – time to failure relationship for samples of normally consolidated London clay is also evident in the remoulded samples of this soil (Figs. 4.20 and 4.21). A possible explanation for this is that the coefficient of consolidation of London clay increases as the sample storage time increases.

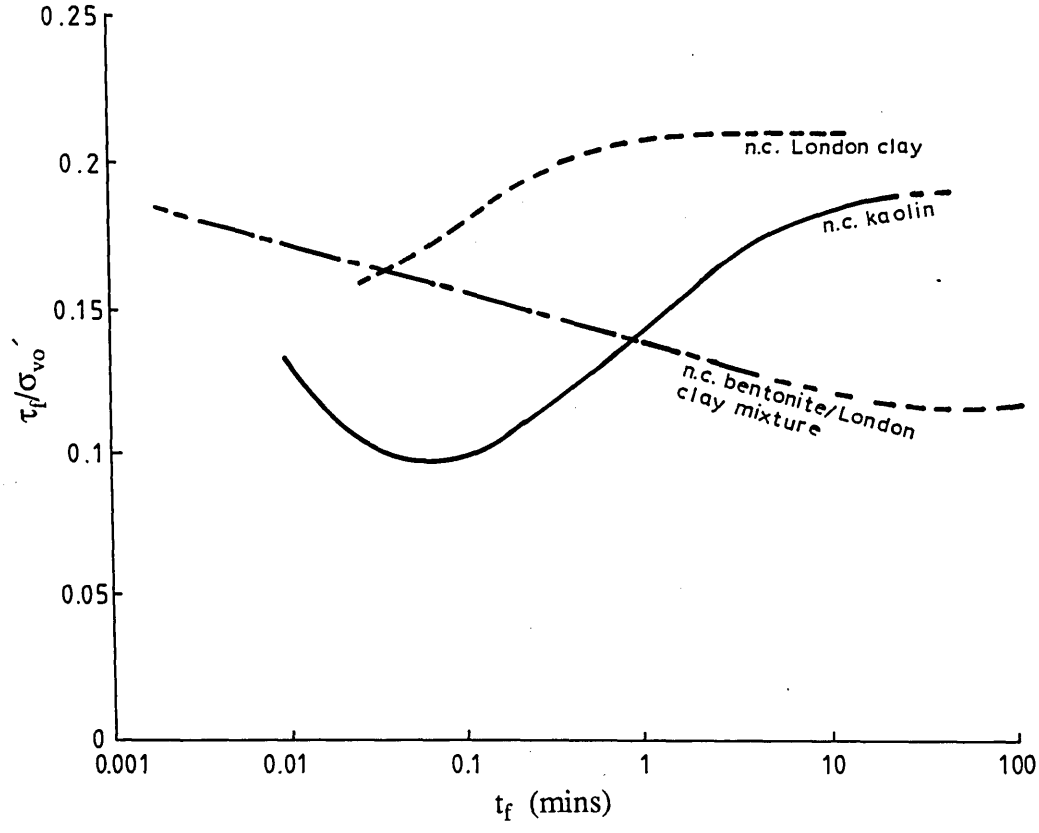


Fig. 4.27 Relationships between normalised peak vane strength and time to failure: 12 mm vane test data.

CHAPTER 5

THE BEHAVIOUR OF VANES WITH DIFFERENT NUMBERS OF BLADES

5.1 INTRODUCTION

The measurement of the undrained strength of soils using the vane is influenced by a number of factors which include (a) the interpretation of the test (Table 3.1), (b) the H/D ratio (Table 3.1), (c) the rate of vane rotation (Chapter 4), and (d) the number of blades on the vane.

In the past it has been suggested that a four-bladed vane would result in the best estimate of the undrained soil strength. However, very little work has been done to justify the use as standard of a vane with four blades. Two phenomena have been considered in this context. On the one hand, it is believed that with decreasing number of blades the possibility of progressive failure is enhanced, resulting from the increasing non-uniformity of the stress distribution around the vane. On the other hand, insertion disturbance effects, which increase as the number of blades increases, are also likely to result in the measurement of a lower shear strength. It is therefore necessary to establish the optimum number of blades which the vane should have in order to obtain the most reliable measurement of the strength of the soil.

This Chapter examines the effect of the number of blades on the behaviour of samples of two soft clays. It will be shown that the relationship between the number of blades and the measured vane strength is dominated by insertion disturbance effects when the number of blades is large, with little or no evidence that progressive failure effects control the relationship when the number of blades is small. In addition, it will become apparent that both the clay type and the vane size have a noticeable influence on the shear stress – rotation characteristics of soils tested with vanes having different numbers of blades.

5.2 TESTING PROGRAMME

A detailed account of the test programme is given in Section 3.4.2C. The tests investigated the effect of different numbers of blades on both the measured vane strength and the shear stress – rotation characteristics of normally consolidated samples of Speswhite kaolin and London clay at zero confining stress. The maximum vertical effective stress to which the samples were consolidated was the same as for the samples tested at different rates of rotation, with $\sigma_{vo}' =$ 250–300 kPa in the case of kaolin, and $\sigma_{vo}' =$ 145–215 kPa in the case of London clay (see Sections 4.2.2 and 4.2.3).

12 and 24mm square vanes with two, three, four and six blades were pushed into the samples to given depths in the range z = 20–60 mm, and rotated through 360° at a constant rate of rotation of (ω =) 6.27 °/min.

A supplementary series of tests was also conducted on kaolin using 12mm square vanes with eight and twelve blades, as well as with a 12mm diameter brass rod, in order to simulate a vane with an 'infinite' number of blades.

The repeatability of the results in each sample was checked.

5.3 SHEAR STRESS – ROTATION CHARACTERISTICS

5.3.1 Introduction

Vanes with the same number of blades yielded very similar shear stress – rotation characteristics. Consequently, throughout this Chapter the averaged shear stress – rotation curves (Section 4.3.3A) for vanes with the same number of blades are presented.

The vane strengths, τ_f, have all been normalised with respect to the maximum consolidation stress that each sample had experienced, σ_{vo}', thereby removing the effect of slight water content variations between the samples (see Section 4.3.2).

In order to examine the influence of the differences in vane size, angles of rotation at failure, θ_f, are plotted against both (a) the number of blades, n, and (b) the segmental distance around the vane periphery between adjacent blades, l (= $2\pi R/n$), where R is the radius of the vane.

A summary of the shear stress – rotation ($\tau/\sigma_{vo}' - \theta$) relationships obtained using the 12 and 24mm square vanes are given in Tables 5.1a and a′ and Tables 5.1b and b′, respectively corresponding to the kaolin and London clay test results; the averaged relationships are shown in Figs. 5.1a and a′ and Figs. 5.1b and b′ (see also Section 4.3.3). Figs. 5.2a and b present both the average [= $(\tau_f/\sigma_{vo}')_{av} = \Sigma(\tau_f/\sigma_{vo}')_i/n$] and the range of results of normalised shear strength, τ_f/σ_{vo}', versus n, whilst Figs. 5.3a and b show the relationships between angle of rotation at failure, θ_f, and n. The variation of θ_f with the segmental distance (l) can be seen in Figs. 5.4a and b. The average values of initial stiffness, K (= $(\tau_m/\sigma_{vo}')/\theta_m$, where τ_m and θ_m are as defined in Section 4.3.3A), and of 'residual' — large displacement — shear strength, τ_r/σ_{vo}' (corresponding to an angle of rotation of θ = 360°), are plotted against the number of blades in Figs. 5.5a and b and Figs. 5.6a and b, respectively.

5.3.2 Kaolin Test Results

Fig. 5.1a shows the averaged results of 12mm square vane tests in terms of normalised shear stress, τ/σ_{vo}', versus angle of rotation, θ; the results of the 24mm square vane tests are shown in Fig. 5.1a′. It is evident that with an increase in the number of blades the amount of rotation to reach failure decreases. It can also be seen that higher strengths are measured with vanes with fewer blades. Figs. 5.2a–5.6a are plotted to explore more fully the trends observed in Figs. 5.1a and a′ for 12 and 24mm square vanes.

The results of 37 tests with both 12 and 24mm vanes with numbers of blades in the range n = 2 to 12 are presented in Fig. 5.2a in terms of τ_f/σ_{vo}' and n; the Figure also shows the results of tests using a 12mm diameter brass rod. The trend is similar irrespective of vane size and shows that the measured strength is high with small values of n and decreases as n increases: the strength measured with a 12-bladed 12mm vane is about 40% less than that measured with one with two blades. The 24mm vane test data show a reduction in the measured strength of about 18% as the number of blades increases from 2 to 6; this proportional decrease in strength as n increases from 2 to 6 is the same for the 12mm vane test data. This trend can be explained in terms of soil disturbance effects due to insertion, which will be greater as the number of blades increases, thus resulting in the measurement of lower strengths.

When tested with a vane with the same number of blades, the 12mm square vane gives strengths which are more than twice the strengths measured with the 24mm vane. This may be explained as a drainage effect (Section 4.4.1). It was demonstrated in

Section 4.4.2F(iv) that partial drainage occurs in the vicinity of the vane when rotated at a rate of rotation of 6.27 °/min. Since the drainage path length is longer for the larger vane size, less consolidation takes place for a given rate of rotation and consequently a lower strength is measured.

The relationship between the angle of rotation required to reach peak torque, θ_f, and the number of blades (n) on the vane is shown in Fig. 5.3a. It is seen that larger angles of rotation are required to reach failure as the number of blades is reduced. Where $n \geq 8$, the rotation required is more-or-less constant at 10°, regardless of the size of the vane. Although the relationships for the 12 and 24mm vanes converge as n increases, different relationships apply for $n \leq 6$; these show that at the same number of blades the 24mm vane reaches failure at significantly larger angles of rotation than the 12mm vane.

In order to examine whether this is a linear scale effect, the data may be plotted against the segmental distance, l (Fig. 5.4a). In this case it can be seen that the rotation required to reach peak torque increases as the segmental distance is increased. Although the lines for the two different vane sizes in Fig. 5.4a do not differ all that much, it appears — on the basis of the trends obtained in Fig. 5.4b for London clay — that the difference between the relationships for the two different vane sizes observed in Fig. 5.3a is not due to a linear scale effect.

The slope of the initial part of the average shear stress – rotation curves, K, has been calculated from $K = (\tau_m/\sigma_{vo}')/\theta_m$, with $\tau_m/\sigma_{vo}' = 0.05$. The trend which emerges from Fig. 5.5a shows that K increases with n in the range n = 2–6 and thereafter it decreases with increasing values of n, reaching a low value for the 12mm diameter brass rod. The 12mm square vanes show a much stiffer response than the 24mm vanes.

Fig. 5.6a shows the relationship between normalised 'residual' strength, τ_r/σ_{vo}', and n. The effect of the number of blades on the measured strength after 360° rotation is seen to be negligible. However, there is a vane-size effect, with the smaller vanes measuring a higher 'residual' strength than the larger ones.

5.3.3 London Clay Test Results

Figs. 5.1b and b´ respectively show the results of 12 and 24mm square vane tests in terms of normalised shear stress, τ/σ_{vo}', and angle of rotation, θ (see also Tables 5.1b and b´). The trends which emerge are not as systematic as those seen in the case of vane tests on kaolin (Figs. 5.1a and a´); this may be due to differences in the samples, possibly arising from the much longer period of time taken for the one-dimensional consolidation of London clay, in which case the London clay samples might have 'aged'. Data extracted from Figs. 5.1b and b´ are presented in Figs. 5.2b–5.6b.

A total of fifteen 2-, 3-, 4-, 6- and 8-bladed 12mm and four 2-, 4- and 6-bladed 24mm square vane tests were carried out; the mean values of the strengths measured with vanes with the same number of blades are presented as τ_f/σ_{vo}' versus n in Fig. 5.2b. Although the 12mm square vanes measure higher strengths than the 24mm vanes having the same number of blades, both vane sizes display a similar trend of behaviour. However, the 12mm vane test data show a greater decrease in strength as the number of blades increases: the strength measured with an 8-bladed 12mm vane is about 20% less than that measured with a 2-bladed vane.

The relationship between the angle of rotation at failure, θ_f, and number of blades, n, is presented in Fig. 5.3b. Clearly, smaller angles of rotation are required to reach failure as the numbers of blades increases. Despite the sparsity of the 24mm vane test data, the results show that the larger vanes require larger angles of rotation to reach failure than the smaller vanes with the same number of blades.

Fig. 5.4b shows the relationship between the angle of rotation at failure, θ_f, and segmental distance, l. At small values of l, values of θ_f are also small but as the segmental distance increases so too does the angle of rotation required to reach peak torque. Furthermore, it seems reasonable to suggest that there are two distinct 'classes' of data, since the lines through the 12 and 24mm vane test results are different.

The relationship between the slope of the initial part of the shear stress – rotation curve (K) and n is shown in Fig. 5.5b; $\tau_m/\sigma_{vo}' = 0.05$. Values of K are almost constant in the range n = 2 to 8, reach a maximum between n = 3 and 6, and then decrease with increasing values of n. The trend through the 24mm vane test data is similar to that for the 12mm vane, although the soil is much 'softer' at similar values of n.

Fig. 5.6b presents the relationship between the normalised 'residual' strength (τ_r/σ_{vo}') and n. Despite the scatter of the data points, it is reasonable to suggest that the measured residual strengths are similar irrespective of the number of blades, with the smaller vane measuring slightly higher values of τ_r/σ_{vo}' than the larger vane.

5.3.4 Summary

The effect of the number of blades on the shear stress – rotation characteristics of the vane tests on Speswhite kaolin (Section 5.3.2) and London clay (Section 5.3.3) can be summarised as follows:

(i) The relationships between the measured vane strength and number of blades for both Speswhite kaolin and London clay show a decrease in strength with an increase in the number of blades. The 24mm square vane test data also show the same trend, although, due to a drainage effect, the 24mm vanes measure lower strengths than do the 12mm vanes with the same number of blades.

(ii) The angle of rotation at failure, θ_f, decreases with increasing number of blades, n. With the same number of blades, the 24mm vanes require much larger angles of rotation to reach failure than the 12mm vanes. The θ_f–n relationship is the same for both Speswhite kaolin and London clay.

(iii) The effect of vane size on the θ_f–n relationship is important because it is still noticeable when the results are presented in terms of θ_f versus the segmental distance, l. At small values of l (large n), small angles of rotation to failure are observed; these increase with increasing values of l. At any particular l, lower values of θ_f are obtained with the 24mm vane than with the 12mm vane.

(iv) The slope of the initial part of the shear stress – rotation curve, K, is small at small values of n, but increases with increasing values of n until it reaches a maximum at n = 6; thereafter K decreases with further increases in n. The effect of n on K is also evident in the 24mm vane test data, although to a much smaller extent. For vanes with the same number of blades, the larger diameter vanes seem far 'softer' than the smaller ones. The observed trend is similar for both Speswhite kaolin and London clay.

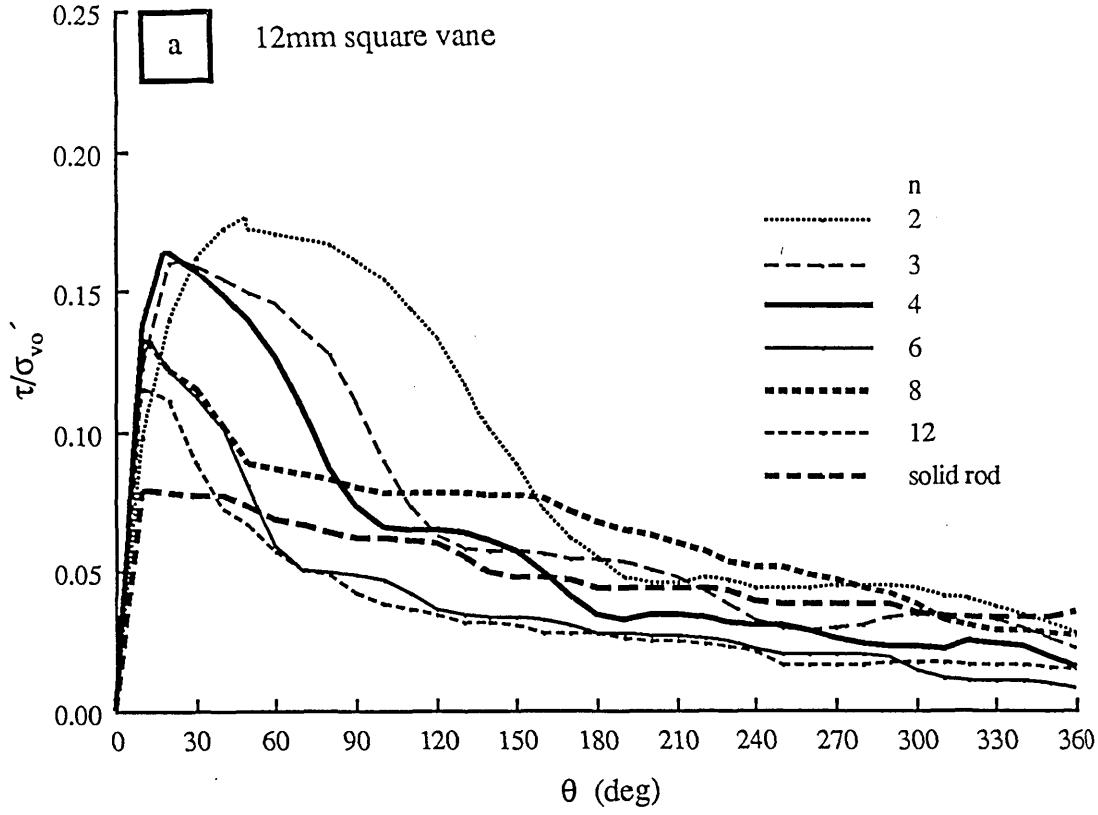
(v) Values of normalised shear strength after 360° rotation, τ_r/σ_{vo}', do not appear to be affected by the number of blades on the vane. Despite greater scatter in the results of tests on London clay (see Fig. 5.6b), the τ_r/σ_{vo}' – n relationship is similar to that observed in the tests on Speswhite kaolin, where the data indicate that τ_r/σ_{vo}' is almost independent of n. A vane-size effect is apparent in that the 12mm vane yields higher strengths than the 24mm vane.

Table 5.1a 12mm square vanes with different numbers of blades tested in normally consolidated kaolin.

No. of Blades	No. of Tests	θ_f			τ_f/σ_{vo}'			τ_r/σ_{vo}'	Segmental distance, l (mm)	Perimeter Ratio, α (%)	Area Ratio A_r (%)
		Average (deg)	Range (deg)		Average	Range		Average			
2	6	48.4	36.2	60	0.1755	0.1446	0.1944	0.0271	18.85	2.42	10.57
3	6	25.2	20	25.3	0.1609	0.1409	0.1803	0.0216	12.57	3.64	12.35
4	6	18.2	14.5	20	0.1636	0.1135	0.1944	0.015	9.43	4.85	14.13
6	5	12.9	12.1	14.7	0.1325	0.1136	0.1506	0.0076	6.28	7.27	17.7
8	2	12.2	8.8	15.6	0.132	0.1038	0.1607	0.0267	4.71	9.7	21.26
12	3	11	8.8	15.3	0.1149	0.0916	0.1368	0.0147	3.14	14.55	28.4
solid rod	2	12.3	10	14.5	0.0792	0.0708	0.0879	0.0353	0	100	100

Table 5.1a′ 24mm square vanes with different numbers of blades tested in normally consolidated kaolin.

No. of Blades	No. of Tests	θ_f			τ_f/σ_{vo}'			τ_r/σ_{vo}'	Segmental distance, l (mm)	Perimeter Ratio, α (%)	Area Ratio A_r (%)
		Average (deg)	Range (deg)		Average	Range		Average			
2	2	87.4	84.7	90	0.0714	0.0618	0.0809	0.0115	37.7	1.21	3.85
3	2	54.6	52.6	56.6	0.0778	0.0652	0.0904	0.0153	25.13	1.82	4.91
4	2	40.9	35.6	46.3	0.0725	0.0683	0.0766	0.0119	18.85	2.43	5.96
6	1	20	–	–	0.0635	–	–	0.0118	12.57	3.64	8.06



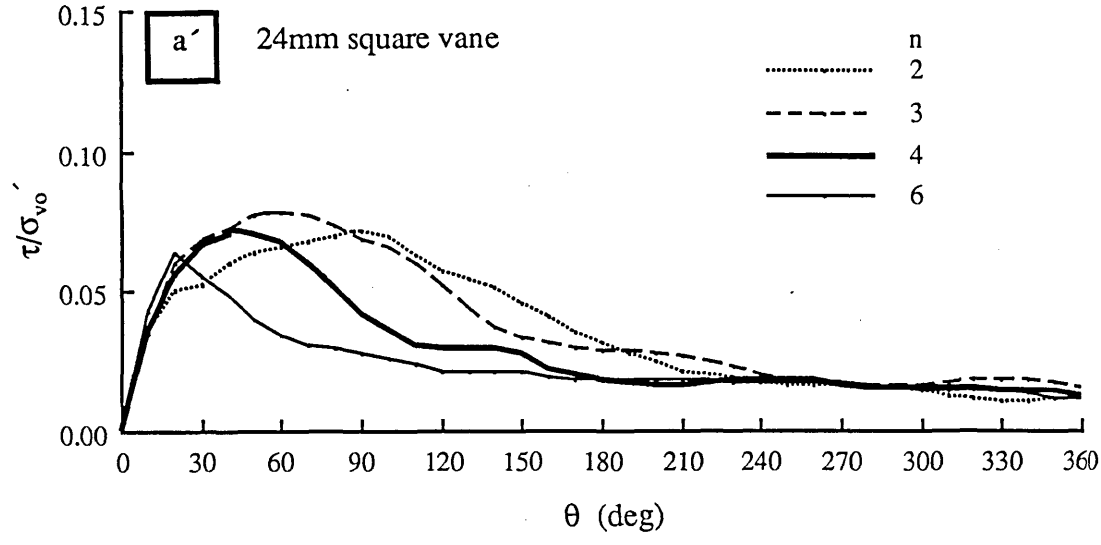


Fig. 5.1 Normalised shear stress — rotation curves for tests in normally consolidated kaolin: Averaged test results ; $\omega = 6.27°/min.$

Table 5.1b 12mm square vanes with different numbers of blades tested in normally consolidated London clay.

No. of Blades	No. of Tests	θ_f			τ_f/σ_{vo}'			τ_r/σ_{vo}'	Segmental distance, l (mm)	Perimeter Ratio, α (%)	Area Ratio A_r (%)
		Average (deg)	Range (deg)		Average	Range		Average			
2	3	66.7	60	70	0.1681	0.1449	0.2035	0.0829	18.85	2.42	10.57
3	3	33.3	20	50	0.1701	0.1498	0.2046	0.0871	12.57	3.64	12.35
4	3	16.7	10	20	0.1422	0.1367	0.1487	0.0515	9.43	4.85	14.13
6	3	9.4	8.2	10	0.1548	0.1367	0.173	0.056	6.28	7.27	17.7
8	3	10.6	5.6	20	0.1426	0.1197	0.1713	0.072	4.71	9.7	21.26

Table 5.1b′ 24mm square vanes with different numbers of blades tested in normally consolidated London clay.

No. of Blades	No. of Tests	θ_f			τ_f/σ_{vo}'			τ_r/σ_{vo}'	Segmental distance, l (mm)	Perimeter Ratio, α (%)	Area Ratio A_r (%)
		Average (deg)	Range (deg)		Average	Range		Average			
2	1	70	–	–	0.1207	–	–	0.0647	37.7	1.21	3.85
4	2	45	30	60	0.1301	0.0947	0.1654	0.0544	18.85	2.43	5.96
6	1	25.8	–	–	0.1371	–	–	0.04	12.57	3.64	8.06

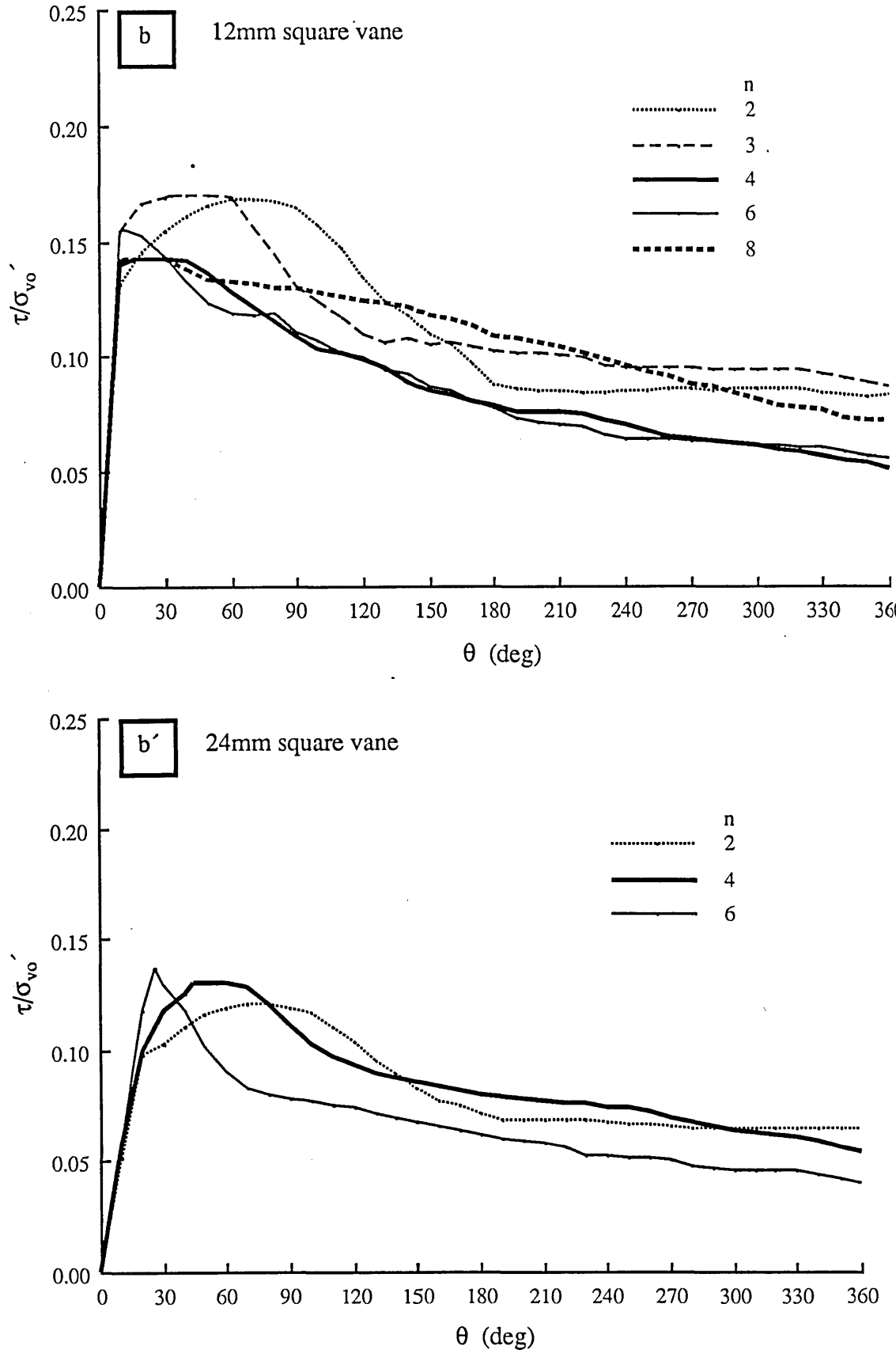


Fig. 5.1 Normalised shear stress — rotation curves for tests in normally consolidated London clay: Averaged test results; $\omega = 6.27°/min.$

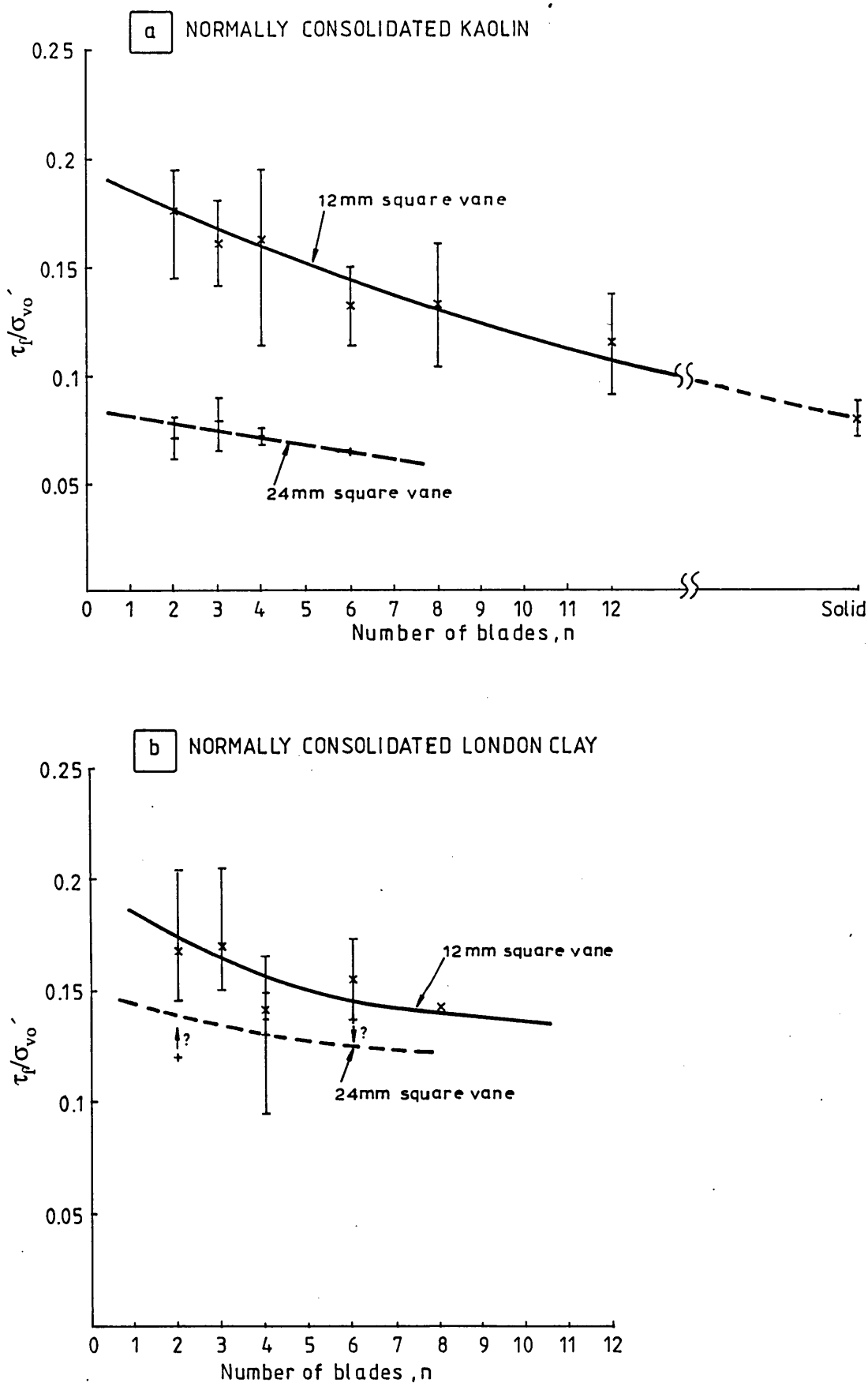


Fig. 5.2 Effect of number of blades on the measured peak vane strength.

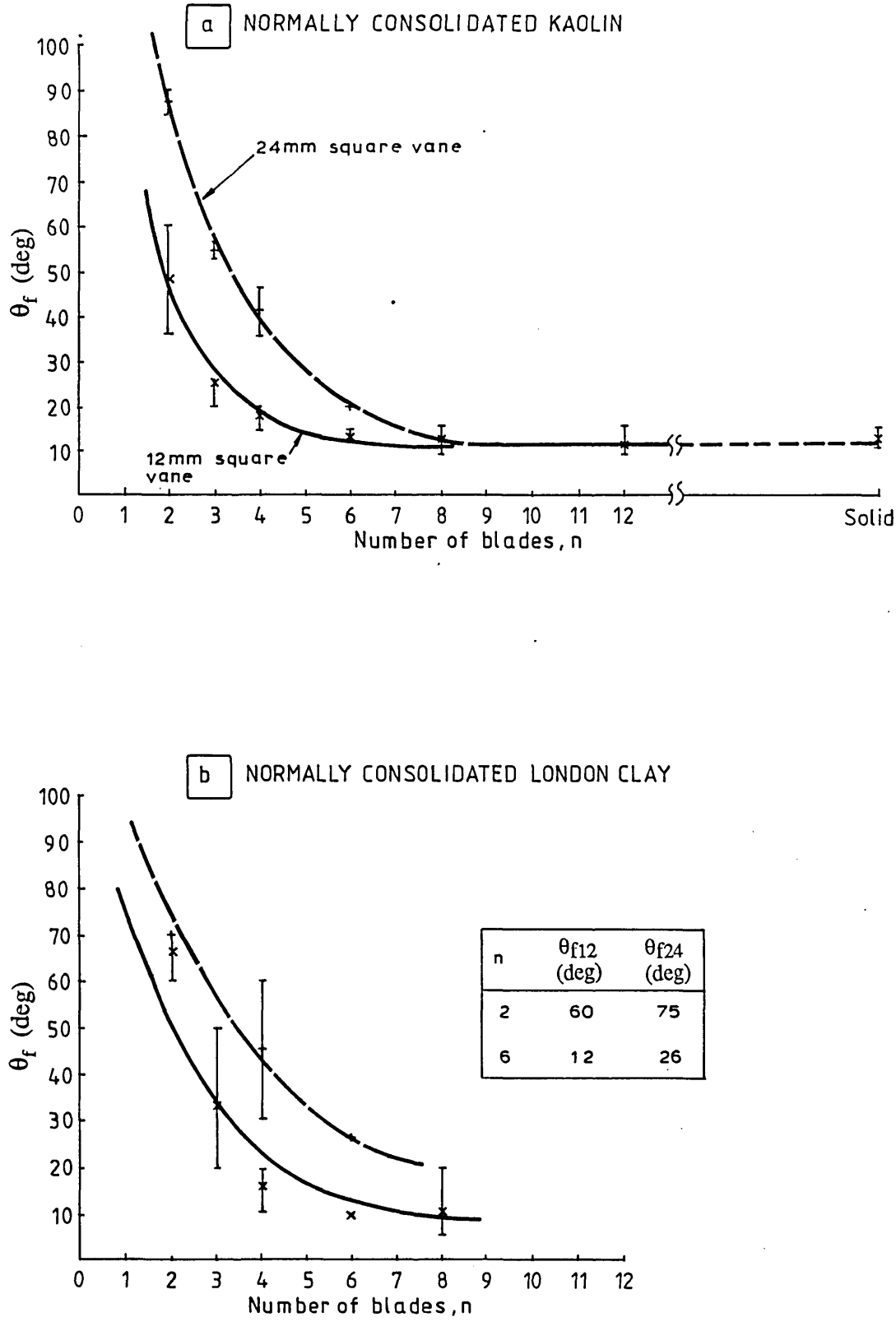


Fig. 5.3 Effect of the number of vane blades on the measured angle of rotation at failure.

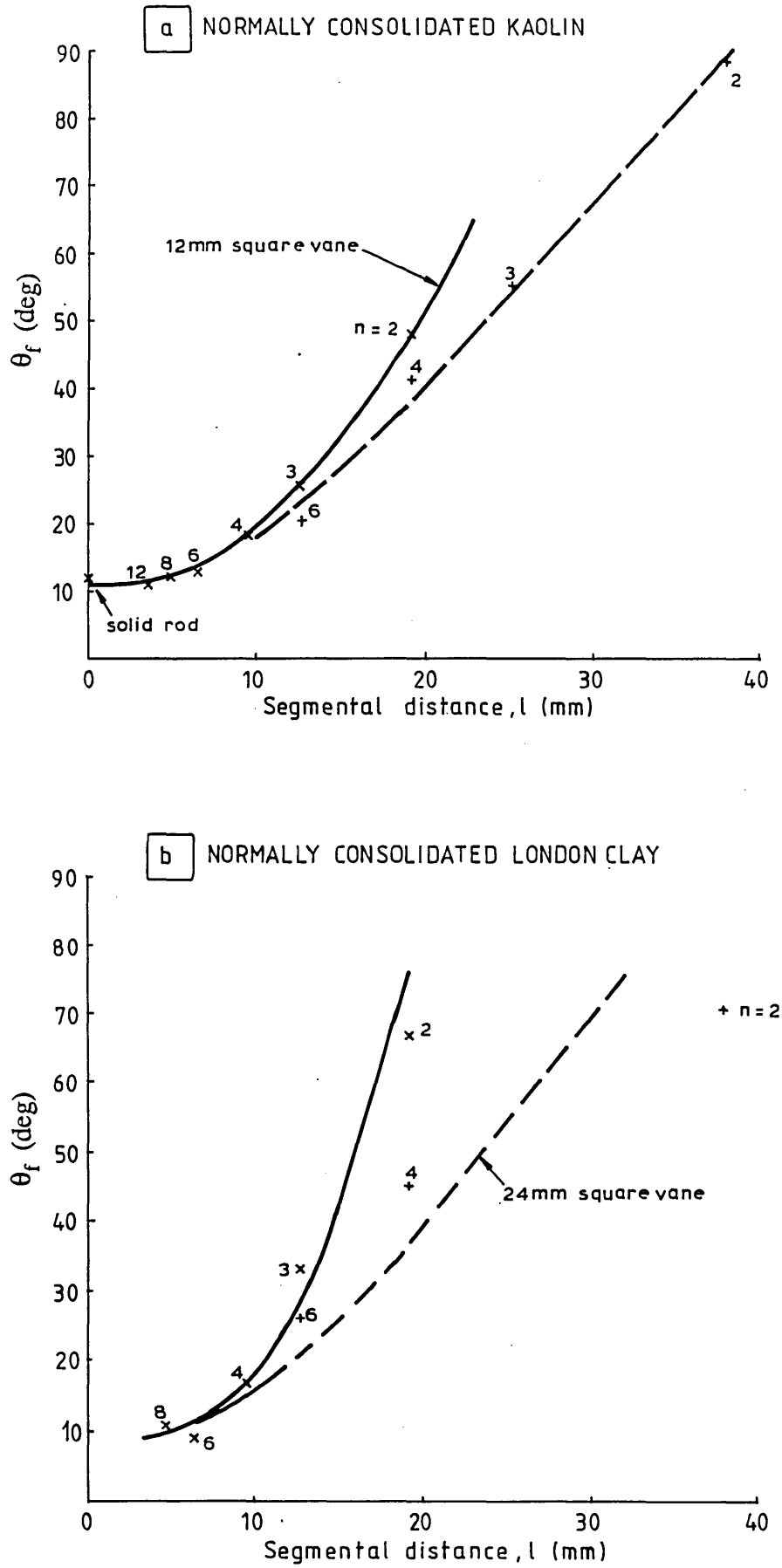


Fig. 5.4 Relations between angle of vane rotation at failure and segmental distance.

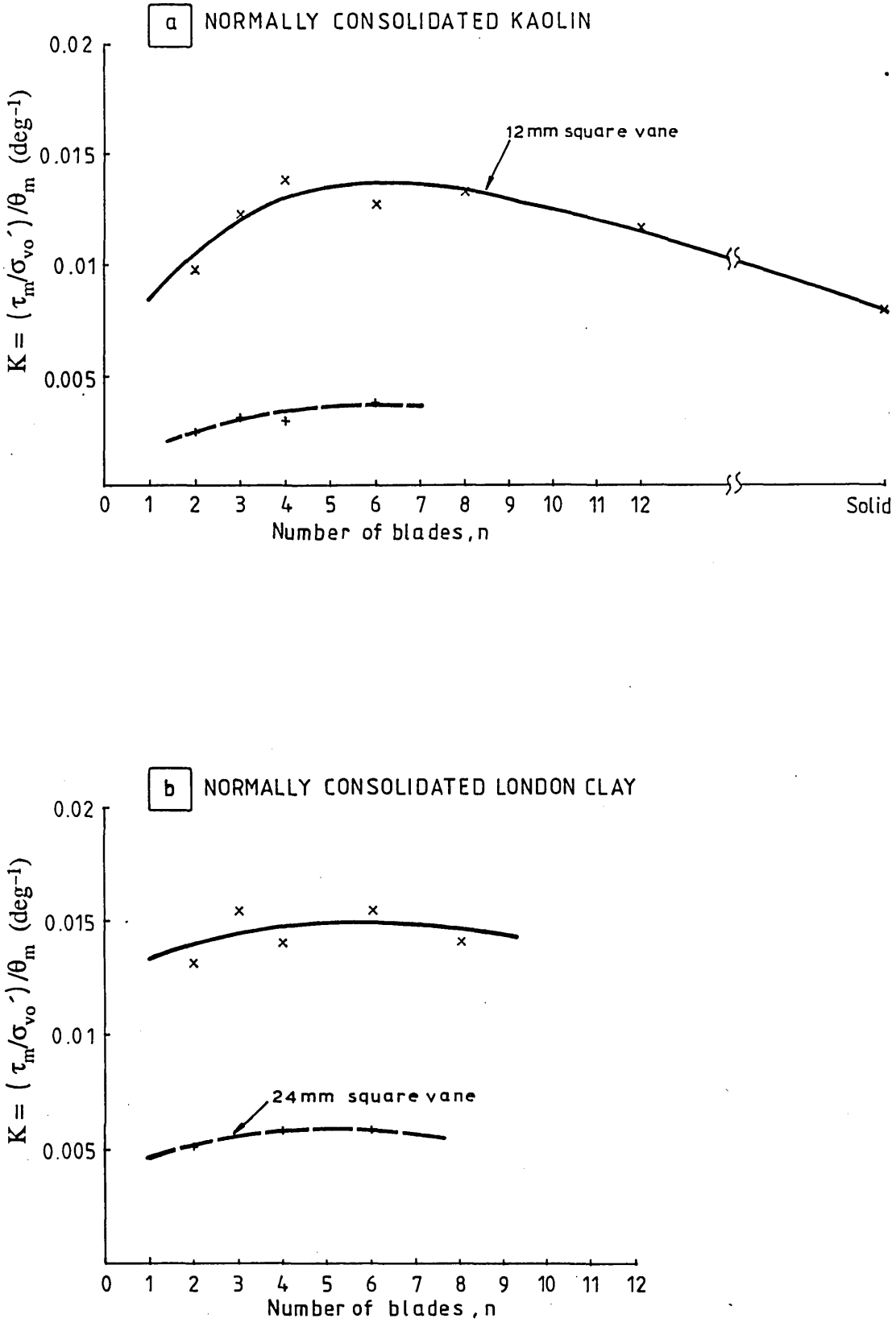


Fig. 5.5 Effect of number of blades on the measured initial soil stiffness.

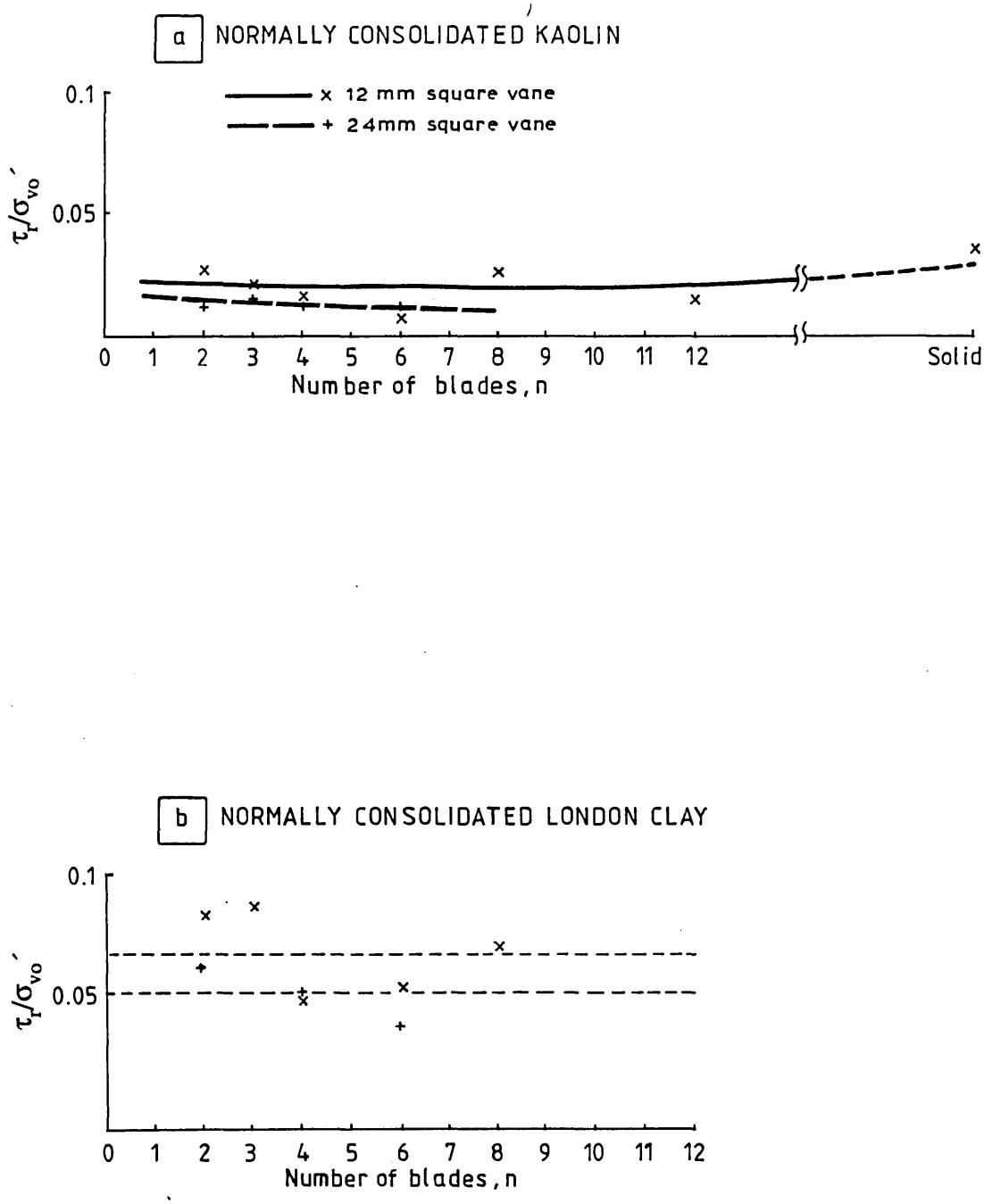


Fig. 5.6 Effect of number of blades on the measured residual vane strength.

5.4 DISCUSSION OF THE RESULTS

5.4.1 Introduction

In this Section an attempt is made to identify the processes which might explain the relationships observed in Section 5.3. Since the 4-bladed vane has been adopted as the standard, the results are normalised to this 'standard'.

Fig. 5.7 shows the parameter W_4 versus n, where $W_4 = (\tau_f/\sigma_{vo}')_n/(\tau_f/\sigma_{vo}')_4$; W_4 is the normalised shear strength of soil tested with an n-bladed vane. Both the results of tests on Speswhite kaolin and London clay are shown. Clearly, the W_4–n relationship is dependent on clay type but there appears to be little or no vane-size effect. Separate trend lines are drawn through each clay type. These are similar and show a gradual decrease in the normalised strength with increasing values of n. The effect of n on the measured strength is less in the case of London clay than in kaolin.

At values of $n < 4$, values of W_4 are in general greater than unity — by about 10% in the case of London clay and by about 5% in the case of kaolin — thus suggesting that if there is a progressive failure effect, it is small. At values of n in the range 4–8, W_4 is still greater than unity in the case of London clay but decreases continuously to about 0.8 at $n = 8$ in the case of kaolin. The 12mm diameter brass rod ($n \equiv 24$) tested in kaolin yields an even lower value of W_4 of about 0.5.

Based on the observed results, it is suggested that the disturbance caused by vane insertion probably outweighs progressive failure effects at $n < 4$, and dominates the behaviour when $n > 4$. The significance of these effects will now be examined.

5.4.2 Progressive Failure Effects

This Section presents a simple highly idealised progressive failure model for the vane test. The sole purpose of this model is to illustrate the mechanics of the phenomenon of progressive failure in relation to the vane test.

The chosen soil element shear stress – rotation model shown in Fig. 5.8 assumes rigid-plastic strain-softening behaviour. The soil element peak strength, τ_p, is maintained up to an angle of rotation of $\theta = 7.5°$, at which instantaneous softening occurs and the residual strength, τ_r ($= \tau_p/2$) is reached, remaining constant for angles of rotation larger than $\theta = 7.5°$.

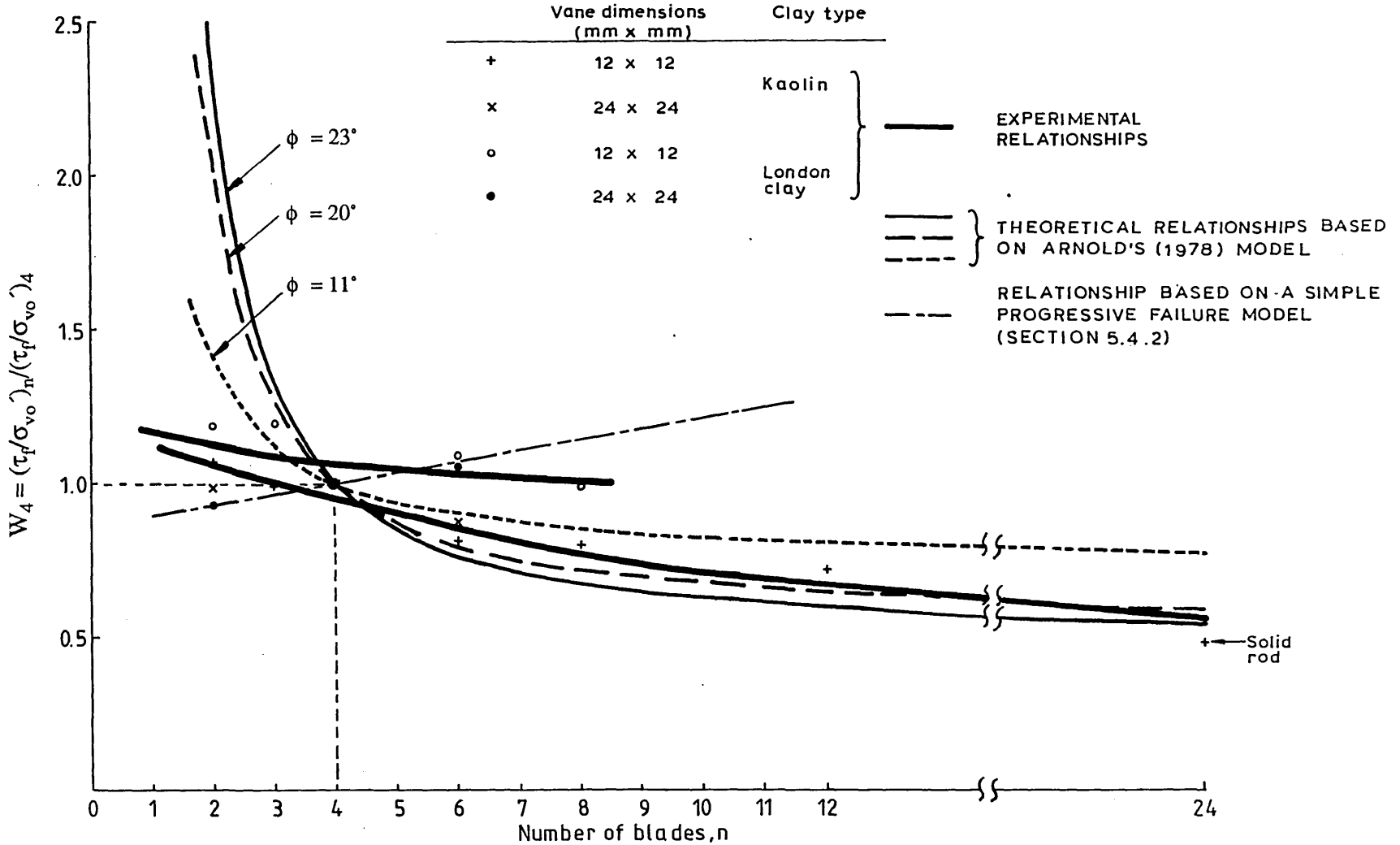


Fig. 5.7 Comparison of experimental and theoretical relationships between normalised vane strength, W_4 and number of blades, n.

Fig. 5.9 shows 7.5°-soil segments between adjacent blades separated by an angle, β (= $2\pi/n$) for a vane with n equally spaced blades. Based on the soil model adopted and the results of thin-section studies reported in Section 6.3.2, it may be assumed that upon vane insertion, which corresponds to zero rotation, the 7.5°-soil segments in front of and behind each vane blade are stressed to the same extent and have already mobilised the peak strength, τ_p (see Fig. 5.9a). The degree of straining in these segments is assumed to be insufficient to have caused strain-softening to the residual strength, τ_r. It is further assumed that the amount of rotation of each 7.5°-soil segment is equal to a 7.5°-rotation of the vane blades. Hence, at 'zero vane rotation', two 7.5°-soil segments are at 'peak' and all the remaining (i.e. ten, if a 4-bladed vane is being considered) 7.5°-soil segments are 'unstressed', i.e. at zero mobilised strength. This is demonstrated in Fig. 5.9a.

Considering that the resistance to torque of each soil 'element' at peak and residual conditions is equal to c_p and c_r respectively, it follows that the contribution of each blade to the torque is given by $m = [(a_p \times c_p) + (a_r \times c_r)] = \Sigma c_i$ (where $c_i = c_p, c_r, 0$), in which a_p and a_r represent the number of soil segments which have reached the peak and residual shear stress conditions respectively. The total calculated torque, therefore, is given by $M = nm (= n\Sigma c_i)$, where n is the number of blades. Therefore, for a 4-bladed vane at zero rotation, $M = 4m = 8c_p$ (see Fig. 5.9c).

Fig. 5.9b shows the soil strength mobilised after a rotation of 7.5°. It illustrates that the segments in front of and behind each blade are now at 'residual', while the segments immediately in front of the former and immediately behind the latter are at 'peak'; the remaining segments are 'unstressed'. Thence, for a 4-bladed vane, the torque after 7.5° rotation is $M = 12c_p$ (see Table 5.2c). Thereby, the 'unstressed' segments progressively reach failure, and thus the peak torque will result when all the segments between adjacent blades have failed, e.g. $M_{max} = 28c_p$ at $\theta_f = 37.5°$ in the case of the 4-bladed vane. Fig. 5.9c shows the torque – rotation plot for the 4-bladed vane; the torque at zero rotation (Fig. 5.9a) and at 7.5° rotation (Fig. 5.9b) are labelled as (1) and (2) respectively.

Table 5.2c presents the calculated torques for the 4-bladed vane on the basis of the simple soil element shear stress – rotation model of Fig. 5.8 and the assumptions outlined in Figs. 5.9a and b. Tables 5.2a, b, d, e and f present the calculated torques for 2-, 3-, 6-, 8- and 12-bladed vanes, respectively.

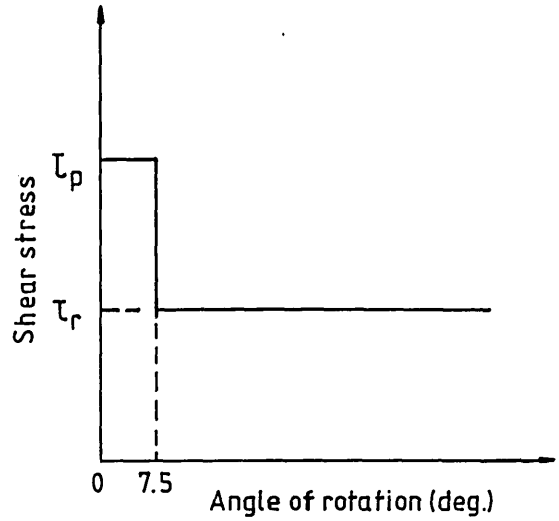
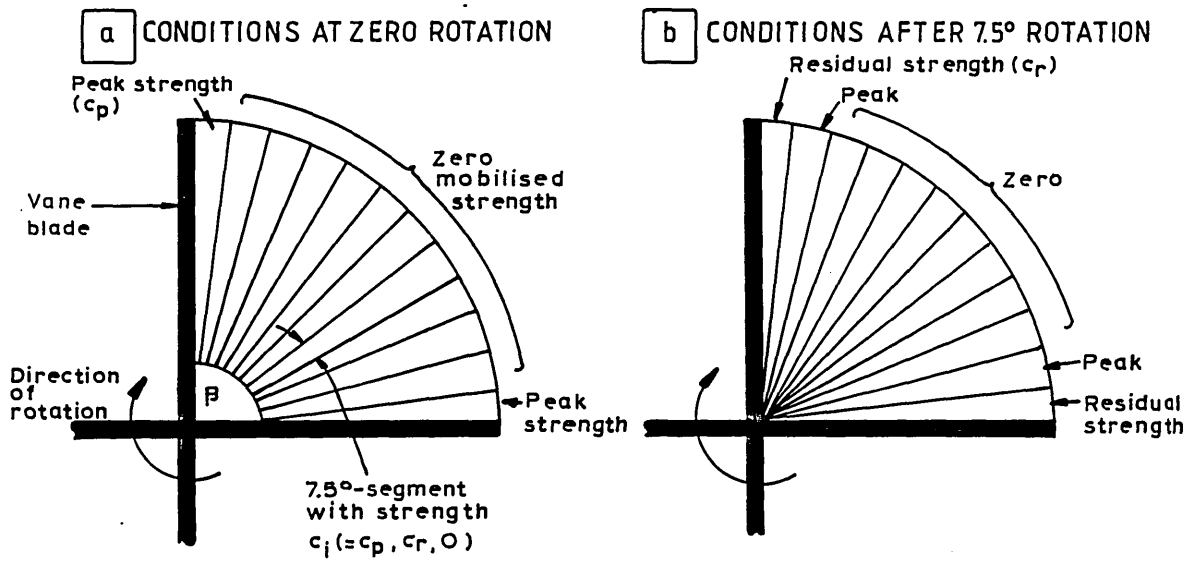


Fig. 5.8 Soil element shear stress — rotation model.



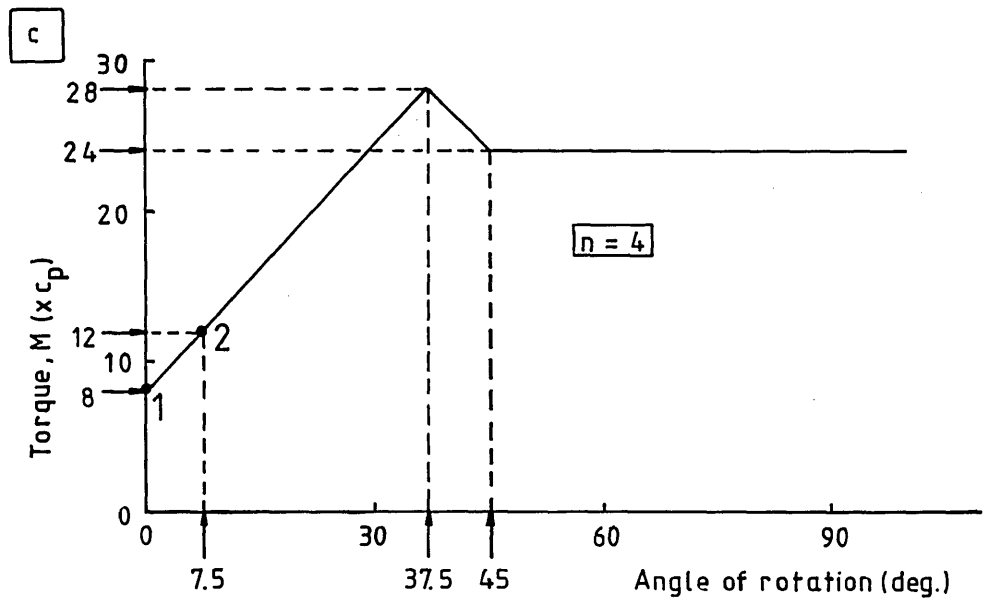


Fig. 5.9 a & b 'State of stress' of 7.5°-soil segments.
c Torque—vane rotation relationship according to a simple progressive failure model.

Angle of Rotation, θ (deg)	No. of Segments			m ($x\ c_p$)	M = 2m ($x\ c_p$)
	at Peak	at Residual	Unstressed		
0	2	0	22	2	4
7.5	"	2	20	3	6
15	"	4	18	4	8
22.5	"	6	16	5	10
30	"	8	14	6	12
37.5	"	10	12	7	14
45	"	12	10	8	16
52.5	"	14	8	9	18
60	"	16	6	10	20
67.5	"	18	4	11	22
75	"	20	2	12	24
82.5	"	22	0	13	26
90	0	24	"	12	24
97.5	"	"	"	"	"
105	"	"	"	"	"
112.5	"	"	"	"	"
120	"	"	"	"	"
127.5	"	"	"	"	"
135	"	"	"	"	"
142.5	"	"	"	"	"
150	"	"	"	"	"
157.5	"	"	"	"	"
165	"	"	"	"	"
172.5	"	"	"	"	"
180	"	"	"	"	"

Table 5.2a
2-bladed vane torques calculated from a progressive failure model.

Angle of Rotation, θ (deg)	No. of Segments			m ($x\ c_p$)	M = 3m ($x\ c_p$)
	at Peak	at Residual	Unstressed		
0	2	0	14	2	6
7.5	"	2	12	3	9
15	"	4	10	4	12
22.5	"	6	8	5	15
30	"	8	6	6	18
37.5	"	10	4	7	21
45	"	12	2	8	24
52.5	"	14	0	9	27
60	0	16	"	8	24
67.5	"	"	"	"	"
75	"	"	"	"	"
82.5	"	"	"	"	"
90	"	"	"	"	"
97.5	"	"	"	"	"
105	"	"	"	"	"
112.5	"	"	"	"	"
120	"	"	"	"	"

Table 5.2b
3-bladed vane torques calculated from a progressive failure model.

Angle of Rotation, θ (deg)	No. of Segments			m ($x\ c_p$)	M = 4m ($x\ c_p$)
	at Peak	at Residual	Unstressed		
0	2	0	10	2	8
7.5	"	2	8	3	12
15	"	4	6	4	16
22.5	"	6	4	5	20
30	"	8	2	6	24
37.5	"	10	0	7	28
45	0	12	"	6	24
52.5	"	"	"	"	"
60	"	"	"	"	"
67.5	"	"	"	"	"
75	"	"	"	"	"
82.5	"	"	"	"	"
90	"	"	"	"	"

Table 5.2c
4-bladed vane torques calculated from a progressive failure model.

Angle of Rotation, θ (deg)	No. of Segments			m ($x c_p$)	M = 6m ($x c_p$)
	at Peak	at Residual	Unstressed		
0	2	0	6	2	12
7.5	"	2	4	3	18
15	"	4	2	4	24
22.5	"	6	0	5	30
30	0	8	"	4	24
37.5	"	"	"	"	"
45	"	"	"	"	"
52.5	"	"	"	"	"
60	"	"	"	"	"

Table 5.2d
6-bladed vane torques calculated from a progressive failure model.

Angle of Rotation, θ (deg)	No. of Segments			m ($x c_p$)	M = 8m ($x c_p$)
	at Peak	at Residual	Unstressed		
0	2	0	4	2	16
7.5	"	2	2	3	24
15	"	4	0	4	32
22.5	0	6	"	3	24
30	"	"	"	"	"
37.5	"	"	"	"	"
45	"	"	"	"	"

Table 5.2e
8-bladed vane torques calculated from a progressive failure model.

Angle of Rotation, θ (deg)	No. of Segments			m ($x c_p$)	M = 12m ($x c_p$)
	at Peak	at Residual	Unstressed		
0	2	0	2	2	24
7.5	"	2	0	3	36
15	0	4	"	2	24
22.5	"	"	"	"	"
30	"	"	"	"	"

Table 5.2f
12-bladed vane torques calculated from a progressive failure model.

Fig. 5.10a is a plot of the calculated torque, M, against angle of rotation, θ. Clearly, as the number of blades increases the calculated peak torque also increases. This is true as long as there are no vane insertion effects, i.e. $c_p/\tau_p = 1$. Fig. 5.10b shows the relationship between calculated torques normalised to the 'standard', W_4, and number of blades, n. It can be seen that there is a linear relationship between W_4 and n such that as n increases, W_4 increases: at $n < 4$, $W_4 < 1$, whilst at $n > 4$, $W_4 > 1$.

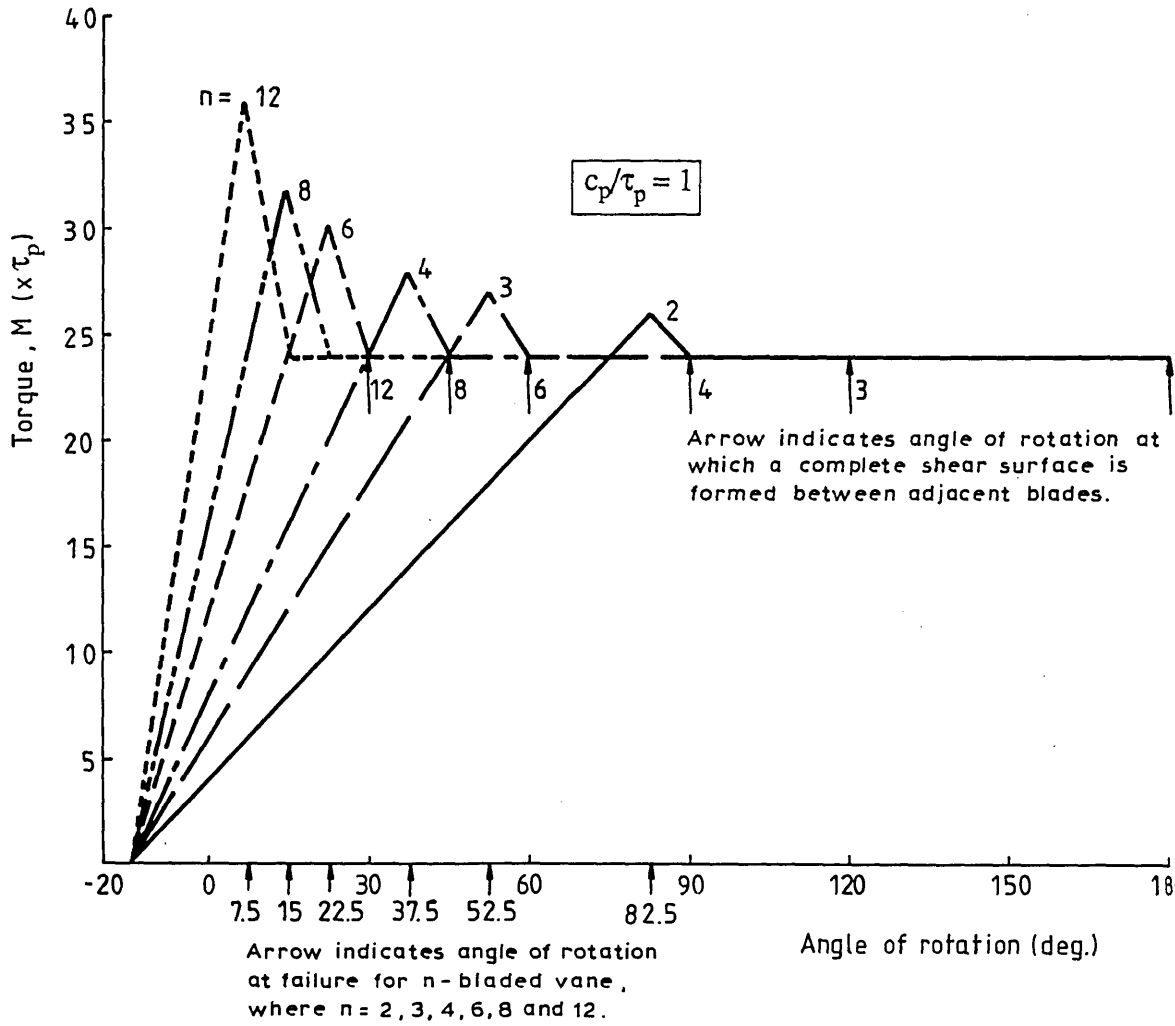


Fig. 5.10a Torque versus angle of rotation for vanes with different numbers of blades : Results obtained from a progressive failure model.

Fig. 5.10c shows the relationship between the angle of rotation at failure, θ_f, and number of blades, n, as predicted by the simple progressive failure model. The observed trend shows that large angles of rotation are required to reach failure when n is small but as n increases, θ_f decreases.

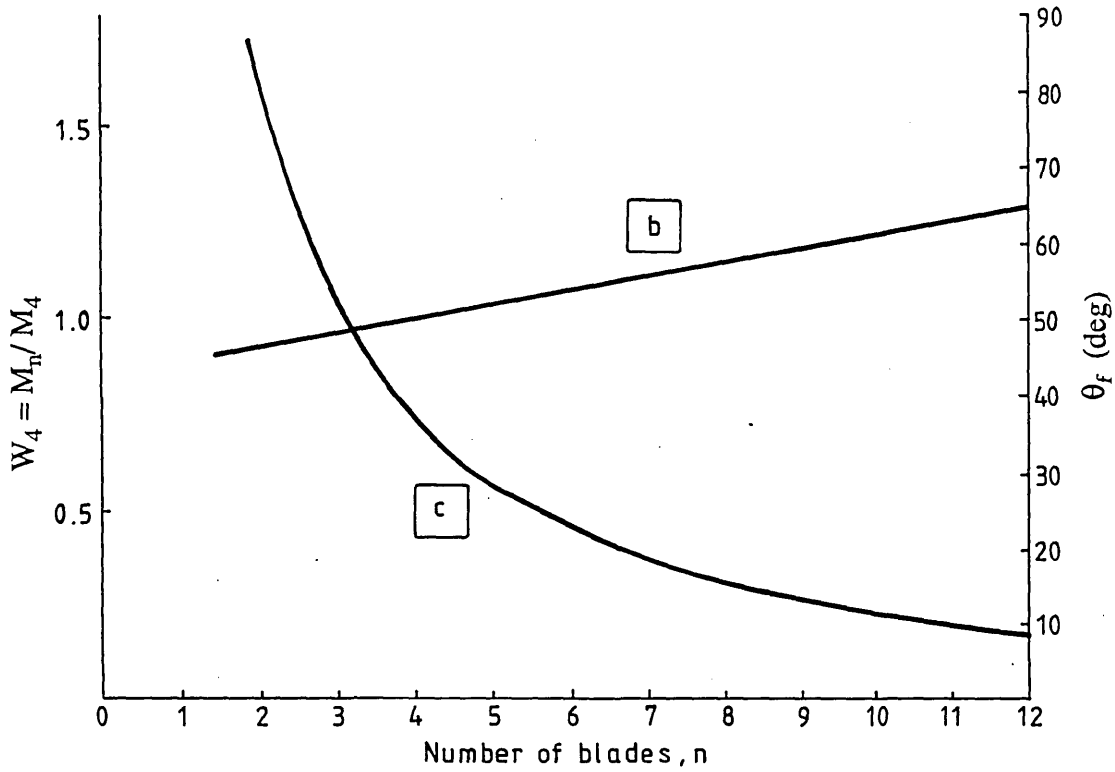


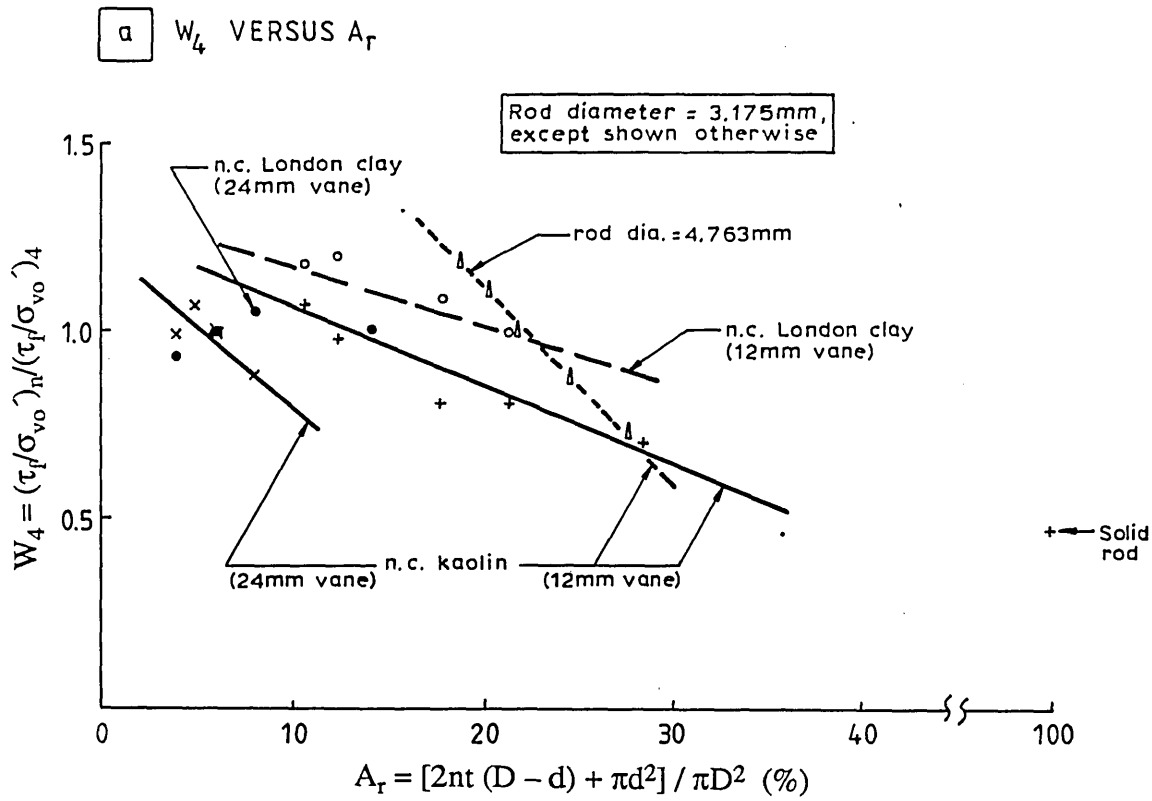
Fig. 5.10 Relationships obtained from a progressive failure model for the vane test
(b) Normalised torque versus n
(c) Angle of rotation at failure versus n.

5.4.3 Insertion Disturbance Effects

It will be seen in Section 6.3.2 that the soil fabric in the vicinity of the vane blades is disturbed as a consequence of vane insertion. Moreover, the results presented in Section 6.3.2 clearly demonstrate that as the number of blades increases, the disturbed volume of soil around the blades also increases (Fig. 6.6). It is therefore useful to examine the effect of insertion disturbance, as a function of the number of blades, on the measurement of the vane shear strength.

Fig. 5.11a shows a number of relationships between the normalised vane shear strength, W_4, and the area ratio, A_r, where A_r denotes the cross-sectional area of the vane as a ratio of the area of the soil swept by the rotated vane (Section 3.2.2A). It presents the results of 12 and 24mm square vane tests on both kaolin and London clay, together with kaolin data from tests with 12mm square vanes having a larger shaft diameter of d = 4.763 mm. It is clear that values of W_4 decrease as A_r increases, thus reflecting the effect of the number of blades on the measured strength. Furthermore, it is evident that both the blade diameter and the rod diameter influence the variation of W_4 with A_r. It is no surprise that the W_4–A_r variation is also affected by the clay type.

Fig. 5.11b shows the relationship between W_4 and the parameter, α, which denotes the "perimeter ratio" and expresses the product of the number of blades (n) and the vane blade thickness (t) as a ratio of the vane peripheral distance (πD); the concept of the perimeter ratio as a measure of the potential fabric disturbance was introduced by La Rochelle et al. (1973). Both the results of 12 and 24mm square vanes on kaolin and London clay are presented; the Figure also shows kaolin data from tests using 12mm square vanes having shaft diameters of 4.763 mm. The results of 4-bladed field vane tests carried out in St. Louis, by La Rochelle et al. (1973), and in both St. Louis and St. Alban by Roy & Leblanc (1988) are also shown for comparison. Although it is readily acknowledged that the clay type influences the W_4–α relationship, it is evident from the data in Fig. 5.11b that there is a certain relationship between W_4 and α, which indicates that the strength decreases as the perimeter ratio increases. It is seen that for values of α < 5% and > 5%, W_4 values are respectively greater than and less than unity.



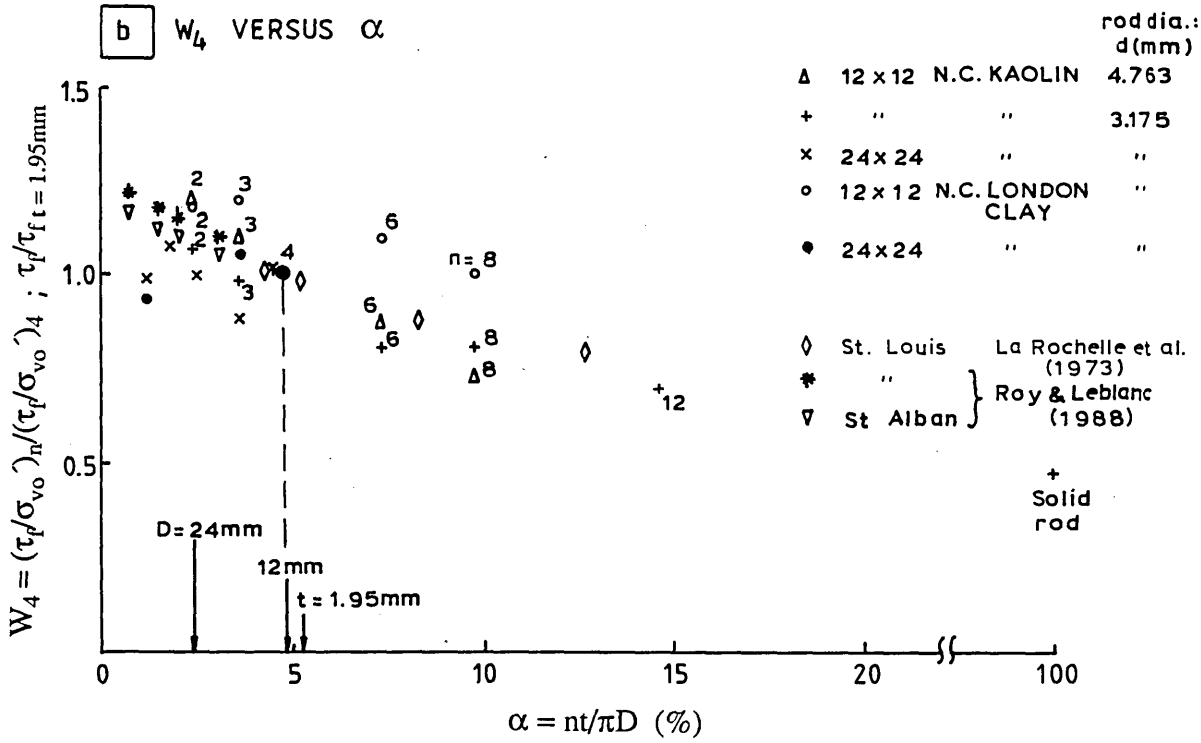


Fig. 5.11 Relationships showing insertion disturbance effects in the vane test.

5.4.4 The Farrent–Arnold Interpretation of the Vane Test

Farrent's (1960) extension of the vane test to c–ϕ materials assumes that the shear stress along the presumed vertical shearing surface between two adjacent blades, A and B, diminishes exponentially in accordance with the expression

$$\tau = \tau_A e^{2\theta \tan\phi} \qquad \text{Eq. 5.1}$$

where τ, τ_A, and θ are defined in Fig. 5.12, and
ϕ is the angle of friction of the soil.

On the basis of the above assumptions, Farrent developed an expression for the total torque measured by the vane, M, given by:

$$M = \frac{\pi D^3}{6}\tau_h + \frac{nHR^2}{2\tan\phi}\tau_A\left[\, e^{2\beta \tan\phi} - 1 \,\right] \qquad \text{Eq. 5.2}$$

where τ_h is the maximum shear stress assumed to apply uniformly over the top and bottom horizontal surfaces circumscribed by the vane, and
β is given by $2\pi/n$, where n is the number of blades on the vane.

A detailed account of the derivation of Eq. 5.2 is given in Appendix A3.

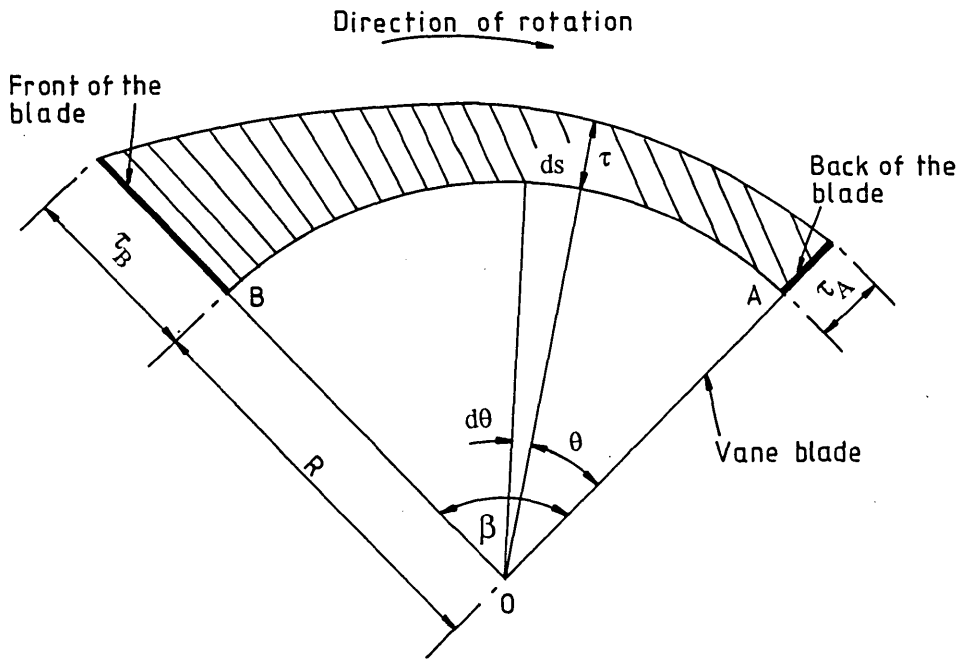


Fig. 5.12 Exponential shear stress distribution along the vertical shearing surface between adjacent blades.

From Mohr-Coulomb considerations, τ_A was expressed by Arnold (1978) as:

$$\tau_A = \frac{c + \sigma_3 \tan\phi}{1 - \dfrac{\tan\phi}{\tan(45 + \phi/2)}} \qquad \text{Eq. 5.3}$$

But due to insertion disturbance effects, c may be taken as zero. Also, $\sigma_3 = \sigma_h = K_0\sigma_v = (1 - \sin\phi)\sigma_v$. Thence, Eq. 5.2 becomes:

$$M = \frac{\pi D^3}{6}\tau_h + \frac{nHR^2}{2\tan\phi}\left[\frac{(1 - \sin\phi)\,\sigma_v \tan\phi}{1 - \dfrac{\tan\phi}{\tan(45 + \phi/2)}}\right]\left[e^{4\pi/n \tan\phi} - 1\right] \qquad \text{Eq. 5.4}$$

From the conventional interpretation of the vane test the expression for M is

$$M = \frac{\pi D^3}{6}\tau_h + \frac{\pi D^2 H}{2}\tau_v \qquad \text{Eq. 5.5}$$

It is then possible to obtain an expression for τ_v/σ_v by equating Eqs. 5.4 and 5.5 and re-arranging, i.e.

$$\frac{\tau_v}{\sigma_v} = \frac{n}{4\pi}\left[e^{4\pi/n \tan\phi} - 1\right]\frac{1 - \sin\phi}{1 - \dfrac{\tan\phi}{\tan(45 + \phi/2)}} \qquad \text{Eq. 5.6}$$

Therefore, for given values of ϕ, the relationship between the maximum shear stress along the vertical cylindrical surface, τ_v, normalised to the vertical stress, σ_v, and the number of blades on the vane, n, can be determined. Values of W_4 can be obtained by normalising values of τ_v/σ_v with respect to the values obtained from the standard 4-bladed vane.

Fig. 5.7 shows the relationship between W_4 and n for different values of ϕ = 11, 20 and 23°, which respectively correspond to the residual angle of friction for kaolin, the peak angle of friction for London clay and the peak angle of friction for kaolin. All three curves show the measurement of higher strengths when the number of blades is small (e.g. $W_4 >> 1$ when n = 2), while lower strengths are attained with increasing numbers of blades (e.g. $W_4 < 1$ when n = 12). It is also evident that the relationship between W_4 and n is influenced by the value of the angle of internal friction, ϕ, such that with decreasing values of ϕ, the effect of the number of blades on the peak strength reduces.

5.4.5 Summary

From a comparison of the W_4–n relationships according to (a) the experimental results for kaolin and London clay (Section 5.3), (b) the simple highly idealised progressive failure model (Section 5.4.2), and (c) the non-progressive failure model developed by Farrent and extended by the writer (Section 5.4.4), there are three phenomena which may explain the observed relationships between the normalised measured strength, τ_f/σ_{vo}', and the number of blades, n. These are given below:

(i) According to Section 5.4.2, progressive failure effects associated with the vane would result in the measurement of lower strengths when n is small, i.e. less than 4, perhaps. Although the experimental results for vanes with less than four blades show that the measurement of the vane shear strength is possibly influenced by progressive failure effects, there is little or no evidence to suggest that such effects dominate the behaviour.

(ii) Vane insertion effects lead to disturbance of the soil fabric, which subsequently results in the measurement of lower strengths with increasing numbers of blades. The results show the existence of an almost linear relationship between the normalised shear strength and the number of blades, as expressed by the perimeter ratio, α.

(iii) An alternative interpretation of the vane test — by Farrent (1960) — is in terms of shear stress strength parameters, c and ϕ, with the assumption of an exponential shear stress distribution along the vertical periphery of adjacent blades. Evidently, the experimental results from tests with vanes having more than four blades are in good agreement with the results obtained using Farrent's interpretation of the vane test.

CHAPTER 6

STUDY OF THE VANE FAILURE MECHANISM

6.1 INTRODUCTION

The basic assumptions of the conventional interpretation of the vane test include the instantaneous and full mobilisation of the peak soil strength, and simultaneous formation of a circular failure surface defined by the vane blades. However, a review of the previous research shows that there are opposing views in connection with both these assumptions (Section 2.6). The available test data indicate a 'vane-sized' circular failure surface in most instances, although there are cases which presume a failure surface with a diameter larger than the vane diameter (Section 2.6.1). Similarly, there is a disagreement regarding the nature of the mode of failure associated with the vane test. On the one hand, there are those who believe that progressive failure does occur, while other authors suggest that the mode of failure is non-progressive in the vane test (Section 2.6.2). Despite the fact that a variety of experimental techniques have been employed in the past, it appears that these conflicting conclusions have arisen as a consequence of one or a number of factors which include:

(a) unsuitability of the technique(s) used;
(b) poor experimental procedures;
(c) absence of clear experimental evidence;
(d) poor appreciation of the fundamental principles of soil mechanics.

Except for an unsuccessful attempt (Veneman, 1977), none of the previous studies has examined the development of the microfabric features which result during vane rotation.

Because of the fundamental nature of these assumptions in the interpretation of the vane test (Section 2.2), it is important to examine, in detail, the validity or otherwise of the above postulates.

This Chapter presents a detailed investigation of the formation of the microfabric features induced in the soil by the rotating vane. For this study, the thin-section technique (Section 3.4.6) was used. The propagation of the shear structures at different stages of the vane test will be clearly demonstrated. Moreover, both the shape and extent of the vane failure surface, and the mode of failure associated with 2-, 3-, 4- and 6-bladed vanes will be shown. It will also become evident that the sample water content

has an influence on the extent of the formation of the shear structures. Furthermore, the importance of the use of suitable soil types in thin-section studies will become obvious. Analyses of the results of 4-bladed vane tests will show that simple shear conditions probably apply at peak torque, with direct shear conditions prevailing post peak. In addition, similarities between the behaviour of the 2-bladed vane and that associated with retaining walls will be examined.

6.2 TESTING PROGRAMME

Sections 3.4.2B and 3.4.3 give a detailed description of the laboratory- and triaxial-vane test programmes, respectively; a summary of each test series will now follow.

6.2.1 Laboratory-vane Tests

Each sample was consolidated to a final height of 125 mm in a U100 tube, and in each sample 12mm square vane tests were carried out at five positions, as shown in Fig. 3.13a. The vanes were inserted to a depth, z = 50 mm, and, after a 'delay time' of less than one minute, rotated to pre-specified angles of rotation at a constant rate of 6.27 °/min (≈ 0.66 mm/min). Each vane was then left 'in situ'. Once the fifth test in a given sample was carried out, the sample was removed from the tube, and specimens were carefully cut and subsequently impregnated with Breox Peg 8000 before thin-sections were prepared. Thereafter, the vane failure mechanism was studied from a visual observation of photographs taken from thin-sections with the aid of a macro-photography system; each thin-section slide was photographed at two different positions, one at 45° to the other (Section 3.4.6D). To examine the development of the microfabric features more fully an optical microscope was used.

A large number of tests was performed to examine the shape and extent of the vane failure surface, and the mode of failure associated with the vane test. Thus, deformation patterns around 12mm square vanes with two, three and six blades, as well as the conventional four, were studied at different angles of rotation corresponding to the following stages of the shear stress – rotation curve: pre-peak, (just prior to peak), at peak, (just after peak), post-peak (and 'residual'). Thereby the effect of different numbers of blades on the development of shear structures during vane rotation was also examined.

Due to the importance attached to the determination of the vane failure mode, particular attention was paid to the examination of the propagation of shear structures around peak torque. Thus an additional series of tests was carried out using the conventional 4-bladed vane in which vane rotation was stopped just pre-peak, at peak and just post-peak shear stress.

The effect of the sample water content on the characteristics of the propagated shear structures was explored by examining the deformation patterns formed at various stages of the shear stress – rotation curves of 2-, 3- and 4-bladed vanes in samples having different water contents in the range w ≈ 40–60%.

Apart from a series of 4-bladed vane tests on normally consolidated samples of London clay ($I_L \approx 0.25$) — aimed at examining the effect of clay type on the propagation of deformation patterns during vane rotation — Speswhite kaolin (normally consolidated from a water content of about 150% to liquidity indices of $I_L \approx 0.25$, 0.53 and 0.82) was used as the test material, since it lends itself so well to microfabric investigations.

6.2.2 Triaxial-vane Tests

To complement the results of the laboratory-vane tests a series of 12mm x 24mm long (conventional) 4-bladed vane tests was also conducted in a large stress path cell.

100mm diameter samples of Speswhite kaolin, which were normally consolidated from a slurry water content of about 150% to 50%, were cut to 150 mm long and subjected to further K_0 consolidation up to vertical stresses approximately twice the preconsolidation stresses. Following the procedures outlined in Sections 3.4.3B and D, each vane was carefully inserted through the centre of the sample and once equilibrium had been reached, rotated at a rate of about (ω =) 0.023 °/min (≈ 0.0025 mm/min; Section 3.4.3E), under drained conditions, to an angle of rotation of about 360°. Two more tests, stopping at peak and pre-peak shear stress conditions, were then carried out at lower depths in the sample by pushing the vane to the subsequent test position at the end of the preceding vane rotation.

On completion of the third test, the sample was unloaded (as described in Section 3.4.3B), and removed from the triaxial cell for subsequent impregnation with Breox Peg 8000. Thin-sections were made from horizons within the sample corresponding to the vane test positions. Deformation patterns resulting from vane rotation were then examined according to the procedures summarised in Section 6.2.1.

6.3 TEST RESULTS

6.3.1 Introduction

This Section is concerned with the presentation of the results of both 12mm square laboratory-vane tests and 12mm rectangular (H/D = 2) triaxial-vane tests with two main objectives:

(i) to determine the diameter of the vane failure surface; and
(ii) to establish the mode of failure associated with the vane test.

After a description of fabric disturbance resulting from vane insertion, special attention is given to the successive development of shear structures at different angles of rotation of the conventional 4-bladed vane. The latter is followed by an examination of the deformation patterns resulting from rotation of 2-, 3- and 6-bladed vanes in kaolin. The effects of sample water content on the characteristics of the propagated shear structures are then studied before the results of 4-bladed vane tests on a sample of reconstituted London clay are presented.

The majority of the tests were carried out on kaolin samples having water contents in the range $w \approx 40$–60%. The London clay specimens had a water content of about $w = 50\%$.

6.3.2 Insertion Disturbance

The disturbance around 4-bladed 12mm square laboratory-vanes, with shaft diameters $d = 3.175$ mm, inserted into samples of Speswhite kaolin with water contents of $w \approx 50$ and 60% can be seen in Figs. 6.1 and 6.2 respectively. Figs. 6.1a and 6.2a are photographs which were taken while the thin-section slide was positioned between crossed polarising filters such that one vane blade assumed the vertical position, whereas Figs. 6.1b and 6.2b show photographs of the same thin-section slide, but now placed so that the same vane blade was at 45° to its position in the previous photograph (see Section 3.4.6D). Figs. 6.3a and b show the fabric disturbance caused by insertion of a 6-bladed 12mm square vane into a kaolin sample with $w \approx 60\%$. The region where the clay fabric has been locally affected by vane insertion shows as a light area around the vane.

The extent of insertion disturbance to the clay fabric around a 4-bladed 12mm rectangular triaxial-vane, having a shaft diameter d = 4.763 mm, can be seen in Figs. 6.4a and b, which respectively show photographs of the same thin-section slide at two different positions (Section 3.4.6D). The effect of the larger shaft diameter, in terms of insertion disturbance to the clay fabric, is seen when Figs. 6.4a and b are compared. Although Fig. 6.4b shows that the reorientation of the clay particles around the blades is similar to the observations made in Figs. 6.1–6.3, Fig. 6.4a clearly demonstrates that the larger vane shaft diameter has resulted in a far greater disturbance to the clay fabric than the insertion disturbance caused by the smaller shaft diameter, as observed in Figs. 6.1–6.3. In this regard, it is of interest to note that Cheah's (1981) radiographic study, using lead threads, also showed that the zone of disturbance in the vicinity of the vane shaft was considerably greater than that around the vane blades, with the lead threads neatly sheared off by the vane blades without any trace of an enlarged disturbed zone, while there was a distinct zone of disturbance extending beyond the shaft by an amount equal to the shaft diameter.

Schematic diagrams of the extent of the reorientation of clay particles as a consequence of vane insertion have been traced from Figs. 6.1–6.4, and are presented in Figs. 6.5a–d. Clearly, the zone of disturbance is similar for both (a) 4-bladed laboratory-vanes pushed into samples having two different water contents (Figs. 6.5a and b), and (b) 4- and 6-bladed laboratory-vanes pushed into samples having the same water content (Figs. 6.5b and c). Fabric disturbance around the tips and edges of the blades is the same in Figs. 6.5a–c; the discrepancies are in the zones of reorientated particles around the intersection of the blades, being greater both in the case of the 6-bladed laboratory-vane (Fig. 6.5c), and when the sample water content is higher (Fig. 6.5b); due to a larger shaft diameter, the zone of disturbed fabric around the triaxial-vane is significantly greater than that around the laboratory-vanes.

Figs. 6.5e* and f* respectively show the zones of disturbed fabric around 2- and 3-bladed laboratory-vanes tested in kaolin having a water content of about w = 40%, while Fig. 6.5g* is a schematic representation of the area of particle reorientation around a 4-bladed laboratory-vane tested in a sample of kaolin with a water content of about w = 50% (cf. Fig. 6.5a). In these tests a small degree of rotation had been applied, but as can be seen, insertion disturbance effects still dominate: except for the 2-bladed laboratory-vane, around which a few early shear structures can be seen, no shear structures had formed as a result of the relatively small angles of rotation through which the vanes had turned. [* Figs. 6.5e–g were obtained by tracing the zones of disturbance around the vane blades from photographs taken while viewing the thin-section slides under crossed polarised light.]

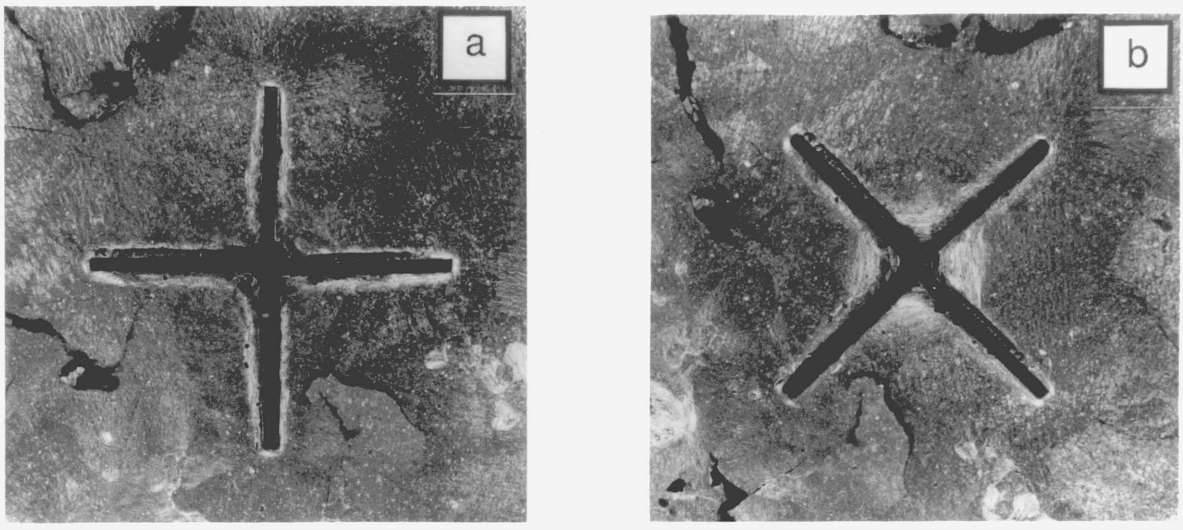


Fig. 6.1 Sample water content ≈ 50%

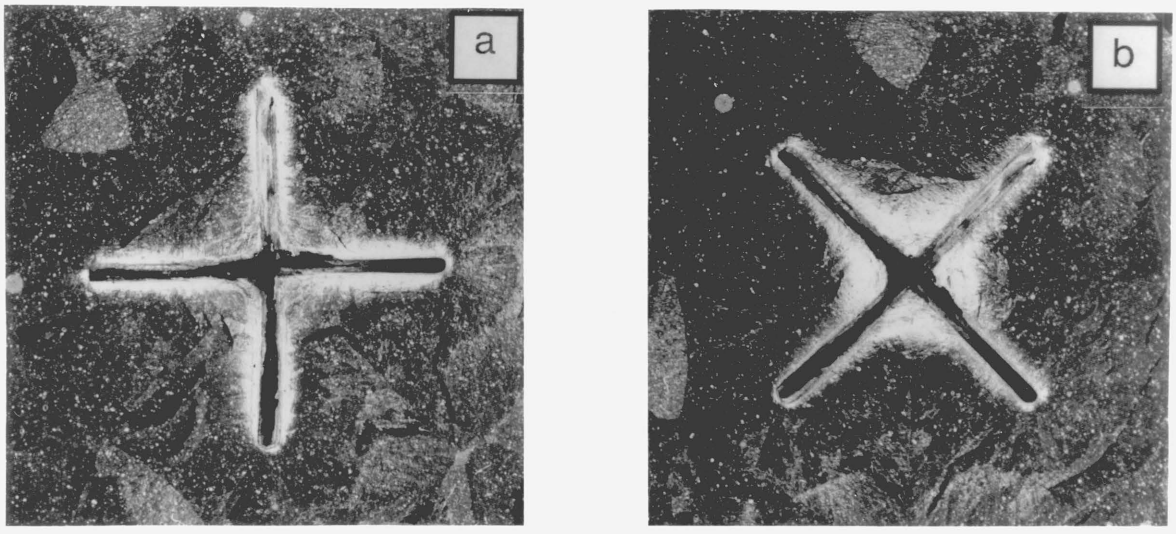


Fig. 6.2 Sample water content ≈60%.

Fabric disturbance around a 4-bladed laboratory-vane in kaolin.

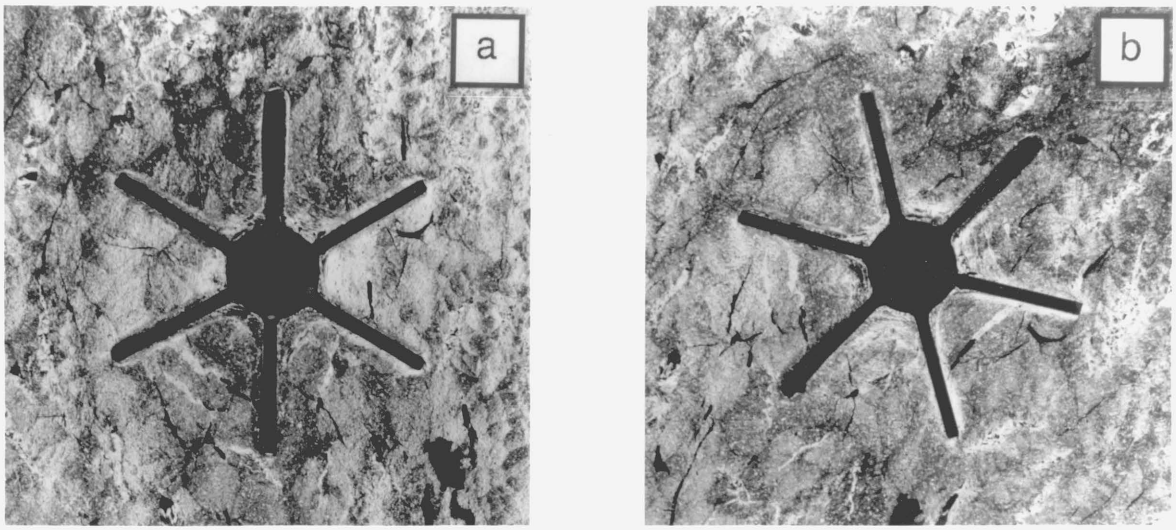


Fig. 6.3 Fabric disturbance around a 6-bladed laboratory-vane in kaolin; $w \approx 60\%$.

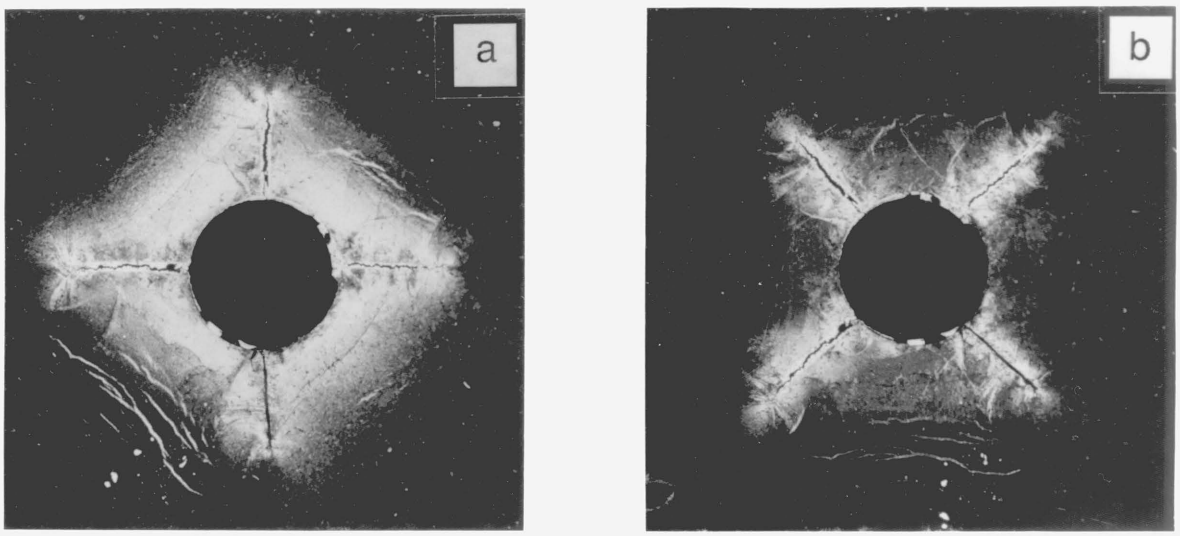


Fig. 6.4 Insertion disturbance around a 4-bladed triaxial-vane in kaolin; $w \approx 46\%$.

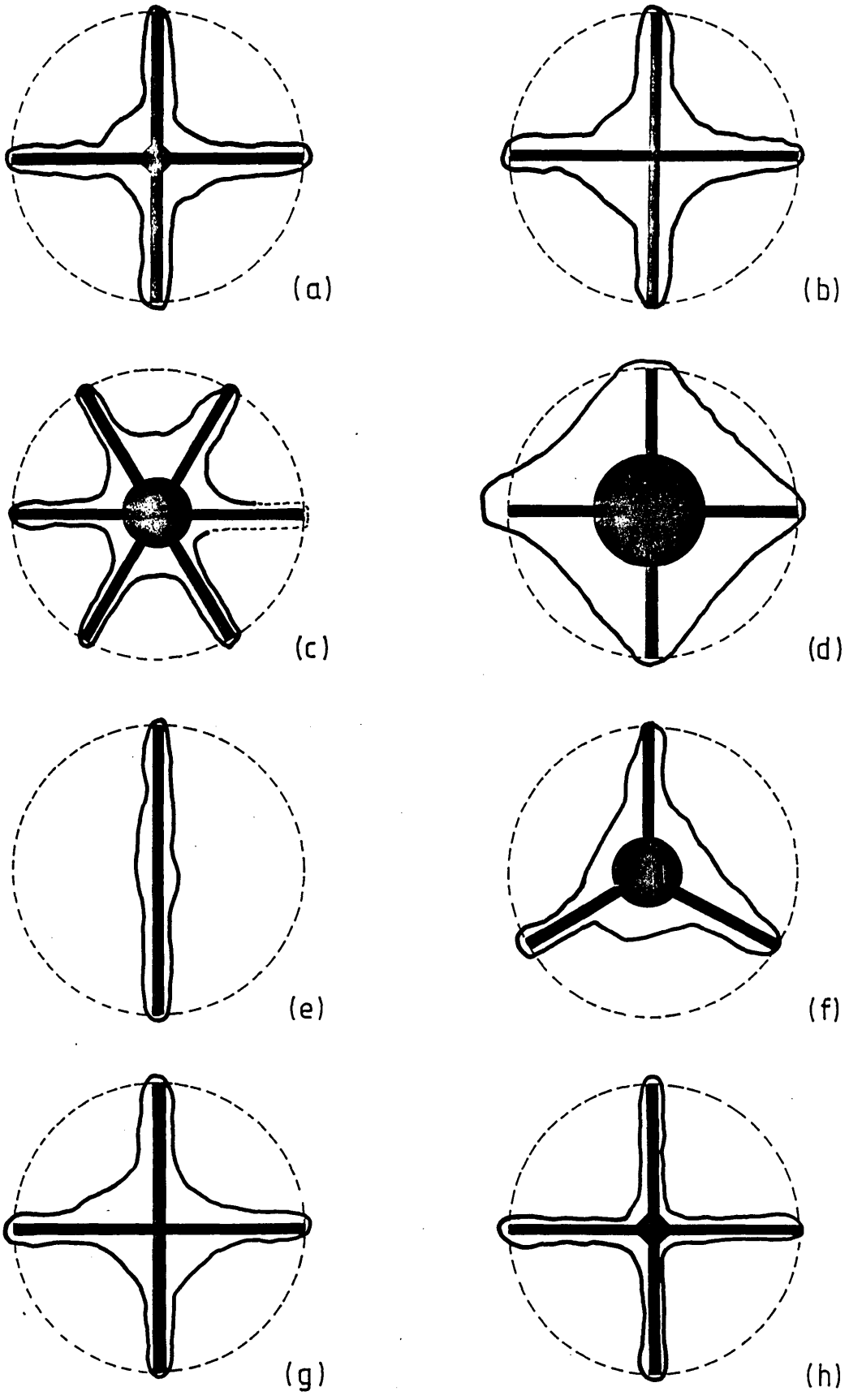


Fig. 6.5 Extent of fabric disturbance following vane insertion.
(a)–(d) Schematic representation of Figs. 6.1 — 6.4
(h) Cadling & Odenstad's (1950) diagrammatic representation.

Fig. 6.5h shows Cadling & Odenstad's (1950) diagrammatic representation of the disturbance to the clay fabric, and it is seen that the suggested zone of disturbance is comparable to that observed, although Figs. 6.5a–g show that there is much greater disturbance in the region of the intersection of the vane blades.

In order to examine the extent of soil disturbance related to the number of blades, the area of reorientated fabric shown in Figs. 6.5a–g has been measured. Fig. 6.6 is a plot of the "disturbance index", I_D, against both the number of blades, n, and the area ratio, A_r; $I_D = D_r/A_r$, where D_r denotes the "disturbance ratio" and represents the area of soil fabric disturbed due to vane insertion, and A_r is related to the cross-sectional area of the vane, with both D_r and A_r expressed as a ratio of the soil area circumscribed by the vane diameter. It can be seen that the disturbance index increases with increasing values of A_r, the latter increasing with increasing values of n, thus showing, as might be expected, that the greater the vane area ratio, the larger the zone of fabric disturbance resulting from vane insertion.

6.3.3 The 4-bladed Vane

6.3.3A Development of shear structures

The progressive development of shear structures at four different stages of the vane test corresponding to pre-peak, peak, post-peak and 'residual' (large displacement) shear stress conditions is shown in Figs. 6.8–6.11. This study was carried out using a sample of Speswhite kaolin normally consolidated to a water content of about w = 60%. Individual shear stress – rotation curves for each stage (1–4) of the test are shown in Fig. 6.7.

Figs. 6.8a to 6.11a are photographs which show the shear structures propagated on the vertical planes around the vane following rotation in the clockwise direction. Each photograph presents the shear structures observed when the corresponding thin-section was viewed with one vane blade assuming the vertical position. The total number of structures and their full extent around the vane periphery at any one stage are shown in Figs. 6.8b to 6.11b. These are tracings of the shear structures taken from photographs of each thin-section at two different positions, one at 45° to the other (see Section 3.4.6D), which ensures that all structures are included.

n	w (%)	θ (deg)	D_r (%)	A_r (%)	I_D
2	40	9.5	8.1	10.6	0.76
3	40	11	18.0	12.4	1.45
4	50	0	16.4	14.1	1.16
"	50	6.5	21.9	14.1	1.55
"	60	1.5	23.2	14.1	1.65
"	46	0	52.7	21.6	2.44
6	60	0	19.4	17.7	1.10

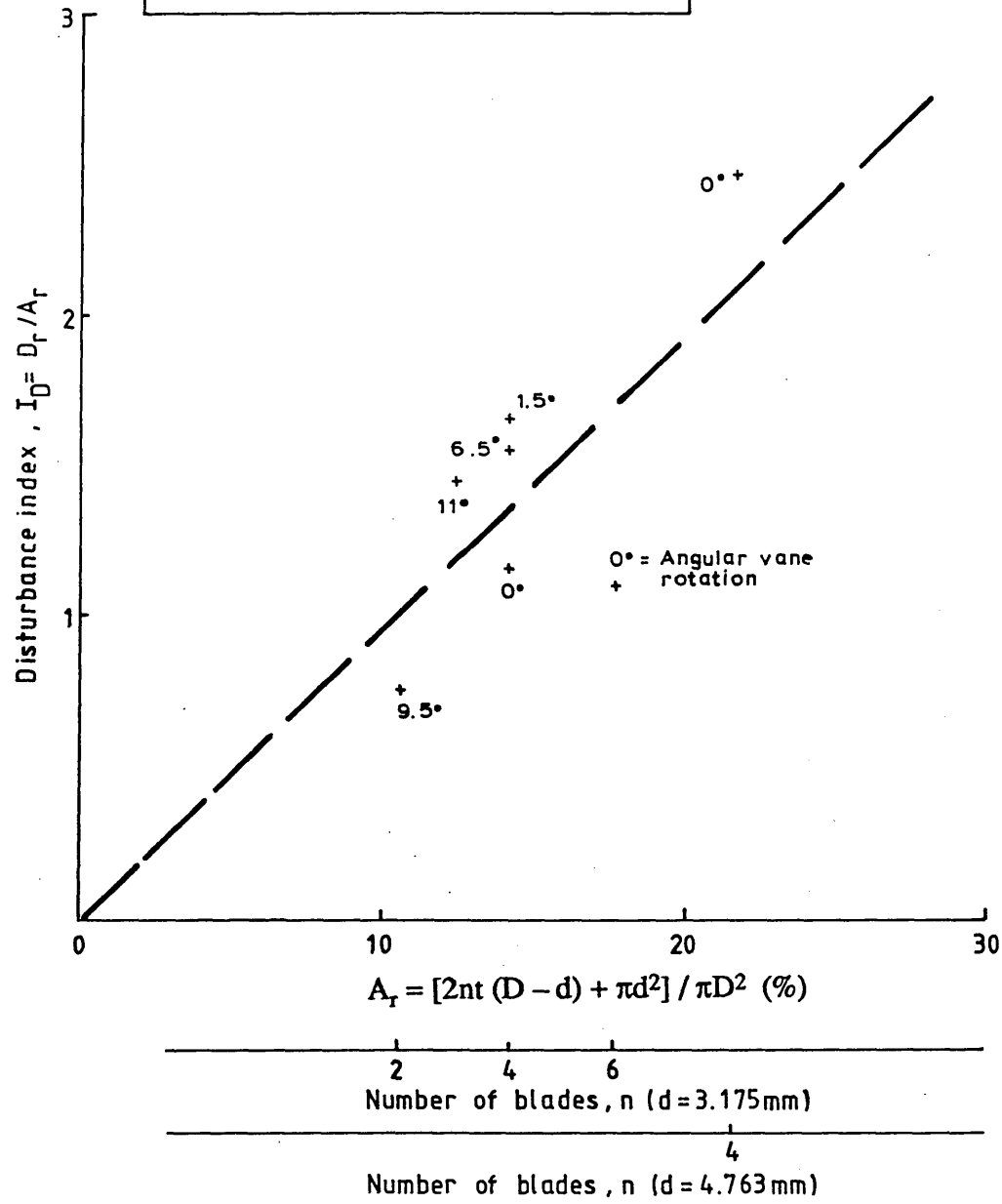


Fig. 6.6 Disturbance index versus vane area ratio/number of blades.

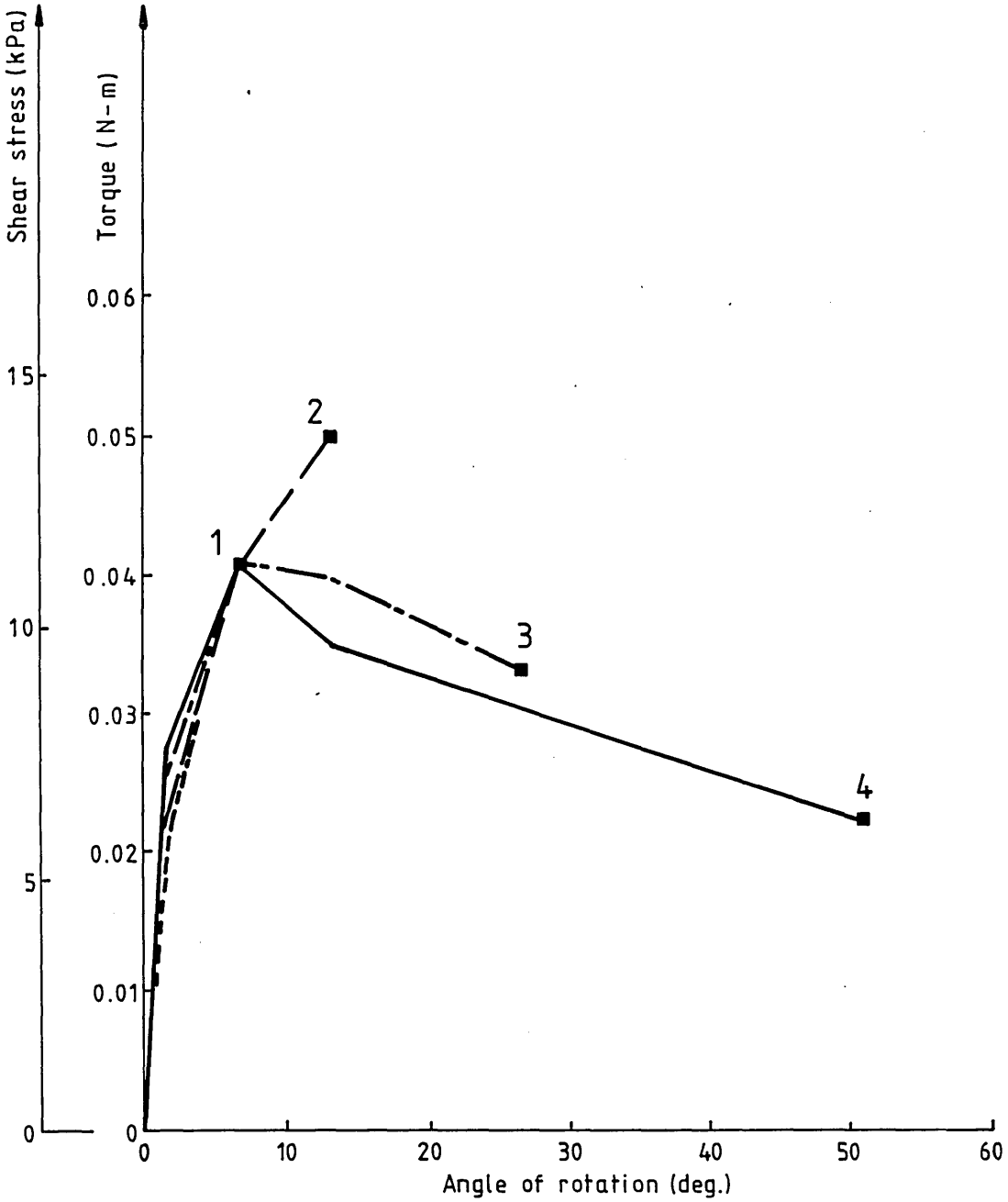


Fig. 6.7 Different stages of 4-bladed vane test in kaolin ; w ≈ 60%.

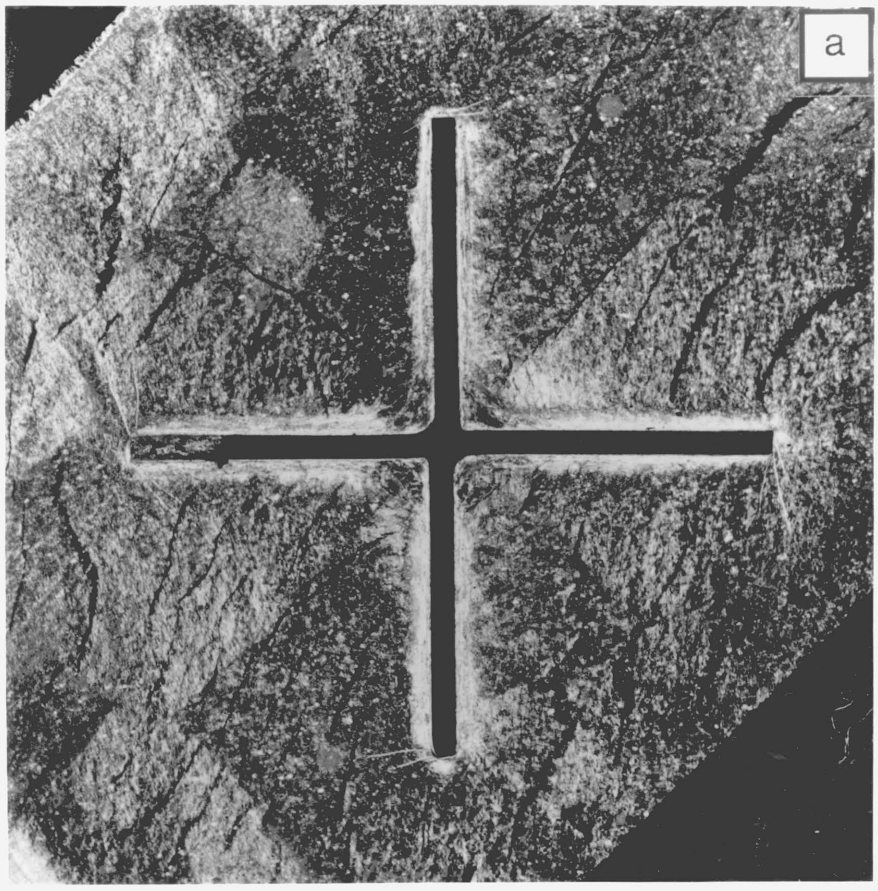
The development of the shear structures after an angle of rotation of about 6.5° (which corresponds to pre-peak conditions; Fig. 6.7) is shown in Figs. 6.8a and b. The repeatability of the structures at the tip of each vane blade is remarkable. Both 'leading' and 'trailing' features, respectively, can be seen in front of and behind each vane blade. In general, there are two (sometimes three) leading and one or two trailing shear structures, all of which appear to have initiated tangential to the tips of the vane blades before further propagation along different angles relative to the blade tips. The leading structures are 'straight' and fall outside the vane circumference, while the trailing structures are 'curvilinear' and lie inside the periphery of the vane. The shear structure characteristics — including number, 'length' and 'angle of propagation' — are described quantitatively in Section 6.4.1.

Figs. 6.9a and b show the characteristics of the shear structures at or about peak torque, corresponding to an angle of rotation of about 12.5°. Both the number and the extent of the shear structures have increased: three leading and three or four trailing shear structures can be seen around each vane blade. The leading shear structures are now longer, and the curvature of the trailing shear structures is much more pronounced. Furthermore, there is no evidence of a circular failure surface around the vane perimeter, although a continuous surface can be seen in one quadrant.

Conditions post peak (angle of rotation of about 26.5°) can be seen in Figs. 6.10a and b, which show that a continuous cylindrical surface has formed around the vane circumference. Again, an increase is evident in both the number and the extent of both the leading and trailing shear structures, although the former are 'remnant' features at this stage. The vane failure zone approximately corresponds to the vane periphery, extending both inside and outside of it.

'Residual' conditions at an angle of rotation of about 51° are evident in Figs. 6.11a and b which show both leading and trailing 'relic' shear structures, and a well-defined 'shear zone', which is particularly clear in one quadrant.

A distinct circular shear surface defined by the vane circumference can be seen in Figs. 6.12a and b, which show photographs of a triaxial-vane test stopped after 365° rotation in normally consolidated kaolin having a water content of about w = 46% (see curve 1, Fig. 8.2); remnant leading shear structures are clearly observed at the vane blade tips.



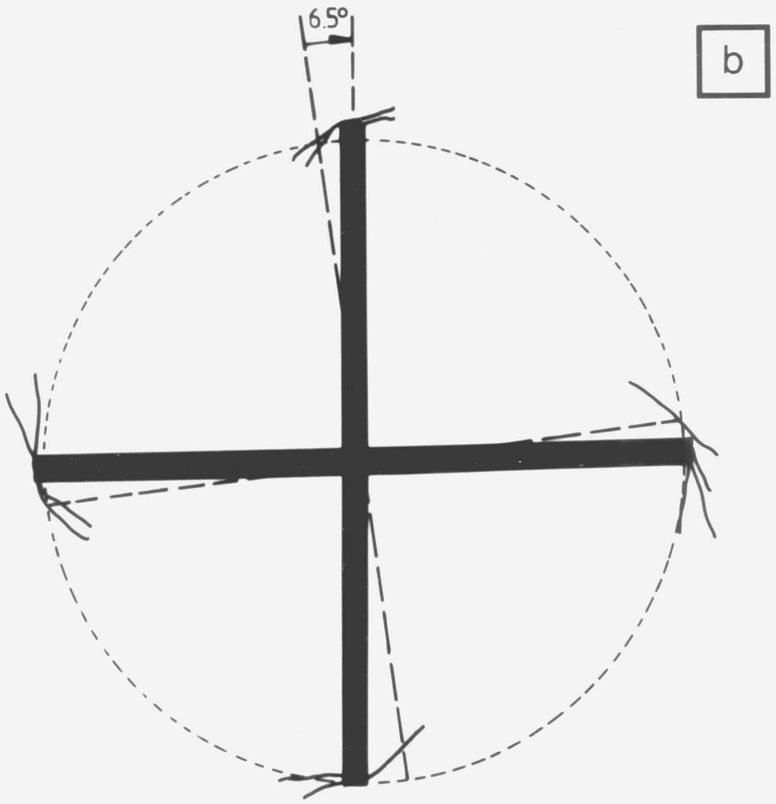
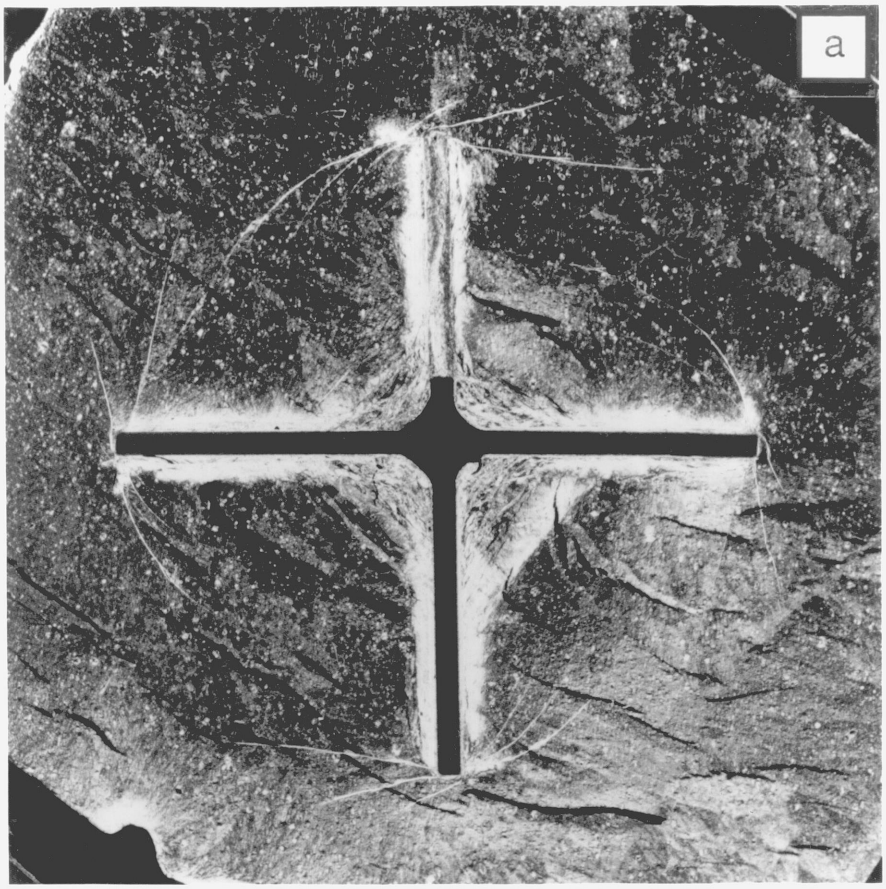


Fig. 6.8 Pre-peak shear structures around a 4-bladed vane in kaolin; stage 1, Fig. 6.7.



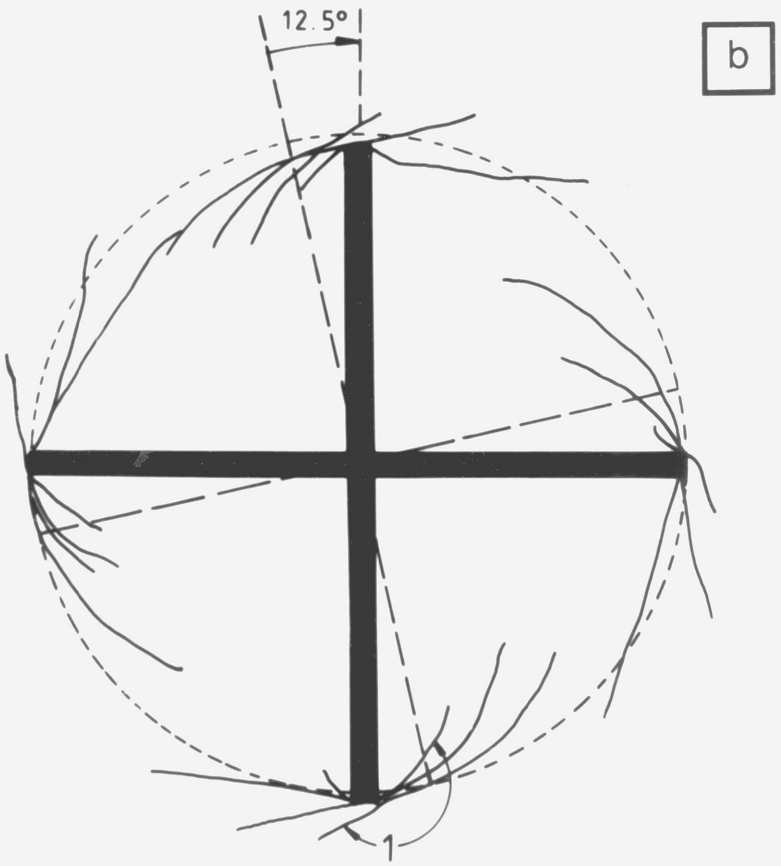
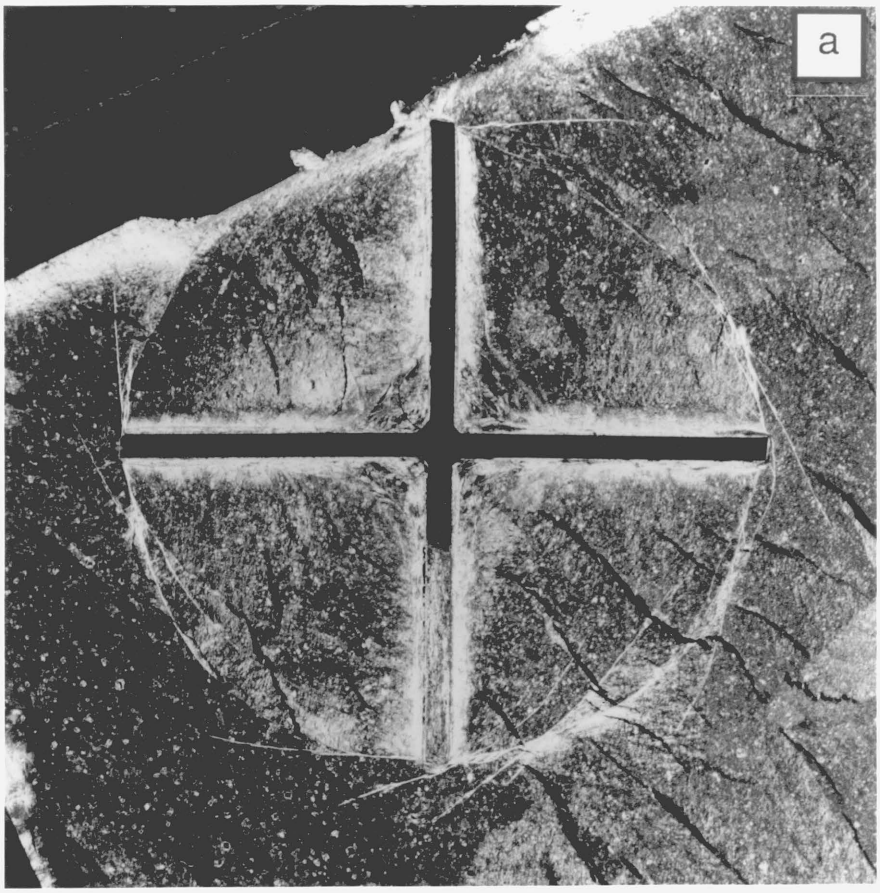


Fig. 6.9 4-bladed vane shear structures propagating at peak shear stress in kaolin; stage 2, Fig. 6.7.



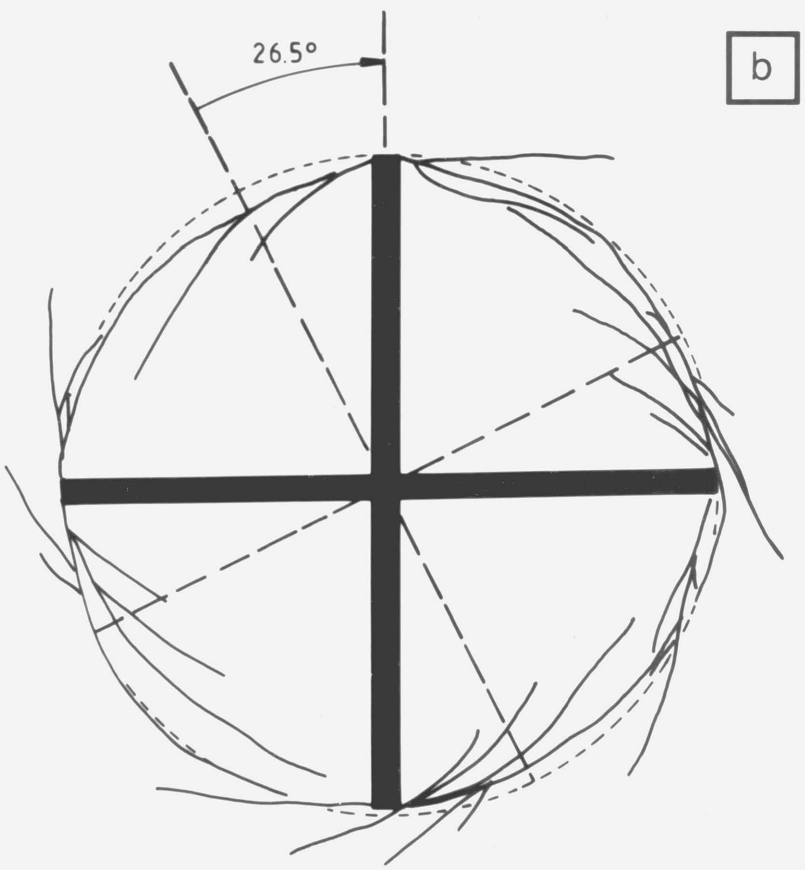
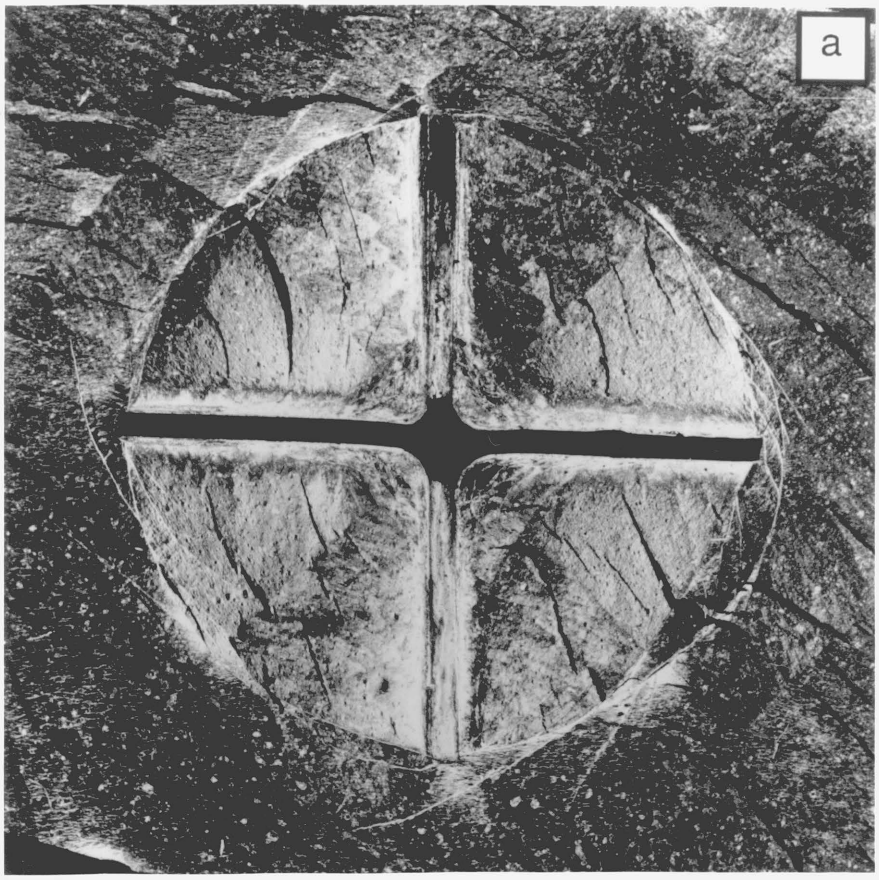


Fig. 6.10 4-bladed vane shear structures developed post peak shear stress in kaolin; stage 3, Fig. 6.7.



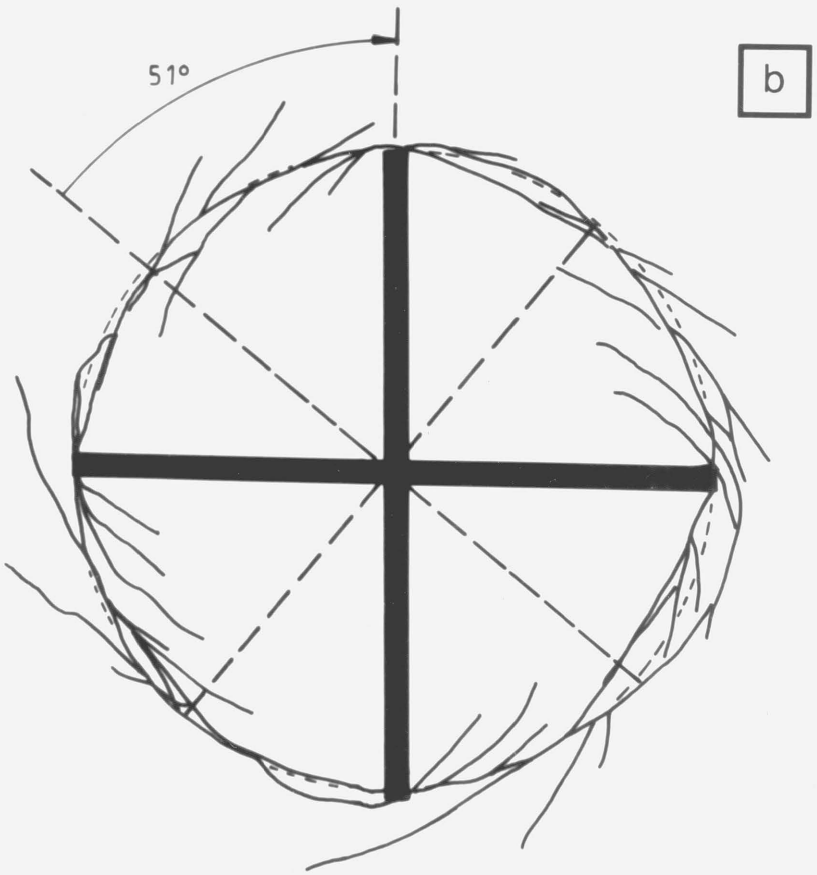
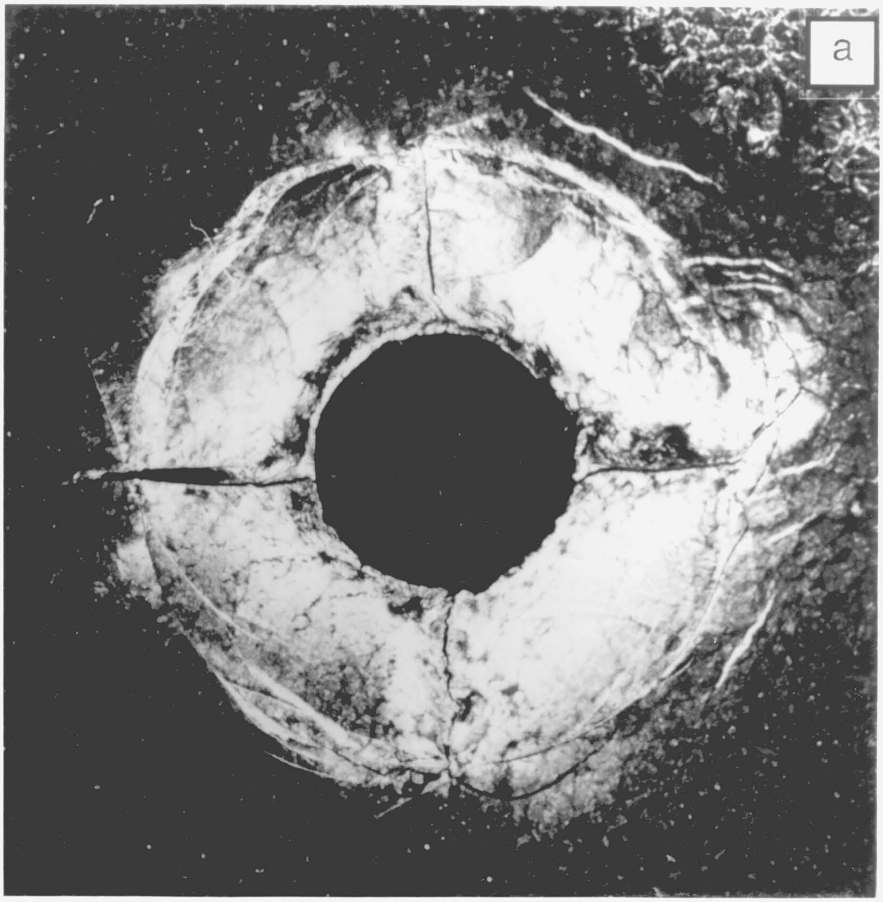


Fig. 6.11 Residual shear structures around a 4-bladed vane in kaolin; stage 4, Fig. 6.7.



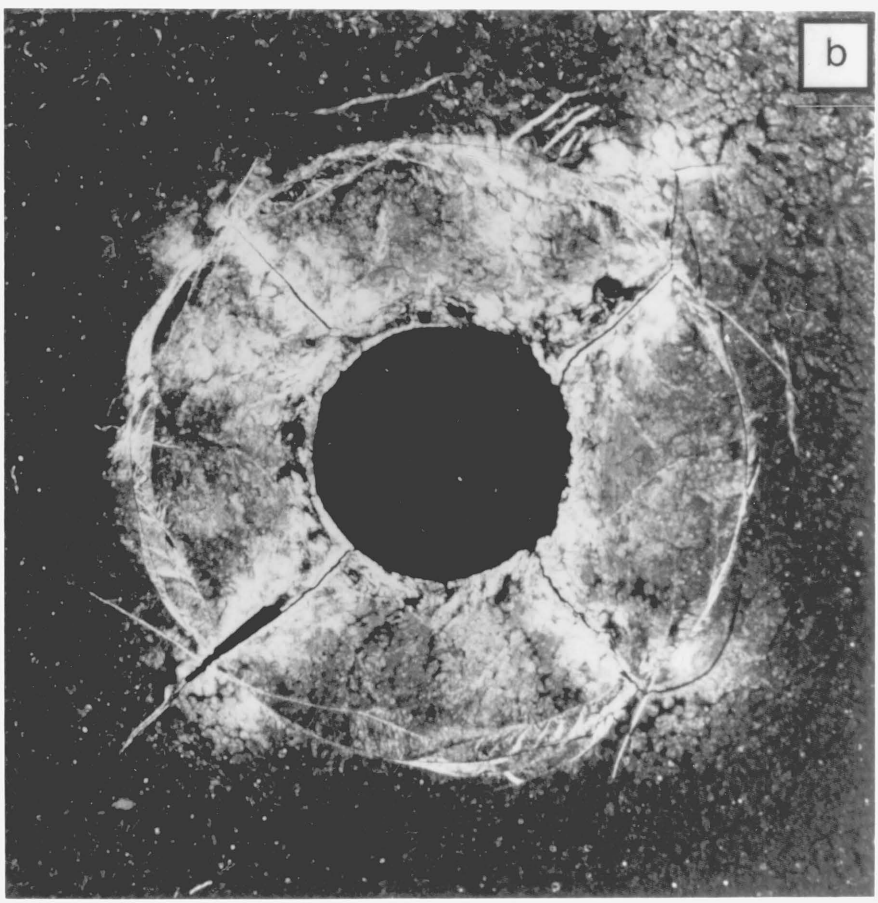


Fig. 6.12 Shear structures around a 4-bladed triaxial-vane rotated through 365°; curve 1, Fig. 8.2.

Observations made from longitudinal thin-sections (Section 3.4.6C) — prepared from samples rotated to peak and 'residual' torque — showed that there was little or no development of shear structures in the vertical direction, with the shear zone around the vane extending vertically by no more than 10% of the vane diameter beyond the top and bottom horizontal surfaces (see Section 3.2.2A(i)).

In summary, each vane blade causes high stress concentrations which lead to intensive local straining and subsequently, to the formation of shear structures. The first leading and trailing shear structures (see, e.g. (1) in Fig. 6.9b), are formed at an early stage of the test, but as vane rotation proceeds, the development of these structures is arrested as new structures develop at successively lower angles of propagation relative to the tips of the vane blades. This progression continues with increasing rotation of the vane. Thus, both the number and the extent of penetration of both leading and trailing shear structures increase up to peak torque, although a continuous shear surface does not develop until post-peak conditions are reached. The vane failure zone forms an annulus, with its inner and outer perimeters extending both inside and outside the vane periphery. At large rotations corresponding to 'residual' conditions, a well-defined circular shear surface circumscribes the vane blades.

The only other set of data cited in the literature which show the deformation patterns in the soil as a consequence of vane rotation, were obtained by Rush (1975) from his tests on Washed Beach sands. The tests were carried out under zero confining stress, similar to the conditions of the laboratory-vane test programme of the present study. Figs. 6.13a and b are tracings of the vane cross-section and the shear structures observed in Figs. 2.6a and b. Although the respective stages of the shear stress – rotation curve were not specified, the propagated shear structures have characteristics which, as can be seen, compare closely with those observed around the vertical periphery of 4-bladed vanes rotated in kaolin (see Figs. 6.8b–6.11b; for comparative purposes, Figs. 6.8b and 6.11b are re-presented here adjacent to Figs. 6.13 a and b). According to Rush, shear structures occurred just prior to failure and increased in length with further rotation until a complete circular failure surface was formed at a rotation of about 12°.

Fig. 6.13a shows both leading and trailing structures at the blade tips, and may be compared with Figs. 6.8b and 6.9b which correspond to conditions prior to and at peak shear stress respectively; there are fewer trailing structures behind the blades of the vane rotated in Washed Beach sands. Remnant leading and trailing shear structures which are evident in Fig. 6.13b are consistent with those relic structures seen in Figs. 6.10b and 6.11b which correspond to post-peak and residual conditions respectively.

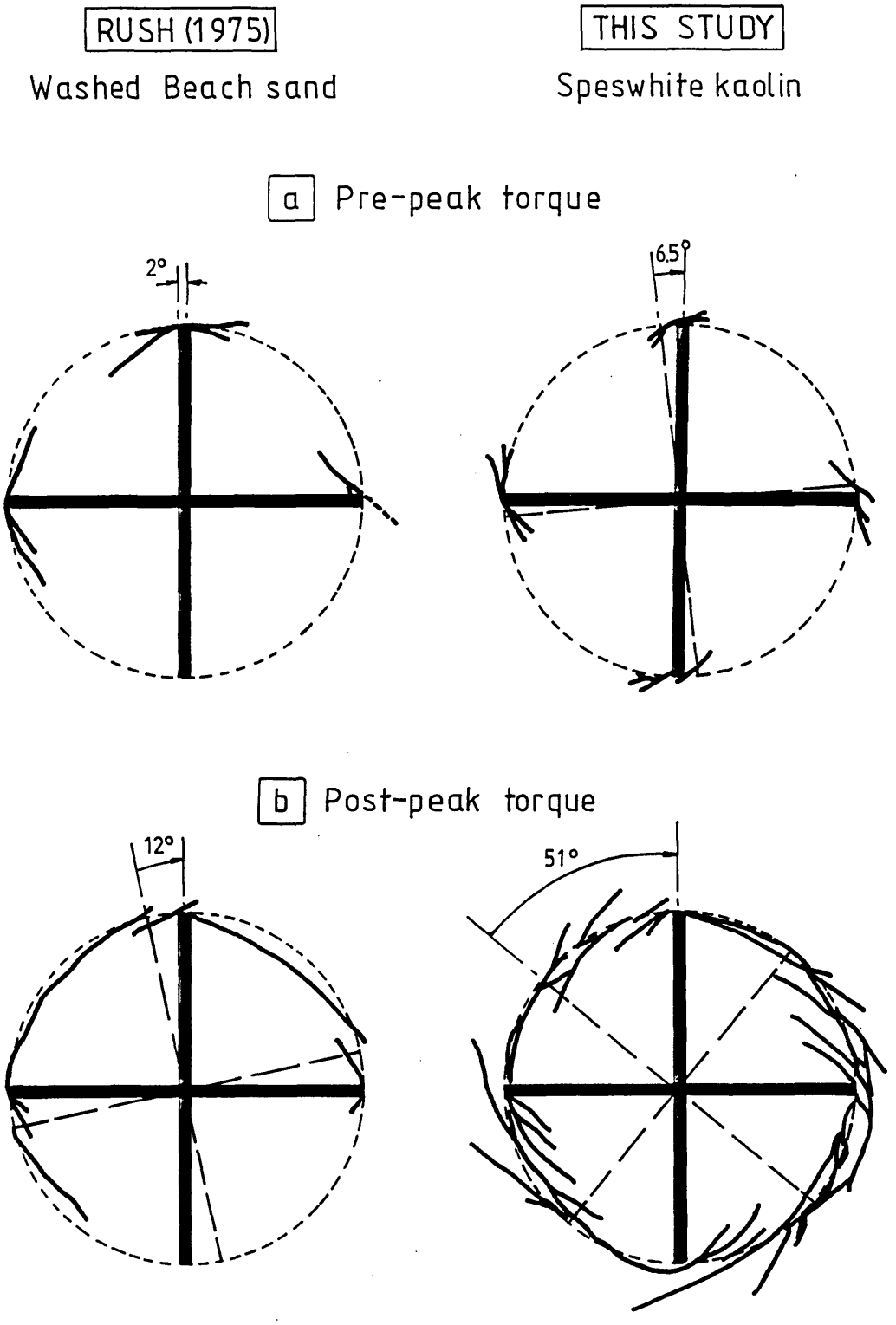


Fig. 6.13 Shear structures propagated in Washed Beach sand compared with vane shear structures in reconstituted kaolin.

It is useful to note that Rush also carried out identical tests on Leighton Buzzard sand, which, when radiographed, failed to show any shear structures. He consequently concluded that the extent of the vane failure zone in cohesionless materials would depend upon index properties such as density and grain size.

6.3.3B Conditions close to peak torque

The tests were performed on normally consolidated kaolin having a water content of about w = 50%. Fig. 6.14 shows the individual shear stress – rotation curves corresponding to four different stages where vane rotation was stopped just pre-peak (stage 1), at peak (stage 2) and just post-peak (stage 3), as well as post-peak (stage 4).

The development of the shear structures at stages 1–4 is respectively presented in Figs. 6.15a to 6.18a. Schematic diagrams which show all the shear structures at the vane tips at stages 1–4 are presented in Figs. 6.15b to 6.18b respectively; as before (see Section 6.3.3A, above) each diagram is a tracing of two photographs of each thin-section taken from two different slide positions, one at 45° to the other. Except for very minor differences which are apparently due to sample water content effects, discussed later in Section 6.3.5, the nature of the shear structures compares well with that described in Section 6.3.3A.

It is clear from Figs. 6.16b and 6.17b that at peak torque a continuous circular surface has not developed around the vane periphery; a cylindrical failure surface circumscribing the vane forms immediately post peak. A similar conclusion may be drawn from the tests presented in Section 6.3.3A.

Figs. 6.19a and b show photographs of the deformation patterns associated with peak torque conditions in a triaxial-vane test on normally consolidated kaolin with a water content of about w = 46% (see curve 2, Fig. 8.1). Despite the large extent of fabric disturbance due to vane insertion effects (see Figs. 6.4a and b), the nature of the leading and trailing shear structures in Figs. 6.19a and b is consistent with that observed in the laboratory-vane tests. In addition, as also observed in Figs. 6.9b and 6.16b, there is no evidence of a continuous shear surface circumscribing the vane blades at failure.

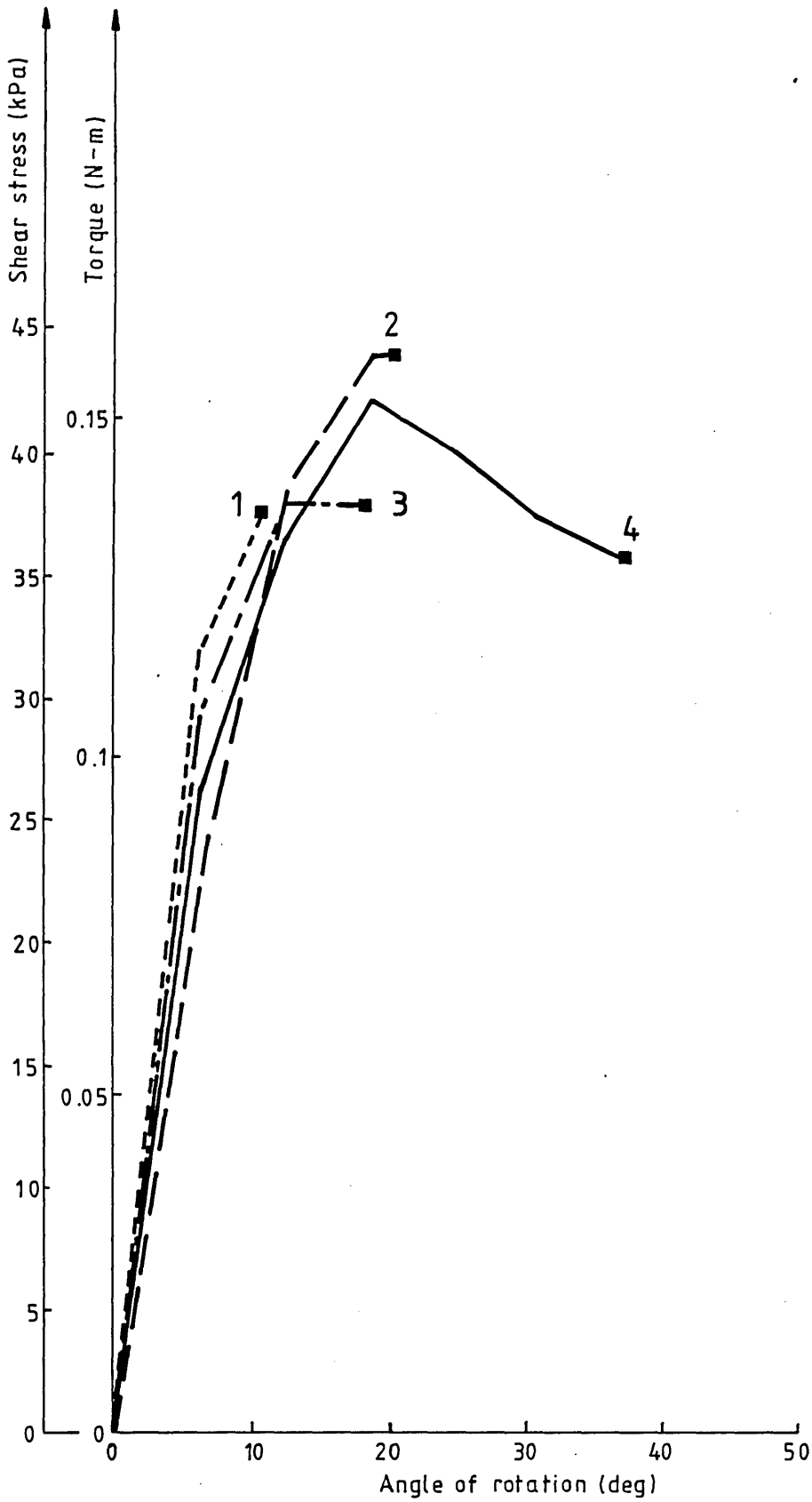


Fig. 6.14 Different stages of 4-bladed vane rotation in kaolin ; $w \approx 50\%$.

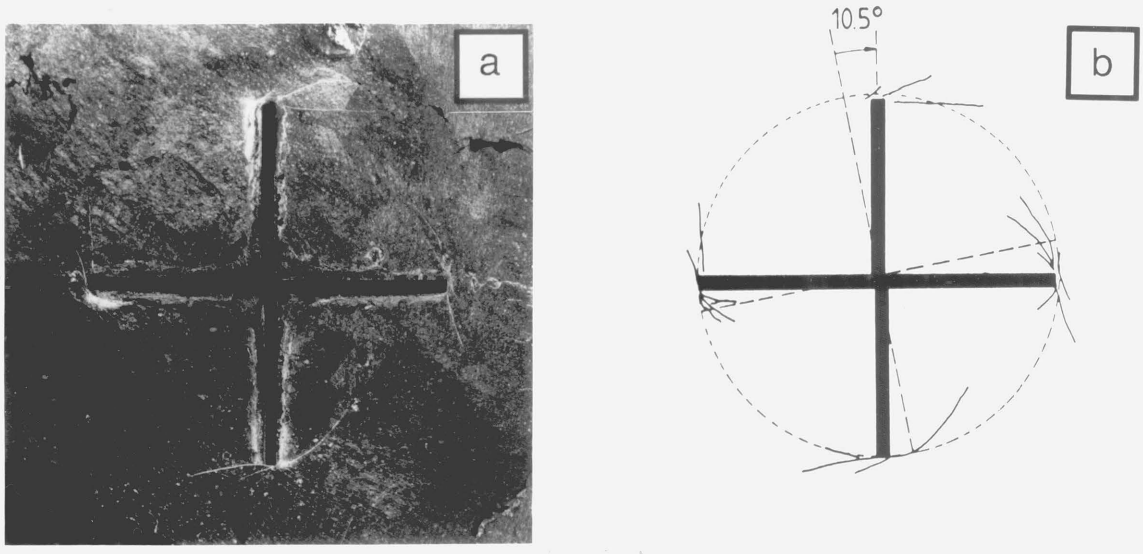


Fig. 6.15 Shear structures propagated immediately prior to peak shear stress ; stage 1, Fig. 6.14.

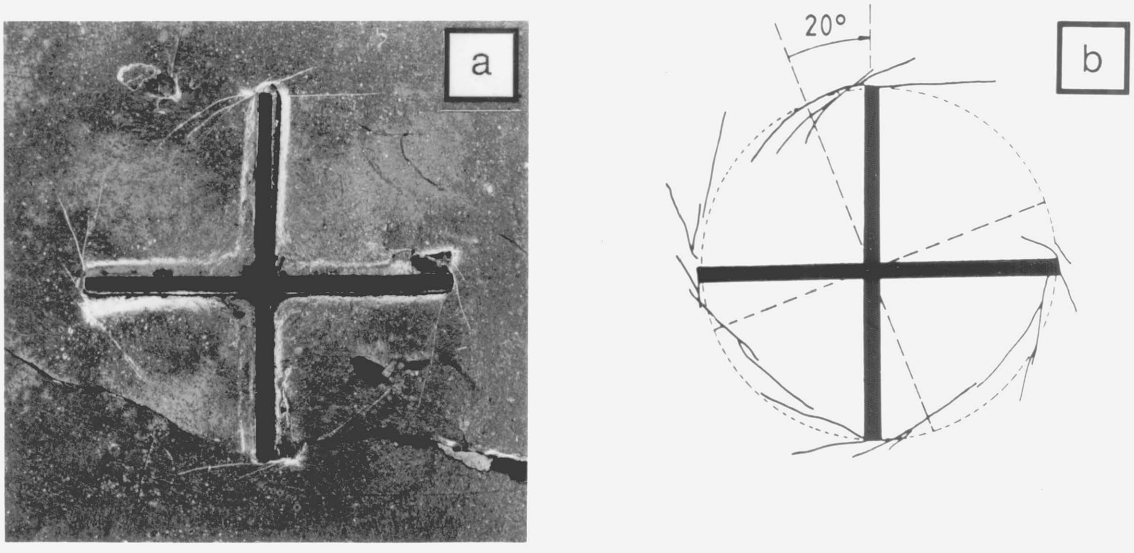


Fig. 6.16 4- bladed vane shear structures developed at peak shear stress; stage 2, Fig. 6.14.

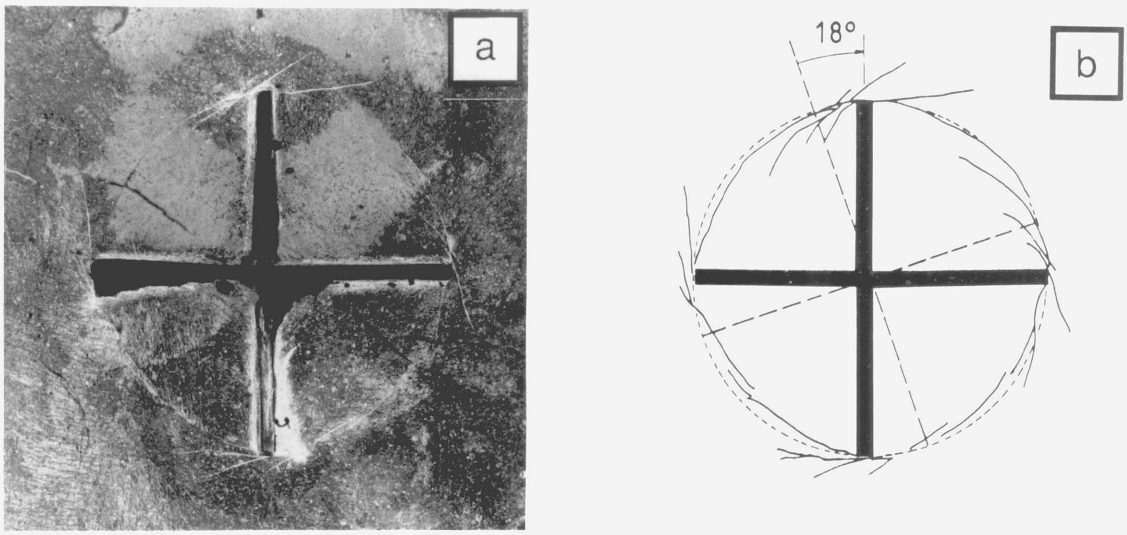


Fig. 6.17 Shear structures propagated immediately post peak shear stress; stage 3, Fig. 6.14.

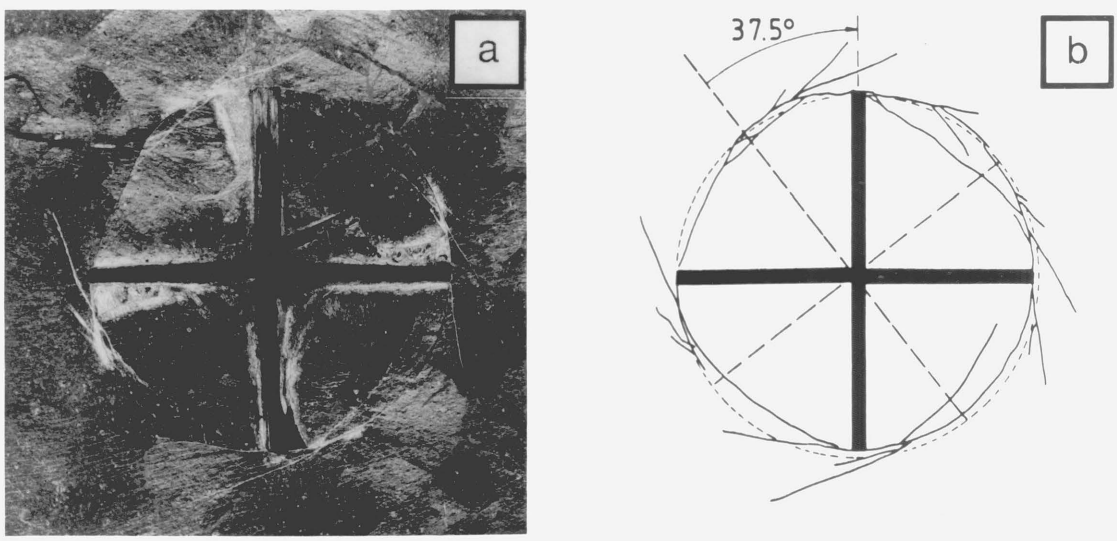


Fig. 6.18 Post-peak shear structures around a 4-bladed vane in kaolin; stage 4, Fig. 6.14.

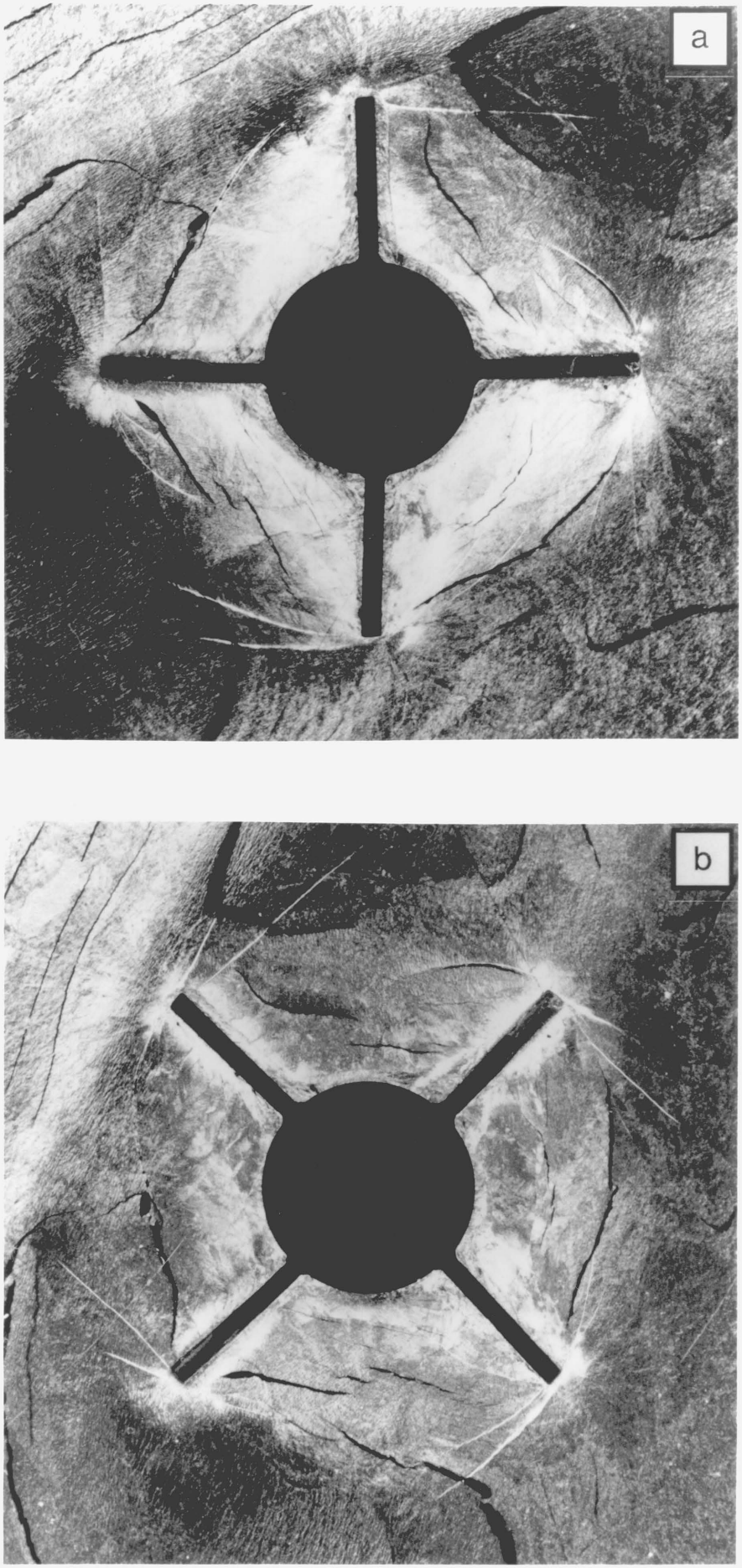


Fig. 6.19 Shear structures developed at peak shear stress around a 4-bladed triaxial-vane in kaolin.

6.3.4 The Effect of Different Numbers of Blades

This series of tests was undertaken in order to examine the influence of the number of vane blades on the vane failure mode.

Kaolin was used exclusively; the samples having been normally consolidated to a water content of about w = 60%, i.e. the same water content as that of the samples used in the first series of tests (see Section 6.3.3A). The vane failure mechanisms associated with vanes with two, three and six blades were investigated; all vanes were 12mm square.

6.3.4A The 2-bladed vane

Fig. 6.20 shows the individual shear stress – rotation curves of 2-bladed vane tests stopped at angles of rotation of 12.5° (stage 1), 25° (stage 2), 37.5° (stage 3) and 62.5° (stage 4); stages 1 to 3 correspond to conditions prior to peak shear stress, while stage 4 represents conditions at peak shear stress. The actual deformation patterns for stages 1–4 are presented in Figs. 6.21a to 6.24a, while Figs. 6.21b to 6.24b are schematic diagrams of all the shear structures observed from the thin-sections.

Figs. 6.21b–6.24b show both leading and trailing shear structures which respectively fall outside and inside the periphery of the vane, although the newly formed leading shear structures lie within the vane perimeter. Moreover, the leading shear structures extend farther than the trailing ones and are therefore far more pronounced — a feature which contrasts with the structures developed around the 4-bladed vanes (Figs. 6.8–6.11). At stages 1–3 there are typically four distinct leading shear structures tangential to each vane blade, whilst the number of tangential structures behind each vane blade is one or two. However, well-defined 'curved' structures can be seen behind each blade extending beyond the point of intersection of the vane blades (Figs. 6.22–6.24). These structures appear to have propagated from the blade tips (Fig. 6.21), but have subsequently become remnant features, probably because of the gap which forms behind each vane blade at larger rotations. With increasing angles of rotation, more of these curved structures are initiated, the latter intersecting the earlier structures and thus forming a shear failure pattern (see, e.g. Fig. 6.23b).

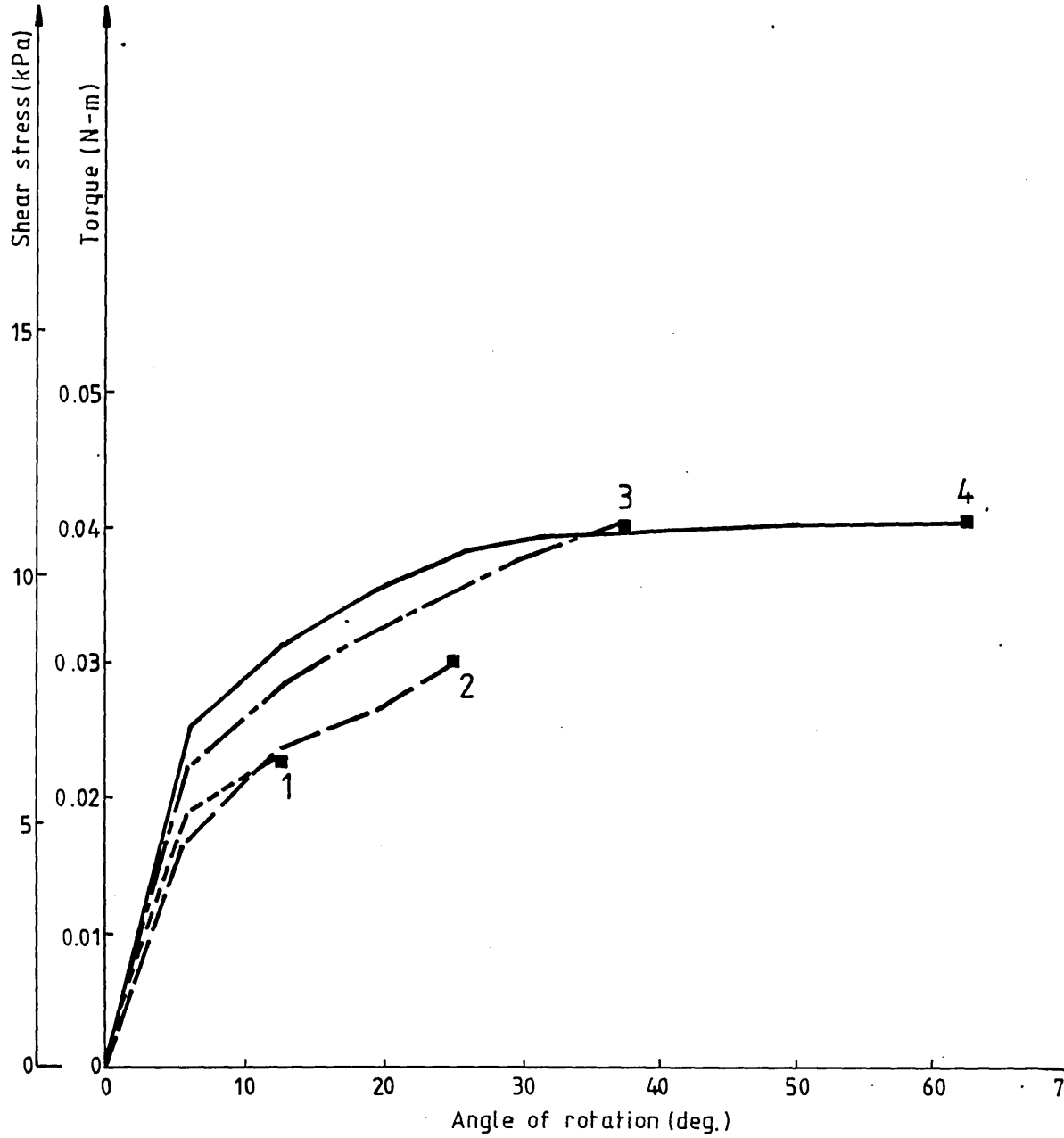
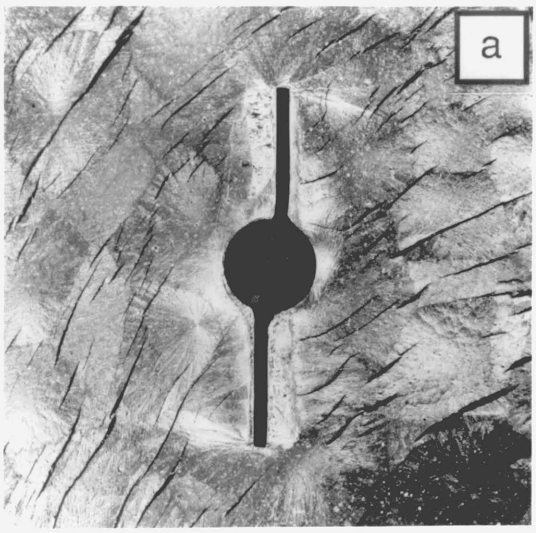


Fig. 6.20 Different stages of 2-bladed vane test in kaolin.



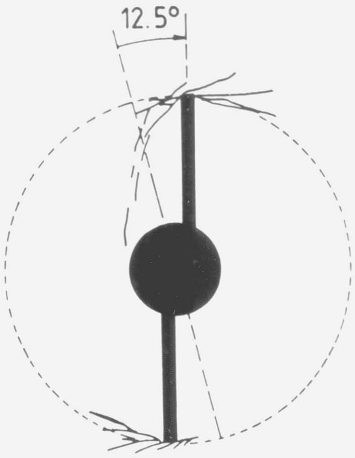
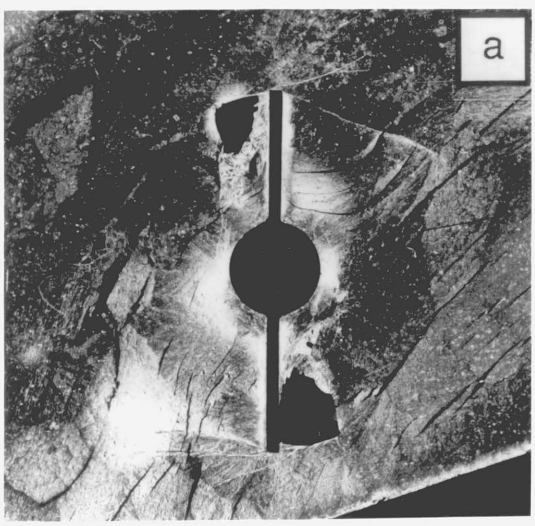


Fig. 6.21 Stage 1, Fig. 6.20.



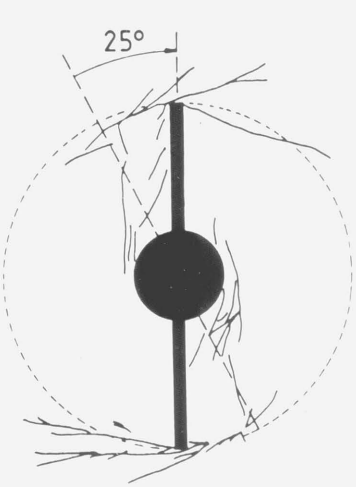


Fig. 6.22 Stage 2, Fig. 6.20.

Pre-peak shear structures around a 2-bladed vane rotated in kaolin.

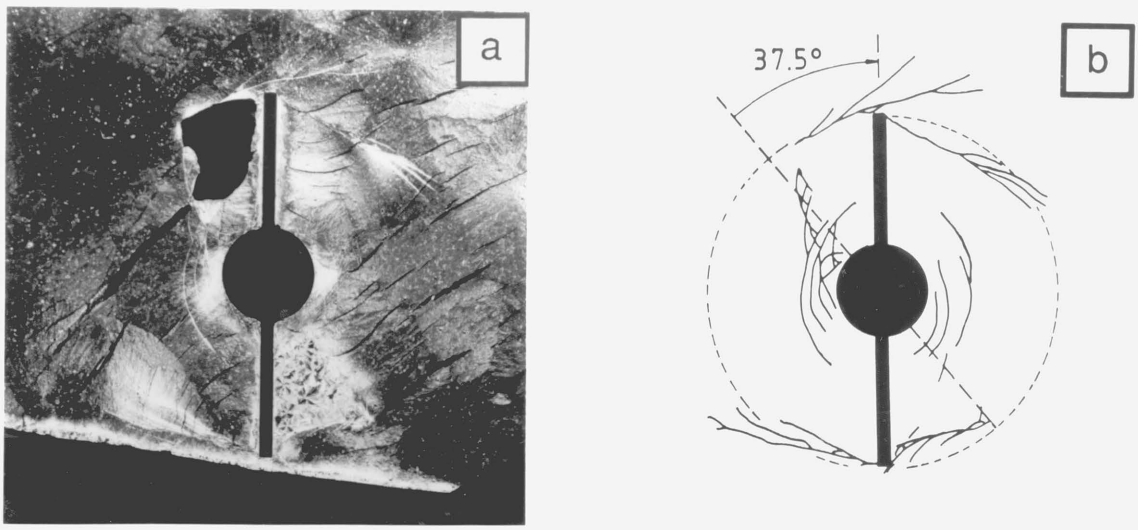


Fig. 6.23 2-bladed vane shear structures developed prior to peak shear stress in kaolin; stage 3, Fig. 6.20.

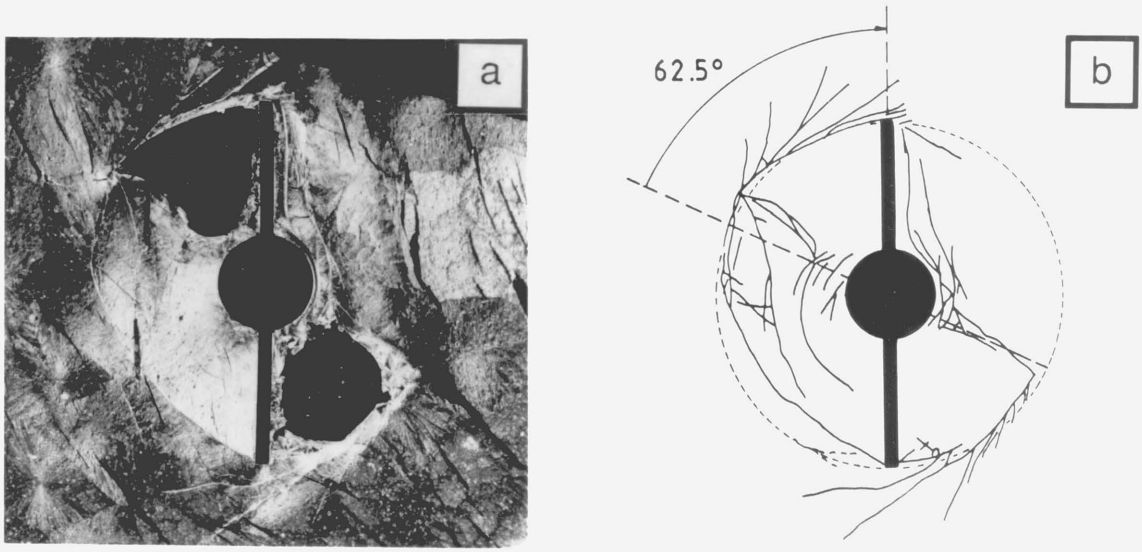


Fig. 6.24 2-bladed vane shear structures propagating at peak shear stress ; stage 4, Fig. 6.20.

Despite some uncertainty associated with the exact angle of rotation at which the peak torque is reached, there is no doubt that a continuous surface is not developed until after the peak shear stress, since in Fig. 6.23b — which shows conditions just pre-peak — there is no evidence of a surface circumscribing the vane blades, and in Fig. 6.24b corresponding to conditions just post-peak, a peripheral surface can be seen only over one semi-circle, lying partly within and partly on the vane perimeter.

The leading shear structures and the curved discontinuities evident behind each blade may respectively be compared with the passive and active rupture surfaces observed in front of and behind retaining walls. In particular, the shear failure pattern which results from the intersection of the curved shear structures behind each blade is similar to the slip-line field which is developed behind a retaining wall subjected to rotation about its top (see, e.g. James, 1971). Section 6.6 examines the similarities between the behaviour of 2-bladed vanes and that of retaining walls.

6.3.4B The 3-bladed vane

The individual shear stress – rotation curves showing the stages at which the 3-bladed vane tests were stopped are shown in Fig. 6.25. Figs. 6.26a to 6.29a show photographs of the shear structures developed around the vane after angles of rotation of 12.5° (stage 1), 25° (stage 2), 37.5° (stage 3) and 62.5° (stage 4), respectively corresponding to pre-peak, peak, just post-peak and post-peak shear stress conditions. Figs. 6.26b to 6.29b are schematic diagrams of all the shear structures observed. Clearly, both leading and trailing shear structures are similar to those observed around the 4-bladed vane. Typically, there are three leading and three or four trailing structures around each vane blade; the former extending beyond the vane periphery, while the latter are longer and lie within the perimeter of the vane.

Fig. 6.27 illustrates 'peak' conditions and shows a continuous surface over two out of the three segments — a more extensive shear surface than that observed at peak torque in the case of both 2- (Figs. 6.23 and 6.24) and 4-bladed (Figs. 6.16 and 6.17) vanes. With increasing angles of rotation, further structures develop both in front of and behind each vane blade, while the structures formed earlier at smaller angles of rotation can be seen as relic features. Conditions 'just post peak' are presented in Figs. 6.28a and b which show a complete continuous circular surface circumscribing the vane blades. 'Post-peak' conditions which are shown in Fig. 6.29 indicate that the continuous surface is closely defined by the vane perimeter.

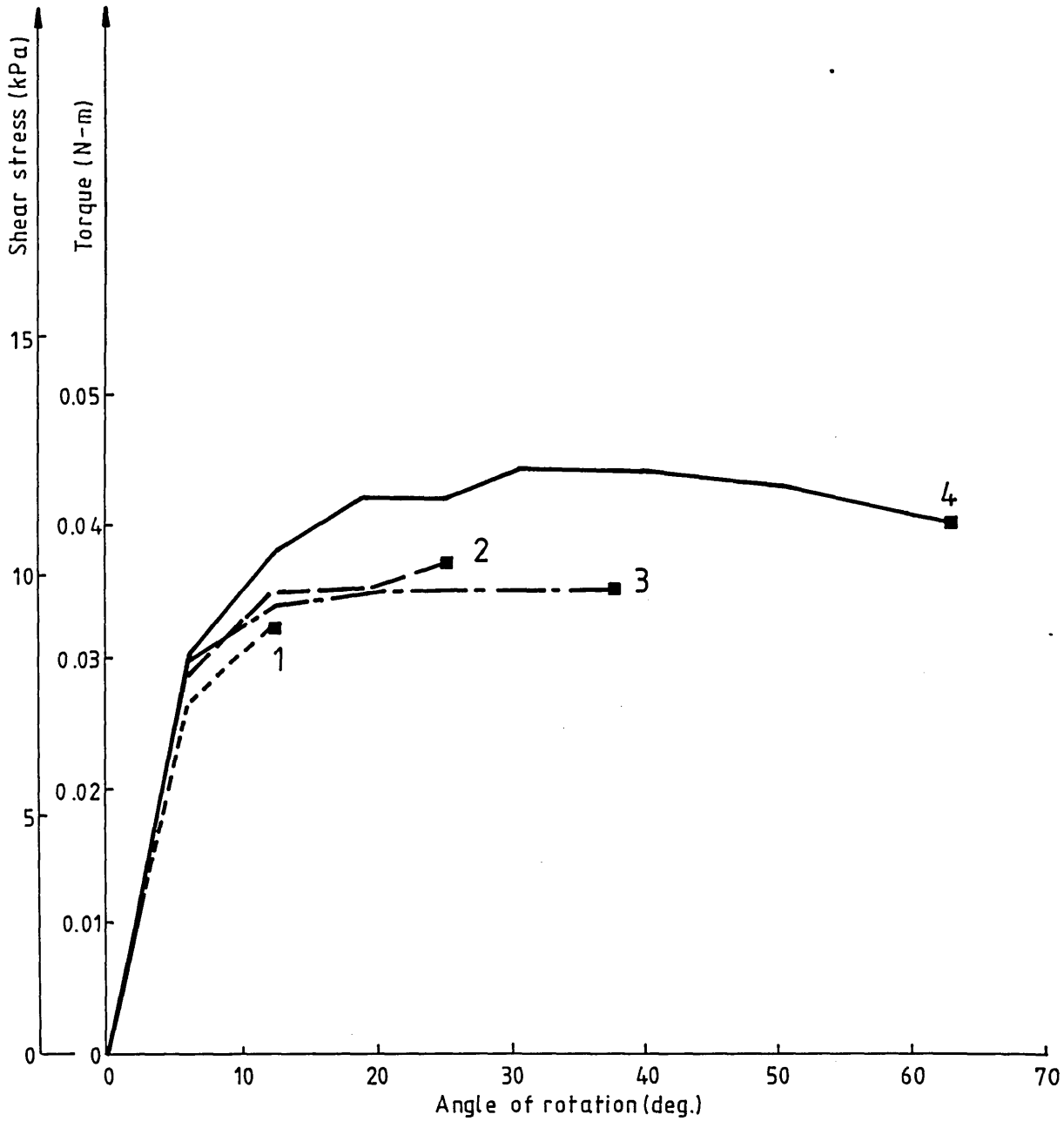


Fig. 6.25 Different stages of 3-bladed vane test in kaolin.

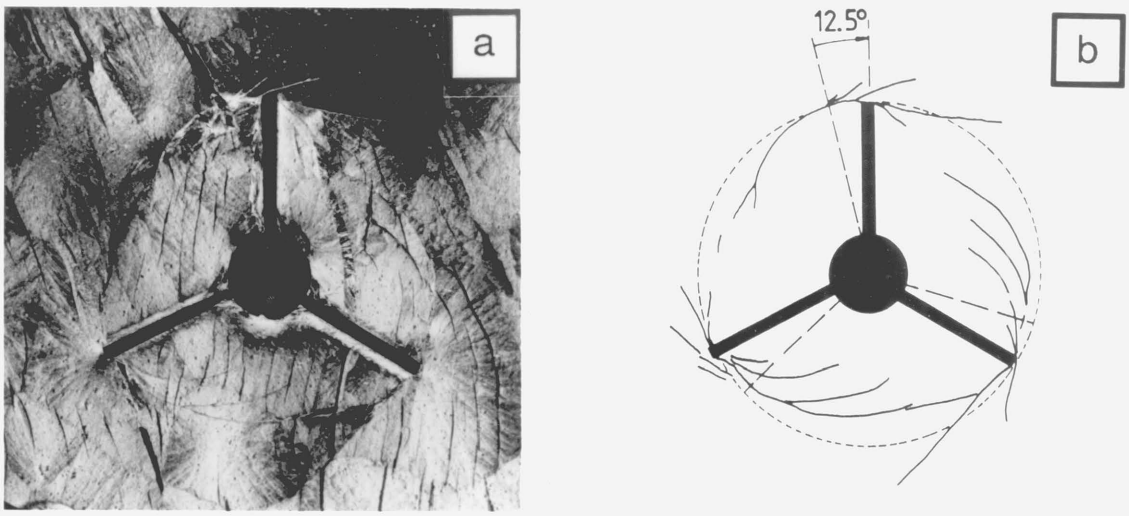


Fig 6.26 Pre-peak shear structures around a 3-bladed vane rotated in kaolin; stage 1, Fig. 6.25.

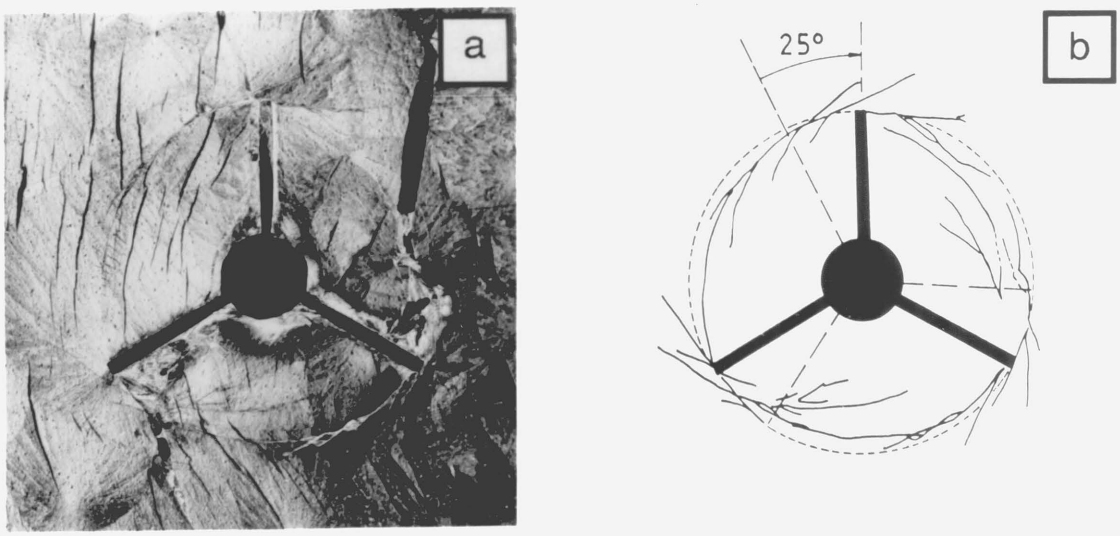


Fig. 6.27 3-bladed vane shear structures developed at peak shear stress; stage 2, Fig. 6.25.

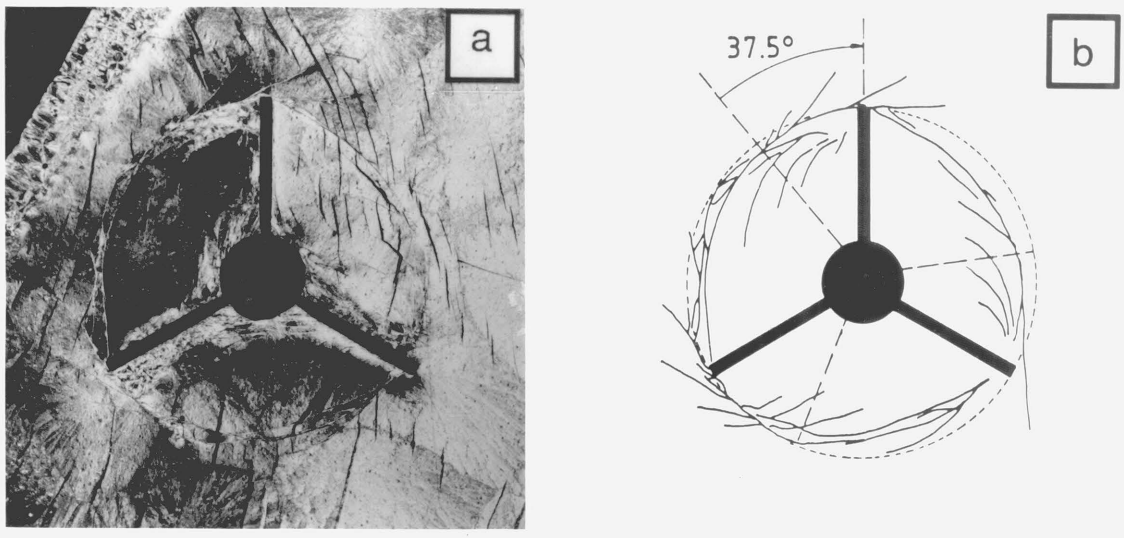


Fig. 6.28 3-bladed vane shear structures propagated immediately post peak shear stress ; stage 3, Fig. 6.25.

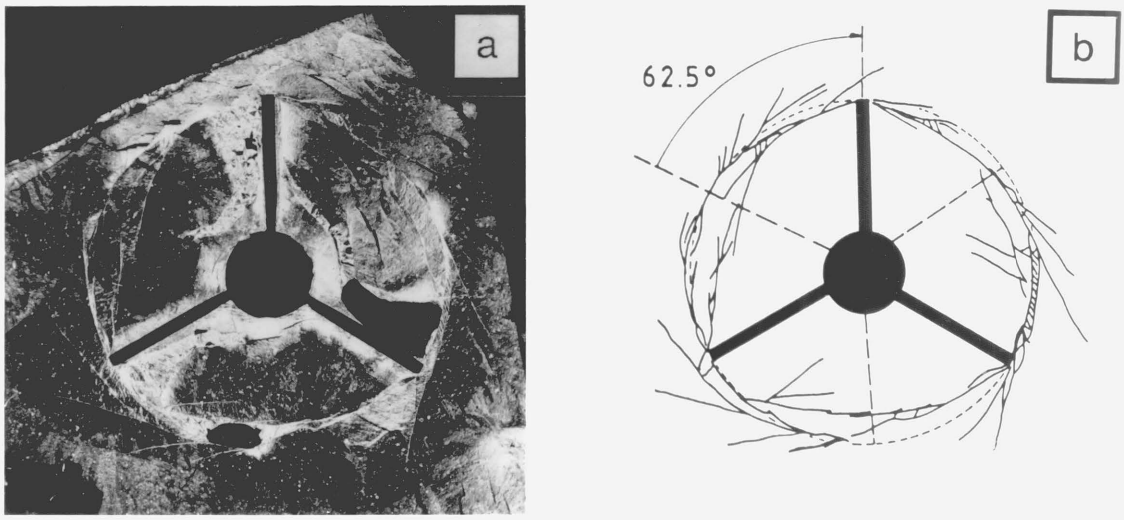


Fig. 6.29 3-bladed vane shear structures developed post peak shear stress; stage 4, Fig. 6.25.

6.3.4C The 6-bladed vane

Fig. 6.30 presents the individual shear stress – rotation curves showing the stages at which the 6-bladed vane tests were stopped. Photographs of the thin-sections are shown in Figs. 6.31a to 6.33a, which demonstrate the development of the shear structures around the vane after angles of rotation of 5° (stage 1), 10° (stage 2) and 11° (stage 3), respectively corresponding to pre-peak, peak and post-peak shear stress conditions. Schematic diagrams of all the shear structures (Section 6.3.3A) around each vane are presented in Figs. 6.31b to 6.33b.

Prior to peak shear stress (Fig. 6.31), one to three leading shear structures can be seen in front of each vane blade, although trailing structures (one or two in each case) are only evident behind three of the blades. Conditions close to peak torque (Fig. 6.32) resemble those observed with the 4-bladed vane (Fig. 6.9), and show more and longer leading and trailing shear structures than those seen prior to peak shear stress. Furthermore, there is no evidence of a continuous circular surface around the vane periphery, though one leading and one trailing structure are almost touching across one of the six segments at peak. Post peak shear stress (Fig. 6.33), a shear failure surface is seen circumscribing the vane, approximately defined by the vane perimeter; remnant shear structures can also be seen.

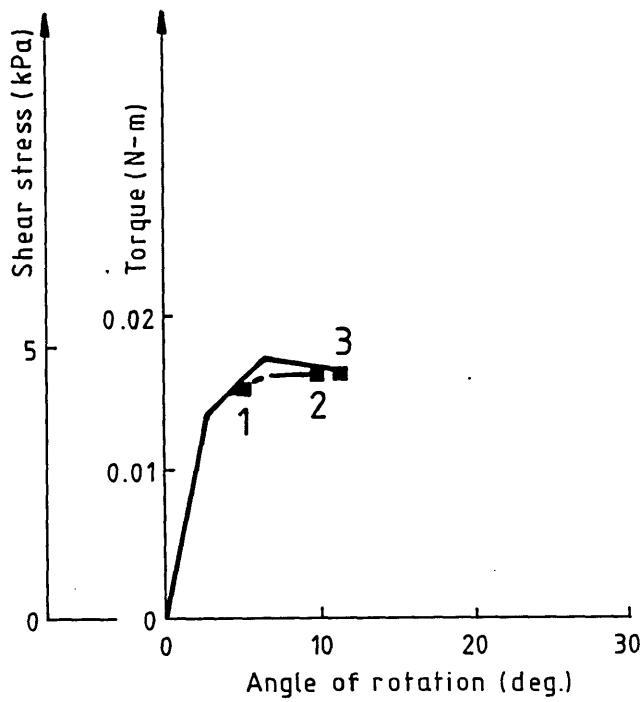


Fig. 6.30 Different stages of 6-bladed vane test in kaolin.

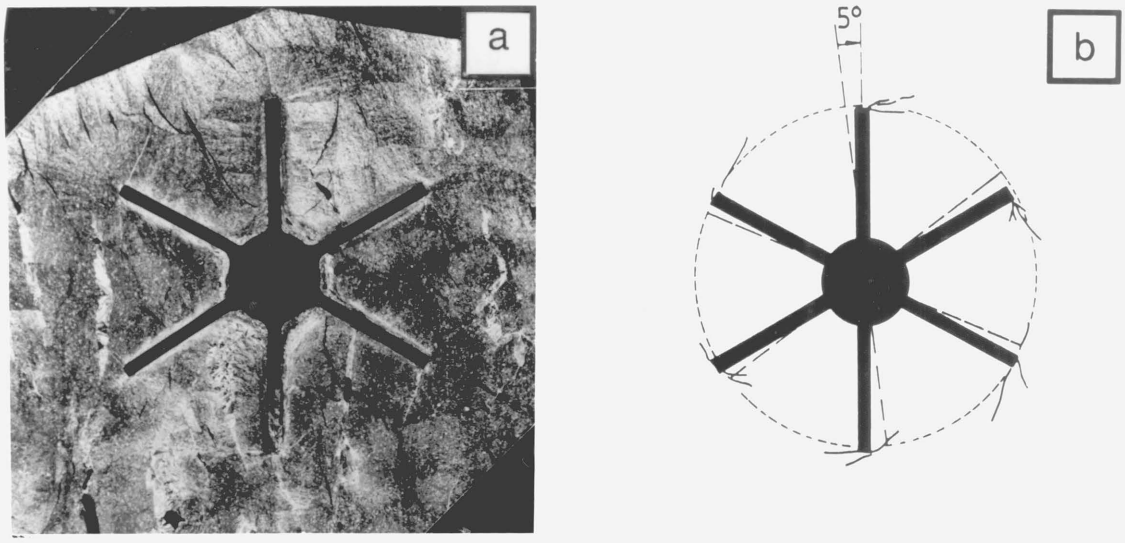


Fig. 6.31 Pre-peak shear structures around a 6-bladed vane in kaolin; stage 1, Fig. 6.30.

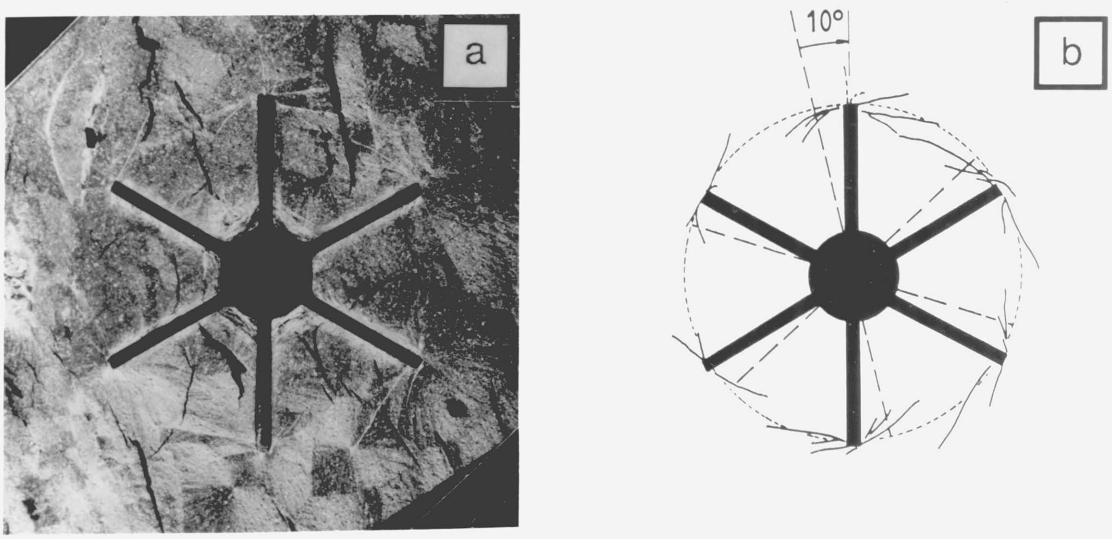
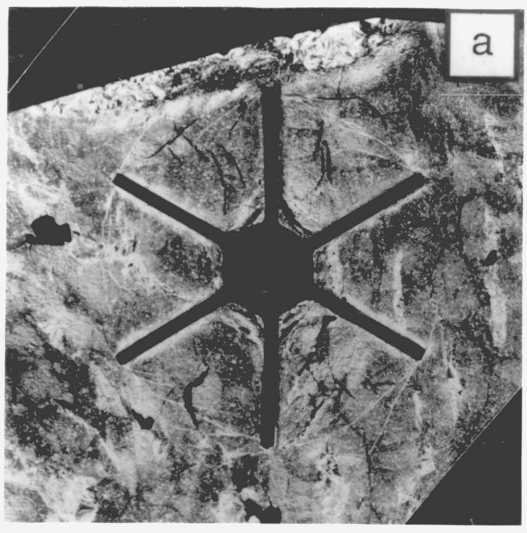


Fig. 6.32 6-bladed vane shear structures propagated at peak shear stress; stage 2, Fig. 6.30.



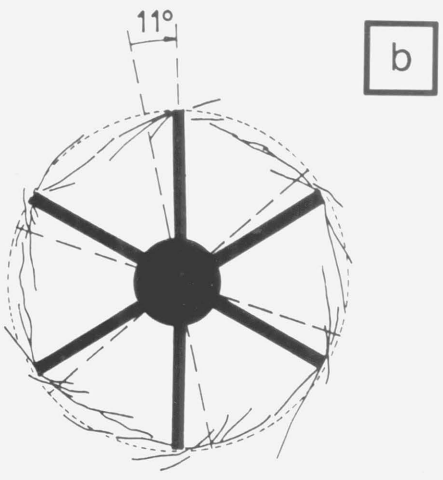


Fig. 6.33 Post-peak shear structures around a 6-bladed vane in kaolin; stage 3, Fig. 6.30.

6.3.4D Summary

Fig. 6.34 shows the average normalised shear stress – rotation ($\tau/\sigma_{vo}' - \theta$) curves of 2-, 3-, 4- and 6-bladed vane tests on reconstituted samples of kaolin having water contents of about w = 60%; values of shear stress were normalised with respect to the maximum consolidation stress on the samples prior to undrained unloading, in order to eliminate slight water content variations which existed between the samples (see Section 4.3.2). Stages at which thin-sections were taken are also presented in Fig. 6.34.

Clearly, there are differences between the normalised shear stress – rotation curves of tests with vanes having different numbers of blades (see Chapter 5); the trend being that lower angles of rotation are required to reach failure as the number of blades increases. In addition to these observations, the characteristics of the propagated shear structures described in Sections 6.3.3A and 6.3.4A–C further suggest that the vane failure mechanism is probably also dependent on the number of blades for the reasons given below:

(a) The pattern of deformation of the soil, as indicated by the propagation of shear structures, is similar around the vertical periphery of the 4- and 6-bladed vanes. However, the shear structures around the 2-bladed vanes differ from the 4-bladed vanes. The nature of the shear structures developed around the vertical periphery of the 3-bladed vanes is largely consistent with that of the 4-bladed vanes, yet with some aspects in common with the 2-bladed vanes.

(b) There is no evidence of the formation of a continuous circular surface around the periphery of any of the vanes at peak torque, although a shear surface circumscribing the blades can be seen over two out of the three segments of the 3-bladed vane.

Furthermore, it is of importance to notice that the final shear surface which circumscribes the vane does not result from a gradual progressive development of a single structure initiated upon vane rotation, although individual leading and trailing shear structures develop successively with increasing rotation until such time that further propagation is arrested due to the kinematic restraints of the vane test. Therefore, there is no indication of a progressive mode of failure in any one of the vanes tested.

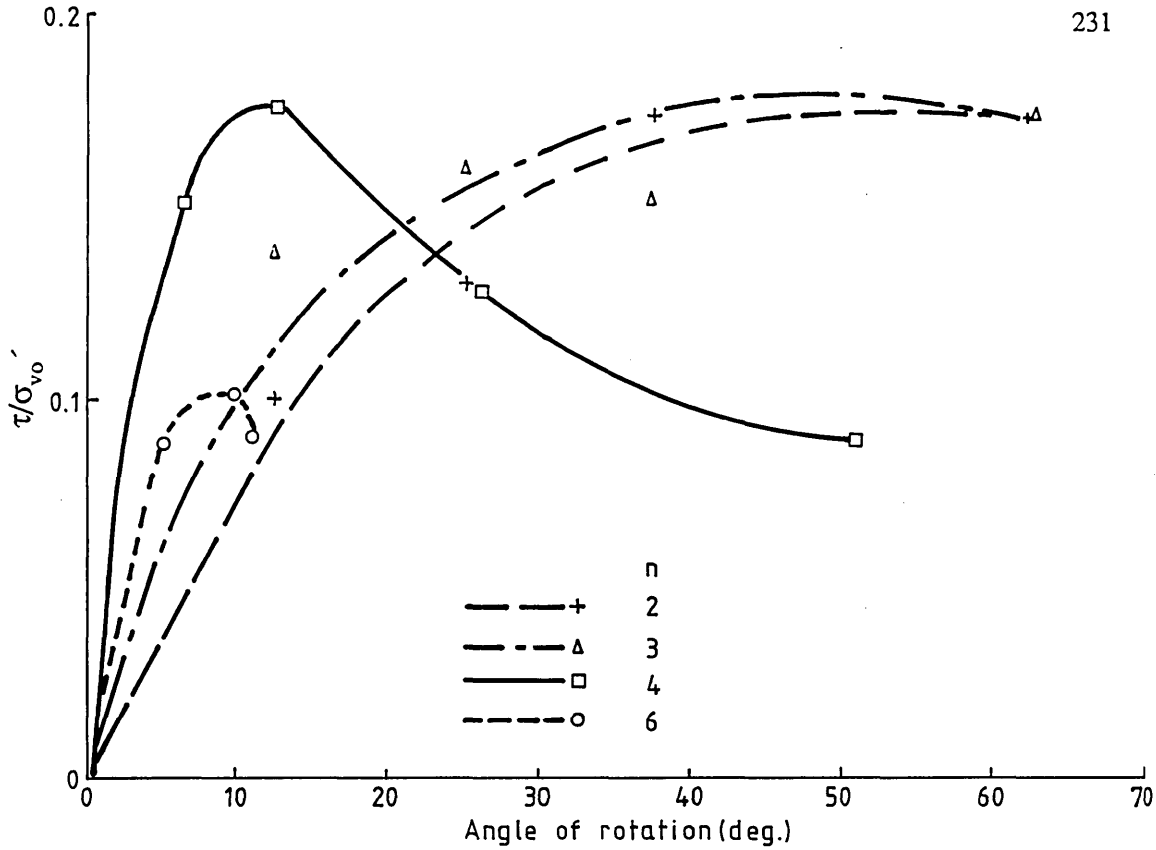


Fig. 6.34 Normalised shear stress — angle of rotation curves for vanes with different numbers of blades.

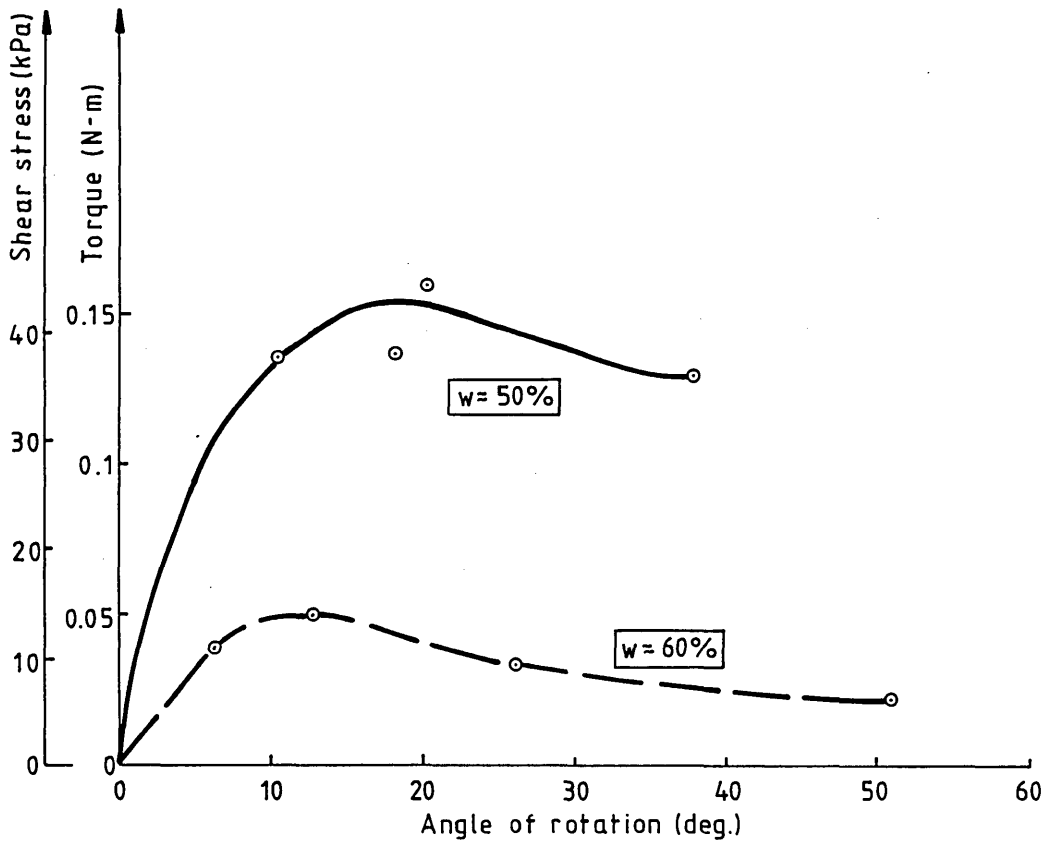


Fig. 6.35 Effect of sample water content on the shear stress — rotation curve.

6.3.5 Sample Water Content Effects

This Section deals with an investigation of the effect of the sample water content on both the shear stress – rotation characteristics and the nature of the propagated shear structures resulting from vane rotation.

Fig. 6.35 presents the results of 4-bladed vane tests in samples of reconstituted kaolin with water contents of about w = 50 and 60% (Sections 6.3.3A and B). The average shear stress – rotation curves were drawn through the corresponding individual shear stress – rotation curves (Figs. 6.7 and 6.14). Clearly, the initial portion of the curve through the 'wetter' sample is much less stiff than that through the 'drier' sample, with the former reaching failure at a lower angle of rotation (i.e. $\theta_f \approx 12.5°$) than the latter, for which $\theta_f \approx 19°$.

The influence of the sample water content on the nature of the developed shear structures is best studied by comparing them at similar stages of the shear stress – rotation curve. Figs. 6.8b and 6.15b both show pre-peak conditions at each water content. There is very little difference between the nature of the propagated shear structures in the two samples, although they extend over a greater distance in the drier sample.

A comparison of the conditions at peak shear stress is made by referring to Figs. 6.9b and 6.16b. Although the leading shear structures are almost identical, there are fewer trailing shear structures in the drier sample. Moreover, a continuous shear surface is more in evidence in the latter (having formed over two of the quadrants of the vane).

Post-peak conditions can be seen in Figs. 6.10b and 6.18b. A continuous circular surface which circumscribes the vane is evident in both samples. Furthermore, the nature of the leading shear structures is similar, as is their presence as relic features. However, the difference between the nature of the trailing shear structures is quite pronounced; there being one structure in the case of the drier sample compared to three or four structures in the case of the wetter sample.

The relative sparsity of the trailing shear structures as a consequence of lower sample water contents is much more obvious in Figs. 6.36 and 6.37, which show the shear structures formed after an angle of rotation of 34.5°, and respectively correspond to pre-peak conditions around 2- and 3-bladed vanes tested in reconstituted kaolin having a water content of about w = 40%. Schematic diagrams of all the shear structures are presented in Figs. 6.36b and 6.37b, both of which show well-developed

leading shear structures with little or no presence of any trailing structures. These may now be compared with Figs. 6.21b and 6.26b, which show pre-peak conditions around the vertical periphery of 2- and 3-bladed vanes rotated through an angle of 12.5° in samples of kaolin having water contents of about w = 60%. Despite the similarity of the nature and extent of the leading shear structures around vanes with the same number of blades (see, e.g. Figs. 6.26b and 6.37b), the relative sparsity of the trailing shear structures propagated around vanes tested in the drier samples is most striking.

In summary, both the number and the extent of the leading and trailing shear structures which develop around the vane decrease with reducing sample water content, ultimately resulting in the absence of trailing shear structures in kaolin having low water contents (of about 40%). The reason for this is a matter for speculation. One explanation is that at lower water contents the samples tend to resist higher shear stresses and consequently, there is less chance of subsequent formation of shear structures once the high shear stress concentrations at the vane blade tips have caused the propagation of the first (series of) shear structure(s). With increasing rotation, further deformation occurs along the same shear structure(s) until the kinematic restraints associated with the vane test can no longer accommodate continued deformation along the same shear structure(s) and the second (series of) shear structure(s) is (are) formed. The relative sparsity of trailing shear structures in samples with comparatively low water contents is perhaps also due to the fact that during vane rotation the formation of gaps behind the blades (see, e.g. Fig. 6.22a) leads to lower stress levels than those in front of the blades, with the local straining concentrated in front of, rather than behind the blades.

6.3.6 Clay-type Effects

A series of 4-bladed vane tests on reconstituted London clay, in which thin-sections were prepared, was carried out for comparison with the kaolin test results. The results of these tests are of interest in the following respects:

(i) The amount of detail of the microfabric features available when viewing thin-sections using the macro-photography system described in Section 3.4.6D was disappointing, since the developed shear structures were not clearly revealed (compared to the excellent clarity of detail of the kaolin thin-sections); shear structures were particularly difficult to observe on the photographs.

(ii) With the aid of an optical microscope it was possible to observe the shear structures induced by the rotating vane. The propagated structures were similar to those observed around the 4-bladed vanes rotated in kaolin.

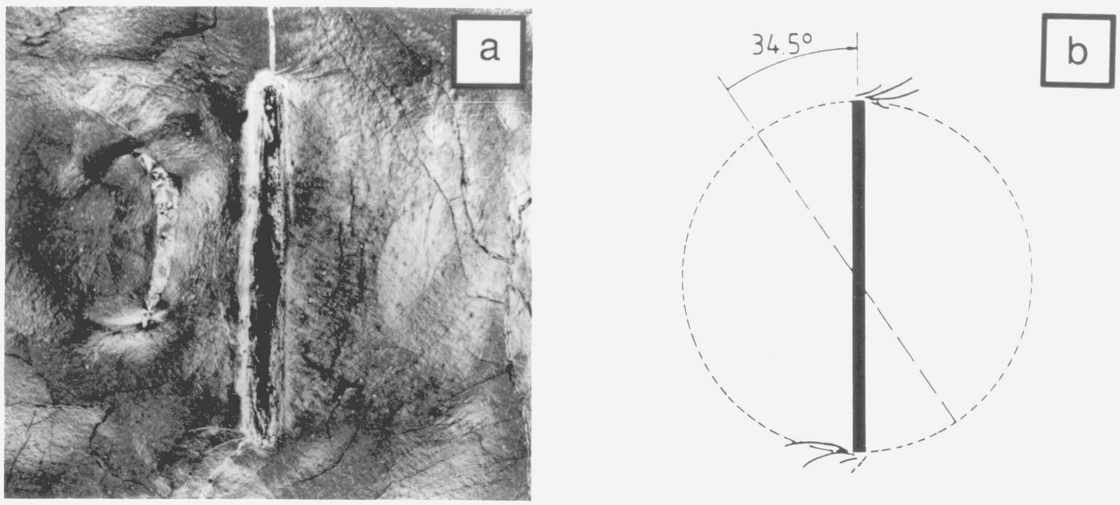


Fig. 6.36 Pre-peak shear structures around a 2-bladed vane in kaolin ; w ≈40 %.

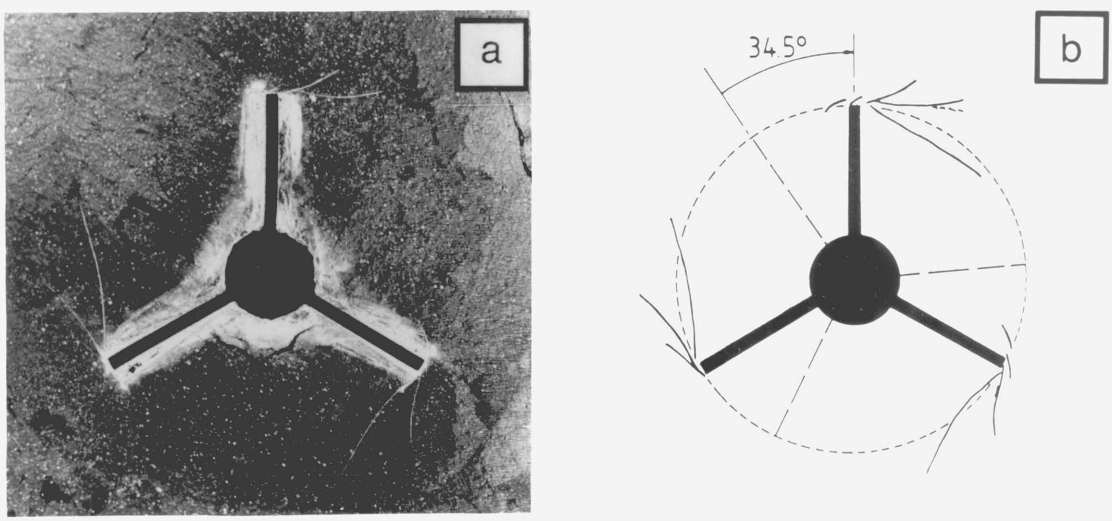


Fig. 6.37 Pre-peak shear structures around a 3-bladed vane in kaolin ; w ≈40%.

6.4 QUANTIFICATION OF THE RESULTS

The kaolin test results described in Sections 6.3.3, 6.3.4 and 6.3.5 are now quantified for the following reasons:

(i) to examine the degree of reproducibility of the shear structures observed at different stages of the shear stress – rotation curve;
(ii) to establish the diameter of the failure surface for vanes with different numbers of blades;
(iii) to determine whether quantification would support a particular mode of failure for the vane test.

Due to the importance attached to the determination of the mode of failure in the vane test, particular attention will be paid to the quantification of the conditions at or near peak shear stress.

6.4.1 Shear Structure Characteristics

'Lengths', 'angles of propagation' (Ω) and numbers of the leading shear structures developed close to peak torque around the vertical periphery of 2-, 3-, 4- and 6-bladed vanes are quantified in this Section; no attempt is made to carry out a similar exercise for the trailing shear structures, due to their curved nature.

6.4.1A Length

The lengths (a) of the leading shear structures propagated around the 4-bladed vanes rotated in kaolin, having a water content of about w = 50% (Figs. 6.15–6.18), are plotted in Fig. 6.38 against the angles of rotation (θ) at which each test was stopped. It can be seen that with proceeding rotation there is a gradual increase in the lengths of the shear structures, although this growth is ultimately arrested, and successive shear structures are subsequently propagated.

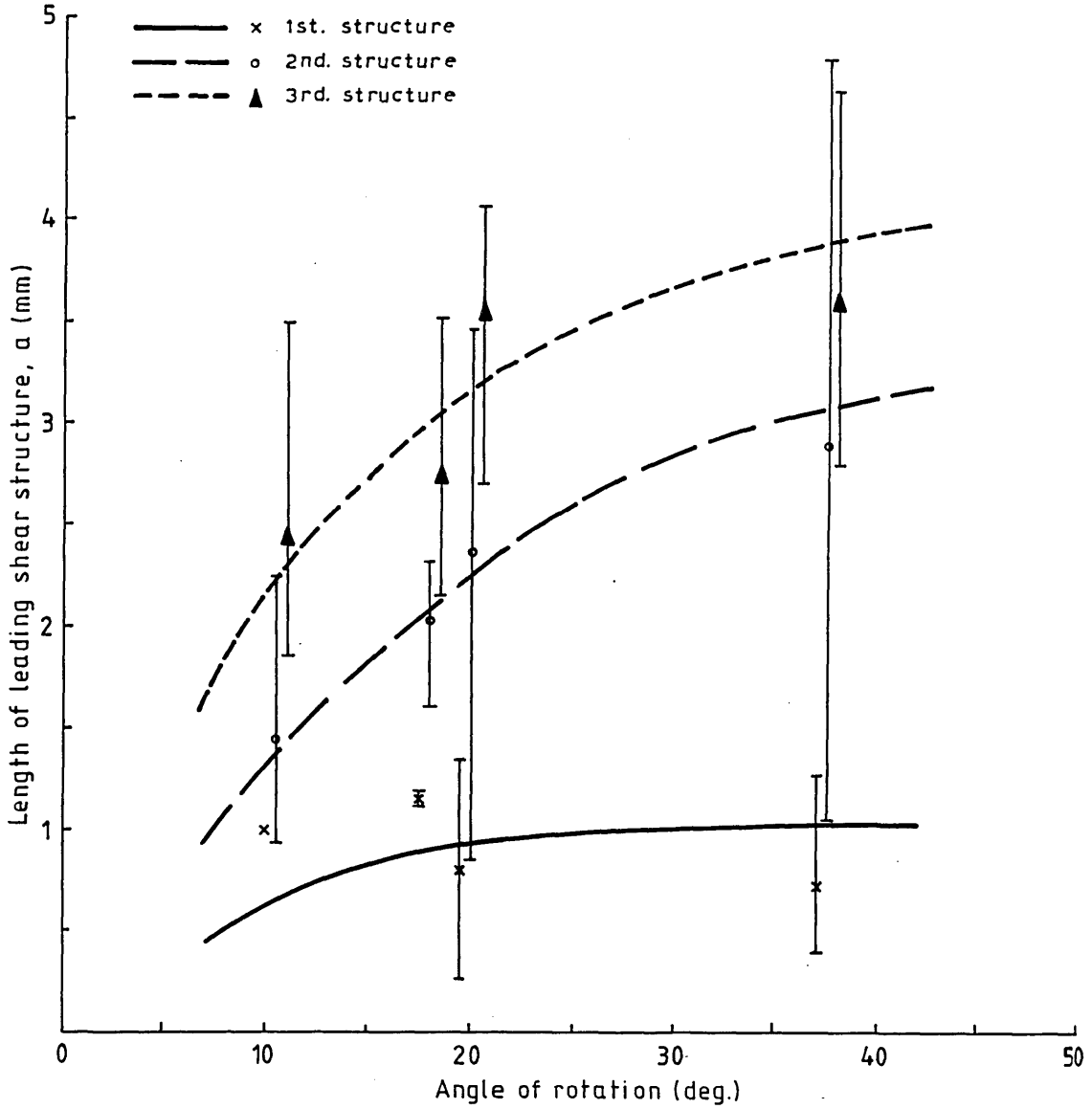


Fig. 6.38 Lengths of leading shear structures versus angle of rotation ; 4-bladed vanes, Figs. 6.15 — 6.18.

6.4.1B Angle of propagation

The variation of the angle of propagation (Ω) of the leading shear structures for samples of kaolin with a water content of about w = 60% is shown in Fig. 6.39. The sign convention used for the measurement of Ω is also shown on that Figure. The adopted datum is the tangent to the point of initiation of each leading shear structure on the vane periphery; Ω is positive when the angle subtended between the datum and the shear structures is in the anti-clockwise direction (see (1) in Fig. 6.39), and it is negative when the same angle is in the clockwise sense (see (2) in Fig. 6.39).

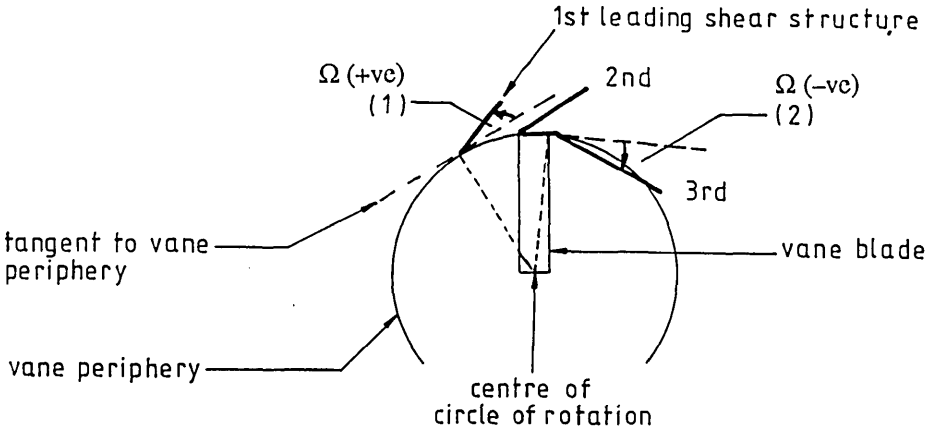
It can be seen that for a vane with any given number of blades, leading shear structures are successively propagated at decreasing values of Ω. Furthermore, the trend which emerges is that the angle of propagation of the leading shear structures reduces as the number of blades (n) increases, with the largest decrease occurring when n increases from 2 to 3 to 4.

6.4.1C Number

Fig. 6.40 presents the relationship between the average number of leading shear structures developed around each blade tip at peak torque, N, and the number of blades on the vane, n, corresponding to the results of tests in kaolin with a water content of about 60%. It shows that N is large when n is small, decreases dramatically in the range n = 2–4, and thereafter becomes asymptotic to about 3 for $n \geq 4$ (6).

6.4.2 Diameter of the Vane Failure Surface

Fig. 6.41 presents relationships between the outer diameter of the vane failure zone, defined as the outermost extent of the shear structures beyond the vane periphery, D_f, normalised to the vane diameter, D, and the number of blades on the vane (n) for vane tests carried out on samples of kaolin with water contents of about w = 60%. The relationships corresponding to conditions prior to peak, at peak and post peak shear stress are shown in Figs. 6.41a–c, respectively. These curves all show the same trend of decreasing D_f/D with increasing n for n in the range 2 to 6, with D_f/D first decreasing rapidly in the range n = 2–4, and then flattening off in the range n = 4–6.



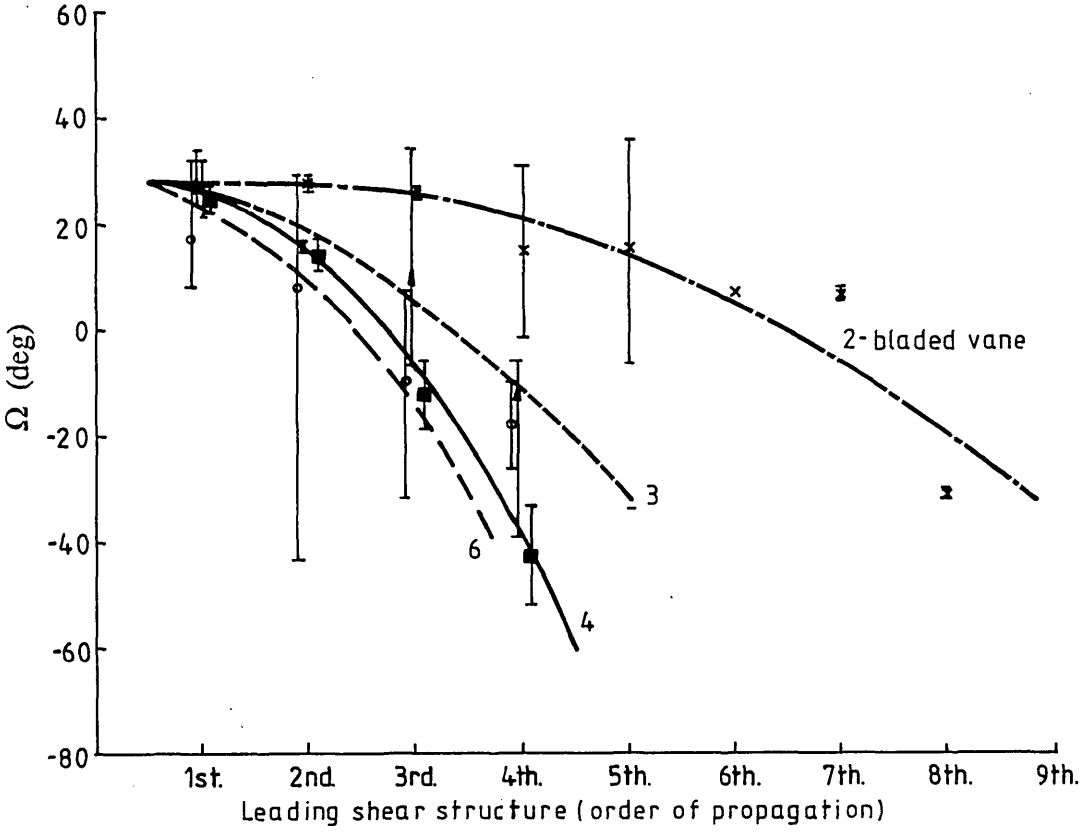


Fig. 6.39 Angles of propagation of leading shear structures for vanes with different numbers of blades.

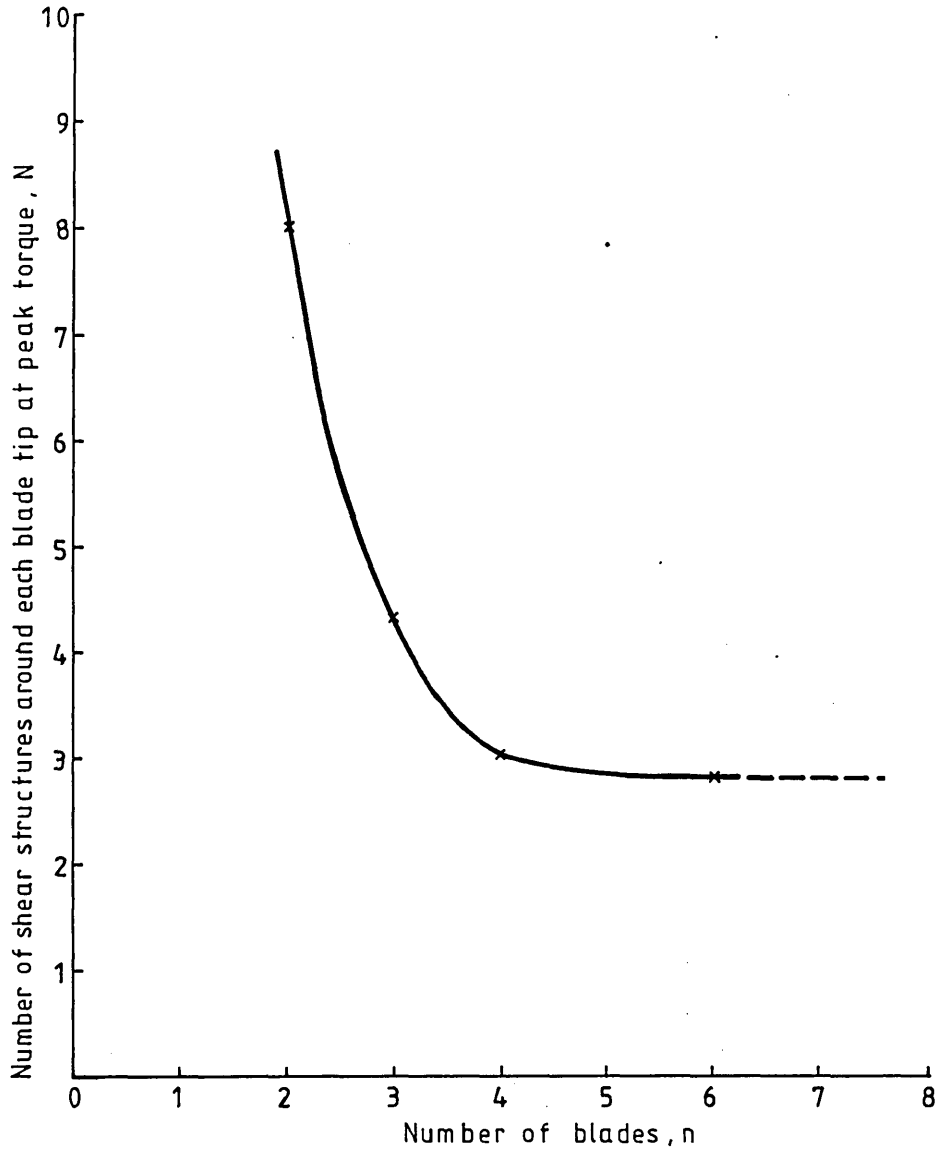


Fig. 6.40 Average number of leading shear structures around each blade tip at peak torque versus number of blades.

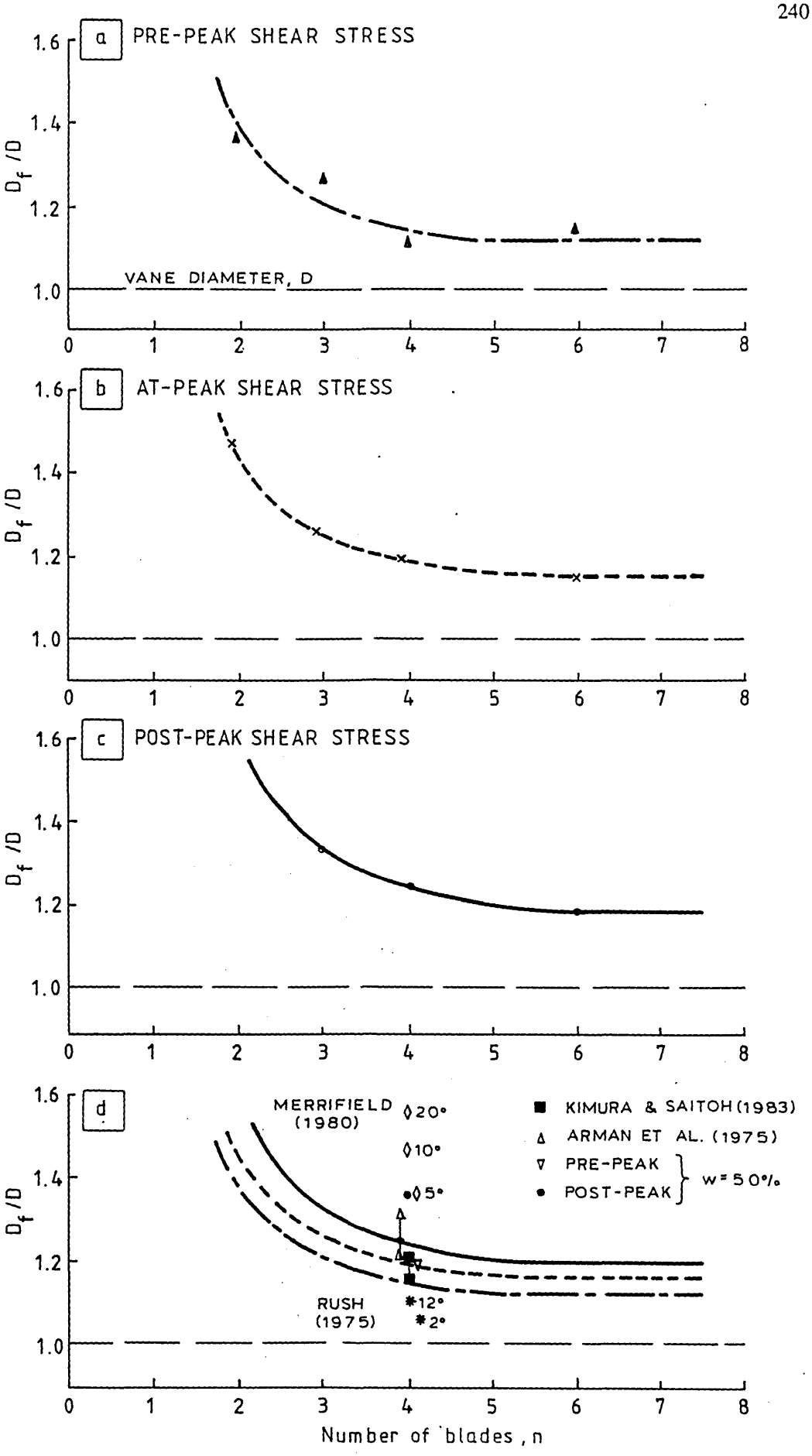


Fig. 6.41 Relationships between the outer diameter of the vane failure zone and number of blades.

The curves shown in Figs. 6.41a–c are re-presented in Fig. 6.41d. From this suite of curves it can be seen that at a given value of n, values of D_f/D increase from pre-peak to peak to post-peak shear stress conditions, which suggests that a greater extent of soil is involved as the test proceeds. For n = 4, the outer diameter of the vane failure zone is ≥ 1.3D, whilst for n > 6, values of D_f/D are in the range 1.12–1.19, always lying above the line which goes through D_f/D = 1.0. (See also Section 8.4.1.) It is therefore concluded that the outer diameter of the vane failure zone is greater than the vane diameter, although the diameter of the vane shear surface is closely defined by the vane perimeter (see Figs. 6.12a and b).

The results of the 4-bladed vane tests on kaolin with a water content of about w = 50% are also shown in Fig. 6.41d. The data points correspond to pre-peak and post-peak shear stress conditions and may be compared with the results of 4-bladed vane tests in samples with w ≈ 60%. At similar stages of the test, values of D_f/D are greater (by about 3.5%) in the case of the drier sample, thus inferring that the shear structures penetrate a longer distance as the sample water content decreases (see Section 6.3.5). The data presented by Arman et al. (1975), Rush (1975), Merrifield (1980) and Kimura & Saitoh (1983) give values of D_f/D which are consistent with the results obtained in this study (see Fig. 6.41d).

6.4.3 Size of the Vane Failure Zone

Fig. 6.42 shows the relationship between the "shear area ratio", S_r, and the number of blades, n, where S_r is given by the area of the shear zone divided by the surface area defined by the outer diameter of the vane failure surface ($\pi D_f^2/4$); area of the shear zone is given by the surface area of the annulus of disturbed soil, bounded by the inner and outer diameters which respectively define the innermost and outermost extent of the shear structures within and beyond the vane periphery (Fig. 6.42). The results presented here correspond to the data points plotted in Figs. 6.41a–c. It can be seen that at n = 2, S_r is slightly less than 100%, rapidly decreases to about 60% at n = 4, and thereafter becomes asymptotic to a value of about 45% at n ≥ 6. It is of interest to note that the shear area ratio remains almost constant at conditions corresponding to pre-peak, peak and post-peak shear stress at n = 2, but as n increases to 3, 4 and 6, S_r becomes more and more dependent on the stage of the shear stress – rotation curve at which its value is determined.

In addition, at peak torque, the 4-bladed vane tested in kaolin with w ≈ 50% gives a value of S_r which is lower, by about 18%, than that given by the 4-bladed vane tested in kaolin with w ≈ 60%, thus suggesting that a lower shear area ratio may result as the sample water content decreases.

Merrifield's (1980) 4-bladed vane tests in Leighton Buzzard sand give values of S_r which are independent of the angle of vane rotation; S_r being about 82%. On the other hand, the results of Rush (1975) obtained from tests on Washed Beach sands give values of S_r of about 37%, i.e. approximately half that obtained from Merrifield's results. This difference of a factor of about two may be attributed to (a) the higher density and single grain-size of Leighton Buzzard sand, and possibly (b) the uniform pressure which was applied to the top of the Leighton Buzzard sand. In this regard, it is noteworthy that Cheah's (1981) radiographic study of the effects of cone penetration in kaolin showed very little soil displacement at the clay surface under σ_v = 0 kPa, whilst noticeable soil displacement was observed when σ_v = 150 kPa.

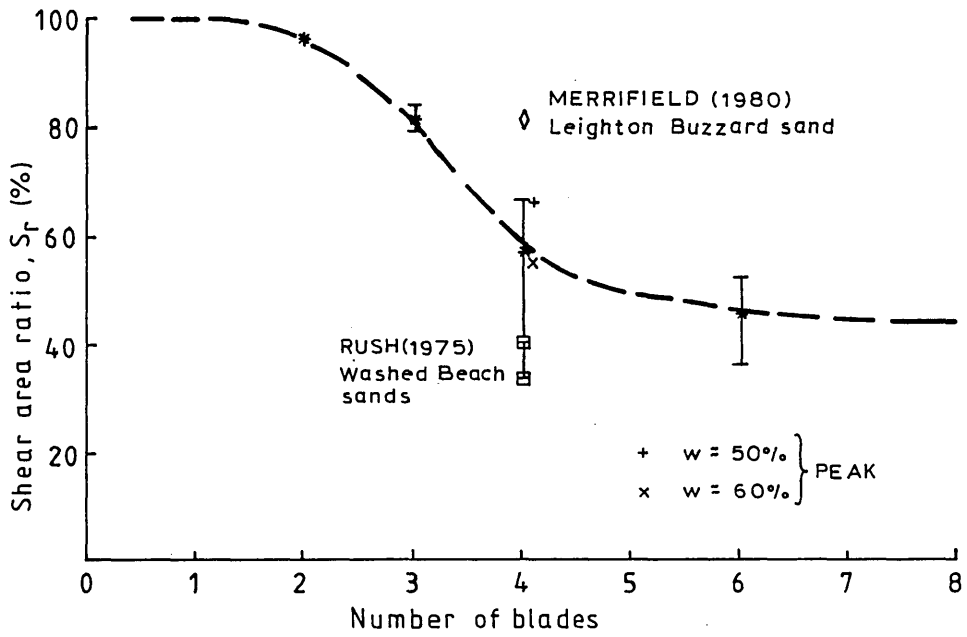


Fig. 6.42 Shear area ratio — number of blades relationship.

6.4.4 Summary

The observations made from Figs. 6.39 to 6.42 are consistent with each other and show:

(a) that the angle of propagation of the leading shear structures (Ω) is a function of the number of blades on the vane;
(b) that the average number of the leading shear structures associated with each blade tip (N) is, in the range n = 2–4, particularly dependent on the number of vane blades, but is almost constant for $n \geq 4$ (6);
(c) that both the outer diameter (D_f) and the size of the vane shear zone are strongly influenced by the number of blades on the vane for n in the range 2 to 6;
(d) that the vane failure zone has an outer diameter which is larger than the vane diameter by approximately 20% (when $n \geq 6$) and 50% (when n = 2), depending on the number of blades;
(e) that, depending on n, between 45% (corresponding to $n \geq 6$) and 100% (corresponding to n = 2) of the volume of soil swept by the rotating vane undergoes permanent deformations, as depicted by the extent of propagation of the shear structures developed;
(f) that, with decreasing sample water content, the vane failure zone outer diameter, D_f, increases, however slightly, while the shear area ratio, S_r, decreases;
(g) that there is a marked change at n = 4 in the shapes of the curves for the N–n, D_f/D – n and S_r–n relationships.

Consequently, it is suggested that the failure mode associated with the 2-bladed vane contrasts with the mechanism which operates in the case of vanes with four or more blades. The above observations further suggest that the failure mechanism associated with the 3-bladed vane is transitional between the modes of failure of the 2- and 4-bladed vanes. These suggestions are also supported by the measurement of different strengths with vanes having different numbers of blades (see Chapter 5 and Section 6.3.4D).

Quantification of the results has shown that the number of blades on the vane, particularly for n in the range 2 to 4, has a significant effect on both the number and angle of propagation of the leading shear structures, and the outer diameter and size of the shear zone developed as a consequence of vane rotation. Hence, it may be implied that different modes of failure govern the response of vanes with different numbers of blades. The following Section will examine the mechanisms of failure associated with the vane test.

6.5 FAILURE MECHANISMS IN THE VANE TEST

6.5.1 Simple Shear Conditions

Despite the disagreement in the literature regarding the progressive or non-progressive nature of the failure mechanism in the vane test, there is very little evidence to support either viewpoint (Section 2.6.2). Moreover, it is difficult to accept Kimura & Saitoh's (1983) conclusion that the vane failure mode is similar to that observed in direct shear tests, since their results do not show whether simple shear or direct shear conditions apply at failure.

Wroth (1984) suggests that the mode of failure in the vane test is one of simple shear, although, owing to the different orientation of the specimens, it is not the same as that caused in a conventional direct shear test (see, e.g. Morgenstern & Tchalenko, 1967). He subsequently derives a mathematical expression for the measured vane strength in terms of the soil friction angle and the horizontal effective stresses (Section 6.6; Eq. 6.1); this, he states, is not at variance with the limited results reported by Law (1979; Section 8.5.1B).

Morgenstern & Tchalenko (1967) present the results of laboratory direct shear tests stopped at different points along the shear stress – displacement curve, with thin-sections taken at each stage of the test, as indicated in Fig. 6.43a (Tchalenko, 1967). Figs. 6.43b–e are tracings of the shear structures observed when viewing thin-sections under crossed polarised light; the kaolin samples having been sheared perpendicular to the original bedding plane. Morgenstern & Tchalenko state that the 'edge' structures — which propagate at the metal 'cutting edges' of the box — are formed as a consequence of high stress concentrations and kinematic restraints at the edges of the specimens.

Conditions at maximum shear stress can be seen in Fig. 6.43c, which show the propagation of shear structures in front of each end of the shear box, without any evidence of a continuous failure surface between the two rigid ends of the box. The final failure plane was not formed until post-peak shear stress conditions were reached (Fig. 6.43d). Morgenstern & Tchalenko subsequently concluded that the observed structures at or near peak shear stress indicate that the central portion of the specimen is failing in simple shear, hence confirming Hill's (1950) interpretation of the shear box test.

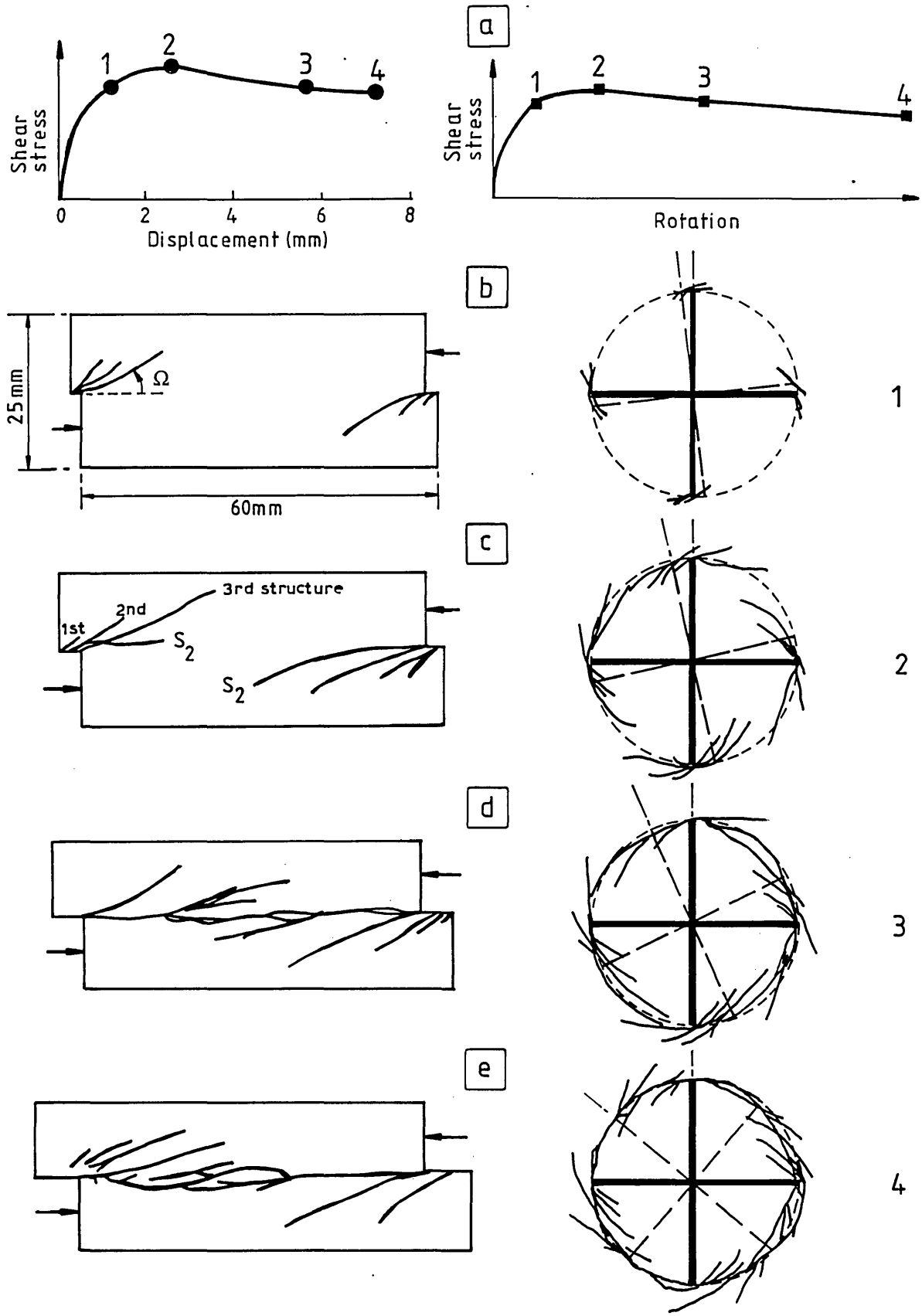


Fig. 6.43 Sequence of shear structures in reconstituted kaolin tested in the direct shear box (after Morgenstern & Tchalenko, 1967) compared with vane shear structures.

An independent study of the shear box test has recently been carried out by Potts et al. (1987). Using the finite element method, they analysed the test for both non-strain-softening and strain-softening soils, and found that the predicted behaviour was very similar to that of ideal simple shear. An analysis in which severe strain-softening was simulated indicated only a slight progressive failure effect. Consequently, they also concluded that the shear box test may be interpreted as if it were a simple shear test.

The finite element method was also used by de Alencar et al. (1988) in an analysis of the vane shear test. They also studied the behaviour of both non-strain-softening and strain-softening soils, and found that the effect of progressive failure was dependent on the strain-softening characteristics of the soil, becoming significant only in soils which show a particularly rapid post-peak reduction of strength (i.e. angle subtended between the horizontal and tangent to post-peak curve = 25° and 70°; $I_B = 0.4$). In spite of the brittle shear stress – rotation characteristics of the kaolin tested in this investigation, however, the thin-section observations of the deformation patterns around 2-, 3-, 4- and 6-bladed vanes show no evidence of progressive failure (Section 6.3.4D).

6.5.2 Comparison of Vane and Shear Box Tests

There is considerable similarity between the structures seen in the shear box and the deformation patterns around the vertical periphery of the conventional 4-bladed vane; the former closely resembling the leading shear structures evident in the vane test (compare Figs. 6.43b–e with Figs. 6.8b–6.11b which are here re-presented adjacent to Figs. 6.43b–e). The leading shear structures at the tips of the vane blades and at the rigid ends of the box both propagate in a similar manner, since in both tests shear discontinuities are initiated at a steep angle (relative to the horizontal) at an early stage of each test, and with further rotation/displacement, the development of the discontinuities is arrested as new shear structures form at comparatively lower angles (relative to the adopted datum) (see Figs. 6.8b and 6.43b). This progression continues beyond post peak shear stress, when in both types of test a continuous failure surface forms (see Figs. 6.10b and 6.43d). Furthermore, a shear failure zone is involved in both the vane and the shear box test (see Figs. 6.11b and 6.43e).

It is important to notice that at maximum shear stress there is no evidence of a continuous shear surface either in the vane or in the shear box test (see Figs. 6.9b and 6.43c), thereby implying that conditions of simple shear are applied by the vane to the

soil mass. A more quantitative examination of the soil deformation patterns, so far described qualitatively, may further support the validity of the simple shear interpretation for the vane test.

Fig. 6.44 shows the variation in the angle of propagation (Ω) of the leading shear structures developed at peak shear stress corresponding to the results of

(a) 4-bladed vane tests on kaolin having a water content of about w = 50%,
(b) Morgenstern & Tchalenko's (1967) shear box tests on kaolin with a water content of about w = 50%, and
(c) the study conducted by Rush (1975) on Washed Beach sands.

It is seen that all three data sets exhibit leading shear structures that are propagated at successively lower angles relative to the adopted datum.

The results of the 4-bladed vane tests and the direct shear tests on kaolin may be compared more readily, since they represent the results of tests on the same clay, at the same water content and at similar overconsolidation ratios (OCR = 1 and 2 respectively). It can be seen that for any given leading shear structure in the range first to fourth (see Fig. 6.44), the value of Ω corresponding to the vane test data is about 25° less than that for the shear box test. In order to examine whether there are any factors which might explain the consistently lower angles at which the leading shear structures are propagated around the 4-bladed vane, differences between the two data sets must be considered.

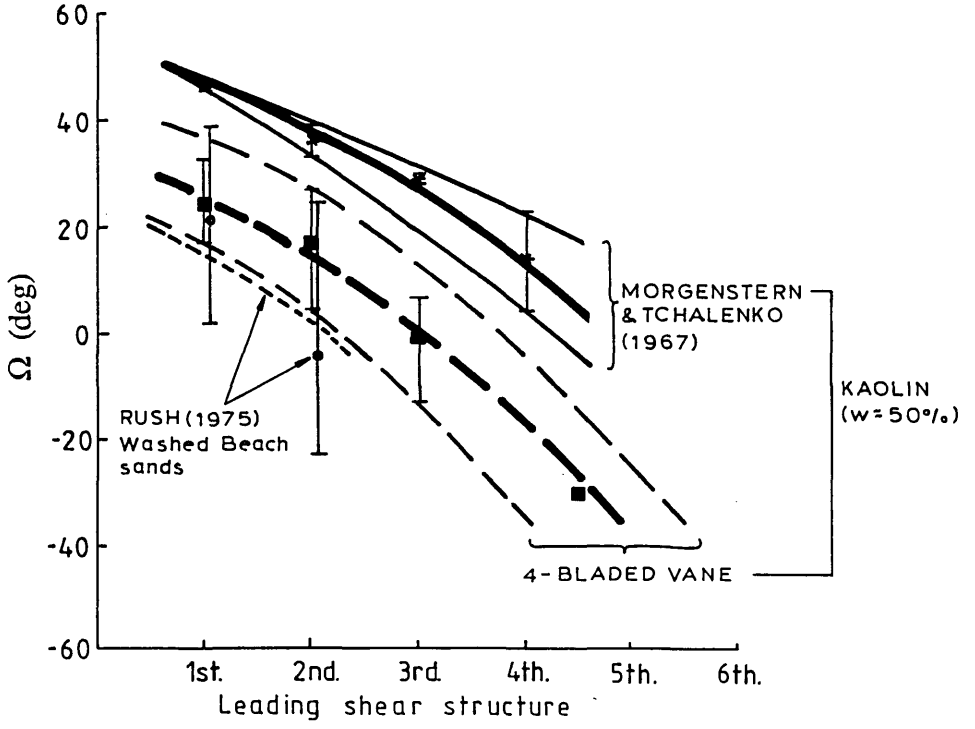


Fig. 6.44 Angle of propagation of the leading shear structures developed at peak shear stress : Comparison of results.

Table 6.1 lists the main features of Morgenstern & Tchalenko's (1967) shear box tests and the 4-bladed vane tests conducted by the writer. It is seen that apart from differences in the normal stresses on the samples, the two test procedures show considerable similarities. The major differences between the two studies concern

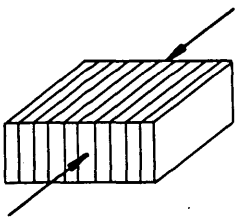
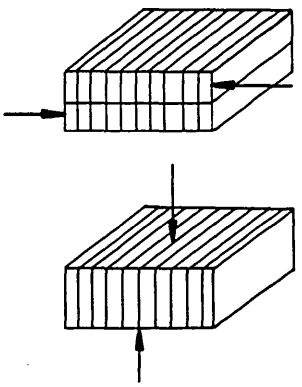
(a) the mode of deformation, and
(b) the direction of shearing relative to the original bedding.

Different modes of deformation will probably lead to different kinematic restraints, which will subsequently impose dissimilar boundary constraints on the soil deformation patterns. It is not unexpected, owing to the 'circular' boundary constraints which result from the rotational mode of deformation in the vane test, that the leading shear structures are confined by the bounds of the affected annulus of soil, and thus propagate at lower values of Ω compared to the angles of propagtion of the structures in the shear box test.

The direction of the original fabric orientation relative to the shearing direction in the shear box test was studied by Morgenstern & Tchalenko (1967). They report that the angle of propagation (Ω) of shear structures (see the kinematic discontinuities labelled S_2 on Fig. 6.43c) developed in samples sheared parallel to the original fabric were about Ω = 20–25°, whilst these same S_2 structures had propagated at angles of about Ω = 12° in samples sheared perpendicular to the original bedding; over the central portion of the box the slip line was propagated at an angle of about Ω = 12° in both families of tests. Therefore, it might reasonably be expected that the earlier developed edge structures could have also formed at angles of propagation which were different in the two test series.

Therefore, it is reasonable to expect shear discontinuities to propagate at different values of Ω once consideration is given to factors such as the orientation of original fabric relative to the shearing direction, and different boundary constraints arising from different types of test. Since the trend displayed by the angle of propagation of successive leading shear structures is similar in both the vane and the direct shear test, it may be implied that quantification of the development of the shear structures propagated at peak shear stress is consistent with the observations discussed earlier qualitatively. Hence, it may be concluded that the mode of failure associated with the 4-bladed vane test is similar to that of the direct shear test, in which simple shear conditions apply at maximum shear stress. Furthermore, it may also be implied that simple shear conditions also apply in the 6-bladed vane test, although the leading shear structures now propagate at smaller angles (Ω) compared with those of the 4-bladed vane (see Fig. 6.39).

Table 6.1 Comparison of the vane test with the direct shear box test.

Parameter	Vane Shear Test	Shear Box Test
o Mode of deformation	rotational displacement	axial displacement
o Sense of shearing	clockwise	'left lateral'
o Direction of movement of rigid metal edges	left to right	left to right
o 'Strain' rate	6.27 °/min ≈ 0.68 mm/min	0.00292 mm/min
o Vertical stress on sample during shearing	0 kPa	215 kPa
o 'Drainage' conditions	assumed to be drained (see Sections 4.4.2F and 4.4.5)	assumed to be drained
o Soil tested	kaolin	kaolin
o Sample water content after unloading	50%	50% (Tchalenko, 1967)
o Maximum vertical stress on sample	200 kPa	430 kPa
o Type of shear structures compared	'leading'	'edge'
o Direction of shearing relative to the original bedding	perpendicular to, and along	perpendicular
		

6.6 ANALYSIS OF THE 2-BLADED VANE IN TERMS OF EARTH PRESSURES

There are considerable similarities between the characteristics of the curvilinear structures developed behind the blades of the 2-bladed vane and the rupture surfaces which develop behind a retaining wall (Section 6.3.4A). In addition, vanes with different numbers of blades result in the measurement of different peak torques (Chapter 5; Section 6.3.4D). Therefore, it is of interest to model the 2-bladed vane in terms of a retaining wall in order to determine how well the peak torque calculated on the basis of active and passive earth pressures compares with the peak torque measured with the 2-bladed vane. This is now examined.

An attempt is made to explore the reasons for the differences in both the measured shear strength and the shear stress – rotation characteristics of 2- and 4-bladed vane tests from a study of the mode(s) of failure associated with vanes with different numbers of blades. This examination is based primarily on the observation of different soil deformation patterns around 2- and 4-bladed vanes (Section 6.3.4D).

Close to peak torque, the development of leading and trailing shear structures around the 4-bladed vane indicates that the mode of failure is one of simple shear (Section 6.5.2). This implies that the vane shear strength (τ_f) may be given by the simple formula

$$\tau_f = \sigma_{ho}' \sin \phi_{ps} \qquad \text{Eq. 6.1}$$

where σ_{ho}' is the 'in situ' horizontal effective stress acting across the vane shear zone, and ϕ_{ps} is the plane strain angle of shearing resistance of the soil.

In obtaining the above relationship (Appendix A4), Wroth (1984) assumed (a) that the soil would behave elastically, and (b) that the peak torque is related to the strength mobilised along the vertical periphery of the vane.

For normally consolidated soils, the expression for the vane shear strength ratio becomes:

$$\frac{\tau_f}{\sigma_{vo}'} = \frac{\sigma_{ho}' \sin\phi_{ps}}{\sigma_{vo}'} = (1 - \sin\phi_{ps}) \sin\phi_{ps} \qquad \text{Eq. 6.2,}$$

since $\sigma_{ho}'/\sigma_{vo}'$ is assumed to be given by the Jaky expression $K_0 = (1 - \sin\phi')$. Note that Wroth adopts the approximation that $K_0 \approx (1 - \sin\phi_{ps})$, since plane strain conditions are assumed in his analysis (Appendix A4).

Fig. 6.45 shows how, owing to symmetry, each (6mm wide x 12mm high) vane blade may be modelled as one retaining wall, with a surcharge σ_{ho}' acting on the ground surface. Thus, the 'wall' is 6mm high and 12mm long, with a width of about 0.5 mm (Section 3.2.2A(i)). Appendix A4 outlines the way in which Eq. 6.2 is used to calculate σ_{ho}' (the horizontal effective stresses in the kaolin sample considered (Section 6.3.3A)).

Since the kaolin is normally consolidated, it is assumed that $c' = 0$. Vane rotation is simulated by clockwise rotation of the retaining wall about its top: only a limited zone of soil (near the foot of the 'wall') will obtain a state of failure, since the magnitude of movement of the top of the 'wall' is comparatively small (see Fig. A4.1). Furthermore, the vane blade is considered rough and consequently, the soil below the base of the 'wall' is not subjected to either compression or extension and therefore restrains the soil above and imposes horizontal shear stresses. Behind the 'wall' (active zone), the soil tends to settle relative to the wall and thus shear stresses acting in an upward direction are imposed on the soil. In front of the 'wall' (passive zone), the soil tends to move upwards and therefore downward acting shear stresses are imposed on the soil. Hence, due to both the mode of wall movement and the wall roughness, the entire soil mass is not in a complete Rankine state of stress and thus the Rankine theory cannot be used for the analysis (see, e.g. Potts & Fourie, 1986).

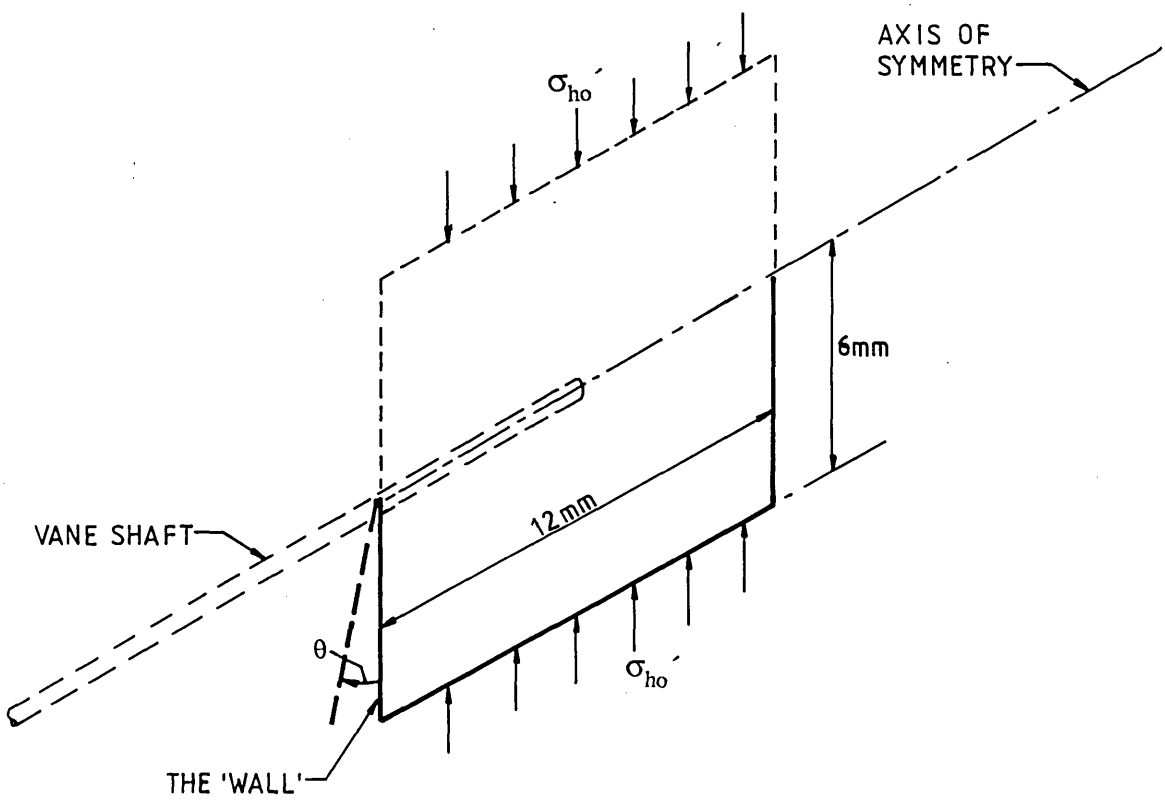


Fig. 6.45 Modelling the vane in terms of retaining walls.

In Coulomb's method of analysis, the inherent assumption that a plane failure surface occurs in the soil adjacent to the wall appears reasonable for the active situation, but for the majority of passive cases it leads to estimates of passive resistance which are much too high and therefore on the unsafe side. Although past experience has shown that the above assumption is reasonable provided that the wall friction angle (δ) $\leq \phi/3$ (Potts, 1984), it is considered reasonable to adopt a wall friction angle of ($\delta =$) $2\phi/3$, since the vane blades were grit-blasted (Section 3.2.2A) and were thus rendered rough. Coulomb's approach is used in Appendix A4 to analyse the 2-bladed vane in terms of earth pressures, with the active thrust and passive resistance on the vertical planes of the 'wall' assumed to act parallel to the ground surface.

The ratio of the peak torque calculated when the 2-bladed vane is modelled as two retaining walls (M_2 = 0.057 N-m) to the reference peak torque corresponding to the 4-bladed vane (M_4 = 0.05 N-m; Fig. 6.7) is about 1.14 (Appendix A4), and is regarded as the 'predicted' M_2/M_4 ratio. There is excellent agreement between the predicted M_2/M_4 ratio and that observed following an extensive programme of laboratory tests with vanes having different numbers of blades (Section 5.5; Fig. 5.7), where $M_2/M_4 \approx$ 1.15. Furthermore, there are considerable similarities between the deformation patterns around the vertical periphery of the 2-bladed vane and the rupture surfaces which result when a retaining wall is subjected to rotation (Section 6.3.4A). It is therefore difficult to escape from the conclusion that it is reasonable to expect considerable similarities between the failure mechanism associated with the 2-bladed vane and that of the retaining wall (see also Section 6.3.4A). Hence, it may be reasonable to attribute the measurement of higher strengths with vanes having fewer blades to:

(a) the presumed difference between the mode of failure associated with vanes with less blades than four and that for vanes with four or more blades, and
(b) vane insertion disturbance effects, with fewer blades resulting in less disturbance to the soil fabric surrounding the vane (Section 6.3.2).

CHAPTER 7

PHOTOELASTIC MODELLING OF THE VANE TEST

7.1 INTRODUCTION

Experimental stress analysis techniques can be used to determine the magnitude and direction of the principal stresses, and thus the shearing stresses in a loaded component. Photoelasticity is the name given to the optical method of stress analysis, which is based upon an examination of the optical conditions in a stressed model by detecting changes in the refractive indices of light passing through the photoelastic material (see Appendix A1). The technique allows a visualisation of the stress field at any point in the model and provides both overall general information and detailed point by point data; this information is easily and permanently recorded by photography and will provide both the magnitudes and the directions of the shearing stresses throughout the loaded material.

The thin-section examination of the deformation patterns around the 4-bladed laboratory- and triaxial-vanes tested in normally consolidated kaolin have provided a clear picture of the initiation and subsequent propagation of the shear discontinuities developed at the blade tips (Section 6.3.3). Now, it is useful to determine the shear stress directions using the technique of photoelasticity, and then compare the directions of the shear stresses at the same points in the vicinity of the vane blade tips as those points where shear structures have been observed from the examination of the kaolin thin-sections. This comparison improves the understanding of the stress field associated with the vane test, although it is important to note that the photoelastic analysis can only be considered relevant until discontinuities (or 'cracks') occur in the soil; it may be appropriate for predicting the nature of initial 'cracking', but not for analysing subsequent behaviour, when it is no longer justifiable to consider that photoelastic materials can comparably simulate the behaviour of soils (see also Section 7.3.3).

Although soils are elasto-plastic materials, it is nonetheless acknowledged that their response in the elastic range may be modelled by materials which exhibit the same behaviour in that range. Both gelatine and polyurethane rubber are linear elastic materials which may be used to establish the shear stress directions around the vane periphery. The stress increments applied to the vane correspond to rotations which are so small that the elastic behaviour of the photoelastic material is ensured. It is

considered that such a model is a reasonable approximation of the stress field in a soil subjected to vane rotations in the elastic range, although it is appreciated that the analysis of the vane test might be more efficiently carried out numerically by the finite element method than by physical modelling techniques.

7.2 TESTING PROGRAMME

The testing programme included a series of experiments on both gelatine and polyurethane rubber models subjected to small torques, corresponding to small rotations of the vane. A detailed account of the experimental procedures is given in Sections 3.5.2B and C.

To check repeatability, two samples of each photoelastic material were tested.

7.3 EXPERIMENTAL RESULTS

The raw experimental results were in the form of photographs which show both the "isochromatics" and the "isoclinics" — both of which are defined in Appendix A1 — around 4-bladed vanes subjected to torques and/or rotations in the elastic range of behaviour of the photoelastic materials used in the experiments. The isoclinics were recorded at orientations (α) of 10°-intervals of the crossed polaroids.

Repeatability of the results was confirmed from a comparison of photographs taken from experiments on two different photoelastic samples, while parameters such as the applied torque on the vane and the orientation of the crossed polaroids were kept constant.

Although the photoelastic patterns which were obtained from both the gelatine and polyurethane model experiments included both the isochromatics and the isoclinics, the isochromatics were much clearer in gelatine than in polyurethane rubber, whilst the isoclinics were more easily observable in polyurethane rubber than in gelatine. The probable reasons are outlined below:

(i) Due to the exceedingly high optical sensitivity of gelatine, the isochromatics, which are particularly evident in circularly-polarised light, still remain pronounced in plane-polarised light and thus severely obscure the observation of the isoclinics. Furthermore, the gelatine model experiments incorporated 45°

surface-silvered mirrors, which apparently do not yield a perfectly plane-polarised light (Allison, 1987), and consequently might also have affected the observation of the isoclinics.

(ii) Since the isoclinics were of particular interest to the present study, and these are best observed when the interference from the isochromatics is least (see Appendix A1), very small torques were applied to the vane in order that the subsequent number of the isochromatics would be a minimum. However, polyurethane rubber is not as optically sensitive as gelatine and consequently the isochromatics were not clear when photographed.

Section 7.3.1 presents the isochromatic patterns obtained from the gelatine model experiments, while Section 7.3.2 shows the isoclinics observed in the experiments in which polyurethane rubber was used to model the soil. Shear stress directions at certain 'points of interest' in the vicinity of the vane blades are presented in Section 7.3.3.

7.3.1 The Isochromatics

The stress distribution around the periphery of a 4-bladed vane is presented in Fig. 7.1, which is a tracing of the photograph showing the isochromatic fringe pattern in gelatine after an angle of rotation of 25°. The letters G, Y and R refer to the fringe colours green, yellow and red, respectively, and the numerals indicate the respective fringe orders, with higher fringe orders representing larger values of principal stress difference; thus, 2G denotes the second order green fringe. The clockwise direction of vane rotation is also shown on this Figure.

Fig. 7.1 shows that maximum shear stress concentrations occur on narrow contours close to each blade, both in front of and behind it. It can further be seen that the distribution of shear stress is asymmetrical about the centre of each quadrant. This may be regarded as experimental evidence for Arnold's (1978) assumption in connection with exponentially (rather than uniformly) distributed shear stresses around the vertical periphery of adjacent vane blades.

Merrifield (1980) also conducted a few photoelastic experiments in order to study the shear stress distribution around a 4-bladed vane rotated in an epoxy gel (Section 2.6.1). Although the photoelastic pattern shown in Fig. 7.1 is very similar to the isochromatic fringe patterns observed by Merrifield, he reported that, because the isochromatic fringes were symmetrical with respect to the centre of each quadrant, his results thus indicated a uniform shear stress distribution.

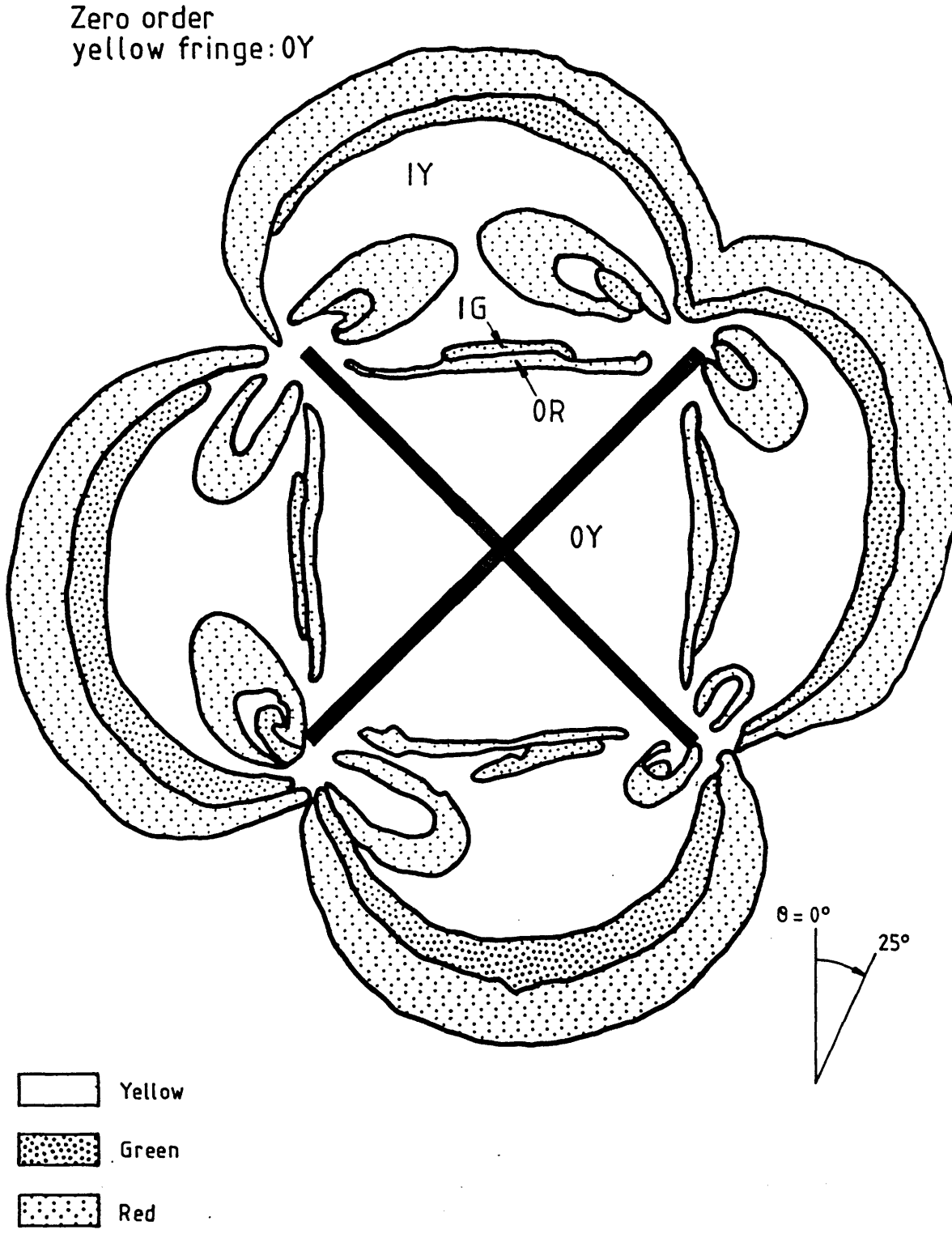


Fig. 7.1 Isochromatic fringe pattern around a 4-bladed vane in gelatine.

7.3.2 The Isoclinics

Fig. 7.2 is a photograph of the (α =) 0°-isoclinics, which was observed when the polyurethane rubber model was subjected to a small torque via two equal 1/2lb dead weights hanging from the offsets of the crossbar (see Fig. 3.18). The orientation of the isoclinics were also recorded photographically as the crossed polaroids were rotated from 0 to 90°, at (α =) 10°-increments; the reference axis was the horizontal line at 45° to the vane blades. To save space, only Fig. 7.3, which shows the 70-° (=25°- = 70°-minus 45°-) isoclinics under the same load conditions as Fig. 7.2, is presented as an example.

Isoclinics corresponding to orientations of the polarisation axis between $\alpha = 0$ and 90° — where α = 0° = 45° = 90°, since when crossed polaroids are used, the images observed from orientations of the polarisation axis of $\alpha = 0$, 45 and 90° are the same — have been traced from the respective photographs, and are presented in Figs. 7.4a–i, which respectively show the 0°-, 5°- (= 50°- = 5°- + 45°-), 10°-, 15°- (= 60°- = 15°- + 45°-), 20°-, 25°- (= 70°- = 25°- + 45°-), 30°-, 35°- (= 80°- = 35°- + 45°-) and 40°-isoclinics; owing to symmetry, the isoclinics are only shown around one of the blades. The shear stress directions along the isoclinics observed around one vane blade, which have been established according to the procedures described in Appendix A1, are also shown in Figs. 7.4a–i. Fig. 7.5 shows the shear stress directions observed from all the isoclinics shown in Figs. 7.4a–i. The directions of the shear stresses were determined on the basis of the following assumptions:

(a) that the polyurethane rubber model was homogeneous and isotropic;
(b) that the model material was linear elastic and thus would obey Hooke's Law;
(c) that the model was in a state of plane strain.

It is particularly useful to determine the shear stress directions both along points where the principal stress differences are a maximum and points along which shear discontinuities were first initiated in kaolin. The points along which the principal stress differences are maximum can be obtained from an examination of Fig. 7.1, while Fig. 6.8b shows the leading and trailing shear structures propagated after at angle of rotation of 6.5° in the vicinity of a 4-bladed vane tested in kaolin ($w \approx 60\%$); the latter shows the 'first series' of shear discontinuities which were observed in the investigation of the vane failure mechanism (Section 6.3.3A). The shear stress directions along the above-mentioned 'points of interest' are determined in the next Section.

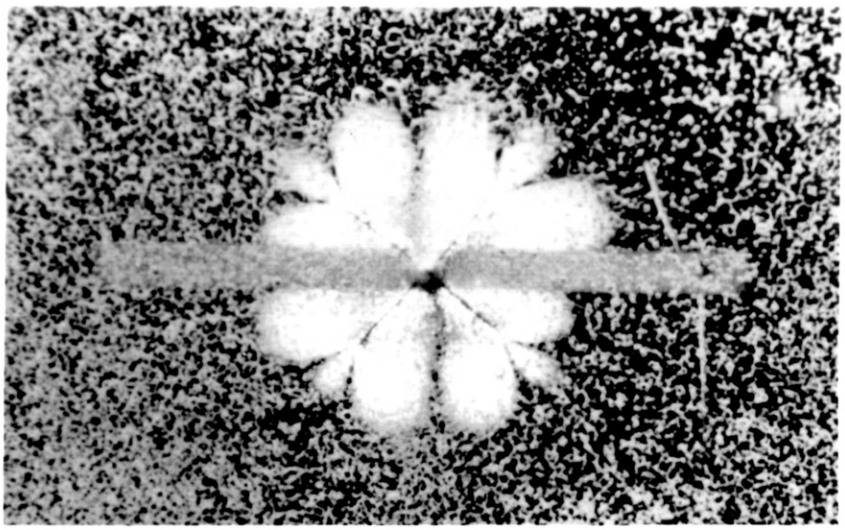


Fig. 7.2 0°-isoclinics around a 4-bladed vane in polyurethane rubber.

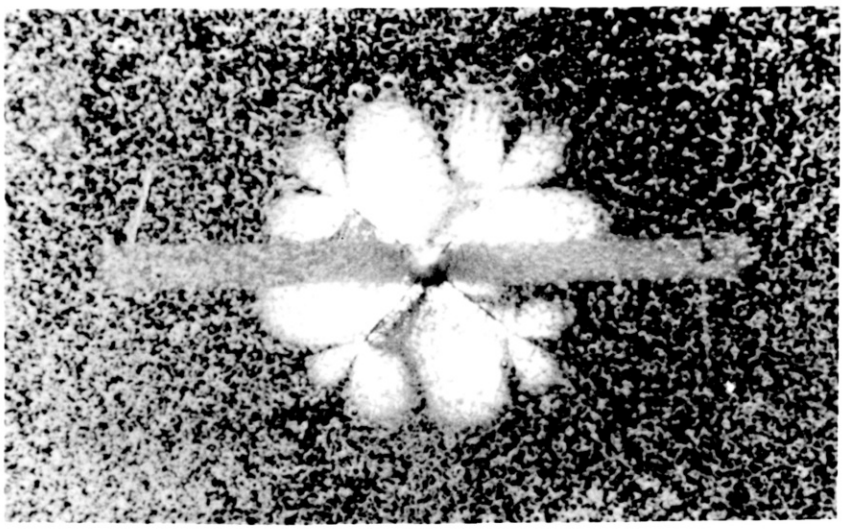


Fig. 7.3 25° -isoclinics around a 4-bladed vane in polyurethane rubber.

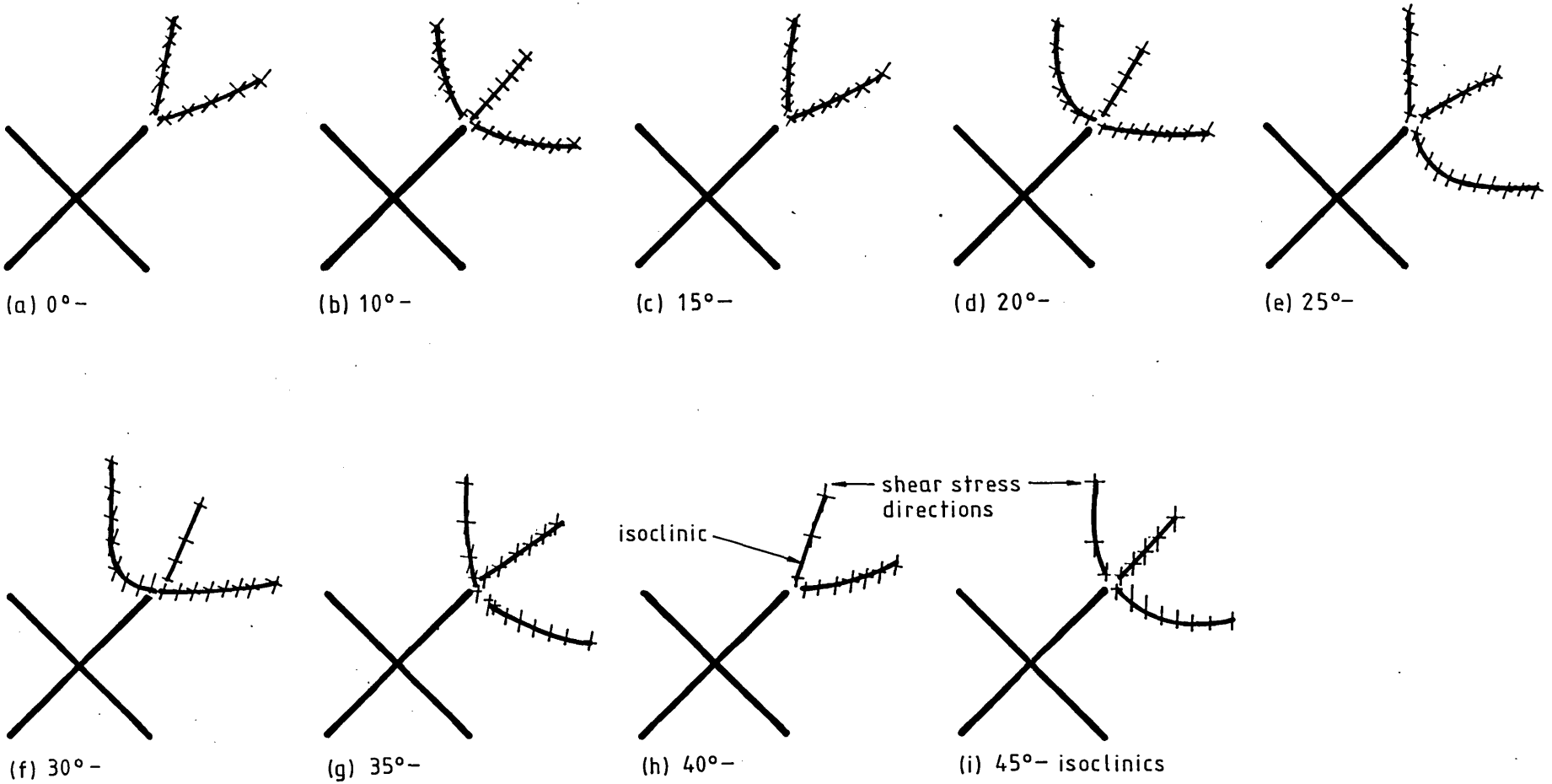


Fig. 7.4 Isoclinics and shear stress directions in the vicinity of a vane blade.

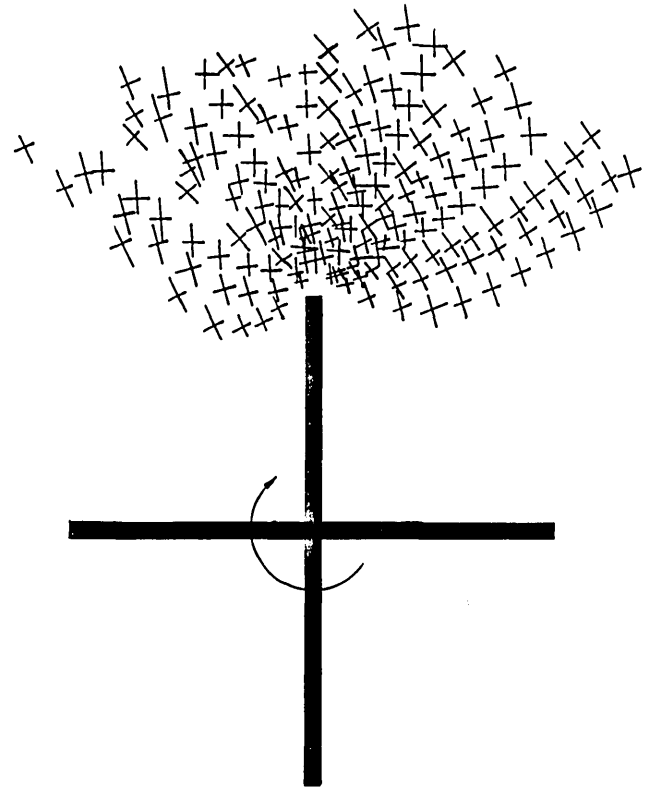


Fig. 7.5 Shear stress directions in the vicinity of a vane blade.

7.3.3 Shear Stress Directions

In order to examine the stress field in the soil around the vane subjected to a small torque at the onset of the propagation of the first shear structures at the vane blade tips, it is reasonable to consider the potential slip-line field under similar circumstances in an elastic material, and construct lines of maximum shear strain, on the basis of the assumption that these coincide with lines of maximum shear stress. Hence, the shear stress directions are determined with regard to the following 'points of interest':

(a) contours of maximum shear stress observed in the gelatine model experiments, and
(b) 'first series' of leading and trailing shear structures observed in kaolin having a water content of about w = 60%.

The shear stress directions along the shear structures in kaolin are shown in Fig. 7.6. These were obtained by determining the shear stress directions along those isoclinics which intersected the shear structures; these being the 20°-, 25°-, 30°- and 40°-isoclinics. The dotted curves shown in Fig. 7.6 represent contours of maximum shear stress, as observed in Fig. 7.1. The results of the photoelastic experiments demonstrate that the directions of the first series of leading and trailing shear structures correspond to contours of maximum shear stress, and are consistent with the directions of the shearing stresses in the vicinity of the 4-bladed vane.

It can be seen that the shear stress directions are in excellent agreement with the direction of the leading shear structure labelled (1) on Fig. 7.6. Furthermore, there is excellent agreement between the shear stress directions and the direction of propagation of one of the trailing shear structures (labelled (4)) over most of its length. This agreement is most encouraging, since it supports the supposition that the shear structures would propagate along lines of maximum shear strain, at least up to the point at which the first leading and/or trailing shear structures are formed. Once failure has taken place, at the instant at which the first leading/trailing shear structure is formed in soil, the material response will no longer be in its elastic range (see Section 7.1). The stress state will change, with accompanying rotation of the principal stress directions, and thus the shear stress directions prior to shear structure propagation will no longer be applicable. Therefore, it does not come as a surprise that the shear stress directions according to the polyurethane rubber model do not coincide with the direction of propagation of the second leading shear structure developed in kaolin (see (2) on Fig. 7.6).

Fig. 7.6 further shows that the photoelastic analysis of the polyurethane rubber model indicates that no isoclinics were observed at any point along the trailing shear structure labelled (3) in Fig. 7.6. This might have arisen as a consequence of the differences between soils and polyurethane rubber.

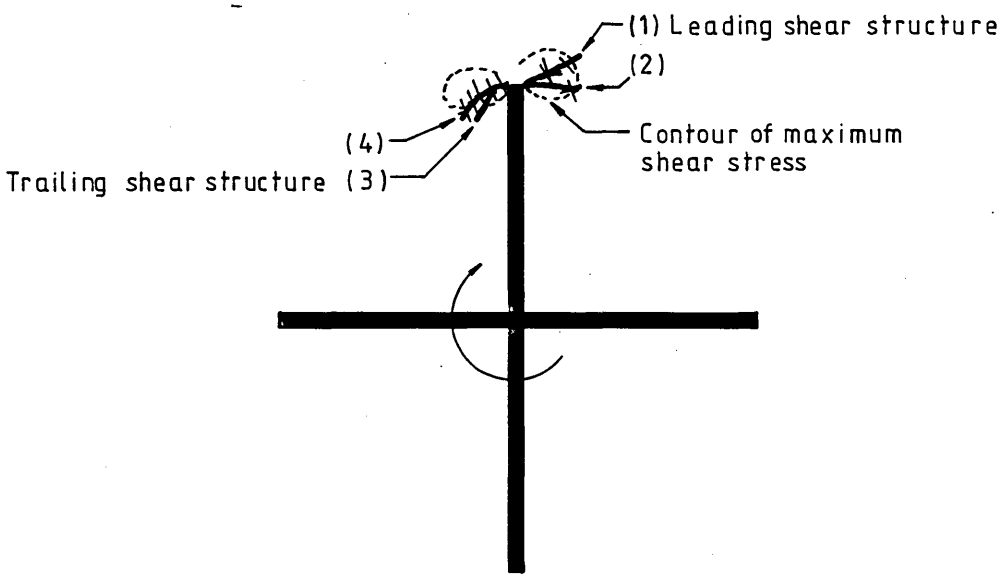


Fig. 7.6 Comparison of maximum shear stress directions in a photoelastic material with angles of propagation of shear structures in kaolin.

CHAPTER 8

ROTATING SHEAR DEVICES UNDER SIMULATED IN SITU CONDITIONS

8.1 INTRODUCTION

The commonest rotating shear device is the 4-bladed vane which is widely used to measure the 'undrained' shear strength of soft clays. Cylindrical piles may be regarded as multi-bladed vanes (Section 2.7, and Chapter 5) and consequently, it is useful to examine the behaviour of piles under torsion in order to determine the validity or otherwise of the above presumption and hence, to establish a test method for the determination of the pile shaft friction. In this light, it is of interest that a few people have carried out torsional pile load tests in order to measure the skin friction developed along the vertical periphery of a cylindrical pile (see, e.g. Stoll, 1972). Although the results of these studies are somewhat inconclusive (Section 2.7), it is possible that torsionally loaded pile tests lead to the determination of soil parameters which may be used in the prediction of soil deformations under other forms of loading (see, e.g. Gens & Potts, 1984, and Kishida et al., 1986). If this suggestion is accepted, there is scope to subject piles to torsion instead of axial load, since rotation of piles is considered both simpler and more economical to perform than loading the piles axially (Stoll, 1972; Poulos, 1975; Randolph, 1981; Kishida et al., 1986). Due to the sparsity of experimental results, it is necessary to conduct more research on this subject.

This Chapter is primarily concerned with a comparison of the shear stress – rotation curves obtained from 12mm diameter 4-bladed vanes having H/D ratios of 2 and 10, with those obtained from 15mm diameter piles (H/D $\approx$ 9), tested under triaxial conditions in similar samples of normally consolidated kaolin. Furthermore, the behaviour of piles under torsion is compared with that of axially loaded piles. In addition, the mode of failure associated with torsionally loaded piles is presented and compared with both the vane failure mechanism and the failure mode of axially loaded piles.

8.2 TESTING PROGRAMME

The testing programme included a series of 12mm diameter 4-bladed vane tests and a number of 15mm diameter 'wished-in-place'* pile tests; both types of test were conducted in a large stress path cell (Section 3.2.2C). [* Note: A'wished-in-place' pile is one which is installed without any disturbance to the surrounding soil fabric. This may be achieved by carefully boring a hole, positioning the pile co-axially, and then grouting up the annulus (see Section 3.4.4B).]

Samples of Speswhite kaolin, which had been normally consolidated to a vertical stress of about 210 kPa, were trimmed nominally to 102mm diameter and 150mm long, and then subjected to further consolidation up to vertical stresses of about 340 kPa, following a K_0 path in the stress path cell. To insert the vanes or to instal the piles, each sample was unloaded decrementally under undrained conditions, as described in Section 3.4.3B. Vane insertion was carried out by attaching the vane to the torsional load cell and carefully lowering the latter through the centre of the sample until the entire vane height was beneath the sample surface (Section 3.4.3C). Pile installation involved drilling a 15mm diameter hole through the central portion of the sample, positioning an 11mm diameter brass pile-core (Fig. 3.2c), and grouting it into the hole using an epoxy resin which was then allowed to set overnight (Section 3.4.4B).

Once the vane/pile was in position (and the resin had set hard), the total radial stress of about 220 kPa was incrementally re-applied to the sample, in accordance with the procedures outlined in Section 3.4.3D. Both vane and pile rotation were carried out under drained conditions at a constant rate of 0.023 °/min (Sections 3.4.3E and 3.4.4C); the axial pile load test was conducted at a rate of displacement of 0.006 mm/min — which was similar to the rate of 0.003 mm/min at which the pile peripheral surface moved in torsional load tests (Section 3.4.4C).

The test programme was concerned with an investigation of both the soil deformation patterns associated with vane and pile rotation (as well as pile displacement) and the shear stress – rotation (/displacement) characteristics of both 4-bladed vanes and rigid model piles. Section 6.2.2 gives a detailed description of the triaxial-vane test programme; vane rotation was stopped at various stages of the test corresponding to conditions prior to and at peak shear stress, as well as to conditions after an angle of rotation of about 360°. The pile test programme involved two torsionally and one axially loaded pile tests; the torsional pile load tests were stopped both when peak shear stress conditions were reached and after an angle of rotation of about 330°, whilst the axial pile load test was stopped when residual conditions appeared to have been attained.

At the end of each test, the sample was unloaded, as outlined in Section 3.4.3B, the stress path cell was disassembled and the sample removed from the pedestal, trimmed and placed in a bath of Breox Peg 8000 for impregnation; water content samples were taken from the trimmings. Finally, thin-sections were prepared and examined according to the procedures described in Section 3.4.6.

The vanes all had H/D ratios of 2, except for one which had an H/D ratio of 10. The piles had H/D ratios of about 9.

8.3 TRIAXIAL-VANE TEST RESULTS

8.3.1 Introduction

The microfabric features which develop in the soil around the vertical periphery of 4-bladed triaxial-vanes at various stages of the shear stress – rotation curve are presented in Sections 6.3.2, 6.3.3A and B. In this Section, first the shear stress – rotation plots for 12mm x 24mm long vanes and then the shear stress – rotation curve for the 12mm x 120mm long vane will be presented.

The tests were carried out under similar triaxial conditions in similar samples of Speswhite kaolin having final water contents of about 46%.

8.3.2 Shear Stress – Rotation Relationships

A summary of five 12mm x 24mm long 4-bladed vane tests in kaolin is given in Table 8.1, together with details of the 12mm x 120mm long vane test. Fig. 8.1 shows the shear stress – rotation curves for vanes having H/D ratios of 2. The initial portions of the curves are almost identical in all cases, except for curve 3 which shows a smaller resistance to shear stress at a given angle of rotation. For angles of rotation < 5°, there are considerable similarities between curves 2, 3, 4 and 5, although these curves correspond to two different samples. It can be seen from curves 1, 2 and 5 that the measured peak strength occurred at similar angles of rotation which were in the range θ_f = 9.1–11.2°. Using the conventional interpretation of the vane test (Eq. 3.2), values of τ_f were respectively 69.5, 74.8 and 61.4 kPa which give an average of about 68.6 ± 6.5 kPa, i.e. 68.6 kPa ± 9.5%, whilst Wroth's interpretation (Eq. 3.1) gives τ_f = 75.8, 81.5 and 66.9 kPa, respectively, resulting in an average peak strength of about τ_f = 74.7 kPa ± 9.5%.

Table 8.1 Results of triaxial-vane tests.

Test No.	Vane H/D Ratio	Sample Height (mm)	Sample Diameter (mm)	σ_r (kPa)	σ_a (kPa)	K_{test}	τ_f 'Conventional' (kPa)	τ_f 'Wroth' (kPa)	θ_f (deg)	τ_r (kPa)	θ_r (deg)	w (%)
1	2	148.95	101.41	218.74	255.5	0.856	69.52	75.78	11.2	21.08	364.9	45.25
2	"	"	"	219.54	259.78	0.845	74.75	81.48	9.8	74.57	10.41	45.96
3	"	"	"	219.27	259.71	0.844	–	–	–	59.41	6.55	45.88
4	"	147.07	101.29	219.66	260.77	0.842	–	–	–	65.19	7.03	46.5
5	"	"	"	219.55	260.84	"	61.41	66.94	9.1	60.89	9.49	46.27
6	10	146.54	101.02	219.7	260.92	"	77.24	78.79	67.7	25.04	361.7	46.02

K_0 = 0.65 for all tests

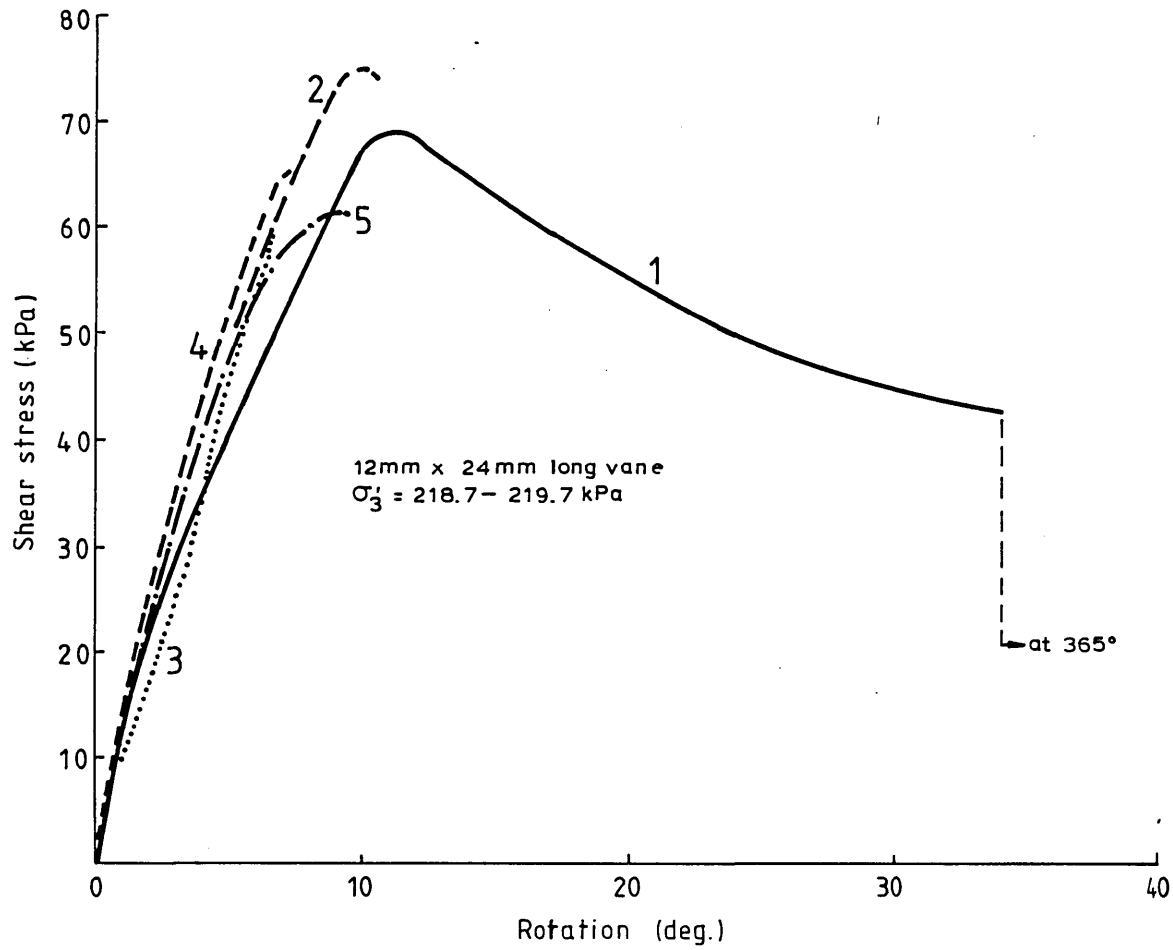


Fig. 8.1 Different stages of 4-bladed triaxial-vane test in reconstituted kaolin.

Post-peak shear stress – rotation characteristics are demonstrated in curve 1 of Fig. 8.1. The complete shear stress – rotation relationship corresponding to approximately one vane revolution is presented (as curve 1) in Fig. 8.2, which also shows the shear stress – rotation curve for the 12mm diameter 120mm long vane test under the same simulated in situ conditions (see Table 8.1). The features of the 'short' and 'long' vane tests, shown respectively by curves 1 and 2 on Fig. 8.2, are of interest in six respects:

(1) Prior to peak shear stress, the short vane exhibits a much stiffer response than the long vane, thus suggesting that the mobilisation of the soil shear strength occurs gradually down the length of the long vane.

(2) The peak shear stress of 77.2 kPa (conventional interpretation) [78.8 kPa (Wroth's interpretation)] is mobilised after an angle of rotation of 67.7° in the case of the long vane, whilst τ_f of 69.5 kPa [75.8 kPa] is mobilised at $\theta_f = 11.2°$ in the case of the short vane. It is noteworthy that the difference between the measured peak strengths of 7.7 kPa [3.0 kPa] is consistent with the range of values of $\tau_{f\,(short)}$ of 68.6 kPa ± 9.5% [74.7 kPa ± 9.5%].

(3) The post-peak rate of reduction of shear stress is similar for both vanes, although it appears somewhat faster in the case of the long vane.

(4) Even after an angle of rotation of 90°, i.e. the angle between two adjacent vane blades, there is no evidence that residual conditions have been attained. Both curve 1 and 2 show a 'step-like' decrease in strength which roughly corresponds to 90° rotations, i.e. between 90 and 180° rotation, 180 and 270° rotation, and 270 and 360° rotation; this phenomenon is associated with slight increases in strength with continued rotation, which is attributed to the probable non-concentric rotation of the vane.

(5) It is seen that after an angle of rotation of 180°, the shear stress measured by the long vane is always higher — by about 15% [5%] — than that measured by the short vane; this observation is a matter for speculation. As a consequence of the more uniform distribution of the normal stresses on the soil mass above and below the vane, an arching effect might have resulted in lower normal stresses on the vertical periphery of the short vane, thus leading to lower radial effective stresses acting on the vane failure surface, and consequently, resulting in the measurement of slightly lower strengths (see also Section 8.5.1). This effect would be minimised in the case of the long vane, since the vane height was almost the same as the sample height and thus, the distribution of the normal stresses on the vane would be very similar to that on any soil mass above and below the vane.

(6) The closer agreement which is obtained between $\tau_{f\,(long)}$ and $\tau_{f\,(short)}$ when Wroth's interpretation is used gives credence to the latter, in preference to the conventional interpretation of the vane test.

Hight (1983) also observed a continuing reduction in the shear stress on the vane failure surface even after one complete revolution of the vane in blocks of reconstituted Lower Cromer Till having OCRs of 1, 4 and 7; the vane had D = 12.5 mm, with H/D = 1.5. Hight attributed this to the substantial reduction in the normal effective stress on the vane shear surface, which he considered was caused by the development of a gap behind the vane blades.

The writer is aware of only one published paper — by Karube et al., 1988 — in which the authors present the shear stress – rotation curves corresponding to tests using vanes of different H/D ratios (of 0.5, 1 and 2); these curves are shown in Fig. 8.3. Although, after incorporating a cylinder shear test result into Fig. 8.3, Karube et al. concluded that the angular rotation at failure increased with reducing H/D ratio, it is difficult to see the emergence of such a definite trend from the data in Fig. 8.3. Karube et al.'s tests were carried out at a rate of rotation of $\omega = 6$ °/min with vanes of different diameters, D = 10 mm (H/D = 2), 15 mm (H/D = 1) and 30 mm (H/D = 0.5).

According to Fig. 2.4b (Section 2.5), which shows strain-rate effects in the case of the soil tested by Karube et al., undrained conditions, corresponding to a 15mm diameter cylinder shear rod, would prevail at a rate of rotation of about 0.2 °/min. Furthermore, on the basis of the arguments presented in Section 4.4.1, the undrained strength would be measured in accordance with the relationship that the rate of rotation corresponding to undrained conditions is inversely proportional to the square of the vane / cylinder shear rod diameter. This suggests that slight viscous effects are probably associated with Karube et al.'s test results and consequently, since viscous rate-effects dominate the results (see Section 4.4.1), the effect of different vane diameters may be negligible in this instance. In spite of this, the writer finds it difficult to agree with Karube et al.'s conclusion regarding the effect of the H/D ratio on the angle of rotation at failure, since (a) the trend exhibited by the vane test results in Fig. 8.3 is unconvincing, and (b) it is believed that the cylinder shear rod reaches failure after a smaller angle of rotation than the 4-bladed vanes because of the more uniform shear stress distribution around the vertical periphery of the rigid pile compared to that around the 4-bladed vanes; this would probably result in the mobilisation of the soil shear strength at an earlier stage, thus implying that the observed behaviour is probably little influenced by the fact that the cylinder shear rod had a larger H/D ratio than the vanes.

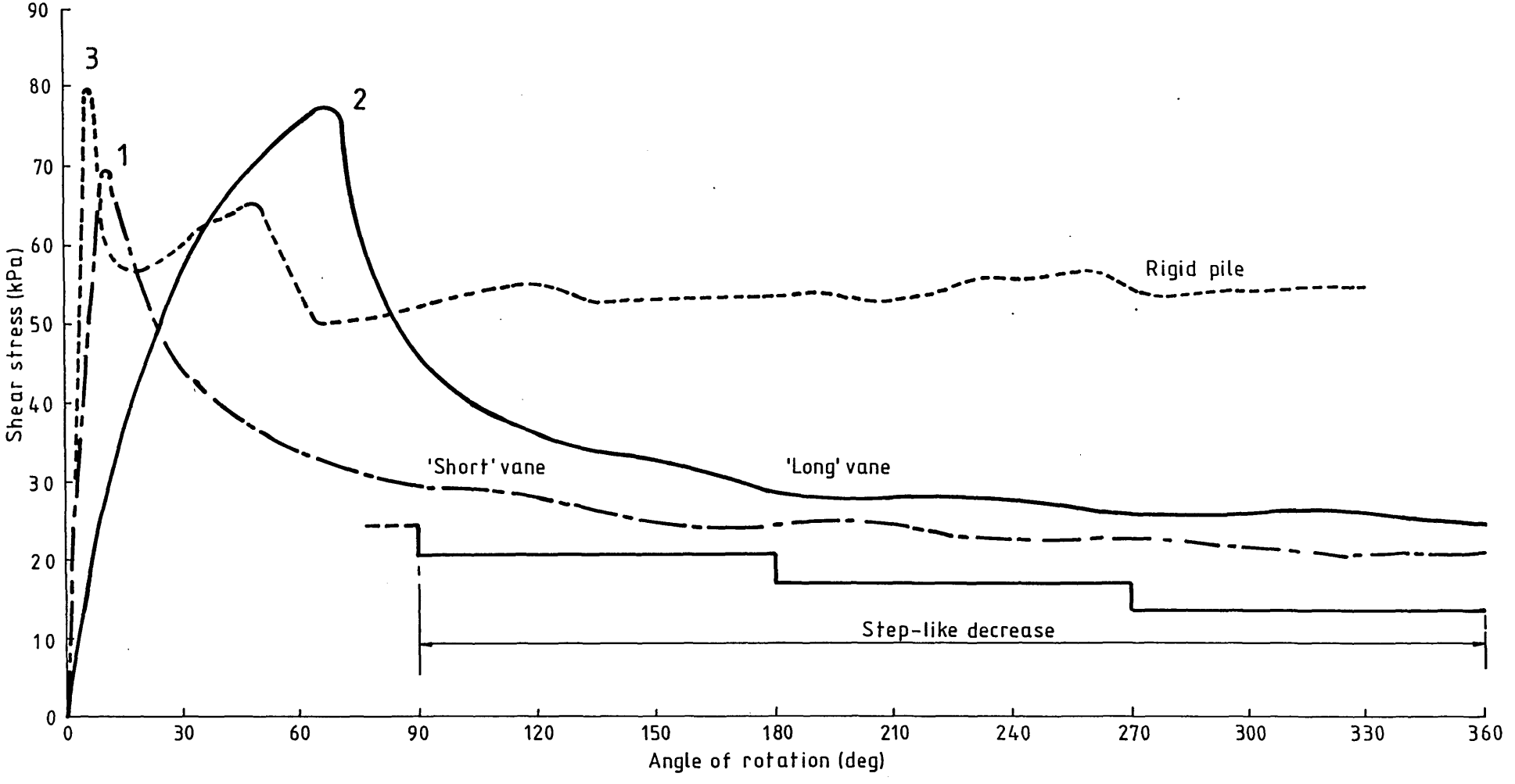


Fig. 8.2 Comparison of the shear stress-rotation behaviour of 4-bladed triaxial-vanes and a model pile.

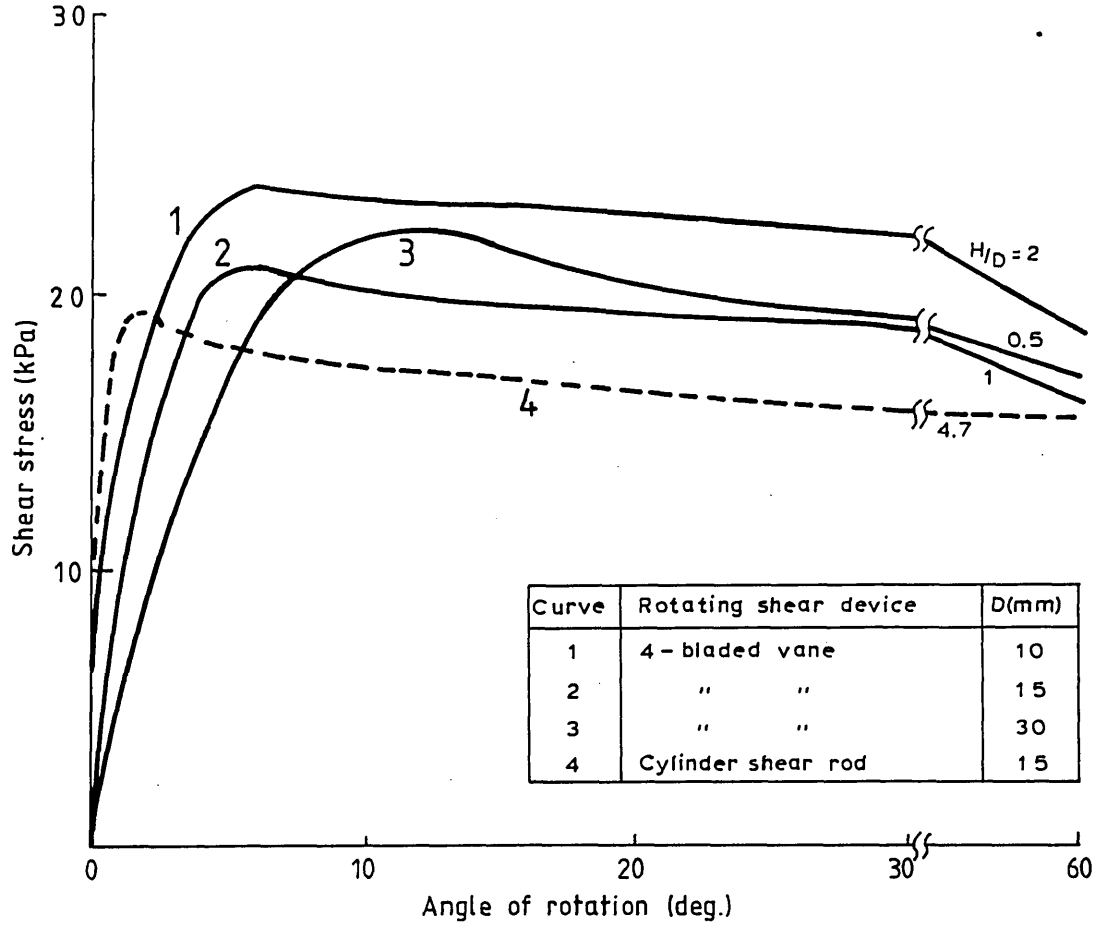


Fig. 8.3 Shear stress—rotation curves for rotating shear devices with different H/D ratios (after Karube et al., 1988).

8.4 MODEL PILE TEST RESULTS

This Section presents the results of 15mm diameter rigid pile tests, with an emphasis on the examination of the behaviour of torsionally loaded piles; axial pile load tests are also described.

The soil deformation patterns observed in thin-sections taken from samples upon pile installation, and at conditions corresponding to the peak and residual (≈ 330° rotation) shear stress are shown in Section 8.4.1, together with the shear stress – rotation curves of torsionally loaded piles. Section 8.4.2 is concerned with the results of axial pile load tests under similar conditions to tests on piles subjected to rotation. The respective shear stress – circumferential/vertical pile displacement curves are given in Figs. 8.4a and b, whilst details of the tests are summarised in Table 8.2.

8.4.1 Piles Subjected to Rotation

8.4.1A Installation disturbance

Fabric disturbance caused by the drilling and reaming operations performed during the course of installing 'wished-in-place' piles was examined from thin-sections — taken from the pile cross-section — observed under crossed polarised light (see Section 3.4.6D). This showed that the disturbance to the fabric was negligible, with features similar to those reported by Martins (1983). To save space, the relevant photographs are not presented and hence, reference should be made to Martins. It is sufficed to say that the reaming operation had resulted in the formation of a few short shear structures, which lie at angles larger than the tangents to the hole, probably caused by the sharp cutting edges of the reaming tool (see Fig. 8.5).

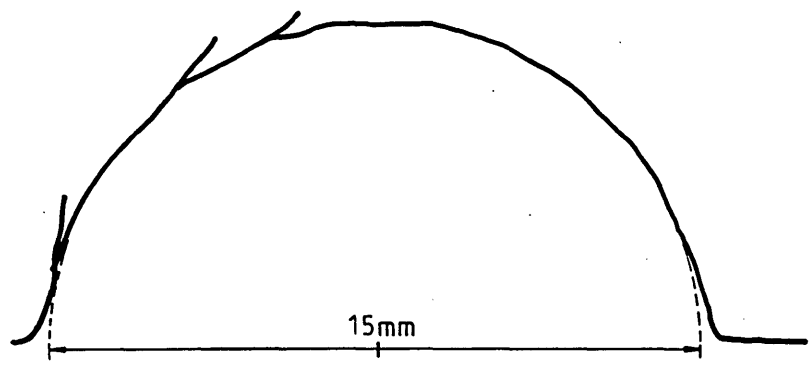


Fig. 8.5 Shear discontinuities caused by the drilling and reaming operations: Schematic representation.

Table 8.2 Results of rigid model pile tests.

Test No.	Sample Height (mm)	Sample Diameter (mm)	σ_r (kPa)	K_{conso}	K_{test}	Pile Length at Peak Shear Stress (mm)	τ_f (kPa)	θ_f x_f	τ_r (kPa)	θ_r x_r	w (%)
MM (R1)	130.08	101.48	219.47	0.65	0.846	105.1	79.7	6.65°	54.61	328.65°	43.8
MM (R2)	138.4	102.1	220.35	"	0.852	113.4	68.69	10.03°	64.6	10.7°	44.8
MM (A1)	136.11	100.9	220.56	"	0.845	120.11	69.26	1.56 mm	18.14	10.56 mm	46.3
JPM (A11)	–	–	210	0.6	0.74	124	88.1	1.33 mm	42.8	13 mm	43.5
JPM (A10)	–	–	260	1.5	1.5	132	98.9	2.55 mm	98.6	2.85 mm	45.7
JPM (A9)	–	–	265	1.49	1.47	131	96.7	2.25 mm	46.5	12.8 mm	44.3

MM: writer
JPM: Martins
A: Axial load
R: Torsion

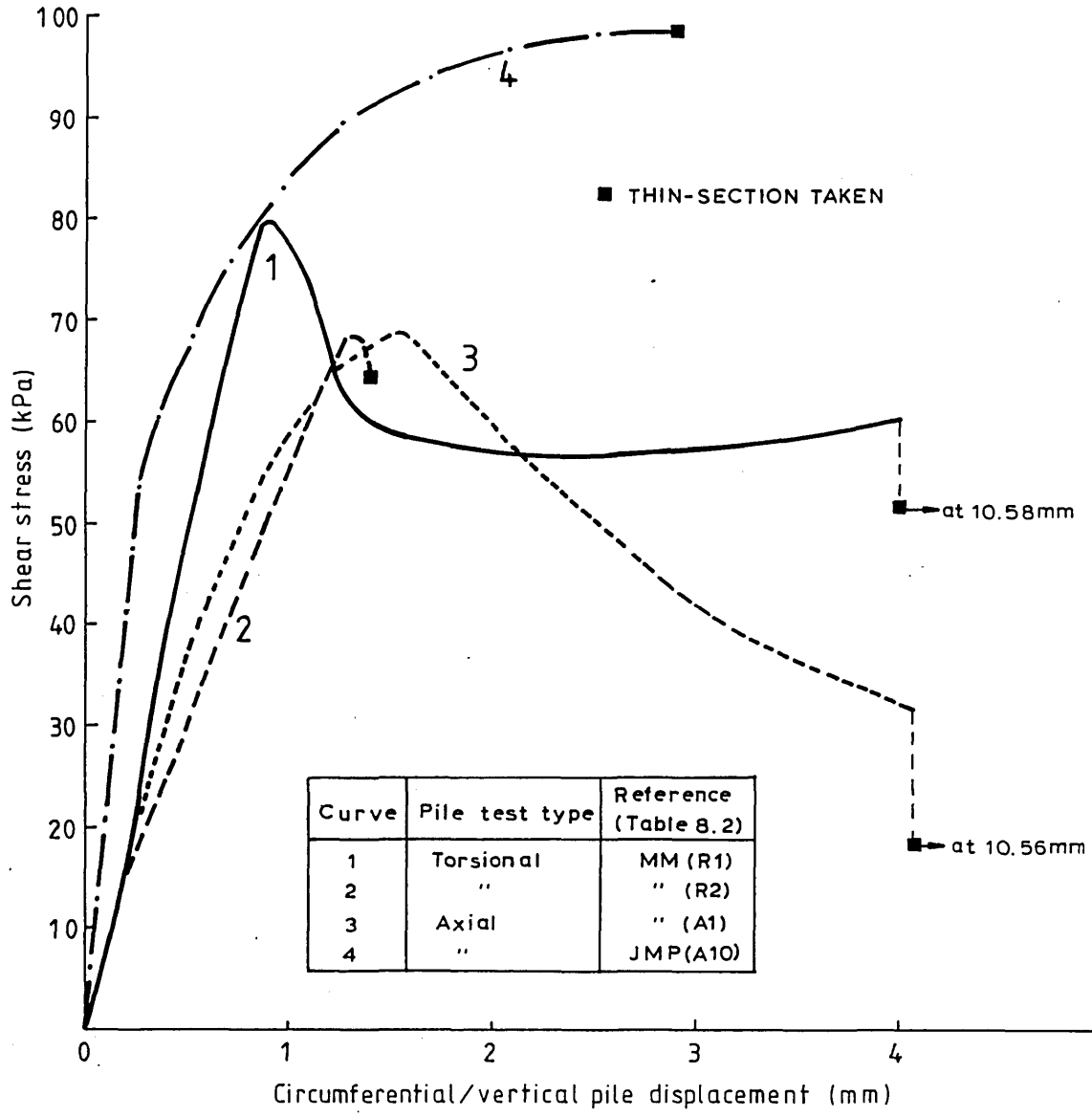


Fig. 8.4a Different stages of axial and torsional model pile tests.

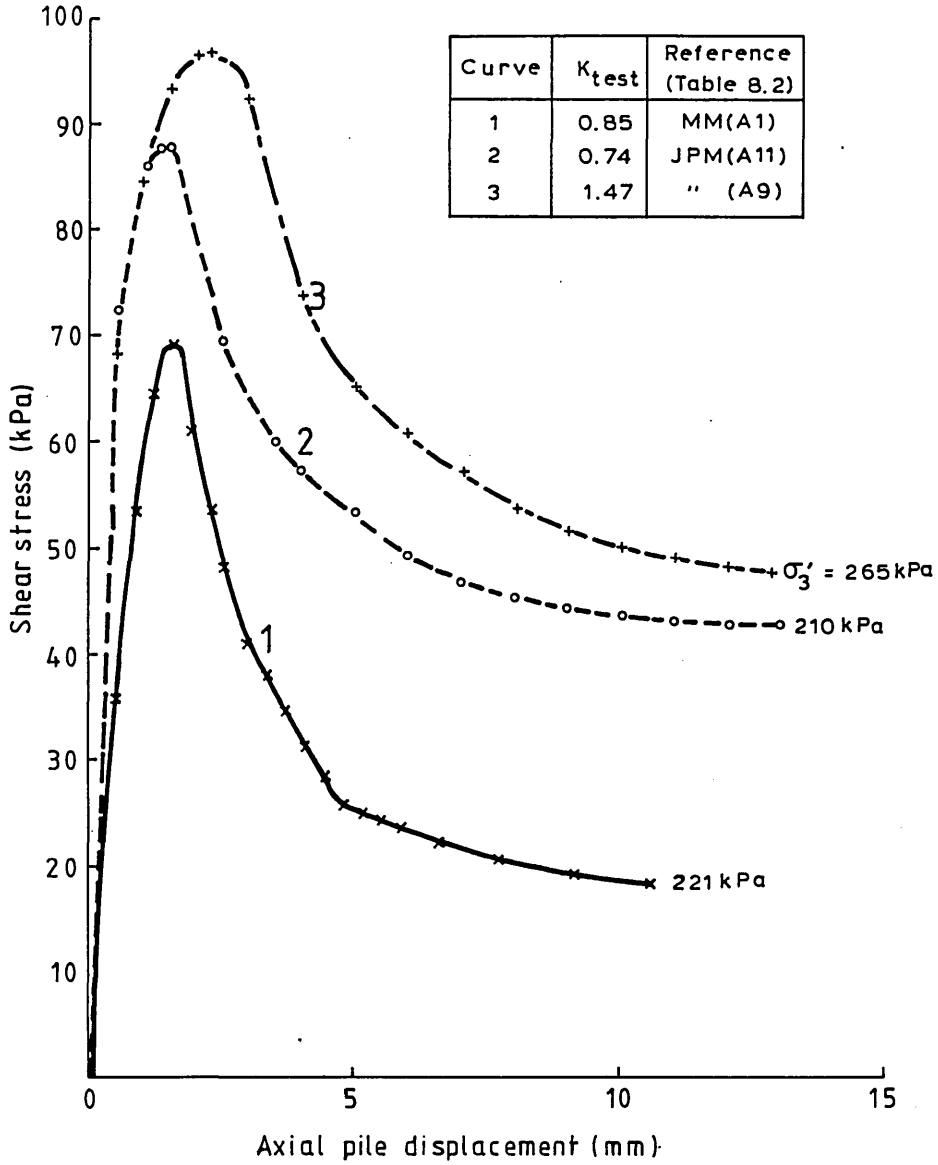


Fig. 8.4b Shear stress – axial displacement curves for model pile tests in kaolin.

8.4.1B Conditions close to peak shear stress

Fig. 8.6 is a photograph showing the propagation of shear structures around the vertical periphery of a pile rotated in the clockwise direction through an angle of about 10.7°, corresponding to conditions at or near the maximum shear stress; the shear stress – rotation characteristics are shown by curve 2 in Fig. 8.4a. The photograph was taken with the orientation of the crossed polarised light selected to show the maximum amount of detail on the thin-section (Section 3.4.6D).

A large number of linear microfabric features, which resemble the leading shear structures developed at the blade tips of a vane (Section 6.3.3), are seen around the pile periphery, extending beyond it by about 0.11–0.12D (where D = pile diameter). (See also Section 6.4.2 and Fig. 6.41.) These microfabric features appear to have initiated from every point on the pile perimeter, propagating at angles which are larger than the tangents to the pile surface. There is no evidence to suggest the presence of a continuous shear surface circumscribing the shear structures; this observation was also made around the vertical vane periphery (see, e.g. Figs. 6.19a and b, and Section 6.3.4D).

It is of interest to compare the propagated shear structures in Fig. 8.6 with the development of the microfabric features around the vertical periphery of an axial pile load test stopped at or near peak shear stress (see curve 4, Fig. 8.4a). Fig. 8.7 was presented by Martins (1983), and shows a photograph of a thin-section taken from the pile cross-section, corresponding to a model pile axial load test in kaolin stopped at conditions close to the maximum shear stress; the model pile was installed using similar procedures to those adopted in the present study, but the kaolin was normally consolidated to a stress ratio of 1.5 (and not 0.85 as was the case in this investigation; see Table 8.2). Martins stated that a continuous displacement discontinuity was not evident. Therefore, the well-defined continuous shear surface observed at a distance of 0.10–0.15D beyond the pile periphery probably represents the locus of the tips of the shear structures developed around the pile surface at the horizon at which the thin-section was taken. It can be seen that the area between this 'apparent' discontinuity and the surface of the pile is disturbed, with a large number of curved shear structures, propagating from the pile perimeter, present within this annulus.

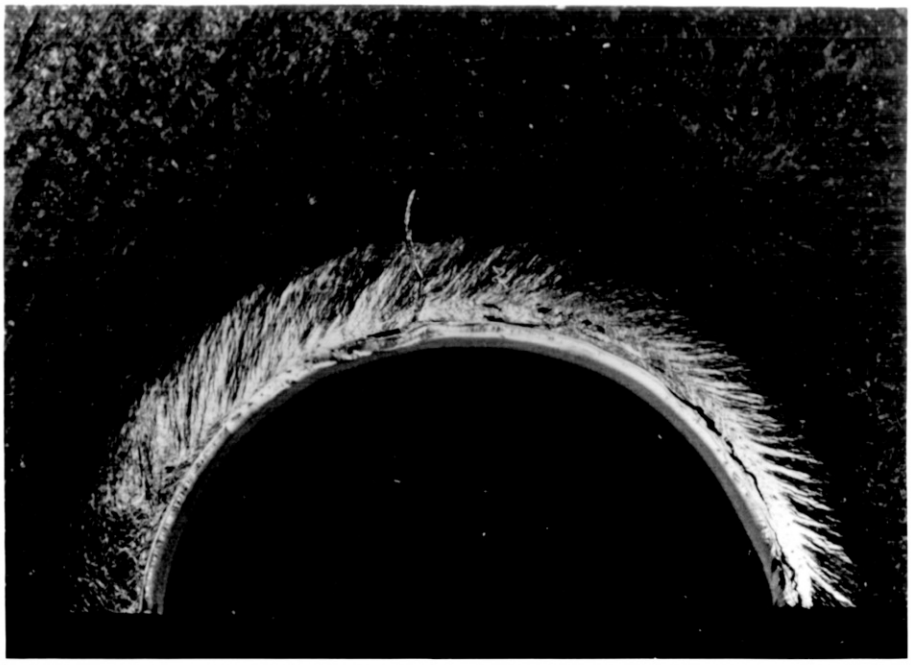


Fig. 8.6 Shear structures propagated at peak shear stress around a rigid pile rotated in the clockwise direction ; curve 2 , Fig. 8.4a.

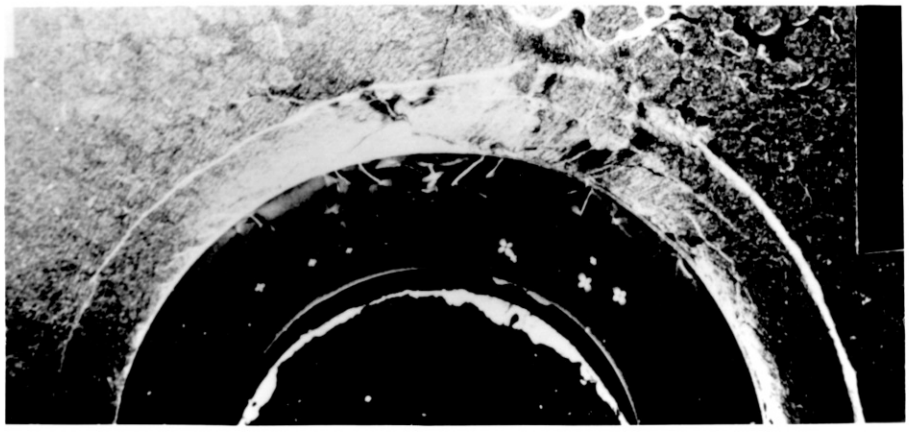


Fig. 8.7 Shear structures developed at peak shear stress around a model pile subjected to axial loading ; curve 4, Fig. 8.4a (after Martins, 1983).

8.4.1C Residual conditions

The development of the shear structures after an angle of rotation of about 330° (which corresponds to residual conditions) is presented in Fig. 8.8; the shear stress – rotation curve for this test is shown both in Fig. 8.2 (by curve 3) and in Fig. 8.4a (by curve 1).

Fig. 8.8 shows a photograph taken from a thin-section prepared from the pile cross-section. The region of soil disturbed as a result of pile rotation through approximately one revolution is seen as the light-coloured annulus around the pile; the latter shows as the black circular area within the annulus. The shear annulus has a width of about 0.12D, with its inner and outer perimeters respectively defined by the circumference of the hole drilled for pile installation purposes and the failure surface bounding the zone of disturbed soil. It is worth remembering that a continuous shear failure surface was also observed circumscribing a vane rotated through to residual conditions (see, e.g. Fig. 6.12); in Section 6.4.2 it was seen that for $n > 6$ the diameter of the vane failure surface (D_f) was about 12–19% larger than the vane diameter, D (see Fig. 6.41d).

Furthermore, a number of distinct shear structures can be seen extending beyond the outer perimeter of the shear zone.

8.4.2 Axially Loaded Pile

The shear stress – displacement relationship for the axial pile load test on kaolin is presented both in Fig. 8.4a (by curve 3) and in Fig. 8.4b (by curve 1). The initial portion (up to the maximum shear stress) of curve 3 shows a shear stress – displacement variation that lies between curves 1 and 2, which portray the response of torsionally loaded piles; curve 3 exhibits a less stiff response than curve 1, whilst it is slightly stiffer than curve 2. It will be remembered that the shear stress – circumferential/vertical displacement curves, according to Gens & Potts (1984), show that the torsionally loaded pile displays a much stiffer response than the axially loaded pile (see Fig. 2.8).

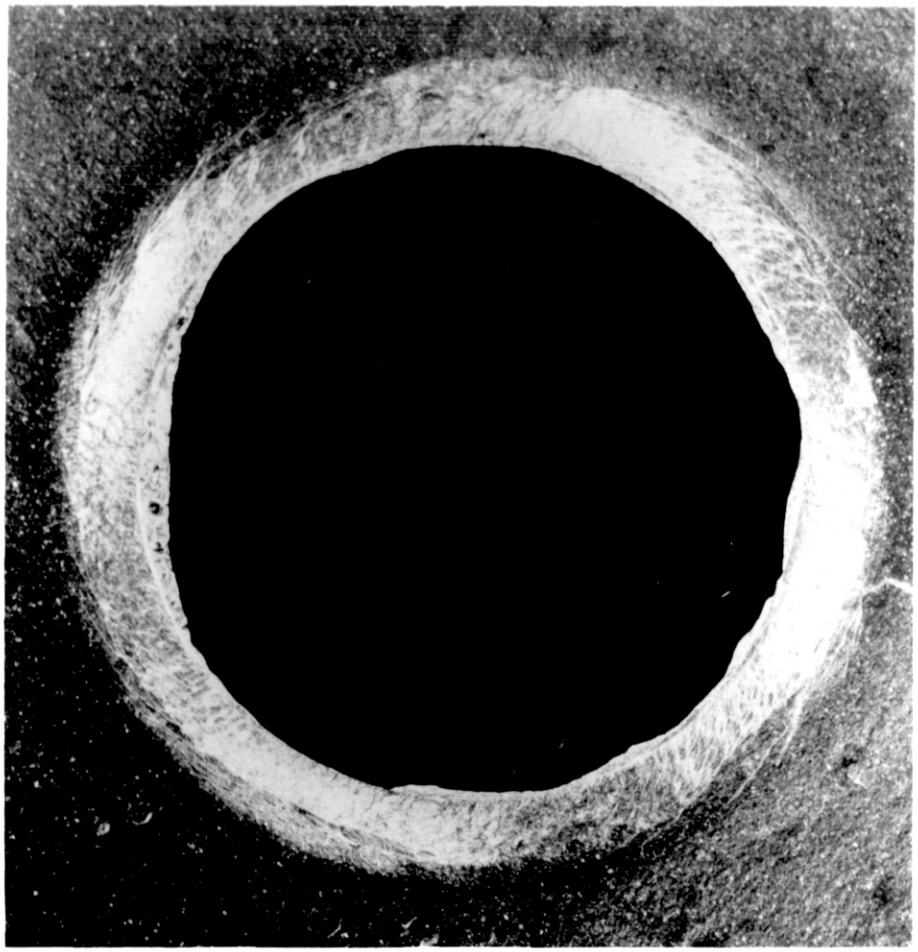


Fig. 8.8 Residual shear structures around a rigid pile rotated in the clockwise direction; curve 3, Fig. 8.2.

Fig. 8.9 is a photograph of a thin-section taken from the pile cross-section after an axial pile displacement of about 10.6 mm, corresponding to residual conditions (see curve 1, Fig. 8.4b); it shows the development of microfabric features around the vertical periphery of the pile. The light-coloured annulus of soil around the pile shows the shear zone, which has a width in the range 0.09–0.18D, and two well-defined shear discontinuities extending beyond the pile perimeter by 0.024–0.044D and 0.09–0.18D, respectively.

Martins (1983) presents a photograph (Fig. 8.10) of a thin-section taken from the cross-section of a pile loaded axially to a residual displacement of about 12.8 mm; the kaolin sample had followed a stress history along $K \approx 1.5$. Curve 3 on Fig. 8.4b shows the relevant shear stress – displacement relationship. There are considerable similarities between Figs. 8.9 and 8.10, although they correspond to axial pile load tests in samples having different initial stress ratios (see also Table 8.2); Martins found that the inclination of the shear structures associated with peak conditions appeared to be independent of the initial stress ratio. Despite the greater clarity of detail which can be observed in Fig. 8.9, both Figures show a shear zone around the pile vertical periphery.

Fig. 8.10 shows the existence of three major thin continuous shear discontinuities parallel to the pile periphery, extending beyond the circumference of the pile by 0.029–0.036D, 0.077–0.097D and 0.13–0.15D, respectively; the latter two are probably 'apparent' features, since Martins observed only one major shear discontinuity in the respective longitudinal thin-section. As can be seen in Fig. 8.7, none of these three discontinuities appears as distinct as that corresponding to the peak shear stress conditions in the sample with a similar initial stress ratio. However, this might be expected to be reasonable, since a greater volume of soil had been disturbed as a result of the larger axial displacement which the pile had undergone in the latter case; consequently, it is possible that any continuous shear discontinuities that might have developed were subsequently obscured by the greater disturbance to the soil fabric.

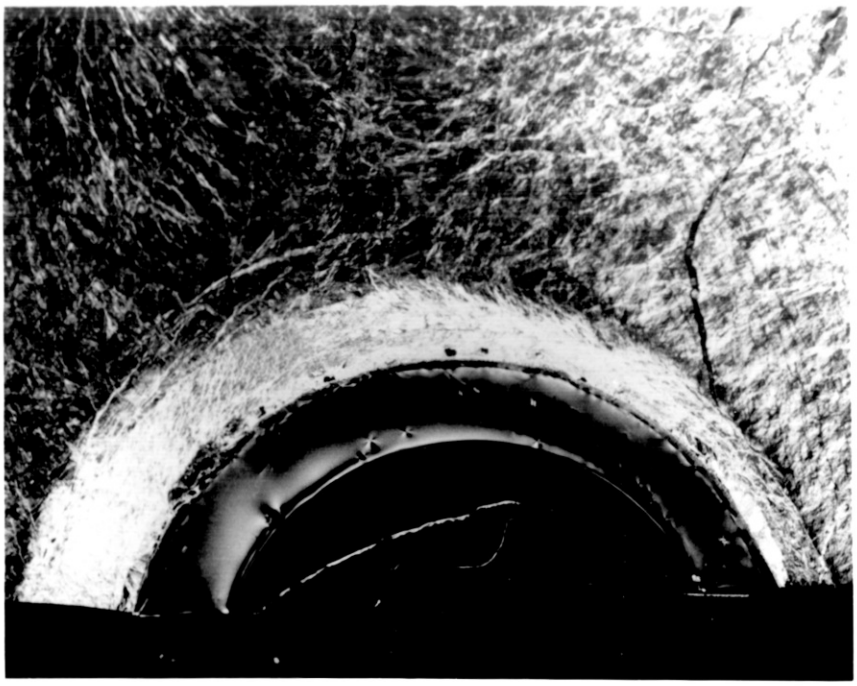


Fig. 8.9 Residual shear structures around a rigid pile subjected to axial loading ; curve 1, Fig. 8.4b.

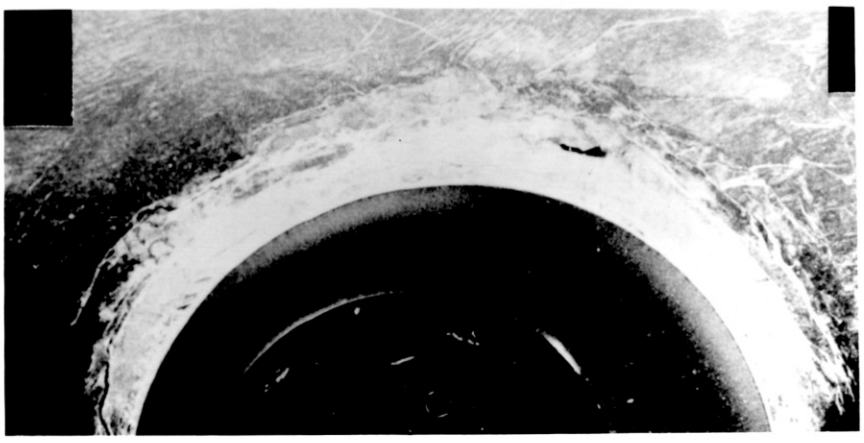


Fig. 8.10 Residual shear structures around a rigid pile subjected to axial loading ; curve 3, Fig. 8.4 b (after Martins, 1983).

8.5 DISCUSSION OF THE RESULTS

8.5.1 The Behaviour of Rotating Shear Devices

This Section is concerned with a comparison of the behaviour of 4-bladed vanes of different H/D ratios and the torsional response of rigid piles having a diameter similar to that of the vanes. The variations in the shear stress – rotation characteristics, as well as the measured shear strength of 4-bladed vanes having different H/D ratios are examined. Moreover, the responses of vanes and rigid piles subjected to rotation are discussed, and the vane test is analysed in terms of effective stress. Finally, a comparison is made between the behaviour of torsionally and axially loaded piles.

8.5.1A Vanes with different H/D ratios

The results of the triaxial-vane tests performed in this investigation have been presented in Section 8.3.2. The shear stress – rotation relationships of vanes having H/D ratios of 2 and 10, tested under similar conditions, have been compared (see Fig. 8.2). Primarily, three points have been noted:

(i) the measurement of a slightly larger shear strength by the long vane;
(ii) the mobilisation of the peak shear strength at an earlier rotation, and following a much steeper soil response at the initial portion of the shear stress – rotation curve, by the short vane;
(iii) the measurement of a higher residual strength by the long vane.

Since the only parameter which was varied is the H/D ratio of the two vanes, it is reasonable to expect that the above variations have probably resulted as a consequence of effects associated with the H/D ratio. Therefore, given that the most important use of the vane test is in the measurement of the soil shear strength, the H/D-ratio effect will first be explored in this connection.

Fig. 8.11 is a plot of the measured shear strength normalised to that shear strength measured with the 'standard' vane with an H/D ratio of 2, against the height to diameter ratio of 4-bladed vanes. It presents the results obtained in this investigation, together with data extracted from the results reported by Cadling & Odenstad (1950), Child (1959), Aas (1967) and Karube et al. (1988); no other data set has been cited in the literature. Based on the data points shown in Fig. 8.11, it is difficult to draw any firm conclusions as to whether or not the vane H/D ratio has any significant influence on

the measurement of the soil shear strength. However, the trend which appears to emerge is that the measured strength is not particularly affected by the vane H/D ratio.

The effect of the H/D ratio on either the angle of rotation at failure (θ_f) and/or the measured residual shear strength (Section 8.3.2) cannot be discussed in any detail, due to the scarcity of experimental data.

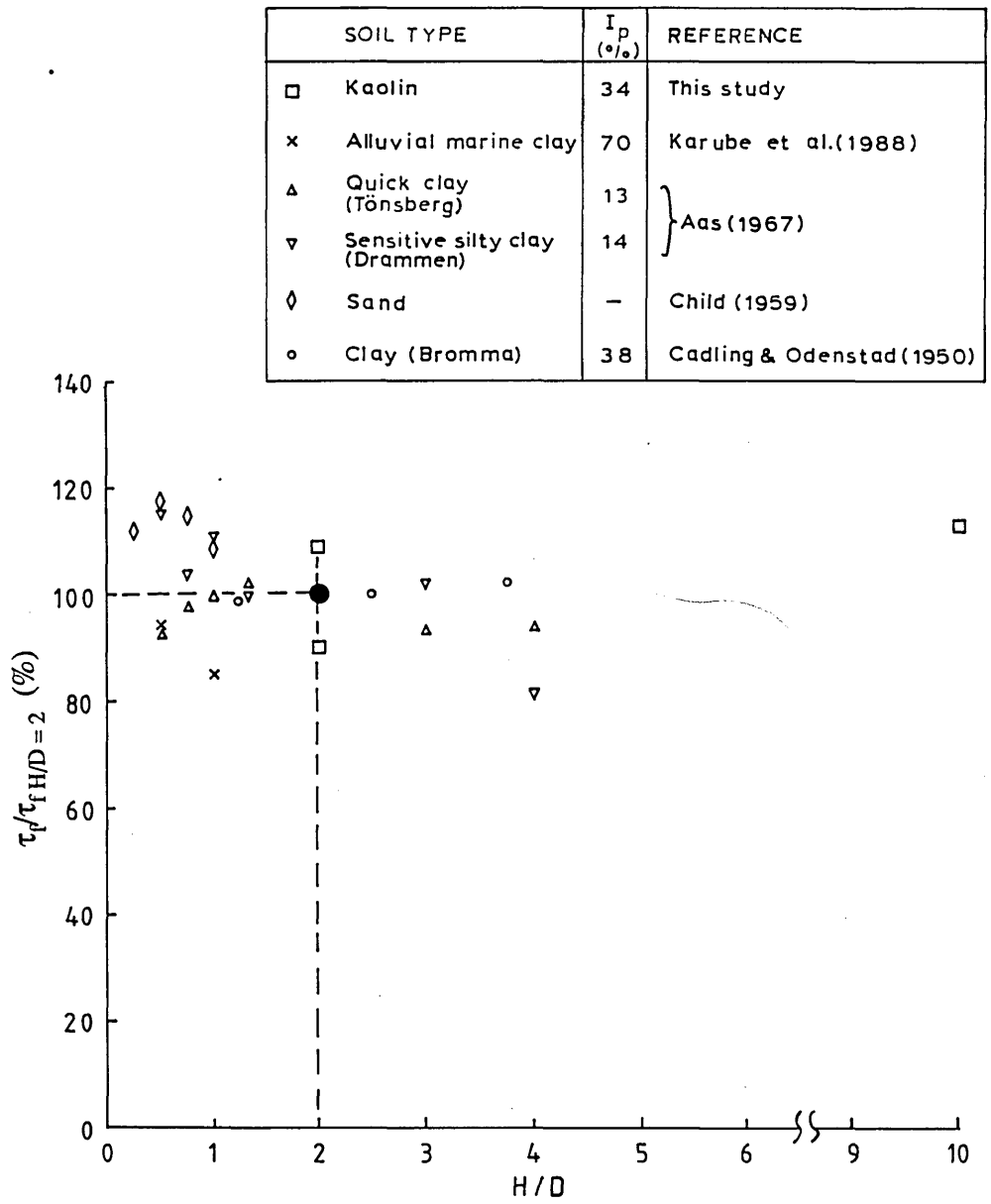


Fig. 8.11 Variation of normalised vane strength with H/D ratio.

8.5.1B Comparison of vane and pile rotation

The behaviour of 4-bladed vanes and rigid piles subjected to rotation under similar test conditions can be examined by comparing the respective shear stress – rotation curves (2 and 3) shown in Fig. 8.2; these curves correspond to similar vane and pile H/D ratios (of 10 and 9 respectively).

Prior to the mobilisation of the peak shear stress, the rigid pile shows a much stiffer response than the vane. This is attributed to the more uniform distribution of shear stresses around the periphery of the rigid pile compared to the less uniform stress state associated with the vane. In addition, the pile reaches failure at a much smaller angular rotation than the vane. This, again, is an observation which may be explained by the differences in the shear stress distributions around these two rotating shear devices. It will be remembered that as the number of vane blades increases, the angle of rotation measured at failure decreases (see Section 5.3.4). The third difference between curves 2 and 3 is associated with the measurement of the residual shear strength; an almost constant residual shear strength is mobilised in the case of the pile soon after the rapid post-peak drop in strength, whilst the shear strength continues to reduce with increasing rotation in the case of the 4-bladed vane, and after about one revolution reaches a value which is approximately half that measured by the pile. The continual reduction in strength with increasing rotation is a matter for speculation. It is possible that the distribution of the normal stresses around the vertical periphery of the 4-bladed vane is less uniform than that around the rigid pile and thus in the case of the former, the soil arches, causing a reduction in the radial effective stresses governing the mode of failure, and thus, leading to the measurement of reducing residual strengths.

It is most interesting that Karube et al.'s (1988) curves 1 and 4 in Fig. 8.3, which respectively correspond to 4-bladed vane (H/D = 2) and cylinder shear rod (H/D $\approx$ 4.7) tests under triaxial conditions, show very similar trends to those discussed above. The main similarities are in the observation of the stiffer pre-peak response and the lower angle of rotation at failure of the cylinder shear rod (curve 4) compared to the behaviour observed in the case of the 4-bladed vane (curve 1). Karube et al. did not concern themselves with such a comparison.

The differences in the post-peak rate of drop in strength between the pile and the 4-bladed vane are also of interest. Rotation of the pile may be considered analogous to soil-brass interface shear, whilst rotation of the 4-bladed vane is analogous to soil-soil shear. Therefore, it is useful to compare the shear stress – displacement curves for soil-brass interface and soil-soil shear tests. Fig. 8.12a shows the results of ring shear

tests for both remoulded London clay on a roughened glass surface (Lemos, 1986) and undisturbed London clay (Garga, 1970; repeated in part in Bishop et al., 1971); the strain rates used in these ring shear tests were of the same order of magnitude as those used for the rotation of the shear devices tested in this investigation. It can be seen that these curves correspond qualitatively to the curves shown in Fig. 8.2.

The results of consolidated drained reconstituted clay-clay and clay-steel interface shear box tests carried out by Littleton (1976) also show a similar trend to that observed in Fig. 8.12a (and Fig. 8.2); the strain rate was not reported. Fig. 8.12b illustrates the shape of the shear stress – displacement curves for illite (I_p = 33%, i.e. similar to the kaolin tested in this investigation), which depicts the difference in the behaviour of clay on clay from that of clay on a smooth steel interface; the 'clay to steel' curve shows both an earlier mobilisation of the peak shear stress and a steeper post-peak response than that seen in the 'clay to clay' curve. In addition, Littleton found that the clay-steel interface tests resulted in the measurement of higher strengths than those in the clay-clay tests (see also Fig. 8.2), although this is not evident in Fig. 8.12b.

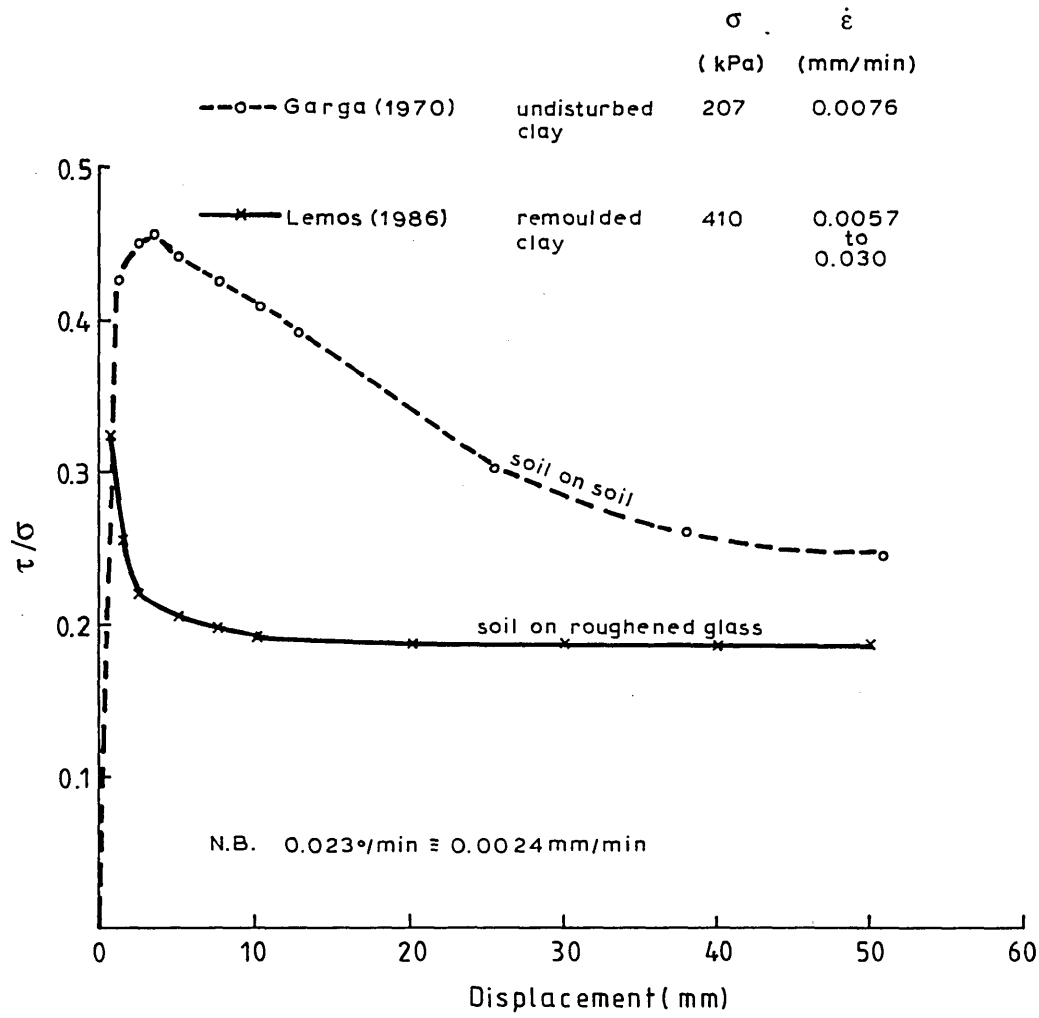


Fig. 8.12a Normalised shear stress — displacement curves for ring shear tests on London clay.

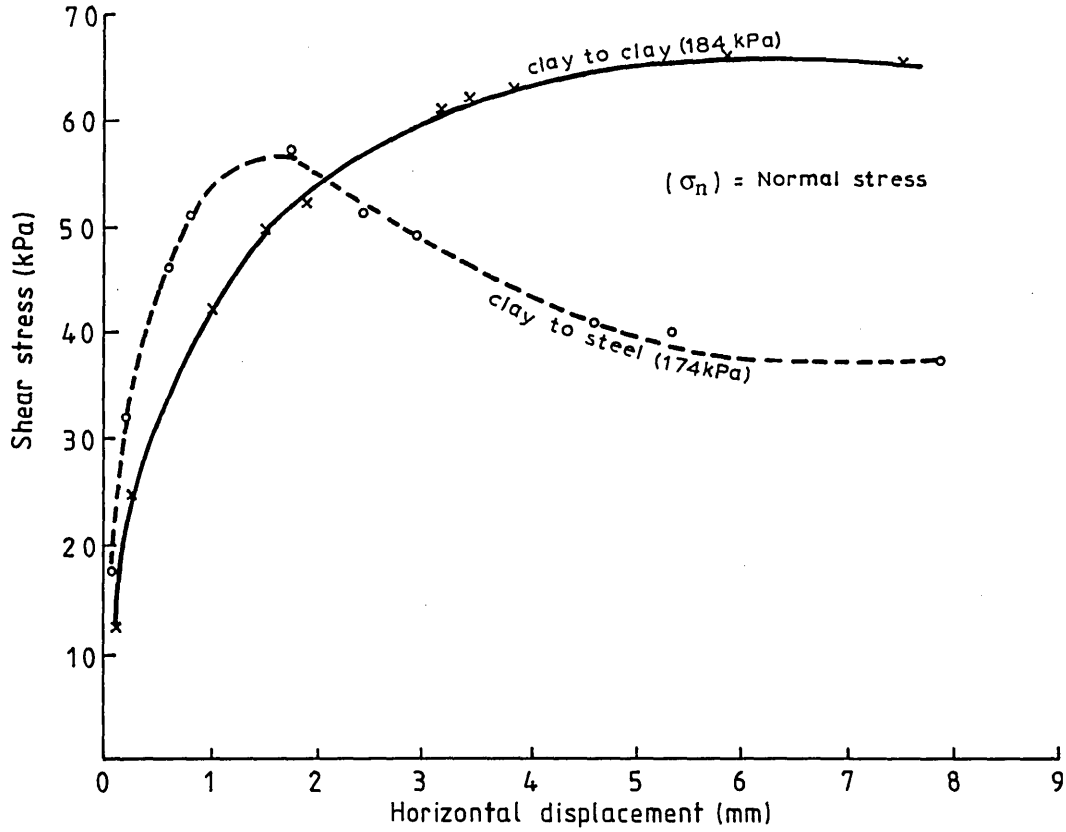


Fig. 8.12b Shear stress – displacement curves for drained shear box tests on reconstituted illite (after Littleton, 1976).

8.5.1C Effective stress analysis of the vane test

Only three other attempts have been made at a fundamental study of the vane test under controlled laboratory conditions (Law, 1979; Matsui & Abe, 1981; Karube et al. 1988). Since the data presented by the above authors include the stresses acting normal to the vertical periphery of the vane, it is useful to examine two hypotheses which are considered appropriate to the analysis of rotating shear devices in terms of effective stress.

Wroth (1984) presents an expression (Eq. 6.1) relating the maximum shear stress measured by the vane, τ_f, to the normal effective stress acting on the vane (σ_h'), by assuming that the strength mobilised is completely dominated by shearing on the vertical periphery of the vane. Eq. 6.1, which is here re-presented by:

$$\tau_f = \sigma_h' \sin\phi'_{ps} \qquad \text{Eq. 8.1,}$$

shows that the mean effective stress remains constant as the vane is rotated, and suggests that simple shear conditions apply at peak shear stress.

An alternative, more conventional interpretation of the vane (/pile) test in terms of effective stress parameters would make use of the relationship:

$$\tau_f = \sigma_h' \tan\phi' \qquad \text{Eq. 8.2.}$$

To explore the validity of the above interpretations in relation to rotating shear devices, the results obtained in this study, and by Law (1979), Matsui & Abe (1981) and Karube et al. (1988) are examined. Table 8.3 lists the relevant parameters corresponding to each study. Values of the angle of shearing resistance, ϕ', have been calculated according to both interpretations. With the exception of Matsui & Abe's data, the 'back-analysed' ϕ' values show good agreement with typical values of ϕ' obtained from Kenney's (1959) well-known relationship between ϕ' and plasticity index (I_P). The examination of the available data has not, however, provided sufficient credence to one interpretation in favour of the other.

Table 8.3 Rotating shear devices under simulated in situ conditions.

Reference	Shear Device	Shear Device		ω	Soil Type	Plasticity Index (%)	σ_h' [σ_v'] (kPa)	K	τ_f/σ_h'			ϕ' (deg)		
		D (mm)	H/D	(°/min)					Mean	Range		*	**	f(Ip)
Law (1979)	4-bladed vane	10	2	5	Leda clay (grey silty marine deposit)	24	19.6–88.3	1	0.5852	0.3871	0.9995	30.3	31.8	30
	"	"	"	"	"	"	"	0.41–0.49	0.6509	0.5863	0.8346	33.1	36.1	"
Matsui & Abe (1981)	4-bladed vane	15	2	6	Kaolin	20	[19.6]	0.40–0.50	1.0659	0.9787	1.2625	46.8	–	30.7
	"	"	"	"	Senri	55	"	0.42–0.52	0.931	0.7959	1.0366	43	61	25.1
	"	"	"	"	Kaolin/Senri Mixture	33	"	0.42–0.51	1.1932	1.0204	1.3133	50	–	28.5
Karube et al. (1988)	cylinder shear rod	15	4.7	6	Osaka Bay clay (alluvial marine deposit)	70	73.5–147	0.50–0.51	0.2646	0.2619	0.2667	14.8	13.6	23.2
	4-bladed vane	"	2	"	"	"	73.5	0.45	0.3252	–	–	18	16.9	"
This Study	4-bladed vane	12	2	0.023	Kaolin	34	218.7–219.6	0.84–0.86	0.3127	0.2797	0.3405	17.4	16.2	28.2
	"	"	10	"	"	"	219.7	0.84	0.3516	–	–	19.4	18.3	"
	Rotating pile	15	9	"	"	"	219.5–220.4	0.85	0.3375	0.3117	0.3632	18.7	17.5	"
	Axially loaded pile	"	"	≈ 0.046	"	"	220.6	0.85	0.314	–	–	17.4	16.3	"
Martins (1983)	Axially loaded pile	"	8–9	≈ 0.032	"	30	210–265	0.74–1.50	0.3883	0.3649	0.4195	21.2	20.3	28.9

* $\tan^{-1}(\tau_f/\sigma_h')$

** $8/9 \sin^{-1}(\tau_f/\sigma_h')$

8.5.2 Comparison of the Behaviour of Torsionally and Axially Loaded Piles

It is the aim of this Section to examine the failure mechanism of torsionally and axially loaded piles, with a view to establishing whether the measurements of shaft friction from torsional pile load tests may be used in the design of piles under vertical load.

It was seen in Section 8.4.1B that the microfabric features developed around the vertical periphery of a torsionally loaded rigid pile (Fig. 8.6) showed considerable similarities to the propagated shear structures around the tips of a 4-bladed vane (Figs. 6.19a and b). In particular, there was no evidence of a continuous shear surface circumscribing the pile at maximum shear stress — a feature which was also observed in the case of the vane. Furthermore, Karube et al. (1988) have suggested that the vane failure mechanism is similar to the mode of shearing around a cylinder shear rod (Section 2.7).

Based on the similarities observed between the peak shear stress microfabric features developed in the shear box test and in the vane test, it was suggested in Section 6.5 that the vane failure mechanism was one of simple shear. Moreover, Martins (1983) has found that the mode of failure associated with an axially loaded 'wished-in-place' pile has characteristics which resemble the development of the shear structures in the shear box test. Consequently, he has also concluded that simple shear conditions probably also apply in the case of piles under vertical load.

Due to the similarities between the propagation of the microfabric features around the vertical periphery of torsionally loaded 'wished-in-place' piles and 4-bladed vanes (as well as considerable similarities between the shear structures developed around the vertical periphery of torsionally and axially loaded piles — Section 8.4.1B — which can be seen in Figs. 8.6 and 8.7), and the conclusions reached regarding the mode of failure associated with 4-bladed vanes (Section 6.5) and axially loaded 'wished-in-place' piles (Martins, 1983), it is reasonable to conclude that the failure mechanism of torsionally loaded 'wished-in-place' piles is also one of simple shear.

If the conclusion that simple shear conditions apply to both torsionally and axially loaded 'wished-in-place' piles is accepted, it would be reasonable to expect similar measurements of shaft adhesion for both modes of testing. It can be seen from Fig. 8.4a that the maximum shear strengths measured by the axially and torsionally loaded piles are similar. Although this study is the only investigation in which 'wished-in-place' piles have been subjected to both rotation and axial load, it should be noted that all other investigations into the behaviour of axially and torsionally loaded piles (Poulos, 1975; Gens & Potts, 1984; Kishida et al. 1986; Tominaga & Hanzawa, 1986) have also concluded that similar shaft adhesions would be measured from these two different modes of pile testing (see Section 2.7).

CHAPTER 9

CONCLUDING REMARKS

9.1 CONCLUSIONS

An extensive experimental and semi-analytical study has been made to examine some of the fundamental aspects of the measurement of the strength of clays using rotating shear devices, including vanes with different numbers of blades and 'wished-in-place' rigid model piles (installed with little or no disturbance to the soil fabric). Conclusions reached regarding each rotating shear device are presented separately.

9.1.1 The Vane Shear Test

Three major aspects associated with the vane shear test have been investigated. These included:

(a) the effect on the measured strength of the rate of rotation of the vane;
(b) the effect of the number of vane blades on the measured strength;
(c) the pattern of soil deformation induced by the vane.

Samples of Speswhite kaolin, London clay and a bentonite/London clay mixture, all prepared in the laboratory, were used in the testing programme. The following conclusions have been drawn.

9.1.1A Strain-rate effects in the vane test

1. Shear stress – rotation characteristics, comprising the peak strength, the angle of rotation at failure and the initial slope of the curve, are strongly influenced by the vane rotation rate. The large displacement ('residual') strength, which corresponds to an angle of rotation of 360°, is not markedly affected by rate-effects.

2. Increasing strengths are measured both at slow rates of rotation, which is associated with consolidation around the vane, and at fast rates where there are accompanying viscous rate-effects. Thus, variation of the measured vane strength with the rate of rotation is a function of both the coefficient of consolidation of the soil, (c_v), and the vane H/D ratio, as well as vane size.

3. Furthermore, the measured vane strength – rate of rotation variation is also a function of plasticity index of the soil.

4. Good agreement is observed between the experimental strengths and relationships based on a proposed hypothetical model which relates viscous rate-effects to the vane diameter, while consolidation effects are related to the square of the vane diameter.

5. Blight's (1968) simple theory of consolidation may be used and extended to establish the rates of rotation required for both undrained and drained conditions to apply during tests with vanes with different H/D ratios. Undrained conditions corresponding to an average degree of pore pressure dissipation (U) of $\leq 5\%$ would apply at a time factor (T) of ≤ 0.04 for vanes with H/D ≥ 2, and at $T \leq 0.015$ for vanes with H/D = 1.

6. (a) Peak-strength measurements obtained from laboratory-vane tests in normally consolidated kaolin, normally consolidated London clay and 47-day old remoulded London clay show large values at slow rates of rotation (ω), these decreasing with increasing ω, and reaching minima before increasing with further increases in shearing rate; 2-day old remoulded London clay and normally consolidated bentonite/London clay mixture show the opposite trend of increasing strengths with increasing rotation rate, with no evidence of points of minima.

   (b) Times to failure corresponding to the measurement of minimum strengths with a 12mm square vane tested in normally consolidated samples of kaolin and a bentonite/London clay mixture are about 0.1 and 60 minutes respectively; these correspond to rates of rotation of approximately 100 and 0.1 °/min respectively.

   (c) Hence, the rate of rotation of 6 °/min, which has been adopted as a standard for the laboratory vane test, is not valid for the measurement of the undrained strength for all soils.

(d) Moreover, the vane tip velocity of 0.15 mm/sec, as recommended by Perlow & Richards (1977), is considered much too general to be adopted as a standard, particularly for soils with high values of c_v.

9.1.1B Effect of the number of blades

1. The highest measurement of strength in a given soil is with a 2-bladed vane, with the measured strength gradually decreasing as the number of blades increases. The strength measured with a solid rod having the same diameter as the vane is the lowest.

2. For vanes with the same number of blades and H/D, increasing vane size results in the measurement of lower peak strengths, higher angles of rotation at failure, and a less stiff soil response. The rate of drop of strength with number of blades is greater in the case of kaolin than with London clay.

3. (a) The foregoing results show that vane insertion disturbance effects — which appear to vary with clay type — influence the measured shear strength for vanes with a small number of blades, and strongly modify the soil response when the number of blades is large.

   (b) There is no evidence of significant progressive failure effects (in the behaviour of vanes with a small number of blades) — a conclusion which is contrary to the speculative comments expressed by some authors in the literature (Section 2.5).

4. An extension of the Farrent–Arnold interpretation of the vane test, which is in terms of shear stress strength parameters and exponentially distributed shear stresses along the vertical periphery of adjacent blades, provides an explanation for the observation of lower strengths being mobilised at smaller angles of rotation for vanes having more than four blades.

5. Thin-section observations show that shear structures which propagate in front of and behind each blade tip, extend both beyond and within the vertical periphery of the vane, thus providing some justification for Arnold's (1978) interpretation of the vane test in which the vane failure surface is assumed to be logarithmic spiral in shape.

6. Furthermore, a photoelastic model analysis of the vane test using gelatine shows isochromatic fringes that demonstrate that the shear stress distribution between adjacent blades may be regarded exponential.

9.1.1C Vane failure mechanism

1. There is disagreement in the literature regarding both the extent of the vane failure surface and the mechanism of failure associated with the vane test, both of which are in connection with the assumption that the mobilisation of the peak soil strength occurs both fully and instantaneously along the entire cylindrical surface circumscribing the vane.

2. (a) In the past, even the apparent sophistication of radiographic techniques has failed to provide the amount of detail required for examining the vane failure mode.

   (b) The soil deformation patterns caused during vane rotation can for the first time be clearly observed from thin-sections prepared from samples of normally consolidated kaolin; similar microfabric features can be observed around vanes rotated in samples of normally consolidated London Clay, although the degree of clarity is inferior compared to that of the kaolin thin-sections.

3. (a) As the vane is rotated, each vane blade causes high stress concentrations and the soil deforms by the formation of 'leading' and 'trailing' shear structures which propagate in front of and behind each blade tip, falling beyond and within the vane perimeter, respectively.

   (b) With increasing angles of vane rotation, the leading and trailing shear structures propagate further, but, ultimately, the development of these structures is arrested as new ones propagate at successively lower inclinations relative to the tips of each vane blades.

   (c) Both the number and extent of penetration of both leading and trailing shear structures increase up to peak torque, although the ultimate, continuous shear failure surface, which is clearly defined by the vane perimeter, does not develop until the onset of post-peak conditions.

(d) There is no progressive element in the formation of this final failure plane.

4. Isoclinic bands obtained from polyurethane rubber photoelastic experiments using 4-bladed vanes show that the directions of the maximum shearing stresses coincide with the directions of propagation of the 'first series' of leading and trailing shear structures in kaolin.

5. (a) The shear zone around the vane extends vertically by no more than 10% of the vane diameter beyond the top and bottom horizontal surfaces, and propagates radially a maximum distance approximately equal to 50% of the vane diameter beyond the vane periphery, depending on the number of vane blades; fewer blades result in longer shear structures penetrating the soil within and beyond the vane circumference.

(b) Between 45% ($n \geq 6$) and 100% ($n = 2$) of the volume of soil swept by the rotating vane undergoes permanent deformations, as indicated by the formation of microfabric features within the soil.

6. Discrepancies between the measured vane strength and the undrained shear strength measured using other test methods should not be attributed to either the assumption of a vane-sized failure surface or the assumption that the vane failure mode is non-progressive. Differences in the boundary conditions and modes of deformation of different test methods should be taken into account.

7. (a) 2-bladed vane shear structures differ from the deformation patterns propagated around the vertical perimeter of 4- and 6-bladed vanes; 3-bladed vane shear structures are largely consistent with those of the 4-bladed vanes, yet with some aspects in common with the 2-bladed vanes.

(b) Quantification has shown that the number of blades on the vane, particularly in the range 2 to 4, has a significant effect on both the number and angle of propagation of the leading shear structures, and the outer diameter and size of the vane shear zone.

8. With reducing sample water content, both the number and the extent of the leading and trailing shear structures developing around the vane decrease, ultimately resulting in the absence of trailing features in kaolin having a water content of about $w \leq 40\%$.

9. The considerable similarities between the shear structures developed around the vertical periphery of the vane and the microfabric features observed by Morgenstern & Tchalenko (1967) in the shear box suggest that the conditions which apply at peak torque are also probably those of simple shear.

10. (a) There are interesting similarities between the 2-bladed vane curvilinear trailing structures and the rupture surfaces which develop behind a retaining wall.

(b) Excellent agreement is obtained between the peak torque derived from an analysis of the 2-bladed vane in terms of earth pressures, and experimental torques normalised with respect to the 4-bladed vane peak torque.

9.1.2 Model Pile Tests

1. Careful installation of 'wished-in-place' rigid model piles in kaolin causes minimal disturbance to the clay fabric.

2. At peak shear stress, the soil microfabric features developed in torsional pile load tests are similar to those observed at maximum torque in the vane test; shear structures initiate from every point on the pile perimeter, but without forming a continuous shear surface circumscribing the pile.

3. There are considerable similarities between the peak shear structures observed around the vertical periphery of torsionally loaded piles and the corresponding features associated with axially loaded piles, with the structures extending a maximum distance of about 15% of the pile diameter beyond the perimeter.

4. A continuous shear band is observed at (large displacement) residual shear stress conditions for both axial and torsional pile load tests. The shear discontinuities extend beyond the pile perimeter a maximum distance of about 12 and 15% of the pile diameter for torsionally and axially loaded piles, respectively.

5. The radial stresses in the soil act normal to the vertical pile periphery and hence are important in controlling the measurement of the pile shaft carrying capacity.

6. Peak strengths measured with torsionally loaded piles compare well with 4-bladed vane strengths, with slightly lower values being recorded by the latter, possibly as a consequence of the less uniform distribution of stresses and perhaps also reducing radial effective stresses due to arching effects.

7. Residual strengths obtained from torsional pile load tests are about two times larger than large displacement ('residual') vane strengths, with the latter not showing any sign of attaining a steady value. This continual reduction in the shear stress on the vane failure surface is due to contractant behaviour of soils (such as normally consolidated kaolin), which results in the substantial simultaneous reduction of the normal effective stresses acting on the vane.

8. Although the shear stress – rotation characteristics of vanes with different H/D ratios show differences, there is little evidence to suggest that the H/D ratio has a marked influence on the measured strengths.

9. The strength measured using rotating shear devices may be interpreted in terms of effective stresses.

10. Simple shear conditions probably apply at maximum shear stress in the case of 'wished-in-place' piles subjected to torsion, as they do for axially loaded piles. Furthermore, similar strengths are measured by torsionally and axially loaded piles tested in kaolin. Hence, soil parameters determined from torsional pile load tests may probably be used in the prediction of soil deformations under other forms of loading.

9.2 PRACTICAL IMPLICATIONS

9.2.1 The Vane Shear Test

The vane shear test is a simple and convenient method for the measurement of the undrained strength of soft clays. Due to its low cost, availability and ease of operation, and due to the worldwide experience gained with the vane test over the past 50 years, its use, in suitable ground conditions, should be encouraged, provided that certain aspects of its performance are appreciated and thus taken into consideration at the outset. Outlined below, are considerations with regard to those particular aspects of the vane test which have been investigated during the course of this research programme.

The vane dimensions, height, H, and diameter, D, are important in the interpretation of the test in two respects. Firstly, due to the non-uniform distribution of shear stress on the two horizontal ends of the vane (Menzies & Merrifield, 1980), the discrepancy between the measured vane strength derived from the conventional interpretation (which assumes a uniform distribution of shear stress around the entire shearing surface) and Wroth's (1984) modified interpretation increases with decreasing values of H/D ratio (Table 3.1), with the conventional interpretation underestimating the soil strength by less than 10% when the standard (H/D = 2) vane is used. Secondly, consolidation effects associated with the vane are also a function of both the vane diameter, D, and the vane H/D ratio (Sections 2.7 and 4.4.5).

For a given rate of rotation, the larger the vane diameter, the greater the vane tip velocity at which the soil is sheared (Perlow & Richards, 1977). Consequently, the drainage conditions corresponding to rotation of two vanes of two different diameters, having the same H/D ratio, rotated at the same rate of rotation, may well vary from those of drained to those of undrained, depending on the difference in the diameters of the vanes and the rotation rate (Section 4.4.2).

With the exception of high plasticity clays (Section 2.4), the selection of the rate of rotation to ensure undrained conditions may be made for vanes with different H/D ratios using theoretical drainage curves derived by Blight (1968) for vanes with H/D = 2, and extended by the writer for both vanes with H/D > 2 and H/D = 1 (Fig. 4.25); in using these theoretical drainage curves it is required that the soil coefficient of consolidation is either known or can be accurately predicted.

The use of the 4-bladed vane as standard is endorsed for the reasons given below:

(a) Vanes with more than four blades cause significant disturbance to the soil fabric during vane insertion (Fig. 6.6, Section 6.3.2), and consequently result in the measurement of a lower shear strength (Fig. 5.7, Section 5.4).

(b) Vanes with less than four blades exhibit a different mode of deformation to the 4-bladed vane, even though the eventual development of a cylindrical vane-sized failure surface is common to all vanes, irrespective of the number of blades.

Given that no progressive element is involved in the formation of the cylinder of revolution which circumscribes the vane periphery, the conventional interpretation may be used for the determination of the undrained strength of soft clays. However, for situations in which the use of shear stress strength parameters is appropriate, Arnold's (1978) interpretation is a valuable improvement, since the assumption of a logarithmic spiral shearing surface which is made in that interpretation has here been substantiated by both

(a) the nature of the microfabric features induced in the soil by the rotating vane at different stages of the test, and
(b) the isochromatic fringe patterns observed from photoelastic stress analysis experiments which suggest that the distribution of the shear stresses around the vertical periphery of the vane is exponential.

9.2.2 Piles Subject To Torsion

It has been shown in Section 8.5.2 that there are considerable similarities in the behaviour of torsionally and axially loaded 'wished-in-place' piles tested in kaolin, particularly with regard to the failure mechanism. In this light, rotation of piles for the determination of the shaft carrying capacity for use in design appears to be satisfactory, although this subject requires further consideration by others.

9.3 SUGGESTIONS FOR FURTHER RESEARCH

Further work is needed to investigate the reason(s) for the discrepancy between the experimental and hypothetical relationships observed in Fig. 4.15, with a view to refining the hypothetical model (Fig. 4.11, Section 4.4.1) proposed as an explanation for the strain-rate effects in the vane test. For this purpose, it is suggested that remoulded samples of London clay, having the same water content and age, should be tested using two square vanes, one twice as large as the other. A second series of tests may be performed by testing similar samples under simulated in situ conditions in a stress path cell (see Section 8.2).

Analytical work using the method of finite elements might be undertaken to study further both the vane failure mechanism and consolidation aspects associated with strain-rate effects in the vane test.

The significance of the H/D ratio on the shear stress – rotation characteristics of vanes could be established by testing vanes with a variety of H/D ratios.

Although the similarities observed from the results of torsional and axial pile load tests on normally consolidated kaolin are very encouraging, further tests should be performed in a different clay type, in order to examine whether the conclusions drawn from the kaolin test results can also be applied to other normally consolidated clays. It would also be of value to investigate the influence of overconsolidation ratio on the response of piles subjected to torsion, thus permitting a comparison with the work of Martins (1983) on axially loaded piles.

Development of an in situ test method for the determination of pile shaft friction is an obvious topic for future research. Possible methods of in situ tests can be investigated in the laboratory using the model pile test cell described in Section 3.2.2C. Types of test to consider could include both 'smooth' and 'rough' (i.e. with small vanes) pile segments tested under torsion and axial load, both in bored hole ('wished-in-place' pile) and driven into place.

REFERENCES

Aas, G. (1965). A study of the effect of the shape of vane and rate of strain on in situ shear strength of clays. *Proc. 6th Int. Conf. S.M. & F.E.*, Montreal, Vol. 1, pp. 141-145.

Aas, G. (1967). Vane tests for investigation of anisotropy of undrained shear strength of clays. *Proc. Geotech. Conf.*, Oslo, Vol. 1, pp. 3-8.

Allison, I.M. (1987). Personal communication.

Arman, A., Poplin, J.K., and Ahmad, N. (1975). Study of the vane shear. *Proc. Specialty Conf. on In-situ Measurement of Soil Properties*, ASCE, Rayleigh, Vol. 1, pp. 93-120.

Arnold, M. (1978). The multi-blade vane in frictional soils. (unpublished).

Atkinson, J.H. (1973). *The deformation of undisturbed London clay*. Ph.D. Thesis, Imperial College, Univ. of London.

Berre, T., and Bjerrum, L. (1973). Shear strength of normally consolidated clays. *Proc. 8th Int. Conf. S.M. & F.E.*, Moscow, Vol. 1, pp. 39-49.

Bhandari, R.K. (1970). *Mudflows in stiff fissured clays*. Ph.D. Thesis, Imperial College, Univ. of London.

Bishop, A.W., and Gibson, R.E. (1963). The influence of provisions for boundary drainage on strength and consolidation characteristics of soils measured in the triaxial apparatus. *Lab. Shear Testing of Soils*, ASTM, STP 361, pp. 435-451.

Bishop, A.W., and Henkel, D.J. (1962). The measurement of soil properties in the triaxial test. 2nd ed., London: Arnold.

Bishop, A.W., and Wesley, L.D. (1975). A hydraulic triaxial apparatus for controlled stress path testing. *Geotechnique*, Vol. 25, pp. 657-670.

Bishop, A.W., Kumapley, N.K., and El-Ruwayih, A. (1975). The influence of pore-water tension on the strength of clay. *Phil. Trans. Royal Soc.*, London, A278, pp. 511-554.

Bishop, A.W., Webb, D.L., and Lewin, P.I. (1965). Undisturbed samples of London Clay from the Ashford Common shaft. *Geotechnique*, Vol. 15, pp. 1-31.

Bishop, A.W., Green, G.E., Garga, V.K., Andresen, A., and Brown, J.D. (1971). A new ring shear apparatus and its application to the measurement of residual strength. *Geotechnique*, Vol. 21, pp. 273-328.

Bjerrum, L. (1971). Effects of rate of strain on undrained shear strength of soft clays. *NGI Publ.* No. 85.

Bjerrum, L. (1973). Problems of soil mechanics and construction on soft clays. *Proc. 8th Int. Conf. S.M. & F.E.*, Moscow, Vol. 3, pp. 111-159.

Bjerrum, L., Simons, N.E., and Torblaa, I. (1958). The effect of time on the shear strength of a soft marine clay. *Proc. Conf. on Earth Pressure Problems*, Brussels, Vol. 1, pp. 148-158.

Blight, G.E. (1961). *Strength and consolidation characteristics of compacted soils.* Ph.D. Thesis, Imperial College, Univ. of London.

Blight, G.E. (1968). A note on field vane testing of silty soils. *Canadian Geotech. J.*, Vol. 5, pp. 142-149.

Blight, G.E. (1977). Discussion on: Influence of shear velocity on vane shear strength. *J. Geotech. Engrg. Div.*, ASCE, Vol. 103, pp. 1349-1350.

British Association for the Advancement of Science Mathemathical Tables. (1950). Vol. VI, Bessel functions, Part I: Functions of orders zero and unity. Prepared by the Committee for the Calculation of Mathematical Tables. Cambridge: University Press for the Royal Society.

BS 1377. (1975). Methods of test for soils for civil engineering purposes. London: British Standards Institution.

Cadling, L., and Odenstad, S. (1950). The vane borer. *Proc. Royal Swedish Geotech. Institute*, No.2.

Carlson, L. (1948). Determination in situ of the shear strength of undisturbed clay by means of a rotating auger. *Proc. 2nd Int. Conf. S.M. & F.E.*, Rotterdam, Vol. 1, pp. 265-270.

Carslaw, H.S., and Jaeger, J.C. (1986). Conduction of heat in solids. 2nd ed., Oxford: University Press.

Chandler, R.J. (1988). The in situ measurement of the undrained shear strength using the field vane.*Vane Shear Strength Testing in Soils : Field & Lab. Studies*, ASTM, STP 1014, A.F. Richards, Ed., Tampa, pp. 13-44.

Cheah, H. (1981). *Site investigation techniques for laboratory soil models.* M.Phil. Thesis, Univ. of Cambridge.

Child, K.T. (1959). *The application of the vane test to sands.* M.Sc. Thesis, Univ. of Leeds.

Coates, R.C., Coutie, M.G., and Kong, F.K. (1980). Structural analysis. 2nd ed., Walton-on-Thames: Nelson.

Cox, J.B. (1967). A review of the vane test. *Trans. I.E. Aust.*, No CE9, pp. 19-30.

Davies, M.C.R. (1981). *Centrifugal modelling of embankments on clay foundations.* Ph.D. Thesis, Univ. of Cambridge.

de Alencar, J., Chan, D.H., and Morgenstern, N.R. (1988). Progressive failure in the vane test.*Vane Shear Strength Testing in Soils : Field & Lab. Studies*, ASTM, STP 1014, A.F. Richards, Ed., Tampa, pp. 150-164.

Donald, I.B., Jordan, D.O., Parker, R.J., and Toh, C.T. (1977). The vane test — a critical appraisal. *Proc. 9th Int. Conf. S.M. & F.E.*, Tokyo, Vol. 1, pp. 81-88.

El-Ruwayih, A.A. (1976). *Stress–strain characteristics of a rock fill, and of clays under high pore water tension.* Ph.D. Thesis, Imperial College, Univ. of London.

Evans, I., and Sherratt, G.G. (1948). A simple and convenient instrument for measuring the shearing resistance of clay soils. *J. of Scientific Instruments and of Physics in Industry*, Vol. 25, pp. 411-414.

Farrent, T.A. (1960). Interpretation of vane tests in soils having friction. *Proc. 3rd Aust.– N.-Z. Conf. S.M. & F.E.*, pp. 81-86.

Flodin, N., and Broms, B. (1981). History of civil engineering in soft clay. *Soft Clay Engineering*, E.W. Brand, and R.P. Brenner, Eds., Amsterdam: Elsevier, pp. 27-308.

Francescon, M. (1983). *Model pile tests in clay: stresses and displacements due to installation and axial loading.* Ph.D. Thesis, Univ. of Cambridge.

Fukuda, M. (1980). A few considerations about the vane test. *Proc. Symp. on the Vane Test*, The Japanese Soc. S.M. & F.E., pp. 65-66. (in Japanese).

Garga, V.K. (1970). *Residual shear strength under large strains and the effect of sample size on the consolidation of fissured clay.* Ph.D. Thesis, Imperial College, Univ. of London.

Geise, J.M., Hoope, J. ten, and May, R.E. (1988). Design and offshore experience with an in-situ vane.*Vane Shear Strength Testing in Soils : Field & Lab. Studies*, ASTM, STP 1014, A.F. Richards, Ed., Tampa, pp. 318-336.

Gens, A. (1982). *Stress–strain and strength characteristics of a low plasticity clay.* Ph.D. Thesis, Imperial College, Univ. of London.

Gens, A., and Potts, D.M. (1984). Formulation of quasi-axisymmetric boundary value problems for finite element analysis. *Engrg. Computation*, Vol. 1, pp. 144-150.

Gibbs, H.J. (1960). Discussion on: Session 4 – Shear strength of undisturbed cohesive soils. *Research Conf. on Shear Strength of Cohesive Soils*, ASCE, Boulder, pp. 1067-1069.

Gibson, R.E., and Henkel, D.J. (1954). Influence of duration of tests at constant rate of strain on measured 'drained' strength. *Geotechnique*, Vol. 4, pp. 6-15.

Goughnour, R.D., and Sallberg, J.R. (1964). Evaluation of the laboratory vane shear test. *Highway Research Record*, No. 48, pp. 19-33.

Hache, R.A.G., and Valsangkar, A.J. (1988). Torsional resistance of single pile in layered soil. *J. Geotech. Engrg. Div.*, ASCE, Vol. 114, pp. 216-220.

Hansen, J.B., and Gibson, R.E. (1948). Undrained shear strengths of anisotropically consolidated clays. *Geotechnique*, Vol. 1, pp. 189-204.

Head, K.H. (1982). Manual of soil laboratory testing. Vol. 2. London: Pentech Press Ltd.

Helenelund, K.V. (1967). Vane tests and tension tsets on fibrous peat. *Proc. Geotech. Conf.*, Oslo, Vol. 1, pp. 199-203.

Hendry, A.W. (1966). Photoelastic analysis. Oxford: Pergamon Press Ltd.

Hill, R. (1950). The mathematical theory of plasticity. Oxford: Clarendon Press.

Hight, D.W. (1983). *Laboratory investigations of sea-bed clays*. Ph.D. Thesis, Imperial College, Univ. of London.

Hoeg, H. (1985). Personal communication.

James, R.G. (1971). Some aspects of soil mechanics model testing. *Proc. Roscoe Memorial Symp.*, pp. 417-440, Cambridge: G.T. Foulis & Co. Ltd.

Jardine, R.J. (1985). Investigations of pile-soil behaviour, with special reference to the foundations of off-shore structures. *Ph.D. Thesis*, Imperial College, Univ. of London.

Jones, R.H. (1961). A preliminary report on the vane test in sands. *Proc. Midlands S.M. & F.E. Soc.*, Birmingham, Vol. 4, pp. 163-175.

Karlsson, R. (1961). Suggested improvements in the liquid limit test, with reference to flow properties of remoulded clays. *Proc. 5th Int. Conf. S.M. & F.E.*, Paris, Vol. 1, pp. 171-184.

Karube, D., Shibuya, S., Baba, T., and Kotera, Y. (1988). Analysis of the vane test based on effective stress.*Vane Shear Strength Testing in Soils : Field & Lab. Studies*, ASTM, STP 1014, A.F. Richards, Ed., Tampa, pp. 131-149.

Kenney, T.C. (1959). Discussion on: Geotechnical properties of glacial lake clays. *J. Geotech. Engrg. Div.*, ASCE, Vol. 85, pp. 67-79.

Kenney, T.C., and Landva, A. (1965). Vane-triaxial apparatus. *Proc. 6th Int. Conf. S.M. & F.E.*, Montreal, Vol. 1, pp. 269-272.

Khan, A.J. (1979). *The influence of stress relief on the engineering properties of clay*. Ph.D. Thesis, Univ. of Strathclyde, Glasgow.

Kimura, T., and Saitoh, K. (1983). Effect of disturbance due to insertion on vane shear strength of normally consolidated cohesive soils. *Soils & Foundations*, Vol. 23, No. 2, pp. 113-124.

Kirkpatrick, W.M., and Khan, A.J. (1981). Interpretation of the vane test. *Proc. 10th Int. Conf. S.M. & F.E.*, Stockholm, Vol. 2, pp. 501-506.

Kirkpatrick, W.M., and Khan, A.J. (1984). The reaction of clays to sampling stress relief. *Geotechnique*, Vol. 34, pp. 29-42.

Kishida, T., Fukaya, T., and Hanzawa, H. (1986). Development of the friction meter for evaluating the skin friction of a pile. *Soils & Foundations*, Vol. 26, No. 1, pp. 122-128.

Krizek, R.J., Edil, T.B., and Ozaydin, I.K. (1975). Preparation and identification of clay samples with controlled fabric. *Eng. Geology*, Vol. 9, pp. 13-38.

Kuske, A., and Robertson, G. (1974). Photoelastic stress analysis. Great Britain: John Wiley & Sons Ltd.

Ladd, C.C., Foott, R., Ishihara, K., Schlosser, F., and Poulos, H.G. (1977). Stress–deformation and strength characteristics: state of the art report. *Proc. 9th Int. Conf. S.M. & F.E.*, Tokyo, Vol. 2, pp. 421-494.

La Rochelle, P., and Lefebvre, G. (1971). Sampling disturbance in Champlain clays. *Sampling of Soil & Rock*, ASTM, STP 483, pp. 143-163.

La Rochelle, P., Roy, M., and Tavenas, F. (1973). Field measurements of cohesion in Champlain clays. *Proc. 8th Int. Conf. S.M. & F.E.*, Moscow, Vol. 1, pp. 229-236.

Law, K.T. (1979). Triaxial-vane tests on a soft marine clay. *Canadian Geotech. J.*, Vol. 16, pp. 11-18.

Lemos, L.J.L. (1986). *The effect of rate on residual strength of soil.* Ph.D. Thesis, Imperial College, Univ. of London.

Littleton, I. (1976). An experimental study of the adhesion between clay and steel. *J. Terramechanics*, Vol. 13, No. 3, pp. 141-152.

Love, J.P. (1984). *Model testing of geogrids in unpaved roads.* Ph.D. Thesis, Univ. of Oxford.

Mahmoud, M. (1988). Vane testing in soft clays. *Ground Engrg.*, Vol. 21, No. 7, pp. 36-40.

Mair, R.J. (1979). *Centrifugal modelling of tunnel construction in soft clay.* Ph.D. Thesis, Univ. of Cambridge.

Martins, J.P. (1983). *Shaft resistance of axially loaded piles in clay.* Ph.D. Thesis, Imperial College, Univ. of London.

Matsui, T., and Abe, N. (1981). Shear mechanisms of vane test in soft clays. *Soils & Foundations*, Vol. 21, No. 4, pp. 69-80.

Menzies, B.K., and Mailey, L.K. (1976). Some measurements of strength anisotropy in soft calys using diamond-shaped shear vanes. *Geotechnique*, Vol. 26, pp. 535-538.

Menzies, B.K., and Merrifield, C.M. (1980). Measurements of shear stress distribution on the edges of a shear vane blade. *Geotechnique*, Vol. 30, pp. 314-318.

Menzies, B.K., and Phillips, A.B. (1972). On the making of rubber membranes. *Geotechnique*, Vol. 30, pp. 153-155.

Menzies, B.K., and Simons, N.E. (1977). Stability of embankments on soft ground, Chapter 11, Developments in S.M.–1, Ed. C.R. Scott, London: Applied Science Publishers Ltd.

Merrifield, C.M. (1980). *Factors affecting the interpretation of the in situ shear vane test.* Ph.D. Thesis, Univ. of Surrey.

Mohan, D., and Jain, G.S. (1957). Field vane tests. *Civ. Engrg. & Public Works Review*, Vol. 52, No. 618, pp. 1387-1388.

Morgenstern, N.R., and Tchalenko, J.S. (1967). Microscopic structures in kaolin subjected to direct shear. *Geotechnique*, Vol. 17, pp. 309-328.

Odeh, M.A. (1980). *The shearing behaviour of kaolin and illite.* M.Sc. Thesis, Univ. of Strathclyde, Gasgow.

O'Neill, M.W., and Dutt, R.N. (1976). Discussion on: Torsional response of piles. *J. Geotech. Engrg. Div.*, ASCE, Vol. 102, pp. 658-660.

Perlow, M., and Richards, A.F. (1977). Influence of shear velocity on vane shear strength. *J. Geotech. Engrg. Div.*, ASCE, Vol. 103, pp. 19-32.

Photolastic, Inc. (1969). Introduction to stress analysis by the photoelastic coating technique. Technical Bulletin TDG-1. USA, Pa., Malvern: Photolastic, Inc.

Potts, D.M. (1984). *Earth pressures*, Soil Mech. M.Sc. Course Notes, Imperial College, Univ. of London.

Potts, D.M., and Fourie, A.B. (1986). A numerical study of the effects of wall deformation on earth pressures. *Int. J. for Numerical & Analytical Methods in Geomechanics*, Vol. 10, pp. 383-405.

Potts, D.M., Dounias, G.T., and Vaughan, P.R. (1987). Finite element analysis of the direct shear box test. *Geotechnique*, Vol. 37, pp. 11-23.

Poulos, H.G. (1975). Torsional response of piles. *J. Geotech. Engrg. Div.*, ASCE, Vol. 101, pp. 1019-1035.

Pugh, R.S. (1978). *The strength and deformation characteristics of a soft alluvial clay under full scale loading conditions.* Ph.D. Thesis, Imperial College, Univ. of London.

Randolph, M.F. (1981). Piles subjected to torsion. *J. Geotech. Engrg. Div.*, ASCE, Vol. 107, pp. 1095-1111.

Reynolds, C.E., and Steedman, J.C. (1981). Reinforced concrete designer's handbook. 9th ed., Mount Durand: Toucan. (A Viewpoint Publication).

Richards, R., and Mark, R. (1966). Gelatin models for photoelastic analysis of gravity structures. *Experimental Mechanics*, pp. 30-38.

Rosenfarb, J.L. (1975). *Effect of fabric on the directional shear strength of a kaolin clay.* Ph.D. Thesis, Northwestern Univ.

Roy, M. (1975). Measurements of in situ shear strength. *Proc. Conf. on In Situ Measurement of Soil Properties*, ASCE, Rayleigh, Vol. 2, pp. 164-167.

Roy, M., and Leblanc, A. (1988). Factors affecting the measurements and interpretation of the vane strength in soft sensitive clays.*Vane Shear Strength Testing in Soils : Field & Lab. Studies*, ASTM, STP 1014, A.F. Richards, Ed., Tampa, pp. 117-128.

Rush, K.J. (1975). *A study of the vane shear test.* M.Sc. Thesis, Univ. of Cambridge.

Schmertmann, J.H. (1975). Measurement of in-situ shear strength. *Proc. Specialty Conf. on In-situ Measurement of Soil Properties*. ASCE, Rayleigh, Vol. 2, pp. 57-138.

Schreiner, H.D. (1977). *An investigation into some factors affecting the strength of underslurry piles*. M.Sc. (Eng.) Thesis, Univ. of Natal, Durban.

Selvadurai, A.P.S. (1979). On the estimation of the deformability characteristics of an isotropic elastic soil medium by means of a vane test. *Int. J. for Numerical & Analytical Methods in Geomechanics*, Vol. 3, pp. 231-243.

Sharifounnasab, M., and Ullrich, C.R. (1985). Rate of shear effects on vane shear strength. *J. Geotech. Engrg. Div.*, ASCE, Vol. 111, pp. 135-139.

Shibuya, S. (1981). *Appraisal of $\phi_u = 0$ method.* M.Sc. Dissertation, Univ. of Kobe, Japan.

Skempton, A.W. (1948). Vane tests in the alluvial plain of the River Forth near Grangemouth. *Geotechnique*, Vol. 1, pp. 111-124.

Skempton, A.W., and Northey, R.D. (1952). The sensitivity of clays. *Geotechnique*, Vol. 3, pp. 30-53.

Sridharan, A., and Madhav, M.R. (1964). Time effects on vane shear strength and sensitivity of clay. *Proc. ASTM*, Vol. 64, pp. 958-967.

Steenfelt, J.S., Randolph, M.F., and Wroth, C.P. (1981). Instrumental model piles jacked into clay. *Proc. 10th Int. Conf. S.M. & F.E.*, Stockholm, Vol. 2, pp. 857-864.

Stephenson, G. (1987). Personal communication.

Stimpson, B. (1970). Modelling materials for engineering rock mechanics. *Int. J. Rock Mech. & Min. Sci.*, Vol. 7, pp. 77-121.

Stoll, U.W. (1972). Torque shear test of cylindrical friction piles. *Civ. Engrg.*, ASCE, Vol. 42, No. 4, pp. 63-65.

Stoll, U.W. (1976). Discussion on: Torsional response of piles. *J. Geotech. Engrg. Div.*, ASCE, Vol. 102, pp. 660-661.

Taylor, R.N. (1984). *Ground movements associated with tunnels and trenches* Ph.D. Thesis, Univ. of Cambridge.

Tchalenko, J.S. (1967). *The influence of shear and consolidation on the microscopic structure of some clays*. Ph.D. Thesis, Imperial College, Univ. of London.

Tominaga, M., and Hanzawa, H. (1986). Skin friction of pile evaluated from the friction meter test in situ. Personal communication to D.W. Hight.

Tomlinson, M.J. (1957). The adhesion of pile driven in clay soils. *Proc. 4th Int. Conf. S.M. & F.E.*, London, Vol. 2, pp. 66-71.

Torstensson, B.A. (1977). Time-dependent effects in the field vane test. *Proc. Int. Symp. on Geotechnical Aspects of Soft Clays*, Bangkok, pp. 387-397.

Veneman, P.L.M. (1977). *Shear strength measurements in representative Wisconsin soils*. Ph.D. Thesis, Univ. of Wisconsin–Madison.

Veneman, P.L.M., and Edil, T.B. (1988). Micromorphological aspects of the vane shear test. *Vane Shear Strength Testing in Soils : Field & Lab. Studies*, ASTM, STP 1014, A.F. Richards, Ed., Tampa, pp. 182-190.

Vey, E., and Schlesinger, L. (1949). Soil shear tests by means of rotating vanes. *Proc. Highway Research Board*, Vol. 29, pp. 544-553.

Wiesel, C.-E. (1973). Some factors influencing in-situ vane test results. *Proc. 8th Int. Conf. S.M. & F.E.*, Moscow, Vol. 1, pp. 475-479.

Wilson, N.E. (1963). Laboratory vane shear tests and the influence of pore-water stresses. *Lab. Shear Testing of Soils*, ASTM, STP 361, pp. 377-389.

Wroth, C.P. (1984). Twenty-fourth Rankine Lecture: The interpretation of in situ soil tests. *Geotechnique*, Vol. 34, pp. 447-489.

APPENDIX A1

BASIC PHOTOELASTICITY

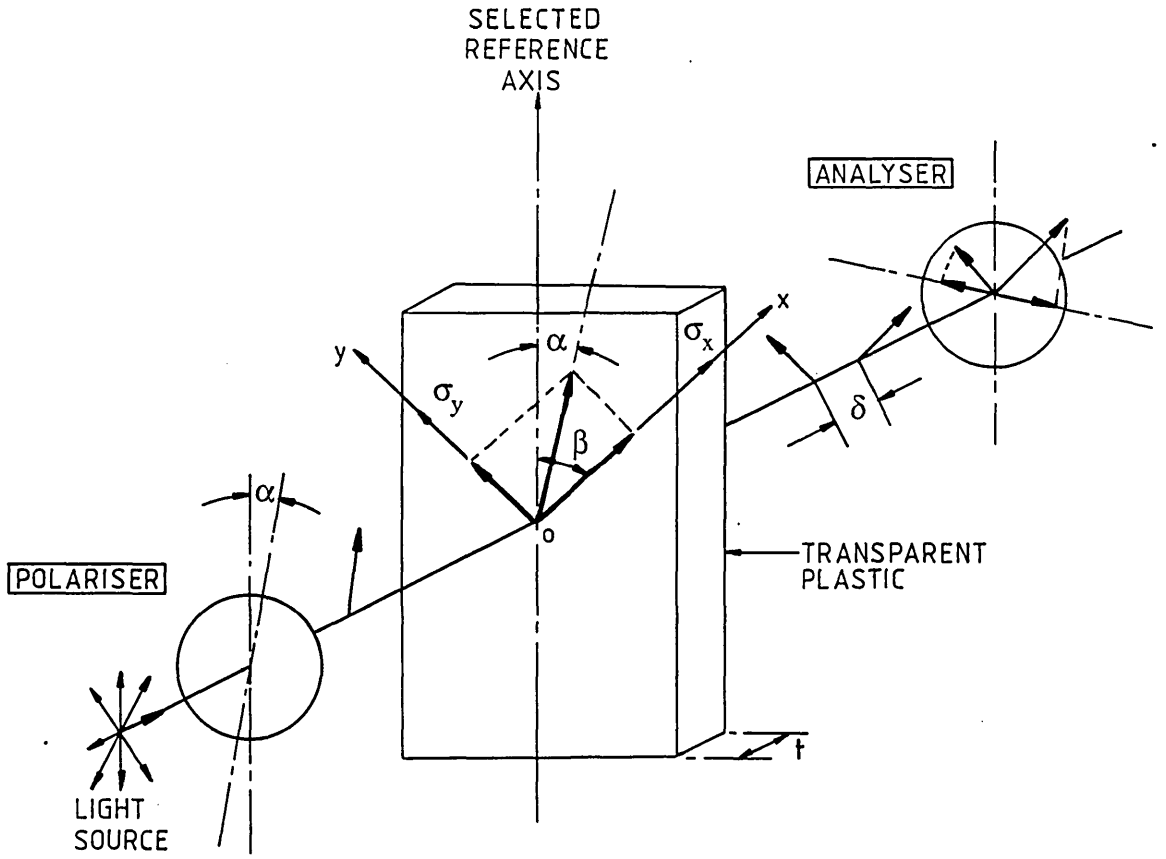
Light propagates in a vacuum or in air at a speed (C) of 3 x 10^8 m/sec. In other transparent media, the speed of light (V) is lower and the ratio C/V is called the "index of refraction". In a homogeneous medium this index is constant regardless of the direction of propagation of light.

Glass, gelatine, polyurethane rubber and certain plastics are transparent materials which are optically isotropic when unstressed, but when stressed become 'anisotropic', owing to changes in the refractive index which result as a consequence of stress changes; the latter are known as "stress birefringent" materials. Thus, plane-polarised light — an organised beam of light contained in one plane only — entering such materials will be split into two components, plane polarised in the directions of the principal stresses at each point in the material (Fig. A1.1). This property, known as "double refraction", makes these materials ideal for photoelastic modelling.

The two components of light will travel through the material at different velocities and will emerge from it having a relative "retardation", δ. This retardation or "phase difference" is directly proportional to the magnitude of the difference of the principal stresses, as well as to the thickness and the stress-optic coefficient of the material; the latter being established by calibration. As a result of the retardation, the light components will interfere with each other upon emerging from the material, with the interference manifesting itself as a photoelastic pattern over the entire material such that the magnitude of the retardation at any point in the model, which is represented by different colours when the light source is white, is proportional to the principal stress difference at that point. These colour "fringes" are known as "isochromatics" and are more clearly observed when a circular polariscope is used (see Fig. A1.2); the isochromatics represent points of equal principal stress difference in the material. "Fringe orders", N (where $\delta = N\lambda$, and λ is the wavelength of the colour fringe), are identified by assigning to every colour fringe its order: 0, 1, 2, 3, etc; the fringes are related to increasing strain.

At all points in the material where the direction of either one of the principal stresses is parallel to the polarising axis of the polaroid filters (i.e. the polariser and analyser), extinction occurs (Fig. 3.16a). These points are continuous forming black bands known as "isoclinics". If the polariser and analyser are kept crossed and rotated, new isoclinics will appear and previous ones will disappear. Since the isoclinics are independent of the magnitude of the load employed, patterns which are not confused by the presence of isochromatics can therefore be obtained by applying small loads which produce only a few or no isochromatic fringes. However, the applied loads should be sufficiently large so that the isoclinics would not be appreciably influenced by any initial or residual stresses present in the material.

The directions of the principal stresses at any point within the model are known as the "stress trajectories", and may be obtained by mapping a complete set of isoclinics throughout the model; the principal stress directions lie along and orthogonal to the directions of the isoclinics, and are measured with reference to a convenient datum, like an axis of symmetry of the test part or structure. The directions of the shear stresses at any point within the model lie at 45° to the stress trajectories.



KEY

x and y	:	planes of propagation of polarised light beams
σ_x and σ_y	:	principal stresses
δ	:	relative retardation between the polarised light beams
$\beta - \alpha$	:	the angle between the analyser and direction of principal stresses ; extinction occurs when the crossed polaroids are parallel to the direction of principal stresses , i.e.

Fig. A1.1 Theoretical aspects of a plane polariscope (after Photolastic , 1969).

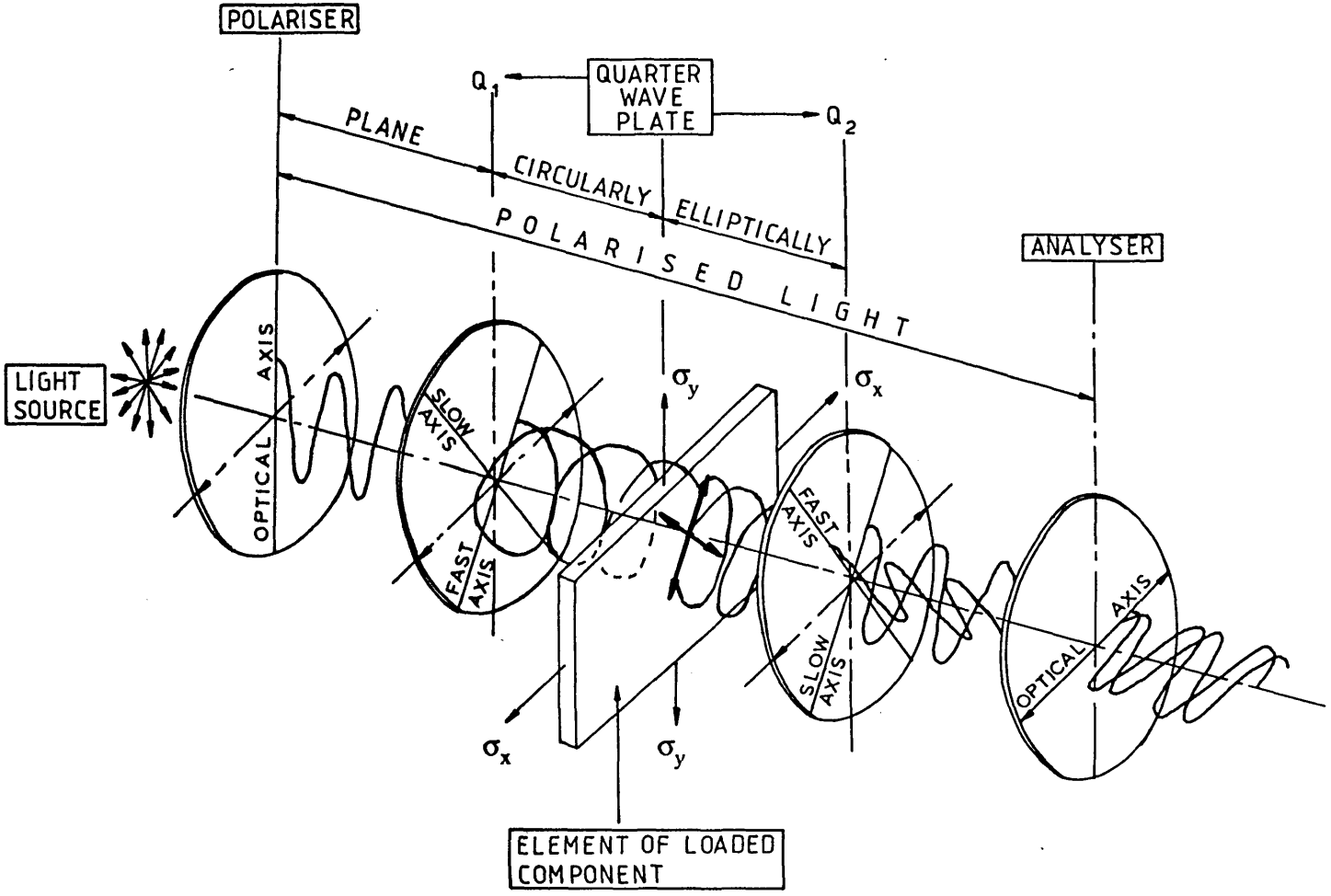


Fig. A1.2 Main components of a circular polariscope.

APPENDIX A2

THEORIES OF CONSOLIDATION FOR THE VANE TEST

A2.1 INTRODUCTION

The process of consolidation involves a decrease in the water content of a saturated soil without replacement of water by air, and is a consequence of stress changes giving rise to an instantaneous increase in the pore pressures within the soil mass. Dissipation of the generated excess pore pressures leads to a change in the volume of voids and subsequently the soil mass consolidates; the stresses in the soil being dependent upon time. An analogy to this process is that of conduction of heat in solids. The generation of heat in a solid at a specified rate per unit time per unit volume is similar to the process of excess pore pressure generation in soils. The variation of temperature within solids is governed by the process of heat conduction and likewise the pore pressure variation in a soil is controlled by the process of pore pressure dissipation. Therefore, it may be considered that the problem of consolidation in soils is mathematically equivalent to the heat conduction problem in solids. Equations which arise in consolidation theory are based on similar equations which occur in the theory of heat conduction.

Table A2.1 lists the parameters relevant in the analysis of problems involving consolidation and the analogous parameters which occur in the analysis of problems of heat conduction in solids.

The aim of this Appendix is to present the theories which have been developed for the analysis of the process of consolidation in relation to the vane test. First, Blight's (1968) theory is presented and discussed, and then, improvements to, and modifications of this theory are suggested.

Heat Conduction in Solids		Consolidation in Soils	
K	thermal conductivity of solid	k	permeability of soil
κ	diffusivity of solid	c_v	coefficient of consolidation
ρ	average density	γ_w	unit weight of water
c	specific heat of solid	m_v	coefficient of volume change of soil
A_0	rate of heat generation per unit time per unit volume	A	rate of change of pore water volume per unit time per unit volume
v	temperature	u	pore water pressure

Table A2.1
Analogy of parameters in consolidation of soils with those in conduction of heat in solids.

A2.2 BLIGHT'S THEORY (THE SPHERICAL CASE)

The simplified theory of consolidation which Blight developed for the vane test enables the pre-selection of the time to failure (or the rate of vane rotation) required to measure the undrained strength. The assumptions made by Blight are as follows:

(a) Before the start of vane rotation, i.e. at t = 0, there are no excess pore pressures due to vane insertion.
(b) The generation of excess pore pressures due to vane rotation is uniform within the volume of soil influenced.
(c) The volume of soil affected during the rotation of the vane is represented by a sphere of radius a, centred at the mid-point of the vane.
(d) Torque and excess pore pressures both increase at a constant rate up to failure but, thereafter, the torque remains constant and pore pressures fall.

These assumptions are considered reasonable for the moment; however, reference should be made to Appendix A2.4 for a discussion of their validity.

The analogous case in problems of heat conduction in solids is that of the sphere $0 \leq r \leq a$, with zero initial and surface temperatures and heat generation at a constant rate A_0 per unit time per unit volume, for which the differential (conduction) equation is given as follows:

$$\frac{1}{r^2}\frac{\partial}{\partial r}\left(r^2\frac{\partial v}{\partial r}\right)-\frac{1}{\kappa}\frac{\partial v}{\partial t}=\frac{-A_0}{K} \qquad \text{Eq. A 2.1}$$

i.e.

$$\frac{1}{r^2}\frac{\partial}{\partial r}\left(r^2\frac{\partial v}{\partial r}\right)+\frac{A_0}{K}=\frac{1}{\kappa}\frac{\partial v}{\partial t}$$

where v = temperature,
$\kappa = K/\rho c$, and
K, ρ, and c are thermal conductivity, average density and specific heat of the solid, respectively.

By letting $w = vr$ and rearranging, Eq. A2.1 becomes

$$\frac{1}{\kappa}\frac{\partial w}{\partial t}=\frac{\partial^2 w}{\partial r^2}+\frac{A_0 r}{K} \qquad \text{Eq. A 2.2}$$

The solution to Eq. A2.2 is given by Carslaw & Jaeger (1986) as:

$$v = \frac{A_0}{K}\left[\frac{(a^2 - r^2)}{6} + \frac{2}{\pi^3}\frac{a^3}{r}\sum_{n=1}^{\infty}\frac{(-1)^n}{n^3}\sin\frac{n\pi r}{a}e^{-n^2\pi^2\kappa t/a^2}\right] \qquad \text{Eq. A 2.3}$$

The consolidation equation analogous to the conduction equation given by Eq. A2.1 is:

$$\frac{1}{r^2}\frac{\partial}{\partial r}\left(r^2\frac{\partial u}{\partial r}\right) + \frac{A\gamma_w}{k} = \frac{1}{c_v}\frac{\partial u}{\partial t} \qquad \text{Eq. A 2.4}$$

where A is the rate of change of pore water volume per unit time per unit volume, and γ_w is the unit weight of water.

The solution to Eq. A2.4 which satisfies the initial and boundary conditions assumed (see assumptions (a) and (c), above), giving an expression for the excess pore water pressure, u, is therefore as follows:

$$u = \frac{A\gamma_w}{k}\left[\frac{(a^2 - r^2)}{6} + \frac{2}{\pi^3}\frac{a^3}{r}\sum_{n=1}^{\infty}\frac{(-1)^n}{n^3}\sin\frac{n\pi r}{a}e^{-n^2\pi^2 c_v t/a^2}\right] \qquad \text{Eq. A 2.5}$$

But

$$A = \frac{\Delta e}{(1+e)\,\Delta t} \qquad \text{Eq. A 2.6}$$

and

$$a_v = \frac{\Delta e}{\Delta u} \quad \text{(a)} \qquad\qquad m_v = \frac{a_v}{1+e} \quad \text{(b)} \qquad \text{Eq. A 2.7}$$

where

e = voids ratio of soil,

a_v = coefficient of compressibilty of soil, and

m_v = coefficient of volume change of soil.

From assumption (d), above, u_0 increases linearly with time and thus:

$$\frac{\Delta u_0}{\Delta t} = \frac{u_0}{t_f} \qquad \text{Eq. A 2.8}$$

At failure, therefore,

$$A = m_v \frac{u_0}{t_f} \qquad \text{Eq. A 2.9}$$

Hence,

$$\frac{A\gamma_w}{k} = \frac{m_v \gamma_w}{k} \frac{u_0}{t_f} = \frac{u_0}{c_v t_f} \qquad \text{Eq. A 2.10 (Eq. 4.7)}$$

Substituting Eq. A2.10 in Eq. A2.5, it follows that

$$\frac{u_f}{u_0} = \frac{1}{c_v t_f}\left[\frac{(a^2 - r^2)}{6} + \frac{2}{\pi^3}\frac{a^3}{r}\sum_{n=1}^{\infty}\frac{(-1)^n}{n^3}\sin\frac{n\pi r}{a}\, e^{-n^2\pi^2 c_v t_f / a^2}\right] \qquad \text{Eq. A 2.11}$$

The above expression was derived by Blight (1968).

The expression for the degree of dissipation of pore pressure, U, is:

$$U = 1 - \frac{u_f}{u_0} \qquad \text{Eq. A2.12 (a) (Eq. 4.5)}$$

The expression for the time factor, T, is:

$$T = \frac{c_v t_f}{D^2} \qquad \text{Eq. A2.12 (b)}$$

where D = vane diameter.

Since maximum shear stresses are measured at the tip of the vane blades (Menzies & Merrifield, 1980), pore pressures at failure (i.e. u_f) would probably occur along the surface circumscribing the tips of the vane blades as well. Hence, the case to consider in Eq. A2.11 is that in which r = D/2.

For vanes with H/D = 2, the drainage surface would probably lie between a = D and a = 3D/2 (Blight, 1968). For vanes with H/D = 1, however, it seems more appropriate that the drainage surface would lie between a = 2D/3 and a = D (writer). This is clearly demonstrated in Figs. 4.23a and b.

By expressing the radius of the sphere of influence, a, in terms of the vane diameter, D, Eq. A2.11 would reduce to a form which can be presented in terms of U and T only. Equations in which U is expressed in terms of T for the different drainage boundaries considered in Section 4.4.5 (and Section 2.4) are given below:

1. a = D, r = D/2 (Blight, 1968)

$$U = 1 - \frac{1}{T}\left[\frac{1}{8} + \frac{4}{\pi^3}\sum_{n=1}^{\infty}\frac{(-1)^n}{n^3}\sin\frac{n\pi}{2}e^{-n^2\pi^2 T}\right] \qquad \text{Eq. A 2.13}$$

2. a = 3D/2, r = D/2 (writer)

$$U = 1 - \frac{1}{T}\left[\frac{1}{3} + \frac{27}{2\pi^3}\sum_{n=1}^{\infty}\frac{(-1)^n}{n^3}\sin\frac{n\pi}{3}e^{-4n^2\pi^2 T/9}\right] \qquad \text{Eq. A 2.14}$$

3. a = 2D/3, r = D/2 (writer)

$$U = 1 - \frac{1}{T}\left[\frac{7}{216} + \frac{32}{27\pi^3}\sum_{n=1}^{\infty}\frac{(-1)^n}{n^3}\sin\frac{3n\pi}{4}e^{-9n^2\pi^2 T/4}\right] \qquad \text{Eq. A 2.15}$$

4. a = 4D/5, r = D/2 (writer)

$$U = 1 - \frac{1}{T}\left[\frac{39}{600} + \frac{256}{125\pi^3}\sum_{n=1}^{\infty}\frac{(-1)^n}{n^3}\sin\frac{5n\pi}{8}e^{-25n^2\pi^2 T/16}\right] \qquad \text{Eq. A 2.16}$$

5. a = 2D, r = D/2 (writer)

$$U = 1 - \frac{1}{T}\left[\frac{5}{8} + \frac{32}{\pi^3}\sum_{n=1}^{\infty}\frac{(-1)^n}{n^3}\sin\frac{n\pi}{4}e^{-n^2\pi^2 T/4}\right] \qquad \text{Eq. A 2.17}$$

A2.3 THE CYLINDRICAL CASE

When the size of the vane is small compared to the volume of soil in which it is rotated, it is valid to examine consolidation effects associated with the vane test on the basis that the volume of soil affected is that of the sphere. However, due to the nature of the mode of failure associated with the vane test (Section 6.3), it is probable that most of the drainage resulting from the dissipation of pore pressures would occur in the radial direction. For the case of a soil sample whose height does not exceed that of the vane, it is perfectly valid to assume that drainage occurs mainly in the radial direction; under such circumstances, an infinite cylinder model, with impermeable boundaries at its top and bottom, would be a better representation of the problem of consolidation around the vane than the spherical model.

For a circular cylinder model representing the volume of soil affected by the vane, the equation of consolidation corresponding to a constant rate of generation of excess pore pressure per unit time per unit volume is:

$$\frac{\partial^2 u}{\partial r^2} + \frac{1}{r}\frac{\partial u}{\partial r} + \frac{A\gamma_w}{k} = \frac{1}{c_v}\frac{\partial u}{\partial t} \qquad \text{Eq. A 2.18}$$

Given that at $t = 0$, $u = 0$ and for $t \geq 0$, $u = 0$ at $r = a$, i.e. the same initial and boundary conditions as those adopted for the spherical case, Carslaw & Jaeger (1986) give the solution to Eq. A2.18 as:

$$u = \frac{A\gamma_w}{k}\left[\frac{(a^2 - r^2)}{4} - \frac{2}{a}\sum_{n=1}^{\infty}\frac{J_0(r\alpha_n)}{\alpha_n^3 J_1(a\alpha_n)} e^{-\alpha_n^2 c_v t}\right] \qquad \text{Eq. A 2.19}$$

where α_n are given by the positive roots of the transcendental equation $J_0(a\alpha_n) = 0$.

Letting $a\alpha_n = \lambda_n$ and considering failure conditions, Eq. A2.19 becomes:

$$\frac{u_f}{u_0} = \frac{1}{c_v t_f}\left[\frac{(a^2 - r^2)}{4} - 2a^2\sum_{n=1}^{\infty}\frac{J_0(r\lambda_n / a)}{\lambda_n^3 J_1(\lambda_n)} e^{-\lambda_n^2 c_v t_f / a^2}\right] \qquad \text{Eq. A 2.20}$$

where λ_n are the positive roots of Bessel's function of order zero, $J_0(\lambda_n) = 0$, which can be found in the British Association Mathematical Tables (1950).

For the case where a = 4D/5 and r = D/2,

$$U = 1 - \frac{1}{T}\left[\frac{39}{400} - \frac{32}{25}\sum_{n=1}^{\infty}\frac{J_0(5\lambda_n/8)}{\lambda_n^3 J_1(\lambda_n)} e^{-25\lambda_n^2 T/16}\right] \qquad \text{Eq. A 2.21}$$

A2.4 CRITICISMS OF BLIGHT'S THEORY

To date, there has not been a thorough review of the assumptions made by Blight in connection with the process of consolidation around the vane during its rotation. Assumptions (a), (c) and (d) — stated in Appendix A2.2 — are acceptable as there is evidence to support them (see Blight, 1968; Matsui & Abe, 1981). However, in assumption (b), it is postulated that the generation of excess pore pressures due to vane rotation is uniform within the sphere of influence. Clearly, this is an incorrect assumption since it is known that excess pore pressures are generated as a result of the rotation of the vane and they therefore would vary with position within the zone of influence, whatever its shape maybe (see, e.g. Davies, 1981). Consequently, it would be wrong to assume that the excess pore pressures (u) are of the same magnitude within the zone of influence: at a radius R + δR from the centre of the zone of influence, it would be expected that u would have a lower value than that at a radius R (where R is the radius of the vane). Therefore, it is wrong to assume that the rate of change of pore water volume, A, is a constant.

A better representation of the processes which occur during vane rotation would result by considering that pore pressure generation is a function of position. For an elastic medium subjected to shear in the horizontal plane, i.e. as is the case in the vane test, the exact expression for the variation of pore pressure in terms of the rate of change of pore water volume per unit time per unit volume of soil is given by:

$$A(r,\theta) = C\frac{\cos\theta}{r^2} \qquad \text{Eq. A 2.22}$$

where C is a constant depending on the soil properties and θ represents variations in the vertical plane of a sphere; the reference point being θ = 90° (Stephenson, 1987).

It is assumed that there is no variation of A in the radial direction, i.e. in the horizontal plane of a sphere, since the 'source' of pore pressure generation is the 'annulus' which circumscribes the vane blades; pore pressure generation is uniform along the annular source.

It should be noted that the expression given by Eq. A2.22 applies to the generation of pore pressures as a consequence of vane rotation and any subsequent pore pressure variation with position. An analogy with the generation of heat in solids and subsequent temperature variation with position is not immediately obvious. However, it is assumed that it is physically possible for the generation of heat in solids to vary with position according to Eq. A2.22.

For the pore pressure variation given by Eq. A2.22, the consolidation equation is:

$$\frac{1}{r^2}\frac{\partial}{\partial r}\left(r^2\frac{\partial u}{\partial r}\right)+\frac{1}{r^2\sin\theta}\frac{\partial}{\partial\theta}\left(\sin\theta\frac{\partial u}{\partial\theta}\right)+\frac{C\sin\theta}{kr^2}=\frac{1}{c_v}\frac{\partial u}{\partial t} \qquad \text{Eq. A 2.23}$$

N.B. When $\theta = 0°$ is taken as the reference point, $A = C\cos\theta/r^2$ becomes $A = C\sin\theta/r^2$.

Since a closed form solution does not exist for Eq. A2.23, numerical methods have to be used; due to time constraints, the latter was not undertaken.

APPENDIX A3

INTERPRETATION OF THE VANE TEST FOR c–ϕ MATERIALS

A number of attempts have been made to develop an interpretation of the vane test for c–ϕ soils (Evans & Sherratt, 1948; Farrent, 1960; Arnold, 1978). The former are based on the concept of a cylindrical failure surface, while Arnold assumes a logarithmic spiral shearing surface which protrudes beyond the perimeter of the circumscribing circle and then appears to lie within the circle.

Using the concept of a spiral failure surface with no progressive failure it is possible to derive an expression for the total torque measured with an n-bladed vane. The moment of resistance of the shearing stress along the surface AB (Fig. 5.12) is given by:

$$\int_{A}^{B} dM$$

where dM is the moment of resistance of an element ds of the shear surface with a shear stress, τ, acting on it.

dM is given by:

$$dM = R\,\tau\,ds \qquad \text{Eq. A3.1}$$

where R is the radius of the vane, $\tau = \tau_A\, e^{2\theta \tan\phi}$, and $ds = R\,d\theta$.

$\therefore$

$$M = \int_{\theta=0}^{\beta} dM = R^2\,\tau_A \int_{\theta=\theta_A=0}^{\beta} e^{2\theta \tan\phi}\, d\theta$$

$$= \frac{R^2\tau_A}{2\tan\phi}\left[e^{2\beta \tan\phi} - 1 \right] \qquad \text{Eq. A3.2}$$

Hence, the total moment of resistance along the vertical shearing surface for an n-bladed vane of height, H, is:

$$M_v = \frac{nHR^2}{2\tan\phi}\tau_A\,(e^{4\pi/n\ \tan\phi} - 1) \qquad \text{Eq. A3.3}$$

Assuming a uniform shear stress distribution along the top and bottom horizontal surfaces, the total moment of resistance along these surfaces is given by

$$M_h = 2\int_0^{D/2} 2\pi R^2 \tau_h\, dR$$

$$= \frac{\pi D^3}{6}\tau_h \qquad \text{Eq. A3.4}$$

where τ_h is the shear stress developed along the vane horizontal surfaces.

Thus, the total torque due to the resistance along both the horizontal and vertical surfaces of the vane is given by

$$M = \frac{\pi D^3}{6}\tau_h + \frac{nHR^2}{2\tan\phi}\tau_A\left[\, e^{4\pi/n\ \tan\phi} - 1 \,\right] \qquad \text{Eq. A3.5}$$

The magnitude of τ_A can be established from Mohr-Coulomb considerations (see Fig. A3.1). It is assumed that the minor principal stress acting across the blade tip at the instance of failure is $\sigma_3 = K_0\sigma_1$. Thence, for a soil with shear stress strength parameters, c and ϕ, the following expressions may be written:

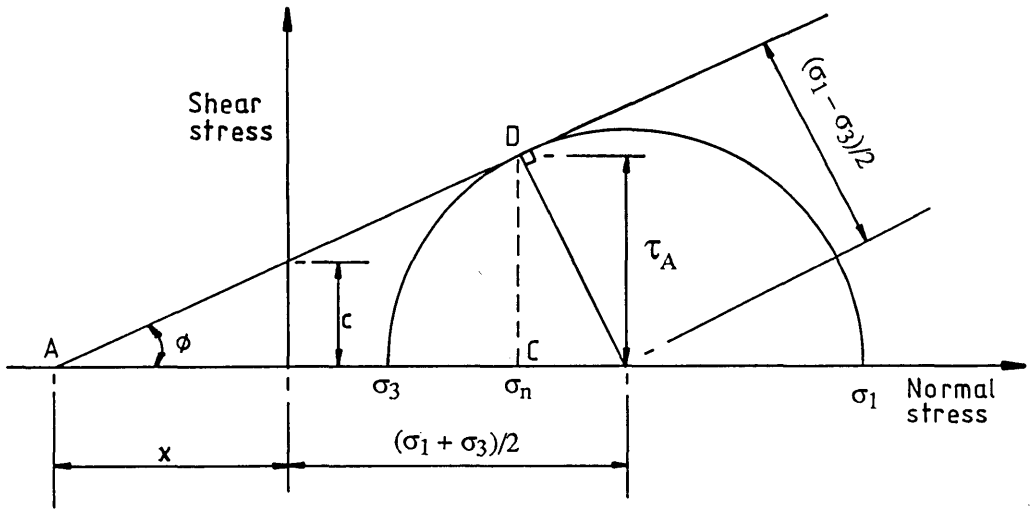


Fig. A3.1 Determination of τ_A from Mohr-Coulomb considerations.

$$\sin\phi = \frac{(\sigma_1 - \sigma_3)/2}{x + (\sigma_1 + \sigma_3)/2}$$

$$= \frac{\sigma_1 - \sigma_3}{2x + \sigma_1 + \sigma_3} \qquad \text{Eq. A3.6}$$

$$\tan\phi = \frac{c}{x} \Rightarrow x = \frac{c}{\tan\phi}$$

$\therefore$

$$\sin\phi = \frac{\sigma_1 - \sigma_3}{\frac{2c}{\tan\phi} + \sigma_1 + \sigma_3} \qquad \text{Eq. A3.7}$$

But

$$\sin\phi = \frac{\tau_A}{AD} \Rightarrow \tau_A = AD \sin\phi \qquad \text{Eq. A3.8}$$

and

$$\tan\phi = \frac{(\sigma_1 - \sigma_3)/2}{AD} \Rightarrow AD = \frac{(\sigma_1 - \sigma_3)}{2\tan\phi} \qquad \text{Eq. A3.9}$$

Substituting Eq. A3.9 in Eq. A3.8:

$$\tau_A = \frac{(\sigma_1 - \sigma_3)}{2\tan\phi} \sin\phi \qquad \text{Eq. A3.10}$$

From Eq. A3.7:

$$\frac{\sin\phi}{1 - \sin\phi} = \frac{\sigma_1 - \sigma_3}{\frac{2c}{\tan\phi} + \sigma_1 + \sigma_3 - (\sigma_1 - \sigma_3)}$$

$$2\frac{\sin\phi}{1 - \sin\phi}\left[\frac{c}{\tan\phi} + \sigma_3\right] = \sigma_1 - \sigma_3 \qquad \text{Eq. A3.11}$$

Substituting Eq. A3.11 in Eq. A3.10:

$$\tau_A = (c + \sigma_3 \tan\phi)\frac{\sin^2\phi}{(1 - \sin\phi)\tan^2\phi} \qquad \text{Eq. A3.12}$$

Simplifying the $\sin^2\phi$ term in Eq. A3.12:

$$\frac{\sin^2\phi}{(1-\sin\phi)\tan^2\phi} = \frac{\cos^2\phi}{1-\sin\phi} = \frac{1}{\sec^2\phi - \dfrac{\tan\phi}{\cos\phi}} = \frac{1}{1+\tan\phi\left[\tan\phi - \dfrac{1}{\cos\phi}\right]}$$

$$\Rightarrow \frac{1}{1-\tan\phi\left[\dfrac{1-\sin\phi}{\cos\phi}\right]} = \frac{1}{1-\dfrac{\tan\phi}{\left[\dfrac{\cos\phi}{1-\sin\phi}\right]}} = \frac{1}{1-\dfrac{\tan\phi}{\left[\dfrac{\cos^2\phi/2 - \sin^2\phi/2}{1-2\sin\phi/2\cos\phi/2}\right]}}.$$

Dividing the denominator of the $\tan\phi$ term by $\cos^2\phi/2$:

$$\Rightarrow \frac{1}{1-\dfrac{\tan\phi}{\left[\dfrac{1-\tan^2\phi/2}{\sec^2\phi/2 - 2\tan\phi/2}\right]}} = \frac{1}{1-\dfrac{\tan\phi}{\left[\dfrac{(1-\tan\phi/2)(1+\tan\phi/2)}{(1-\tan\phi/2)^2}\right]}}$$

$$\Rightarrow \frac{1}{1-\dfrac{\tan\phi}{\tan(45+\phi/2)}}$$

$\therefore$

$$\tau_A = \frac{c+\sigma_3\tan\phi}{1-\dfrac{\tan\phi}{\tan(45+\phi/2)}} \qquad \text{Eq. A3.13}$$

APPENDIX A4

ANALYSIS OF THE VANE TEST IN TERMS OF EARTH PRESSURES

Section 6.6 outlined the assumptions made in, and the results obtained from a 'retaining wall analysis' of the 2-bladed vane. The calculations which were carried out, leading to the conclusions reached in Section 6.6, are presented below.

The case considered is that of the 4-bladed vane test series on normally consolidated kaolin with a water content of about w = 60% (Section 6.3.3A; Fig. 6.7). The measured peak torque was about M_4 = 0.05 N-m, which according to the conventional interpretation corresponds to a vane shear strength of τ_f = 13.8 kPa. This reference value of M_4 will be compared with the peak torque obtained by modelling the 2-bladed vane in terms of two retaining walls.

Assume that each vane blade simulates one rough retaining wall subjected to rotation about its top (Figs. 6.45 and A4.1). Coulomb's limit equilibrium method (Section 6.6) may be used to analyse the model: in this approach, the resultant force on the wall, P_R, is given by the difference between the passive resistance, P_P, and the active thrust, P_A, which would act in front of and behind the 'wall' respectively.

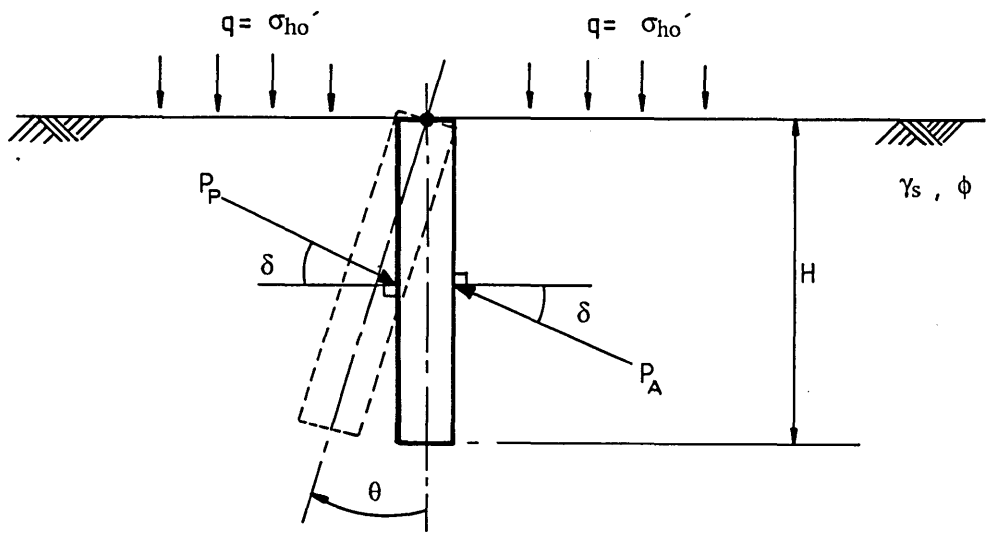


Fig. A4.1 Retaining wall subjected to rotation about its top.

For the case under consideration, P_P and P_A may, to a first approximation, be represented by the following formulae:

$$P_P = \frac{1}{2}\gamma_s H^2 K_P + qHK_P \qquad \text{Eq. A4.1}$$

$$P_A = \frac{1}{2}\gamma_s H^2 K_A + qHK_A \qquad \text{Eq. A4.2}$$

in which γ_s = saturated unit weight of soil,
H = 'wall' height,
q = surcharge, and
K_P and K_A are coefficients of passive and active earth pressures respectively.

Given that drained conditions may be assumed (see Sections 4.4.1, 4.4.2 and 4.4.5), the expressions for K_P and K_A (see, e.g. Potts, 1984) are as follows:

$$K_P = \left[\frac{\cos\phi}{1 - \left[\frac{\sin(\phi+\delta)\sin\phi}{\cos\delta}\right]^{1/2}}\right]^2 \qquad \text{Eq. A4.3}$$

$$K_A = \left[\frac{\cos\phi}{1 + \left[\frac{\sin(\phi+\delta)\sin\phi}{\cos\delta}\right]^{1/2}}\right]^2 \qquad \text{Eq. A4.4}$$

where ϕ = soil friction angle, assumed to equal ϕ_{ps};
δ = 'wall' friction angle, assumed to equal $2\phi/3$.

Calculations using the above formulae will lead to an estimation of the resultant force per unit length of 'wall', P_R. The total resultant force on the entire length of 'wall' is thus given by:

$$F_R = P_R L \qquad \text{Eq. A4.5}$$

where L = 'wall' length (= 12×10^{-3} m; Fig. 6.45).

Hence, the torque about the top of the 'wall' is given by:

$$M_R = F_R\, l \qquad \text{Eq. A4.6}$$

where l is the lever arm, and denotes the position of the centre of gravity of the net pressure distribution (diagram) through which F_R acts.

For the case under consideration, the relevant parameters are as follows:

$\gamma_s = \{(G+e)/(1+e)\}\ \gamma_w = 16.0$ kN/m^3, since G = 2.61 (Table 3.2), $\gamma_w = 9.81$kN/m^3, and $e = wG = 0.6 \times 2.61 = 1.57$

$H = 6 \times 10^{-3}$ m

$q = \sigma_{ho}'$ (see Fig. 6.45, Section 6.6, and Fig. A4.1); $\sigma_{ho}' = K_0\sigma_{vo}'$

where $K_0 \approx 1 - \sin\phi_{tc} \approx 0.61$, since for one-dimensional normal consolidation, the conditions are axially symmetric and thus it is considered more appropriate to express K_0 in terms of ϕ_{tc} (= 23°; Table 3.3), and not ϕ_{ps} (see, e.g. Wroth, 1984), and σ_{vo}' may be obtained by using Eq. 6.2, from which the vane shear strength ratio is equal to

$(\tau_f/\sigma_{vo}')_{n.c.} = (1 - \sin 26)\sin 26 = 0.246$, since $\phi_{ps} = 9\phi_{tc}/8 \approx 26°$.

Thence, $\sigma_{vo}' = 13.8 / 0.246 \approx 56$ kPa, and $\sigma_{ho}' = 0.61 \times 56 \approx 34.2$ kPa.

$K_p = 4.199$; $K_A = 0.331$.

Hence, $P_P = 0.8628$ kN/m length of 'wall',
$P_A = 0.0680$ kN/m length of 'wall', and
$P_R = 0.7948$ kN/m length of 'wall'.

Along the whole length of 'wall'

$F_R = 9.54 \times 10^{-3}$ kN.

The position of the centre of gravity of the net pressure distribution (diagram) from the top of the 'wall' is given by:

$l \approx 0.5H$.

Therefore, the torque about the top of the 'wall' is:

$M_R = 2.862 \times 10^{-5}$ kN-m, which for two 'walls', will equal:
$M_{2R} = 2M_R = 5.72 \times 10^{-5}$ kN-m ≈ 0.057 N-m.